



**Faculté de génie
Département de génie civil et de génie du bâtiment**

**DÉVELOPPEMENT DES BÉTONS NANO-MODIFIÉS AUX
PERFORMANCES AMÉLIORÉES**

***(NANO-ENGINEERING CONCRETE PROPERTIES FOR ENHANCED
PERFORMANCE)***

Thèse de doctorat
Spécialité : Génie civil

Thèse présentée au département de génie civil et de génie du bâtiment en
vue de l'obtention du grade Docteur en philosophie en génie

*(A dissertation submitted in partial fulfillment
of the requirements for the degree of Doctor of Philosophy in
Civil Engineering)*

Ousmane Ahmat HISSEINE

Jury: Arezki Tagnit-Hamou (directeur de these/ Thesis director)

Ammar Yahia (Président de jury/jury president)

Richard Gagné (rapporteur/reporter)

Carmel Jolicoeur (évaluateur interne/internal examiner)

Surendra P. Shah (évaluateur externe/external examiner)

Victor C. Li (évaluateur externe/external examiner)

Le 24-juillet-2019

Le jury a accepté la thèse de Monsieur Ousmane Ahmat Hisseine dans sa version finale
(*The jury has accepted the thesis of Mr. Ousmane Ahmat Hisseine in its final version*)

Jury:

Professeur Arezki Tagnit-Hamou
Directeur de thèse/ Thesis director
Université de Sherbrooke, Canada

Professeur Ammar Yahia
Président de jury/Jury president
Université de Sherbrooke, Canada

Professeur Richard Gagné
Rapporteur/Reporter
Université de Sherbrooke, Canada

Professeur Carmel Jolicoeur
Évaluateur interne/Internal examiner
Université de Sherbrooke, Canada

Professeur Surendra P. Shah
Évaluateur externe/External examiner
Northwestern University, USA

Professeur Victor C. Li
Évaluateur externe/External examiner
University of Michigan, USA

RÉSUMÉ

Compte tenu de la nature multi-échelle des défauts dans le béton, il s'ensuit que les diverses tentatives existantes en technologie de béton fibré (BF)—visant à atténuer la tendance intrinsèque du béton à la fissuration—demeurent toujours relativement inefficaces. Ceci est attribué non seulement au fait que le grand espacement interfibrillaire des macro-fibres (dans un BF) ne favorise pas un pontage efficace des fissures multi-échelles, mais aussi au fait que le phénomène de fissuration commence tout d'abord à l'échelle nanométrique. En conséquence, des travaux de recherche et de développement considérables ont été investis au cours de la dernière décennie pour développer des bétons incorporant des particules nanométriques. Ainsi, les nanofibres ont émergé comme un outil efficace permettant la manipulation du béton au niveau de sa nanostructure tel que celle-ci soit conçue de manière à contrôler le comportement du béton à l'échelle macroscopique pour obtenir des bétons à performances améliorées. Dans ce contexte, bien que les nanomatériaux à base de carbone tels que les nanofibres de carbone et les nanotubes de carbone ont acquis une popularité relative, certaines préoccupations liées à leur coût actuel ainsi qu'à la santé humaine et environnementale favoriseraient plutôt les matériaux nano-cellulosiques. Ces derniers ont apparu récemment comme un enjeu permettant de conférer des propriétés composites améliorées nécessaires pour des applications aussi variées telles que les adhésifs, les nano-composites, et les électroniques transparentes.

La présente étude vise à explorer les possibilités d'améliorer les propriétés du béton à l'aide d'un nouveau type de matériaux nano-cellulosiques, notamment, les filaments de cellulose (FC), afin d'obtenir des performances améliorées nécessaires pour des applications ciblées. Les FC sont des fibrilles cellulosiques de diamètre nanométrique (30 à 400 nm) et de longueur micrométrique (100 à 2000 μm), présentant ainsi le ratio d'aspect le plus élevé (100 à 1000) parmi tous les matériaux nano-cellulosiques actuellement disponibles. L'étude se concentre sur l'impact de FC comme un outil permettant d'améliorer les propriétés du béton dans ses trois principaux états (frais, durcissant et durci). En conséquence, trois applications en relation avec ces états du béton ont été identifiées grâce à un programme expérimental compréhensif: (i) amélioration des propriétés du béton frais en utilisant le FC comme agent modificateur de viscosité (VMA), (ii) amélioration des propriétés du béton durcissant en utilisant le FC comme un agent réducteur de retrait (iii) amélioration de la performance du béton à l'état durci en utilisant le FC comme un renforcement nanométrique pour conférer un pontage de fissures à l'échelle des hydrates. L'étude vise, en outre, à mettre en vigueur ces différentes améliorations

(en propriétés du béton) apportées par l'utilisation de FC pour développer une nouvelle formulation de béton, ainsi optimisant les apports de FC.

L'amélioration des propriétés du béton à l'état frais a été entamée dans le cadre de valoriser l'aspect hydrophile des FC, leur taille nanométrique et leur flexibilité afin de conférer un effet VMA dans les bétons autoplaçants (BAP) dont la formulation nécessite un équilibre délicat entre la fluidité et la stabilité. Dans ce contexte, les FC ont été incorporés à des concentrations de 0,05-0,30% en masse de liants dans des pâtes de ciment et des BAP. Les résultats démontrent que les FC peuvent servir d'un adjuvant VMA permettant non seulement d'améliorer la rhéologie, mais aussi de conférer des effets positifs collatéraux aux performances mécaniques (amélioration de 12–26% de la résistance en compression, traction brésilienne et flexion) par rapport aux bétons contenant de VMA conventionnels de type Welan Gum. L'effet VMA des FC est attribué à la formation des réseaux de fibrilles de FC nanométriques et flexibles permettant de percoler les particules cimentaires et accroître la stabilité des mélanges tel que démontré à travers un modèle de percolation géométrique ainsi que par les études de la microstructure. A ce propos, Il est à noter que l'effet de VMA conféré par les FC est également accompagné d'un effet rhéofluidifiant attribuable à la tendance des FC flexibles à s'aligner dans la direction de l'écoulement du mélange sous un cisaillement croissant.

La potentialité des FC d'améliorer les propriétés des bétons durcissant a été évaluée dans le contexte d'exploiter les caractères hydrophiles et hygroscopiques des FC pour atténuer le retrait endogène dans les bétons fibrés à ultra hautes performances (BFUP). Ainsi, alors que les BFUP peuvent contenir jusqu'à 25% de fumée de silice (pour accroître la compacité et maximiser la résistance mécanique), cette teneur élevée en fumée de silice rend la matrice vulnérable au retrait endogène. Cependant, la réduction de la teneur de la fumée de silice jusqu'à 15% résulte à une matrice moins vulnérable au retrait endogène, néanmoins présentant une faible résistance mécanique. Dans ce sens, l'incorporation des FC à des taux de 0-0,30% par masse de liant a permis produire des BFUP ayant 25% de fumée de silice et présentant une réduction en retrait endogène allant jusqu'à 45% et 35% au cours des premières 24 heures et 7 jours, respectivement.

Enfin, la potentialité des FC en tant que renforcement nanométrique a été étudiée sur des pâtes de ciment et sur des bétons. Dans le premier cas, des propriétés mécaniques améliorées (résistance à la compression, résistance à la flexion et module d'élasticité) allant jusqu'à 25% ont été obtenues. Dans le deuxième cas, des améliorations de résistance allant jusqu'à 16% (en compression), 34% (en traction brésilienne), 22% (en flexion) et 96% (en ténacité) ont été obtenues. Pour identifier les mécanismes sous-jacents à l'effet des FC sur la résistance

mécanique des composite cimentaires, les observations ci-dessus ont été supplémentées par des études de la microstructure, notamment le degré d'hydratation et les propriétés micromécaniques (dureté, module d'indentation, et le fluage par contact) de phases de microstructure en utilisant la méthode de *Nanoindentation coupled with quantitative energy-dispersive spectroscopy* (NI-QEDS). Ainsi, il a été constaté que les performances macro-mécaniques améliorées découlaient d'un double effet des FC sur la microstructure, à savoir : un degré d'hydratation augmenté (15%) et des propriétés micromécaniques supérieures dans la matrice de C-S-H (~ 12-25%).

Pour une mise en valeur des différents apports de la nano-modification des composites cimentaires par l'incorporation des FC, en particulier l'effet nano-renforçant et la synergie entre les FC à l'échelle nanométrique et les macro-fibres, une nouvelle formulation d'un béton de haute performance de type béton écrouissant (*Strain-hardening cementitious composites*) a été développée. La conception de ce nouveau béton a suivi une nouvelle approche articulant l'optimisation de la compacité granulaire avec les modèles micromécaniques. Ainsi, la poudre de verre (PV) provenant du concassage des bouteilles de verre a été incorporée en remplacement de la cendre volante (CV) – souvent utilisée dans cette application – de manière à optimiser la compacité de la matrice pour améliorer la résistance mécanique. Par la suite, les FC ont été introduits comme un renforcement nanométrique permettant d'obtenir un béton renforcé à multi-échelle. Les résultats démontrent que les FC ont permis de nano-renforcer la matrice ainsi que d'améliorer les propriétés d'interface entre la matrice et les macro-fibres d'alcool polyvinylique (PVA), permettant ainsi d'améliorer le comportement d'écrouissage. Ainsi, des bétons écrouissant contenant jusqu'à 100% de PV en remplacement de CV ont été développés. Les formulations obtenues ont un caractère autoplaçant (≈ 250 mm d'étalement) et présentent (à 28 jours) une résistance à la compression de 60-75 MPa, une capacité de flexion de 9-15 MPa, une résistance à la traction de 3-6 MPa, une capacité de contrainte en traction de 2-5% et une résistivité électrique améliorée. Les bétons formulés présentent, alors, des performances mécaniques supérieures à celles des bétons écrouissants contenant la CV. Néanmoins, bien que l'amélioration en résistance mécanique obtenue avec la PV ne compromette pas la ductilité du composite jusqu'à une teneur de 40% de PV, une ductilité réduite a été observée quand la teneur en PV dépasse 40%. Pour ce, le FC a été utilisé pour conférer un effet nano-renforçant ainsi que pour améliorer les propriétés d'interface entre la matrice et les macro-fibres. L'incorporation des FC a démontré un double effet sur le comportement des bétons écrouissants : (i) le module d'élasticité de la matrice plane des bétons écrouissant est très important en présence des FC. Ceci a contribué à réduire la ténacité de la fissuration, (ii) les FC ont atténué la friction excessive

– entre les macro-fibres et la matrice – rencontrée à des teneurs élevées en PV (limitant la ductilité du béton). Les FC ont aussi conféré un effet écrouissant à l'arrachement des macro-fibres de PVA permettant ainsi d'accroître la capacité de contrainte en traction. Une amélioration en capacité de déformation et en ductilité au-delà de 200% par rapport aux bétons écrouissants sans FC a été obtenue. Ainsi, avec l'incorporation de FC, il était possible de produire des bétons écrouissant contenant jusqu'à 100% de PV en remplacement de CV tout en présentant des résistances mécaniques et ductilités plus importantes.

Pour une mise à l'échelle des performances mécaniques améliorées (particulièrement la ductilité importante) démontées par la nouvelle formulation de béton écrouissant, cette dernière a été utilisée comme un surbéton pour développer un nouveau type de dalles composites à échelle réelle (allant jusqu'à 2400 × 900 mm). La nouvelle dalle composite est envisagée de bénéficier de la ductilité améliorée de son surbéton écrouissant de manière à accroître la compatibilité structurale entre le tablier métallique et son surbéton. Ceci a pour but d'améliorer la résistance à la détérioration de l'adhésion d'interface tablier-béton, un des principaux types de ruptures des dalles composites. Les résultats indiquent que, comparément à des dalles composites construites de béton à haute performance ayant la même résistance en compression que le nouveau béton écrouissant, les dalles composites au béton écrouissant ont démontré une amélioration de 35 et 42% en capacité maximum de chargement et en ductilité, respectivement. De même, les dalles composites au béton écrouissant ont démontré une résistance plus élevée à la détérioration de l'adhésion d'interface tablier-béton, autrement dit, une amélioration à la capacité cisaillement-adhésion connue par *shear-bond capacity*.

À cet égard, la nouvelle formulation du béton écrouissant développée dans le cadre cette étude (et implémentée de l'échelle nano/micro jusqu'à l'échelle structurale réelle) s'est vue bénéficiée de deux aspects liés à l'éco-efficacité. Le premier concerne la valorisation du verre recyclé dans un béton à haute performance, contribuant ainsi à alléger le fardeau socio-économique important créé par l'enfouissement de verre de post-consommation. Le deuxième concerne la mise en exergue de la cellulose—le polymère naturel le plus abondant et le plus renouvelable sur la planète—vers le développement de bétons à haute performance (renforcés à multi-échelle) nécessaires pour des infrastructures en béton plus performantes.

Mots clés : Béton écologique ; Béton fibré ; béton nano-modifié ; composites cimentaires écrouissant ; matériaux nano-cellulosiques ; micromécanique ; optimisation de compacité granulaire ; poudre de verre recyclée.

ABSTRACT

In light of the well-established multi-scale nature of flaws in concrete, it follows that existing diverse attempts in fiber-reinforced concrete (FRC) technology—intended to mitigate the inherent tendency of concrete to cracking—remain relatively inefficient. This is majorly attributed to the fact that the large inter-fiber spacing in conventionally used macrofibers does not promote an effective bridging of multiscale cracks. As a result, increasing research and development are currently being invested to develop concretes incorporating nanoscale particles. Thus, nanoscale fibers emerged as a promising tool for manipulating concrete nanostructure towards a controlled macrobehavior necessary for enhanced overall performance. In this context, while carbon nanostructure (CNS) such as carbon nanofibers (CNF) and carbon nanotubes (CNT) have gained a relative popularity, it should be noted that eco-efficiency incentives would favor the currently emerging nanocellulose materials (NCM) extracted from cellulose-based systems, the most abundant and renewable resource on the planet. NCM have been demonstrated as a means to engineer superior composite properties necessary for versatile applications including optics, biomedical applications, and transparent electronics.

The current study is aimed at disclosing the possibilities of re-engineering concrete properties using a new type of NCM, namely, cellulose filaments (CF) in order to achieve superior concrete performance necessary for specific applications. CF are cellulosic fibrils with a nanometric diameter (30–400 nm) and micrometric length (100–2000 μm), thereby exhibiting the highest aspect ratio (100–1000) among all currently available NCM. The study focuses on the influence of CF as a tool for nano-tailoring the properties of concrete in its three major states (fresh, hardening, and hardened). As a result, three applications in relation to the above concrete states were identified through intensive experimentation: (i) enhancing the properties of fresh concrete by using CF as a viscosity modifying admixture (VMA), (ii) enhancing the properties of hardening concrete by using CF as a shrinkage reducing admixture (SRA), and (iii) improving the performance of concrete at the hardened state by using CF as a nanoscale reinforcement. The study further aims at leveraging those different enhancements in concrete properties obtained with CF towards developing a new concrete formulation that optimizes the advantages of CF.

The enhancement of concrete properties at fresh state was undertaken in the context of valorizing the hydrophilic and flexible nanoscale CF to function as a VMA in self-consolidating concrete (SCC) whereby the design of flowable (yet stable and robust) mixtures requires a

delicate balance between flowability and stability. For this, CF were incorporated at concentrations ranging from 0.05 to 0.30% per weight of binder in cement pastes and SCC. CF were demonstrated as a valuable tool not only for rheology modification, but also to impart collateral positive effects on mechanical performance (strength enhancement of 12–26% in compression, splitting-tension, and flexure) when compared to commercially available VMA of Welan Gum type. CF were found to serve as a VMA due to the buildup of flexible nanoscale networks as demonstrated by a geometry-based percolation model as well as by microstructure investigations. Interestingly, this effect was found to be accompanied by a shear thinning effect attributable to the streamlining of flexible nanocellulose fibrils in the direction of flow under increasing shear rates, thereby potentially enhancing pumpability.

The potential of CF to enhance the properties of hardening concrete was attempted in the context of exploiting the hydrophilic and hygroscopic characters of CF to mitigate autogenous shrinkage (AS) in ultra-high-performance concrete (UHPC). While such, when UHPC formulation was adjusted to accommodate CF at rates of 0–0.30% per cement mass, and silica fume content was varied (from 15 to 25%), CF were found to be more beneficial in reducing AS at early-age with a reduction of up to 45% during the first 24 hours and 35% at 7 days. On the other hand, adjusting SF content from 25 to 15% had a negligible effect on AS at early-age (0–4% reduction at 1 day) but a higher effect at later-age (28% reduction at 7 days) attributable to the time-dependent pozzolanicity of silica fume. However, this alternative was found to have adverse effects on mechanical performance (32% lower flexural capacity).

Finally, the potential of CF as a nanoscale reinforcement was investigated on cement pastes and on concrete. In the former, strength enhancement in engineering properties (compressive strength, flexural capacity, and elastic modulus) of up to 25% were achieved. In the latter, strength improvements of up to 16% (in compression), 34% (in splitting tension), 22% (in flexure), and 96% (in energy absorption) were obtained. To disclose the mechanisms underpinning the effect of CF on strength of cement systems, the above findings were supplemented by microstructure investigations, namely, degree of hydration and micromechanical properties (indentation modulus M , hardness H , and contact creep modulus C) of major microstructure phases using nanoindentation coupled with quantitative energy-dispersive spectroscopy (NI-QEDS). As a result, the improved macromechanical performance was found to sprout from a twofold microstructure change, i.e.: an increased degree of hydration and higher micromechanical properties of C-S-H gel matrix (~12–25%).

To leverage the above different advantages offered by CF on cement and concrete composites, particularly the nanoreinforcing effect and the potential synergy between the nanoscale CF and macrofibers, a novel multi-scale fiber-reinforced strain-hardening cementitious composite (SHCC) was developed. The design of this SHCC followed a new approach that couples packing density optimization with micromechanical tailoring. Thus, high-volume ground-glass pozzolans (HVGP) were incorporated under the guidance of particle packing optimization to replace fly ash (FA) commonly used in SHCC such that composite strength can be increased. The newly formulated SHCC was further improved in terms of ductility and strain-hardening capacity by the incorporation of CF whereby the latter was a useful tool to nanomodify SHCC matrix and interface properties towards enhanced strain-hardening behavior. In outcome, HVGP-SHCC formulations with GP replacement of fly ash of up to 100% were developed. The resulting formulations have self-consolidation ability (mini-slump diameter in the range of 250 mm) and exhibited (at 28 days) 60-75 MPa compressive strength, 9-15 MPa flexural capacity, 3-6 MPa tensile strength, 2-5% tensile strain capacity, and a significantly increased electrical resistivity (up to 60% enhancement). Thus, the mechanical properties of the newly developed HVGP-SHCC exceed those reported in the commonly used high-volume fly ash (HVFA)-SHCC. Nevertheless, while the strength enhancement obtained with GP does not jeopardize composite ductility up to 40% GP content, a reduced ductility was noticed at GP>40%. As a result, CF were used to impart a nanoreinforcing effect to HVGP-SHCC as well as to nanomodify the interface properties of PVA fibers. In outcome, a twofold effect was obtained by nanomodifying SHCC with CF: (i) CF imparted higher elastic modulus to the bulk cementitious matrix (E_m) thereby contributed to attenuating the crack tip toughness ($J_{tip} = K_m^2/E_m$) with K_m being matrix fracture toughness, (ii) CF led to attenuating the excessive frictional bond encountered at higher GP content (densifying the matrix and increasing its strength, but limiting strain-hardening behavior) and imparted a characteristic slip-hardening effect (β) which contributed towards improving composite strain-hardening capacity and ductility. Thus, enhancement in ultimate strain-capacity above 200% as compared to systems without CF were obtained. Therefore, with the incorporation of CF, it was possible to produce SHCC with up to 100%GP replacement of FA while exhibiting higher strength and ductility.

To scale-up the enhanced mechanical performance (particularly the high strength and ductility) demonstrated by the new SHCC, the latter was used as a topping to develop a novel type of composite deck slabs at full-scale (dimensions of up to 2400 × 900 mm). The composite deck slabs thus constructed are intended to benefit from the improved strength and ductility of

nanomodified HVGP-SHCC topping such that better compatibility between the steel deck and its concrete topping can be obtained. This has the potential to increase the performance of composite deck slabs under shear bond failure, a major failure mode in composite deck slabs. Results indicated that, compared to composite deck slabs with a high-strength concrete topping having similar compressive strength as the nanomodified HVGP-SHCC, the slabs constructed with the SHCC exhibited up to 35 and 42% enhancement in ultimate load-carrying capacity and ductility, respectively. Furthermore, composite deck slabs with nanomodified HVGP-SHCC exhibited higher shear bond capacity.

Considering these results, it is perceivable that the newly developed SHCC (implemented from the material level at the nanoscale to the structural level at the macroscale) has benefited from a twofold ecoefficiency perspective. The first concerns the valorization of post-consumer recycled glass into the development of high-performance concrete, thereby contributing to relieve a significant socio-economical burden created by landfilling post-consumer glass. The second concerns exploiting the power of cellulose, the most abundant naturally occurring polymer on the planet, towards a biomimetic design of high-performance multiscale-reinforced cement composites necessary for sustainable and resilient concrete infrastructure systems.

Key word: Ecological concrete; fiber-reinforced concrete; micromechanics; nanocellulose materials; nanomodified concrete; particle packing optimization; recycled glass powder; strain-hardening cementitious composites.

DEDICATION

To my parents for withstanding all life challenges to provide schooling to us (their offspring) though they missed that chance,

To my wife Sarra for the endless support and love,

To my kids Ousman, Razan, and Amir for sweetening my life.

To my siblings and friends for their valuable support

À mes parents pour avoir surmonté des défis énormes dans mon

parcours scolaire,

À mon épouse Sarra et mes enfants Ousman, Razan et Amir pour

pour le soutien et l'amour inconditionnel,

À mes frères, sœurs et amis pour le soutien continue.

ACKNOWLEDGEMENT

Praise to God, Lord of the Worlds for endowing me with the resilience to timely accomplish this challenging project while trying to equilibrate between my research responsibilities and my family commitments.

Thanks to my supervisor Prof. Arezki Tagnit-Hamou for his continuous support not only in this project but in the whole academic endeavor. Specific appreciation to Arezki goes for offering access to high-caliber research resources and for providing quality supervision in streamlining research activities towards project milestones while offering me an adequate margin of research independence.

My thanks are also extended to the Natural Sciences and Engineering Research Council of Canada (NSERC) for offering me the Vanier Scholarship (the most competitive and prestigious scholarship nation-wide) as part of the Canada Graduate Scholarships for the 2016-2019 term. Although my field of specialization takes often a bit longer PhD duration, the generous financial support offered to me through Vanier Scholarship, the prestige of this award and its fixed term of 3 years as well as the networking with elite peers were indeed determinants for motivation and powerful catalysts for productivity in quality research. My thanks also go to Kruger Biomaterials Inc. and to Euclid Chemicals for the support and the useful communications indispensable for project deliverables.

My thanks also go to the department of Civil and Building Engineering for facilitating research and administrative logistics, to Prof. Ammar Yahia for his cooperation through his research resources, to Prof. Richard Gangé for the useful discussions, to Dr. Ahmed Omran for his indispensable support, to my colleagues with whom I collaborated in some phases of my research (Nancy Soliman and William Wilson), to my colleagues who offered me assistance (Aghiles Begresh, Ablam Zidol, Jafar Rashidi, and Masoud Hosseinpour), and the valuable support offered by our lab technicians (Frédéric, Denis, Rajko, Ghislaine, and Josée).

My appreciations are also extended to the jury members (Carmel Jolicoeur, Richard Gagné, Surendra Shah, and Victor Li) for accepting to revise my work and particular thanks go to Surendra Shah, and Victor Li for accepting to travel to Sherbrooke to physically attend my thesis defense.

Last and most importantly, my thanks go to my wife Sarra for the love and support, particularly for understanding my research commitments and to my kids Ousman, Razan, and Amir for the joy and fun contributing to equilibrate research and family life.

Thanks to anyone else who contributed somehow, but his name did not appear mistakenly.

Hisseine, Ousmane Ahmat

Sherbrooke, 17 April 2019

TABLE OF CONTENTS

(Table de matière)

RÉSUMÉ	i
ABSTRACT	ixv
DEDICATION	ix
ACKNOWLEDGEMENT	x
TABLE OF CONTENTS	xi
LIST OF FIGURES	xiii
LIST OF TABLES	xv
ABBREVIATIONS AND SYMBOLS	xvi
CHAPTER 1. Introduction	22
1.1 Research Background and Context	22
1.2 Research definition	25
1.3 Research objectives	26
1.4 Research methodology	27
1.5 Thesis structure and original research contributions	32
1.6 References	35
CHAPTER 2. Literature Review	38
2.1 General	38
2.2 Fiber reinforced concrete	38
2.2.1 Historical overview	38
2.2.2 Classification of fiber reinforced concrete based on fiber type	40
2.2.2.1 Steel Fiber Reinforced Concrete (SFRC)	40
2.2.2.2 Synthetic fiber reinforced concrete (SNFRC)	41
2.2.2.3 Glass fiber reinforced concrete (GFRC)	42
2.2.2.4 Natural fiber-reinforced concrete (NFRC)	42
2.2.3 Strengthening mechanism of FRC	44
2.2.4 Effect of fibers on pre- versus post-cracking mechanism	45
2.3 Nanomodified concrete	51
2.3.1 Nano-powders in cement composites	52
2.3.1.1 Nano-SiO ₂	53
2.3.1.2 Nano-TiO ₂	53
2.3.2 Carbon-nanostructures	55
2.3.2.1 carbon nanotubes (CNT) and carbon nanofibers (CNF)	56
2.3.2.2 Graphene oxide (GO)	59
2.3.3 Nanocellulose Materials (NCM)	61
2.3.3.1 Structure of cellulose	61
2.3.3.2 Hierarchical structure of cellulose	63
2.3.3.3 Nanocellulose materials and opportunities for composite design	64
2.3.3.4 Common types of nanocellulose materials (NCM)	67

2.3.3.5	Mechanical properties of nanocellulose materials (NCM).....	67
2.3.3.6	Nanocellulose materials in cement and concrete composites.....	70
2.3.3.6.1.	<i>Cement hydration and structuration</i>	70
2.3.3.6.2.	<i>Potential role of NCM on cement hydration and in FRC mechanism.</i>	75
2.3.3.6.3.	<i>Concluding remarks on the effect of NCM on cement systems</i>	90
2.3.4	Nanoengineering fiber-reinforced cementitious composites (FRCC)	91
2.3.4.1	Stain-hardening cementitious composites (SHCC)	94
2.3.4.2	Nanoengineered stain-hardening cementitious composites.....	97
2.3.4.3	Structural application of SHCC.....	100
2.4	References	103
CHAPTER 3:	Effect of Cellulose Filaments (CF) on Rheology	121
3.1	Introduction.....	121
3.2	Article 1-Feasibility of using CF as a viscosity modifying agent in SCC	122
CHAPTER 4:	Effect of Cellulose Filaments (CF) on Hardening Concrete	165
4.1	Introduction.....	165
4.2	Article 2-Controlling autogenous shrinkage UHPC with CF	166
CHAPTER 5:	Effect of Cellulose Filaments on Hardened Concrete	208
5.1	Introduction.....	208
5.2	Article 3- Influence of Cellulose Filaments on Cement Paste and Concrete.....	209
CHAPTER 6:	Effect of Cellulose Filaments on Microstructure	254
6.1	Introduction.....	254
6.2	Article 4- Microstructure study for the effects of CF on cement systems	255
CHAPTER 7:	Nanomodification of Interface Properties of HVGP-SHCC	300
7.1	Introduction.....	300
7.2	Article 5- Nano-engineering interface properties of SHCC.....	301
CHAPTER 8:	Development of SHCC with high-volume GP	349
8.1	Introduction.....	349
8.2	Article 6- Development of ecological SHCC with high-volume GP.....	350
CHAPTER 9:	Nano-engineered SHCC	401
9.1	Introduction.....	401
9.2	Article 7- Nanocellulose for nano-engineered SHCC with high-volume GP	402
CHAPTER 10:	Structural application of HVGP-SHCC	461
10.1	Introduction.....	461
10.2	Article 8- Nanoengineered SHCC for high performance composite slabs.....	462
CHAPTER 11:	Conclusions and Perspectives (English)	484
CHAPTER 12:	Conclusions et Recommendation (Francais)	489

LIST OF FIGURES

(Lise des figures)

Chapter 1

Fig. 1. 1 Schematic illustration of research methodology	31
Fig. 1. 2 Schematic view of overall thesis organization.....	34

Chapter 2

Fig. 2.1: Common fibers used in FRC technology.....	40
Fig. 2.2: Microstructure and molecular structures of natural fiber cell wall	43
Fig. 2.3: Fracture mechanism of FRC	45
Fig. 2.4: Schematic illustration of the effect of different fiber scale on fracture behavior	47
Fig. 2.5: Relationship between particle size and specific surface area.....	52
Fig. 2.6: The <i>Dives in Misericordia</i>	54
Fig. 2.7: Carbon nanostructures.....	55
Fig. 2.8: Crack bridging in cement-CNT composites.....	58
Fig. 2.9: Cement hydration products in the presence of graphene oxide (GO)	60
Fig. 2.10: Mechanism of formation of petal-like hydration products in GO systems.....	61
Fig. 2.11 Structure of cellulose.....	63
Fig. 2.12: Hierarchical structure of cellulose	64
Fig. 2.13: Length-to-width relationship (aspect ratio) in NCM	68
Fig. 2.14: Micrographs of cellulose NCM.....	69
Fig. 2.15: Schematic illustration of cement hydration	71
Fig. 2.16: Microstructure of hydrating Portland cement pastes	72
Fig. 2.17: Microstructure of cementitious matrix and interfacial transition zone (ITZ)	74
Fig. 2.18: Nanoengineering with CF	77
Fig. 2.19: Effect of different addition rates of nanofibrillated cellulose	81

Fig. 2.20: Hydration products in the presence of CNC	82
Fig. 2.21: SEM image of microcrystalline cellulose (MCC).....	84
Fig. 2.22: Flexural performance of cement pastes with CNC.....	85
Fig. 2.23: Synerby between nananocellulose and microfibers.	87
Fig. 2.24: Classification of fiber-reinforced cementitious composites.....	93
Fig. 2.25. Fiber birding stress – crack opening width relationship	95
Fig. 2.26: Overall view of hierarchical structure of abalone shell.	98
Fig. 2.27: Effect of different fiber scale on fracture behavior.....	99
Fig. 2.28: Effect of nanocellulose materials on the performance of.....	99
Fig. 2.29: Application of ECC for Bridge Deck Link Slabs	101
Fig. 2.30: SHCC Structural applications	102

Chapters 3-10

Individual List of Figures are provided in each chapter as part of the journal article requirements

LIST OF TABLES

Chapter 2

Table 2.1. Properties of cellulose and other reinforcing materials.	66
Table 2.2. Mechanical properties of common nanocellulose materials	66
Table 2.3: Summary of literature on NCF cement composites	89

Chapters 3-10

Individual List of Tables are provided in each chapter as part of the journal article.

ABBREVIATIONS AND SYMBOLS

1. ABBREVIATIONS

BC	Bacterial cellulose
CF	Cellulose filaments
CH	Calcium hydroxide
CNF	Carbon nanofibers
CNT	Carbon nanotubes
CPM	compressible packing model
C-S-H	Calcium-silicate-hydrate
EA	Expansive agents
ECC	Engineered cementitious composites
ECC	Engineered cementitious composites
EDS	Energy dispersive spectroscopy
FA	Fly ash
FEG	Field emission gun
FRC	Fiber-reinforced concrete
GP	Glass powder = Ground glass pozzolans
GU	General Use
HPC	High-performance concrete
HPFRCC	High-performance fiber-reinforced cementitious composites
HRWRA	High-range water-reducer admixture
HVFA	High volume fly ash
HVGP	High-volume GP
ITZ	Interfacial transition zone
LWA	Lightweight aggregates
MC	Moisture content
MCC	Microcrystalline cellulose
MWCU	Molecular weight cut-off
NCM	Nanocellulose materials
NF	Natural fibers

NFC	Nanofibrillated cellulose
NI-QEDS	Nanoindentation coupled with quantitative energy-dispersive spectroscopy
PCE	Poly-carboxylate
PVA	Polyvinyl alcohol
QS	Quartz sand
RH	Relative humidity
SAP	Superabsorbent polymers
SCC	Self-consolidating concrete
SCM	supplementary cementitious material
SEM	Scanning electron microscopy
SF	Silica fume
SFP	Single-fiber pull-out
<i>SG</i>	specific gravity
SHCC	Strain-hardening cementitious composites
SRA	Shrinkage reducing admixture
TEC	Thermal expansion coefficient
TZ	Time-zero for measuring
UHPC	Ultra-high-performance concrete
VMA	Viscosity modifying admixture
VSI	Visual stability index
WG	Welan gum
WRC	Water release capacity
WWR	Water retention capacity

2. SYMBOLS

C	Contact creep modulus
CB_w	Chemically bound water
CB_∞	Maximum value CB_w
CO_{loss}	Mass loss due to decarbonation
d_{50}	Mean particle diameter
d_f	Fiber diameter
D_h	Degree of hydration
d_{max}	Maximum particle size
E	Elastic modulus
E_m	Elastic modulus of matrix
E_f	Elastic modulus of fiber
f	Fiber snubbing effect
f'	Fiber strength reduction factor
f_c	Compressive strength
f_l	flexural capacity
f_{sp}	Splitting-tensile strength
G_d	Chemical bond energy
H	Indentation hardness
J_b	Complementary energy
J_{tip}	Crack tip toughness
k	Spalling effect
K_m	Matrix fracture toughness
M	Indentation modulus
β	Slip-hardening coefficient
$\dot{\gamma}$	Shear rate
T_{500}	Time required to reach a 500 mm spread diameter
T_b	Flexural toughness
τ	shear stress

τ_0	Frictional bond strength (in the context of interface properties)
τ_0	Yield stress (in the context of rheology)
V_f	Volume fraction of fiber,
V_m	Volume of matrix
δ_0	Pullout length corresponding to full fiber debonding
θ	Fiber orientation
μ_{ap}	Apparent viscosity
μ_{pl}	Plastic viscosity
$\sigma(\delta)$	Fiber bridging stress versus crack-opening response
σ_0	Maximum bridging stress
σ_{mu}	Matrix tensile strength
w/b	Water-to-binder ratio
w/c	Water-to-cement ratio

Part I: Background

Chapter 1: Introduction

- 1.1 Research context
- 1.2 Research definition
- 1.3 Research objectives
- 1.4 Research methodology
- 1.5 Thesis structure
- 1.6 References

Chapter 2: Literature Review

- 2.1 General
- 2.2 Fibe-reinforced concrete
 - 2.2.1 Brief history
 - 2.2.2 Classification
 - 2.2.3 Strengthening mechanism
 - 2.2.4 Effect of fiber scale on FRC mechanism
- 2.3 Nanomodified concrete
 - 2.3.1 Nanopowders
 - 2.3.2 Carbon-nanostructures
 - 2.3.3 Nanocellulose materials
 - 2.3.4 Nanoengineered FRC composites

In this part of the thesis, the fundamental elements of the current research (in terms of problem statement, research objectives & methodology, etc.) are first presented. Later, to facilitate the reader's grasp of the subject of Nanoengineering Concrete Properties, the latter is attempted within the overall topic of fiber-reinforced concrete where the use of nanoscale fibers is presented as a complementary measure to the conventionally used micro/macroscale fibers.

CHAPTER I . Introduction

1.1 Research context

While concrete represents by far the most widely used man-made material (with a global annual production of more than 4.3 billion tons [ECA, 2015] and a Canadian production exceeding 36 million m³ (or ≥ 1 m³ par capita) [CAC, 2018]), it still remains that the intrinsic brittleness of concrete and its consequent inherent affinity for cracking shape a salient drawback. The tendency of concrete for cracking can be manifested in varying magnitudes of aggressivity depending on the driving (endogenous/exiguous) forces of cracking. This can jeopardize the structural performance and durability of concrete infrastructures thereby creating a significant socio-economical burden, particularly in terms of infrastructure maintenance. As such, most of the major leaps in concrete technology have been intended, in a way or another, to control the cracking phenomenon in concrete. From the incorporation of steel rebars, to the introduction of macrofibers, to the use of microfibers, all these attempts (decreasing in scale) envisioned overcoming the tensile strength deficiency of concrete. As a result, the tensile capacity and crack bridging ability offered by the separate or coupled effect of these reinforcing systems can lead to higher cracking resistance, enhanced ductility, and improved toughness particularly with fiber reinforced concrete (FRC) [Shah, 1983; Banthia and Mindess , 1995; Li, 2002].

In that regard, while fiber-bridging represents the fundamental mechanism underpinning the FRC effect on concrete, it remains that the increased inter-fiber spacing in fibers conventionally used in FRC does not promote an effective crack bridging *vis-à-vis* the multiscale (nano, to micro, to macro) nature of cracking. As such, macro-size fibers conventionally used in FRC can only handle cracks at their size, without a noticeable effect on micro and nano flaws. Furthermore, the effect of macrofibers is rather reflected at the composite scale without actually affecting the property of the cementitious matrix at the martial scale due to the law adherence between the fibers and the host matrix. Similarly, macrofibers (at conventionl dosages of 2-3% per volume) have a marginal effect on the pre-cracking mechanism, but rather influence the post-cracking strength [Balaguru and Shah, 1992]. It follows that the performance of cement

and concrete composites can be further enhanced, should nanoscale reinforcement be considered. Nanoscale reinforcement can have better intimate adherence to the matrix due to their increased surface reactivity dictated at their molecular scale. This may allow nanoscale reinforcement to interfere with cracks from the stage of inception and hinder nanocracks from growing into microcracks then coalescing into macrocracks, thereby delaying damage localization. This has stimulated increasing research attention paid during the last decade in nanofibers, particularly, carbon nanofibers (CNF) and carbon nanotubes (CNT) [Konsta-Gdoutos *et al.*, 2010a; Sanchez and Sobolev, 2010]. These materials were found to impart significant enhancement in composite flexural strength, tensile capacity, and particularly elastic modulus [Konsta-Gdoutos *et al.*, 2010b]. The enhancement in composite properties were found to stem from the capacity of these nanoinclusions to alter not only the composite performance (as the typical case with macrofibers), but also to further modify the properties of the materials at the scale at which these nanomaterials are acting and interacting with their surrounding environment inside the matrix, namely, the hydrates such as calcium silicate-hydrate- (C-S-H) gel and calcium-hydroxide (CH) crystals [Konsta-Gdoutos *et al.*, 2010b; Raki *et al.*, 2010].

Nonetheless, it remains that the cost of carbon-nanostructure (CNS) at the current state of the art is prohibitively high and may hinder large-scale applications [Raki *et al.*, 2010]. Additionally, the use of CNS (particularly at dry state rather than liquid suspensions) face some concerns pertaining to human health [Davis, 1993; Poland *et al.*, 2008; Donaldson *et al.*, 2010]. One way to exploit the power of nanofibers while responding to environmental and human health concerns may lay in the use of nanocellulose materials (NCM). NCM cover a wide spectrum of plant-based nanoscale materials, such as microcrystalline cellulose (MCC), bacterial cellulose (BC), cellulose nanocrystals (CNC), nanofibrillated cellulose (NFC), microfibrillated cellulose (MFC), and cellulose filaments (CF).

Leveraging the power of natural systems such as that offered by the complex hierarchical structure of cellulose (the fundamental building block) of all NCM is believed to allow elevating nanocellulose-modified-concrete to mimic the inherent features of natural system improved until perfection during millions of years by the effect of the hidden Force behind mother nature. This is largely attributable to the complex hierarchical structure exhibited by natural systems in

general and plants in particular [Torgal and Jalali, 2011]. Bones, for instance, exhibit unique mechanical properties in terms of stiffness, strength and lightweight [Filipponi and Sutherland, 2013]. Likewise, plants exhibit high tensile strength, and remarkable on-axis stiffness, elastic modulus, and toughness while remaining relatively lightweight through their porous structure allowing for the complex fluid-mechanics and dynamics phenomena associated with liquid transport [Wang and Dixon, 2012].

Ongoing research related to NCM in concrete technology is focusing on CNC [Cao *et al.*, 2015], MFC and NFC [Ardanuy *et al.*, 2012; Onuaguluchi *et al.*, 2014]; and recently our works on CF [Hisseine *et al.*, 2018a; Hisseine *et al.*, 2018b; Hisseine *et al.*, 2018c; Hisseine *et al.*, 2019a; Hisseine *et al.*, 2019b; Hisseine *et al.*, 2019c]. CF are cellulosic fibrils with a nanometric diameter (30–400 nm) and micrometric length (100–2000 μm), thereby exhibiting the highest aspect ratio (100–1000) among all currently available NCM. Owing to their nanoscale size, fibril morphology, and large surface area ($>80 \text{ m}^2/\text{g}$), CF have been proven as a powerful new means to nanoengineer superior composite properties necessary for versatile applications such as adhesives, polymer reinforcement, nanocomposites, transparent flexible electronics [Moon *et al.*, 2001; Habibi and Dufresne, Goodsell *et al.*, 2014] and recently cement products [Onuaguluchi *et al.*, 2014; Cao *et al.*, 2015; Hisseine *et al.*, 2018a; Hisseine *et al.*, 2018b; Hisseine *et al.*, 2019c]. The use of CF in such versatile applications is primarily catalyzed by two NCM features: (i) the highly functionalizable cellulose polymers, and (ii) the remarkable nanoscale reinforcing potential of cellulose chains forming highly ordered domains of nanoparticles [Foster *et al.*, 2018]. Thus, CF offer significant opportunities in composite design by providing functionalizable nanoscale reinforcement. Such opportunities cannot be achieved with macroscale natural fibers (for being too large to exhibit surface reactivity) or with molecular cellulose (for being too tiny to impart reinforcing effect) [Moon *et al.*, 2001]. As such, the increased surface area of CF ($>80 \text{ m}^2/\text{g}$) is perceivable to allow intimate adherence with the host matrix through chemical reactions driven by hydrogen bonding fostered by the omnipresent hydroxyl (OH^-) groups (not evident with macroscale natural fibers) [Hisseine *et al.*, 2019a], while conserving high transversal isotropic stiffness, thereby providing an effective nanoscale reinforcement (not evident with molecular cellulose). Additionally, considering the nanometric

scale of CF (allowing exploiting the power of cellulose that imparts strength to plant-based materials) as well as their extraction process (involving delignification and removal of degradable compounds causing instability at high pH and inconsistency in mechanical properties), it follows that CF may offer an opportunity to overcome the drawbacks of cement composites reinforced with macroscale natural fibers, such as the low elastic modulus [Jarabo *et al.*, 2012], poor compatibility between fiber and matrix [Faruk *et al.*, 2012], and inconsistency in fiber properties leading to variation in concrete quality and performance [Aziz *et al.*, 1981].

That said, the current study hypothesizes that the versatile advantages of the nanoscale CF may be leveraged towards reengineering concrete properties to achieve enhanced performance required for specific applications, more precisely: (i) enhancing the rheological properties of fresh concrete, (ii) controlling the volumetric instability of hardening concrete, and (iii) improving the mechanical properties of hardened concrete.

1.2 Research definition

In line with the above hypothesis, the current study is contributing to a new research direction where concrete properties can be nanoengineered towards higher performance using green material, namely cellulose filaments (CF). More specifically, this study fills a niche research gap in fiber-reinforced concrete (FRC) technology where conventionally used macrofibers do not promote an effective crack bridging owing to the large inter-fiber spacing *vis-à-vis* the multiscale nature of cracks in concrete. Thus, the incorporation of the nanoscale CF would provide a nanoreinforcing system, which, when used in synergy with macro fibers would result in a multiscale FRC with better performance. This has been validated through a newly developed multi-scale strain-hardening cementitious composite incorporating a blend of PVA fibers and CF. Furthermore, given the multifunctional properties of CF, its incorporation in concrete collaterally enhances further concrete properties such as rheological performance (via a viscosity modifying effect) and the volumetric instability (via an internal curing effect). The former offers an alternative option to commercially available VMA used in flowable concretes, while the latter provides a novel tool for mitigating autogenous shrinkage in ultra-high-performance concrete (UHPC).

1.3 Research objectives

In light of the aforementioned hypothesis, the current study is aimed at valorizing cellulose filaments (CF) to nanoengineer the properties of concrete at its three major phases (fresh, hardening, and hardened). As such, the nanoscale of CF, its hydrophilicity, flexibility and high aspect ratio are expected to be exploited to impart better rheological properties to fresh concrete. Similarly, CF nanoscale, fibrillar morphology, reinforcing ability, hydrophilicity, and hygroscopicity may be utilized to control the volumetric instability of hardening concrete. On the other hand, the reinforcing effect of the nanoscale CF can be utilized to impart a nanoreinforcing effect to allow a more efficient crack control. Additionally, the project aims at valorizing CF for the development of multiscale FRC where CF can serve as a nano-reinforcement in parallel to macro fibers. To this end, the following specific objectives are considered:

1. Characterizing the overall effect of CF on fresh properties, rheological behavior, heat of hydration, volumetric instability, microstructure, and mechanical performance of cement pastes and concrete.
2. Valorising CF as an alternative viscosity modifying agent (VMA) to allow formulating flowable, yet stable, self-consolidating concrete (SCC) mixtures with enhanced mechanical performance.
3. Taking advantage of the nanoreinforcing effect of CF as well as its water retention and release capacities to control the autogenous shrinkage, particularly, in low water-to-cement systems such as ultra-high-performance concrete (UHPC).
4. Exploiting the nanoreinforcing ability of CF to nanoengineer the strength properties of hardened concrete (particularly, the elastic modulus, the flexural capacity, and toughness) and to disclose the mechanism underpinning the way CF influences the strength of cement systems.
5. Leveraging CF advantages to develop a novel multi-scale FRC, namely, a nanomodified-strain-hardening cementitious composite.

1.4 Research methodology

To achieve the aforementioned project objectives, a comprehensive research program with four main parts and eight phases was conducted as schematized in Fig. 1.1

Part I: This part addresses the research background and involves a comprehensive literature survey pertaining to fiber-reinforced-concrete, nanoengineered concrete, and nanocellulose modified concrete. This part also sets the research problem, the hypothesis put forward to address this problem, research objectives, along with the methodology established to achieve those objectives.

Part II: This part involves evaluating CF characteristics (e.g. density, morphology, dispersion, water retention capacity, and water release capacity) and their implications on properties of cement and concrete composites. Four phases are included in this part:

- **Phase 1-*Effect of CF on rheological properties of concrete*:** This phase is aimed at valorizing CF as viscosity modifying admixture (VMA). Several CF rates were considered in cement pastes and self-consolidating concrete (SCC). A possible mechanism underlying CF effect as a VMA was proposed. CF addition rates necessary to ensure rheological performance comparable to that of conventional Welan-Gum VMA were established. Results of this phase are presented in article 1 [[Hisseine et al., 2018a](#)].
- **Phase 2- *Effect of CF on concrete properties during the hardening stage*:** This phase is aimed at valorizing the hydrophilic and hygroscopic CF as a tool to mitigate autogenous shrinkage. To examine CF effect in this perspective, an ultra-high-performance concrete mixture (UHPC) with a water-to-binder ratio of 0.25 was selected for nanomodification with CF. The influence of CF on autogenous shrinkage of UHPC was compared to when the mixture content in silica fume was varied. Results of this phase are presented in article 2 [[Hisseine et al., 2018b](#)].
- **Phase 3- *Effect of CF on hardened properties*:** This phase is aimed at utilizing CF as nano-reinforcement to enhance the mechanical performance. Cement pastes and concrete were

considered. For cement pastes, the effect of CF on mechanical performance was also evaluated in function of the curing regime (wet curing versus dry-sealed curing). The effect of CF on tensile strength, flexural capacity, and toughness was evaluated. This was supplemented by autogenous shrinkage during the first 7 days of curing as well as by microstructure investigations to disclose CF effect on the interfacial transition zone (ITZ). Results of this phase are presented in article 3 [Hisseine *et al.*, 2018c].

- **Phase 4- *Effect of CF on microstructure properties***: This phase is intended to disclose and the mechanisms underpinning the influence of CF on the mechanical performance of cement systems. For this, this phase provides a *top-down* approach establishing a link between the mechanical performance at the engineering scale (i.e. compressive strength, elastic modulus, flexural capacity and toughness) and the microstructure properties (i.e. the micromechanical properties of main microstructure phases) using nanoindentation coupled with quantitative energy-dispersive spectroscopy (NI-QEDS) approach. Possible microstructure reasons for CF effect on micromechanical performance were proposed. Results of this phase are presented in article 4 [Hisseine *et al.*, 2019a].

Part III: This part is designed to leverage the opportunities offered by CF for enhancing concrete properties towards developing a new formulation with enhanced properties. It consists of developing a strain-hardening cementitious composite (SHCC) also known as engineered cementitious composite (ECC) using high-volume ground-glass pozzolans (HVGP) in replacement of fly ash. A new approach coupling particle packing optimization with micromechanical tailoring was proposed to allow optimizing strength and ductility. Three phases make up this part:

- **Phase 5- *Characterization and nanomodification of interface properties of strain-hardening cementitious composites incorporating high-volume ground-glass pozzolans (HVGP-SHCC)***: Here, single-fiber pull-out tests were performed to characterize the interface properties of HVGP-SHCC. Further, CF was used as a tool to nanoengineer the interface properties to impart improved strain-hardening behavior. In outcome, fiber-bridging capacity versus crack opening response $\sigma(\delta)$ for the different formulations was

developed. The ensuing σ (δ) response are to serve for the micromechanical tailoring of HVGP-SHCC. Results of this phase are presented in article 5 [Hisseine *et al.*, 2019b].

- **Phase 6-Development of strain-hardening cementitious composites incorporating high-volume ground-glass pozzolans (HVGP-SHCC):** In this phase, the results of σ (δ) response developed in Phase 5 were used to micromechanically tailor the different formulations of HVGP-SHCC. The resulting formulations were further validated with tests at the composite level (uniaxial tensile test and flexural capacity test). In outcome, HVGP-SHCC with 0-100% replacement of fly ash by GP and exhibiting improved strength characteristics were developed. Results of this phase are presented in article 6 [Hisseine *et al.*, 2019c].
- **Phase 7-Development of nanomodified strain-hardening cementitious composites incorporating high-volume ground-glass pozzolans (nHVGP-SHCC):** In this phase, optimized HVGP-SHCC mixtures from phase 6 were chosen for nanomodification with CF. The influence of CF as a nano-reinforcement (presented in Phase 4) as well as CF effect on nanoengineering interface properties (attempted in Phase 5) are leveraged to further improve the ductility and strain-hardening behavior of HVGP-SHCC. The use of CF provided a multi-scale reinforcing system which allowed obtaining composites with higher strength and ductility than conventional SHCC with high volume fly ash (HVFA-SHCC). Results of this phase are presented in article 7 [Hisseine *et al.*, 2018d].

Part IV: *Scale-up of nanomodified strain-hardening cementitious composites incorporating high-volume ground-glass pozzolans (nHVGP-SHCC).* In this part, the newly developed nHVGP-SHCC was scaled-up for structural application (Phase 8). The objective is to transpose the high-strength and high strain-hardening capacity obtained at the engineering scale toward structural-size application. An optimized HVGP-SHCC formulation from Phase 7 was scaled-up to construct nine full-scale composite deck slabs (with dimensions of up to 2400 × 900 mm). Test variables include: (i) deck geometry (trapezoidal versus re-entrant), (ii) shear-span (800 and 600 mm), (iii) secondary reinforcement (with or without welded wire reinforcement), (iv) concrete topping (conventional SCC mixture and the newly developed nHVGP-SHCC), and (v)

loading regime (static versus cyclic). To provide a comparative assessment, eight composite deck slabs of similar dimensions to those with HVGP-SHCC were constructed with a commercial SCC mix designed with similar compressive strength (f_c) as the selected HVGP-SHCC in an attempt to attenuate the effect of f_c on structural performance across the two different concrete types (nHVGP-SHCC and SCC). Results of this part are presented in article 8.

Part V: Here, the different research findings as well as future perspectives are summarized through chapter 11 (English version) and chapter 12 (French version).

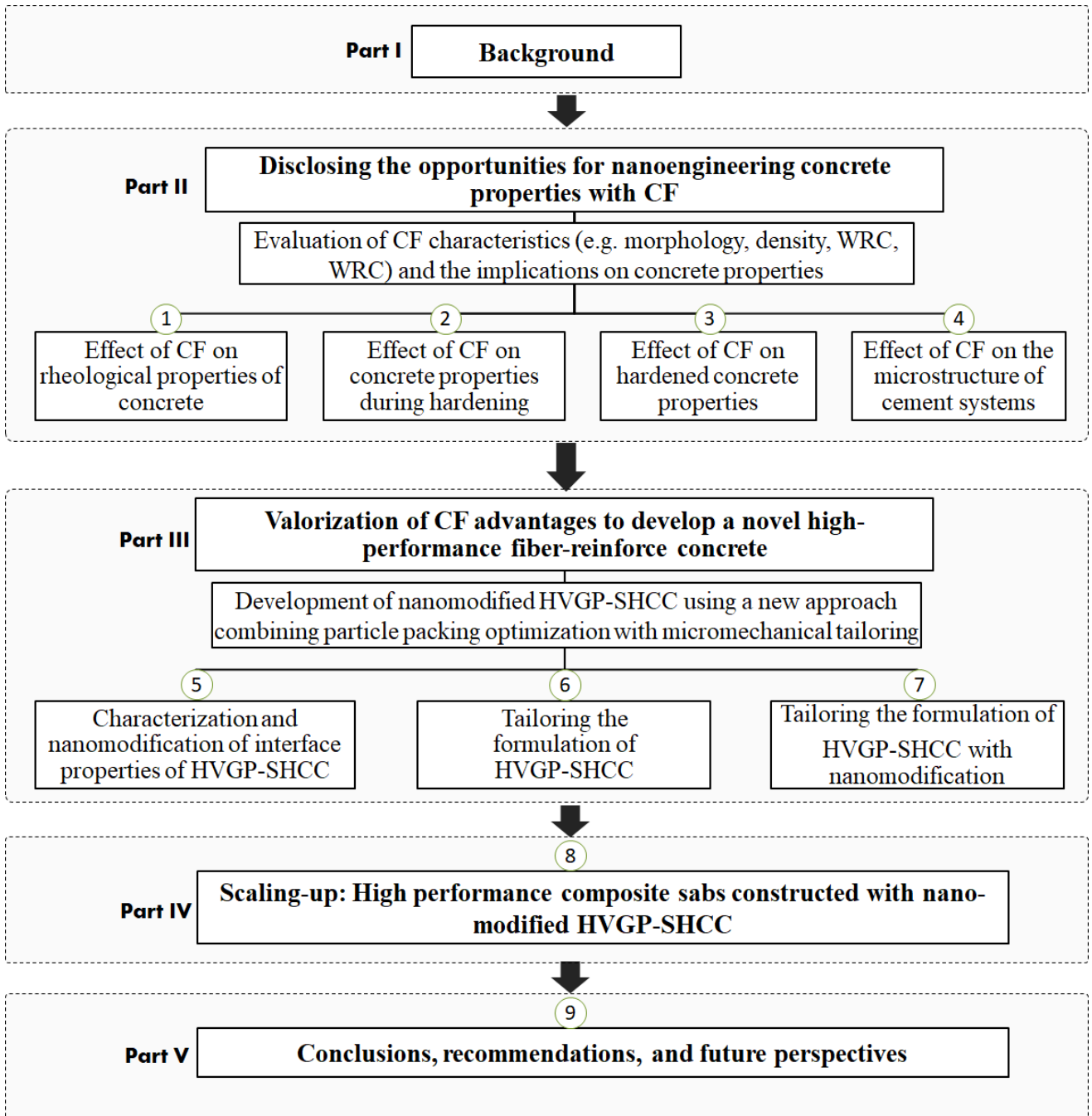


Fig. 1. 1 Schematic illustration of research methodology.

1.5 Thesis structure and original contributions

In line with project phases outlined in the previous section, this thesis comprises eleven chapters (a schematic of the structure of the thesis is depicted in Fig. 1.2). This includes an introductory chapter (Chap. 1), a chapter on literature review (Chap. 2), seven chapters (Chap. 3–Chap. 9) corresponding to seven original research contributions in the form of journal articles, a supplementary chapter (Chap. 10) on structural application in the form of an article under preparation, and a concluding chapter (Chap. 11). Chapter 12 is the French version of Chapter 11. In total, eight journal publications were produced from this thesis as detailed below:

Article 1: Hisseine O. A., Omran, A. F., N. Basic, and Tagnit-Hamou, A. (2018) Feasibility of using cellulose filaments as a viscosity modifying agent. *Cement and Concrete Composites* 94: 327–340.

Article 2: Hisseine, O.A., Soliman, N., and Tagnit-Hamou, A. (2018) Cellulose filaments for controlling autogenous shrinkage in ultra-high-performance concrete. Under review by the journal of *Cement and concrete research*.

Article 3: Hisseine, O. A., Omran, A.F., and Tagnit-Hamou, A. (2018) Influence of Cellulose Filaments on Cement Pastes and Concrete. *ASCE Journal of Materials in Civil Engineering*, 30(6): 04018109.

Article 4: Hisseine, O. A, Wilson, W., Sorelli, L., and Tagnit-Hamou, A. (2019) Nanocellulose for improving mechanical properties of concrete: A macro-to-micro investigation for disclosing the effects of cellulose filaments on strength of cement systems. *Construction and Building Materials* 206: 84–96.

Article 5: Hisseine, O.A., and Tagnit-Hamou, A. (2019). Characterization and nano-engineering the interface properties of high-volume glass powder strain hardening cement composites: Under review by the journal of *Construction and Building Materials*.

Article 6: Hisseine, O.A., and Tagnit-Hamou, A. (2019). Development of strain-hardening cementitious composites incorporating high-volume ground-glass pozzolans: Under review by the journal of *Construction and Building Materials*.

Article 7: Hisseine, O.A., and Tagnit-Hamou, A. (2019d). Nanocellulose for the development of nano-engineered strain-hardening cementitious composite incorporating high-volume ground-glass pozzolans: Under review by the journal of *Cement and Concrete Campsites*.

Article 8: Hisseine, O.A., and Tagnit-Hamou, A. (2019). Nano-engineered strain-hardening cementitious composite incorporating high-volume ground-glass pozzolans for high performance composite deck slabs with improved shear bond capacity: Under preparation, to be submitted to the journal of *Engineering Structures*.

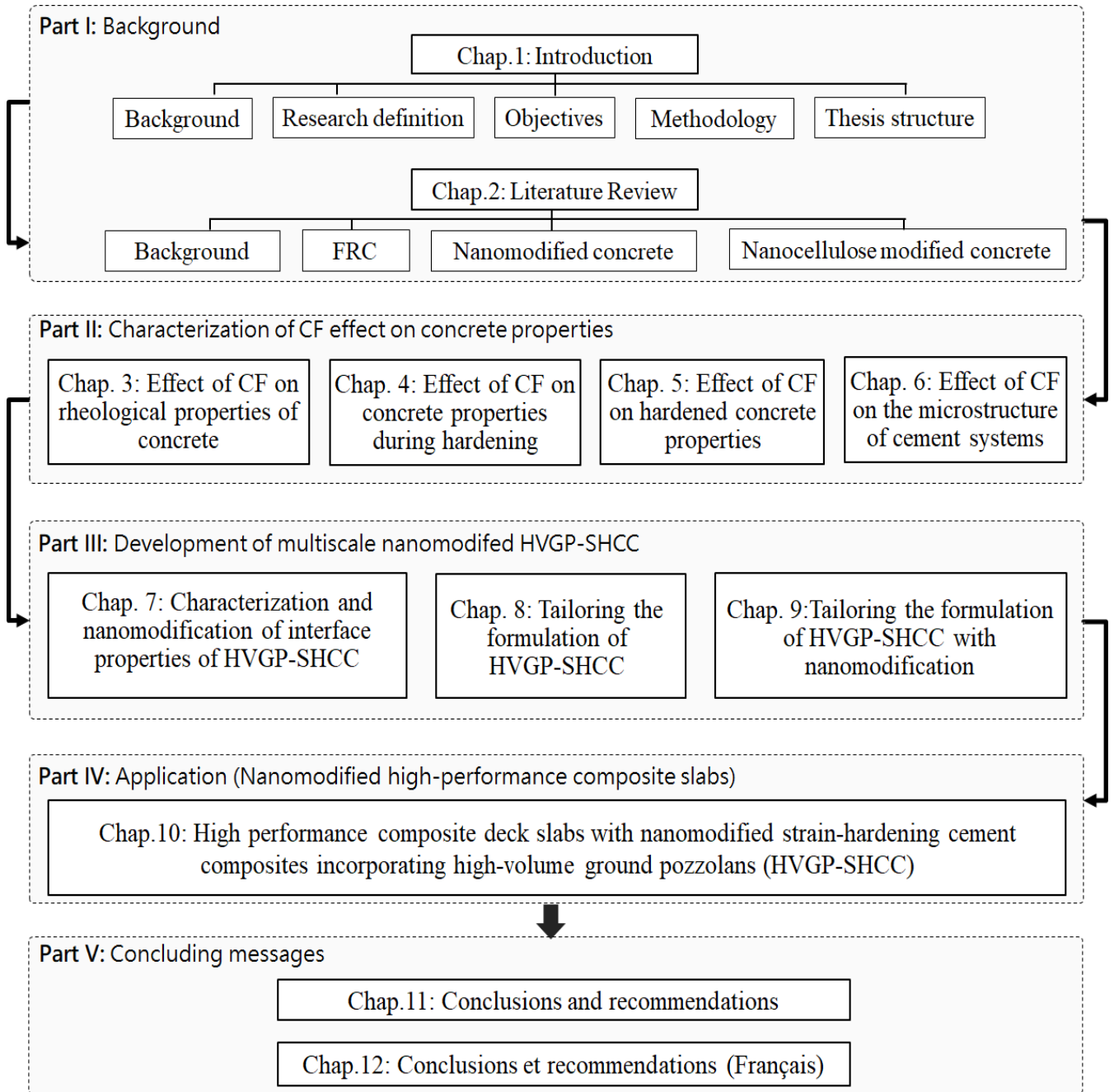


Fig. 1. 2 Schematic view of overall thesis organization.

1.6 References

- Abu Al-Rub, K. R., Tyson, M. B., Yazdanbakhsh, A., and Grasley Z. (2012) Mechanical Properties of Nanocomposite Cement Incorporating Surface-Treated and Untreated Carbon Nanotubes and Carbon Nanofibers, *J. Nanomech. Micromech.*, vol. 2: p. 1-6.
- Altoubat, S. Ousmane, H., and Barakat, S. (2016) Experimental study of in-plane shear behaviour of fiber-reinforced concrete composite deck slabs, *J. Struct. Eng.* vol. 142, no 3: 04015156.
- Ardanuy, M., Claramunt, J., Arevalo, R., Pares, F., Aracri, E., and Vidal, T. (2012) Nanofibrillated-cellulose as a potential reinforcement for high performance cement mortar composites, *BioResources*, vol. 7, n° 3, p. 3883–3884.
- Aziz, M. A., Paramasivam, P., and Lee, S. L. (1981) Prospects for natural fiber-reinforced concrete in construction, *Int. J. Cem. Compos. Lightweight Concr.*, vol. 3, n° 2, p. 123–132.
- Banthia, N., Moncef, A., Chokri, K., and Sheng, J. (1994) Micro-fiber reinforced cement composites: Uniaxial tensile response. *Can J Civil Eng.*, vol. 2, n° 6, p. 999–1011.
- CAC (2018). Canadian Cement Association, Available online at www.cement.ca [accessed on June 7, 2018]
- Cao Y., Zavaterri, Youngblood, P. J. Moon, R., and Weiss, J. (2015) The influence of cellulose nanocrystal additions on the performance of cement paste, *Cem. Concr. Compos.*, vol. 56, p. 73–83.
- Davis, J. M. G. (1993) The need for standardized testing procedures for all products capable of liberating respirable fibers—the example of materials based on cellulose, *Br. J. Ind. Med.*, vol. 50, n° 2, p. 187-190.
- Donaldson, K., Murphy, F. A., Duffin, R., Poland, C. A. (2010) Asbestos, carbon nanotubes and the pleural mesothelium: a review of the hypothesis regarding the role of long fibre retention in the parietal pleura, inflammation and mesothelioma Part. *Fibre Toxicol.*, vol. 7, p.5.
- ECA (2018). European Cement Association (CEMBUREAU). Available online at <https://cembureau.eu/> [accessed on March 30, 2019].
- Faruk, O., Bledzki, A.K., Fink, H.S., and Sain, M. (2012) Biocomposites reinforced with natural fibers, *Prog. Polym. Sci.*, vol. 37, p. 552–1596.
- Foster, E. J., Moon, R. J., Agarwal, U. P. et al. (2018) Current characterization methods for cellulose nanomaterials, *Chem. Soc. Rev.*, vol. n° 47, p. 2609–2679.

- Goodsell, J. E., Moon, R. J., Huizar, A., Pipes, R. B. (2014) A strategy for prediction of the elastic properties of epoxy-cellulose nanocrystal-reinforced fiber networks, *Nord. Pulp Pap. Res. J.* vol. 29, n° 1, p. 85–94.
- Habibi, Y., and Dufresne, A. (2008) Highly filled bionanocomposites from functionalized polysaccharide nanocrystals, *Biomacromolecules*, vol. 9, n° 7, p. 1974–1980.
- Hisseine, O. A., and Tagnit-Hamou, A. (2019b) Characterization and nano-engineering the interface properties of high-volume glass powder strain hardening cement composites: Under review by the journal of *Composites Part B*.
- Hisseine, O. A., Basic, N., Omran, A. F., and Tagnit-Hamou, A. (2018a) Feasibility of using cellulose filaments as a viscosity modifying agent in self-consolidating concrete, *Cem. Concr. Compos.*, vol. 94, p. 327–340.
- Hisseine, O. A., Omran, A. F., and Tagnit-Hamou, A. (2018c) Influence of cellulose filaments on cement pastes and concrete, *J. Mater. Civ. Eng.*, vol. 30, n° 6: 04018109.
- Hisseine, O. A., Wilson, W., Sorelli, L., Tolnai, B., and Tagnit-Hamou, A. (2019a) Nanocellulose for improved concrete performance: A macro-to-micro investigation for disclosing the effects of cellulose filaments on strength of cement systems, *Constr. Build. Mater.*, vol. 206, p. 84-96.
- Hisseine, O.A., and Tagnit-Hamou, A. (2019c). Development of high volume-glass powder strain-hardening cement composites: Under review by the journal of *Cement and Concrete Research*.
- Hisseine, O.A., and Tagnit-Hamou, A. (2019d). Development of nano-engineered strain-hardening cement composite with high volume-glass powder using cellulose filaments: Under review by *Cement and Concrete Campsites*.
- Hisseine, O.A., Soliman, N., and Tagnit-Hamou, A. (2018b) Cellulose filaments for controlling autogenous shrinkage in ultra-high-performance concrete. Under review by the journal of *Cement and concrete research*.
- Jarabo, R., Fuente, E., Monte, M. C., Savastano, H., Mutjé, P., Negro, C. (2012) Use of cellulose fibers from hemp core in fiber-cement production: effect on flocculation, retention, drainage and product properties, *Ind. Crops Prod.*, vol. 39, p. 89–96.
- Khaloo, A. R., Afshari, M. (2005) Flexural behaviour of small steel fibre reinforced concrete slabs, *Cem Concr Compos*, vol. 27, n°1, p.141–149.
- Konsta-Gdoutos, M. S., Metaxa, Z. S., and Shah, S. (2010a) Highly dispersed carbon nanotube reinforced cement-based materials. *Cem. Concr. Res.*, vol. 40, p. 1052–1059.

- Konsta-Gdoutos, M. S., Metaxa, Z. S., and Shah, S. (2010b) Multi-scale mechanical and fracture characteristics and early-age strain capacity of high-performance carbon nanotube/cement nanocomposites, *Cem. Concr. Compos.*, vol. 32, p.110–115.
- Löfgren, I. (2005) Fibre-reinforced Concrete for Industrial Construction-a fracture mechanics approach to material testing and structural analysis. PhD Thesis, *Chalmers University of Technology*.
- Moon, R. J., Martini, A., Nairn, J., Simonsen, J., and Youngblood, J. (2011) Cellulose nanomaterials review: structure, properties and nanocomposites, *Chem. Soc. Rev.*, vol. 40, n° 7, p. 3941–3994.
- Onuaguluchi, O., Panesar, D., and Sain, M. (2014) Properties of nanofibre reinforced cement composites, *Constr. Build. Mater.*, vol. 63, p. 119–124.
- Poland, C. A., Duffin, R., Kinloch, I., Maynard, A., Wallace, W.A.H., Seaton, A., et al. (2008) Carbon nanotubes introduced into the abdominal cavity of mice show asbestos-like pathogenicity in a pilot study, *Nat. Nano.*, vol. 3, n° 7, p. 423-428.
- Raki, L., Beaudoin, J., Alizadeh, R., Makar, J., Sato, T. (2010) Cement and concrete nanoscience and nanotechnology, *Materials*, vol. 3, p. 918–42.
- Sanchez, F., and Sobolev, K. (2010) Nanotechnology in concrete - a review. *Constr. Build. Mater.* vol. 24, p. 2060–2071.

CHAPTER 2 . Literature Review

2.1 General

In this chapter, the background on nanofiber-modified concrete is attempted within the overall context of fiber-reinforced concrete (FRC). For this, an overview of FRC is first presented in section 2.2 [including a brief history of FRC (2.2.1); fiber-type-based classification of FRC (2.2.2), strengthening mechanism of FRC (2.2.3), and the effect of different fiber scale (macro, micro, and nano) on FRC strengthening mechanism (2.2.4)]. The discussion on the effect of different fiber scale on FRC strengthening mechanism attempted in section 2.2.4 is later linked to the necessity for multi-scale FRC (a blend of nano and macro fibers). As such, nanomodified concrete is introduced in section 2.3 as a tool to allow designing multi-scale FRC. In this context, most common nanomaterials in the construction industry [nanopowders (section 2.3.1); and carbon nano-structures (section 2.3.2)] are reviewed first to provide a ground to facilitate understanding the general effect of these nano-particles on cement systems before nanocellulose materials (NCM) are introduced (in section 2.3.3). Finally, the perspectives for leveraging NCM towards designing nanoengineered fiber-reinforced cementitious composites are attempted in section 2.3.4.

2.2 Fiber reinforced concrete

2.2.1 Historical overview

The term fiber-reinforced concrete (FRC) is defined by AC1, as a concrete containing dispersed randomly oriented fibers such as steel, synthetic, glass, or natural fibers [ACI 116R-00, 2005]. The primary purpose of adding fibers to concrete is to inhibit the inherent cracking propensity of concrete, control its brittleness, and provide reliable post-cracking behavior. While the use of fibers in modern construction practice emerged with the use of asbestos fibers in the early 1900s, the original concept of using fibers to reinforce brittle construction materials is not new:

Horsehair and straw were used to enhance the tensile strength of mortars and sun-baked bricks since antiquity. However, major research and development in FRC picked-up in the 1960s (with steel, glass, and synthetic fibers) following the identification of health risk associated with the use of asbestos [Romualdi and Mandel, 1964]. A more detailed historical review of FRC can be found in Naaman [1985], Zollo [1997], and Beddar [2004].

While initial research and development in FRC focused mainly on steel fibers for their high strength and elastic modulus allowing improved crack resistance, ductility, and toughness to cement composites [Dixon and Mayfield, 1971; Johnston and Colin, 1974; Naaman, 1985], currently, a wide-spectrum of fibers are commercially available (Fig. 2.1) for different FRC applications. This includes mainly, steel fibers, synthetic fibers, glass fibers, and natural fibers [ACI 544, 2002]. Continuous research and development in FRC resulted in fibers with enhanced strength and geometry to respond to specific application requirements. Thus, different fibers with high tensile strength, elastic modulus, and adapted geometry (e.g. hooked-end, flat-end, crimped etc. for steel fibers and twisted, fibrillated, waved, etc. for polymeric fibers) have also been made available. Depending on the application, fibers with desirable mechanical properties and geometry may be chosen. Thus, some fibers such as steel and high strength polymeric fibers can be used for structural applications to reduce the amount of passive reinforcement in reinforced concrete elements such that reinforcement congestion may be attenuated [Johnston and Colin, 1974; Soltanzadeh *et al.*, 2015]. Some other fibers (e.g. polymeric fibers) may be used to impart crack resistance and enhance post-peak strength. Other types (e.g. polymeric fibers, natural fibers, etc.) may be utilized for controlling temperature/shrinkage cracking, plastic shrinkage in fresh concrete or drying shrinkage [Onuaguluchi and Banthia, 2016]

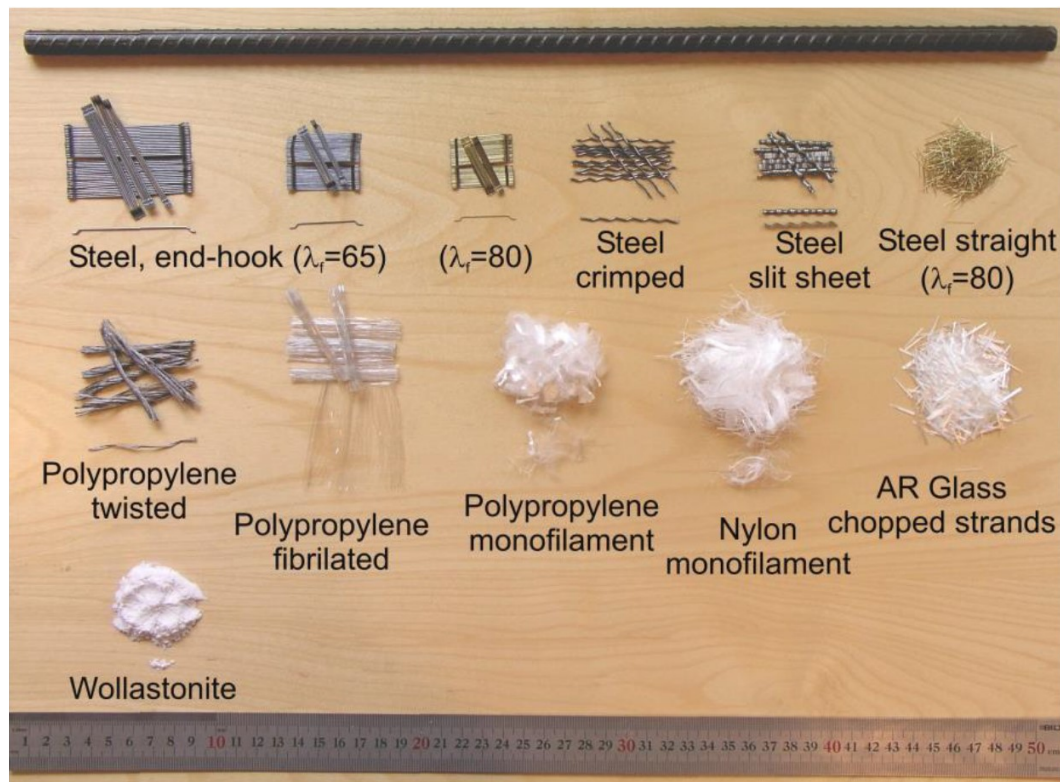


Fig. 2.1: Common fibers used in FRC technology, adapted from Löfgren [2005].

2.2.2 Classification of FRC based on fiber type

Based on fiber type, four major categories of FRC can be identified: (i) steel fiber FRC; (ii) synthetic fiber FRC; (iii) glass fiber FRC; and (iv) cellulose fiber FRC.

2.2.2.1 Steel Fiber Reinforced Concrete (SFRC)

Steel fibers are the most commonly used in FRC owing to their elastic modulus compared to that of concrete as well as their high tensile strength thereby providing concrete with higher tensile capacity and significantly enhanced post-cracking strength and toughness [Altun *et al.*, 2007]. Major effects of steel fibers on fresh properties consist of the balling of fibers (for long thin fibers), the increased demand in superplasticizer dosage necessary to compensate for slump loss as well as the increased demand in vibration to avoid fiber balling [Balaguru and

Ramakrishnan, 1986]. For hardened properties, steel fibers impart higher post-crack strength and ductility to the matrix. The effect of steel fibers on compressive strength is moderate (0-15%) at 1.5 vol. % of fibers, however the effect on tension capacity is more phenomenal (30 to 40%) at 1.5 vol. % of fibers [Johnston, 1974]. This was also found to lead to enhanced durability aspects due to the reduced cracking which lowers the ingress of deteriorating agents [Rapoport *et al.*, 2002; Grzybowski and Shah, 1990]. The most characteristic feature of SFRC is toughness, which is determined by the standardized slow flexure methods, JSCE SF-4 [JSCE, 1986] and ASTM C 1018 method [ASTM, 1997].

2.2.2.2 Synthetic fiber reinforced concrete (SNFRC)

Synthetic fibers (SNF) are man-made fibers ensuing from the petrochemical industry. Common SNF types are acrylic, carbon, nylon, polyester, polyethylene, polypropylene, and polyvinyl alcohol. Some advantages of SNF include the high strength to weight ratio. However, melting at high temperature is a concern. Some researchers report that the melting of SNF would rather create internal channels to release the thermal stresses, thereby attenuating cracking predilection of concrete [Altoubat and Housseine, 2016]. Fresh properties of SNFRC vary across the various types of SNF. However, the salient feature is the reduced workability (due to the increased surface area of fibers) if superplasticizers were not used. Yet, SNFs reduce bleeding and segregation [Vondran, 1990]. Hardened properties of SNFRC depend on the loading type. For instance, there is no noticeable effect on the compressive strength apart from altering the failure mode into a less brittle one. Much effect of SNFs is in flexural toughness and post-cracking behavior. The toughness of SNFRC is determined using the ACI method [ACI 544.2R, 2002] and ASTM C1018 [ASTM, 1997]. In both cases the toughness index depends to a large extent on the loading method (load-controlled Vs deflection controlled) and the estimate of the first-crack load. Therefore, caution should be exercised in interpreting published toughness results. SNFs are also effective in controlling cracking resulting from volume changes due to plastic and drying shrinkage [Noushini *et al.*, 2014].

2.2.2.3 Glass fiber reinforced concrete (GFRC)

Glass fibers (GF) are fine filaments manufactured from silicate-based substances with the most common types being the E-glass (alumino-borosilicates) and A-glass (alkali-lime). For the high silicates content of glass fibers, the first attempts of their use in cement were hampered by their embrittlement. This stimulated the development of alkali-resistant glass fibers. The most salient application of GFRC composites is for aesthetical elements. The hardened properties of GFRC in such applications is a function of several factors including fiber content, polymer content, water-cement ratio, and curing. GFRC composites typically possess considerable load and strain capacity beyond the matrix cracking strength [ACI 544.2R, 2002].

In spite of their high strength, GFRC composites were found to soon lose strength due to either the alkali attack on the fibers which reduces fiber tensile strength, or due to the infiltration of the hydration products to fiber bundles, increasing the bond to individual glass filaments, reducing fiber pull-out [Mobasher and Shah, 1989]. Preventive measures include the addition of polymers to protect individual glass filaments from alkali attack and partially fill the spaces between the filaments; thereby reducing the effects of fiber embrittlement [Van der Plas, 1991]. Another strategy is to apply to the fibers an alkali resistant coating to reduce the affinity of GF for calcium hydroxide. Zirconium oxide (ZrO_2) was also found to impart noticeable improvements in fiber tensile strength retention.

2.2.2.4 Natural fiber-reinforced concrete (NFRC)

Natural fibres (NF) are natural composites with a cellular structure and have different proportions of cellulose, hemicelluloses, and lignin content (Fig. 2.2). Whereas cellulose is a polymer containing glucose units and hemicellulose is a polymer made of various polysaccharides, the lignin is an amorphous and heterogeneous mixture of aromatic polymers and phenyl-propane monomers. Additionally, NF also contain other minority components such as water, proteins, peptides and inorganics.

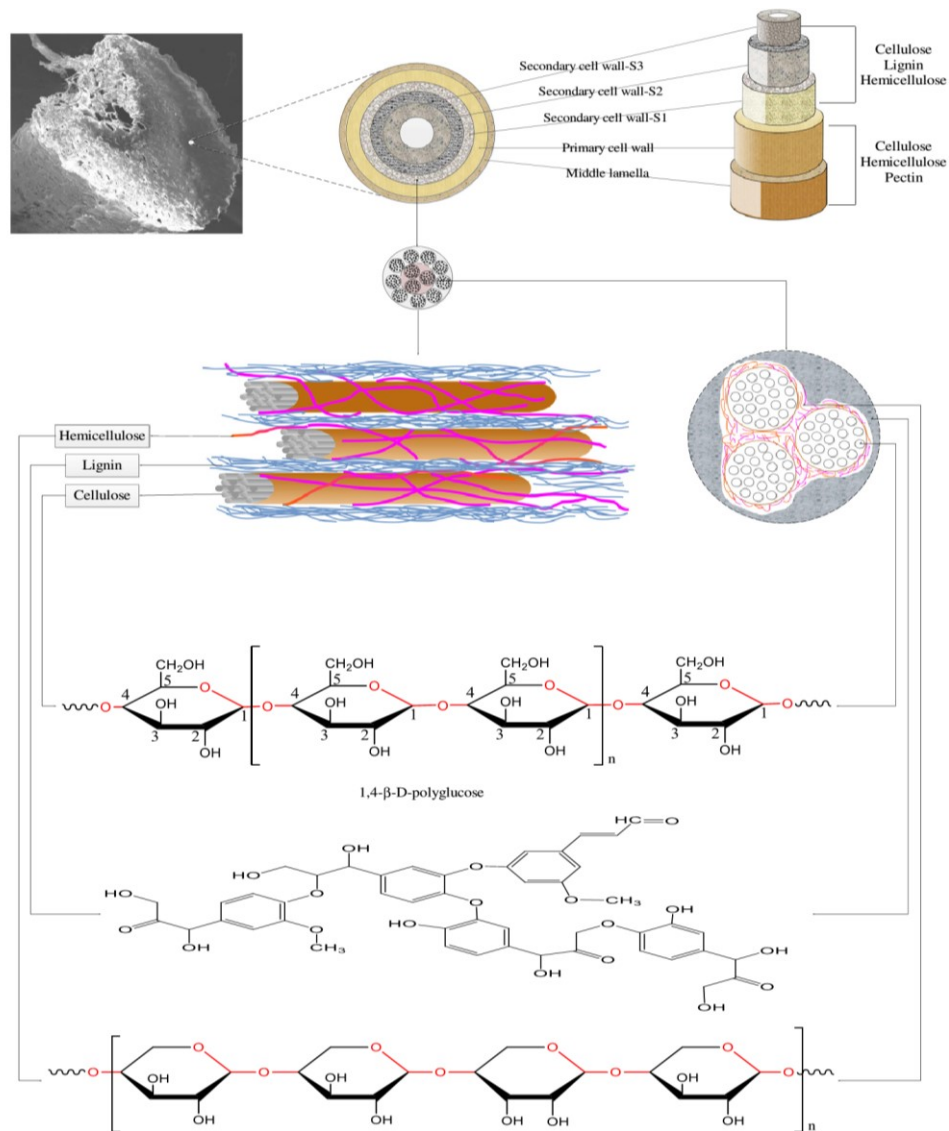


Fig. 2.2: Microstructure, Molecular structures of natural fiber cell wall [Wei and Meyer, 2015].

NF were demonstrated efficient in controlling plastic shrinkage [e.g., 99% reduction in crack width and total crack area with only 0.3% by volume [Boghossian and Wegner, 2008], mitigating drying shrinkage [e.g., 86% reduction in crack width with only 1% by volume [Kawashima and Shah, 2011], and improving the mechanical performance of cement composites [e.g., 20–50% enhancement in flexural strength and fracture toughness when an NF dosage of 2–16% by weight was considered [Sedan *et al.*, 2008; Morton *et al.*, 2010; Merta and

Tschegg 2013]. However, untreated NF exhibit two major handicaps: (i) variation of fiber properties, and vulnerability to the alkaline medium of cement [Ardanuy *et al.*, 2011].

The composition of NF varies largely across fiber origin (wood, non-wood), part of the plant where the NF is extracted (bast, leaf, stalk, seed), and form of the fibers (strand, staple, pulp). These varieties can lead to inconsistency in fiber mechanical properties, which in turn result in variations in concrete performance [Aziz *et al.*, 1981]. On the other hand, the vulnerability of NF in the alkaline medium of cement is attributable to the alkaline degradation of some fiber components such as lignin, hemicellulose, pectin, and soluble sugars [Onuaguluchi and Banthia, 2016]. NF degradation in cement systems is mainly attributed to the fiber mineralization owing to the migration of calcium hydroxide (CH) from cement hydration toward fiber lumen [Ardanuy *et al.*, 2011]. Currently, a set of proven techniques are available to overcome the drawbacks of NF. Fiber pre-treatment techniques such as hornification (stiffening the polymer structure of NF upon water removal) are used to enhance fiber stability and performance in cement composites [Ferriria *et al.*, 2016]. Another preventive measure is the accelerated carbonation. It allows the quick reaction of CH with CO₂ resulting in calcium carbonate CaCO₃, thereby not reducing the risk of fiber mineralization by CH, but also reducing matrix porosity, enhancing matrix strength and durability through the formation of CaCO₃ [Tonoli *et al.*, 2010; Soroushian *et al.*, 2012]

On the other hand, supplementary cementitious materials (SCM) are also used to mobilize pozzolanic reaction to consume CH, reduce fiber embrittlement, and produce supplementary C-S-H to densify the matrix and improve its mechanical performance [Toledo Filho *et al.*, 2003; Mohr *et al.*, 2007; Melo Filho, 2013].

2.2.3 Strengthening mechanism of FRC

Properties of FRC are influenced by the underlying strengthening and toughening mechanism offered by the fibers. This is primarily governed by the three composite constituents (fiber, matrix, and fiber/matrix interface properties) [Li and Stang, 1997]. Consequently, the properties of FRC composites are influenced directly by (i) the ability of the fibers to transfer loads across

cracked sections (also referred to as fiber bridging capacity), which is mobilized by (ii) fiber/matrix interfacial bond and, (iii) fiber capacity to withstand rupture [Lin *et al.*, 2009]. These are known to consume increasing fracture energy depending on fiber characteristics, particularly, length, tensile capacity, bond with the matrix, and fiber count. As such, Anderson [2005] showed that the fracture of steel fiber-reinforced concrete composite undergoes a 5-step process that includes: Fiber rupture, fiber pull-out, fiber bridging, fiber/matrix debonding, matrix cracking, and crack front debonding (as shown in the figure below).

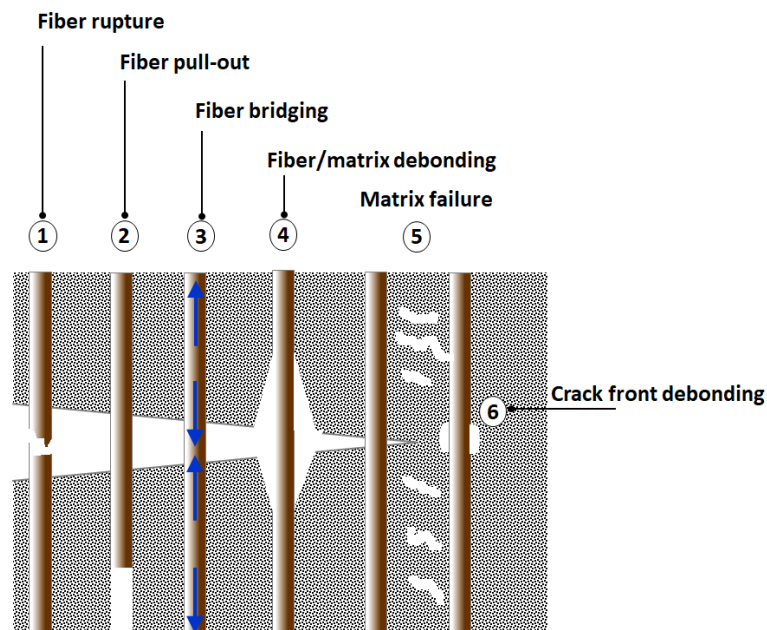


Fig. 2.3: Fracture mechanism of FRC; reproduced from Anderson [2005].

2.2.4 Effect of fibers on pre- versus post-cracking mechanism

In light of the above-described mechanism, it should be noted that conventionally used fibers in FRC often control the post-cracking mechanism, once the initial cracking of matrix takes place. Here, fibers bridge the cracks and transfer stresses across matrix-cracked sections. In this regard, when fibers having a tensile strength higher than that of the matrix are used, the presence of fibers can limit crack propagation by the bridging effect [Narwal *et al.*, 2013; Mo and Yap, 2014]. Fiber bridging mobilizes fundamentally fiber/matrix interfacial bond; the reason for which deformed fibers (hooked end, twisted, corrugated, flat ended, etc.) significantly enhance

the post-cracking response owing to the higher energy consumed during fiber pull-out [Yan *et al.*, 1999; Naaman, 2003]. Nevertheless, it should be noted that considering the multiscale nature of cracking in concrete, the effect of conventionally used macrofibres in effectively arresting multiscale cracking is not evident. This justifies why macrofibers commonly used in FRC (within practical fiber dosages) have limited influence on cracking strength, but rather influence the post-cracking stage. Thus, it is legitimate to believe that composites incorporating more than one scale of fibers will exhibit improved performance.

In the context of this research [where nanoscale cellulose filaments (CF) are to be valorized to enhance the performance of concrete], it is perceivable that when CF is used in conjunction with macrofibers, a multiscale FRC may be obtained. Based on the work of Rossi *et al.* [1987] on the influence of two scales of fibers (micro and macro), and that of Löfgren [2005] on macrofibers, a novel description for the combined effect of three-scale fibers (nano, micro, macro) was proposed in this study as shown in Fig. 2.4. For this, three scales of cracks were inferred from the multiscale nature of cracking in concrete [Afroughsabet, 2016]. This includes: (i) nanocracks, (ii) microcracks, and (iii) macrocracks.

Nanocracks are those cracks intrinsic to the heterogenous microstructure of the cementitious system and thus they exist in the matrix even before any external loading is applied [Kwak and Filippou, 1990]. These cracks are attributable to residual mechanisms such as residual thermal strains or volumetric instabilities accompanying cement hydration (such as chemical, autogenous, plastic, and drying shrinkage). In this perspective, nanocracks exist within the microstructure of the bulk cementitious matrix itself and contribute to forming the porous network. Those are the cracks which can be found between the hydrates (e.g. C-S-H, CH, Aft, Afm, etc.) and the bulk matrix or within the skeleton of the hydrated system itself. Therefore, pre-existing nanocracks prevail within the elastic stage designated by *A* in Fig. 2.4. Microcracks are initiated as a result of widening-up of pre-existing cracks (nanocracks) upon loading which extends the nanocracks [in the hydrated system, the bulk cementitious matrix, and the paste-aggregate interfacial transition zone (ITZ)] to the microscale. Thus, microcracks are considered to prevail once the linear elastic stage designated by *B* is surpassed. Macrocracks, on the other

hand, emerge as a result of loading levels exceeding the elastic limit. Thus, as stresses are increased from the elastic limit B to a point of microcrack saturation C , microcracks coalesce and lead to damage localization into macrocracking at point D which correspond to ultimate capacity. The extension of the curve beyond point D depends majorly on the presence of fibers or not and on the scale of fibers used (nano, micro, macro) as to be elaborated in the following paragraphs.

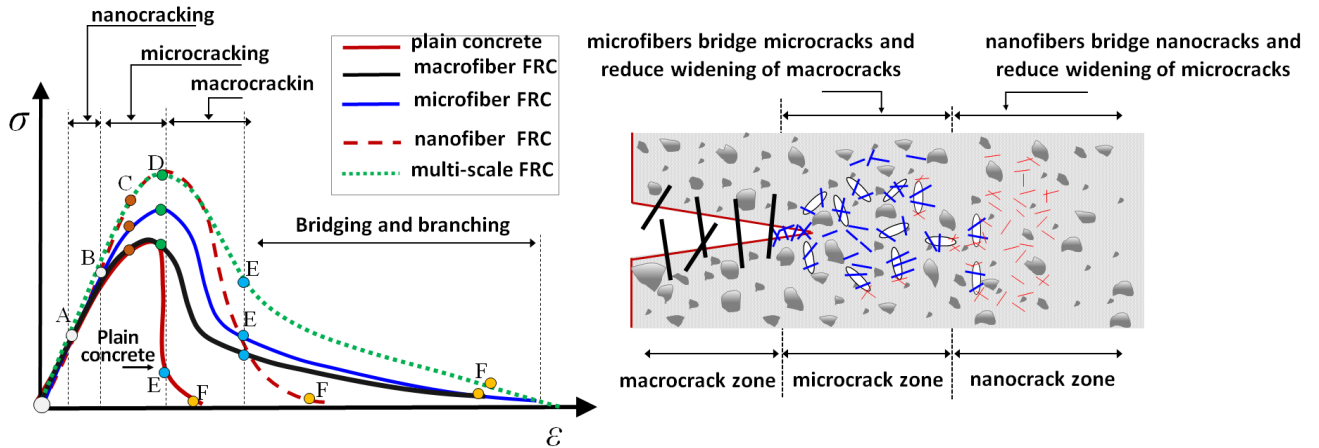


Fig. 2.4: Schematic illustration of the effect of different fiber scale (nano, micro, macro) on the fracture behavior of concrete, inspired from the work of Löfgren [2005] on macrofibers.

The effect of different fiber scales on FRC mechanism can be interpreted in light of the above-described multi-scale cracking nature in concrete. Generally, macrofibers are efficient in improving the post-cracking performance once macrocracks are already formed. Micro and nanofibers, on the other hand, can alter the fracture mechanics at, respectively, the micro and nanoscale which can govern the response prior to the rupture strength. Nonetheless, the effect of micro and nanofibers on the post-cracking stage can be restrained by their smaller size such that when macrocracks are formed, controlling their growth with micro /nanofibers is not evident.

As such, a plain system (the curve in red) would experience a rapid loss in load-carrying ability as the applied stresses exceed the elastic limit B causing saturation of microcracks (C) and their localization into macrocracks marking the ultimate capacity (D). This can be followed by a small

bridging and branching tail at end of the curve corresponding to aggregate bridging effect [Shah *et al.*, 1995]. The addition of macrofibers (curve in black) will not affect the elastic limit B , nor will it affect the growth of microcracks (C) or the ultimate capacity (D). It will rather influence the drop in the load-carrying capacity DE whereby the presence of macrofibers mobilizes a transfer of stresses from the cracked matrix to the bridging fibers such that the drop DE is attenuated. Furthermore, the branching tail FE can be enhanced compared to that of the plain system. This corresponds to a coupled effect of a small contribution from aggregate bridging and a significant contribution from macrofiber bridging [Li and Maalej, 1996] where the energy consumed in pulling-out or rupturing bridging fibers extends the branching tail.

The use of microfibers (curve in blue) will influence the elastic limit (B), delay the point of microcrack saturation (C); thereby enhancing the ultimate capacity (D). This can be associated with the ability of microfibers to interfere with the widening-up of microcracks prevailing in the bulk cementitious matrix as well as in the paste-aggregate ITZ. Furthermore, microfibers can reduce the drop in the load-carrying capacity (DE) and enhance the branching tail (EF) by blunting the mouth of advancing macrocracks and resisting its widening-up by a bridging effect. However, for microfibers to be effective in this perspective, a relatively high aspect ratio and stiffness are indispensable such that the fibers can have sufficient length and strength to restrain microcracks from unstable growth leading to crack saturation (C) then localization (D) as suggested by Rossi *et al.* [1987], Betterman *et al.* [1995], Nelson *et al.* [2002], Lawler *et al.* [2003], and Stang [1987].

The advantageous effect of microfibers as compared to that of macrofibers on controlling the growth of microcracks and delaying matrix rupture can be attributed to the fact that at similar volume fraction to macrofibers, the higher fiber count in microfibers increases their likelihood to interfere with microcrack saturation (C) and eventually delay the ultimate capacity (D). Findings by Betterman *et al.* [1995] support that peak-stress (D) is increased with increasing fibre volume or decreasing fibre diameter. On the other hand, in the context of the improved pre-peak behavior with microfibers versus the reduced effect on post-peak behavior, observations by Lawler *et al.* [2003] proved that in the presence of microfibres, microcracks

were prevented from widening. However, the presence of microfibers had reduced effect on the length growth of microcracks which eventually saturated (*C*), coalesced into macrocracks (*D*), and eventually degradation in load-carrying capacity was inevitable as microcracks have a lesser effect on post-peak behavior. Comparable observations were made by Nelson *et al.* [2002] in their investigation on polyvinyl alcohol (PVA) microfibers as well as on cellulose microfibers.

Finally, for nanofibers, considering their nanoscale dimension allowing them to interact with cement hydrates which are also nanometric in size, it can be perceived that incorporating nanofibers in the cementitious matrix can allow intercepting the nanocracks which are intrinsic to the heterogenous microstructure of cement system. Thus, nanofibers can allow reducing or otherwise interfering with pre-existing cracks caused by residual mechanisms such as residual thermal strains or volumetric instabilities accompanying cement hydration. In this regard, a nanofiber-reinforced system (the curve in dotted red) can exhibit the following: (i) higher elastic limit (*B*) due to the effect of nanofibers on interacting with cement hydrates and enhancing the micromechanical properties of C-S-H [Konsta-Gdoutos *et al.*, 2009; Sanchez and Sobolev, 2010], (ii) delayed microcrack saturation (*C*) by blunting the edges of microcracks and interfering with their growth into macro-cracks, thereby improving the peak stress (*D*). Nonetheless, the effect of nanofibers remains significantly pronounced at the pre-peak stage (i.e. prior to the formation of macro-cracks). This is because nanofibers offer a toughening effect which is nonetheless limited by their nanoscale size such that bridging nano/microcracks is quite evident while the formation of macrocracks (once started) causes an abrupt degradation in load carrying capacity. This is reflected by the curve segment *DEF* showing more drop in the load-carrying capacity (*DE*) and a reduced effect on the branching and bridging tail (*EF*). Consequently, a cementitious system combining more than one scale (nano, micro, macro) (curve in dotted green) is expected to result in a synergetic effect, such that both pre-peak and post-peak behaviors are improved as suggested by Betterman *et al.* [1995], Markovic *et al.* [2004] and Meda *et al.* [2004].

It should be noted that the enhanced elastic properties and pre-peak behavior with nanofibers are not only the result of increased fiber count owing to the reduced fiber size, but also the result

of intrinsic properties of nanomaterials. For instance, the higher elastic modulus reaching the order of tera pascals (TPa) in carbon nanostructures [Lee *et al.*, 2008] or that of nanocellulose materials (NCM) where the crystalline portion can have elastic modulus in the order of 138 GPa [Sakurada *et al.*, 1962] can mobilize higher composite elastic modulus. Moreover, the nanometric scale of those materials can catalyze reactivity and provide nucleation sites for the growth of hydration products. In carbon nanotubes (CNT), for instance, nanoindentation assessment by Konsta-Gdoutos *et al.* [2009] suggest that CNT can strongly modify and reinforce the nanostructure of the cementitious matrix such that higher amount of high stiffness C-S-H and reduced nano-porosity can be achieved with as little CNT addition as 0.10% per cement mass. This was found to particularly improve the elastic modulus by more than 50%. The significant improvement in elastic properties offered by CNT were found elsewhere to buttress substantial enhancement in overall mechanical performance, particularly in tensile strength, flexural capacity and fracture properties. See Lee *et al.* [2008]; Konsta-Gdoutos *et al.* [2009]; Konsta-Gdoutos *et al.* [2010a]; and Konsta-Gdoutos *et al.* [2010b].

With NCM, on the other hand, the high surface area and omnipresence of surface hydroxyl (OH⁻) groups [Khazraji and Robert, 2013] can lead to surface reactivity and interactions with hydrates containing hydrogen in their structure, namely C-S-H and CH [Hoyos *et al.*, 2013]. As a result, C-S-H gel matrix with higher micromechanical properties can be obtained as reported by Cao *et al.* [2016a] indicating that the use cellulose nanocrystals (CNC) increases the stiffness of high-density calcium-silicate-hydrate (C-S-H) surrounding unhydrated cement particles. Similarly, Flores *et al.* [2017] reported that the incorporation of CNC results into a larger volume fraction of high-density C-S-H and a smaller volume fraction of low-density C-S-H. The above reported effect of NCM on altering the microstructure properties of cementitious systems can explain the substantial increase in macromechanical performance. Onuaguluchi *et al.* [2014] reported enhancement in flexural strength and flexural toughness of up to 108 and 186% when nanofibrillated cellulose (NFC) was incorporated of 0.05-0.40% per cement mass into cement paste matrix with water-to-cement ratio (w/c) of 0.50. Cao *et al.* [2015] recorded flexural strength enhancement of 20%-30% upon the incorporation of CNC at rates of 0.1-1.2% per cement mass in cement paste with w/c=0.35. These findings were also supported by those of

Peter *et al.* [2009] and Ardanuy *et al.* [2012] on CNF; and that of Hoyos *et al.* [2013] on microcrystalline cellulose (MCC). In light of the former discussion on the effect of macrofibers on the post-peak behavior, the enhancements imparted by nanofibers on pre-peak properties offer an opportunity to design FRC composites with improved pre-peak and post-peak performance. Further details about nanofibers in concrete will be covered in the next section within the overall context of nanomaterials in concrete.

2.3 Nanomodified concrete

Nanotechnology involves manipulating matter and materials at scales below 100 nm [Ashby *et al.*, 2009]. The application of nanotechnology in the concrete industry is still an emerging field where research is presently very active. Nonetheless, it is well established that nanomaterials can be incorporated into concrete matrices such that a nanomodified concrete is obtained. Nanomodified concrete refers to a concrete obtained by incorporating nanometer objects to engineer concrete nanostructure and control its macrobehavior [Jennings *et al.*, 2008] in order to achieve tailored and multifunctional cementitious composites with superior mechanical performance and durability [Sanchez and Sobolev, 2010]. The opportunities offered with nanomodification of concrete stem from the radically different material properties as well as material purity and compositional consistency dictated at a lower scale. Furthermore, the reduction in particle size significantly increases specific surface area (Fig. 2.5), which in turn has a significant effect on microstructure properties and eventually on mechanical performance. The following sections are dedicated to reviewing existing research on the effect of nanoparticles in concrete including (briefly) nanopowders (section 2.3.1), carbon nanostructures (section 2.3.2), and (more detailly) nanocellulose materials (NCM) (section 2.3.3).

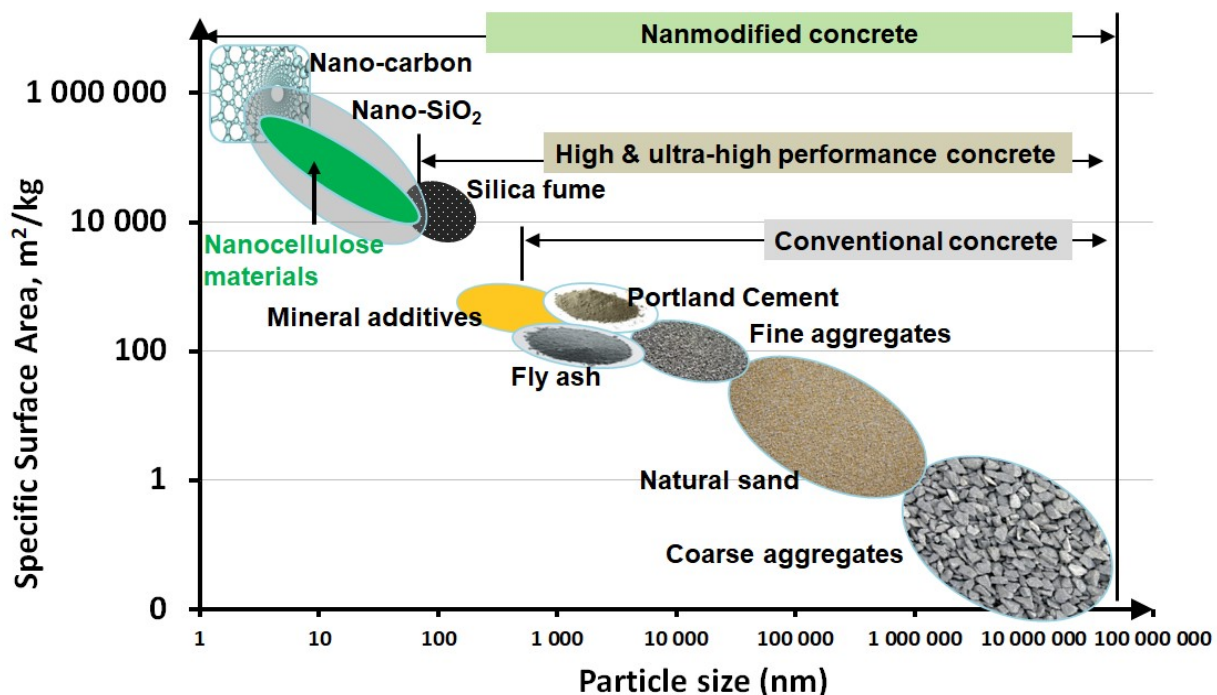


Fig. 2.5: Relationship between particle size and specific surface area as related to the constituents of different classes of concrete reproduced from [Sanchez and Sobolev \[2010\]](#).

2.3.1 Nano-powders in cement composites

The term nanopowder has been introduced herein to make a distinction between nanoparticles with spherical or irregular shape as contrasted to nanoparticles with rod-like shape exhibiting high aspect ratio, also referred to as nanofibers (such as graphene-based nanofibers, calcium carbonate nanowhiskers, and nanocellulose materials). The addition of nanopowders is primarily motivated by enhancing the microstructure of the cementitious matrix as well as to impart some specific desirable properties at fresh state (such as rheological modification) or at hardened state such as surface finishability or self-cleaning features. Existing investigations on nanopowders covered mainly nanometal oxides, namely, nano-SiO₂, nano-TiO₂, nano-Fe₂O₃, nano-Al₂O₃. Among these, nano-SiO₂ and nano-TiO₂ have been the most widely researched. For further depth, the reader is invited to consult [Sanchez and Sobolev \[2010\]](#); [Singh *et al.* \[2012\]](#); and [Kontoleonos *et al.* \[2012\]](#).

2.3.1.1 Nano-SiO₂

Owing to their extreme finesse and high surface area (50-750 m²/g) [AkzoNobel, 2010], nano-SiO₂ particles exhibit a remarkable filler effect which can mobilize higher packing density, reduced capillary porosity, and significantly enhanced mechanical performance. For this, nano-SiO₂ were found to influence the properties of cement matrices through a twofold effect, physical and chemical. In the physical effect, the high surface area of nano-SiO₂ grains allows nucleation sites to accelerate the hydration process by fostering the precipitation of Ca²⁺ ions. See Jo *et al.* [2007]; Senff *et al.* [2009]; Ltifia *et al.* [2011]; Madani *et al.* [2012]; and Hou *et al.* [2013]. For the chemical effect, the highly silicate-rich nano-SiO₂ promote a pozzolanic reaction consuming the relatively cleavable CH crystals and producing supplementary C-S-H gel, disconnecting porosity and enhancing mechanical and durability aspects [Singh *et al.*, 2012]. The accelerated hydration with nano-SiO₂ was also accompanied with higher heat of hydration [Bjornstrom *et al.*, 2004], while the above-mentioned combined effect of nucleation and pozzolanicity promote denser microstructure with lesser amount of CH crystals as demonstrated by Jo *et al.* [2007]; Singh *et al.* [2012]; Kontoleonos *et al.* [2012]. As an example of enhancement in mechanical performance, the incorporation of 5% nano-SiO₂ into cement paste was found to increase the compressive strength at 1 day and 28 days by, respectively, 64 and 35% [Singh *et al.*, 2012].

2.3.1.2 Nano-TiO₂

Nano-TiO₂ is a mineral present under two forms (rutile and anatase) and serves as a photocatalyst under UV light as it oxidizes water to create hydroxyl (OH) groups. It can also oxidize oxygen or organic materials directly. As such, nano-TiO₂ is added to confer sterilizing, deodorizing and antifouling properties to paints, cements, windows and tiles. The photocatalysis effect of nano-TiO₂ allows to nano-engineer cement composites with auto-cleaning features [Sanchez and Sobolev, 2010]. An example of actual applications of this feature is depicted in Fig. 2.6. On the other hand, the high density of nano-TiO₂ (3.9 g/cm³) and the higher hardness can be leveraged to impart higher mechanical strength and durability aspects to cement

composites. Nano-TiO₂ was found to promote cement hydration through providing germination sites for C-S-H. [Jalal *et al.* \[2013\]](#) reported that the incorporation of nano-TiO₂ in partial replacement of cement at 4wt.% accelerated the formation of C-S-H gel as a result of increased crystalline Ca(OH)₂ amount at the early age of hydration. This resulted in an improved microstructure, reduced porosity, and enhanced mechanical and durability features. Findings by [Zhang *et al.* \[2011\]](#) as well as by [Nazari and Riahi \[2011\]](#) suggest that at an optimum nano-TiO₂ of 1% per volume, reduced porosity, enhanced microstructure, and higher compressive strength can be obtained. Investigations by [Chen *et al.* \[2012\]](#) showed enhancement in compressive strength of up to 20% when nano-TiO₂ was incorporated at contents of 0-10 wt.% of rutile and anatase nano particles. For detailed information on the effect of nano-TiO₂ on cement systems, the reader is invited to consult [Katyal *et al.* \[1999\]](#); [Nazari and Riahi \[2011\]](#); [Jalal *et al.* \[2013\]](#); [Sikora *et al.* \[2015\]](#).



Fig. 2.6: The *Dives in Misericordia*, a church (in Rome, Italy) constructed of TiO₂ (Photo courtesy of Frener & Reifer).

2.3.2 Carbon-nanostructures

Carbon nanostructures (CNS) cover a spectrum of graphene-based nanomaterials such as graphene, graphene oxide (GO), carbon nanotubes (CNT), and carbon nanofibers (CNF) [Fig. 2.7 (a)-(e)]. Compared to traditional macroscale carbon fibers [Fig. 2.7 (f) and (g)], CNS have recently attracted an increasing research attention owing to their extremely high aspect ratio, exceptional strength, elastic behavior and excellent thermal properties. CNS exhibit tensile strength in the order of GPa and elastic modulus in the order of TPa in addition to unique thermal, electronic and chemical properties. See [Trtik and Bartos \[2001\]](#); [Sobolev and Ferrada-Gutiérrez \[2005\]](#); [Sanchez and Sobolev \[2010\]](#). Graphene and GO [Fig. 2.7 (a) and (b), respectively], the simplest form of CNS, represent allotropes of carbon consisting of a single layer of carbon atoms arranged in a hexagonal lattice. So far, these 1-atom thick almost transparent structures shape the strongest material ever tested, even stronger than diamond, while exhibiting high electrical and thermal properties. The fundamental difference between graphene and GO is that in the latter, the hexagonal carbon networks bear hydroxyl epoxide, carboxyl or carbonyl groups as a means to foster functionalization. See [Lee *et al.* \[2008\]](#); [Balandin *et al.* \[2008\]](#); [Sheehy *et al.* \[2009\]](#); [Zhu *et al.* \[2014\]](#); [Chuah *et al.* \[2014\]](#); and [Lin *et al.* \[2017\]](#).

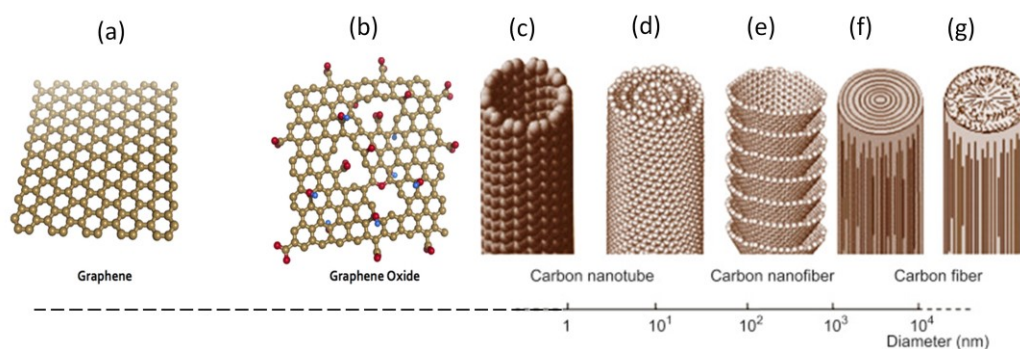


Fig. 2.7: A variety of carbon nanostructures (CNS): (a) Graphene, (b) Graphene oxide (GO), (c) Single-walled carbon nanotubes (SWCNT), (d) Multi-walled carbon nanotubes (MWCNT), (e) Stacked-cup carbon nanotubes (carbon nanofibers), and (f and g) conventional carbon fibers. Adapted from [Radic *et al.* \[2013\]](#) and [Hiremath and Bhat \[2017\]](#).

2.3.2.1 Carbon nanotubes (CNT) and carbon nanofibers (CNF)

CNT are hollow cylindrical graphene structures obtained by rolling graphene sheets. Precise rolling results into single-walled carbon nanotubes (SWCNT) [Fig. 2.7 (c)] while multiple rolling yields multi-walled carbon nanotubes (MWCNT) [Fig. 2.7 (d)] [Lijima and Ichihashi, 1993]. SWCNT have a wall of one atom thick, diameter of 0.3–2 nm, and length > 200 nm, while MWCNT have multiple walls, diameter of 10–50 nm, and length of 1–50 μm , with properties slightly lower than those of SWCNT, but at a relatively reduced cost [Kang *et al.*, 2006].

CNF are composed of multiple concentric nested tubes with walls inclined relative to the longitudinal axis. CNF are analogous to large diameter MWCNT, but CNF are not continuous tubes as their surfaces show steps at the termination of each tube wall [Fig. 2.7 (e)], and for this, CNF are also referred to as stacked-cup carbon nanotubes (SCCNT). CNF have diameters of 65–130 nm, 50–100 μm length [Kang *et al.*, 2006]. They have moderate electrochemical properties compared to those of CNT, but their relatively larger size compared to CNT allows better dispersion and easier incorporation into composites. Furthermore, their numerous exposed edge planes along the surface [Fig. 2.7 (e)] allow higher interaction with the host matrix. Building upon the initial works of Iijima [1991] on MWCNT and that of Benning *et al.* [1992] on SWCNT, considerable possibilities of composite nano-tailoring opened-up in versatile applications including cement composites. In the latter, significant research (particularly for CNT) has been conducted by Shah and collaborators [Shah *et al.*, 2009; Konsta-Gdoutos *et al.*, 2009; Konsta-Gdoutos *et al.*, 2010a; Konsta-Gdoutos *et al.*, 2010b]. See also Makar *et al.* [2004]; Makar *et al.* [2005]; Li *et al.* [2005]; Li *et al.* [2007] and much more other investigators.

Owing to their high surface area, aspect ratio (> 1000) [Xie *et al.*, 2005; Alain *et al.*, 2001], and excellent mechanical properties, the incorporation of CNT into cement composites opens significant opportunities for enhancement in composite mechanical performance. Nonetheless, the major handicap is the dispersion of these hydrophobic materials (with high self-attraction tendency) inside the hydrophilic cementitious mixtures. This is the reason why early

investigations on CNT recorded contradicting enhancement in mechanical performance. As a result, an effective dispersion technique is a fundamental pre-requisite for enhanced composite mechanical performance.

Makar *et al.* [2005] dispersed SWCNT and MWCNT by sonication in isopropanol followed by cement addition, evaporation, and grinding. This produced cement particles coated with CNT. The authors showed that when CNT are added to cement paste as a pre-mix with gum Arabic (a water-soluble gum used as a dispersing agent), early-age hydration was increased and that a strong bond is possible between the cement paste and the CNT. Furthermore, higher nanoindentation modulus M and hardness H were obtained, while adverse results were obtained when no dispersing agent was used.

On the other hand, when Cwirzen *et al.* [2008] introduced MWCNT (0.006–0.042 wt.% loadings) as a water suspension with surfactant admixtures added, the compressive and flexural strength didn't record any improvement. Rather, the bond between the MWCNT and the matrix was quite weak. Similarly, when Musso *et al.* [2009] used 0.5 wt.% MWCNT (dispersed using acetone, ultrasonic vibration, superplasticizer, and a viscosity modifying agent that were added during the mixing stage) to investigate the effect of MWCNT surface structure (pristine, annealed, and carboxyl group functionalized), the flexural and compressive strengths were significantly decreased for functionalized MWCNT. For pristine and annealed MWCNT, flexural and compressive strengths enhancements of 10–20% recorded.

At improved dispersion of MWCNT using functionalization by grafting polyacrylic acid polymers to MWCNT, Cwirzen *et al.* [2008] demonstrated to achieve high mixture workability and improvement in compressive strength of up to 50% at MWCNT content of 0.045-0.15 wt.%. Furthermore, when Shah *et al.* [2009] dispersed CNT in water using surfactant and ultrasonic energy, CNT content of 0.048 wt.% and 0.08 wt.% was able to increase the elastic modulus of cement paste by up to 50%. This enhancement can be crosslinked with the microstructure alterations lead by CNT as supported by the subsequent investigation on nanoindentation of CNT-cement paste by Konsta-Gdoutos *et al.* [2009] where CNT was found to modify the C–S–H, increase the quantity of high stiffness C–S–H, reinforce the cement paste matrix at the

nanoscale, and decrease the porosity. An example of cement microstructure being altered by the addition of CNT is shown in Fig. 2.8 where CNT appear to provide a nanoreinforcing agent to the matrix.

On the basis of some of the above promising results and much others, several recent investigations have leveraged CNS for the development of cement composites with improved performance. To mention only a few, we have, self-sensing CNT-cement composite for traffic monitoring [Baoguo *et al.*, 2009]; self-sensing CNT-reinforced ultra-high-performance concrete (UHPC) [Seung *et al.*, 2018], improved mechanical performance in CNF-reinforced UHPC [Sbia *et al.*, 2014]; reduced crack resistance due to drying shrinkage in cement mortars [Hogancamp *et al.*, 2017]; synergetic effect between nanofibers and macrofibers for hybrid-reinforced UHPC [Ngoc and Kim, 2017], increased tensile strength, flexural capacity and energy absorption capacity with CNS-reinforced UHPC [Meng and Khayat, 2016], and blending MWCNT with macrofibers for enhancing the initial cracking fracture toughness to produce high toughness cementitious composites [Xu *et al.*, 2019].

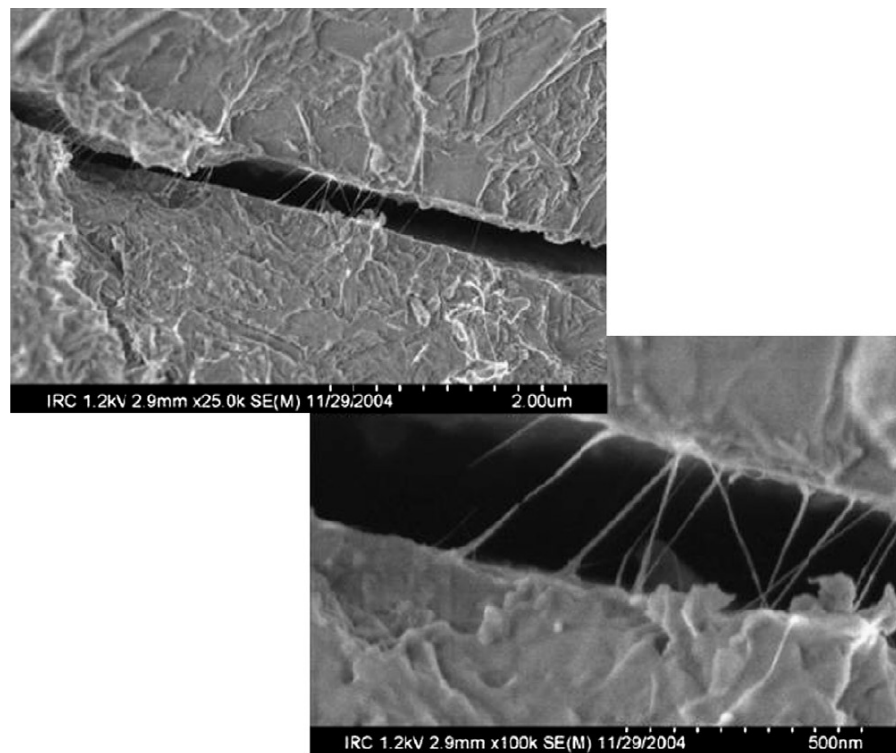


Fig. 2.8: Crack bridging in cement-CNT composites [Makar *et al.* 2005].

2.3.2.2 Graphene oxide (GO)

Among all carbon nanostructures (CNS), GO is the latest material introduced following its discovery in 2010. Massive investigations about this new material started right after its 2010 Nobel prize extraction process developed by Geim and Novoselov from the university of Manchester, UK. Using graphite and simple regular tools such as adhesive and tape, Geim and Novoselov were able to obtain a flake of carbon with a thickness of one single atom exhibiting the highest possible strength of so far tested materials. Coupled with exceptional electrical, sensing, thermal, and transparent features, GO has now found a way in versatile applications particularly in transparent electronics, biomedical, water treatment, etc. By 2011, investigations on the use of GO in cement composites have also appeared.

Additional to the intrinsic properties of all CNS such as high strength, elastic properties, and high surface area, what distinguishes GO is the extremely thin structure (at 1-carbon atom thickness) with hexagonally arranged carbon atoms providing extreme strength. Investigations in GO-cement composites indicate that the atomic-size GO has a significant effect on cement hydration kinetics [Lv *et al.*, 2013a; Lv *et al.*, 2014; Lv *et al.*, 2016]. One of the most debated features of GO-cement composites is the petal-like hydration products observed by Lv *et al.* [2013] whereby cement hydrates tend to be well-ordered in crystalline or petal-like shapes [see Fig. 2.9]. For this, Lv *et al.* [2013] reported that the incorporation of GO led to smaller and more uniform pores. He ascribed this feature to the high strength and ordered structure of GO favoring the growth of cement hydration products in a more ordered manner, imparting the so-called *template effect*. Later on, investigations by Wang *et al.* [2015], and recently by Jiang and Wang [2017] supported the finding of Lv *et al.* [2013]. However, Horszczaruk *et al.* [2015] showed that no significant effect on cement hydration product can be obtained with GO. Subsequently, Cui *et al.* [2017] further rebutted the *template effect* and the consequent formation of petal-like hydration products, which, for him are not part of hydration products, but just calcium carbonate due to the carbonation reaction when preparing the sample of cement composites.

Despite this controversy, what is well-established is that incorporating such tiny materials with high strength and ordered structure as GO should alter the microstructure. For this, further work

by [Lv et al. \[2016\]](#) and [Lv et al. \[2017\]](#) explored the mechanism underpinning the formation of petal-like hydration products in GO-cement composite as illustrated in [Fig. 2.10](#). This opened further opportunities to target a controlled altering of the microstructure of cement composites reinforced by GO in order to achieve the desired performance of composite materials [[Xu et al., 2018](#)]. That said, despite the controversy regarding the *template effect*, available investigations on GO-cement composites are in concord about increased mechanical performance. A wide range of strength increase rate of GO-reinforced composites, from 15% to 160% in compressive strength, 18%–185% in split tensile strength increase was recorded, with a wide range of strength increase being partly associated with mixture percentage differences of GO in cement composites (i.e., from 0.02% to 4%) as well as the preparation of GO samples. See [Lv et al., \[2013\]](#); [Chen et al. \[2015\]](#); [Shang \[2015\]](#); and [Horszczaruk et al. \[2015\]](#).

Having addressed the overall behavior of cement composites incorporating nanopowders in section [2.3.1](#) and carbon nanostructures in section [2.3.2](#), the general effect of these already widely investigated nano-inclusions in cementitious systems has set the basic concepts to understand the effect of nanocellulose materials (the main topic of this research) on cementitious composites. NCM have been utilized in the field of polymer composites for several years, but their incorporation into cement composites is a new research direction that has just emerged. Section [2.3.3](#) is devoted to recapitulating existing literature on NCM characteristics as well as the limited available investigation on their effect on cement composites.

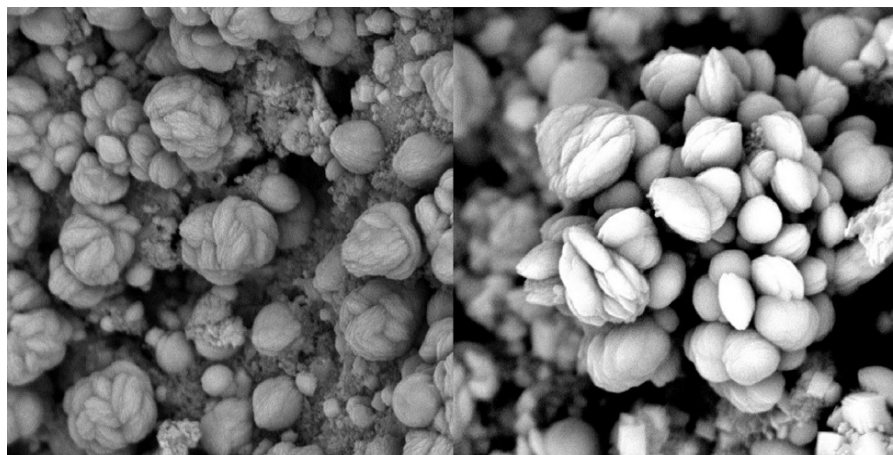


Fig. 2.9: Cement hydration products in crystalline or petal-like shapes in the presence of graphene oxide (GO) (adapted from [Lv et al. \[2013\]](#)).

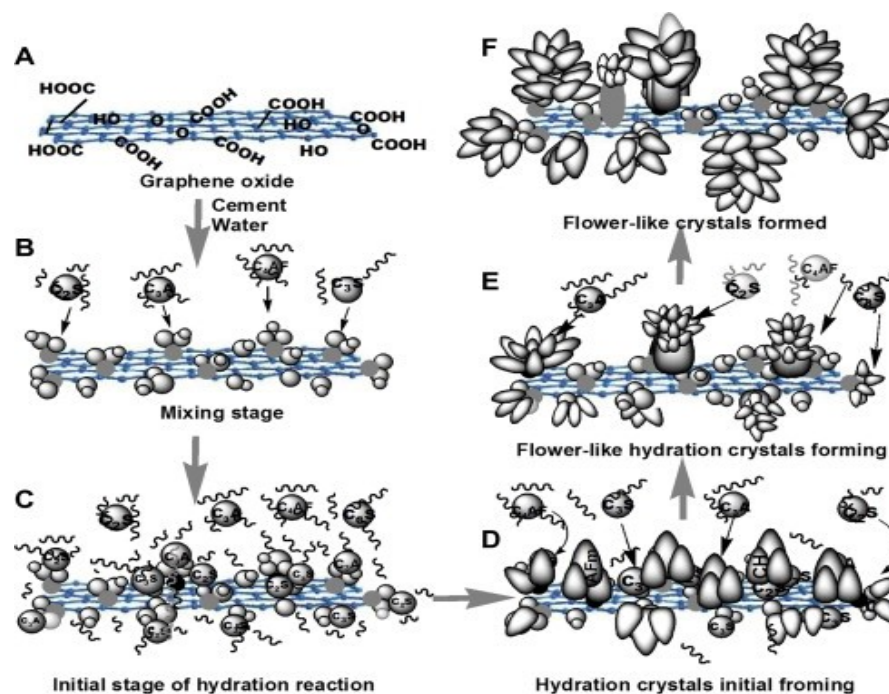


Fig. 2.10: The mechanism of formation of petal-like hydration products in graphene-oxide cement composite. Figure adapted from Lv et al. [2016].

2.3.3 Nanocellulose Materials (NCM)

NCM are plant-based cellulosic materials of nano/micro dimensions with cellulose being the fundamental building block.

2.3.3.1 Structure of cellulose

Cellulose is an organic compound belonging to the family of polysaccharides and is the primary structural component of the cell wall of green plants and many forms of algae. Moon et al. [2011] describe cellulose as a naturally occurring polymer consisting of a linear chain of ringed glucose molecules with a flat ribbon-like conformation. Fig. 2.11 (a) illustrates the repeat unit of cellulose polymers. The repeat unit consists of two anhydroglucose rings $[(C_6H_{10}O_5)_n]$; with $n = 10\,000$ to $15\,000$, where n depends on the cellulose source material. These two anhydrous

rings are linked together via oxygen covalently bonded to C1 (of one glucose ring) and C4 (of the adjoining ring) resulting into the so-called *1→4 linkage* also known as β *1–4 glucosidic bond* [Samir *et al.*, 2005].

The above-described molecular structure stimulates several intrinsic properties of cellulose polymer: (i) a stable linear configuration (promoting on-axis stiffness) resulting from the intrachain hydrogen bonding between hydroxyl groups and oxygens of the adjoining ring, (ii) an intrinsic tendency to parallel staking of multiple cellulose chains (fostering the formation of elementary fibrils that further aggregate into larger microfibrils) due to van der Waals and intermolecular hydrogen bonds between hydroxyl groups and oxygens of adjacent molecules, (iii) high axial stiffness (imparting inherent strength to plant-based materials) due to intra- and inter-chain hydrogen bonding network culminating into stiff cellulose microfibrils [Fig. 2.11 (b)]. Those microfibrils constitute the fundamental building block in trees, plants, some marine creatures (tunicates), algae, and some bacteria [Moon *et al.*, 2011].

The structure of cellulose fibrils (resulting from parallel stacking of cellulose chains) consists of regions with highly arranged cellulose chains (also referred to as crystalline regions) interrupted with less ordered regions (also referred to as amorphous regions). During the extraction process of NCM, the amorphous regions are eliminated via acid hydrolysis for instance to yield cellulose nanocrystals (CNC) [Fig. 2.11 (c)].

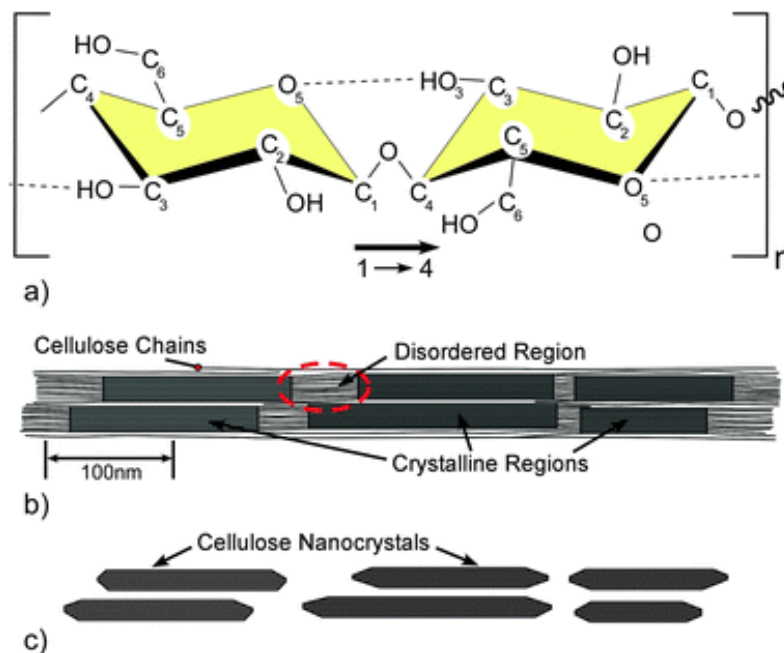


Fig. 2.11 Schematics illustration the structure of cellulose: single cellulose chain repeat unit (a), idealized cellulose microfibril configurations of the crystalline and amorphous regions (b), and (c) cellulose nanocrystals after acid hydrolysis. Figure adapted from Moon *et al.* [2011].

2.3.3.2 Hierarchical structure of cellulose

The structure of cellulose addressed earlier is the driving force for the inherent strength in cellulose-based systems. This can also be linked to the complex hierarchical structure of cellulose spanning from the atomic/molecular scale (cellulose units), to the nanometric-scale (cellulose individual fibers), to the micrometric scale (cellulose microfibrils), to the centimeter-scale (cellulose macrofibers), to the macro-scale (trees). In a top-down approach, we can see that wood pulp is made of a large amount of cellulose macrofibers. The wall structure of cellulose macrofibers is composed of bunches of closely stacked cellulose microfibrils organized around a cavity called a fiber lumen. A single cellulose macrofibril is composed of tiny bands of cellulose microfibrils, which, when peeled axially, individual microfibrils are obtained (Fig. 2.12). Each individual microfibril is composed of crystalline and amorphous domains such that when the amorphous domains are removed with acid hydrolysis, cellulose nanocrystals (CNC) are obtained. As the research in NCM has just picked up and is currently very active, there is not yet a consensus on terminologies. Thus, the end individual cellulose

microfibrils (containing amorphous regions interrupted with crystalline regions) are also termed as microfibrillated cellulose (MFC), or nanofibrillated cellulose (NFC)/cellulose nanofibers (CNF), or cellulose filaments (CF), bearing in mind the difference in the extraction process leading to variation in microfibrils diameter, length, and consequently aspect ratio. However, for the crystalline regions, there is a terminology consensus which is cellulose nanocrystals (CNC) or alternatively nanocrystalline cellulose (NCC) which are interchangeably used to refer to the same element.

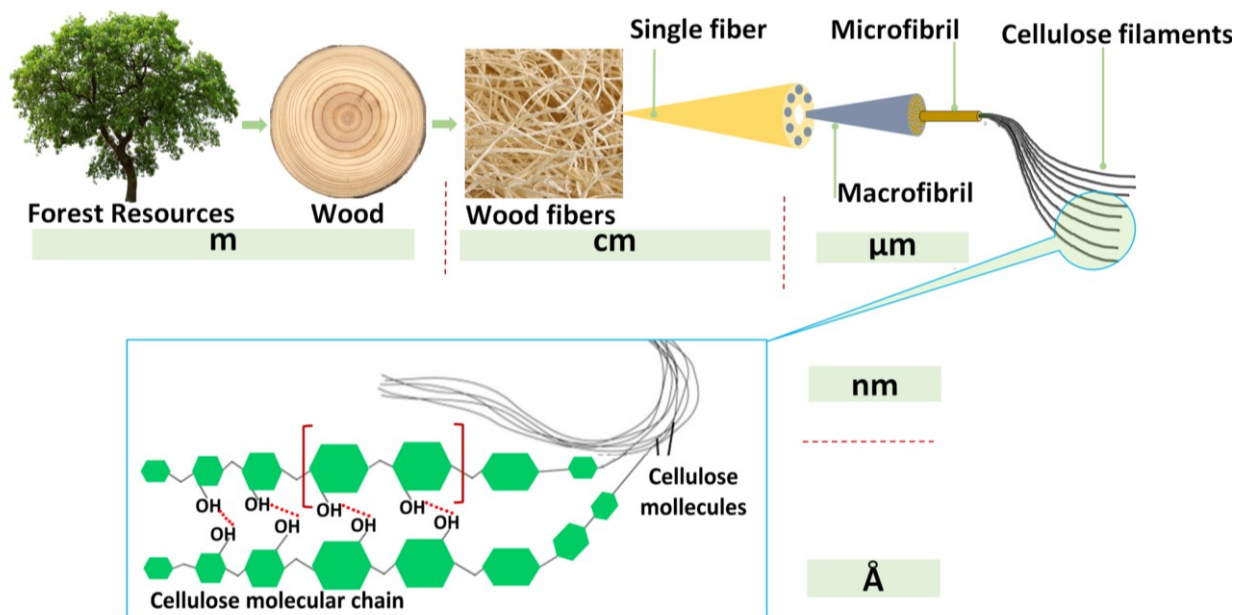


Fig. 2.12: Hierarchical structure of cellulose. The figure depicts cellulose as an intrinsic building block within a structured hierarchy (from the molecular/atomic scale to the macro scale) imparting inherent strength to plant-based systems. Figure adapted from article 4 [Hisseine *et al.*, 2019a] published in the context of this research.

2.3.3.3 Nanocellulose materials and opportunities in composite

The complex hierarchical structure of NCM as well as the intrinsic properties such as the high surface area, high on-axis stiffness, and high functionality additional to excellent strength properties surpassing those of some traditional reinforcing materials (Table 2.1), NCM paved a path to versatile application as a sustainable candidate for the development of green high-

performance bio-composites. The versatility of NCM is mainly driven by the highly functionalizable cellulose polymers as well as from the remarkable nanoscale reinforcing potential of the axially-very stiff cellulose chains [Foster *et al.*, 2018]. In this regard, NCM unveiled opportunities in composite design which were impossible to achieve with macroscale natural fibers (for being too large to exhibit surface reactivity) or with molecular cellulose (being too tiny to impart a reinforcing ability to composites) as highlighted by Moon *et al.* [2011]. The increased surface area of NCM allows intimate adherence with the host matrix through chemical reactions driven by hydrogen bonding (not evident with macroscale natural fibers), while conserving high transversal isotropic stiffness, which provides an effective nanoscale reinforcement (not evident with molecular cellulose). NCM provide further capabilities to overcome some of the drawbacks of cement composites reinforced with macroscale natural fibers, such as the low elastic modulus [Jarabo *et al.*, 2012], poor compatibility between fiber and matrix [Faruk *et al.*, 2012], and inconsistency in fiber properties leading to variation in concrete quality and performance [Aziz *et al.*, 1981].

With this, NCM have emerged in the last few years as highly potential candidates to respond to the ever-increasing demand for products made from renewable and sustainable resources. Products that are biodegradable, non-petroleum based, carbon neutral. Products which are exhibiting the lowest environmental, animal/human health and safety risks Moon *et al.* [2011]. As such, NCM have found applications in such versatile applications as adhesives, polymer reinforcement, nanocomposites, transparent flexible electronics, cosmetics, and bio-based polymer composites [Moon *et al.*, 2011; Goodsell *et al.*, 2014; Habibi *et al.*, 1980].

Table 2. 1. Properties of cellulose and other reinforcing materials Moon *et al.* [2011].

Material	Density ρ (g/cm ³)	Tensile strength, σ_f (GPa)	Axial elastic modulus, E_A (GPa)	Transversal elastic modulus, E_T (GPa)	References
Kevlar-49 fiber	1.4	3.5	124-130	2.5	Kawabata <i>et al.</i> [1993]; Callister <i>et al.</i> [1994]
Carbon fiber	1.8	1.5–5.5	150-500	–	Callister <i>et al.</i> [1994]
Steel Wire	7.8	4.1	210	–	Callister <i>et al.</i> [1994]
Clay Nanoplatelets	–	–	170	–	Hussain <i>et al.</i> [2006]
Carbon Nanotubes	–	11-63	270-950	0.8–30	Yu <i>et al.</i> [2000; Salvetat <i>et al.</i> [2006]
Boron nanowhiskers	1.6	2–8	250-360	–	Ding <i>et al.</i> [2006]
Crystalline cellulose		7.5–7.7	110-220	10–50	Source references in Table 2.2

Table 2. 2. Mechanical properties of common nanocellulose materials (compiled from different sources by Moon *et al.* [2011].

Material	Axial elastic modulus, E_A (GPa)	Transversal elastic modulus, E_T (GPa)	Tensile strength, σ_f (GPa)	Tensile strain ϵ (%)	Protocol
Wood fiber	14–27	–	0.3–1.4	4–23	Tensile test
Plant fiber	5–45	–	0.3–0.8	13–8	Tensile test, Raman spectroscopy
MCC	25±4	–	–	–	
MFC and NFC	N/A	–	–	–	
Plant CNC	57	–	–	–	Raman spectroscopy
Wood CNC	–	18–50	–	–	AFM Indentation
BC	78±17	–	–	–	AFM–3-point bend
	114	–	–	–	Raman spectroscopy
CelluloseI β -Experimental	120-138		–	–	XRD
-Modeling	220±50	15 ± 1	–	–	IXS

MCC: Microcrystalline cellulose; MFC: Microfibrillated cellulose; NFC: Nanofibrillated cellulose; CNC: Cellulose nanocrystals; BC: Bacterial cellulose

2.3.3.4 Common types of nanocellulose materials

Nanocellulose materials (NCM) includes an array of cellulosic materials of nano/micro scale such as nanofibrillated cellulose (NFC), microfibrillated cellulose (MFC), cellulose nanocrystals (CNC), bacterial cellulose (BC), and cellulose filaments (CF). NFC consists of alternating crystalline and amorphous domains made of bundles of stretched cellulose chain molecules with long, flexible, and entangled cellulose nanofibers of approximately 1–100 nm diameter and 500–2,000 nm length [Moon *et al.*, 2011]. CNC consists of rod-like highly crystalline cellulose particles of 2–20 nm diameter and 50–500 nm length, thereby exhibiting a lower aspect ratio compared to NFC and limited flexibility due to the absence of amorphous portions [Brinchi *et al.*, 2013]. BC particles are microfibrils secreted by various bacteria and have different morphologies, but they are typically rectangular like, 6–10 nm wide and 30–50 nm long [Eichhorn *et al.*, 2010]. CFs are mechanically processed cellulose fibrils with micrometric length and nanometric diameter. CF exhibit some structural similarities with NFC, but they have an extended length (100–2,000 μm) compared to their diameter (30–400 nm), thereby resulting in a significantly higher aspect ratio (100–1,000). For this, Fig. 2.13 provides a comparison between the aspect ratio of commonly available NCM and that of CF used in this current study. On the other hand, Fig. 2.14 shows micrographs of wood pulp fibrils [Fig. 2.14 (a)] as compared to other currently available NCM [Fig. 2.14 (b)–(e)] and the CF [Fig. 2.14 (f)], the high aspect ratio NCM being investigated in the current project. For further details about the characteristics of NCM see Eichhorn *et al.* [2010]; Moon *et al.* [2011]; Brinchi *et al.* [2010].

2.3.3.5 Mechanical properties of nanocellulose materials (NCM)

A full understanding of the intrinsic mechanical properties of NCM has not been developed and is a topic of ongoing research. Thus, the characterization of mechanical properties of NCM remains quite challenging for the following factors: (i) the small particle size combined with the limited metrology techniques available to characterize NCM, (ii) Multiple axes behavior in NCM. Additionally, several factors may influence the measured mechanical properties and will contribute to the significant variation in measurement due to the crystal structure ($I\alpha$, $I\beta$, II), percent crystallinity,

anisotropy, defects, as well as the measurement protocol itself [Moon *et al.*, 2011]. For further insight into this crucial part of NCM, the reader is invited to consult the recent review on *Current characterization methods for cellulose nanomaterials* by Foster *et al.* [2018].

Table 2.2 shows the mechanical properties of common NCM where in most cases only the elastic properties (more readily measurable axial direction of cellulose) are reported. Measurement of direct mechanical properties of individual fibrils (such as NFC, MFC, or CF) have often been hindered by anisotropy of crystalline cellulose, that's the non-symmetric crystalline structure of cellulose [Moon *et al.*, 2011].

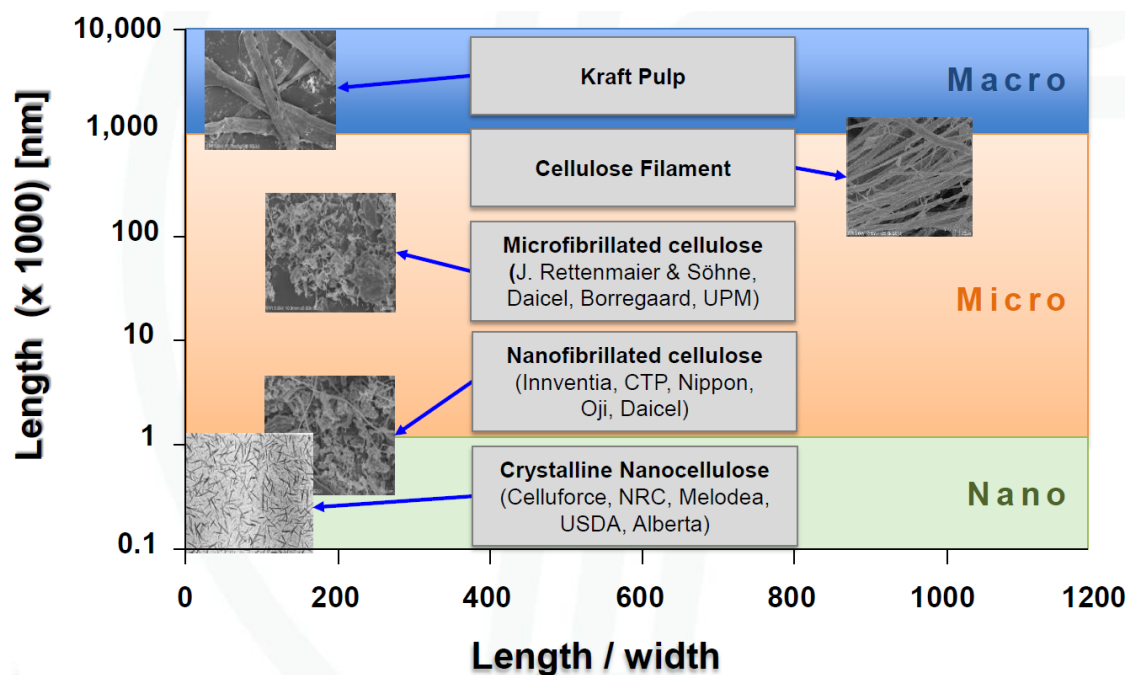


Fig. 2.13: Length-to-width relationship (aspect ratio) in commercially available nanocellulose materials (NCM) as compared to that of cellulose filaments (CF) being investigated in the current project. Figure reproduced with the permission of CF supplier [Kruger Biomaterials Inc., Montréal (QC), Canada].

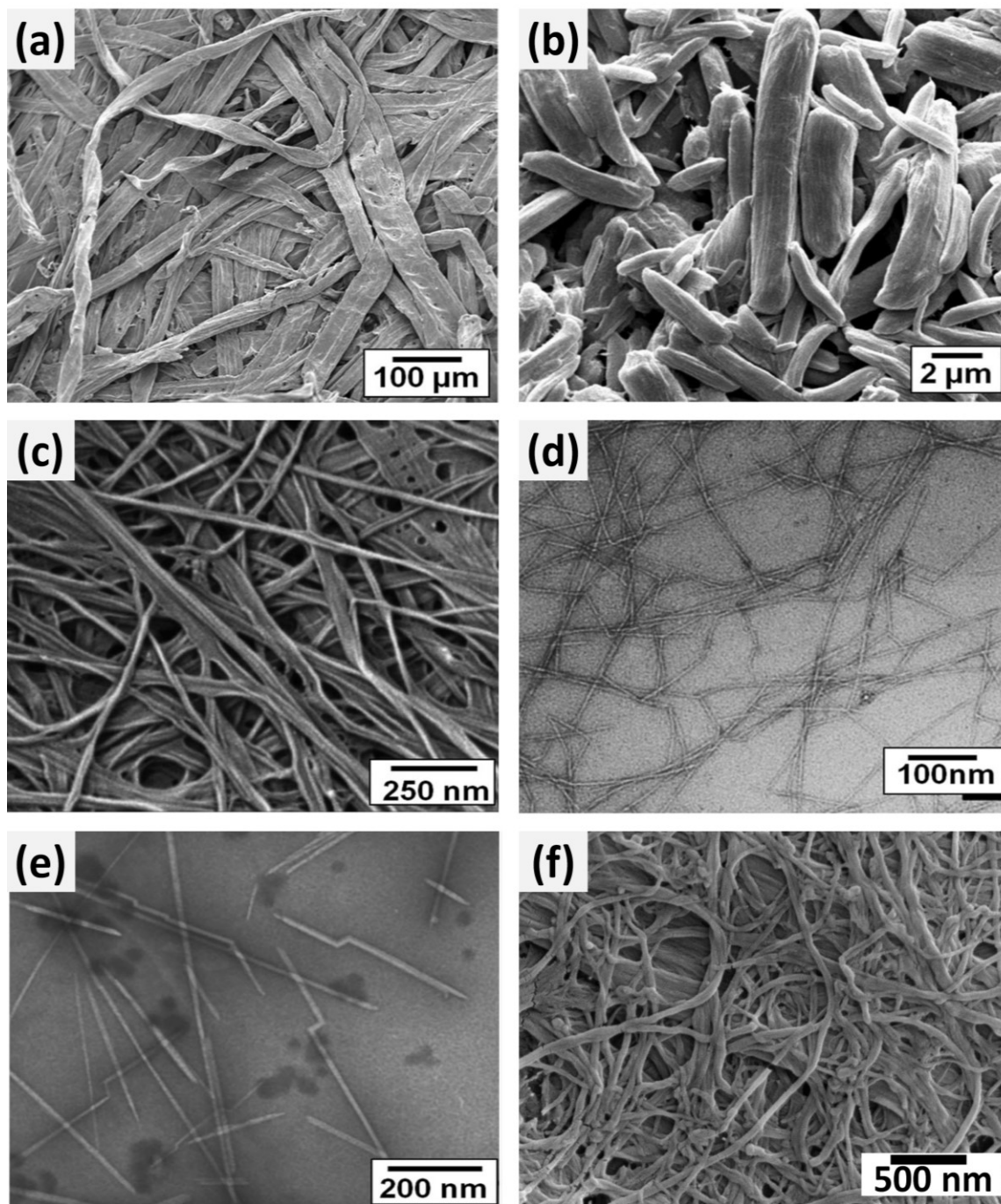


Fig. 2.14: Micrographs of cellulose pulp (a) as compared to common nanocellulose materials: Microfibrillated cellulose (MFC) (b) adapted from [Dufresne *et al.* \[1997\]](#); Bacterial cellulose (BC) (c) adapted from [Ifuku *et al.* \[2007\]](#); Nanofibrillated cellulose (NFC) (d) adapted from [Saito *et al.* \[2007\]](#); cellulose nanocrystals (CNC) (e) adapted from [Moon *et al.* \[2011\]](#) and; cellulose filaments (CF) (f) adapted from article 1 published in the current study [[Hisseine *et al.* 2018a](#)].

2.3.3.6 Nanocellulose materials in cement and concrete

Building on the potential reinforcing ability of nanocellulose materials (NCM) as well as their high functionality demonstrated in versatile applications including polymer reinforcement, nanocomposites, transparent flexible electronics, optics et., [Dufresne *et al.*, 2000; Yano *et al.*, 2005; Moon *et al.*, 2011; Goodsell *et al.*, 2014; Habibi *et al.*, 1980], very recently NCM found applications in concrete technology. However, the available literature is very is limited. The effect of NCM on properties of cement composites can be attempted in light of NCM features addressed in previous sections (from one side) and in light of the intrinsic properties of cement composites associated with their transformation from fresh to hardened state (the hydration), from another side.

2.3.3.6.1 Cement hydration and structuration

In cement composites, the bulk matrix phase [mainly a mixture of Portland cement and water and possibly supplementary cementitious materials (SCM), high-range water reducing admixtures (HRWRA), and other admixtures)] develops strength through cement hydration reaction. The latter is an exothermal reaction through which cement grains hydrate leading to the development of a stiff microstructure. This is a transformation from a liquid-like phase to a solid state within a few hours, giving cement composites the so-called name of *man-made rock*.

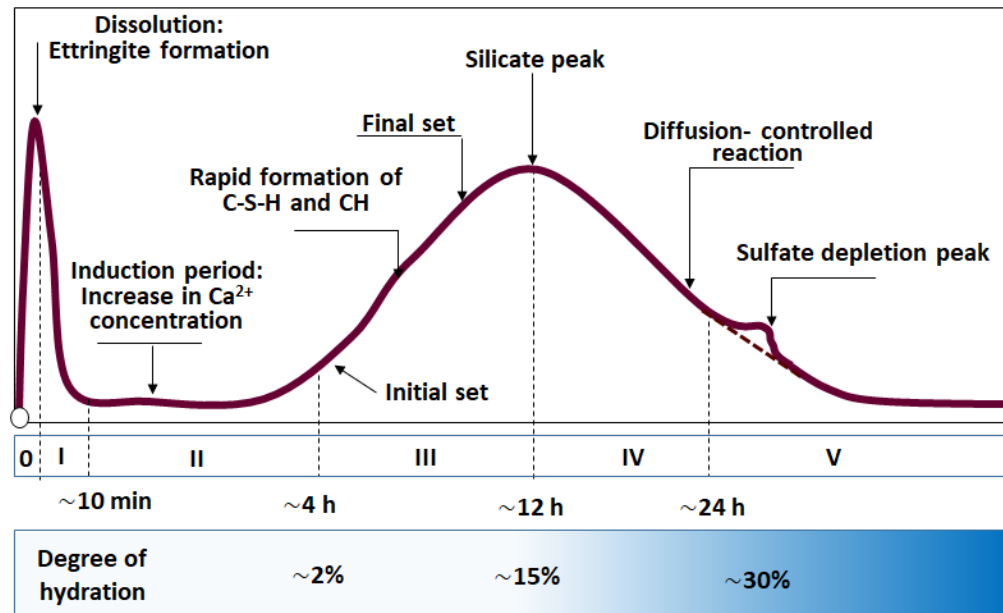


Fig. 2.15: Schematic illustration of cement hydration inspired from Gartner *et al.* [2002].

Based on vast literature [Aitcin, 2000; Neville, 2000; Gartner *et al.*, 2002, Mindess *et al.*, 2003], the structuration of cement composites goes through a four-phase transformation (Fig. 2.15) involving complex physiochemical interactions between clinker active phases, calcium sulphate, and water. At the onset of water contact with cement, vigorous reactions take place leading to significant heat release corresponding to the initial dissolution of cement active phases (stages 0 to I). A so-called *dormant period* (which is actually not dormant for the increase in the concentration of Ca^{2+} ions as well as in electrical conductivity) occurs (stage II). Later, as structuration continues, when the initially formed hydrated construct a percolated network of connected particles, a rigidification threshold is attained (or setting time), the onset of a solid-like phase (III). This is dominated by the hydration of tri-calcium silicate (C_3S) and is characterized by a remarkable heat rise (silicate depletion peak) following the induction period. Thereafter, heat intensity declines where hydration reactions are rather controlled by ion diffusion (IV), while hydration does not completely stop, but rather continues in a less vigorous manner (V) as far as there is water available to dissolve cement grains and as long as there is available space to accommodate hydrates. This transformation results in the formation of cement hydrates, the most dominant of which is Calcium Silicate Hydrate phase (C-S-H), a gel matrix responsible for the mechanical strength.

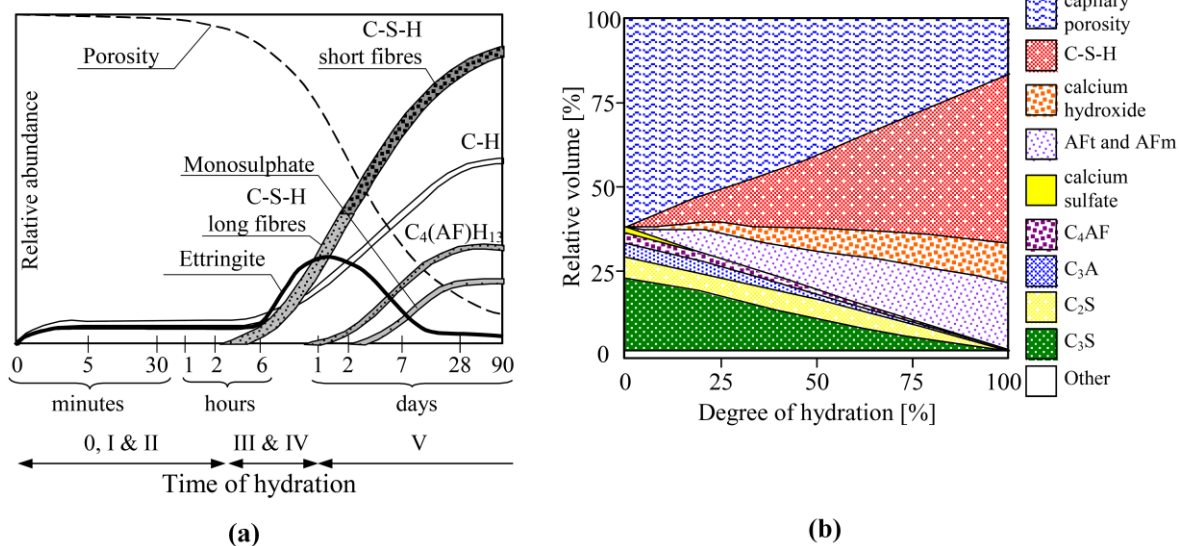


Fig. 2.16: Relative volumes of the major compounds in the microstructure of hydrating Portland cement pastes: as a function of time (a) [Locher *et al.*, 1976]; and as a function of the degree of hydration as estimated by a computer model for a w/c-ratio of 0.5 (b) [Tennis and Jennings, 2000].

The overall output of the hydration reaction is depicted in (Fig. 2.16) where C-S-H occupies 50–60% of the volume of solids while the porosity dominates the overall volume. This porous network, multiscale in nature, is made up of a continuous distribution of pore sizes, from air voids with a size of 50–200 μm to capillaries of about 0.05–10 μm diameter and gel pores less than 0.5 nm in diameter. The porous network also includes the porosity at the interfacial transition zone (ITZ) between aggregates (as well as macrofibers in FRC) and the bulk cementitious matrix. The ITZ is generally perceived to have lower structural properties, much coarser pores, and easily cleavable highly soluble calcium hydrate (CH) crystals compared to the bulk cementitious matrix [Ollivier *et al.*, 1995; Wang *et al.*, 2009; Erdem *et al.*, 2012]. This is generally associated with the *wall effect* in which the aggregates (and macrofibers) appear locally flat relative to cement grains, which disrupts cement packing [Scrivener *et al.*, 2004], or to the *microbleeding* effect that leads to the accumulation of mixture water beneath the aggregates during consolidation [Goldman and Bentur, 1992]. This makes the ITZ the weakest link of the microstructural system, where cracking initiates, and thus it has a phenomenal effect on the mechanical and transport properties of concrete [Nemati *et al.*, 1998; Wong *et al.*, 2009]. According to Mindess *et al.* [2003], the ITZ

in a typical concrete can be as thick as 20–50 μm , while making up 20–40% of the total bulk cementitious matrix.

While it is well established that the addition of macrofibers does not substantially alter cement hydration kinetics (described in this section) nor does it change the development of the microstructure of the bulk cementitious matrix, it should be elucidated that the formation of ITZ around the fibers (as part of microstructure development) significantly affects the pull-out behavior of fibers. This has also a relatively moderate influence on FRC pre-cracking strength being matrix-governed, and a significant effect on the post-cracking strength predominantly controlled by fiber pull-out. Therefore, the microstructure of the cementitious matrix influences the interface behavior which in turn governs the interfacial micromechanical response such as a frictional bond, chemical bond, and slip hardening in polymeric fibers. This makes understanding the microstructure an indispensable part of the strengthening and toughening effect in FRC [Bentur *et al.*,1995]. Figure (Fig. 2.17) shows micrographs of a bulk cementitious matrix [Fig. 2.16 (a)] as well as a close-look at the porous layer prevailing at the ITZ [Fig. 2.17 (b)] as also confirmed by Fig. 2.17 (c), while Fig. 2.16 (d) describes the composition of the ITZ.

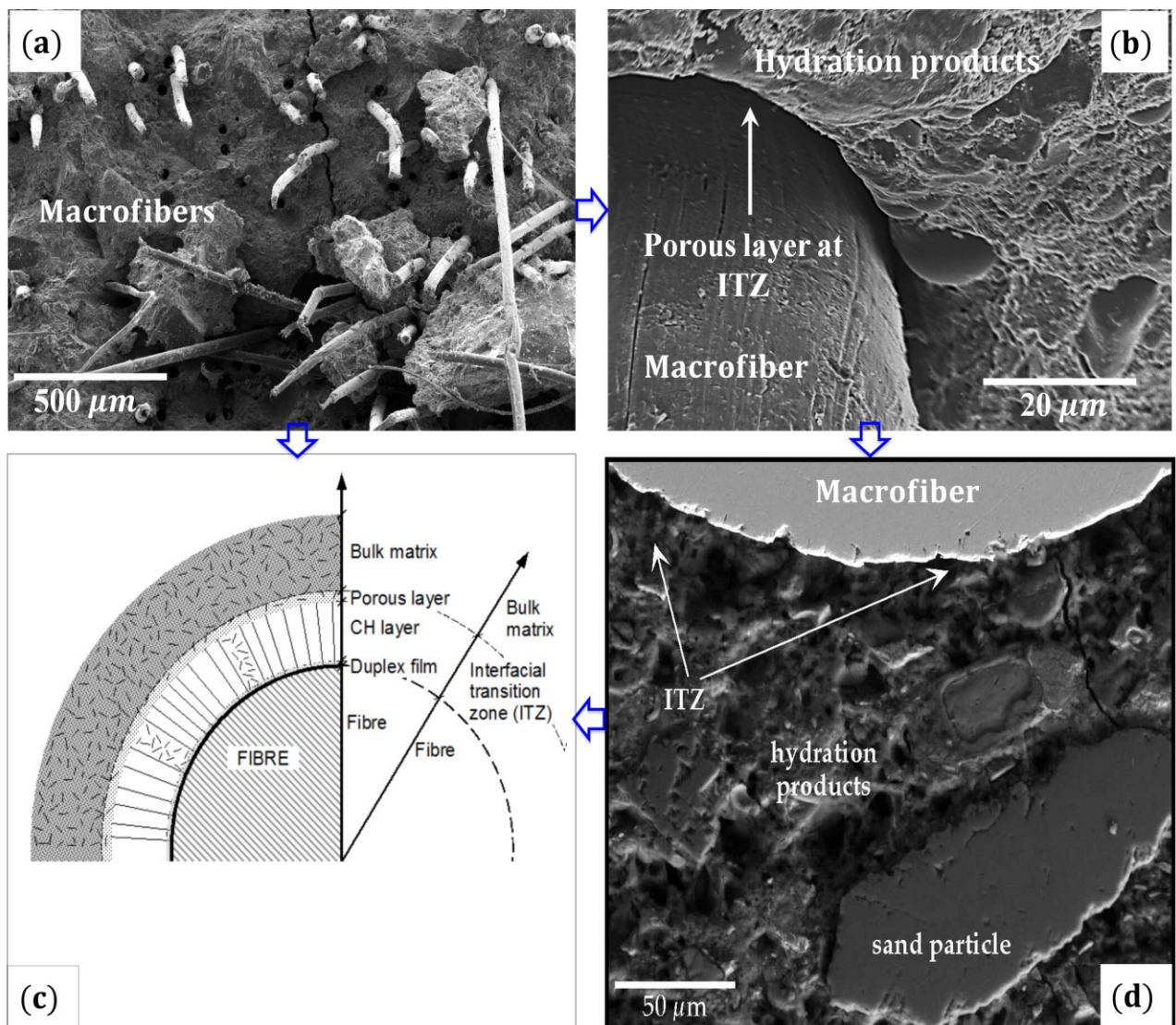


Fig. 2.17: Microstructure of cementitious matrix and interfacial transition zone (ITZ): (a) Bulk cementitious matrix reinforced with macrofibres [micrograph performed on strain-hardening cementitious composites (SHCC) as part of the current study as will be addressed later in [Chapters 7–9](#)]; (b) ITZ between a macrofiber and cement matrix (micrograph performed on SHCC as part of the current study); (c) schematic description of the ITZ around a macrofiber [[Bentur, 1991](#)]; (d) Cross-section of macrofiber, ITZ, and concrete microstructure [[Credit of Easley and Faber, Northwestern University](#)].

2.3.3.6.2 *Potential role of NCM in cement hydration and in FRC mechanism*

While the effect of macrofibers on the above-described cement hydration is minimal and the major importance lies in the interaction between the fibers and the matrix through the ITZ, the scenario is quite different with nanocellulose materials (NCM) for the following reasons:

1. The nanometric scale of NCM implies a seeding effect that can accelerate cement hydration,
2. The nanoscale fibers may also interact with cement hydrates such that NCM provide sites for the germination of C-S-H. This may possibly provide stiffness to C-S-H and result in higher micromechanical properties (at the microstructure level) leading to higher macroscale mechanical strength,
3. The hydrophilic/hygroscopic nature of NCM may provide supplementary source of water to foster the solubilization of cement grains, hence promote cement hydration,
4. The alkaline hydrolysis of cellulose which is also an exothermal reaction may overlap with the exothermal hydration reaction leading to higher heat release,
5. In situations where NCM contain soluble sugars, the hydration reaction may be decelerated by extending the dormant period. This is, however, a rare case since NCM are obtained by delignification (elimination of lignin) and removal of soluble sugars thereby leading to high cellulose purity (>95%).
6. The hydrophilic and hygroscopic nature of NCM may allow a hybrid effect of internal curing and matrix bridging such that volumetric instabilities in the bulk cementitious matrix may be attenuated. This can have direct implications on the porous networks where residual cracking due to autogenous shrinkage can be reduced in the presence of NCM.
7. NCM may provide a nanoreinforcing effect interacting with hydrates (which are also nanometric) to bridge nanoscale cracks and hinder them from growing to micro then coalescing to macrocracks.
8. NCM may also interfere at level of ITZ such that this weakest link in the bulk cementitious matrix may be improved. (viii) NCM may also work in synergy with macro fibers such that their nanoreinforcing effect may provide a secondary reinforcement,

while their enhancement of ITZ may affect the pull-out behavior of macrofibers towards enhanced ductility.

Through the research conducted herein as well as from the limited available literature on NCM, several pieces of evidence supporting the above statements were collected. For this, Fig. 2.18 provides some of the evidence collected in this study demonstrating the opportunities offered with nanoscale cellulose filaments (CF) to nanoengineer cementitious composites in several perspectives. This includes: (i) the hydrophilic and hygroscopic CF providing water pathways from the bulk matrix towards anhydrous grains [Fig. 2.18 (b) and (b)], (ii) the nanoscale CF bridging hydrates [Fig. 2.18 (c)] and serving as germination platform for hydrates [Fig. 2.18 (d)], (iii) CF reinforcing the ITZ [Fig. 2.18 (e)] and bridging nanocracks [Fig. 2.18 (f)].

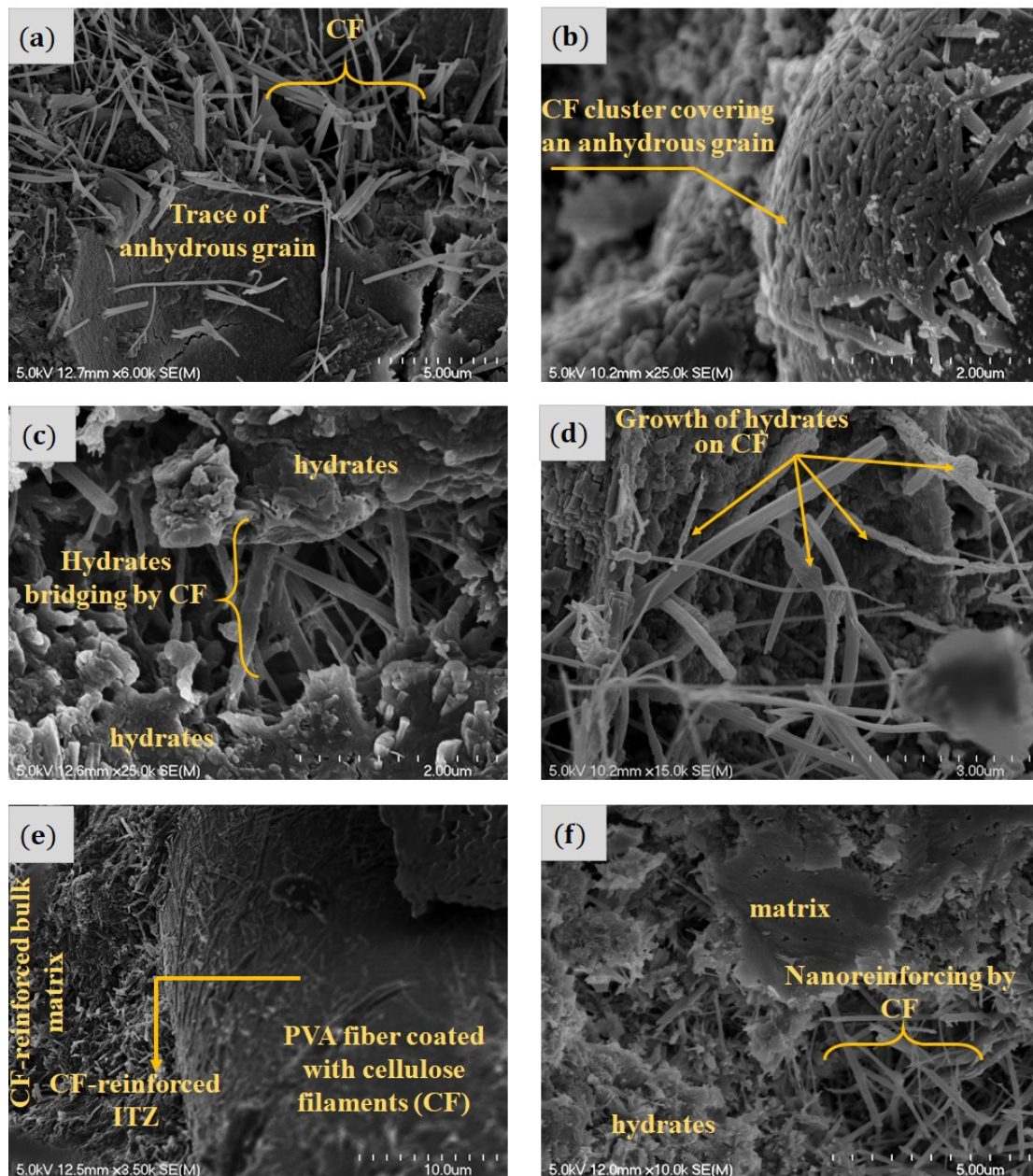


Fig. 2.18: Nanoengineering with CF: (a) and (b) CF linking matrix to anhydrous grains (most probably providing water pathway); (c) CF bridging hydrates; (d) CF serving as germination platform for hydrates; (d) CF reinforcing the ITZ; and (f) CF bridging nanocracks. Micrographs collected as part of the current study in the context of developing nanoengineered SHCC as to be addressed later in [Chapters 7–9](#).

In light of the above-discussed effect of CF on the microstructure of cement composites, the following sub-sections address the available limited literature on the effect of NCM on the behavior of cement and concrete composites. The survey of literature has been organized around six major themes such that the effect of NCM on the behavior of cement composites is attempted in a progressive manner starting from the dispersing of nanomaterials inside the fresh mixture and culminating to composite performance at hardened state. This includes the dispersion of NCM (Section 2.3.3.6.2.1), fresh properties (Section 2.3.3.6.2.2), hydration kinetics (Section 2.3.3.6.2.3), microstructure (Section 2.3.3.6.2.4), mechanical performance (Section 2.3.3.6.2.5), and synergy between macro/micro fibers and nanofibers (Section 2.3.3.6.2.6)

2.3.3.6.2.1 Dispersion of nanocellulose materials

Dispersion refers to the process of separating bundles or aggregates of nanoinclusions into individual objects. For NCM, the high surface area, the intra-chain hydrogen bonding, the inherent tendency for close stacking, and the flexibility of some NCM (such as NFC, MFC, and CF) lead to a high tendency for self-assembly. Effective dispersion is a pre-requisite for enhanced composite performance, or the agglomerates will create a weakness spot in the matrix leading to stress concentrations thereby adversely effecting composite performance. Among reported techniques for dispersion of nanofibers (in general), we have: (i) mechanical approach through which nanofibers are separated by means of high-shear mixing or ultrasonication (subjecting a nanofiber water-suspension to repeated electromechanical waves to facilitate separating it to individual fibrils), and (ii) a chemical approach which involves chemical alteration of nanofiber surface by crating either covalent or noncovalent bonds. Covalent bonds include functionalizing the surface of nanofibers at the defect sites, the end caps, or the entire surface. Noncovalent bonding methods use chemical surfactants to maintain long-term suspension within a variety of liquid solutions [Rashid *et al.*, 2012].

Owing to the hydrophilic nature of NCM, their dispersion in the water medium (required for cement mixtures) remains less challenging as compared to the case of hydrophobic nanofibers such as carbon nanotubes (CNT) and carbon nanofibers (CNF). For NCM, high shear mixing has been the most used technique [Hoyos *et al.*, 2013; Cao *et al.*, 2015; Peter *et al.*, 2009]. Hoyos

et al. [2013] reported that MCC shows no traces of agglomeration due to a noticeable affinity between the hydrophilic MCC and the host cementitious matrix. In some cases, to further enhance dispersion, NCM may be subjected to high-shear mixing followed by ultrasonication. Onuaguluchi *et al.* [2014] mixed a CNF suspension gel (containing 98.1% water) into the batch water. The resulting suspension was pre-mixed for 5 min in a beaker using a hand mixer. To further enhance the dispersion, a polycarboxylate-based high-range-water reducing admixture (HRWRA) was added to the mixing water at a maximum dosage rate of 1.6% by mass of cement. The resulting suspension (CNF-HRWRA-batch water) was then agitated for 10 min in an ultrasonic bath.

Cao *et al.* [2016a] explored effective ways to disperse CNC and studied the relationship between CNC dispersion, rheological properties, and strength of CNC–cement composite. For sonication, they used Hielscher Sonic Processor to transfer mechanical vibrations into the suspension, thereby resulting into continuous formation and collapse of microscopic bubbles, and the energy release by the bubbles enables the dispersion of the CNC agglomerates. To avoid, the rise of temperature during sonication, they placed the suspension container in an ice bath. Later, CNC suspension was mixed with an artificial cement pore solution to determine the critical CNC concentration necessary to reach the lowest yield stress. Based on rheological measurements, this was found to be 0.18 vol% which approaches an experimentally determined optimum dosage (of 0.2 vol%) necessary for enhanced mechanical performance [Cao *et al.* 2015].

As stated earlier that ultrasonication can help further dispersion of NMC, Cao *et al.* [2016b] used ultrasonication to aid dispersion of CNC. They found that after ultrasonication the flexural strength of CNC– cement composite was increased by up to 50%. This research provides insights into how to use CNC more efficiently with cementitious systems for future applications. To supplement further evidence on the effectiveness of sonication for dispersing CNC, Energy-dispersive X-ray (EDX) spectroscopy findings by Cao *et al.* [2016b] demonstrated that: (1) for CNC–cement composites that were not sonicated, CNC tend to concentrate along the interfacial regions between the cement particles and the paste; (2) for sonicated CNC–cement composites,

more CNCs are dispersed into the paste. Nanoindentation results showed that regions of the cement paste that are rich in CNC exhibited higher elastic modulus.

2.3.3.6.2.2 Fresh properties and rheology

The high surface area of nanofilaments is associated with increased water demand. Furthermore, the inherent hydrophilic nature of NCM, and the tendency to form a viscous nanocellulose suspension have high potential to alter mixture rheology. Thus, the effect of nanofilament on the rheology and workability of the mixes is evident. For instance, at higher CNC loading (more than 0.2% by volume of cement, without adequate dispersion scheme), the yield stress of cement pastes increases significantly due to agglomeration [Cao *et al.*, 2015]. Hoyos *et al.* [2013] reported an increase in yield stress of 2.6 times relative to the paste with no MCC due to the presence of hydroxyl groups on nanocellulose surface (hence the interaction of MCCs with cement particles, hydration products, and water). These findings are also supported by Stephenson [2011] who indicated that the addition of NC fibers significantly decreased the workability of the UHPC mix. Reza *et al.* [2010] studied the influence of CNCs as compared to bentonite on reducing water filtration in oil well cement paste. They found that CNCs were more effective than bentonite in altering the yield stress and the flow behavior of the mix. They also reported that CNCs increased the viscosity of bentonite suspensions and made them stable at low shear rates. Additionally, the addition of CNC to colloids leads to shear thinning which in turn results in a lower slump for the cement-based slurry. Similarly, findings by Nilsson and Sargenius [2011] on MFC-reinforced mortar, revealed that the use of MFC leads to higher plastic viscosity of fresh mortar.

2.3.3.6.2.3 Hydration kinetics

While macrofibers have no influence on hydration kinetics, nanoscale NCM do have an effect on the hydration process. At early-age (within the first few hours of casting) for instance, [Onuaguluchi *et al.*, 2014] reported that nanofibrillated cellulose (NFC) reduce the mixture conductivity and delay the hydration process. This is due to the reduced rate of cement dissolution and ion diffusion induced by the viscous nanofibers suspension. However, this delayed cement dissolution had and no deleterious effect beyond the first few hours. Rather,

higher heat release was observed at later ages in the presence of NFC (Fig. 2.19). Similarly, the increase in NFC content was found to be accompanied by an increase in the hydration peak and in the cumulative heat of hydration. At 28 days, cement pastes containing cellulose nanofibers exhibited higher degree of hydration than those exhibited by the unreinforced reference mixture. This increase is attributed to the process of internal curing provided by these fibers as also supported by Mezenzevova *et al.* [2012] and Jongvisuttisun *et al.* [2013].

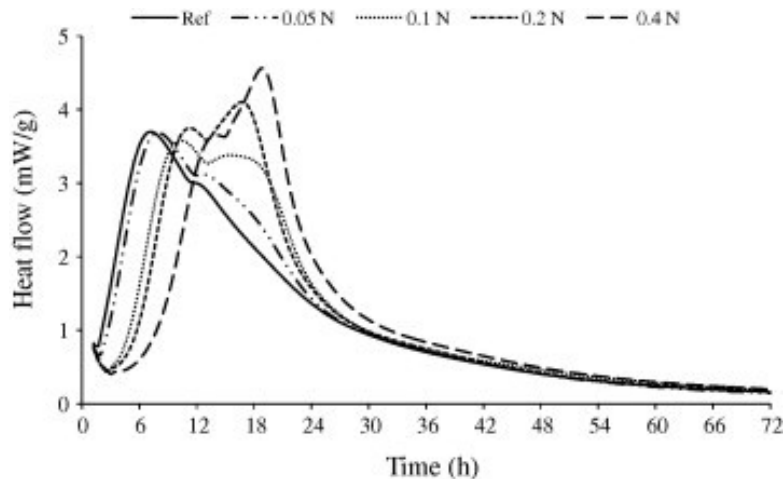


Fig. 2.19: Effect of different addition rates of nanofibrillated cellulose (from 0.05 to 0.4% per cement mass) on heat of hydration [Onuaguluchi *et al.* 2014].

A similar observation about the delayed hydration at early ages and accelerated hydration thereafter was noticed for cement paste incorporating microcrystalline cellulose (MCC) by Hoyos *et al.* [2013] whereby at early ages, the ability of MCC to interact with the matrix promoted the solubilisation of CH and the formation of a waterproofing barrier on the anhydrous particles of cement. This was found to delay the hydration reaction and decrease the maximum adiabatic temperature. At later stages, the existence of MCC in the cement paste increased the degree hydration as the MCC released their water content into the cement mortar, which favored the creation of more hydration products. Another study [Mishra *et al.*, 2003] reported a similar pattern of increase in the heat of hydration with increasing content of cellulose-based polymer, but up some extent, after which an increase in nanocellulose content is accompanied by a reduction in heat of hydration.

Cao *et al.* [2015] reported an increased degree of hydration when CNC were used at rates of 0%, 0.1%, 0.15%, 0.2%. They ascribed the increased hydration degree to two mechanisms: (1) *Steric stabilization*: responsible for dispersing the cement particles, a mechanism also exhibited by water reducing admixtures to improve workability, and (2) *short-circuit diffusion*: which describes how the CNCs appear to provide a channel for water transporting through the hydration products ring (i.e., high density CSH) to the unhydrated cement particle and thereby improving hydration (Fig. 2.20). Investigation on bacterial cellulose (BS) by Mohammadkazemi *et al.* [2015] also indicate higher heat release in the presence of BC.

Generally, the addition of NCM may lead to instantaneous reduced heat leads to a net higher heat release. The instantaneous reduction in heat release observed in some studies is linked to a diluting effect lead by NCM which interfere with the initial dissolution of cement active phases. On the other hand, the increased heat of hydration and the improved degree of hydration can ascribe to a better dispersion effect of cement grains, which an analogous effect the dispersing function of high-range water reducing admixtures. The increased degree of hydration can also be linked with the alkaline hydrolysis of cellulose which is also an exothermic reaction overlapping with the cement hydration.

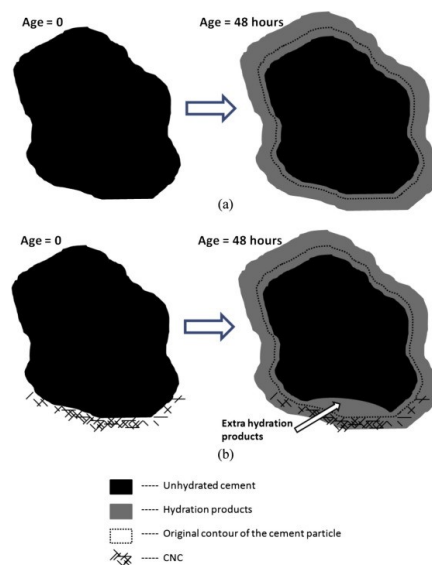


Fig. 2.20: A schematics illustration of the proposed hydration products forming around the cement grain from the age of 0–48 h in the (a) plain cement and (b) cement with CNC on a portion of the cement particle showing SCD [Cao *et al.*, 2014].

2.3.3.6.2.4 Microstructure

Nanoparticles can potentially allow better void filling due to their extremely low particle size [Ashby *et al.*, 2009], thereby enhancing the concrete microstructure. Thus, the addition of NCM can alter the microstructure [Sanchez and Sobolev, 2010]. In fact, some nanoparticles such as nano-SiO₂ and anatase-TiO₂ organise themselves in an efficient close-packed configuration [Ashby *et al.*, 2009]. Other nanomaterials such as CNF, CNC, and CNT fill-up the nanogaps existing between the hydration products, bridge cracks the nanoscale, reinforce the ITZ between aggregates and bulk cementitious matrix. A driving force for enhanced microstructure with NCM is the omnipresence of OH⁻ hydroxyl groups on NCM surface. This promotes surface reactivity leading to higher likelihood of interactions with hydration products containing hydrogen in their structure.

Microstructure analysis of cement past incorporating MCC by Hoyos *et al.* [2013] showed that MCC have the ability to interact with the hydration products, namely C-S-H and CH (Fig. 2.21). This is due to the highly hydrophilic character and the higher water retention capacity of MCC. The study attributed this to the fact that MCCs are constituted of several bonded chains of cellulose with three hydroxyl groups per anhydroglucose unit. The free-OH groups allow MCC to interact through hydrogen bonds with other compounds containing hydrogen atoms in their structure such as CSH and CH. The high specific surface area of MCC provides an enhanced fiber matrix-interaction as well as an increase of cellulose hydroxyl groups available for hydrogen bond with the cementitious matrix [Hoyos *et al.*, 2013].

Further effects of NCM on the microstructure of cement systems can be traced down to the higher elastic modulus of the crystalline portion of NCM (120-138 GPa) [Diddens *et al.*, 2008]; In this regard, Cao *et al.* [2016b] indicated that the use of cellulose nanocrystals (CNC) increases the stiffness of high-density C-S-H surrounding unhydrated cement particles. Similarly, Flores *et al.* [30] reported that the incorporation of CNC results into a larger volume fraction of high-density C-S-H and a smaller volume fraction of low-density C-S-H.

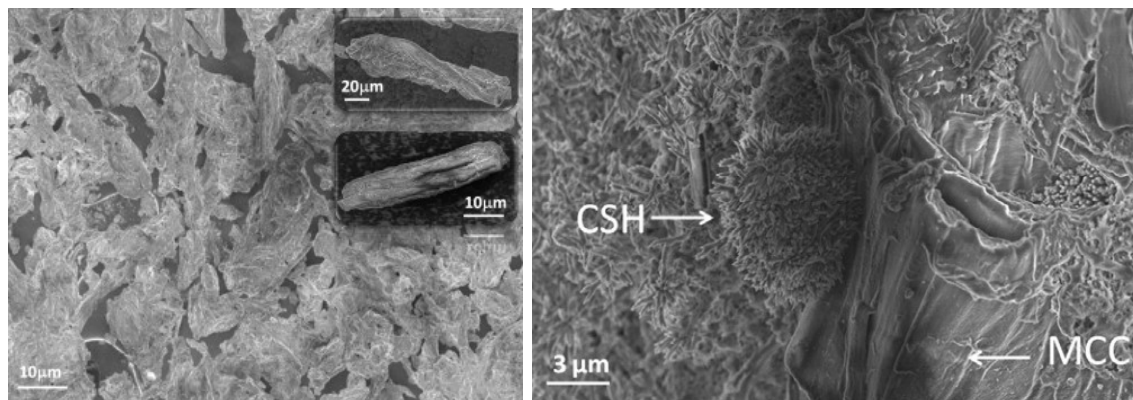


Fig. 2.21: SEM image of microcrystalline cellulose (MCC) (left), and SEM images of cement-based materials with 3 wt.% of MCC (right) [Hoyos *et al.*, 2013].

2.3.3.6.2.5 Mechanical Properties

The enhanced microstructure imparted by NCM as discussed in the previous section has a direct effect on the mechanical properties of cement matrices. Onuaguluchi *et al.* [2014] reported that NFC were found efficient in increasing the flexural strength and energy absorption of cement pastes. Mixtures with 0.1% nanofiber showed optimum mechanical properties with an increase (relative to the reference paste) in flexural strength and energy absorption by approximately 106% and 184%, respectively. However, reduced mechanical performance was observed at nanofiber contents of 0.2% and 0.4% due to fiber agglomeration.

A similar observation was made by Cao *et al.* [2015] on CNC, indicating that at early ages, flexural strength increases with increasing concentration of CNCs. For older ages, the strength reaches a peak at around 0.2% of CNC and then decreases due to the agglomeration of CNCs at higher concentrations. Cao *et al.* [2015] also reported a strong correlation between the flexural strength and the degree of hydration (DH) up to a DH of 58%, and that the flexural strengths of cement pastes with modest concentrations of CNC were about 20% to 30% higher than the cement paste without CNCs. The study attributes this increase to the increase in DH of the cement pastes when CNCs are used, which in turn is attributed to the two mechanisms explained above.

The use of NFC was also found to improve the fracture properties of concrete as was addressed by Stephenson [2011] who performed three-point bending tests on notched beams made from ultra-high-performance concrete (UHPC) containing NFC at 0.1%, 0.5%, and 1.0% - by weight of cement. The study showed that the 0.5% NFC reinforcement is optimal in improving fracture properties of UHPC. The average fracture energy of specimens of this reinforcement level was higher than that of all others. The study attributes the outperformance of the reinforcement percentage of 0.5% to the dispersion and workability associated with this reinforcement level and reported that an amount of 0.1% was likely not enough to properly disperse throughout the mix and produce a noticeable effect, while mixes containing 1.0% were often much less workable, hence not consistent.

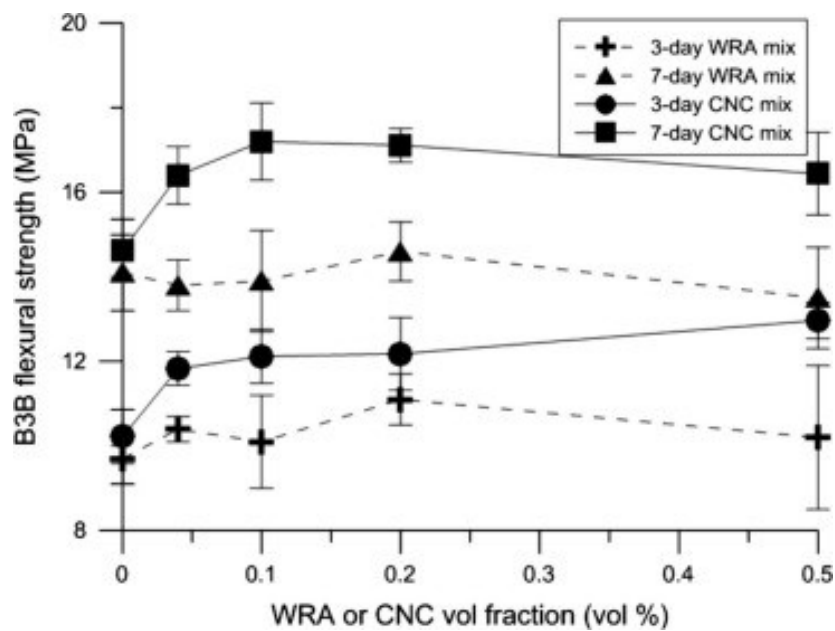


Fig. 2.22: Flexural performance of cement pastes with CNC Cao Y. et al [2015].

The effect of the level of reinforcement of cellulose-based polymer on the mechanical properties of cement pastes were addressed by Mishra *et al.* [2003]. Their study used a constant water to cement ratio of 0.32 and cellulose polymer addition percentage fractions of 0; 0.05, 0.10, 0.25, 0.50, 1.00, 2.00, 3.00, and 4.00 by mass of cement. According to their study, the increase in cellulose-polymer content was observed to have a negative effect on the compressive strength

at early ages (7 and 28 days). However, at late curing stages, increase in cellulose polymer content (up to an optimum content of 1.0%) was found to enhance the compressive strength of cement pastes. This may be ascribed to the increase in cement hydration at late ages as reported earlier in the findings of [Onuaguluchi *et al.*, 2014].

Likewise, longer curing periods resulted in higher fracture toughness with the maximum value obtained with a cellulose polymer content of 0.5%. Van [1989] suggested that the higher fracture toughness values observed at longer curing periods is due to alternative forces (caused by hydrodynamics) developed between the polymer and the cementitious material. These hydrodynamic forces are repulsive in nature, which appear when the cementitious particles try to move against the viscosity of the polymer solution during setting. As the curing time increase these forces gradually change into electrostatic attractive forces.

Obreinmoff [1930] and Dickinson [1981] suggested that the electrostatic forces can be mobilized in dry atmosphere when the crack faces become charged during the fracturing process, thereby leading to a potential self-healing mechanism. Clarke *et al.* [1987] attribute the increase in fracture toughness to the fact that some cellulose-polymer molecules act as a bridging force between adjacent cementitious particles. Such forces, according to Evans *et al.* [1989], can form a robust link holding the cementitious particles intact through a hydrogen/chemical bonding which may eventually resist crack propagation, if not crack inception.

2.3.3.6.2.6) Synergetic effect between micro and nanofibers

Considering the potential ability of NCM to increase the pre-peak strength, and the proven effectiveness of micro/macro fibers for enhancing the post-cracking strength, Ardanuy *et al.* [2012] investigated the effect of both types of reinforcement on the mechanical properties of concrete matrices. NFC was found to impart notable enhancement in flexural strength and modulus, due an intrinsic higher strength and stiffness compared to micro cellulose. However, the cement matrix with NFC exhibited brittle behavior compare to the matrix with micro cellulose (Fig. 2.23 Fig. 2.23: Flexural stress-displacement curves of cement composites with CF compared to micro-cellulose fibers [Ardanuy *et al.*, 2012]).

The study ascribed this behavior to the low crack bridging capacity of nanofibers associated with the short length of NCF which is not enough to prevent crack growth, and the reduced composite toughness owing to an increased fiber-matrix bonding. In fact, when the interfacial properties are maximized rather than optimized, the high energy absorption mechanism involved in the composite fracture such as debonding and fiber pullout, are hindered in favor of fiber rupture, bringing about a brittle fracture, and therefore, low fracture energy. In addition, the high specific surface area of NCF provides an enhanced fiber matrix-interaction as well as an increase of cellulose hydroxyl groups available for hydrogen bond with the cementitious matrix [Coutts 2005; Hoyos *et al.*, 2013], leading to an embrittlement of the composite.

On the other hand, the matrix reinforced with micro cellulose fibers exhibited a more plastic behavior due to the fibers being long, hence efficient in engaging in bridging cracks, and due to the interfacial regions were weaker owing to low specific surface area of fibers which favors toughening by debonding and fiber pullout.

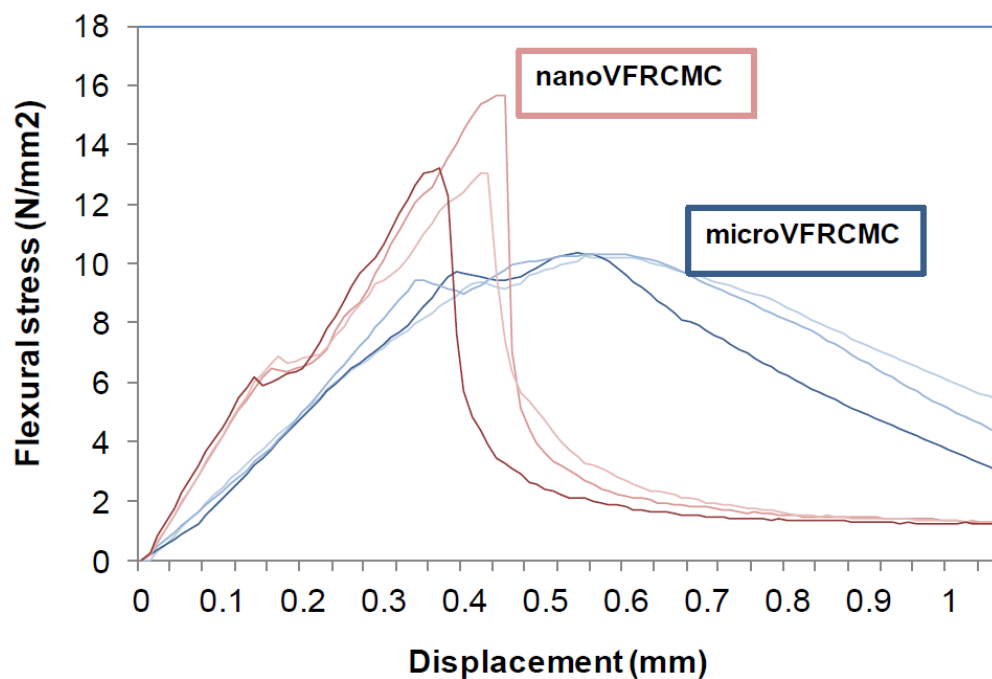
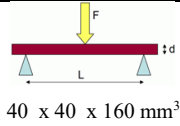
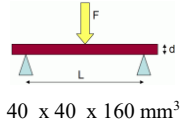
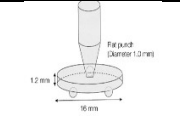
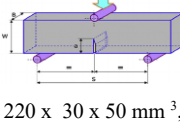
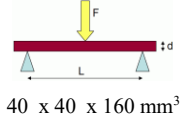
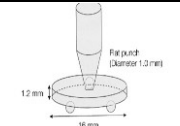


Fig. 2.23: Flexural stress-displacement curves of cement composites with CF compared to micro-cellulose fibers [Ardanuy *et al.*, 2012].

Peters *et al.* [2010] studied the effect of a combination of micro and nanocellulose fibers on the fracture toughness of the otherwise brittle, ultra-high-performance concrete (UHPC). Micro and nanocellulose fibers were used both separately and in combination, at volume fractions of 0, 1%, 3% and 5%. Results from split cylinder and three-point bend notched beam tests indicated that 3% micro cellulose reinforcement is most effective in increasing the fracture energy performance of the material. And that the inclusion of microfibers into the concrete increased the fracture energy by 53%. A hybrid mix consisting of both micro and nanocellulose fibers increased the fracture energy by 26% relative to the unreinforced material.

Table 2. 3: Summary of literature on NCF cement composites with emphasis on mechanical performance.

Reference	Matrix	W/C	NCM type	Dosage	Superplasticizer	Dispersion	Protocol for testing mechanical performance	Increase in mechanical performance
Onuaguluchi <i>et al.</i> 2014	Paste	0.5	NFC	0%, 0.05%, 0.1%, 0.2%, 0.4% by binder mass	Polycarboxylate-based superplasticizer: 1.6% by mass of binder	Ultrasonic mixing	 40 x 40 x 160 mm ³	Flexural strength: 108% Flexural toughness: 186%
C. Gómez Hoyos <i>et al.</i> 2013	Mortar	0.45	MCC	0%, 3%	-	High shear mixing	 40 x 40 x 160 mm ³	Normal curing: Reduced flexural strength Accelerated curing: Increased flexural strength
Cao <i>et al.</i> 2015	paste	0.35	CNC	0%, 0.04%, 0.1%, 0.2%, 0.5%, 1.0%, 1.5%, Per volume	-	High shear mixing	 12 mm 16 mm	Flexural strength: 20% - 30%
Peter <i>et al.</i> 2009	Reactive-powder Concrete	Micro: 0.24, 0.29, 0.35 Nano: 0.24	micro -cellulose nanocellulose	0, 1%, 3%, 5% 0, 1%, 3%, 5% by mass of binder	Polycarboxylate-based superplasticizer: 1.6% by mass of binder	High shear mixing	 220 x 30 x 50 mm ³ , Span 180mm, Notch: 13 mm	Fracture energy: 53%
Ardanuy <i>et al.</i> 2012	Mortar	0.67	NFC	3.3%	-	-	 40 x 40 x 160 mm ³	Flexural strength: 40% Flexural Modulus: 66%
F. Mohammadkazemi <i>et al.</i> 2015	Mortar		BC)	0.1% BNC coated on Bagasse fibers	Calcium chloride: 5% + Polycarboxylate based superplasticizer: 0.5% by cement weight	Ultrasonic mixing	DIN EN 13986:2005-03	Modulus of rupture: 46% - 68%
Cao <i>et al.</i> 2016	Paste	0.35	Nano Crystalline Cellulose	0%, 0.04%, 0.1%, 0.2%, 0.5%, 1.0%, 1.5% Per volume	-	• Ultrasonic, Polycarboxylate-based HRWR	 12 mm 16 mm	Flexural strength: 50%

2.3.3.6.3 Concluding remarks on the effect of nanocellulose materials on cement systems

Subject to adequate dispersion which is a key factor to ensure the effectiveness of NCM (owing to their inherent tendency for self-assembly driven by their high surface area), the most salient effects of NCM include a viscosity modifying effect, increased heat of hydration, alteration in the microstructure, and improvement in mechanical properties. The viscosity modifying effect is driven by the hydrophilicity of NCM as well by the tendency of NCM particles towards forming a nanoscale network linking cement particles and promoting mixture stability. The effect of NCM on hydration kinetics can be summarized by an overall higher heat release attributable to: (i) the nanoscale materials working as nucleation sites to accelerate the hydration, (ii) the internal curing effect of the hydrophilic and hygroscopic NCM either providing supplementary water to solubilize further anhydrous cement grains or providing a pathway for water from the bulk matrix toward anhydrous particles (also termed as short circuit diffusion) an internal curing agent promoting, and (iii) the alkaline hydrolysis of cellulose which is also an exothermic reaction overlapping with the mainstream cement hydration. This leads to an overall higher degree of hydration in cement systems incorporating NCM.

The microstructure of cement systems is altered by the nanoscale NCM interfering with nanoscale cracks, altering the porous network at the interfacial transition zone (ITZ), interaction with cement hydrates, and enhancing the micromechanical properties of C-S-H. Consequent to this effect on the microstructure and the above-recorded increased degree of hydration, higher mechanical properties (particularly flexural capacity and toughness) were recorded with NCM. Bearing in mind the nano/micro length of NCM particles, NCM enhance more the pre-peak flexural behavior than the post-peak behavior whereby the load-carrying capacity is limited by fiber length not promoting extended pull-out effect. Consequently, mixtures combining NCM and macro fibers record enhanced pre-peak and post-peak flexural performance. This opens the opportunity for valorizing NCM in designing fiber reinforced cement composites (FRCC) with superior performance as addressed in the coming section (2.3.4)

2.3.4 Nanoengineering fiber-reinforced cementitious composites

Generally, a cementitious matrix subjected to uniaxial tension will either exhibit: (i) a brittle, (ii) a quasi-brittle or (iii) a strain-hardening. In the first case, the tensile response is limited by the first cracking strength (σ_{cc}) which is the case of plain concrete (PC). In the latter two cases, the tensile response is rather controlled by the post-peak strength (σ_{pc}) whereby for a strain-hardening behavior to prevail, the condition $\sigma_{pc} \geq \sigma_{cc}$ must be met [Naaman and Reinhardt, 2003]. Furthermore, for strain-hardening to be maintained and multiple cracking to be developed, a steady-state crack growth is mandatory [Li, 1998]. Strain-hardening is also referred to as pseudo strain-hardening or quasi strain-hardening [Naaman, 2007].

To further discuss fiber-reinforced cementitious composites (FRCC) and the perspectives to nanoengineer their formulation, it is necessary to first attempt the different categories of FRCC. For this, the most widely-accepted categorization of FRCC is the one classifying them on the basis of their stress-strain response in direct tension and their load-deflection response in flexure [Stang and Li 2004; Naaman and Reinhardt, 2006]. Based on this approach, Naaman and Reinhardt [2006]'s plot in Fig. 2.24 suggests that an FRCC exhibiting strain-hardening behavior in direct tension is referred to as high-performance fiber-reinforced cementitious composite (HPFRCC). When an FRCC not strain-hardening in direct tension can still exhibit this behavior under bending, this FRCC is called deflection-hardening FRCC, a type of ductile fiber-reinforced cementitious composites (DFRCC) [Matsumoto and Mihashi, 2002]. Deflection-hardening is also influenced by the dimension and cross-section geometry of a specimen and is therefore not a material property in the strict sense as highlighted by Trub (2011). Furthermore, strain-hardening is more of material property and may be taken into account in structural design as it is scale-invariant [Stang and Li, 2004]. Deflection-hardening, in contrast, is a structural property (influenced by the dimension and cross-sectional geometry of test specimen) and therefore is not a material property in the strict sense [Naaman and Reinhardt, 2003]. As such, strain-hardening composites are also deflection-hardening ones, but the vice-versa is does not hold. A Fiber Reinforced Cementitious Composite which falls into neither of these two categories is called deflection-softening FRCC.

Stain-softening and deflection-softening composites include conventional FRC which may occasionally exhibit strain-hardening in bending but would show strain-softening in tension. In this regard, although the material shows ductility in bending, the fact that it strain-softens in tension leads to localizing the failure in a small segment of the member. Consequently, damage localization (associated with a limited fracture process zone and large crack opening) takes place, leading to softening behavior [Trub, 2011]. This type of ductility is often not transposable to the structural level.

In contrast, strain-hardening FRCC, having the ability to develop multiple-cracking, turn to delay failure localization and are also called high-performance fiber-reinforced cementitious composites (HPFRCC) such as: Slurry Infiltrated Fiber Concrete (SIFCON), Slurry Infiltrated Mat Concrete (SIMCON) and Engineered Cementitious Composites (ECC)

SIFCON and SIMCON are types of HPFRCC with very high fiber content, typically 5-12% with sizes 30-60 mm and aspect ratio 60-100. Such high addition rates of fibers are achieved by randomly placing the fibers in molds, then infiltrating highly flowable cement slurry to the molds. These HPFRCC show significant strain-hardening in direct tension. However, the high fiber content and casting methods lead to prohibitive costs and thus restrict large-scale and/or *in-situ* applications. For more detailed information about these HPFRCC, the reader is invited to consult Balaguru and Shah [1992].

Engineered Cementitious Composites (ECC) also known as Strain-Hardening Cementitious Composites (SHCC), on the other hand, are ultra-ductile FRCC exhibiting exceptional ductility and strain-hardening behavior with as low fiber content as 2% vol, while using casting and placing protocols similar to the ones used for normal concrete. In line with the objective of this study to valorise cellulose filaments (CF) for the development of nanomodified SHCC, next sections are devoted to providing the reader with general background about SHCC (2.3.4.1), perspectives for nanoengineering SHCC (2.3.4.2), and some of SHCC applications (2.3.4.3).

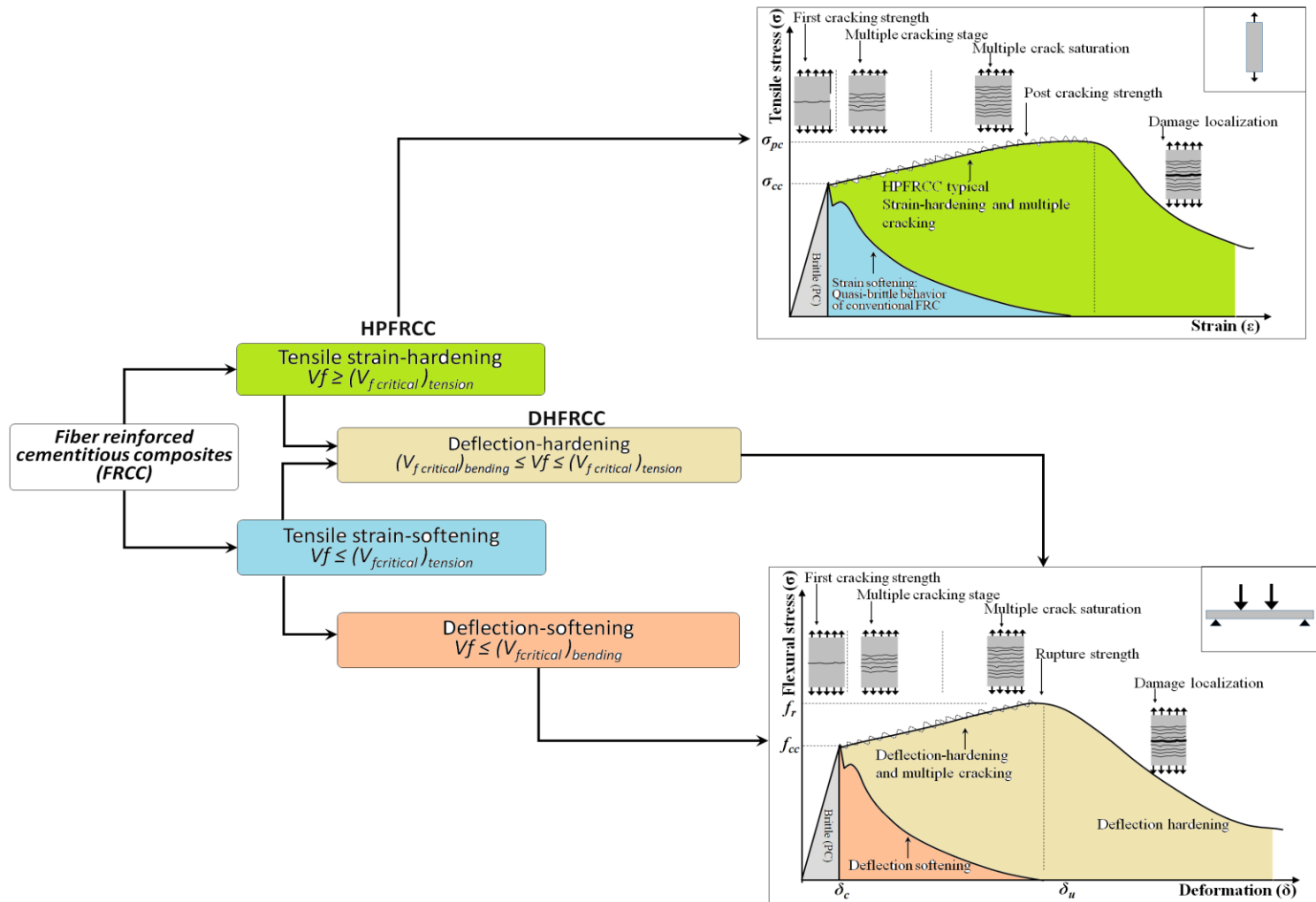


Fig. 2.24: Classification of fiber-reinforced cementitious composites, based on Naaman and Reinhardt [2006].

2.3.4.1 Stain-hardening cementitious composites (SHCC)

Engineered Cementitious Composites (ECC) alternatively called Strain-Hardening Cementitious Composites (SHCC) are ultra-ductile FRCC developed by Victor Li and co-workers at the University of Michigan at the early 1990s [Li, 1993]. The most salient feature of ECC is the exceptional ductility and strain-hardening behavior with as low fiber content as 2% vol., while using concrete batching and placing protocols similar to the ones used for normal concrete. The formulation of SHCC follows micromechanical and fracture mechanics guidelines such that the three composite constituents (matrix, fiber, and fiber/matrix interface) are tailored to obtain a composite exhibiting a smooth transition from the quasi-brittle behavior (of conventional fiber-reinforced cement composites) to a metal-like behavior [Li *et al.*, 1995]. This transition is characterized by (i) a sustained or even higher load carrying capacity after matrix first cracking associated with the steady state cracking, (ii) sequential tight multiple cracking until matrix peak capacity is reached, and (iii) high ultimate tensile strain capacity reaching 2-5% (200-500 times that of plain cement matrices or conventional FRC) [Li, 1998].

The design of SHCC mixtures is based on tailoring matrix, fiber, and fiber/matrix interface along with their associated parameters: [(fiber volume fraction, length, diameter, strength, and elastic modulus, etc. for fiber); (fracture toughness, elastic modulus, and tensile strength etc. for the matrix); and (chemical and frictional bonds, slip-hardening behavior, etc. for fiber/matrix interface)]. The process of micromechanical tailoring is thus the one that quantitatively accounts for the mechanical interaction between these three groups of composite constituent parameters when the composite is subjected to loading [Li and Leung, 1992; Kanda and Li, 1998]. This process elevates composite development from the serendipity of trial-and-error tests to a systematic and guided selection (or otherwise modification) of these micromechanical parameters so that their coupled effect culminates into a composite exhibiting pseudo-ductility at fairly low fiber volume fraction commonly $\leq 2\%$ [Li, 1998; Li and Wang, 2001; Li, 2003]. Emanating from flat crack analyses of ceramics composites reinforced with continuous aligned fibers [Marshall and Cox, 1988], micromechanical tailoring model was first introduced in cement and concrete composites by Li and collaborators [Li, 1993; Li, 1998; Li and Wang,

2001; Li, 2003] and was later improved by Lin *et al.* [1999], Yang *et al.* [2007] and Kanda and Li [1998].

The development of pseudo-ductile composites following micromechanics tailoring dictates that for a given composite to exhibit strain-hardening behavior featured by steady-state (flat) crack growth, two criteria must be met, or the more common Griffith crack propagation mode will prevail, leading to quasi-brittle failure of traditional FRC matrices. The two criteria are (i) strength criterion and (ii) energy criterion. Strength criterion requires the matrix first-crack strength (σ_{fc}) controlled by matrix fracture toughness (K_m) and initial flaw sizes to be less than fiber bridging capacity (σ_0) on any given potential crack plane as presented in Eq. (1).

$$\sigma_{fc} \leq \sigma_0 \quad (1)$$

On the other hand, the energy criterion stipulates that, for a crack (once generated) to grow in a steady-state mode [the state where tensile strength uncouples from crack length, in contrast to the well-known Griffith residual strength concept relating a decreasing tensile strength to increasing crack size [Marshall and Cox 1988], the following energy balance [Eq. (2)] has to be satisfied.

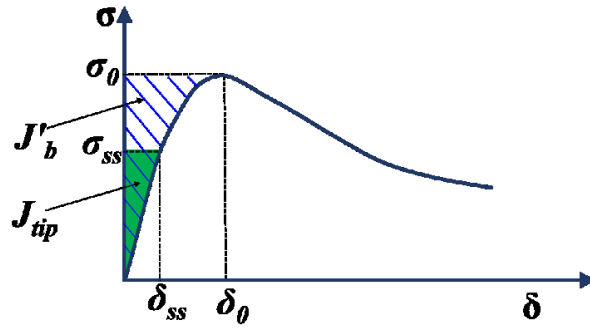


Fig. 2.25: Fiber bridging stress – crack opening width relationship as liked to pseudo-ductility conditions.

$$J_{tip} = \sigma_{ss} \delta_{ss} - \int_0^{\delta_{ss}} \sigma(\delta) d\delta \quad (2)$$

In Eq. (2), it is observable J_{tip} reaches its upper limit under the following conditions:

$$\begin{cases} \sigma_{ss} = \sigma_0 \\ \delta_{ss} = \delta_0 \\ \sigma_0 \delta_0 - \int_0^{\delta_0} \delta(\delta) d\delta \equiv J'_b \end{cases} \quad (3)$$

where σ_{ss} is the steady-state cracking stress; δ_{ss} is the flat crack opening corresponding to σ_{ss} (Fig. 2.25); J_{tip} is the crack tip toughness, which can be approximated as the cementitious matrix toughness if fiber volume fraction is less than 5%, calculated as in [Eq. (2)]; σ_0 is the maximum bridging stress which corresponds to the crack opening δ_0 and J'_b is the complementary energy controlled by fiber bridging stress and determined from the σ - δ curve.

$$J_{tip} = \frac{K_m^2}{E_m} \quad (4)$$

where K_m is the matrix fracture toughness and E_m is the matrix Young modulus of elasticity.

In consequence of Eq. (3), for crack growth to follow a steady-state mode (necessary for pseudo-ductility behavior), the crack tip toughness should not exceed the complementary energy as below:

$$J_{tip} \leq J'_b \quad (5)$$

As such, for a matrix to exhibit a tensile strain-hardening behavior, both criteria (strength and energy) must be satisfied. Otherwise, the tension-softening behavior of traditional FRC will prevail. In this regard, while some conventional FRC may satisfy the strength criteria (governing the range of matrix flaw size), the energy criteria (governing the propagation of steady-state crack) excludes most conventional FRC and can be satisfied only when micromechanically principle are taken into account [Li, 1998; Li and Wang, 2001; Li, 2003].

Different types of SHCC with different formulation characteristics tailored for specific functionality (such as highly-flowable [Kong *et al.*, 2003], pigmentable [Yang *et al.*, 2012], sprayable [Kim *et al.*, 2003], printable [Figueiredo *et al.*, 2019], spray-applied fire resistive [Zhang and Li, 2015] and so on) are now available. Similarly, significant development has been made in terms of fostering SHCC ductility by tailoring interface properties, use of cost-effective

PVA fibers, improving the ecoefficiency, reducing the cement content, using high-volume supplementary cementitious materials, and promoting the use of locally available materials. For elaborated details, the reader is invited to consult Victor Li's comprehensive review on this topic [Li, 2003].

2.3.4.2 Nanoengineered strain-hardening cementitious composites

While it is well established that SHCC demonstrates exceptional ductility characteristic elevating it to a metal-like behavior (as highlighted earlier), the fact that cracking in cement composites is multiscale in nature opens a window for further tailoring the performance of SHCC. After all, the initial development of SHCC by Li and coworkers was inspired by the structure of nacre (known as mother of pearl – the iridescent inner lining layer of abalone shells) show in Fig. 2.26. This substance is known to be of high mechanical performance and exceptional ductility and has the primary role of protecting the abalone by allowing the shell to withstand the impact of shock (by predators attempting for breaking it) without fracturing [Jackson *et al.*, 1988; Mayer, 2005].

As a structural biomaterial, nacre has a very complex hierarchical structure that spans over multiple length scales from macroscale to nanoscale (Fig. 2.26 (a)-(d), respectively). Nacre consists of 95 wt.% brittle aragonite [Fig. 2.26 (c)], a crystallographic form of calcium carbonate (CaCO_3), and 5 wt.% of organic polymers [Fig. 2.26 (d)] and polysaccharides [Menig *et al.*, 2000]. This gives nacre a structure made primarily of brittle constituents (aragonite tablets) glued together with a soft multi-scale biopolymer thereby forming a brick-and-mortar structure [Meyers *et al.*, 2008]. The inter-tile biopolymers [Fig. 2.26 (d)] were reported to be made of chitin fibers [Meyers *et al.*, 2011]. This composition underpins the complex hierarchical structure of nacre that has, surprisingly, a fracture toughness ~ 3000 times higher than that of its major constituent – pure aragonite [Currey, 1977; Jackson *et al.*, 1988].

In SHCC, the brittle cementitious matrix at $\sim 98\%$ of total volume plays the role of aragonite tiles, while the PVA fibers at $\sim 2\%$ volume play the role of chitin fibers in nacre. In spite of this low fiber volume fraction, the micromechanical tailoring approach detailed earlier culminates

into composites with strain capacity 200-500 times higher than that of normal concrete or conventional FRC [Li, 1998]. The common fiber used in SHCC design has length in the range of 8-12 mm, a typical diameter of 38 μm , an elastic modulus of 40 GPa, and a tensile strength of 1400 MPa.

In this regard, and considering the role of multi-scale fiber reinforcement attempted earlier in section 2.2.4 as summarized in Fig. 2.27, as well as the complex hierarchical structure of cellulose (in Fig. 2.12) and the inherent on-axis high mechanical properties of nanocellulose materials (NCM) detailed in Table 2.1 and Table 2.2, it follows that re-engineering SHCC formulation using nanoscale NCM in conjunction with PVA microfibers can offer a forward step in the *biomimetic design* of SHCC. This hypothesis can also be supported by the varied potential advantages offered by NCM to nanomodify SHCC matrix [Fig. 2.28 (a)] as well as interface properties [Fig. 2.28 (c)].

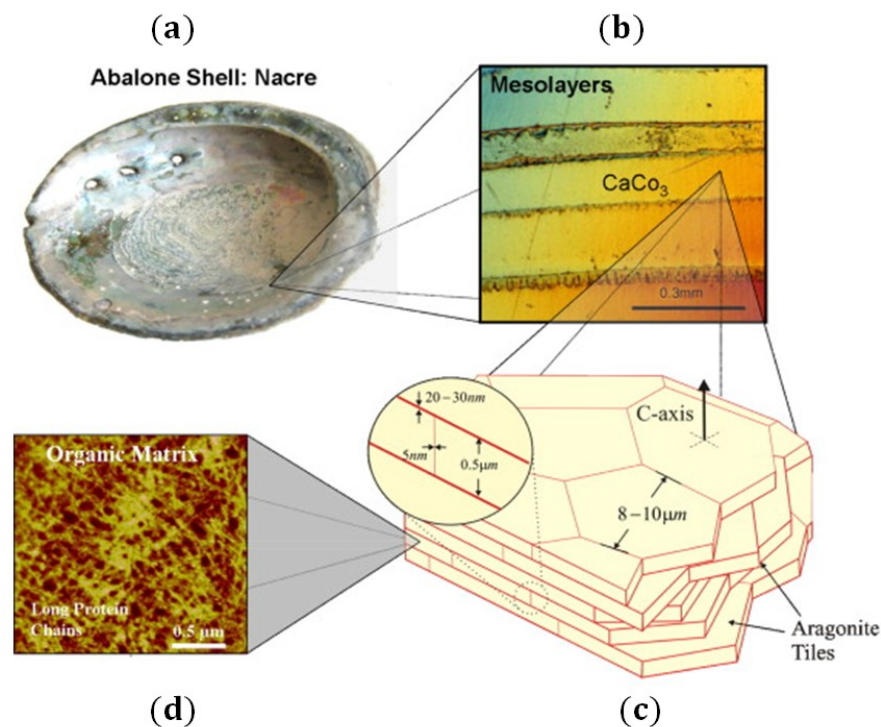


Fig. 2.26: Overall view of the hierarchical structure of abalone shell spanning from the macroscale shell (a), to the microscale CaCO_3 layers (b), to the mesoscale Aragonite tiles (c), to the nanoscale organic polymers (d). Figure adapted from Meyers *et al.* [2008].

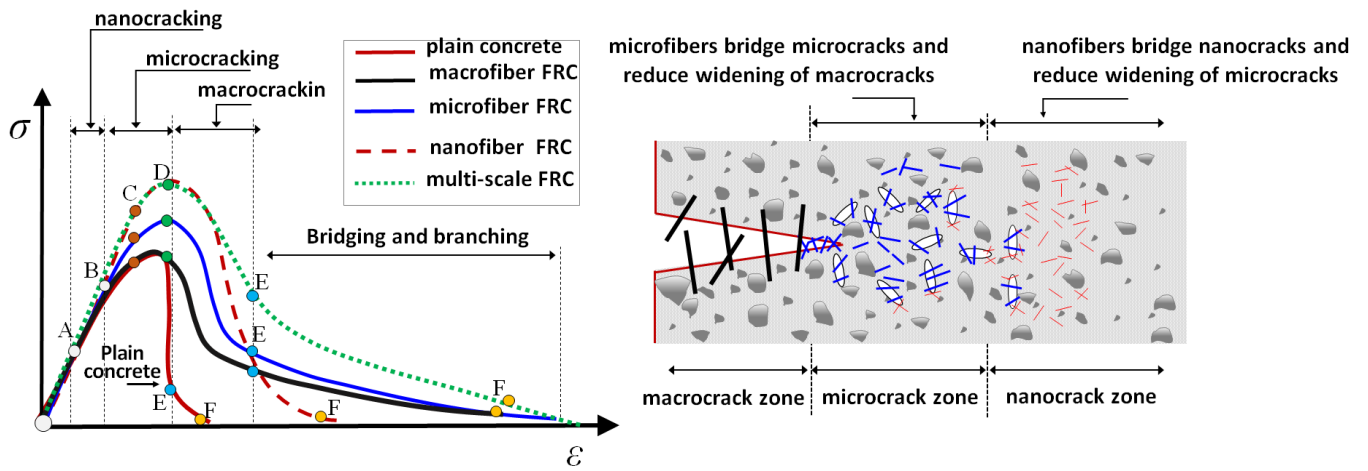


Fig. 2.27: Schematic illustration of the effect of different fiber scale on fracture behavior. NB: This figure is the same as Fig. 2.4. It has been called once again here to facilitate the discussion in this section

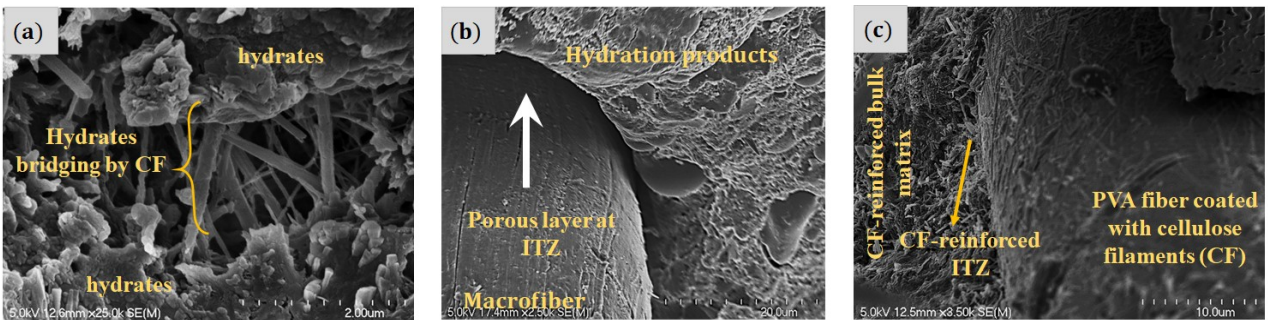


Fig. 2.28: Effect of nanocellulose materials on the performance of strain-hardening cementitious composites: (a) Bridging nanoscale cracks and interacting with hydrates, (b) SHCC without NCM showing a porous interfacial transition zone (ITZ), and (c) nanocellulose-modified SHCC showing an ITZ stiffened with NCM [SEM micrographs collected as part of the development of nanocellulose modified strain-hardening cementitious composites attempted later in Chapters 7-9 of this thesis].

2.3.4.3 Structural application of SHCC

As a result of the strict design guidelines described in section 2.3.4.1, SHCC exhibit remarkable metal-like ductility characteristics accompanied with substantial fracture toughness elevating SHCC to closely replicate the features of aluminum alloys [Maalej and Hashida, 1995]. Interestingly, these features are scale-invariant and can be transposed from millimetric-scale elements to structural-size elements [Stang and Li, 2004]. This encouraged the use of ECC in several structural applications including: (i) structural strength and ductility of reinforced beams under cyclic loads [Kanda *et al.*, 1998] where the load carrying capacity was increased by 50% and the ultimate deformation by 200% under shear tension failure mode, (ii) the use of ECC in the hinging zone of beam-column connections [Mishra, 1995] where the total energy absorption was increased by 2.8 times relative to the R/C specimen, (iii) the use of SHCC as a protective layer for enhancing the corrosion durability of R/C structures [Maalej and Li, 1995], (iv) use of SHCC for interior beam-column connections for enhanced seismic resistance [Qudah and Maalej, 2014]. On the other hand, owing to the featured ductility, SHCC show high compatibility with reinforcing steel before its tensile strain capacity is achieved [Fischer and Li, 2002]. This allows SHCC reinforced elements to exhibit high strength [Moreno and Trono, 2014] and strain hardening behavior that can be taken into consideration in the design of reinforced ECC members under bending moments [JSCE, 2008].

SHCC have also been used in reinforced SHCC beams where greater shear resistance under static loading conditions was obtained with SHCC compared to reinforced concrete beams [Shimizu *et al.*, 2004; Varela and Saiidi, 2013; Xu *et al.*, 2013]. SHCC reinforced members subject to cyclic load reversals also demonstrated better damage tolerance and energy dissipation capacity [Fukuyama *et al.*, 2000; Fischer and Li, 2002]. SHCC have also been used in shear critical members such as beam-column joints where shear failure was prevented and stirrups in the joints could even be eliminated under cyclic loading [Parra-Montesinos, 2005; Yuan *et al.*, 2013; Parra-Montesinos *et al.*, 2005]. The enhanced structural performance of SHCC members was found to underpin the use of SHCC in several real-life structural

applications including bridge deck link slabs (Fig. 2.29) [Lepech *et al.*, 2009] dam repairs, and coupling beams in high rise buildings (Fig. 2.30) [Kanda *et al.*, 2011].

The enhanced SHCC performance transposable to the structural level has also motivated new applications such as in structural extruded elements, FRP reinforced concrete, and steel-concrete composite structures (particularly composite steel floor deck-slabs). In the particular case of composite steel floor deck-slabs, the use of SHCC has the potential to increase the compatibility between the ductile steel deck and its brittle concrete topping thereby improving the composite action and enhancing the resistance to shear bond failure (one of the major failure types in composite slabs due to the steel-concrete slip). In this regard, and for the sake of limiting redundancy in literature survey between the current chapter and chapter 10 (on the use of a newly developed SHCC to develop fatigue-induced shear-bond efficient composite slabs), a contextualized literature survey on composite slabs is provided in Section 10.2 (Chapter 10).

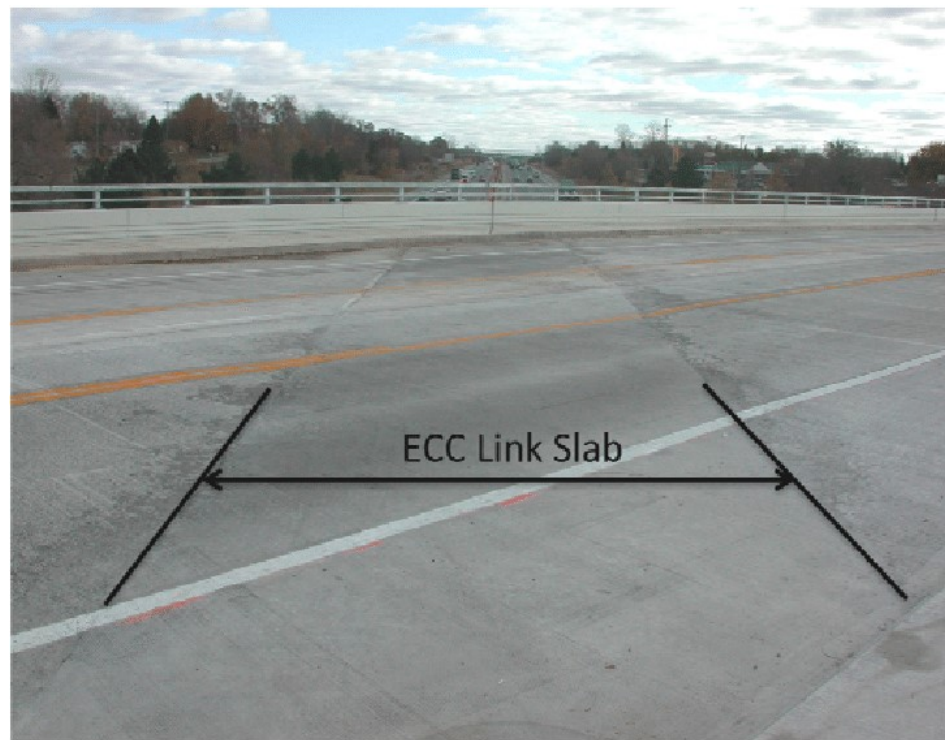


Fig. 2.29: Application of ECC for Bridge Deck Link Slabs [Lepech and Li, 2009]

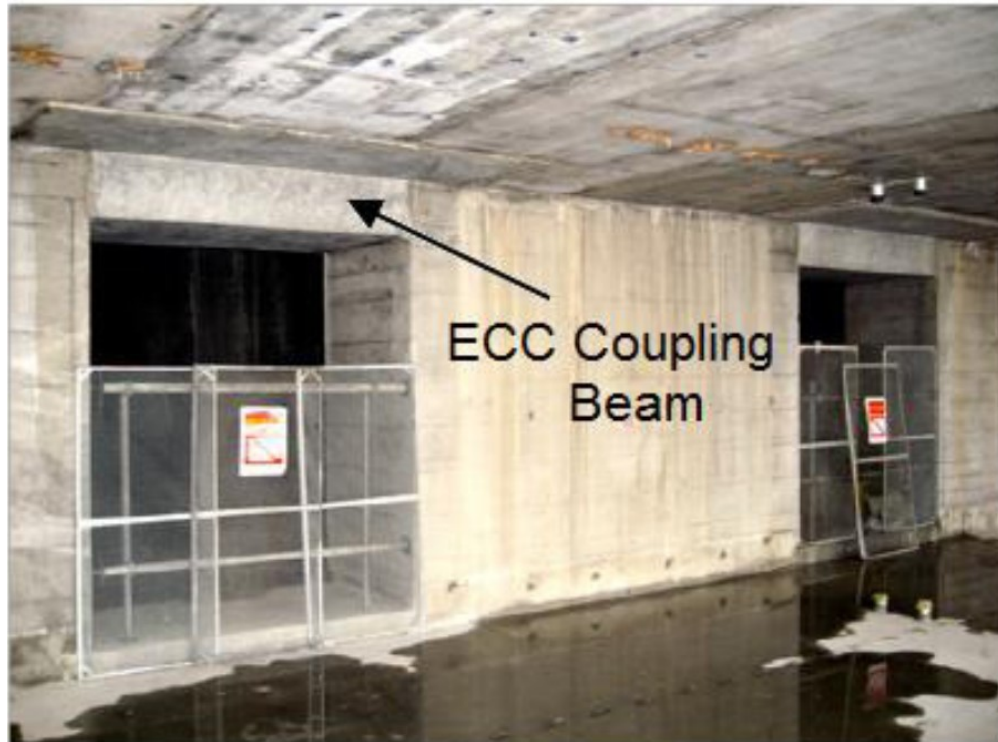


Fig. 2.30: SHCC (ECC) Coupling Beams in a 60-story high-rise reinforced concrete structure in Osaka Japan where SHCC was used enhance seismic safety and durability by absorbing energy during an earthquake [Kanda *et al.*, 2011]

2.4 References

- ACI Committee 544 (2002) State-of-the-Art Report (ACI 544 .1R-96) on Fiber Reinforced Concrete, ACI JOURNAL, Proceedings, 70 (11) pp. 727-744.
- Afroughsabet, V., Biolzi, L., and Ozbakkaloglu, T. J. (2016). *Mater Sci.*, 51, 6517
<https://doi.org/10.1007/s10853-016-9917-4>.
- Aïtcin, P.-C. (2000) Cements of yesterday and today – Concrete of tomorrow, *Cement and Concrete Research*, 30 (9), pp. 1349-1359.
- AkzoNobel (2010), Annual Report 2010, p. 4.
- Alain, P., Christophe, C., Emmanuel, F., Revathi, B., and Rousset, A. (2001) Specific Surface Area of Carbon Nanotubes and Bundles of Carbon Nanotubes, *Carbon.*, 39, pp. 507-514.
- Altoubat, S., Ousmane, H., and Barakat, S. (2016), Experimental study of in-plane shear behaviour of fiber-reinforced concrete composite deck slabs, *J. Struct. Eng.*, 10.1061/(ASCE) ST.1943-541X.0001413, 04015156.
- Altun, F., Haktanir, T., and Ari, K. (2007) Effects of steel fiber addition on mechanical properties of concrete and RC beams, *Constr Build Mater.*, 21 (3), pp. 654–661.
- Anderson, T. L. (2005) Fracture mechanics: fundamentals and applications: *CRC press*, FL, USA.
- Ardanuy, M., Claramunt, J., García-Hortal, J. A., and Barra, M. (2011) Fiber-matrix interactions in cement mortar composites reinforced with cellulosic fibers, *Cellulose*, 18, pp. 281–289.
- Ardanuy, M., Claramunt, J., Arevalo, R., Pares, F., Aracri, E., and Vidal, T. (2012) Nanofibrillated-cellulose as a potential reinforcement for high performance cement mortar composites, *BioResources*, 7 (3), pp. 3883–3884.
- ASCE (1992) Standard for the Structural Design of Composite Slabs, ANSI/ASCE 3-91 American Society of Civil Engineers, New York.
- Ashby, M., Ferreira, P., and Schodek, D. (2009). *Nanomaterials, nanotechnologies and design: an introduction for engineers and architects*. Boston, MA: Elsevier Science Ltd.
- ASTM C 1018–Test Method for Flexural Toughness and First Crack Strength of Fiber- Reinforced Concrete (Using Beam with Third-Point Loading).
- Aziz, M.A., Paramasivam, P., and Lee, S.L. (1981) Prospects for natural fibre reinforced concretes in construction, *Int. J. Cem. Compos, Lightweight Concr.*, 3 (2), pp.123–132.
- Balaguru, P., and Ramakrishnan, V. (1986) Mechanical Properties of Superplasticized Fiber Reinforced Concrete Developed for Bridge Decks and Highway Pavements, *Concrete in Transportation*, SP-93, American Concrete Institute, Detroit, 1986, pp. 563-584.
- Balaguru, P.N. and Shah, S.P (1992) *Fiber-reinforced cement composites*, McGraw-Hill, 1992.

- Balandin, A. A., Ghosh, S., Bao, W., Calizo, I., Teweldebrhan, D., Miao, F., and Lau, C. N (2008) Superior Thermal Conductivity of Single-Layer Graphene, *Nano Letters*, 8 (3), pp. 902–907. doi:10.1021/nl0731872. ISSN 1530-6984. PMID 18284217.
- Banthia, N. and Mindess, S. (eds.) (1995) Fiber Reinforced Concrete – Modern Developments. The Second University-Industry Workshop on Fibre Reinforced Concrete and Other Composites held in Toronto, Canada, March 26-29, 1995.
- Beddar, M. (2004) Fibre-reinforced concrete – Past, present and future, *Concrete*, April 2004 (38) 4, *ABI/INFORM Trade & Industry*, pp. 47-49.
- Benning, P. J., Poirier, D. M., Ohno, T. R., Chen, Y., Jost, M. B., Stepniak, F., et al. (1992) C-60 and C-70 fullerenes and potassium fullerides. *Phys Rev B*, 45, pp. 6899–6913.
- Bentur, A. (1991) Microstructure, interfacial effects and micromechanics of cementitious composites, in *Advances in Cementitious Materials* (ed. S. Mindess), The American Ceramic Society, USA, pp. 523-547.
- Bentur, A., Wu, S.T, Banthia, N., Baggott, R., Hansen, W., Katz, A., Leung, C.K.Y., Li, V.C., Mobasher, B., Naaman, A.E., Robertson, R., Soroushian, P., Stang, H., and Taerwe, L.R. (1995) Fibre-matrix interfaces. In *High Performance Fibre Reinforced Cementitious Composites*, eds. Naaman and Reinhardt. Chapman and Hall, London, 1995, pp. 149-191
- Betterman, L.R., Ouyang, C., and Shah, S.P. (1995) Fiber-matrix interaction in microfiber-reinforced mortar, *Advanced Cement Based Materials*, 2, pp. 53-61.
- Bjornstrom, J., Martinelli, A., Matic, A., Borjesson, L., and Panas, I. (2004) Accelerating effects of colloidal nano-silica for beneficial calcium–silicate–hydrate formation in cement, *Chem Phys Lett*, 392, pp. 242–248.
- Boghossian, E., and Wegner, L. D. (2008) Use of flax fibres to reduce plastic shrinkage cracking in concrete, *Cem. Concr. Compos.*, 30 (10), pp. 929–937.
- Brinchi, L., F. Cotana, E. Fortunati, and J.M. Kenny (2013) Production of nanocrystalline cellulose from lignocellulosic biomass: technology and applications, *Carbohydr. Polym.* 94, pp.154–169.
- BS 5950, Part 4: Code of Practice for Design of Floors with Profiled Steel Sheeting, *British Standards Institution*, London (1994).
- Callister Jr. W. D. (1994) In *Materials Science and Engineering: An Introduction*, ed. W. D. Callister, Jr., *John Wiley & Sons, Inc.*, New York, 1994, p. 530.
- Cao, Y., Zavaterra, P., Youngblood, J., Moon, R., and Weiss, J. (2015) The influence of cellulose nanocrystal additions on the performance of cement paste, *Cem. Concr. Compos.*, 56, pp. 73–83.
- Cao, Y., Tian, N., Bahr, D., Zavattieri, P. D., Youngblood, J., Moon, R. J., et al. (2016b) The influence of cellulose nanocrystals on the microstructure of cement paste, *Cem Concr Compos*, 74, pp. 164–173.

- Cao, Y., Zavattieri, P. D., Youngblood, J., Moon, R. J., and Weiss, W. J. (2016a) The relationship between cellulose nanocrystal dispersion and strength, *Constr Build Mater.*, 119, pp. 71–79.
- CCA (2018). The Canadian Cement Association. Available on www.cement.ca [accessed on 07/06/2018].
- Chen, J., Zhao, D., Ge, H., and Wang, J. (2015) Graphene oxide-deposited carbon fiber/cement composites for electromagnetic interference shielding application, *Constr. Build. Mater.* 84, pp. 66–72.
- Chen, J., Kou, S. C., and Poon, C. S. (2012) Hydration and properties of nano-TiO₂ blended cement composites, *Cement and Concrete Composites*, 34, pp. 642–649.
- Chuah, S., Pan, Z., Sanjayan, J. G., Wang, C. M., and Duan, W. H. (2014) Nano reinforced cement and concrete composites and new perspective from graphene oxide, *Construction and Building Materials*, 73, pp. 113-124.
- Colin, D. J., and Ronald A. C. (1974) Strength and Deformation of Steel Fiber Reinforced Mortar in Uniaxial Tension, *Fiber Reinforced Concrete, SP-44*, American Concrete Institute, Detroit, pp. 177-207.
- Cui, H., Yan, X., Tang, L., and Feng Xing, F. (2017) Possible pitfall in sample preparation for SEM analysis - A discussion of the paper “Fabrication of polycarboxylate/graphene oxide nanosheet composites by copolymerization for reinforcing and toughening cement composites” by Lv et al., *Cement and Concrete Composites*, 77, pp. 81-85.
- Currey, J. (1997) Mechanical properties of mother of pearl in tension, *Proc. R. Soc. Lond. Ser. B Biol. Sci.*, 196 (1125) pp. 443-463.
- Cwirzen, A., Habermehl-Cwirzen, K., Nasibulin, A.G., Kaupinen, E.I., Mudimela, P.R., and Penttala, V. (2008) SEM/AFM studies of cementitious binder modified by MWCNT and nano-sized Fe needles, *Materials Characterization*, 60 (7), pp. 735-740.
- Cwirzen, A., Habermehl-Cwirzen, K., and Penttala, V. (2008) Surface decoration of carbon nanotubes and mechanical properties of cement/carbon nanotube composites, *Adv Cem Res.*, 20 (2), pp. 65–73.
- Daniel, E. S., and Jörg, S. (2009) Optical transparency of graphene as determined by the fine-structure constant, *Physical Review B.*, 80 (19).
- Davis, J. M. G. (1993), The need for standardized testing procedures for all products capable of liberating respirable fibers—the example of materials based on cellulose, *Br. J. Ind. Med.*, 50 (2), pp. 87-190.
- Diddens, I., Murphy, B., Krisch, M., and Muller, M. (2008), *Macromolecules*, 41, pp. 9755 -9759.
- Dixon, J., and Mayfield, B. (1971) Concrete Reinforced with Fibrous Wire, *Journal of the Concrete Society, Concrete*, 5 (3), pp. 73-76.

- Donaldson, K., Murphy, F. A., Duffin, R., and Poland, C. A. (2010) Asbestos, carbon nanotubes and the pleural mesothelium: a review of the hypothesis regarding the role of long fibre retention in the parietal pleura, inflammation and mesothelioma *Part. Fibre Toxicol.*, 7, p. 5.
- Dousti, M. R., Boluk, Y., and Bindiganavile, V (2010). The influence of cellulose nanocrystals on the fresh properties of oil well cement pastes. Unpublished work. 2010.
- Dufresne, A., Cavaille, J. Y., and Vignon, M. R. (1997) *J. Appl. Polym. Sci.*, 64, pp. 1185–1194.
- Dufresne, A., Dupeyre, D., and Vignon, M. R. (2000) *J. Appl. Polym. Sci.*, 76, pp. 2080–2092.
- Eichhorn, S. J., Dufresne, A., Aranguren, M., et al. (2010) Review: current international research into cellulose nanofibres and nanocomposites, *J. Mater. Sci.*, 45, pp. 1–33.
- Eldib, M. E., Maaly, H. M., Beshay, A. W., and Tolba, T. (2009) Modelling and analysis of two-way composite slabs, *J. Constr. Steel Res.*, 65 (5), pp. 1236-1248.
- Erdem, S., Dawson, A. R., and Thom, N. H. (2012). “Influence of the micro- and nanoscale local mechanical properties of the interfacial transition zone on impact behavior of concrete made with different aggregates, *Cem. Concr. Res.*, 42 (2), pp. 447–458.
- Eurocode 4-(1994) Design of Composite Steel and Concrete Structures, Part 1. 1: General Rules and Rules for Buildings. EN1994-1-1 European Committee for Standardization, Brussels.
- Faruk, O., Bledzki, A. K., Fink, H. S., and Sain, M. (2012) Biocomposites reinforced with natural fibers, *Prog. Polym. Sci.*, 37, pp. 552–1596.
- Ferreira, S. R., et al. (2016) Effect of Natural Fiber Hornification on the Fiber Matrix Interface in Cement Based Composite Systems, *Key Engineering Materials*, 668, pp. 118-125.
- Filipponi, L., and Sutherland, D. (2013) Nanotechnologies: Principles, Applications, Implications and Hands-on Activities European Commission, Directorate-General for Research and Innovation, EUR 24957.
- Fischer, G., and Li, V. C. (2003) Deformation behavior of fiber-reinforced polymer reinforced engineered cementitious composites (ECC) flexural members under reversed cyclic loading conditions, *ACI Struct. J.*, 100, pp. 25-35.
- Flores J., Kamali, M., Ghahremaninezhad, A. (2017) An investigation into the properties and microstructure of cement mixtures modified with cellulose nanocrystal, *Materials*, 10 (5), p. 498, 10.3390/ma10050498.
- Foster E. J., Moon, R. J., Agarwal, U. P., et al. (2018) Current characterization methods for cellulose nanomaterials, *Chem. Soc. Rev.*, 47, pp. 2609-2679.
- Fukuyama, H., Sato, Y., Li, V. C., Matsuzaki, Y., Mihashi, H. (2000) Ductile Engineered Cementitious Composite Elements for Seismic Structural Application. In: Proceedings of the 12th World Conference on Earthquake Engineering. New Zealand.

- Gartner, E. M., Young, J. F., Damidot, D. A., and Jawed, I. (2002) Hydration of portland cement. Chapter 3 in *Structure and performance of cements* (eds. Bensted and Barnes) Spoon Press, London, 2002.
- Goldman, A., and Bentur, A. (1992) Effects of pozzolanic and non-reactive micro fillers on the transition zone in high-strength concretes, *Proc., RILEM Int. Conf. (Toulouse) on Interfaces in Cementitious Composites*, Vol. 18, E & FN Spon, London, 53–61.
- Goodsell, J. E., Moon, R. J., Huizar, A., and Pipes, R. B. (2014) A strategy for prediction of the elastic properties of epoxy-cellulose nanocrystal-reinforced fiber networks, *Nord. Pulp Pap. Res. J.*, 29 (1), pp. 85–94.
- Grzybowski, M., and Shah, S. P. (1990) Shrinkage cracking of fiber reinforced concrete, *ACI Mater J.*, 87 (2), pp. 138–148.
- Habibi, Y., and Dufresne, A. (2008) Highly filled bionanocomposites from functionalized polysaccharide nanocrystals, *Biomacromolecules*, 9 (7), pp. 1974–1980.
- Han, B., Yu, X., and Eil Kwon, E. (2009) A self-sensing carbon nanotube/cement composite for traffic monitoring, IOP Publishing Ltd, *Nanotechnology*, 20 (44).
- Hiremath, N., and Bhat, G. (2017) 4 - High-performance carbon nanofibers and nanotubes, Editor(s): Gajanan Bhat, In *Woodhead Publishing Series in Textiles, Structure and Properties of High-Performance Fibers*, Woodhead Publishing, pp. 79-109.
- Hisseine, O. A., Wilson, W., Sorelli, L., and Tagnit-Hamou, A. (2019a) Nanocellulose for improving mechanical properties of concrete: A macro-to-micro investigation for disclosing the effects of cellulose filaments on strength of cement systems, *Construction and Building Materials*, 206, pp. 84–96.
- Hisseine, O. A., Omran, A. F., and Tagnit-Hamou, A. (2018c) Influence of Cellulose Filaments on Cement Pastes and Concrete, *ASCE Journal of Materials in Civil Engineering*, 30 (6): 04018109.
- Hisseine, O. A., Omran, A. F., Basic, N., and Tagnit-Hamou, A. (2018a) Feasibility of using cellulose filaments as a viscosity modifying agent, *Cement and Concrete Composites*, 94, pp. 327–340.
- Hisseine, O. A., and Tagnit-Hamou, A. (2019b). Characterization and nano-engineering the interface properties of high-volume glass powder strain hardening cement composites. Under review by *Composites Part B*.
- Hisseine, O. A., and Tagnit-Hamou, A. (2019c). Development of nano-engineered strain-hardening cement composite with high volume-glass powder using cellulose filaments. Under review by *Cement and concrete composites*.
- Hisseine, O. A., Soliman, N., and Tagnit-Hamou, A. (2018a) Cellulose filaments for controlling autogenous shrinkage in ultra-high-performance concrete. Being considered for publication by *Cement and concrete research*.

- Hogancamp, J., and Grasley, Z. (2017) The use of microfine cement to enhance the efficacy of carbon nanofibers with respect to drying shrinkage crack resistance of portland cement mortars, *Cement and Concrete Composites*, 83, pp. 405-414.
- Horszczaruk, E., Mijowska, E., Kalenczuk, R. J., Aleksandrak, M., and Mijowska, S. (2015) Nanocomposite of cement/graphene oxide – Impact on hydration kinetics and Young's modulus, *Constr. Build. Mater.*, 78, pp. 234–242.
- Hossain, K. M. A., Alam, S., Anwar, M. S., and Julkarnine, K. M. Y. (2016) High performance composite slabs with profiled steel deck and Engineered Cementitious Composite – Strength and shear bond characteristics, *Construction and Building Materials*, 125, pp. 227-240.
- Hou, P., Kawashima, S., Kong, D., David, J., Qian, J., and Shah, S. P. (2013) Modification effects of colloidal nanoSiO₂ on cement hydration and its gel property, *Composites: Part B*, 45, pp. 440–448.
- Hoyos, C. G., Cristia, E., and Vázquez, A. (2013) Effect of cellulose microcrystalline particles on properties of cement-based composites, *Materials & Design*, 51 (1), pp. 810-818.
- Hussain, F., Hojjati, M., Okamoto, M., and Gorga, R. E. (2006) *J. Compos. Mater.*, 40, pp.1511–1575.
- Ifuku, S., Nogi, M., Abe, K., Handa, K., Nakatsubo, F., and H. Yano (2007) *Biomacromolecules*, 8, pp. 1973–1978.
- Iijima, S. (1991) Helical microtubules of graphitic carbon, *Nature*, 56, pp. 56–58.
- Iijima, S., and Ichihashi, T. (1993) Single-shell carbon nanotubes of 1-nm diameter, *Nature*, 363, pp. 603–605. <http://dx.doi.org/10.1038/363603a0>.
- Jackson, A. P., Vincent, J. F. V., and Turner, R. M. (1988) *Proc. R. Soc.*, 234(B), 415. doi: 10.1098/rspb.1988.0056.
- Jalal, M., Fathi, M., and Farzad, M. (2013) Effects of fly ash and TiO₂ nanoparticles on rheological, mechanical, microstructural and thermal properties of high strength self-compacting concrete. *Mech. Mater.*, 61, pp. 11–27.
- Jarabo, R., Fuente, E., Monte, M.C., Savastano, H., Mutjé, P., and Negro, C. (2012) Use of cellulose fibers from hemp core in fiber-cement production: effect on flocculation, retention, drainage and product properties, *Ind. Crops Prod.*, 39, pp. 89–96.
- Jennings, H. M., Bullard, J. W., Thomas, J. J., Andrade, J. E., Chen, J. J., and Scherer, G. W. (2008) Characterization and modeling of pores and surfaces in cement paste: Correlations to processing and properties, *J. Adv. Concr. Technol.*, 6 (1), pp. 5–29.
- Jiang, R.S., and Wang, B.M. (2012) Mechanical properties and microstructure of graphene cement composites, *Key Eng. Mater.*, 748, pp. 295–300.
- Jo, B. W., Kim, C. H., Lim, and J. H. (2007) Characteristics of cement mortar with nano-SiO₂ particles, *ACI Mater J*, 104 (4), pp. 404–407.

- Johnston, C. D. (1974) Steel Fibre Reinforced Mortar and Concrete — A Review of Mechanical Properties, Fiber Reinforced Concrete, SP-44, American Concrete Institute, Detroit, pp. 127-142.
- JSCE (2008) Recommendations for design and construction of high-performance fiber reinforced cement composites with multiple fine cracks (HPFRCC), *Japan Society of Civil Engineers*, Concrete Engineering Series 82.
- JSCE-SF4 (1984) Standard for Flexural Strength and Flexural Toughness, Method of Tests for Steel fiber Reinforced Concrete, Concrete Library of JSCE, No. 3, *Japan Concrete Institute (JCI)*, pp. 58-66.
- Kanda, T., and Li, V. C. (1998) Multiple cracking sequence and saturation in fiber reinforced cementitious composite, *Concr. Res. Technol.*, JCI, 9 (2), pp. 19–33.
- Kanda, T., Nagai, S., Maruta, M., and Yamamoto, Y. (2011) New High-Rise R/C Structure using ECC Coupling Beams. Second Intl. RILEM Conference on Strain-hardening Cementitious Composites, Rio de Janeiro, Brazil, pp. 289-296.
- Kang, I., Heung, Y. Y., Kim, J. H., Lee, J. W., et al. (2006) Introduction to carbon nanotube and nanofiber smart materials, *Composites Part B: Engineering*, 37 (6), pp. 382-394.
- Katyal, N. K., Ahluwalia, S.C., and Parkash, R. (1999). Effect of TiO₂ on the hydration of tricalcium silicate. *Cem. Concr. Res.*, 29, pp. 1851–1855.
- Kawabata, S., Sera, M., Kotani, T., Katsuma, K., Niwa, M., and Xiaoxin, C. (1993) 9th *International Conference on Composite Materials*, Madrid, Spain.
- Kawashima, S., and Shah, S. P. (2011) Early-age autogenous and drying shrinkage behavior of cellulose fiber-reinforced cementitious materials, *Cem. Concr. Compos.*, 33, pp. 201–208.
- Khazraji, A.C., and Robert, S. (2013), Self-assembly and intermolecular forces when cellulose and water interact using molecular modeling, *J. Nanomater.*, Article ID 745979.
- Kim, Y. Y., Kong, H. J., Li, V. C. (2003) Design of engineered cementitious composite (ECC) suitable for wet-mix shotcreting, *ACI Mater J.*, 100 (6), pp. 511-518.
- Kong, H-J., Bike, S. G., V, and Li, V. C. (2003), Development of a self- consolidating engineered cementitious composite employing electrosteric dispersion/stabilization, *Cement and Concrete Composites*, 25 (3), pp. 301-309.
- Konsta-Gdoutos, M. S., Metaxa, Z. S., and Shah, S. P. (2010a). Multi-scale mechanical and fracture characteristics and early-age strain capacity of high-performance carbon nanotube/cement nanocomposites, *Cement and Concrete Composites*, 32 (2), pp. 110–115.
- Konsta-Gdoutos, M. S., Metaxa, Z. S., and Shah, S. P. (2010b). Highly dispersed carbon nanotubes reinforced cement-based materials, *Cement and Concrete Research*, 40 (7), 1052–1059.

- Kontoleonos, F., Tsakiridis, P. E., Marinos, A., Kaloidas V, and Katsioti, M. (2012) Influence of colloidal nanosilica on ultrafine cement hydration: physicochemical and microstructural characterization, *Constr. Build. Mater.*, 35, pp. 347–360.
- Kunieda, M., and Rokugo, K. (2006) Recent progress on HPFRCC in Japan required performance and applications, *J. Adv. Concr. Technol.*, 4 (1), pp. 19–33.
- Kwak, H. G., and Filippou, F. C. (1990) Finite element analysis of reinforced concrete structures under monotonic loads. Berkeley, CA: Department of Civil Engineering, University of California, pp 33–39.
- Löfgren, I. (2005) Fibre-reinforced Concrete for Industrial Construction-a fracture mechanics approach to material testing and structural analysis. PhD Thesis, Chalmers University of Technology.
- Land, G., and Stephen, D. (2012) The influence of nano-silica on the hydration of ordinary Portland cement. *J. Mater. Sci.*, 47, pp. 1011–1017.
- Lawler, J. S., Wilhelm, T., Zampini, D., and Shah, S. P. (2003): Fracture processes of hybrid fiberreinforced mortar, *Materials and Structures*, 36, pp. 197-208.
- Lee, S. H., Kim, S., and Yoo, D. Y. (2018) Hybrid effects of steel fiber and carbon nanotube on self-sensing capability of ultra-high-performance concrete, *Construction and Building Materials*, 185, pp. 530-544.
- Lee, C., Wei, X., Kysar, J. W., and Hone, J. (2008). Measurement of the Elastic Properties and Intrinsic Strength of Monolayer Graphene, *Science*, 321 (5887), pp. 385–388. doi:10.1126/science.1157996. ISSN 0036-8075. PMID 18635798.
- Lepech, M. D., and Li, V. C. (2009), Application of ECC for Bridge Deck Link Slabs, *RILEM J. of Materials and Structures*, 42 (9), pp. 1185-1195.
- Li, G. Y., Wang, P. M., and Zhao, X. (2005). Mechanical behavior and microstructure of cement composites incorporating surface-treated multi-walled carbon nanotubes, *Carbon*, 43, pp. 1239–1245.
- Li, G. Y., Wang, P. M., and Zhao, X. (2007) Pressure-sensitive properties and microstructure of carbon nanotube reinforced cement composites, *Cem. Concr. Compos.*, 29 (5), pp. 377–382.
- Li, V. C. (1993) From micromechanics to structural engineering – the design of cementitious composites for civil engineering application, *J. Struct. Eng. Earthquake Eng.*, 10 (2), pp. 37–48.
- Li, V. C. (1998) Engineered Cementitious Composites (ECC) – Tailored Composites Through Micromechanical Modeling, Fiber Reinforced Concrete: Present and the Future, *Canadian Society for Civil Engineering*, Montreal, 1998, pp. 64–97.
- Li, V. C. (2002) Large volume, high-performance applications of fibers in civil engineering, *Journal of Applied Polymer Science*, 83, John Wiley & Sons, pp. 660-686.

- Li, V. C. (2003) On engineered cementitious composites (ECC) – a review of the material and its application, *J. Adv. Concr. Technol.*, 1, pp. 215–230.
- Li, V. C. (2004) Strategies for high performance fiber reinforced cementitious composites development, in: S. Ahmad, M. di Prisco, C. Meyer, G.A. Plizzari, S. Shah (Eds.), *Fiber Reinforced Concrete: From Theory to Practice*, Proceedings of the North American/European Workshop on Advances in Fiber Reinforced Concrete, Bergamo, Italy, pp. 93–98.
- Li, V. C. and Maalej, M. (1996a) Toughening in Cement Based Composites. Part II: Fiber Reinforced Cementitious Composites, *Cement and Concrete Composites*, 18, pp. 239–249.
- Li, V. C. and Maalej, M. (1996b) Toughening in Cement Based Composites. Part I: Cement, Mortar, and Concrete, *Cement and Concrete Composites*, 18, pp. 223–237.
- Li, V. C., and Leung C. K. Y. (1992) Steady state and multiple cracking of short random fiber composites, *ASCE J. Eng. Mech.*, 118 (11), pp. 2246–2264.
- Li, V. C., Mishra, D. K., and Wu, H. C. (1995) Matrix design for pseudo strain-hardening fiber reinforced cementitious composites, *RILEM J. Materials and Structures*, 28 (183), pp. 586–595.
- Li, V. C., Wang, S., and Wu, C. (2001) Tensile strain-hardening behavior of polyvinyl alcohol engineered cementitious composite, *ACI Mater. J.*, 98 (6), pp. 483–492.
- Li, V. C., and Stang, H. (1997) Interface property characterization and strengthening mechanisms in fiber reinforced cement-based composites, *Adv. Cem. Based Mater.*, 6 (1), pp. 1–20.
- Lin, T., Jia, D., He, P., Wang, M., and Liang, D. (2009). Effects of fiber length on mechanical properties and fracture behavior of short carbon fiber reinforced geopolymer matrix composites, *Mater. Sci. Eng. A*, 497 (1–2), pp. 181–185.
- Lin, X., Zhao, W., Zhou, W., Liu, P., et al. (2017), Epitaxial Growth of Aligned and Continuous Carbon Nanofibers from Carbon Nanotubes, *ACS Nano*, 11 (2), pp. 1257–1263.
- Ltifia, M., Guefrechb, A., Mounangab, P., and Khelidj, A. (2011) Experimental study of the effect of addition of nano-silica on the behaviour of cement mortars. *Proc Eng*, 10, pp. 900–905.
- Lv S. H., et al. (2013) Study on reinforcing and toughening of graphene oxide to cement-based composites, *Gongneng Cailiao, J. Funct. Mater.*, 44 (15), pp. 2227–2231.
- Lv, S., et al. (2013b) Regulation of GO on cement hydration crystals and its toughening effect, *Mag. Concr. Res.*, 65 (20), pp. 1246–1254.
- Lv, S., Zhang, J., Zhu, L., and Jia, C. (2016) Preparation of cement composites with ordered microstructures via doping with graphene oxide nanosheets and an investigation of their strength and durability, *Materials*, 9 (12), p. 924.

- Lv, S., Zhang, J., Zhu, L., Jia, C., and Luo, X. (2017) Preparation of regular cement hydration crystals and ordered microstructures by doping GON and an Investigation into its compressive and flexural strengths, *Crystals*, 7 (12), p 165.
- Lv, S., Liu, J., Sun, T., Ma, Y., and Zhou, Q. (2014) Effect of GO nanosheets on shapes of cement hydration crystals and their formation process, *Construction and Building Materials*, 64, p. 231-239.
- Maalej, M., Hashida, T., and Li, V. C. (1995) Effect of Fiber Volume Fraction on the off- Crack-Plane Fracture Energy in Strain-Hardening Engineered Cementitious Composites, *J. Amer. Ceramics Soc.*, 78 (12), pp. 3369-3375.
- Madani, H., Bagheri, A., and Parhizkar, T. (2012) The pozzolanic reactivity of monodispersed nanosilica hydrosols and their influence on the hydration characteristics of Portland cement, *Cem. Concr. Res.*, 42, pp. 1563–1570.
- Makar, J. M., and Beaudoin, J. J. (2004), Carbon nanotubes and their application in the construction industry. Proc., 1st Int. Symp. on Nanotechnology in Construction, P. J. M. Bartos, J. J. Hughes, P. Trtik, and W. Zhu, eds., *Royal Society of Chemistry*, Paisley, Scotland, 331–341.
- Makar, J. M., Margeson, J. C., and Luh, J. (2005). Carbon nanotube/ cement composite—Early results and potential applications. Proc., 3rd Int. Conf. on Construction Materials: Performance, Innovation and Structural Implications, The Univ. of British Columbia, Vancouver, BC, Canada, 1–10.
- Markovic, I., Walraven, J.C., and van Mier J. G. M. (2004): Tensile behaviour of high-performance hybrid fibre concrete. In *Fracture Mechanics of Concrete Structures*, Vol 2, eds Li et al., Proceedings of FRAMCOS-5, Vail, Colorado, USA, April 2004, pp. 1113-1120.
- Marshall, D. B., and Cox, B. N., A J-integral method for calculating steady-state matrix cracking stresses in composites, *Mech. Mater.*, 8, pp. 127–133.
- Matsumoto, T., and Mihashi, H. (2002) JCI-DFRCC Summary Report on DFRCC Terminologies and Application Concepts. In *Proceedings of the JCI International Workshop on Ductile Fiber Reinforced Cementitious Composites— Application and Evaluation*, pp. 59–66.
- Mayer, G. (2005) *Science*, 310:1144. doi: 10.1126/science.1116994.
- Meda, A., Plizzari, G. A., and Sorelli, L. (2004): Uni-axial and bending test for the determination of fracture properties of fiber reinforced concrete. In *Fracture Mechanics of Concrete Structures*, Vol. 2, eds. Li et al., Proceedings of FRAMCOS-5, Vail, Colorado, USA, April 2004, pp. 1163-1170.
- Melo Filho, J. D. A., Silva, F. D. A., and Toledo Filho, R.D. (2013) Degradation kinetics and aging mechanisms on sisal fiber cement composite systems, *Cem Concr Compos*, 40, pp. 30–39.
- Meng, W., and Khayat, K. M. (2016), Mechanical properties of ultra-high-performance concrete enhanced with graphite nanoplatelets and carbon nanofibers, *Composites Part B: Engineering*, 107, pp. 113-122.

- Menig, R., et al. (2000) Quasi-static and dynamic mechanical response of *Haliotis rufescens* (abalone) shells, *Acta Mater.*, 48 (9) pp. 2383-2398.
- Merta, I., and Tschegg, E. K. (2013) Fracture energy of natural fibre reinforced concrete, *Constr. Build. Mater.*, 40, pp. 991–997.
- Metaxa, Z. S., Konsta-Gdoutos, M. S., and Shah, S. P. (2009) Carbon nanotube reinforced concrete, *ACI Special Publication*, 267, pp. 11–20
- Meyers, M. A., Lin, A. Y., Po-Yu Chen, P. Y., and Muyco, J. (2008), Mechanical strength of abalone nacre: Role of the soft organic layer, *Journal of the Mechanical Behavior of Biomedical Materials*, 1 (1), pp. 76-85.
- Mindess, S., Young, J. F., and Darwin, D (2003) Concrete, 2nd ed. Prentice Hall, Upper Saddle River New Jersey, 2002.
- Mo, K. H., Yap, K. K. Q., Alengaram, U. J., and Jumaat, M. Z. (2014) The effect of steel fibres on the enhancement of flexural and compressive toughness and fracture characteristics of oil palm shell concrete, *Constr. Build. Mater.*, 55, pp. 20–28.
- Mobasher, B., and Shah, S. P. (1989), Test Parameters for Evaluating Toughness of Glass-Fiber Reinforced Concrete Panels, *ACI Materials Journal*, 86 (5), pp. 448-458.
- Mohammadkazemi, F., Doosthoseini, K., Ganjian, E., and Azin, M. (2015) Manufacturing of bacterial nano-cellulose reinforced fiber - cement composites, *Constr Build Mater*, 101(1), pp. 958–964.
- Mohammed, B. S., Aswin, M., Beatty W. H., and Hafiz, M. (2016), Longitudinal shear resistance of PVA-ECC composite slabs, *Structures*, 5, pp. 247-257.
- Mohammed, B. S. (2010) Structural behavior and m_k value of composite slab utilizing concrete containing crumb rubber, *Constr. Build. Mater.*, 24 (7), pp. 1214–1221.
- Mohammed, B. S., Al-Ganad, M. A., and Abdullahi M. (2011) Analytical & experimental studies on composite slabs utilizing palm oil clinker, *Constr. Build. Mater.*, 25 (8) pp. 3550–3560.
- Moon, R. J., Martini, A., Nairn, J., Simonsen, J., and Youngblood, J. (2011) Cellulose nanomaterials review: structure, properties and nanocomposites, *Chem. Soc. Rev.*, 40 (7), pp. 3941–3994.
- Moreno, D. M., Trono, W., Jen, G., Ostertag, C., and Billington, S. (2014) Tension stiffening in reinforced high-performance fiber reinforced cement-based composites, *Cement Concr. Compos.*, 50, pp. 36-46.
- Morton, J. H., Cooke, T., and Akers, S. (2010) Performance of slash pine fibers in fiber cement products, *Constr. Build. Mater.*, 24 (2), pp. 165–170.
- Musso, S., Tulliani, J-M., Ferro, G., Tagliaferro, A. (2009) Influence of carbon nanotubes structure on the mechanical behavior of cement composites, *Compos. Sci. Technol.*, 69 (11–12), pp. 1985–1990.

- Naaman, A. E. (2003) Engineered steel fibers with optimal properties for reinforcement of cement composites, *J. Adv. Concr. Technol.*, 1 (3), pp. 241–252.
- Naaman, A. E. (2007) Tensile strain-hardening FRC composites: Historical evolution since the 1960. *Advances in Construction Materials*, pp. 181–202.
- Naaman, A. E., Fiber Reinforcement for Concrete, *Concrete International: Design and Construction*, 7 (3), pp. 21-25.
- Naaman, A. E., and Reinhardt, H. W. (2003) Setting the stage: Toward a performance-based classification of FRC composites, In ‘High Performance Fiber Reinforced Cement Composites (HPFRCC4). Proceedings of the Fourth International RILEM Workshop’. (eds.) A. E. Naaman and H. W. Reinhardt. RILEM Publications S.A.R.L., pp. 1-4.
- Naaman, A. E., and Reinhardt, H. W. (2006) Proposed classification of HPFRC composites based on their tensile response, *Materials and Structures*, 39 (5) pp. 547–555.
- Narwal, J, Goel, A., Sharma, D., Kapoor, D. R., and Singh, B. (2013) An experimental investigation on structural performance of steel fibre reinforced concrete beam, *Int. J. Eng. Adv. Technol.*, 2 (6), pp. 301–304.
- Nazari, A., and Riahi, S. (2010) The effect of TiO₂ nanoparticles on water permeability and thermal and mechanical properties of high strength self-compacting concrete, *Mater.Sci. Eng. A*, 528, pp. 756–763.
- ~~Nazari, A., and Riahi, S. (2011) The effects of TiO₂ nanoparticles on physical, thermal and mechanical properties of concrete using ground granulated blast furnace slag as binder, *Materials Science and Engineering: A*, 528 (4–5), pp. 2085–2092.~~
- Nazari, A., and Riahi, S. (2011) The effects of TiO₂ nanoparticles on physical, thermal and mechanical properties of concrete using ground granulated blast furnace slag as binder, *Mater. Sci. Eng. A*, 528 (4-5), pp. 2085–2092.
- Nelson, P. K, Li, V. C, and Kamada, T. (2002) Fracture Toughness of Microfiber Reinforced Cement Composites, *Journal of Materials in Civil Engineering*, 144 (5), pp. 384–391.
- Nemati, K. M., Monterio, P. J. M., and Scrivener, K. L. (1998) Analysis of compressive stress induced cracks in concrete, *ACI Mater. J.*, 95 (5), p. 617–630.
- Neville, A. M. (2000) *Properties of Concrete*, fourth edition. Pearson Education Limited.
- Nilsson, J., and Sargenius, P. (2011) Effect of microfibrillar cellulose on concrete equivalent mortar fresh and hardened properties. Swedish Cement and Concrete Research Institute, Stockholm, Sweden.
- Noushini, A., Vessalas, K., Arabian, G., and Samali, B. (2014) Drying Shrinkage Behaviour of Fibre Reinforced Concrete Incorporating Polyvinyl Alcohol Fibres and Fly Ash, *Advances in Civil Engineering*, Article ID 836173, 10 pages.

- Ollivier, J. P., Maso, J. C., and Bourdette, B. (1995), Interfacial transition zone in concrete, *Adv. Cem. Based Mater.*, 2 (1), pp. 30–38.
- Onuaguluchi, O., and Banthia, N. (2016), Plant-based natural fibre reinforced cement composites: A review, *Cem. Concr. Compos.*, 68, pp. 96–108.
- Onuaguluchi, O., Panesar, D., and Sain, M. (2014) Properties of nanofibre reinforced cement composites, *Construct. Build. Mater.*, 63, pp. 119–124.
- Parra-Montesinos, G. J. (2005) High-performance fiber-reinforced cement composites: an alternative for seismic design of structures, *ACI Struct. J.*, 102, pp. 668-675.
- Parra-Montesinos, G. J., Peterfreund, S. W., and Chao, S.-H. (2005). Highly damage-tolerant beam-column joints through use of high-performance fiber-reinforced cement composites, *ACI Struct. J.*, 102, pp. 487-495.
- Peters, S. J., Rushing, T. S., Landis, E. N., and Cummins, T. K. (2011) Nanocellulose and Microcellulose Fibers for Concrete, Transportation Research Record, *Journal of the Transportation Research Board*, 2142, pp. 25–28.
- Poland, C. A., Duffin, R., Kinloch, I., Maynard, A., Wallace, W.A.H., Seaton, A., et al. (2008) Carbon nanotubes introduced into the abdominal cavity of mice show asbestos-like pathogenicity in a pilot study, *Nat. Nano.*, 3 (7) pp. 423-428.
- Qian, S., Lepech, M. D., Yun, Y. K., and Li, V. C. (2009) Introduction of transition zone design for bridge deck link slabs using ductile concrete, *ACI Struct. J.*, 106 (1), pp. 96–105.
- Radic, S., Geitner, N. K., Podila, R., Käkinen, A., Chen, P., Ke, P. C., and Ding F. (2013) Competitive Binding of Natural Amphiphiles with Graphene Derivatives, *Scientific Reports*, 3, Article number: 2273.
- Raki, L., Beaudoin, J., Alizadeh, R., Makar, J., and Sato, T. (2010) Cement and concrete nanoscience and nanotechnology, *Materials*, 3, pp. 918–942.
- Rapoport, J., Aldea, C. M., Shah, S. P., Ankenman, B., and Karr, A. (2002) Permeability of cracked steel fiber-reinforced concrete, *J. Mater. Civ. Eng.*, 14 (4), pp. 355–358.
- Romualdi, J. P., and Mandel, J. A. (1964) Tensile Strength of Concrete Affected by Uniformly Distributed Closely Spaced Short Lengths of Wire Reinforcement, *ACI JOURNAL, Proceedings*, 6 (6), pp. 657-671.
- Rossi, P., Acker, P., and Malier, P. (1987): Effect of steel fibres at two different stages: the material and the structure, *Materials and Structures*, 20, pp. 436-439.
- Saito, T., Kimura, S., Nishiyama, Y. and Isogai, A. (2007) *Biomacromolecules*, 8, pp. 2485–2491.
- Sakurada, I., Nukushima, Y., and Ito, T. (1962) Experimental determination of the elastic modulus of crystalline regions in oriented polymers, *J. Polym. Sci.*, 57, pp. 651–660.

- Salvetat, J. P., Bhattacharyya, S. and Pipes, R. B. (2006) *J. Nanosci. Nanotechnol.*, 2006, 6, pp. 1857–1882.
- Samir, M. A. S. A., Alloin, F., and Dufresne, A. (2005) *Biomacromolecules*, 6, pp. 612–626.
- Sanchez, F., and Sobolev, K. (2010). Nanotechnology in concrete – A review, *Construction and Building Materials*, 24 (11), 2060–2071.
- Sbia, L. A, Peyvandi, A., Soroushian, P., Lu, J., and Balachandra, A. M. (2014) Enhancement of Ultrahigh Performance Concrete Material Properties with Carbon Nanofiber, *Advances in Civil Engineering*, Article ID 854729, 10 pages.
- Scrivener, K. L., Crumbie, A. K., and Laugesen, P. (2004) The interfacial transition zone (ITZ) between the cement paste and aggregate in concrete, *Interface Sci.*, 12 (4), pp. 411–421.
- Sedan, D., Pagnoux, C., Smith, A., and Chotard, T., (2008) Mechanical properties of hemp fibre reinforced cement: influence of the fibre/matrix interaction, *J. Eur. Ceram. Soc.* 28, pp. 183–192.
- Senff, L., Labrincha, J. A., Ferreira, V. M., Hotza D., and Repette, W. L. (2009) Effect of nano-silica on rheology and fresh properties of cement pastes and mortars, *Constr. Build. Mater.*, 23, pp. 2487–2491.
- Shah, S. P., Ouyang, C., and Swartz, S. E. (1995) Fracture mechanics of concrete: Applications of fracture mechanics to concrete, rock, and other brittle materials, *John Wiley and Sons*, New York.
- Shah, S. P. (1983), Fiber Reinforced Concretes, Handbook of Structural Concrete, edited by F. K. Kong, R. H. Evans, E. Cohen, and F. Roll, McGraw-Hill, U.K., 1983.
- Shah, S. P., Konsta-Gdoutos, M. S., Metaxa, Z. S., and Mondal, P. (2019) Nanoscale modification of cementitious materials In: Bittnar Z, Bartos PJM, Nemecek J, Smilauer V, Zeman J, editors. Nanotechnology in construction: proceedings of the NICOM3 (3rd international symposium on nanotechnology in construction). Prague, Czech Republic, pp. 125–130.
- Shang Y., Zhang, D., Yang, C., Liu, Y., Liu, Y. (2015) Effect of graphene oxide on the rheological properties of cement pastes, *Constr. Build. Mater.*, 96, pp. 20–28.
- Shimizu, K., Kanakubo, T., Kanda, T., and Nagai, K. (2004) Shear behavior of steel reinforced PVA-ECC beams. In: Proceedings of the 13th world conference on earthquake engineering. Vancouver, Canada.
- Sikora, P., Horszczaruk, E., and Rucinska, T. (2015) The effect of nanosilica and titanium dioxide on the mechanical and self-cleaning properties of waste-glass cement mortar, *Procedia Engineering*, 108, pp. 146-153.
- Singh, L. P., Bhattacharyya, S. K., and Ahalawat, S. (2012) Preparation of size-controlled silica nanoparticles and its functional role in cementitious system, *J. Adv. Concr. Technol.*, 10, pp. 345–352.

- Singh, L. P., Bhattacharyya, S. K., and Mishra, G., Ahalawat, S. (2012) Reduction of calcium leaching in cement hydration process using nanomaterials. *Mater. Technol.: Adv. Perform. Mater.*, 27 (3), pp. 233–238.
- Sobolev, K., and Ferrada-Gutiérrez, M. (2005) How nanotechnology can change the concrete world: Part 1, *American Ceramic Society Bulletin*, 10, pp. 14–17.
- Soltanzadeh, F., Barros, J. A. O, and Santos, R. F. C (2015) High performance fiber reinforced concrete for the shear reinforcement: experimental and numerical research, *Constr. Build. Mater.*, 77, pp. 94–109.
- Soroushian, P., Won J-P., and Hassan, M. (2012) Durability characteristics of CO₂-cured cellulose fiber reinforced cement composites, *Constr. Build. Mater.*, 34, pp. 44–53.
- Stang, H. (1987) A double inclusion model for microcrack arrest in fibre reinforced brittle materials. *J. Mech. Phys. Solids.*, 35 (3), pp. 325-342.
- Stang, H. and Li, V. C. (2004) Classification of Fibre Reinforced Cementitious Materials for Structural Applications. In 6th RILEM Symposium on Fibre-Reinforced Concretes (FRC), pages 197–218, Varenna, Italy, September 2004. RILEM Publications.
- Stefan, C. F., Claudia, R. R., Zeeshan, A., Bos, D.H., et al. (2019) An approach to develop printable strain hardening cementitious composites, *Materials & Design*, 169, 107651.
- Stephenson, K. M. (2011) Characterizing the behavior and properties of nanocellulose reinforced ultra-high-performance concrete. Orono, ME: University of Maine; 2011.
- Tennis, P. D., and Jennings, H.M. (2000): A Model for Two Types of Calcium Silicate Hydrate in the Microstructure of Portland Cement Pastes, *Cement and Concrete Research*, 30 (6), pp. 855-863.
- Tolêdo-Filho, R. D., Ghavam, K., England, G. L., Scrivener, K. (2003) Development of vegetable fibre-mortar composites of improved durability, *Cem. Concr. Compos.*, 25 (2), pp. 185–196.
- Tonoli, G. H. D., Santos, S. F., Joaquim, P., and Savastano, H. (2010) Effect of accelerated carbonation on cementitious roofing tiles reinforced with lignocellulosic fibre, *Constr. Build. Mater.*, 24, pp. 193–201.
- Torgal, P. F., and Jalali, S. (2011) Nanotechnology: advantages and drawbacks in the field of construction and building materials, *Constr. Build. Mater.*, 25, pp. 582-590.
- Tran, T. N., and Dong Joo Kim, J. D. (2017) Synergistic response of blending fibers in ultra-high-performance concrete under high rate tensile loads, *Cement and Concrete Composites*, 78, pp. 132-145.
- Trtik, P., and Bartos, P. J. M. (2001) Nanotechnology and concrete: What can we utilise from the upcoming technologies? Proceeding of the 2nd Anna Maria workshop: Cement & Concrete: Trends & Challenges, pp. 109–120. Anna Maria, FL, USA.

- Trub, M. C., Numerical Modeling of High-Performance Fiber Reinforced Cementitious Composites, PhD Thesis, ETH, 2011.
- Van der Plas, C. (1991) The Many Improvements of GRC by Polymer Addition, Eighth Biennial Congress of the Glassfibre Reinforced Cement Association, Maastricht, The Netherlands, pp. 13-21.
- Varela, S., and Saiidi, M. S. (2013) Shear behavior of engineered cementitious composite structural members. In: Second conference on smart monitor, assessment and rehabilitation of civil structures. Istanbul, Turkey.
- Vondran, G. L., Nagabhushanam, M., and Ramakrishnan, V. (1990) Fatigue Strength of Polypropylene Fiber Reinforced Concretes, Fiber Reinforced Cements and Concretes: Recent Developments, edited by R. N. Swamy and B. Barr, Elsevier Applied Science, London and New York, 1990, pp. 533-543.
- Wang, Q., Wang J., Lu, C-X, Liu, B-W, Zhang, K., and Li, C-Z. (2015), Influence of graphene oxide additions on the microstructure and mechanical strength of cement, *New Carbon Materials*, 30 (4), pp. 349-356.
- Wang, H. Z., and Dixon, R. A. (2012) On-off switches for secondary cell wall biosynthesis, *Mol. Plant*, 5 (2), pp. 297-303.
- Wang, X. H., Jacobsen, S., He, J. Y., Zhang, Z. L., and Lee, S. F. (2009) Application of nanoindentation testing to study of the interfacial transition zone in steel fiber reinforced mortar, *Cem. Concr. Res.*, 39 (8), pp. 701–715.
- Wei, J., and Meyer, C. (2015) Degradation mechanisms of natural fiber in the matrix of cement composites, *Cement and Concrete Research*, 73, pp. 1-16.
- Xie, X. L., Mai, Y. W., and Zhou, X. P. (2005) Dispersion and alignment of carbon nanotubes in polymer matrix: a review, *Mater. Sci. Eng. R.*, 49 (4), pp. 89–112.
- Xu, S., Hou. L.-J., and Zhang, X.-F. (2012) Shear behavior of reinforced ultrahigh toughness cementitious beams without transverse reinforcement, *J. Mater. Civ. Eng.*, 24, pp. 1283-1294.
- Xu, S., Lyu, Y., Xu, S., and Li, Q. (2019), Enhancing the initial cracking fracture toughness of steel-polyvinyl alcohol hybrid fibers ultra-high toughness cementitious composites by incorporating multi-walled carbon nanotubes, *Construction and Building Materials*, 195, pp. 269–282.
- Xu, Y., Zeng, J., Chen, W., Jin, R., Li, B., and Pan, Z. (2018) A holistic review of cement composites reinforced with graphene oxide, *Construction and Building Materials*, 171 pp. 291-302.
- Yan, H., Sun. W., and Chen, H. (1999) The effect of silica fume and steel fiber on the dynamic mechanical performance of high strength concrete, *Cem. Concr. Res.*, 29 (3), pp. 423–426.

- Yang, E. H., Garcez, E. and Li, V. C. (2012) Development of pigmentable engineered cementitious composites for architectural elements through integrated structures and materials design, *Materials and Structures*, 45 (3), pp. 425-432.
- Yano, H., Sugiyama, J., Nakagaito, A. N., Nogi, M., Matsuura, T., Hikita, M. and Handa, K. (2005) *Adv. Mater.*, 17, pp. 153–155.
- Yu, M. F., Lourie, O., Dyer, M. J., Moloni, K., Kelly, T. F., and Ruoff, R. S. (2000) *Science*, 287, pp. 637–640.
- Yuan, F., Pan, J., Xu, Z., and Leung, C. K. Y. (2013) A comparison of engineered cementitious composites versus normal concrete in beam-column joints under reversed cyclic loading, *Mater. Struct.*, 46, pp. 145-159.
- Zhang Q., and Li, V. C. (2015) Development of durable spray-applied fire-resistive Engineered Cementitious Composites (SFR-ECC), *Cement and Concrete Composites*, 60, pp. 10-16.
- Zhang, M., and Li, H. (2011) Pore structure and chloride permeability of concrete containing nanoparticles for pavement, *Construction and Building Materials*, 25 (2), pp. 608-616.
- Zhu, S. E., Yuan, S., and Janssen, G. C. A. M. (2014) Optical transmittance of multilayer graphene, *EPL*, 108 (1): 17007.
- Zollo, R. F. (1997) Fiber-reinforced Concrete: An Overview after 30 Years of Development, *Cement and Concrete Composites*, 19 (2), pp. 107-122.
- Zyganitidis, I., Stefanidou, M., Kalfagiannis, N., and Logothetidis, S. (2011) Nanomechanical characterization of cement-based pastes enriched with SiO₂ nanoparticles, *Mater. Sci. Eng. B*, 176, pp. 1580–1584.

Part II:

Disclosing the opportunities for nanoengineering concrete properties using Cellulose Filaments (CF)

- Chapter 3: Effect of CF on rheological properties of concrete
- Chapter 4: Effect of CF on hardening concrete properties
- Chapter 5: Effect of CF on hardened concrete properties
- Chapter 6: Effect of CF on concrete microstructure

This part of the thesis contributes towards achieving project objectives 1 through 4, which focus on the effect of CF on the three major concrete states (fresh, hardening, and hardened) as well as on the influence of CF on the microstructure of cement composites

CHAPTER 3 .

Effect of Cellulose Filaments on Rheological Properties of Cement and Concrete Composites

3.1 Introduction

The current chapter is devoted to exploring the potential of CF to serve as a viscosity modifying agent (VMA) in self-consolidating concrete (SCC). SCC mixture should typically be designed to exhibit enough flowability necessary for placing them without mechanical vibration (while maintaining adequate homogeneity). For this, the use of VMA is an intrinsic feature of SCC formulation to produce flowable yet stable mixtures. VMAs are polymers introduced to enhance mixture consistency and stability via varied mechanisms such as: (i) increasing the yield stress and viscosity of the liquid phase, (ii) increasing mixture viscosity by interaction with mixture particles; and (iii) increasing the water retention capacity by a hydrophilic action. In this regard, this chapter is aimed at valorising the hydrophilic and flexible nanoscale cellulose filaments (CF) [diameter of (30–400 nm) and length of (100–2000 μm)] with high aspect ratio (up to 000) to enhance the properties of fresh concrete by a VMA effect. CF hydrophilicity implies high water retention capacity capable of imparting a VMA effect. Similarly, the nanoscale, high aspect ratio, and omnipresence of hydroxyl groups may favor interactions between CF and cement particles such that mixture consistency can be improved. To this end, the effect of CF (at 0.05-0.30% per weight of binder) on rheological properties (fresh properties, flow behavior, yield stress, plastic viscosity, and apparent viscosity) of cement paste and SCC were evaluated and compared to the effect of a commercially available VMA of Welan Gum type. A mechanism responsible for the VMA effect of CF was also proposed and validated with a geometry-based percolation model as well as by microstructure assessment. With a demonstrated VMA effect that has collateral positive impact on mechanical properties via nanoreinforcing action of CF, Therefore, this chapter contributes to offering a multifunctional VMA with strength enhancement functions transposed from the multifunctional aspect of biosystems (cellulose polymers). Full details of these findings are reported as par of [Article 1](#) published in this study (section 3.2 below).

3.2 Article 1-Feasibility of using cellulose filaments as a viscosity modifying agent (VMA) in self-consolidating concrete (SCC)

Article information

Authors and affiliations:

O.A. Hisseine, PhD candidate and Canada Vanier Scholar of NSERC, Cement and Concrete Research Group, Department of Civil Engineering, Université de Sherbrooke

N. Basic, PhD candidate, Cement and Concrete Research Group, Department of Civil Engineering, Université de Sherbrooke

A. F. Omran, Research associate, Cement and Concrete Research Group, Department of Civil Engineering, Université de Sherbrooke

A. Tagnit-Hamou, Professor and director of Cement and Concrete Research Group, Department of Civil Engineering, Université de Sherbrooke

Article status: Published

Journal: Cement and Concrete Composites

Reference: Hisseine O. A., Basic, N., Omran, A. F., and Tagnit-Hamou, A. (2018a) Feasibility of using cellulose filaments as a viscosity modifying agent. *Cement and Concrete Composites* vol. 94, pp. 327–340. DOI: <https://doi.org/10.1016/j.cemconcomp.2018.09.009>

Titre français: Faisabilité d'utiliser les filaments de cellulose comme agent modificateur de viscosité dans les bétons autoplaçants

Contribution of this article to the thesis: With the primary goal of valorising cellulose filaments (CF) as a viscosity modifying admixture (VMA), the current articles contributes towards realising objectives 1 and 2 of this thesis, namely: (i) characterizing the overall effect of CF on fresh properties, rheological behavior, heat of hydration, microstructure, and mechanical performance of cement pastes and concrete, and (ii) valorising CF as an alternative VMA to allow formulating flowable, yet stable, self-consolidating concrete (SCC) mixtures with enhanced strength performance.

Feasibility of using cellulose filaments as a viscosity modifying agent in self-consolidating concrete

Ousmane A.Hisseine^{a,b,*}, N.Basic^a, Ahmed F.Omran^a, Arezki Tagnit-Hamou^a

^a Cement and Concrete Research Group, Department of Civil Engineering, Université de Sherbrooke, 2500, Boulevard de l'Université, Sherbrooke, QC, J1K 2R1, Canada

^b Vanier Scholar of the Natural Sciences and Engineering Research Council of Canada (NSERC), Canada

*Corresponding author

Published in Cement and Concrete Composites (2018), Vol. 94, pp. 327-340.

Abstract

Nanomodification of concrete represents one of the phenomenal leaps in concrete technology providing innovative tools for engineering cement composites with improved performance. In self-consolidating concrete (SCC), for instance, designing flowable–yet stable and robust–SCC mixtures requires an optimum balance between flowability and stability. This is conventionally achieved by optimizing the dosage of high range water reducing admixtures (HRWRA) indispensable for flowability, while increasing the binder content or introducing viscosity modifying agents (VMA) necessary for stability. This study shows how cellulose filaments (CF)—a new type of nanocellulose materials—can be used as a novel tool for rheology modification and strength enhancement in SCC. CF were incorporated at concentrations ranging from 0.05 to 0.30% per weight of binder in cement pastes and SCC. Rheological and mechanical properties of CF systems were compared to those of plain systems and systems incorporating a commercially available VMA of Welan Gum type. Results showed that CF serve as a VMA due to the buildup of flexible nanoscale CF networks. As such, a geometry-based percolation model showed that at a concentration of 0.12 wt.%, a network of percolating CF was formed. Beyond this CF content, the yield stress, the plastic viscosity, as well as the HRWRA demand exhibited a substantial increase. CF networks increased mixture viscosity—essential for stability—at low shear rates. On the other hand, at high shear rates, CF networks led to lower apparent viscosity essential for improving pumpability; owing to the streamlining of the flexible nanocellulose fibrils in the direction of flow, thereby imparting

a shear thinning behavior. Furthermore, CF imparted improvement in mechanical performance of 12–26% in compression, splitting-tension, and flexure. Research outcomes are expected to contribute towards offering an alternative VMA with strength improvement potential while contributing towards the implementation of sustainable materials for concrete technology.

Keywords: Cellulose filaments, Mechanical performance, Nanocellulose materials, Rheology enhancement, Self-consolidating concrete, Viscosity modifying agents

1. Introduction

Nanomaterials have recently emerged as promising tools for engineering concretes with enhanced performance and improved sustainability [1]. Thus, nanocellulose materials (NCM)—being extracted from the most bounteous and renewable resource on the planet, and exhibiting several remarkable properties such as increased elastic modulus, hydrophilicity, and surface reactivity—are believed to shape a promising green candidate. The sustainability dimensions of NCM stem from their intrinsic features such their biodegradability, low toxicity, low environmental and health risks associated with their production, and low production cost [2, 3, 4]. NCM cover an array of nanoscale plant-based materials with high cellulose purity [2,5]. Common NCM with emerging applications in concrete technology include nanofibrillated cellulose (NFC) [6]; microcrystalline cellulose (MCC) [7]; cellulose nanocrystals (CNC) [8]; bacterial nanocellulose (BC) [9]; and cellulose filaments (CF) [10]. Among these NCM, CF represent a relatively new class with highly promising applications in concrete technology owing to its hydrophilicity, high surface area, and high aspect ratio (100–1000) stemming from its nanometric diameter (30–400 nm), but micrometric length (100–2000 μm).

CF have demonstrated enhancement in flexural strength and tensile-splitting capacity of 15–25% in cement pastes and concrete [10] owing to higher degree of hydration and enhancement of C-S-H phase micromechanical properties (indentation modulus and hardness) [11]. These enhancements, though, were achieved with relatively very low concentrations (0.05–0.20%) where filament dispersion is thought to be the most effective. This is possibly attributed to the high surface area of CF ($>80 \text{ m}^2/\text{g}$) which increases the propensity of the filaments for self-assembly at high concentrations. CF tendency for self-assembly is believed to foster creating a

fibrillated network. In light of the flexibility of CF fibrils, their inherent tendency for self-assembly has the potential to provide a micro/nano reinforcing mesh to stabilize the rheological behavior of cement and concrete composites. This can increase mixture consistency and homogeneity, enhance mixture stability and robustness, and translate into improved mechanical performance in the hardened product. Such impacts on the properties of cement and concrete composites may be viewed analogous to the well reported effect of viscosity modifying agents (VMA).

VMA are polymeric materials which are introduced in mixtures and suspensions to increase their viscosity and enhance their consistency [12]. In cement-based composites, commonly used VMA consist of polysaccharides [13], microbial-source polysaccharides, and acrylic-based polymers [12]. The mode of action of those different VMA depends mainly on their type. Some water-soluble polymers such as cellulose ethers and polyethylene oxides act by increasing the viscosity of the mixing water. This is also true for some polysaccharides (e.g. Diutan Gum) which are more effective in increasing the yield value of the liquid phase [13]. However, some other polysaccharides (e.g. starch) increase mixture viscosity by interaction with mixture particles [13]. This is also the case of organic water-soluble flocculants (e.g. natural gum) which act by adsorption onto cement grains. These VMA increase the viscosity due to an enhanced inter-particle attraction between cement grains [14]. On the other hand, water-swelling materials of high surface area—such as milled asbestos and bentonites—increase the water retaining capacity [14].

Typical applications of VMA in concrete include underwater concreting intended for repairing marine structures where mixtures should exhibit an adequate level of flowability, yet show a reduced tendency to segregation and a minimal intermixing with the surrounding water. VMA are also used in shotcrete applications where high cohesiveness and adequate resistance to sagging are required at low shear rates without affecting concrete pumpability. Introducing VMA in such concretes increases their pseudoplasticity. At increasing pseudoplasticity, mixtures exhibit higher apparent viscosity at low shear rates—necessary to withstand sagging—while demonstrating a relatively low resistance to flow at high shear rates, typically encountered during pumping [15]. The most common use of VMA in concrete technology is in high-

flowability concretes. These are the type of concretes where the optimum balance between deformability and stability is a challenge. A very common type of flowable concrete where VMA is used is self-consolidating concrete (SCC). A well-designed SCC mixture should exhibit two key features: (i) an adequate deformability, while maintaining (ii) an excellent stability. For SCC to fulfill deformability requirements, the mixture is adjusted such that it contains increased quantities of high-range water-reducing admixtures (HRWRA) and a reduced maximum size of coarse aggregates. To respond to stability requirements, however, SCC mixtures should conventionally contain higher amount of binders. Alternatively, for sustainability incentives, concrete practitioners use VMA to reduce the mixture demand in binders [16]. The introduction of VMA in those concretes increases the mixture viscosity and enhances its homogeneity. As a result, the separation propensity of the variable-density constituents is attenuated, and the performance of the hardened product is improved. However, some commercially available VMA such as Welan Gum (WG) are expensive and add to the invoice of SCC, thereby rendering it a speciality concrete [17].

In this regard, and in light of CF characteristics described earlier (i.e., high surface area, high aspect ratio, and high water-retention capacity), it is hypothesized herein that CF have a significant potential to serve as an alternative VMA. In light of this hypothesis, the objective of this study is to produce stable SCC mixtures using CF as a VMA. Initial applications of CF emerged in the paper and pulp industry and its implementation in concrete technology as a VMA is a relatively new research frontier. To achieve the above objective, the effect of CF—at solid concentrations ranging from 0.05 to 0.30% by weight of binder—on hydration kinetics, flow properties, rheological behavior, and mechanical performance was evaluated in cement pastes and SCC. With cellulose being the most copious polymeric raw material on the planet (imparting inherent strength to plant-based materials), it may be legitimate to believe that CF can serve as a viable alternative VMA which can also have collateral functions such as internal curing and reinforcing—which are not evident in conventionally used VMA. This is expected to contribute towards the development of next-generation green cement composites with improved performance and multifunctional characteristics.

2. Experimental program

2.1. Materials properties

2.1.1. Basic concrete constituents

General Use (GU) Portland cement (CSA A3001) equivalent to Type I cement (ASTM C1157) and class F-fly ash (FA) were used in this study. The particle size distribution for each of these binders is shown in Fig. 1, while their physical properties and oxide-based chemical compositions by X-ray fluorescence analysis are reported in Table 1. In the SCC mixtures, crushed limestone coarse aggregates with 5–14 mm maximum aggregate size, 2.77 specific gravity (*SG*), and 0.52% water absorption rate were used. Natural river sand with a *SG* of 2.65 and an absorption rate of 0.9% was employed. A HRWRA with 32% solid content—fulfilling the requirements of ASTM C494 Type F admixtures [18]—was added at a dosage of 2.5 L/m³ to secure the target flowability. A Welan Gum (WG)-based VMA with a solid content of 39% and was introduced at a solid concentration of 0.05% by weight of binder. It is compliant with requirements of ASTM C494 Type S admixtures [18].

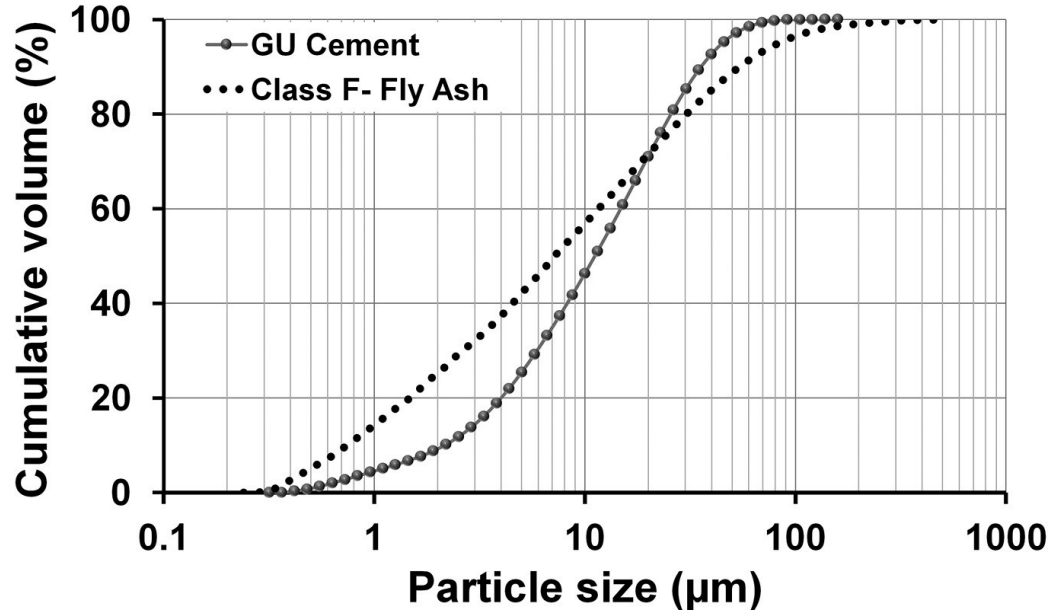


Fig. 1. Particle size distribution of general use (GU) cement and class F-fly ash used in the current study.

Table 1. Chemical composition and physical properties of binders used in the study.

Chemical analysis (%)	Type	GU	Class F-fly ash
SiO ₂	20.5		53.7
Al ₂ O ₃	4.0		17.5
Fe ₂ O ₃	2.0		5.6
CaO	63.2		12.4
MgO	2.2		2.1
SO ₃	3.4		1.4
Na ₂ O	0.2		1.6
K ₂ O	0.9		2.0
Free lime	1.1		3.90
Loss-on-ignition	2.9		1.8
Insoluble residues	0.1		0.1
Blaine fineness (m ² /kg)	431		287
Fineness, passing on 45 µm sieve (%)	91		95

2.1.2. Cellulose filaments

The CF used in this study were provided by Kruger Biomaterials Inc. (Trois-Rivières, Québec, Canada) in a semi-dispersed form having a nominal moisture content of 70%. CF represent an intrinsic part of the hierarchical structure of cellulose which impart intrinsic strength to plant-based materials (Fig. 2). According to the supplier, the filaments were derived from FSC®-certified Kraft wood pulp using only virgin fibers to ensure optimum performance and consistent properties. Additional to the intrinsic sustainability features of CF, the extraction process of this material follows a green approach with a yield value of 100%. In fact, as per the supplier, the filaments were extracted through a patented process that uses only mechanical energy and does not involve any chemical or enzymatic treatment, nor does it produce effluent. In addition, the production facility is almost entirely powered by renewable energy, thereby minimizing the carbon footprint of CF.

The filaments have high flexibility and an extended length. They have a diameter of 30–400 nm, a length of 100–2000 µm, and an aspect ratio of 100–1000. CF exhibit high surface area of more than 80 m²/g. Owing to the above-mentioned extraction process, CF have high cellulose purity (cellulose >95% and hemicelluloses <5%). As such, it is free from impurities such as lignin, pectin, wax, and soluble sugars. Fig. 3 shows a picture of water suspensions with varying CF

contents, while Fig. 4 depicts a scanning electron microscope (SEM) image of a CF diluted aqueous suspension at a concentration of 0.10%.

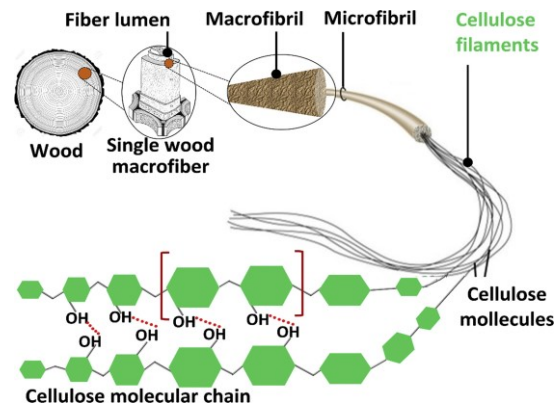


Fig. 2. Schematic illustration of the hierarchical structure of cellulose filaments (CF) used in this study. Picture adapted from Hisseine et al. [11] with permission from ASCE.

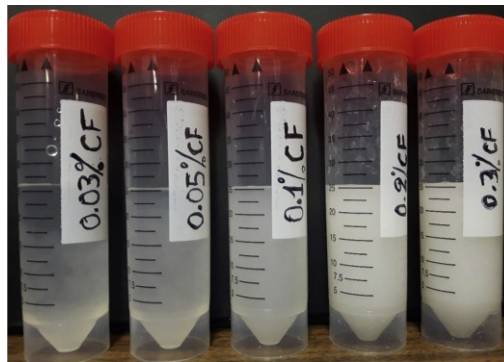


Fig. 3. Aqueous suspensions of cellulose filaments (CF) used to prepare the different cement systems considered in this study.

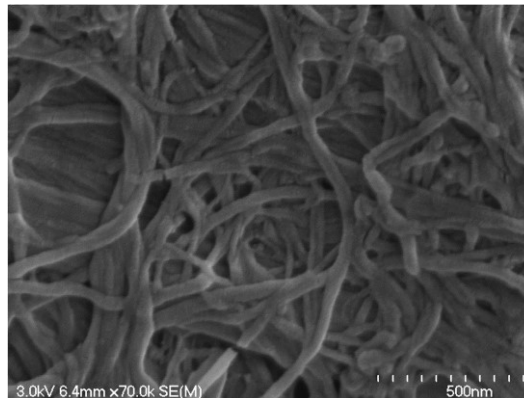


Fig. 4. Scanning electron microscope (SEM) image of a diluted aqueous suspension of cellulose filaments (CF). Adapted from Hisseine et al. [11] with permission from ASCE.

2.2. Mixture proportioning and procedures

To provide a more comprehensive assessment for the effect of CF on cement systems, both paste and concrete systems were considered in this study. Six paste mixtures were designed with a water-to-cement ratio (w/c) of 0.5. This includes a plain mixture (designated herein as Ref.), a mixture with 0.05% of a Welan Gum-based VMA designated as (0.05% WG), and four mixtures with CF concentrations of 0.05, 0.10, 0.20, and 0.30% by weight of binder (Table 2). For concrete mixtures, two series of SCC with a water-to-binder (w/b) ratio of 0.42 were considered. In the first test series, the mixture content in HRWRA was kept constant at 2.5 L/m^3 . In these mixtures, the effect of CF—at concentrations of 0%, 0.10%, 0.15%, and 0.20%—on fresh, rheological, and mechanical properties was evaluated. In the second test series, in an attempt to produce rheologically equivalent SCC systems (necessary for a better evaluation of the influence of CF on SCC properties), the mixture demand in HRWRA required to achieve a slump-flow of $700 \pm 35 \text{ mm}$ was adequately adjusted when CF were incorporated at concentrations of 0%, 0.05%, 0.10%, 0.15%, and 0.20%. In both test series, a mixture with a commercially available VMA (Welan Gum) fulfilling the requirements of ASTM C494 Type S VMA was used at a solid concentration of 0.05% by weight of binder (Table 3).

To produce the different CF concentrations, CF aqueous suspensions were prepared by diluting the as-received material in water by applying high shear mixing. Further details about the procedure followed for preparing the different CF concentrations can be found elsewhere [10]. To prepare paste mixtures (where no HRWRA was used), CF suspension was added to the total adjusted batch water then the mixing process for the different pastes was carried out in compliance with ASTM C305 guidelines [19]. For SCC mixtures (where the addition of HRWRA was imperative), the batch water (apart from the water used in preparing the CF suspension) was mixed with the HRWRA and divided into two parts, one of which was mixed with the CF suspension.

The mixing procedure of SCC mixtures consisted of homogenizing the sand and coarse aggregates for 1 min. The first half of the mixing water containing CF was then added, and the mixing process continued for another 1 min. Later, the cementitious materials were added and mixed for 0.5 min, followed by adding the second half of the mixing water and the material was

mixed for 2.5 min. Following 2 min of rest, the material was remixed for another 2 min. At the end of mixing (7 min from the initial cement-water contact), the concrete mixture was cast for the various tests. Specimens for mechanical properties were cast from each batch then demolded at the age of 24 ± 1 h. Samples for 1-day compressive strength were then tested, while the rest was kept in a controlled curing room at 100% RH and 23 °C until the age of testing.

Table 2. Mix proportions of cement pastes.

Paste mixtures	Mass(g)			Volume (cm ³)			(CF/cement) vol.%
	Cement	Water	CF	Cement	Water	CF	
Ref.	500	250	0	159.2	250	0	
0.05% WG	500	250	0	159.2	250	0	
0.05% CF	500	250	0.25	159.2	250	0.17	0.10%
0.10% CF	500	250	0.50	159.2	250	0.33	0.21%
0.20% CF	500	250	1.00	159.2	250	0.67	0.42%
0.30%CF	500	250	1.50	159.2	250	1.00	0.63%

Table 3. Concrete mix proportions, kg/m³.

Component	Ref.	0.05% WG	0.05% CF*	0.10%	0.15%	0.20% CF
WG VMA (solid content)		0.244	-	-	-	-
Cellulose filament (solid content)	-	-	0.244	0.487	0.731	0.974
HRWRA, L/m ³	Test series I	2.5	2.5	2.5	2.5	2.5
	Test series II	2.0	2.8	2.8	3.0	5.2
Type GU cement				365		
Class F fly ash				122		
Total binder				487		
Water				200		
Sand (0-5 mm)				804		
Coarse Aggregate (5-14 mm)				825		

*Mixture tested only in test series II

2.3. Testing procedures

2.3.1. Tests on paste mixtures

2.3.1.1. Rheology

The rheology of paste mixtures was assessed using a coaxial cylinder rheometer with a serrated surface providing a shear gap of 1.126 mm. The rheological parameters [i.e., yield stress (τ_0) and plastic viscosity (μ_p)] were determined from the mathematically modified Bingham model [20] described as:

$$\tau = \tau_0 + \mu_p \gamma' + c \gamma'^2 \quad (1)$$

Where τ_0 = yield stress (Pa), μ_p = plastic viscosity (Pa.s), γ' = shear rate (s^{-1}), and c = constant with most common values ≤ 0.001 which can be considered to be equal to zero when compared to the values of yield stress and plastic viscosity [21].

2.3.1.2. Isothermal calorimetry

The effect of CF on heat of hydration was evaluated by assessing the heat evolution in paste mixtures using a TAM Air isothermal calorimeter. From each mixture, a 3.0-g sample was placed into the calorimetric chamber kept at a constant temperature of 22 ± 0.1 °C. Heat measurements were collected for a continuous period of 48 h.

2.3.2. Tests on concrete mixtures

2.3.2.1. Flow properties

For concrete mixtures, the assessment of fresh properties was conducted using common SCC fresh property tests which include: (i) the slump-flow diameter, the time required to reach a 500 mm spread diameter (T_{500}), and the visual stability index (VSI) (ASTM C 1611) [22]; (ii) the J-Ring spread diameter and blockage ratio (ASTM C 1621) [22]; and (iii) the V-Funnel (EFNARC 2005) [23].

The VSI is a visual assessment tool for SCC stability. It was originally developed by BASF and subsequently incorporated in ASTM standards (ASTM C 1611) [22]. It consists of visually inspecting the concrete mixture (once spread and its flow stopped) then assigning a VSI index (0–3) by: (i) observing the distribution of coarse aggregates within the concrete mass, (ii) the

distribution of the mortar fraction particularly along the perimeter, and (iii) the bleeding characteristics. The VSI is assigned on the basis of the following criteria: 0 = highly stable mixture with no evidence of segregation or bleeding. 1 = stable mixture with no evidence of segregation, but slight bleeding observed as a sheen on the concrete mass. 2 = unstable mixture with a slight mortar halo ≤ 0.5 in. (≤ 10 mm) and/or aggregate pile in the center of the concrete mass. 3 = highly unstable, clearly segregating by evidence of a large mortar halo ≥ 0.5 in. (≥ 10 mm) and/or a large aggregate pile in the center of the concrete mass.

2.3.2.2. Rheology

The rheology of concrete mixtures was assessed using a ConTec 5 rheometer which consists of a fixed outer cylinder and an inner rotating bladed cylinder. The rotation speed was adjusted to increase from 0.025 to 0.5 revolutions per sec (rps) in 10 points such that 50 resistance-time measurements are recorded at each point.

2.3.2.3. Strength development

For all SCC mixtures, compressive strength (ASTM C39) [24] on 100×200 mm cylinders (at 1, 7, and 28 days), splitting-tensile capacity (ASTM C496) [25] on 100×200 mm cylinders (at 28 days), and flexural strength (ASTM C78) [26] on $100 \times 100 \times 400$ mm prisms (at 28 days) were assessed. The flexural strength assessment of concrete was conducted using a four-points bending configuration in a displacement controlled mode at a displacement rate of 0.0008 mm/s.

2.3.2.4. Microstructural analysis

To investigate the interaction between CF and the cementitious matrix, a high resolution field emission gun (FEG) scanning electron microscopy (SEM) of type Hitachi S-4700 equipped with an Oxford Energy Dispersive Spectroscopy (EDS) of type X-Max was employed. Analysis was conducted on fresh fractured surfaces at 28+ days for typical paste and SCC mixtures. Specimens were glazed with a gold palladium coat during 60 s to attenuate the effect of surface charges induced by the ultra-high energy electron beam. A double-face adhesive carbon film was placed between the specimens and the specimen-holding plate to foster conductivity.

A secondary electron (SE) detector, operated at 3.0 kV accelerating voltage and an emission current of 10 μA , was adopted for the analysis of fractured specimens.

3. Results and discussion

3.1. Results and discussion of paste mixtures

3.1.1. Rheological performance

Figures 5-7 present the results of rheological measurement for the different paste mixtures considered in this study. Fig. 5 presents the flow behavior fitted to the modified Bingham model, while Fig. 6 illustrates the variations of rheological parameters [i.e., yield stress (τ_0) and plastic viscosity (μ_p)] in the different pastes. Fig. 5 indicates that the modified Bingham model describes quite well the flow behavior of tested paste mixtures with a coefficient of determination $R^2 \geq 0.93$ throughout all mixtures. The figure also indicates that the incorporation of CF increased both the yield stress and the plastic viscosity for all ranges of shear rate ($\dot{\gamma}$). However, it appears that CF had a relatively more significant effect on yield stress than on plastic viscosity. This is further confirmed by Fig. 6 indicating that the use of 0.05%WG increased the yield stress from 8.4 to 13.4 Pa (or 1.6 times). On the other hand, the use of CF at 0.05, 0.10, 0.20 and 0.30% increased the yield stress to 12.5, 18.1, 30.1, and 34.8 Pa, respectively. This corresponds to increments in yield stress of 1.5, 2.2, 3.6, and 4.1 times, respectively. As for the plastic viscosity, the use of 0.05% WG increased the plastic viscosity of the reference mixture from 0.225 to 0.298 Pa.s (1.3 times). For CF mixtures, CF dosages of 0.05, 0.10, 0.20 and 0.30% increased the plastic viscosity of the reference system (0.225 Pa.s) to 0.294, 0.384, 0.594, and 0.770 Pa.s, respectively. This corresponds to 1.3, 1.7, 2.6, and 3.4, respectively.

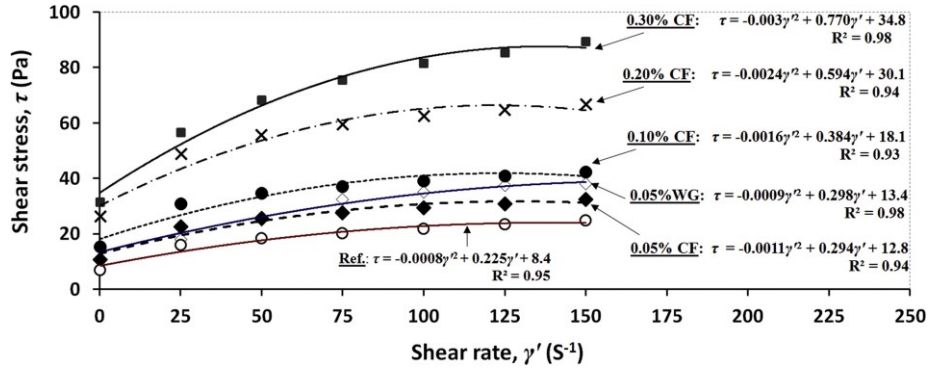


Fig. 5. Shear stress (τ)–shear rate (γ') response for the different paste mixtures.

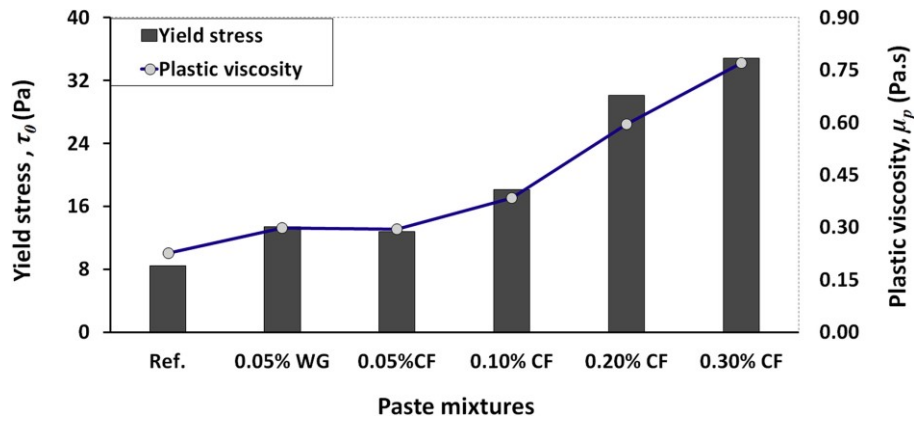


Fig. 6. Rheological parameters of cement pastes.

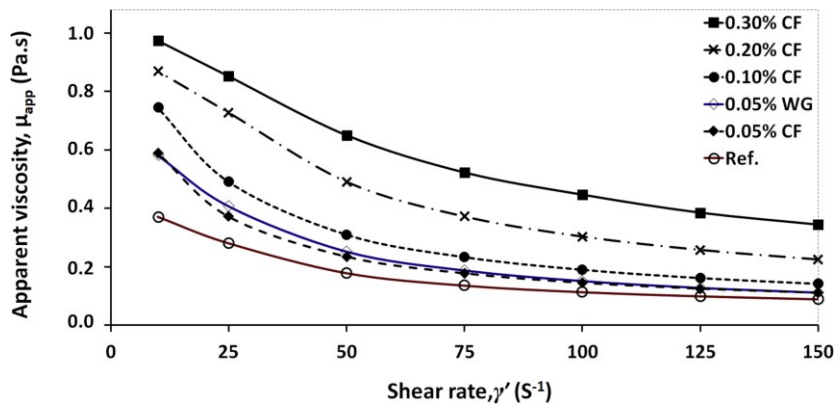


Fig. 7. Variation in apparent viscosity (μ_{ap}) in function of shear rate (γ') in the different paste mixtures.

The above results demonstrate the significant effect of CF on altering the rheology of cement pastes. At the same concentration of 0.05% in WG and CF, and in the absence of HRWRA, WG and CF showed comparable behavior in both yield stress and plastic viscosity. Further increase in CF dosage led to substantial increase in both yield stress and plastic viscosity with a sort of inflection point (in the trend of yield stress and plastic viscosity) between CF dosages of 0.10 and 0.20%.

On the other hand, the trend of yield stress and plastic viscosity described above reveals that the increase in the plastic viscosity is relatively lower in magnitude than the increase in the yield stress. This can be linked to the shear thinning effect exhibited in mixtures with CF. This is further confirmed by Fig. 7 illustrating the variation of apparent viscosity (μ_{ap}) in function of shear rate. The figure indicates that while the apparent viscosity in mixtures with CF is significantly high at low shear rates, it experiences substantial drop as shear rate increases. For instance, the apparent viscosity at the low shear rate of 10 s^{-1} for the different mixtures (Ref.; 0.05% WG; 0.05, 0.1, 0.2, and 0.30% CF) was respectively, 0.390, 0.602, 0.610, 0.765, 89, and 0.995 Pa.s. At high shear rate of 150 s^{-1} , the apparent viscosity for the above mixtures decreased to 0.109, 0.131, 0.131, 0.161, 0.244, 0.363 Pa.s, respectively. This corresponds to a decrease of 72, 78, 78, 79, 73, and 64%, respectively. This describes the pseudoplastic behavior exhibited by the paste mixtures. This behavior appears to be more significant in the mixture with WG and the ones with CF up to 0.10%. However, the percentage drop in the apparent viscosity in the mixture with 0.20% CF appears comparable to that of the plain mixture., while the mixture with 0.30% CF had a relatively lower percentage drop in apparent viscosity perhaps due to the very high CF content. Nonetheless, the shear thinning behavior can still be noticed.

The effect of CF on altering the rheological performance of cement systems is attributed to the hydrophilic nature of the filaments and to their nano-fibrillated structure. The hydrophilicity of CF and the omnipresence of hydroxyl (OH^-) groups on the surface of cellulose molecules foster water adsorption whereby water molecules adhere to the periphery of CF via hydrogen bonding [27]. This may allow CF to fix and imbibe part of the mixing water. The high water retention capacity of CF may also sprout from the high

molecular weight of cellulose molecular chains making up CF [28], since high molecular weight correlates well with higher water retention capacity in cellulose polymers [29].

On the other hand, the higher effect of CF on the yield stress than on the plastic viscosity as reflected by the shear thinning effect exhibited in mixtures with CF can be ascribed to the formation and buildup of CF networks. The nano-fibrillated structure, flexibility, and high aspect ratio of CF promote the intertwining and entanglement of individual filaments and/or the formation of filament networks. This increases the viscosity at low shear rates, hence the higher yield stress. At high shear rates, however, CF entanglements and networks are more likely to be dislodged whereby individual filaments would be streamlined in the direction of flow. Thus, mixture resistance to deformation may be decreased. In light of the above results, the VMA effect imparted by CF appears to be significantly influenced by the formation of CF networks. In this regard, it is believed that at the addition of low CF concentrations (e.g. 0.05%), a network of scattered filaments is formed. Upon further addition of CF, the network increases in complexity until a dosage where all filaments are connected or percolated. Beyond such a dosage, also called percolation threshold, mixture rheology would most probably exhibit some remarkable changes. Therefore, the next section is dedicated to evaluating whether there exists a correlation between a geometry-based percolation threshold and the rheological measurements.

3.1.2. Build-up of CF networks and percolation threshold

The result discussed in the previous section shed the light on the significant effect of CF on the rheology of cement systems even at low CF concentrations. The exact mechanism responsible for the effect of CF as a VMA, however, is yet to be fully understood. It may involve physical parameters (e.g., water retention associated with the hydrophilic CF, steric shielding due to the significantly high surface area and aspect ratio, and formation of a CF network due to the high aspect ratio coupled with the flexibility of filaments). The mechanism may include also chemical parameters such CF interaction with the different charged systems in pore solution as well as the interaction with HRWRA. Nonetheless, it appears that the tendency of the filaments to form a network has a major contribution in their VMA effect. To elaborate this,

let's consider a plain cement paste with high w/c. In such a system, cement particles are well suspended in the mixing water [Fig. 8 (a)]. Owing to the high surface area and aspect ratio of CF, it is perceptible that the addition of even a small amount of CF will obstruct the aqueous gaps between cement grains and create some bridges between some cement particles [Fig. 8 (b)]. This increases relatively the mixture viscosity. The addition of further CF intensifies these bridges which consequently lead to even higher viscosity. The formation of these bridges would continue spatially in a three-dimensional scale until an eventually continuous network of filaments is formed [Fig. 8 (c)]. The minimum amount of CF necessary to form a three-dimensional continuous network of connecting particles corresponds to the so-called percolation threshold [30]. While the formation of a CF network and the associated concept of percolation threshold are perceived herein to play a pivotal role in the VMA effect of CF, this VMA effect can be even transposed into enhancement in mechanical performance in the hardened product. In fact, research works on nanocellulose-reinforced polymer composites indicate that a mechanically percolating network of nanocellulose particles can form within the host matrix in a way that fosters the mechanical solicitation [31,32]. In this regard, the percolation threshold that depends mainly on the aspect ratio of the nanoparticles plays a fundamental role [31, 32, 33]. Deep-rooted in nanocomposites and polymer sciences [30, 34], the percolation theory has also been used in cement systems [35, 36, 37]. In this study, a geometry-based percolation model developed by Garboczi et al. [38] has been employed to predict the percolation threshold. The model estimates the percolation threshold on a volume basis, based on the geometry of particles without considering the interactions between the particles and between the particles and the medium. The model is expressed as:

$$p_c = \frac{sx+x^2}{h+fx+gx^{3/2}+cx^2+dx^3} \quad (2)$$

Where $h=7.742$, $f=14.61$, $g=12.33$, $c=1.763$, $d=1.658$, and $s=9.875$.

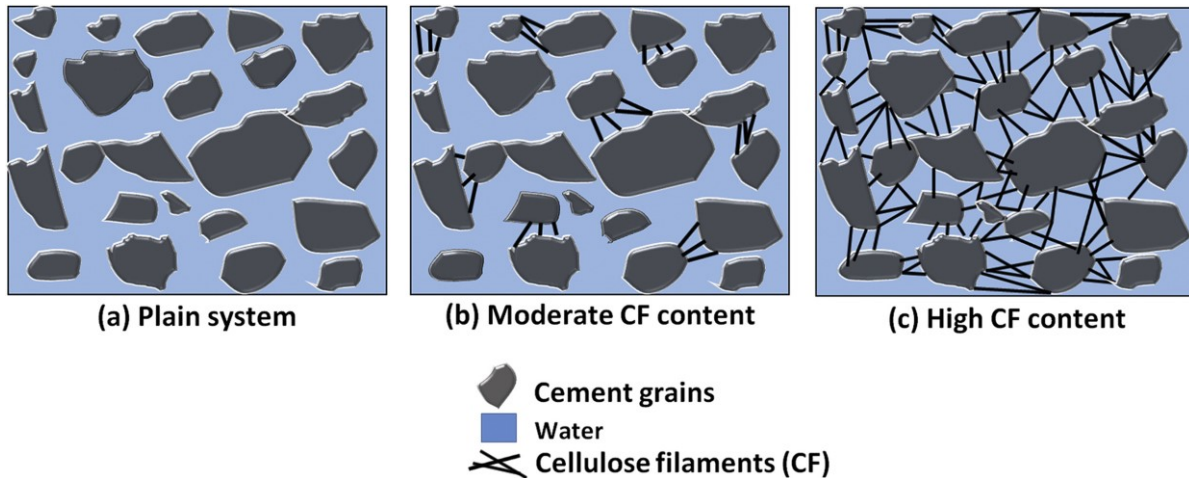


Fig. 8. Schematic illustration of the proposed mechanism contributing to explaining the viscosity modifying effect of cellulose filaments (formation and buildup of network of CF).

To implement Eq. (2), the supplier-provided aspect ratio of CF (100–1000) was used. While this initial aspect ratio of CF varies across a large range, it has been reported that fiber processing such as pre-treatment or dispersion process can lead to significant fiber shortening, thereby decreasing the aspect ratio [39]. Depending on fiber processing prior to incorporation into the matrix, the final aspect ratio can drop to 25-500 [2]. As such, in light of the morphological similarities between CF and microfibrillated cellulose (MFC)-also having nanometric diameter but micrometric length, an aspect ratio of 250 has been inferred from MFC dimensions reported in the literature [2, 40, 41, 42]. This value still represents the highest aspect ratio among all common nanocellulose materials, namely, NFC (≈ 100) [2], CNC (≈ 50) [5], and BC (≈ 10) [2]. At the aspect ratio of 250 adapted for CF, the above percolation model estimates the percolation threshold at a CF volume fraction of 0.249%. This corresponds to a CF mass fraction of 0.12%. Considering that the above model predicts the percolation threshold in an inert medium, the geometrical percolation threshold of 0.12 wt. % is expected to be slightly different in the cement matrix due to the effect of different charged species. Nonetheless, it may be used as an indicator for the concentration of CF where a continuous network of filaments develops in an inert medium.

Physically, when a dispersed material reaches a percolation threshold, its bulk material properties undergo some sudden transitions such as from insulation to conductivity in electric conductors [43] and from shear thinning to shear thickening in rheology [37]. In this regard, the rheological measurements of paste mixtures discussed in the previous section indicate that both the yield stress and plastic viscosity undergo a sudden increase beyond a CF concentration of 0.10%. This is quite close to the CF percolation threshold of 0.12% predicted by the percolation model. While more research is needed to understand further mechanisms underpinning the VMA effect of CF, the above observations substantiate that CF—additional to their water retention capacity—can alter mixture viscosity via the formation a fibrillated network. The latter is more likely to increase in complexity when the filaments develop a continuous three-dimensional mesh. At this stage, the mixture rheological parameters would experience abrupt changes as observed in the rheological measurements of tested paste mixtures.

3.1.3. Isothermal calorimetry

Fig. 9 and Fig. 10 present the results of isothermal calorimetry for the different paste mixtures considered in this study. Evaluation of the effect of CF on heat of hydration was deemed necessary because conventionally used VMA often interfere with the kinetics of cement hydration. This is ascribable to the adsorption of the VMA polymer chains onto cement particles, thereby impeding the solubilisation of mineral species in pore solution and influencing the hydration kinetics, in consequence [33]. Fig. 9 shows the heat evolution in the different paste systems. The figure indicates that while the effect of CF can't be clearly captured within the first 6 h or so, higher heat release can be observed beyond the first 6 h in all CF mixtures. Furthermore, the figure shows that in mixtures with CF, the time required to reach the silicate hydration peak was comparable to that of the reference mixture. Moreover, the heat release corresponding to the silicate hydration peak was slightly higher in all mixtures with CF. Additionally, the sulfate depletion peak—particularly for the mixture with 0.30% CF—was slightly higher. On the other hand, the mixture with 0.05% WG exhibited a reduction in heat release ($\approx 5\%$) as well as a noticeable retardation effect as compared to the plain system. While the reference mixture and all mixtures with CF reached the silicate hydration peak at ~ 8.75 h,

the mixture with the 0.05% WG reached the silicate hydration peak 2 h later. This indicates that when CF were used as a VMA at the above tested dosages, no adverse effects on hydration kinetics were noticed. This is, however, not the case in most common VMA which cause retardation such as cellulose-ether-based VMA [44] and some polysaccharides such as Welan Gum [45].

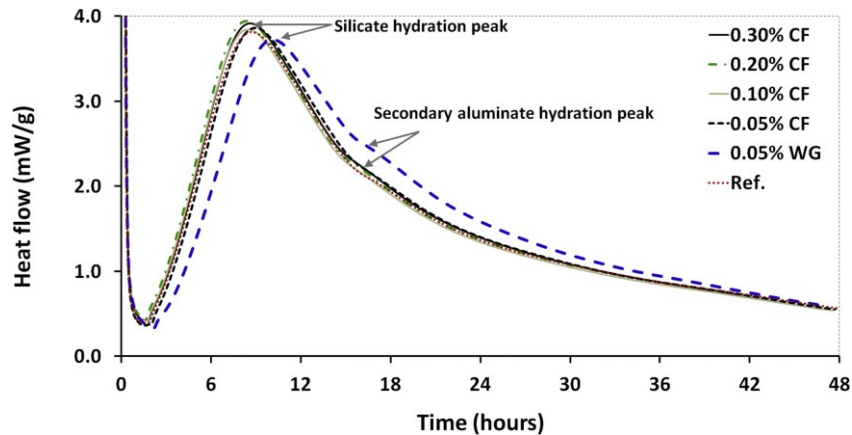


Fig. 9. Evolution of heat of hydration over time for the different paste mixtures.

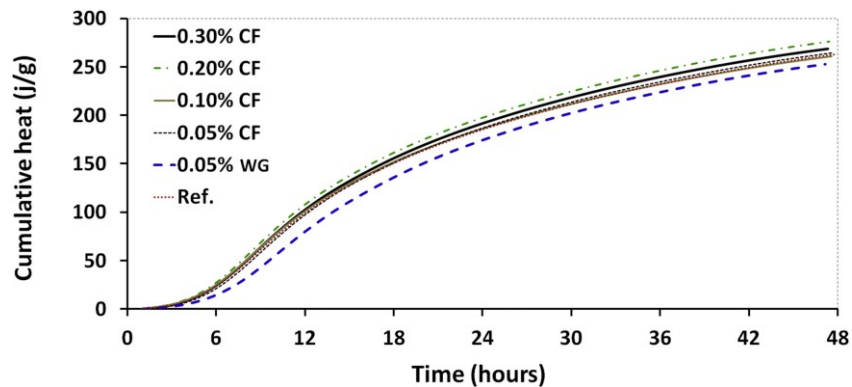


Fig. 10. Cumulative heat release in function of time for the different paste mixtures.

The effect of CF on heat evolution is further confirmed by the cumulative heat release (Fig. 10), whereby the total released heat was relatively higher in all CF mixtures compared to that of the reference. The mixture with 0.30% CF and the one with 0.20% CF, for instance, exhibited, respectively, 7 and 5% higher cumulative heat than that of the reference.

The increased heat of hydration observed in CF-mixtures can be associated with the alkaline hydrolysis of cellulose (at early ages of hydration) or with an curing effect at later ages. At early ages (within the first 24 hrs), the exothermic alkaline hydrolysis reaction of cellulose—producing organic acids and non-acidic products—promotes cement hydration [46]. On the other hand, at relatively later ages (beyond 24 hrs), as the cementitious matrix hardens, the hydrophilic and hygroscopic CF is more likely to serve as an internal curing agent. In this regards, CF could provide supplementary water to foster the hydration process by promoting the solubilisation of further anhydrous cement grains [11].

The increased heat of hydration observed in mixtures with CF is consistent with other relevant studies on nanocellulose materials where increased heat of hydration was reported in a more pronounced manner in cement systems incorporating MCC [7], CNC [8], BC [9], and cellulose-based polymers [47]. This can result in a higher degree of hydration which can influence the mechanical performance [8, 11, 48, 49].

Nonetheless, it should be elucidated that the net effect of cellulose materials on hydration kinetics is primarily contingent on the product of cellulose alkaline hydrolysis [50]. Onuaguluchi et al. [51] indicated that cellulose nanofibers showed some retardation effect at first few hours—due to the viscous nanocellulose suspension impeding the solubilisation of cement active phases—but lead to higher heat release at later ages. Cao et al. [8] reported slight retardation, but overall higher heat with CNC when the latter was used in Type V cement—low C3A—owing to the adherence of CNC to anhydrous cement particles. Tongfei et al. [48] reported attenuated retardation with CNC when Type I/II cement was used owing to the higher content in C3A which has a higher propensity for absorbing CNC. On the other hand, they showed that both CNC source and cement type can significantly influence hydration kinetics.

The correlation between the alkaline hydrolysis of cellulose and the hydration kinetics in cellulose-based cement systems may also explain the retardation effects commonly encountered in conventional natural fibers such as hemp, flax, jute, coir, bamboo, and others. In fact, these fibers contain—in addition to cellulose—other compounds such as hemicelluloses, lignin, and pectin for which the alkaline hydrolysis leads to the formation of water soluble sugars that can impede cement hydration [52]. The dissolution of those soluble sugars produces calcium

compounds which act as inhibitors against the formation of calcium-silicate hydrates (C–S–H), thereby decreasing the heat release [53]. However, this is not exactly the case with nanocellulose materials such as the tested CF composed of mainly cellulose. As such, with the high cellulose purity of CF (cellulose content >95% and hemicellulose content <5% as supported by liquid chromatography), and in the absence of lignin and pectin and other soluble sugars [10], it is expected that the enhancement in cement hydration (due to the alkaline hydrolysis of cellulose) may overcome the impediment of cement hydration (associated with the dissolution of soluble sugars). This may result in a net higher hydration heat as observed herein.

Overall, while test results suggest that the incorporation of CF slightly increases the heat of hydration and does not cause retardation, it can conservatively be concluded that using CF as a VMA does not affect the hydration kinetics. This is particularly important in light of the adverse effects on hydration kinetics encountered when high dosages of conventional VMA are used, though some researchers ascribe such negative effects to the sharp increase in the HRWRA required to maintain a desirable balance between stability and flowability [54].

3.2. Results and discussion of SCC mixtures

As mentioned earlier, two series of SCC mixtures were considered in this study. To facilitate the discussion, each test series is addressed in a separate section. In test series I, in an attempt to capture the bare effect of CF on flow properties and rheological parameters of SCC, the content of HRWRA was kept constant across all mixtures. In test series II, the demand in HRWRA necessary to maintain a target slump-flow diameter of 700 ± 35 mm was adjusted across all mixtures, in an attempt to obtain rheologically comparable systems which are to be assessed for their fresh properties and mechanical performance.

3.2.1. Results of test series I-SCC mixtures (constant HRWRA)

3.2.1.1. Flow properties

The fresh properties of series I-SCC mixtures are displayed in Table 4. Measurements of slump-flow show that while the reference mixture had a spread diameter of 785 mm, the addition of

0.05% WG reduced the spread diameter to 560 mm. On the other hand, SCC mixtures containing CF at 0.10%, 0.15%, and 0.20% recorded further reduction in the spread diameter, namely, 540, 320, and 305 mm, respectively. Thus, mixtures with CF, particularly at 0.15 and 0.20% marked a significant drop in workability. These observations are also consistent with the measurements collected from the J-Ring spread diameter. The reduction in the spread diameter in the mixtures with WG or CF was reflected on the extended flow time. The V-Funnel flow time in the mixture with 0.05% WG and the one with 0.10% CF increased by more than twice as compared to that of the reference mixture. For CF dosages of 0.15% and 0.20%, this increment was more than 7 and 9 times, respectively. Since the dosage of HRWRA was kept constant across all mixtures, the effect of CF on reducing the workability was so significant that for CF dosages of 0.15% and 0.20%, the measurement of T_{500} was not possible since mixtures exhibited very high viscosity. The higher viscosity imparted by CF, enhanced mixture stability. Nonetheless, the stability imparted by CF in this series should be regarded with precaution. This is because the dosage of HRWRA was maintained the same in all mixtures to capture the bare effect of CF on flow properties and rheological parameters. Consequently, reduction in slump-flow, increment in flow-time, and increase in VSI were obviously imperative. The slump-flow of the reference being 780 mm, would definitely imply high fluidity and high risk of segregation. On the other hand, the slump-flow in all other mixtures was far lower than that of the reference, which by itself influences the stability. For this reason, it is remarkable that for a recommended slump-flow diameter between 500 and 700 mm and a T_{500} between 2 and 5 s as suggested by Nagataki and Fujiwara [55] and a V-Funnel flow time between 6 and 12 s as recommended by EFNARC [23], only the mixture with 0.05% WG and the one with 0.10% CF can be viewed as satisfactory since the dosage of HRWRA was kept constant in all mixtures.

Table 4. Fresh properties of series I-SCC mixtures.

SCC (series I)	Mixtures	Air content (%)	Unit weight (kg/m ³)	Slump flow		VSI	J-Ring Diameter (mm)	V-Funnel flow time (sec)
				Diameter (mm)	T ₅₀₀ (sec)			
Ref.		1.0	2315	785	1.83	2	770	2.13
0.05%WG		2.3	2386	560	2.83	1	470	5.22
0.10% CF		1.5	2373	540	5.12	1	455	5.34
0.15% CF		3.0	2316	320	-	0	310	14.75
0.20% CF		3.1	2320	305	-	0	300	20.34

3.2.1.2. Rheology

Fig. 11 and Fig. 12 present the rheological measurements of series I-SCC mixtures. Fig. 11 displays the rheological response represented by the relationship between the shear stress (τ) and the shear rate (γ'). This was done by fitting the flow behavior to the Bingham model:

$$\tau = \tau_0 + \mu_p \gamma' \quad (3)$$

Where τ_0 = yield stress and μ_p = plastic viscosity.

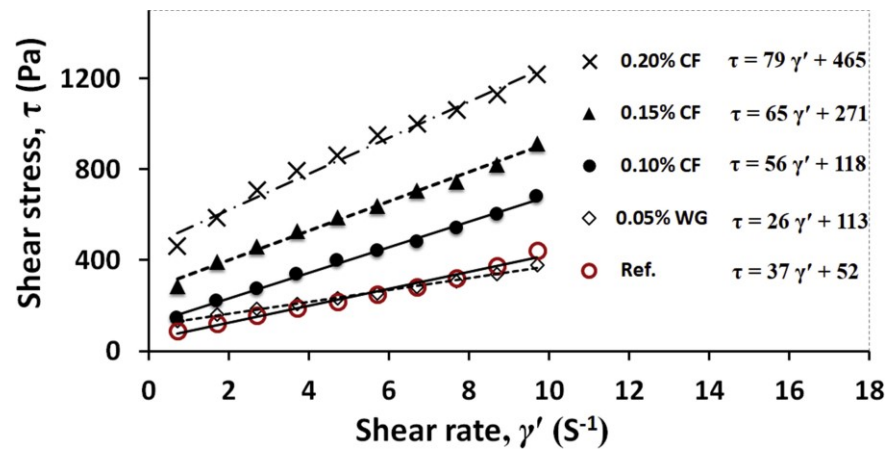


Fig. 11. Shear stress (τ)–shear rate (γ') response in series I–SCC mixtures.

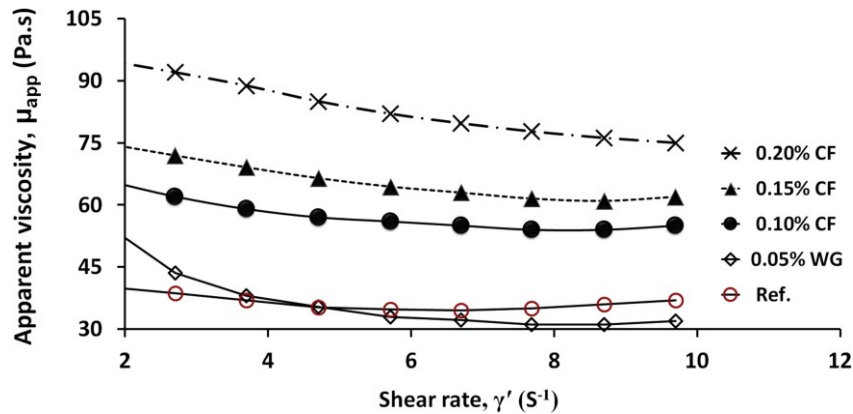


Fig. 12. Variation of apparent viscosity (μ_{ap}) in function of shear rate (γ') in series I–SCC mixtures.

Fig. 11 shows increased viscosity at low shear rates as expressed by the higher yield stress when CF were used. The yield stress in the reference mixture was 52 Pa. In the mixture with 0.05 WG and the mixtures with CF (0.1, 0.15, and 0.20%), the yield stress was 113, 118, 271, 465 Pa. This corresponds to increments in yield stress of, respectively, 2.2, 2.3, 5.2, and 8.9 times that of reference. In contrast to the sharp increase in the yield stress, the increment in plastic viscosity was relatively less sharp as can be inferred from the flow curves which are almost parallel to that of the reference (with the exception of the mixture with 0.30% CF). The plastic viscosity of the reference mixture was 37 Pa s. In the mixture with 0.05%WG and the mixtures with CF (0.1, 0.15, and 0.20%), the plastic viscosity was equal to 26, 56, 65, and 79 Pa s, respectively. This corresponds to increments in plastic viscosity of, respectively, 0.7, 1.5, 1.8, and 2.1 times that of the reference.

The increased yield stress (hence the higher viscosity at low shear rates) observed herein is also consistent with the reduced workability in CF-mixtures observed in the previous section. On the other hand, the relatively attenuated plastic viscosity at high shear rates can be associated with shear thinning—or pseudoplastic—behavior imparted by CF. This is better illustrated in Fig. 12 showing the relationship between the apparent viscosity (μ_{ap}) and shear rate (γ'). The figure indicates that SCC mixtures with WG or CF exhibited a shear thinning behavior where the apparent viscosity decreases with the increase in shear rate. Such a trend was not evident in the

reference mixture where the variation in the apparent viscosity as shear rate increases was very subtle. The shear thinning behavior observed in mixtures with CF is traceable to the fact that at low shear rates, the long and flexible nanocellulose fibrils may intertwine and entangle to inhibit deformation, thereby accelerating the viscosity buildup and increasing the apparent viscosity. As CF concentration increases, the intertwining and entanglements may form a structured network. This further increases the yield stress and the apparent viscosity. With increasing shear rates, however, most likely CF entanglements are dislodged, CF networks are pulverized, and individual filaments are streamlined in the direction of the flow, thereby decreasing the mixture resistance to deformation and yielding a reduction in apparent viscosity as observed.

The pseudoplasticity is an interesting feature in cement mixtures as the high apparent viscosity at low shear rates enhances the capacity of mixtures to maintain their constituents in suspension, thereby reducing the rate of sedimentation of fines and segregation of aggregates. On the other hand, the reduced apparent viscosity exhibited at high shear rates—due to the shear thinning behavior—facilitates pumping and placing [15].

3.2.2. Results of series II-SCC mixtures (variable HRWRA dosage)

3.2.2.1. Flow properties

Table 5 presents the flow properties of series II-SCC mixtures. Measurements of slump-flow show that all tested mixtures exhibited a slump-flow of approximately 700 ± 35 mm. The slump-flow of 710 mm in the reference mixture in this test series—as compared to 785 mm in series I—is due to the reduction in HRWRA from 2.5 to 2.0 L/m³. This adjustment was deemed necessary in an attempt to reduce the risk of segregation in the reference mixture. While increasing the HRWRA dosage in mixtures with WG or CF was imperative to achieve a target slump-flow comparable to that of the reference, the demand in HRWRA was substantially high at increasing CF dosages (Fig. 13). The increase in HRWRA demand in the mixtures with 0.05% WG, 0.05% CF, and 0.10% CF was, respectively, 15, 15, and 27% relative to the reference. For the mixtures with 0.15 and 0.20% CF, however, this increase corresponds to 58 and 138%, respectively. The above slump-flow results are within the EFNARC range for slump-flow class II (660–750 mm) and are also consistent with the measurements of J-Ring spread. While all mixtures had

comparable slump-flow, it is observable that with increasing CF content, mixtures have high resistance to deformation particularly in the presence of obstacles. This was reflected in the results of J-ring test where relatively lower spread diameter was recorded in mixtures with high CF (0.15 and 0.20% CF). Likewise, the blockage ratio for both J-ring and L-box was relatively lower as CF dosage increases. However, this trend is not the same in the flow time. The flow time evaluated by the T_{500} , the V-funnel passing time, and the L-Box passing time was observed to increase with the incorporation of CF up to a content of 0.10%. Beyond 0.10% CF, the flow time was observed to reduce relatively. While further work is needed to reconcile between the increased viscosity with the reduced flow-time in mixtures with high CF content, this feature may be linked to the significant amount of HRWRA—used in mixtures with CF content beyond 0.10%—which may reduce the flow time. However, this reduced flow-time may not be necessarily translated into higher passing ability due to the effect of CF on creating a fibrillated network, thereby increasing the self-assembly of mixture constituents and interfering with the obstacles (bars) in the J-ring and L-Box test. The self-assembly feature imparted by CF on SCC enhances mixture homogeneity and stability. As a result, all mixtures with CF recorded higher visual stability index (0 = highly stable or 1 = stable) than the reference mixture (2 = unstable) as expected.

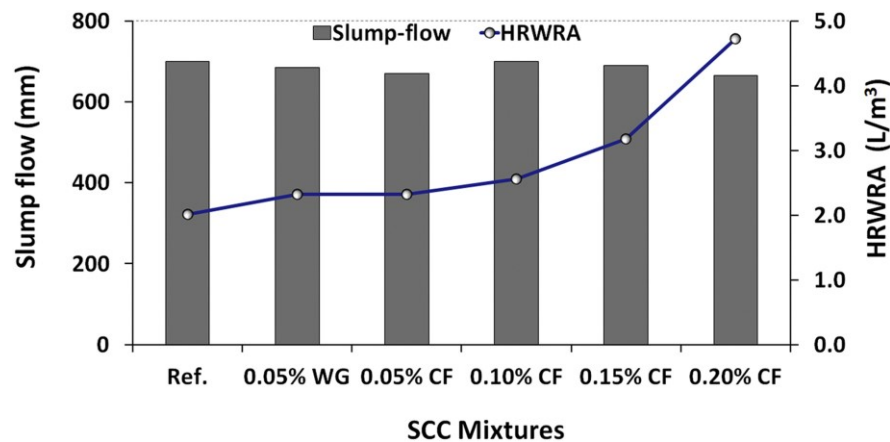


Fig. 13. Variation of mixture demand in high range water reducer (HRWR) across the different series II–SCC mixtures.

Table 5. Fresh properties of series II-SCC mixtures.

SCC mixtures (series II)	Air content (%)	Unit weight (kg/m ³)	Slump flow		VSI	J-Ring		V-Funnel flow time (sec)	L-Box	
			Diameter (mm)	T_{500} (sec)		Diameter (mm)	Blockage ratio		Time (s)	Blockage ratio
Ref.	1.7	2328	700	1.94	2	685	0.86	3.47	1.92	0.83
0.05% WG	3.5	2351	685	2.10	1	660	0.83	5.02	1.89	0.83
0.05% CF	2.1	2369	670	2.20	1	620	0.82	5.06	1.97	0.83
0.10% CF	2.3	2336	700	1.85	1	630	0.82	4.73	1.86	0.82
0.15% CF	2.6	2341	690	1.75	0	600	0.81	4.01	1.81	0.81
0.20% CF	3.1	2352	665	1.60	0	570	0.81	3.50	1.78	0.81

3.2.2.2. Rheology

Fig. 14 and Table 6 present the rheological measurements of test series II-SCC mixtures. Fig. 14 displays the rheological response fitted to the Bingham model. Results indicate that for the mixture with 0.05%WG and the one with 0.05% CF, the rheological parameters were quite comparable to that of the reference: yield stress ~ 28 Pa and plastic viscosity ~ 15 Pa s. However, for the mixtures with 0.01, 0.15 and 0.20% CF, the yield stresses (38.12, 48.39, 57.95 Pa s, respectively) and plastic viscosities (16.95, 17.15, and 19.62, respectively) were higher. Furthermore, the increase in plastic viscosity is lower than the increase in yield stress. The increase in yield stress and plastic viscosity at high CF dosage explains the significant demand in HRWRA (Fig. 13). On the other hand, the increase in HRWRA in function of CF dosage reveals that at approximately 0.15% CF, the HRWRA demand increases substantially as reflected by the inflection in the trend. The CF dosage of 0.15% is in the vicinity of the percolation threshold of 0.12% identified earlier. These observations further confirm the existence of a CF content beyond which rheological measurements undergo abrupt changes due to the formation of a network of interconnected CF fibrils. This obviously increases mixture resistance to deformation and leads to a substantial increase in the HRWRA necessary to achieve a target slump-flow diameter.

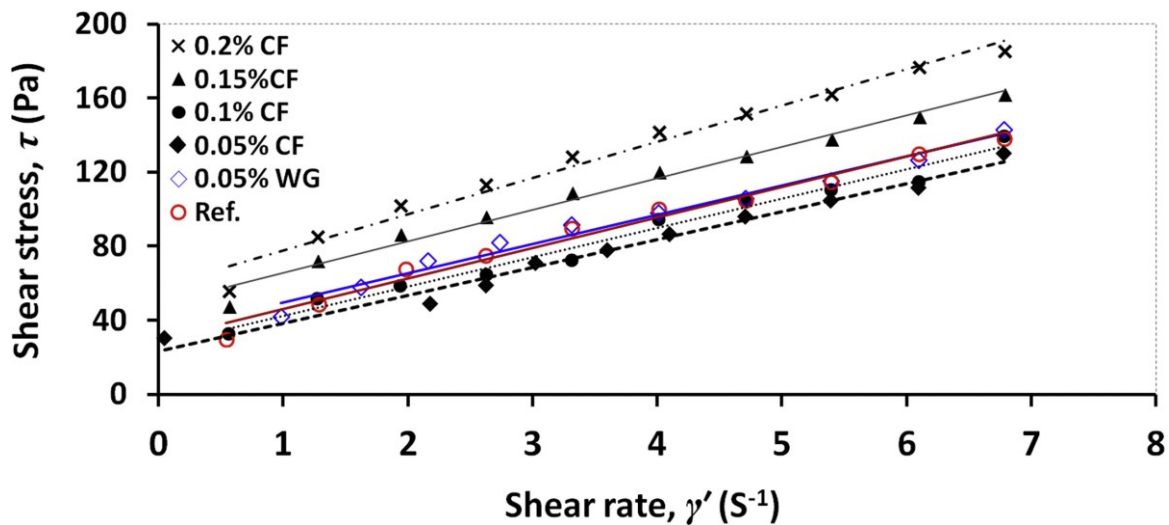


Fig. 14. Shear stress (τ)–shear rate (γ') response in series II-SCC mixtures.

Table 6. Rheological parameters of series II-SCC mixtures

SCC Mixtures	Yield stress (Pa)	Plastic viscosity (Pa.s)
Ref.	16,445	29,558
0.05%wg	15,79	29,75
0.05% CF	15,847	26,585
0.10% CF	16,85	38
0.15% CF	17,035	48,39
0.20% CF	19,616	57,947

3.2.2.3. Strength development

3.2.2.3.1. Compressive strength

Table 7 shows all tested mechanical properties for series II-SCC mixtures. Results indicate that the overall effect of tested dosages of WG and CF on compressive strength varies with the curing age. At one day for instance, all mixtures recorded slightly lower strength relative to the that of the reference, except the mixture with 0.05% CF which had about 8% higher strength. From 7 to 28 days, strength parity or enhancement was achieved by all mixtures. The enhancements in compressive strength in the mixtures with 0.05% WG, 0.05%CF, 0.10%CF, and 0.15% CF correspond to 10, 12, 10, and 3% respectively. On the other hand, the mixture with 0.20% exhibited a comparable strength to that of the reference. The lower compressive strength recorded at early age (1 day) in the mixture with 0.05% WG may be correlated with the possible interference between the VMA polymer chains adsorbed on cement grains and the precipitation of cement active phases. This may affect the hydration kinetics and delay the strength development [45] as observed herein. This is also consistent with the calorimetry results depicted earlier in Fig. 9, Fig. 10 where the mixture with 0.05% WG exhibited about 2 h retardation in the time required to reach the silicate hydration peak, 5% lower heat release at silicate hydration peak, and 4% lower cumulative heat release. On the other hand, in mixtures with CF, the decreased 1-day strength with higher CF dosage can be linked to poor CF dispersion at higher dosages [10], while the enhanced strength afterwards can be attributed to the time-dependent development of bond between nanocellulose materials and cement hydrates [49]. Interpretations by Hoyos et al. [7] indicate that as cement hydration proceeds, the

omnipresence of OH⁻ groups on the surface of nanocellulose materials can promote the formation of hydrogen bonds with hydration products containing hydrogen in their structure such as calcium-silicate-hydrate (C-S-H) and calcium hydroxide (CH). The increased strength in mixtures with CF is also in harmony with the higher heat release (up to 7%) observed in all mixtures containing CF.

Table 7. Mechanical properties of series II-SCC mixtures

SCC Mixtures (series II)	Mechanical properties				
	Compressive strength, f_c (MPa) in function of curing age (days)			Splitting-tensile strength, f_{sp} (MPa) at 28 days	Flexural capacity, f_{fl} (MPa) at 28 days
	1	7	28		
Ref.	22.2±0.15	35.6±1.52	42,6±1.25	3.41± 0.12	6.90±0.42
0,05% WG	22.0±0.31	36.8±1.25	46,9±0.44	3.48± 0.14	7.53±0.15
0.05% CF	24.0±1.62	38.1±1.37	47,8±3.37	4.31± 0.11	8.49±0.55
0.10% CF	22.0±0.87	34.3±0.97	46,8±1.50	4.27± 0.21	7.80±0.10
0.15% CF	20.0±0.85	33.0±1.00	44,0±1.30	4.15± 0.32	7.62±0.15
0.20% CF	19.1±0.80	33.3±1.38	42,1±1.85	4.01± 0.22	7.31±0.37

3.2.2.3.2. Flexural capacity and splitting-tensile strength

The effect of CF on mechanical properties of concrete is more evident on the flexural capacity (f_{fl}) and the splitting-tensile strength (f_{sp}) where the fibrillated morphology of CF is more likely to reinforce the matrix at the micro/nano scale. While the measurements of f_{sp} and f_{fl} shown in Table 7 indicate that overall all mixtures had higher capacity than the reference (due to the stability imparted by the VMA effect thereby enhancing the homogeneity in the hardened product), it should be noted that mixtures incorporating CF exhibited further enhancement in both f_{fl} and f_{sp} . In flexural capacity for instance, the mixture with 0.05% WG had an enhancement of 8% relative to the reference. In mixtures with CF (0.05, 0.10, 0.15, and 0.20%), this enhancement corresponds to 21, 12, 9, and 5%, respectively. Similar trend can be observed for the f_{sp} where mixtures containing WG or CF recorded higher strength compared to the reference, with higher enhancement in f_{sp} obtained at low CF concentrations. In fact, the mixture with 0.05 WG showed comparable (2%) strength to that of the reference. For mixtures

with CF (0.05, 0.10, 0.15, and 0.20%), however, the enhancement in f_{sp} was, respectively, 26, 25, 22, and 18% relative to the reference mixture.

As such, whereas all tested CF dosage have a positive effect on both f_{sp} and f_{fl} , the highest gain shows at lower CF dosages (between 0.05 and 0.10%) where CF dispersion and hence the reinforcing effect are believed to be more prominent. The increased tensile and flexural properties in mixtures with CF may stem from the higher elastic modulus of the crystalline portion of nanostructured cellulose materials approaching 138 GP [56]. It can also be attributed to the hydrophilic and hygroscopic CF serving as an internal curing agent. In this regard, Hisseine et al. [10] showed that, with the incorporation of CF, the autogenous shrinkage (at 7 days) of low water-to-binder ratio cement pastes was reduced by up to 36%. Moreover, microstructure investigations and nanoindentation assessments indicated that CF can increase the degree the hydration and result into a hydrated system with a C-S-H having higher micromechanical properties (indentation modulus M and hardness N) [11]. Similarly, Cao et al. [8] suggested that the use of cellulose nanocrystals improves the flexural capacity owing to an improved degree of hydration and an increased stiffness of high density (C-S-H) surrounding unhydrated cement particles. Likewise, interpretations by Flores et al. [49] indicate that the incorporation of CNC could result in a larger volume fraction of high density C-S-H and a smaller volume fraction of low-density C-S-H. Such effects on the microstructure can have direct implications on macro-mechanical performance as observed in this experimental campaign. The above results suggest that while conventionally used VMA can still improve mechanical performance via enhancing mixture stability and homogeneity, the use of CF in this perspective can have the further advantage of providing a nanoreinforcing system to the matrix. Such a feature is not evident with commercially available VMA some of which are water soluble.

On the other hand, while the mechanical performance reported herein is limited to test series II-SCC having comparable flow properties, the effect of CF on increasing the mechanical performance was also evident even in series I-mixtures (having similar HRWRA content) as reported elsewhere [10]. In fact, in this test series where the HRWRA content was kept constant, the plain mixture has obviously higher flowability compared to mixtures with CF. As a result,

the amounts of rheologically-active water and HRWRA are higher in the reference mixture than in counterpart mixtures. This leads to better deflocculation of cement flocks, thereby fostering cement dispersion and increasing the degree of cement hydration in the plain mixture than in mixtures with CF. Nonetheless, the effect of CF on enhancing the mechanical performance was quite evident. Strength improvements of up to 16% (in compression), 34% (in splitting tension), 22% (in flexure), and 96% (in energy absorption) were obtained [10].

3.2.2.3.3. Microstructure analysis

Microstructure investigations conducted by FEG-SEM on cement pastes and SCC samples revealed that CF adhere intimately into the structure of the cementitious matrix. Fig. 15 shows a fresh fractured paste sample with 0.20% CF. The figure shows several CF well cemented into the matrix, bridging hydrates, and interfering with the matrix porous network. Furthermore, Fig. 16 depicts a fresh fractured SCC mixture with 0.20% CF. The figure shows an aggregate surrounded by a paste layer with the interfacial transition zone (ITZ) between the paste and the aggregate being reinforced by several filaments. While the micromechanical properties of the ITZ in the presence of CF are still to be evaluated to disclose the effect of CF on strengthening this region most often perceived as the weakest link in the bulk cement matrix, the observed presence of CF in the ITZ may favor increasing the micro-mechanical properties. This may also substantiate the enhanced mechanical performance at the macroscale, particularly flexural capacity and splitting-tensile strength discussed in the previous section.

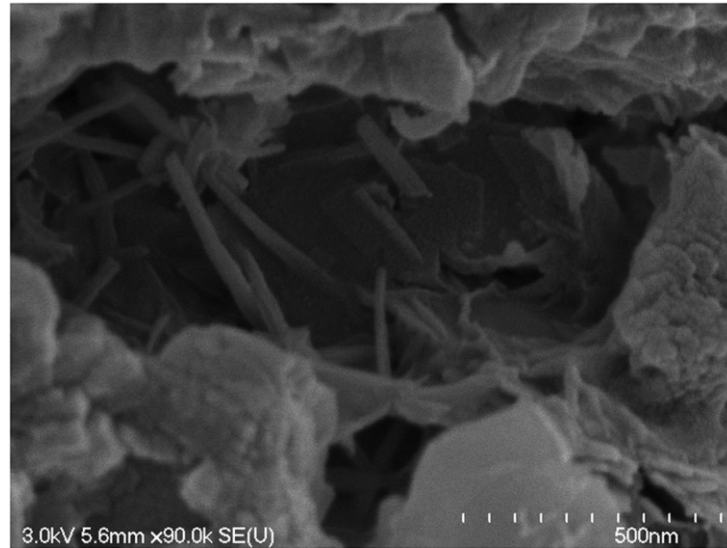


Fig. 15. Scanning Electron Microscopy (SEM) image of a cement paste with 0.20% CF. The image illustrates a network of cellulose filaments (CF) reinforcing the matrix

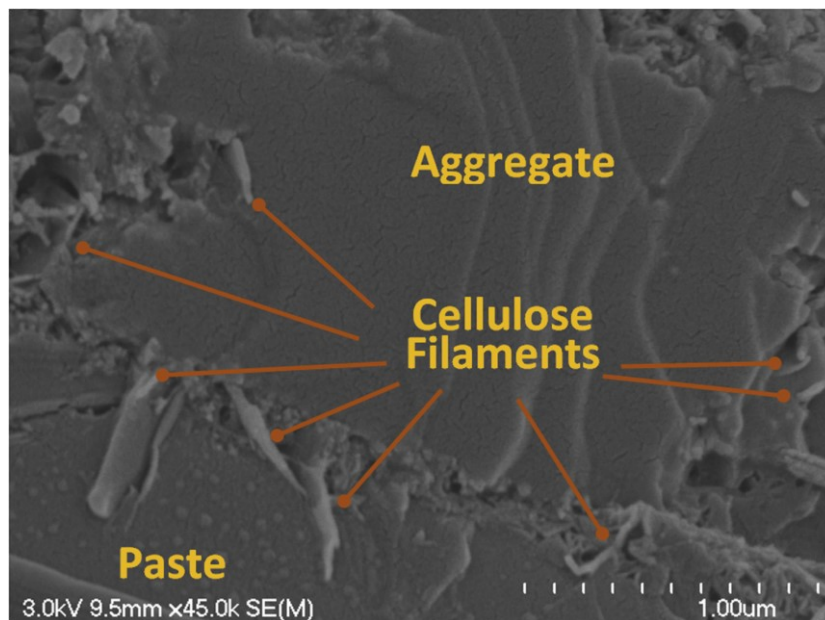


Fig. 16. SEM image of an SCC mixture with 0.20% CF. The image shows a transition zone (between cement paste and an aggregate) reinforced and with CF. Adapted from Hisseine et al. [10].

4. Summary and conclusions

This study was aimed at investigating the viability and limitations of using cellulose filaments (CF)—a new type of nanocellulose materials—as a viscosity modifying admixture (VMA) for self-consolidating concrete (SCC) applications. The properties of cement pastes and SCC incorporating CF (at concentrations of 0.05, 0.10, 0.15, 0.20, and 0.30% per weight of binder) were examined and compared to those obtained from plain systems and systems incorporating a commercial VMA of Welan Gum (WG) type at a dosage of 0.05%. In cement pastes, the effect of CF on heat of hydration was also evaluated. Overall, results indicate that the incorporation of CF (even at low concentrations) slightly increases the heat of hydration, but significantly influences fresh properties, rheology, and mechanical performance. Specific findings are as follows:

- Within the tested CF dosages, no adverse effects on hydration kinetics were noticed. Rather, slightly higher heat release (up to $\approx 7\%$) can be obtained without any retardation effects, in contrast to many commercially available VMA causing some retardation.
- CF have a significant viscosity modifying effect. The filaments improve mixture stability by increasing the yield stress and the plastic viscosity of cement pastes and SCC. However, the effect of CF on the yield stress appears to be higher than that on the plastic viscosity. This is attributed to the shear thinning effect imparted by the nanocellulose fibrils to CF mixtures. This feature allows CF systems to have high apparent viscosity—at low shear rates—necessary for stability, but low apparent viscosity—at high shear rates—necessary for improving pumpability.
- Additional to the water retention capacity (which is an intrinsic feature of the hydrophilic CF), results indicate that the long and flexible CF fibrils can form a network which significantly increases mixture viscosity. A geometry-based percolation model indicated that at a CF concentration corresponding to the percolation threshold (0.12 wt.%), the rheological properties (yield stress and plastic viscosity) of paste mixtures undergo abrupt increases. In SCC mixtures, at CF concentrations between 0.10 and 0.15% (the interval that includes the percolation threshold), the mixture demand

in HRWRA recoded a noticeable increase. As a result, within the limits of CF dispersion technique used in this study, a CF content below 0.12% is recommended to produce stable SCC mixtures having a HRWRA demand comparable to that of a typical mixture with a conventional VMA, but with higher mechanical performance.

- While both WG and CF showed positive effects on mechanical performance due to the enhanced homogeneity and stability, results indicated that mixtures with CF have further improved the flexural capacity and tensile splitting strength of SCC by up to 21 and 26%, respectively. This is attributed to the fibrillated morphology and reinforcing ability of CF (as also substantiated by the microstructural assessments). Such features are, though, not evident with conventional VMA.
- The effectiveness of CF is more prominent at lower concentrations where CF dispersion is more evident. This is associated with the high surface area leading to filament self-assembly and formation of CF networks at increasing CF content. While this feature plays an important role in the VMA effect of CF, the higher mechanical performance achieved at lower CF concentrations than at higher ones, as well as the substantial increase in HRWRA demand when CF content exceeds the percolation threshold, indicate that CF dispersion significantly influences composite performance. Therefore, further research with better CF dispersion is recommended to allow achieving optimum composite performance.

Acknowledgments

This project is jointly supported by a Collaborative Research and Development (CRD) grant from the Natural Sciences and Engineering Research Council of Canada (NSERC), Canada Vanier Graduate Scholarship (CGS) program award no: 360284 offered to the first author, Kruger Inc., and Euclid Chemicals. The authors are grateful to the gracious support from the different partners. The authors also acknowledge the contribution of Prof. Ammar Yahia through the research facility of his Industrial Research Chair for the Development of Fluid Concretes with Adaptive Rheology.

References

- [1] F. Sanchez, K. Sobolev, Nanotechnology in concrete – a review, *Construct. Build. Mater.* 24 (11) (2010) 2060–2071.
- [2] R.J. Moon, A. Martini, J. Nairn, J. Simonsen, J. Youngblood, Cellulose nanomaterials review: structure, properties and nanocomposites, *Chem. Soc. Rev.* 40 (2011) 3941–3994.
- [3] J.E. Goodsell, R.J. Moon, A. Huizar, R.B. Pipes, A strategy for prediction of the elastic properties of epoxy-cellulose nanocrystal-reinforced fiber networks, *Nord. Pulp Pap Res. J.* 29 (1) (2014) 85–94.
- [4] Y. Habibi, A. Dufresne, Highly filled bionanocomposites from functionalized polysaccharide nanocrystals, *Biomacromolecules* 9 (7) (2008) 1974–1980.
- [5] L. Brinchi, F. Cotana, E. Fortunati, J.M. Kenny, Production of nanocrystalline cellulose from lignocellulosic biomass: technology and applications, *Carbohydr. Polym.* 94 (2013) 154–169.
- [6] S.J. Peters, T.S. Rushing, E.N. Landis, T.K. Cummins, Nanocellulose and microcellulose fibers for concrete, *Transport. Res. Rec.* 2142 (2010) 25–28.
- [7] C.G. Hoyos, E. Cristia, A. Vázquez, Effect of cellulose microcrystalline particles on the properties of cement-based composites, *Mater. Des.* 51 (2013) 810–818.
- [8] Y. Cao, P. Zavaterra, J. Youngblood, R. Moon, J. Weiss, The influence of cellulose nanocrystal additions on the performance of cement paste, *Cement Concr. Compos.* 56 (2015) 73–83.
- [9] F. Mohammadkazemi, K. Doosthoseini, E. Ganjian, M. Azin, Manufacturing of bacterial nano-cellulose reinforced fiber-cement composites, *Construct. Build. Mater.* 101 (2015) 958–964.
- [10] O.A. Hisseine, A.F. Omran, A. Tagnit-Hamou, Influence of cellulose filaments on cement pastes and concrete. *ASCE Journal of Materials in Civil Engineering*, 30(6): 04018109.
- [11] Hisseine, O. A, Wilson, W., Sorelli, L., and Tagnit-Hamou, A. (2019a) Nanocellulose for improving mechanical properties of concrete: A macro-to-micro investigation for

- disclosing the effects of cellulose filaments on strength of cement systems. *Construction and Building Materials* 206: 84–96.
- [12] K.H. Khayat KH, Z. Guizani, Use of viscosity modifying admixtures to enhance stability of fluid concrete, *ACI Mater. J.* 94 (1997) 332–340.
- [13] W. Schmidt, H.J.H. Brouwers, H.C. Kühne, B. Meng, Interactions of polysaccharide stabilising agents with early cement hydration without and in the presence of superplasticizers, *Construct. Build. Mater.* 139 (2017).
- [14] K.H. Khayat, Viscosity-enhancing admixtures for cement-based materials — an overview, *Cement Concr. Compos.* 20 (2–3) (1998) 171–188.
- [15] V.A. Ghio, P.J.M. Monteiro, Bond strength of reinforcing bars in reinforced shotcrete, *ACI Mater. J.* 94 (1997) 111–118.
- [16] K.H. Khayat, J. Assaad, Air void stability of self-consolidating concrete, *ACI Mater. J.* 99 (2002) 408–416.
- [17] M. Lachemi, K.M.A. Hossain, V. Lambros, P.C. Nkinamubanzi, N. Bouzoubaa, Performance of new viscosity modifying admixtures in enhancing the rheological properties of cement paste, *Cement Concr. Res.* 34 (2004) 185–193.
- [18] ASTM C494/C494M-16 Standard Specification for Chemical Admixtures for Concrete, ASTM International, West Conshohocken, PA, 2016.
- [19] ASTM C305-14 Standard Practice for Mechanical Mixing of Hydraulic Cement Pastes and Mortars of Plastic Consistency, ASTM International, West Conshohocken, PA, 2014.
- [20] K.H. Khayat, A. Yahia, Simple field tests to characterize fluidity and washout resistance of structural cement grout, *Cem. Concr. Aggregates* 20 (1) (1998) 145–156.
- [21] M. Sonebi, Rheological properties of grouts with viscosity modifying agents as diutan gum and welan gum incorporating pulverised fly ash, *Cement Concr. Res.* 36 (2006) 1609–1618.
- [22] ASTM C1611/C1611M-14 Standard Test Method for Slump Flow of Self-consolidating Concrete, ASTM International, West Conshohocken, PA, 2014.

- [23] EFNARC 2005, Specification and Guidelines for Self-consolidating Concrete, European Federation of Producers and Contractors of Specialist Products for Structures, Surrey, 2005, p. 32.
- [24] ASTM C39/C39M-16 Standard Test Method for Compressive Strength of Cylindrical Concrete Specimens, ASTM International, West Conshohocken, PA, 2016.
- [25] ASTM C496/C496M-11 Standard Test Method for Splitting Tensile Strength of Cylindrical Concrete Specimens, ASTM International, West Conshohocken, PA, 2004 (Reapproved 2011).
- [26] ASTM C78/C78M-16 Standard Test Method for Flexural Strength of Concrete (Using
- [27] Simple Beam with Third-Point Loading), ASTM International, West Conshohocken, PA, 2016.
- [28] A.C. Chami-Khazraji, S. Sylvain Robert, Self-assembly and intermolecular forces when cellulose and water interact using molecular modeling, *J. Nanomater.* (2013) 745979, <https://doi.org/10.1155/2013/745979>.
- [29] J. George, S. Sabapathi, Cellulose nanocrystals: synthesis, functional properties, and applications, *Nanotechnol. Sci. Appl.* 8 (2015) 45–54 S64386.
- [30] J. Pouchez, A. Peschard, P. Crosseau, R. Guyonnet, B. Guilhot, F. Vallée, HPMC and HEMC influence on cement hydration, *Cement Concr. Res.* 36 (2) (2006) 288–294.
- [31] R. Schueler, J. Petermann, K. Schulte, H.-P. Wentzel, Agglomeration and electrical percolation behavior of carbon black dispersed in epoxy resin, *J. Appl. Polym. Sci.* 63 (13) (1997) 1741–1746.
- [32] A. Dufresne, Nanocellulose: a new ageless bionanomaterial, *Mater. Today* 16 (6) (2013) 220–227.
- [33] J. Bras, D. Viet, C. Bruzzese, A. Dufresne, Correlation between stiffness of sheets prepared from cellulose whiskers and nanoparticles dimensions, *Carbohydr. Polym.* 1 (2011) 211–215.
- [34] S. Iwamoto, A. Nakagaito, H. Yano, *Appl. Phys. A* 89 (2) (2007) 461–466. A.K. Kota, B.H. Cipriano, M.K. Duesterberg, A.L. Gershon, D. Powell, S.R. Raghavan, et al.,

- Electrical and rheological percolation in polystyrene/MWCNT nanocomposites, *Macromolecules* 40 (2007) 7400–7406.
- [35] [35] D.P. Bentz, E.J. Garboczi, Percolation of phases in a three-dimensional cement paste microstructural model, *Cement Concr. Res.* 21 (2) (1991) 325–344.
- [36] K.L. Scrivener, K.M. Nemati, The percolation of pore space in the cement paste/aggregate interfacial zone of concrete, *Cement Concr. Res.* 26 (1) (1996) 35–40.
- [37] Y. Cao, P. Zavattieri, J. Youngblood, R. Moon, J. Weiss, The relationship between cellulose nanocrystal dispersion and strength, *Construct. Build. Mater.* 119 (2016) 71–79.
- [38] E. Garboczi, K. Snyder, J. Douglas, Geometrical percolation threshold of overlapping ellipsoids, *Phys. Rev. E* 52 (1) (1995) 819–828.
- [39] M.J. Lundahl, V. Klar, L. Wang, M. Ago, O.J. Rojast, Spinning of Cellulose Nanofibrils into Filaments: A Review, *Ind. Eng. Chem. Res.* 56 (1) (2017) 8–19, <https://doi.org/10.1021/acs.iecr.6b04010>.
- [40] A. Dufresne, J.Y. Cavaille, M.R. Vignon, Mechanical behavior of sheets prepared from sugar beet cellulose microfibrils, *J. Appl. Polym. Sci.* 64 (1997) 1185–1194.
- [41] A.K. Turbak, F.W. Snyder, K.R. Sandberg, Microfibrillated cellulose, a new cellulose product: properties, uses, and commercial potential, *J. Appl. Polym. Sci.: Appl. Polym. Symp.* 37 (1983) 815–827.
- [42] C. Rondeau-Mouro, B. Bouchet, B. Pontoire, P. Robert, J. Mazoyer, A. Buleon, Structural features and potential texturising properties of lemon and maize cellulose microfibrils, *Carbohydr. Polym* 53 (2003) 241–252.
- [43] W. Tian, R. Yang, Effect of interface scattering on phonon thermal conductivity percolation in random nanowire composites, *Appl. Phys. Lett.* 90 (2007) 2631051–2631053.
- [44] J. Pourchez, P. Grosseau, R. Guyonnet, B. Ruot, HEC influence on cement hydration measured by conductometry, *Cement Concr. Res.* 36 (9) (2006).
- [45] K.H. Khayat, A. Yahia, Effect of welan gum-highrange water reducer combinations on rheology of cement grout, *ACI Mater. J.* 94 (1997) 365–372.

- [46] C.J. Knill, J.F. Kennedy, Degradation of cellulose under alkaline conditions, *Carbohydr. Polym.* 51 (2003) 281–300.
- [47] P.C. Mishra, V.K. Singh, K.K. Narang, N.K. Singh, Effect of carboxymethyl-cellulose on the properties of cement, *Mater. Sci. Eng.* 357 (2003) 13–19.
- [48] [T. Fu, F. Montes, P. Suraneni, J. Youngblood, J. Weiss, The influence of cellulose nanocrystals on the hydration and flexural strength of portland cement pastes, *Polymers* 9 (24) (2017) 424.
- [49] J. Flores, M. Kamali, A. Ghahremaninezhad, An investigation into the properties and microstructure of cement mixtures modified with cellulose nanocrystal, *Materials* 10 (5) (2017) 498 <http://doi.org/10.3390/ma10050498>.
- [50] K.M.A. Glaus, L.R. Van Loon, Complexation of calcium by α -isosaccharinic acid under alkaline conditions, *Acta Chem. Scand.* 53 (1999) 241–246.
- [51] O. Onuaguluchi, D. Panesar, M. Sain, Properties of nanofibre reinforced cement composites, *Construct. Build. Mater.* 63 (2014) 119–124.
- [52] R. Sudin, N. Swamy, Bamboo and wood fibre cement composites for sustainable infrastructure regeneration, *J. Mater. Sci.* 41 (2006) 6917–6924.
- [53] D. Sedan, C. Pagnoux, A. Smith, T. Chotard, Mechanical properties of hemp fibre reinforced cement: influence of the fibre/matrix interaction, *J. Eur. Ceram. Soc.* 28 (2008) 183–192.
- [54] K.H. Khayat, Effects of anti-washout admixtures on fresh concrete properties, *ACI Mater. J.* 92 (1995) 164–171.
- [55] S. Nagataki, H. Fujiwara, V.M. Malhotra (Ed.), *Self-consolidating Property of Highly-flowable Concrete*, Second Conference on Advances in Concrete Technology, ACI SP-154, American Concrete Institute, June, 1995, pp. 301–304.
- [56] K. Abe, S. Iwamoto, H. Yano, Obtaining cellulose nanofibers with a uniform width of 15 nm from wood, *Biomacromolecules* 8 (2007) 3276–3278.

List of Figures

- Fig. 1. Particle size distribution of general use (GU) cement and class F-fly ash used in the current study.
- Fig. 2. Schematic of the hierarchical structure of cellulose filaments (CF) used in this study. Picture adapted from Hisseine et al. [11] with permission from ASCE.
- Fig. 3. Aqueous suspensions of cellulose filaments (CF) used to prepare the different cement systems considered in this study.
- Fig. 4. Transmission electron microscope (TEM) image of a diluted aqueous suspension of cellulose filaments (CF). Picture adapted from Hisseine et al. [11] with permission from ASCE.
- Fig. 5. Shear stress (τ)–shear rate ($\dot{\gamma}$) response for the different paste mixtures
- Fig. 6. Rheological parameters of cement pastes
- Fig. 7. Variation in apparent viscosity (μ_{ap}) in function of shear rate ($\dot{\gamma}$) in the different paste mixtures
- Fig. 8. Schematic illustration of the formation and buildup of network of cellulose filaments (CF).
- Fig. 9. Evolution of heat of hydration over time for the different paste mixtures.
- Fig. 10. Cumulative heat release in function of time for the different paste mixtures.
- Fig. 11. Shear stress (τ)–shear rate ($\dot{\gamma}$) response in series I–SCC mixtures.
- Fig. 12. Variation of apparent viscosity (μ_{ap}) in function of shear rate ($\dot{\gamma}$) in series I–SCC mixtures.
- Fig. 13. Variation of mixture demand in high range water reducer (HRWR) across the different series II–SCC mixtures.
- Fig. 14. Shear stress (τ)–shear rate ($\dot{\gamma}$) response in series II–SCC mixtures
- Fig. 15. Scanning Electron Microscopy (SEM) image of a cement paste with 0.20% CF at 120 days. The image illustrates a network of cellulose filaments (CF) reinforcing the matrix.
- Fig. 16. Scanning Electron Microscopy (SEM) image of an SCC mixture with 0.20% CF at 28 days. The image shows a transition zone (between cement paste and an aggregate) reinforced and with CF.

List of Tables

Table 1. Chemical composition and physical properties of binders used in the study.

Table 2. Mix proportions of cement pastes.

Table 3. Concrete mix proportions, kg/m³.

Table 4. Fresh properties of series I-SCC mixtures.

Table 5. Fresh properties of series II-SCC mixtures.

Table 6. Rheological parameters of series II-SCC mixtures.

Table 7. Mechanical properties of series II-SCC mixtures

CHAPTER 4 .

Effect of Cellulose Filaments on the Properties of Hardening Concrete

4.1 Introduction

This chapter aims at valorizing cellulose filaments (CF) to enhance the properties of concrete during the hardening phase. The chapter focusses on leveraging the hydrophilic and hygroscopic feature of CF (implying respectively high water-retention and release capacities) as well as its nanoscale fibrillated morphology associated with the intrinsic high on-axis strength and stiffness to mitigate autogenous shrinkage in ultra-high-performance concrete (UHPC). The formulation of UHPC with a water-to-binder ration of 0.25 was adjusted to accommodate CF at rates of 0-0.30% per cement mass. The effect of CF (at rates of 0-0.30%) and that of silica fume content (15-25%) on autogenous shrinkage behavior was evaluated with high precision vibrating-wire gauges from the onset of casting until 91 days. UHPC mixtures with reduced autogenous shrinkage (while maintaining adequate mechanical capacity) were obtained using CF. Therefore, the current chapter contributes into valorising CF as a tool for controlling volumetric instabilities in UHPC through a coupled effect of internal curing (transposed by the hydrophilicity and hygroscopicity of CF) and matrix nanoreinforcing (transposed by the inherent reinforcing effect of nanocellulose). Details on these findings are reported as par of [Article 2](#) of this study (section 4.2 below)

4.2 Article 2-Controlling autogenous shrinkage of ultra-high-performance concrete (UHPC) with cellulose filaments (CF): A novel application of nanocellulose

Article information

Authors and affiliations:

O.A. Hisseine, PhD candidate and Canada Vanier Scholar of NSERC, Cement and Concrete Research Group, Department of Civil Engineering, Université de Sherbrooke

Nancy A. Soliman, Post-doctoral fellow, Department of Civil and Environmental Engineering Massachusetts Institute of Technology

Balázs Tolnai, General Manager Technology, Kruger Inc.

A. Tagnit-Hamou, Professor and director of Cement and Concrete Research Group, Department of Civil Engineering, Université de Sherbrooke

Article status: At final review

Initial submission date: October 8, 2018

Journal: Cement and Concrete Research

Manuscript ID: CEMCON_2018_1071

Reference: Hisseine O. A., N. A. Soliman, B. Tolnai, A. Tagnit-Hamou (2018a), Controlling autogenous shrinkage of ultra-high-performance concrete with cellulose filaments: A novel application of nanocellulose. Under review by *Cement and Concrete Research* .

Titre français: Contrôler le retrait autogène des bétons à ultra-haute-performance (UHPC) en utilisant les filaments de cellulose: une nouvelle application de la nanocellulose

Contribution of this article to the thesis: This article contributes into achieving the objective 3 of this thesis, namely, taking advantage of the nanoreinforcing effect of CF as well as its water retention and release capacities to control the autogenous shrinkage, particularly, in low water-to-cement systems such as ultra-high-performance concrete (UHPC).

Controlling autogenous shrinkage of ultra-high-performance concrete with cellulose filaments: A novel application of nanocellulose

Ousmane A. Hisseine¹; Nancy A. Soliman²; Balázs Tolnai³ and Arezki Tagnit-Hamou⁴

Under review by Cement and Concrete Research

Abstract

Nanoengineering of concrete properties with nanocellulose materials has the potential to unveil remarkable opportunities for enhancing concrete performance. This study introduces the use of nanoscale cellulose filaments (CF) as a novel tool for engineering ultra-high performance concrete (UHPC) with attenuated autogenous shrinkage. A UHPC mix was tailored to accommodate the incorporation of CF at 0.3 wt. %. The effects of incorporating CF and that of varying silica fume (SF) content (15 and 25%) were assessed. CF was more beneficial in reducing autogenous shrinkage at early-age. A reduction in autogenous shrinkage of up to 45% was obtained during the first 24 hours before stabilizing at 35% at 7 days. On the other hand, adjusting SF content from 25 to 15% had negligible effect on autogenous shrinkage at early-age (0–4% reduction at 1 day) but higher effect at later-age (28% reduction at 7 days). However, this option led to reduced mechanical performance (32% lower flexural capacity). The hydrophilic and hygroscopic CF fibrils reduce autogenous shrinkage through a hybrid effect of internal curing and matrix bridging. Thus, CF allows designing UHPC with reduced autogenous shrinkage while maintaining satisfactory mechanical performance.

¹ (Corresponding author) PhD Candidate and NSERC Canada Vanier Scholar, Cement and Concrete Research Group, Université de Sherbrooke, Canada. Address: 2500, Boul. de l'Univ., Sherbrooke, QC J1K 2R1, Canada. Tel: +1 819 919 2615. Email: O.Hisseine@USherbrooke.ca

² Post-doctoral fellow, Cement and Concrete Research Group, Université de Sherbrooke, Canada. Email: nancy.ahmed.soliman@usherbrooke.ca

³ General Manager Technology, Kruger Inc., 3285 Bedford Road, Montreal, Quebec, Canada, H3S1G5, balazs.tolnai@kruger.com, 514-343-3100 / ext.12193

⁴ Professor and Head of the Cement and Concrete Research Group, Université de Sherbrooke, Canada. Email: A.Tagnit@USherbrooke.ca

Author Keywords: Autogenous shrinkage, cellulose filaments, mechanical performance, nanocellulose, recycled glass powder, ultra-high-performance concrete

1. Introduction

Improving concrete eco-efficiency is contingent to a challenging quest for more ecological (yet robust) materials in order to meet the stringent sustainability and resiliency requirements for modern infrastructure systems. In this respect, nano-modification of concrete has recently emerged as a major advancement in concrete technology allowing designing concretes with improved performance [1]. This is primarily ascribable to the radically different material properties exhibited at the nanoscale [2]. As such, nanocellulose materials (NCM)—with their remarkable properties such as the hydrophilicity, high surface reactivity, increased elastic modulus [3], and high strength to weight ratio [4] have the potential to revolutionize the performance of cement composites. This can also be accompanied by an improved eco-efficiency of concrete products for the fact that NCM stem from the most bounteous and renewable materials on the planet [5].

Typical NCM include cellulose nanocrystals (CNC); nanofibrillated cellulose (NFC); bacterial cellulose (BC); and cellulose filaments (CF). The latter remains relatively the most recent cement additive with promising application in concrete technology [6-8]. CF was found to increase the flexural capacity and toughness of cement systems via internal curing and nanoreinforcing effects [6]. CF was also found to increase the degree of hydration and alter the mechanical properties of matrix microstructure phases, namely calcium-silicate hydrate (C-S-H) and calcium hydroxide (CH), thereby enhancing the mechanical performance [7]. Considering the hydrophilic and hygroscopic features of CF (implying high water retention and release capacities) and in light of the effect of filaments on fostering the degree of hydration and on enhancing the phase-micromechanical properties of cement systems, it may be legitimate to believe that CF has a promising potential to alter the volumetric instabilities of concrete.

Volumetric instabilities shape a concern in versatile types of concretes including mass concrete; self-consolidating concrete (SCC); and low water-to-binder ratio (w/b) concretes (e.g.

engineered cementitious composites (ECC), high-performance concrete (HPC), and ultra-high-performance concrete (UHPC)). Primarily, concrete type, its w/b, and curing conditions define the most dominant volumetric instability (e.g., plastic shrinkage, drying shrinkage, autogenous shrinkage, and others). With the increasing recent interest towards low-w/b-cement composites, the autogenous shrinkage is broadly viewed as a prevailing form of volumetric instability jeopardizing structural health and durability of structures built with low w/b concretes [9].

Autogenous shrinkage represents the macroscopic volumetric changes (other than those due to temperature gradient, loss or ingress of substances, the application of external forces or restraint) as cement hydrates [10]. The volumetric changes occurring in cement systems as the hydration proceeds (chemical shrinkage) create fine pores due to the restraint created by the structuring of the hydrated cement system, or the aggregate skeleton, or the reinforcing steel. In the absence of external water supply, the pores drain water from coarser capillary networks where menisci are developed, in a process that does not involve mass loss (called self-desiccation). The developed menisci, however, create tensile stresses which can exceed the tensile capacity of the yet young concrete. As the generated tensile stresses are balanced by compressive forces developed on the pore walls, volumetric changes are developed in a phenomenon called autogenous shrinkage [11]. While the contribution of autogenous shrinkage to the total long-term deformations in high-w/b-concretes can be as low as 5-10% [12], it can reach up to 50% in low-w/b-concretes [13]. Under restrained conditions, autogenous shrinkage can be significantly deleterious and may jeopardize mechanical performance and durability [14].

As a typical concrete application susceptible to volumetric instability, UHPC has a matrix intrinsically prone to autogenous shrinkage. UHPC is a mortar-based, very high-strength, and high-durability material designed with high packing density, low w/b, high content of cement, and high dosage of high-range water reducing admixtures (HRWRA) [15,16]. While these characteristics endow UHPC with very high strength properties associated with its optimally-packed and water-starved microstructure, these features, however, render UHPC vulnerable to early-age deformations particularly autogenous shrinkage. The higher packing density, for instance, refines matrix pores and increases capillary pressure [17, 18]. The high cement content, on the other hand, mobilizes chemical shrinkage, the driver of self-desiccation which leads to

autogenous shrinkage [11]. The high content in pozzolans, particularly silica fume (SF), further refines the pore structure, increases the capillary pressure, and exacerbates matrix instability as large Portlandite (CH) crystals are converted to relatively less volumetric calcium-silicate-hydrate (C-S-H) gels [14,18,19]. In the absence of coarse aggregates and with the reduction of maximum particle size to around 200-600 μm , fresh UHPC mixtures exhibit an intrinsic reduced stiffness which further increases volumetric instability [20]. Volumetric instabilities in UHPC are particularly of phenomenal importance at early ages when the still-hardening young concrete hasn't yet developed sufficient strength. Consequently, shrinkage-induced cracks may be deleterious to strength and durability of UHPC [18, 19, 21]. Autogenous deformations popped-up at the top of issues pertaining to the implementation of UHPC when this class of concrete started to make its way from the precast industry to in-situ casting or when conventional curing (rather than hot/steam curing) regimes were adopted instead.

Several noteworthy efforts have been invested towards mitigating autogenous shrinkage in UHPC. This includes replacing cement and SF with different supplementary cementitious materials (SCM) [22-27], incorporating coarse aggregates [28], using saturated light weight aggregates (LWA) [29], introducing shrinkage reducing admixtures (SRA) [9,30], using super-absorbent polymers (SAP) [9], incorporating expansive agents (EAs) [30], improving curing conditions [31-33], and incorporating nanofibers such as carbon nanofibers (CNF) and carbon nanotubes (CNT) [34].

Despite all efforts made so far in this direction, autogenous shrinkage, however, remains a major concern. This is partially associated with the fact that some current shrinkage-mitigation techniques have adverse effects on mechanical properties, thereby increasing the production cost of UHPC [35, 36]. For instance, whereas the net effect of SAP on concrete strength depends on the w/b , matrix maturity, and SAP dosage [37], it is reported that high dosages of SAP lowers the hardened properties of concrete due to the apparition of supplementary voids in the skeleton of the hardened system [38]. On the other hand, while the inclusion of SRAs and EAs can effectively mitigate autogenous shrinkage, it was reported that these additives increase the air content, significantly reduce mixture fluidity, and adversely affect the mechanical performance when used at relatively high dosages [39]. On the other hand, major challenges encountered in

the use of carbon-based nanofibers, particularly CNF and CNT, include the difficulty of ensuring an effective dispersion of those hydrophobic materials in the hydrophilic cementitious matrix [40]; and the health risks associated with their handling (high toxicity coupled with high risk of inhalation) [41- 43].

Owing to the hydrophilic and hygroscopic nature of CF (allowing high water retention and release) coupled with the fibrillated morphology of CF (allowing for nanoreinforcing effect), it is hypothesized herein that CF can serve as an internal curing agent to reduce autogenous shrinkage in UHPC. When using CF as a shrinkage reducer, it appears that the most interesting feature of CF (not exhibited by conventionally used shrinkage reduction techniques) is that additional to controlling autogenous shrinkage via internal curing, the filaments have the further advantage of potential crack resistance through their fibrillated morphology. The hybrid effect of internal curing and matrix bridging that CF may exhibit can be juxtaposed to that obtained by blending SRA and synthetic fibers in the same matrix such that the former reduces shrinkage deformations, while the latter provides crack resistance [46]. Moreover, the fact that CF are extracted from the most abundant natural resources, and present very low health and environmental risks associated with their production [5,44,45], may shape substantiate CF potential as an effective shrinkage reducing agent. To this end, the current study is aimed at producing an UHPC mixture with reduced autogenous deformations using CF as a novel shrinkage reducing admixture, while enhancing both performance and ecoefficiency dimensions of UHPC.

To achieve project objective, a sustainable ultra-high-performance glass concrete (UHPGC) recently developed at the University of Sherbrooke using recycled glass [24] was considered. The formulation of the UHPC was tailored to accommodate the inclusion of CF at 0.3% by weight, while the content of SF (principal source of autogenous shrinkage) was adjusted from 25 to 15%. The performance of the UHPC was assessed in terms of fresh properties, autogenous shrinkage, and mechanical performance to answer a fundamental question: What are the separate and joint effects of incorporating CF or reducing the SF content (from 25 to 15%) on the development of autogenous shrinkage and mechanical properties? Research outcomes are expected to contribute towards the implementation of UHPC for in-situ applications while

providing a twofold-sustainable alternative: Bio-sourced, nanostructured CF for mitigating autogenous shrinkage of a recycled glass-based sustainable UHPC.

2 Experimental Program

2.1 Materials properties

2.1.1 Cellulose filaments

The cellulose filaments (CF) used in this study were received from Kruger Biomaterials Inc. (Trois-Rivière, QC). CF consist of mechanically processed cellulose fibrils with nanometric diameter (30–400 nm) but micrometric length (100–2,000 μm) which results into their significantly high aspect ratio (100–1,000) and very high surface area (more than 80 m^2/g). The filaments have a specific gravity (*SG*) of 1.5 and were received in a colloidal form (water suspension with 1.2% CF solid content). In their dispersed form, the filaments have a water absorption capacity of 220% of their mass. According to the supplier, the filaments were derived from FSC®-certified Kraft wood pulp using only virgin fibers to ensure optimum performance and consistent properties. Additional to the intrinsic sustainability features of CF, the extraction process of this material follows a green approach with a yield value of 100%. In fact, as per the supplier, the filaments were extracted through a patented process that uses only mechanical energy and does not involve any chemical or enzymatic treatment, nor does it produce effluent. In addition, the production facility is almost entirely powered by renewable energy; thereby minimizing the carbon footprint of CF. CF represent an intrinsic part of the hierarchical structure of cellulose (Fig. 1), which imparts inherent strength to plant-based materials. The extraction process of CF involves removal of matrix impurities such as lignin, pectin, wax, and soluble sugars. As such, CF (Fig. 2) contains mainly cellulose (>95%) and a small amount of hemicellulose (<5%). This is consistent with the two types of saccharides (glucose and xylose) detected by liquid chromatography tests conducted on CF, where typically the former is found in cellulose while the latter is found in hemicellulose. As CF is used in this study to control

autogenous shrinkage, details about CF-water interaction in terms of water retention and release capacity are detailed later in section 2.4.1.

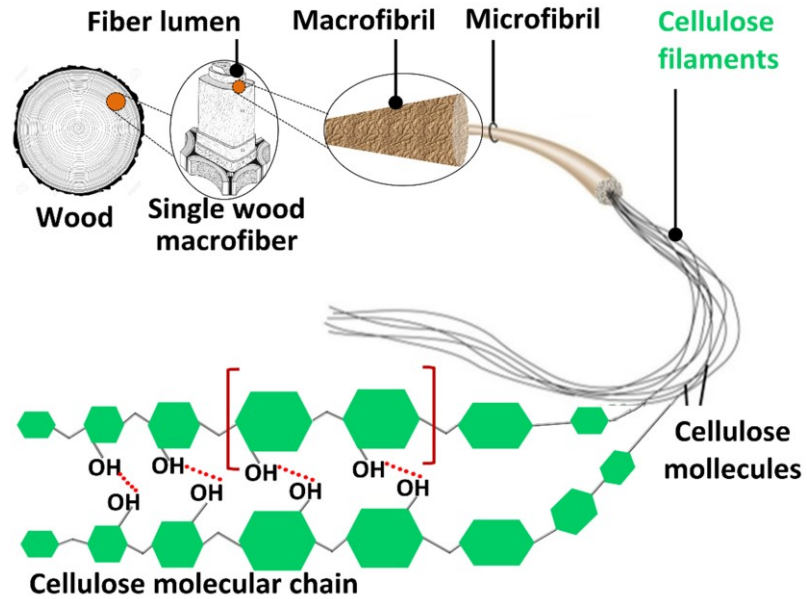


Fig. 1. Schematic of hierarchical structure of cellulose filaments (CF).

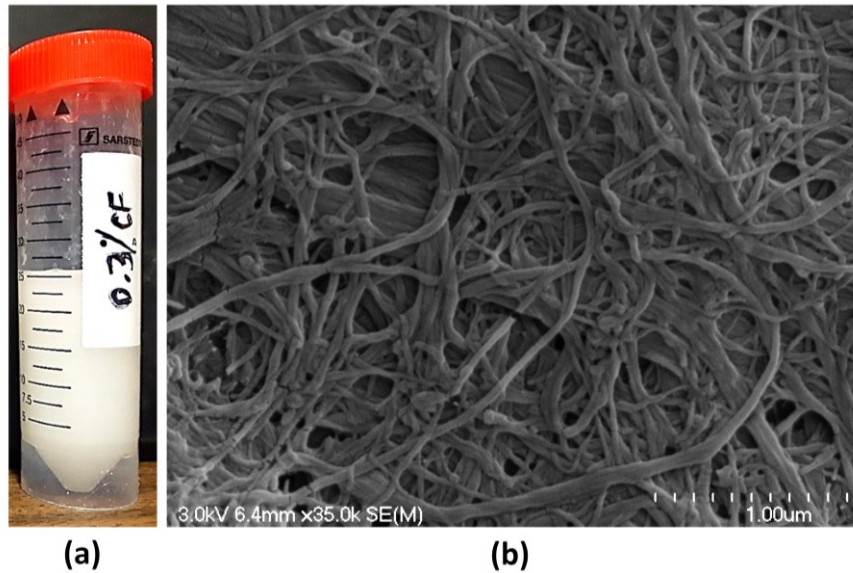


Fig. 2. Cellulose filaments (CF): (a) aqueous suspension at 0.3%CF; (b) scanning electron microscope (SEM) image of a dried aqueous suspension illustrating the fibrillated morphology of CF.

2.1.2 UHPC basic constituents

To formulate UHPC mix, an informed selection of mixture constituents is necessary for optimizing the performance of the end product. The flowability, for instance, is strongly influenced by increasing cement fineness and by cement content in C_3A and C_3S [16]. This is more pronounced in UHPC as cement particles are closely packed due to the very low w/b . Considering the effect of the hydrophilic CF on mixture fluidity; it appears that enhancing the rheology of UHPC dictates the selection of cement with the lowest C_3A and C_3S contents. As such, a high-sulfate-resistance cement (type HS) with low C_3A content, was selected. The cement has an SG of 3.21, Blaine fineness of $370 \text{ m}^2/\text{kg}$, and mean particle diameter (d_{50}) of $11 \text{ }\mu\text{m}$. Silica fume (SF) fulfilling the requirements of CAN/CSA A3000 specifications and having a SG of 2.20, Blaine surface area of $20,000 \text{ m}^2/\text{kg}$, and d_{50} of $0.15 \text{ }\mu\text{m}$ was employed. Quartz sand (QS) with a SG of 2.70, maximum particle size (d_{max}) of $600 \text{ }\mu\text{m}$, and mean particle size (d_{50}) of $250 \text{ }\mu\text{m}$ was also used. Additionally, a high-alkali-glass powder (G_H) with a SG of 2.6 and d_{50} of $12 \text{ }\mu\text{m}$ was also used. Table 1 shows the chemical composition of the materials used in this study. Fig.3 provides the PSD of the cement, G_H , SF, and QS [24]. A polycarboxylate (PCE)-based HRWRA with a SG of 1.09 and solid content of 40% was used.

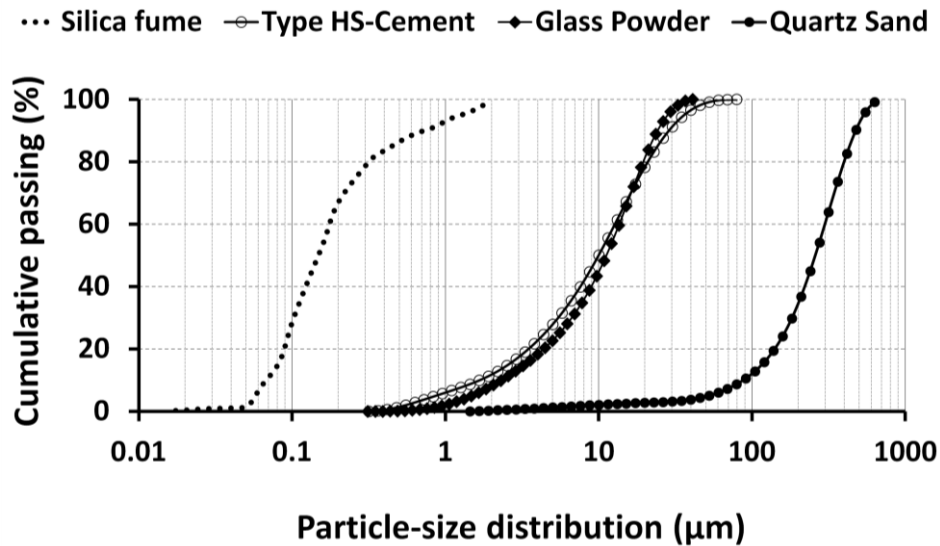


Fig. 3. Particle-size distribution of granular materials used in this study

Table 1. Chemical compositions of powders and granular materials used in the study.

Identification	Quartz Sand	Glass Powder	Type HS Cement	Silica Fume
Silicon dioxide (SiO ₂)	99.8	73.00	22	99.8
Iron oxide (Fe ₂ O ₃)	0.04	0.40	4.3	0.09
Aluminum oxide (Al ₂ O ₃)	0.14	1.50	3.5	0.11
Calcium oxide (CaO)	0.17	11.30	65.6	0.4
Titanium dioxide (TiO ₂)	0.02	0.04	0.2	—
Sulfur trioxide (SO ₃),	—	—	2.3	—
Magnesium oxide (MgO)	0.008	1.20	1.9	0.20
Sodium oxide (Na ₂ O)	—	13.00	0.07	0.20
Potassium oxide (K ₂ O)	0.05	0.50	0.8	0.50
Equivalent alkali (Na ₂ O _{eq})	—	—	0.9	—
Zinc oxide (ZnO)	—	—	0.09	0.25
Loss on ignition (LOI)	0.2	0.60	1.0	3.50
C ₃ S	—	—	50	—
C ₂ S	—	—	25	—
C ₃ A	—	—	2.0	—
C ₄ AF	—	—	14	—

2.2 Mixture proportions

The tested UHPC mixture was designed by optimizing the particle-size distribution and packing density, as detailed elsewhere [24, 47]. The mix design was tailored by incorporating CF and varying the SF content across four mixtures (0nCF/15SF, 0.3CF/15SF25, 0CF/SF25, and 0.3CF0.3/SF25) as depicted in Table 2 in order to examine the impact of these formulations on autogenous shrinkage behavior as well as on fresh and hardened properties. All mixtures had a constant QS, and SF/G_H to cement weight ratio and were designed with a *w/b* of 0.25, and a solid HRWRA content of 1.25% of cement weight. Each mixture label is a combination of two parts, representing the content in CF and SF, respectively. For example, the mixture 0.3CF/15SF15 contains 0.3% CF and 15% SF.

Table 2. Ultra-high-performance concrete (UHPC) mixture proportions (CF for cellulose filaments and, SF for silica fume. Numbers preceding CF/SF indicate content in % weight).

Mixture Composition (kg/m ³)	UHPC mixtures			
	0CF/15SF	0CF/25SF	0.3CF/15SF	0.3CF/25SF
Type HS cement	601	569	600	568
Silica fume (SF)	120	190	120	189
Water	230	237	230	237
Water-to-binder ratio (<i>w/b</i>)	0.25	0.25	0.25	0.25
Quartz sand	962	911	960	909
Glass powder	440	417	440	417
HRWRA (solid extract)	11	10	11	10
Cellulose filaments, CF (solid extract)	—	—	2.4	2.3

2.3 Specimen Preparation

Concrete batching was carried out using a pan mixer of type Mortartman 360 (Imer, CA, USA). In an attempt to enhance mixture homogeneity and avoid particle agglomeration, all powder materials were dry-mixed for 10 min prior to adding water and HRWRA. A water HRWRA suspension was prepared by diluting the required HRWRA into the mixing water. Approximately half of that suspension was gradually added to the batch over 5–7 min of mixing. The rest of the water HRWRA suspension was gradually added over an additional 5–7 min of mixing. For mixtures containing CF, the as-received colloidal CF was added to the water–HRWRA suspension while taking in consideration the adjustment of the net water demand determined after subtracting the amount of water brought by the CF water suspension (1.2% solid CF content).

After mixing, concrete was cast for the different tests. Specimens for mechanical properties were covered with plastic sheets and kept in a room with a relative humidity and temperature of approximately 50% and 23 °C, respectively, for 24±1 h then demoulded and transferred for storage in a fog room at 100% RH and 22 °C temperature until the age of testing. UHPC specimens for autogenous shrinkage were cast directly inside a controlled room (50% RH and 22 °C). The moulds containing the pastes were hermetically sealed with adhesive plastic wraps immediately after casting and remained so until demolded 24±0.5 h later. Immediately after

demolding (within 2±1/2 min), the specimens were sealed with an adhesive aluminum foil and kept in a controlled environment (50% RH and 22 °C) for 91+ days. The different test methods adopted to execute the experimental program are elaborated in the following sections.

2.4 Test Methods

2.4.1 Tests on the CF–water interaction

As CF are employed in this study to attenuate autogenous shrinkage (partially through an internal curing effect), the assessment of CF's water retention capacity (WRC) and water release rate (WRR) was deemed necessary. The WRC of CF was determined following the approach detailed in a previous work in the same project [6] where CF was found to have a WRC of 125% of their mass when the WRC was assessed on semi–dispersed CF (34% solid content). For fully dispersed CF, the WRC was as high as 220% due to the increased surface area exposed to interaction with water molecules. To assess the WRR, the following methodology was adopted: A 30 g sample of semi–dispersed CF (34% solid content) was kept in an oven at 60 °C until its mass loss stabilized at final mass of 10.2 g of dry CF. Several CF suspensions were prepared by mixing 0.1 g of dry CF (referred herein as M_0) with 1.9 g of distilled water then the samples were hermetically sealed and kept at 22 °C and 50% RH for 72 hours to allow full saturation. Samples were then subjected to centrifugation at 3000 rpm for 25 min using 2 ml centrifugal filters of 100,000 molecular weight cut-off (MWCU) to drain out water. The resulting CF was accurately weighted for its wetted mass (M_1). The samples were thereafter stored in humidity-controlled room where the temperature was kept constant at 25 ± 1 °C while the RH was varied as follows: 20, 50, 70, and 90%. This was an attempt to better capture the WRR of CF, particularly at high RH levels in an attempt to simulate the RH encountered in hydrating UHPC. Loukili et al. [19] reported that RH in HUPC reaches 73% in 8 days then slows down to 68% in 90 days. CF Samples exposed to each RH level for a series of exposure durations (from 0.17 h up to 14 days) were accurately weighed for their mass (M_2) after moisture loss, and the WRR was calculated as follows:

$$\text{WRR} = \left(\frac{M_1 - M_2}{M_1 - M_0} \right) \times 100\% \quad (1)$$

2.4.2 Fresh properties

UHPC fresh properties were measured right after mixing. This includes the unit weight, the air content (ASTM C 185), and the slump–flow [flow–table test (ASTM C 1437)]. For the latter, when a mixture’s slump flow diameter is below 250 mm, the flow diameter is also measured after subjecting the sample to 25 blows on the flow–table. This was more applicable in mixtures incorporating CF where the initial slump was relatively low prior to applying the blows, but significantly high after applying the blows.

2.4.3 Autogenous shrinkage

Specimens for autogenous shrinkage test were cast soon after casting. The different UHPC mixtures were cast in 80×80×350 mm prismatic molds instrumented with an embedded vibrating–wire strain gauges of type EM–5 (Roctest Ltd., Saint-Lambert, QC, Canada) with 144 Ω resistance and a strain range of 3000 $\mu\epsilon$ (Fig.4). This instrumentation allows continuous measurement of deformations. Additional to measuring deformations resulting from autogenous shrinkage, the gauge is also equipped with a thermocouple to record temperature evolutions in the paste throughout the testing period so that temperature–borne deformations can be subtracted from the total deformation. To ensure full embedment of the gauge within the matrix, the gauge was set centered in the mold (in all directions) using attachment wires so as to allow it a free rotation and axial translation (necessary to respond to the matrix linear deformations). The fresh UHPC mixtures were placed in the mold in two layers and were consolidated following the procedures detailed in ASTM C157-14. Data were continuously recorded via an acquisition system at 30-240 min frequency so that the early–age behavior can be captured. To measure only effective autogenous deformations (beyond the liquid phase), the zero-time (TZ) for measuring autogenous deformations was determined following the method proposed by Meddah and Tagnit-Hamou [48]. The method consists of using the rate of deformation [the first derivative of deformation with respect to time ($\partial\epsilon/\partial t$)] as a tool for identifying the TZ. The latter is defined as the peak of the maximum rate of deformation which is considered as an indicator of a phenomenal change in the microstructure of the hydrating system and the onset of the

hardening phase or the solidification threshold [48]. Additionally, the rate of temperature evolution over time or thermal flux ($\partial T/\partial t$) was also determined and correlated with the rate of thermal deformation. This correlation provides an additional indicator of the time corresponding to the solidification threshold, because at the onset of solidification, a sudden drop in electrical conductivity occurs due to the formation of hydrates and the consequent disconnection in the interstitial solution [49]. As the rate of dissolution decreases substantially at the onset of solidification, the latter is quite at the vicinity of the maximum flux [48].

A further point worth elucidating is the determination of autogenous deformations from total deformations recorded by the vibrating wire-gauge. This was performed by subtracting thermal deformations from total deformation considering the manufacturer-provided thermal expansion coefficient (TEC) of the vibrating wire gauge [$11(10)^{-6}$] and that of UHPC. For UHPC, during the first few hours (3-24 h) as the matrix is still plastic (hence highly sensitive to thermal variations), the dynamic model proposed by Holt [50] for determining TEC ($TEC = 193.9 \times t^{0.86}$ where $3 \leq t \text{ (hr)} \leq 24$) was used. Beyond 24 hr, once the matrix has solidified, a TEC of $12(10)^{-6}$ proposed by RILEM [51] was used. Considering that test samples were kept hermetically sealed throughout the experiment, and that in low w/c ratio systems autogenous shrinkage contributes predominantly to the total shrinkage [52], drying shrinkage was not considered.

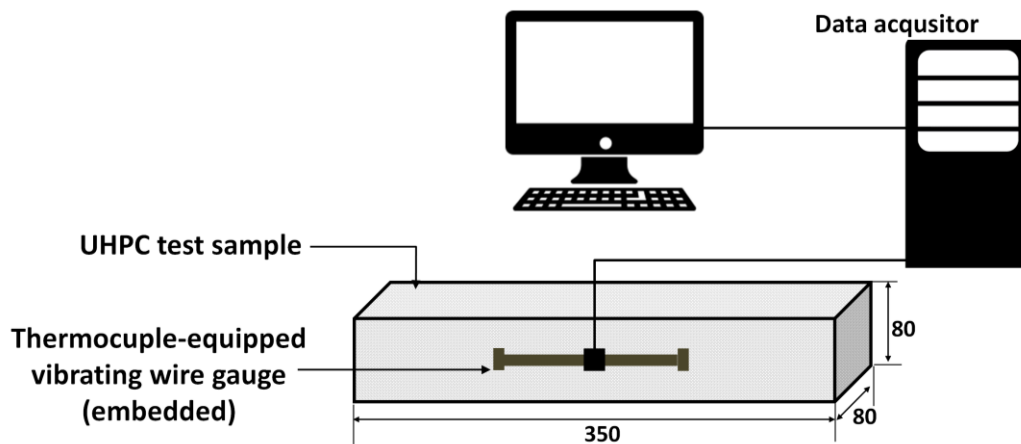


Fig. 4. Schematic diagram of test set-up for autogenous shrinkage (all dimensions in mm).

2.4.4 Mechanical properties

The tested mechanical properties included the compressive strength (f_c) and the flexural capacity (f_{fl}). The f_c was assessed on 50×50×50 mm cubes at 1, 7, 28, 56, and 91 days according to ASTM C109-16 guidelines. The f_{fl} [ASTM C78-16] was evaluated on 100×100×400 mm prisms at 28 and 91 days. Flexural tests were performed under four-point bending configuration in a displacement-controlled mode using a displacement rate of 0.0008 mm/s.

3 Results analysis and discussions

Test results and discussions are presented in the following sequence: Results of tests on water-CF interaction were first discussed since the water-absorption/desorption of the hydrophilic CF plays an important role on both fresh and hardened properties of CF-cement systems. The effect of CF on altering the fresh properties of tested UHPC mixtures were then addressed and the implications of the hydrophilic CF on fresh properties were discussed. Later, the effect of incorporating CF or adjusting SF content on autogenous shrinkage was discussed. The discussion of mechanical properties was kept at the end to unveil possible repercussions on this parameter from mixture behavior at fresh state and matrix volumetric stability at early ages.

3.1 Results of tests on water–CF interaction

Previous tests on WRC of CF showed that it exceeds 100% by 6 h of saturation and stabilizes at 125% when semi-dispersed CF was saturated in distilled water for 72 hours. For fully dispersed CF, the WRC reached 220% owing to the higher exposed surface area implicated in the desorption process. The difference between the two absorption rates is attributable to the entanglements in the former case (semi-dispersed), which leads to reducing the effective surface area involved in water desorption. Samples obtained from WRC tests at 72 h of saturation followed by centrifugation at 3000 rpm for 25 min and exposure to a controlled medium released their absorbed water according to the trend shown in Fig. 5. The figure indicates that irrespective of the RH, fully saturated CF can release all imbibed water. The WRR is, however, fast at low

RH but very slow at high RH as expected. At 20% RH, for instance, CF released all the retained water within 6 hours. In contrast, for RH levels of 50, 70, and 90%, the plateauing of the WRR slowed down to 1, 7, and 14 days, respectively. The observed slow WRR at higher RH levels can be viewed advantageous since CF releases its water over an extended period as cement hydrates and self-desiccation takes place. On the other hand, slower WRR at high RH levels would also prevent CF from releasing water to the batch water during the mixing process or soon afterwards. While the RH has been used in this study as a driving force to stimulate the water desorption capacity of CF, it should be noted that the water diffusion in hydrating cement systems is influenced by several other factors such as the capillary pressure, the average pore size, the pore solution surface tension [53] which have not been taken into consideration in this study for simplicity.

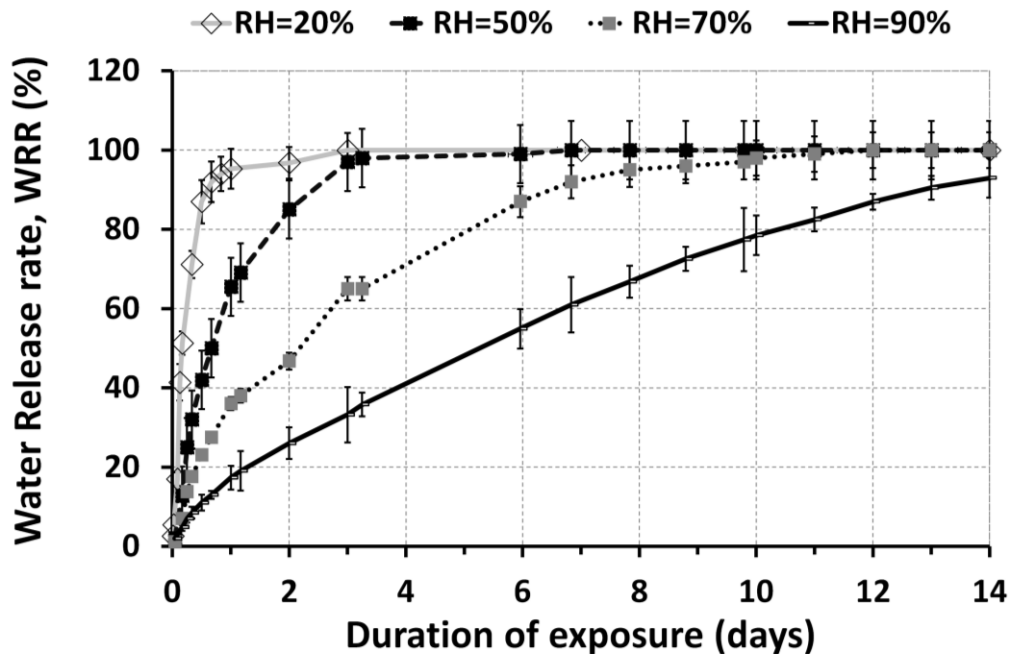


Fig. 5. Water release rate of cellulose filaments (CF) in function of duration of exposure to different relative humidity (RH) levels

3.2 Fresh properties

3.2.1 Effect of cellulose filaments (CF) on fresh properties

The fresh properties of tested UHPC mixtures are presented in Table 3. Results indicate that, relative to the mixtures with no CF, those incorporating CF had slightly higher air content. This effect is observable at both SF contents of 15 and 25% and can be ascribed to the increased surface area of CF which could lead to slight air entrapment. The effect of CF on air entrapment may also be influenced by the interaction between CF and the PCE-HRWRA used herein which has not been attempted in this study. Further investigation is necessary to clarify this point. As for the slump-flow, measurements reveal a decreasing trend with the addition of CF. When SF content was maintained at 15%, the slump-flow decreased from 305 mm in the mixture without CF to 170 mm in the mixture with 0.3% CF. Similarly, when SF content was increased to 25%, the incorporation of CF decreased the slump-flow from 295 mm to 160 mm. The drop in slump-flow in mixtures with CF is associated with the hydrophilic and fibrillar aspects of CF. The former leads to peripherally fixing water molecules or imbibing part of the mixing water, thereby reducing the slump-flow [6]. The latter, however, when coupled with the flexibility and high aspect ratio of CF, promotes the formation of filament networks, thereby increasing the viscosity buildup [7]. Nonetheless, it should be highlighted that while the incorporation of CF reduced the slump-flow, test observations indicate that UHPC mixtures with CF exhibit reduced viscosity when agitated. This confirms the shear thinning behavior identified in previous tests conducted on CF- SCC [6].

Table 3. Fresh properties of tested ultra-high-performance concrete (UHPC) mixtures.

	Mixtures			
	0CF/15SF	0.3CF/15SF	0CF/25SF	0.3CF/25SF
Air content (%)	3.98	4.9	3.4	4.0
Slump flow (mm)	305	170	295	160
Fresh unit weight (kg/m ³)	2271	2246	2252	2238

3.2.2 Effect of silica fume (SF) on fresh properties

Table 3 indicates that reducing SF content from 25% in the mixture 0CF/25SF to 15% in the mixture 0CF/15SF had slightly increased the slump-flow (from 295 to 305 mm). This slight improvement is attributable to the reduction in total surface area of SF particles (for their extreme fineness). Consequently, the water demand required to lubricate the surface of SF particles decreased. Hence, the slump-flow for the same w/b increased slightly. Another explanation for the slight workability enhancement with decreasing SF content is that SF particles require more HRWRA to be dispersed and reach a certain slump-flow. According to the interpretations of [54], charged species in cement pore solution of UHPC are not only from cement grains, but also from SF particles which possess positive surface charges. Thus, SF particles compete with cement grains for adsorption of PCE molecules onto their surface. In this regard, while the tested UHPC has lower SF content than cement, the surface area of SF exceeds that of cement. Hence, a PCE molecule dissolved in UHPC pore solution would predominantly recognize SF surface for adsorption. This suggests that an effective dispersion of SF, and not forcedly that of cement alone, would be necessary to achieve flowable UHPC mixture. As a result, when SF content is decreased, the PCE dosage necessary to disperse the particles decreased due to the decrease in the net particle surface area. This would lead to higher slump-flow at the same PCE dosage.

However, with the significantly high surface area of SF, the adjustment of SF content from 25 to 15% is rather expected to lead to substantial drop in water demand and consequently to more significant increase in flowability than the recorded 10 mm difference. However, some competing actions may have led to the observed results. Possible reasons include the relatively lower cement content but higher packing density in mixtures with 25% SF than in mixtures with 15% SF. Cement content in mixture with 25% SF as compared to that of UHPC with 15% correspond to 601 versus 569 kg/m³, respectively, in mixtures with no CF and 600 versus 568 kg/m³ in mixtures with CF. The relatively lower cement content in mixtures with 25% SF can contribute to slightly reducing the water demand, thereby interfering with higher water demand resulting from higher SF content. From packing density perspectives, the increased packing density (0.79) in mixtures with 25% SF as compared to 0.75 in mixtures with 15% SF can reduce

the matrix voids, thereby allowing for the availability of more rheologically- active water to coat the particles' surface [55]. Nonetheless, further studies are required to cover these points.

3.3 Autogenous shrinkage

This section presents results of autogenous shrinkage of all tested UHPC mixtures. To facilitate the discussion of autogenous shrinkage measurements, three distinct ages have been identified, namely, very-early-age (0 – 12 h), early age (12 h – 7 days), and later-age (7-91 days). The very-early-age corresponds to the plastic phase where autogenous deformations are relatively less effective. The early-age contains the transition phase and expands to the hardened phase, while the later-age corresponds to long-term deformations. Section 3.3.1 addresses the evolution of autogenous shrinkage at the very-early-age where as-recorded autogenous deformations are presented. As-recorded deformations are later calibrated at the time-zero (for measurement of autogenous shrinkage) as addressed in section 3.3.2. Section 3.3.3 is devoted to the evolution of autogenous deformations (beyond the time-zero) which correspond to what we refer to as early-age deformations, while section 3.3.4 addresses long-term deformations.

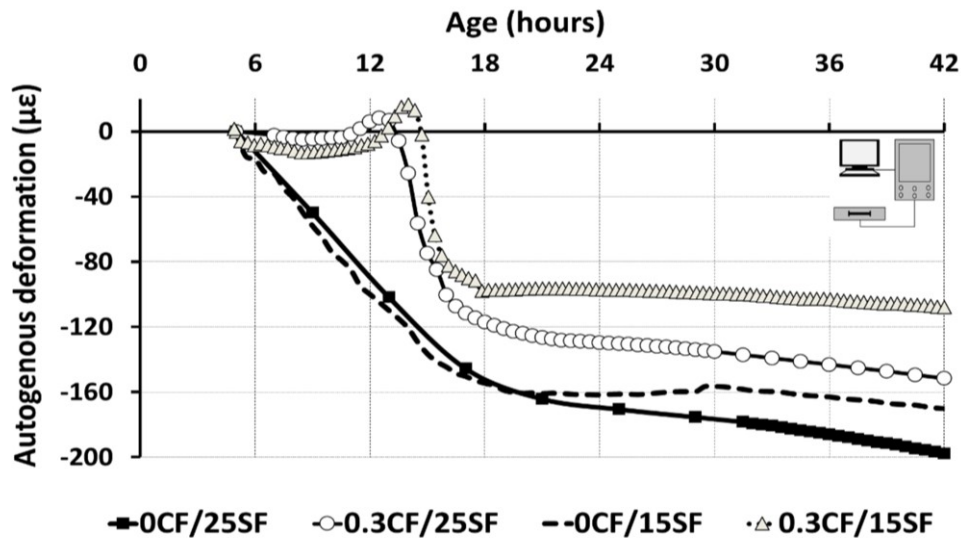


Fig. 6. Evolution of very-early-age (0-12 hours) autogenous deformations in the different ultra-high-performance concrete (UHPC) mixtures.

3.3.1 Effect of CF and SF on very-early-age autogenous shrinkage

Fig. 6 presents the evolution of very-early-age autogenous deformations for all tested UHPC mixtures. To capture well the profile of volumetric instability at very-early-age (0 – 12 h) and early-age (12 h – 7 days), as-recorded deformations have been used to plot the curves shown in Fig. 6. As-recorded data reflect negligible deformations during the first 5 h after which a distinct behavioral difference in very-early-age deformations in the absence or presence of CF was observed. The two mixtures without CF but having varying SF content (0CF/25SF and 0CF/15SF) recorded quite steep deformations which reached up to $100 \mu\epsilon$ at 12 h. Moreover, the deformations recorded during this time interval were quite comparable for both mixtures despite the substantial variation in SF content (15-25%).

In contrast, very-early-age deformations in mixtures containing CF (0.3CF/25SF and 0.3CF/15SF) were the least. This corresponds to deformations from $\sim 0 \mu\epsilon$ to even a sort of expansion (as compared to $100 \mu\epsilon$ in the mixtures without CF). This is equivalent to a percentage reduction of $\approx 100\%$ during the first 12 h. Furthermore, autogenous deformations recorded in these two mixtures with similar CF dosage (0.3%) but very different SF contents (15 and 25%) were also very comparable during this time interval. Beyond the very-early-age period, however, drastic changes in autogenous deformations were observed at approximately 20 h in mixtures without CF and 15.5 h in mixtures with CF.

The above results suggest that the incorporation of CF has influenced the evolution of autogenous shrinkage at very-early-age. Major effect of CF sprouts from the matrix expansions not evident in counterpart mixtures. One possible reason for very-early-age expansion exhibited in mixtures with CF can be the volume refill associated with CF water release (Fig. 4) replenishing the emptying cement pores as hydration proceeds. These volumetric expansions may be juxtaposed to those observed in super-absorbent polymers (SAP) [32,37] such that the gradual release of imbibed water (Fig. 4) as cement hydrates [56] leads to relatively widening capillary pores, thereby enlarging menisci curvature [57] and attenuating the capillary surface tension, in consequence. This would eventually lead to volumetric expansions [32] as observed herein. The above expansions observed pronouncedly in mixtures with CF are advantageous as

they have been reflected by far less very-early-age deformations. While autogenous deformations during the plastic phase are considered less effective and are often discarded, the corresponding expansions can be advantageous in reducing the net early-age deformations and long-term deformations to be detailed in subsequent sections. These findings are substantiated by mainstream investigations on shrinkage mitigating strategies via internal curing such as with LWA or SAP [32, 57-61].

On the other hand, while the incorporation of CF has significantly influenced the very-early-age autogenous behavior, results do not support a noticeable effect of tested SF contents (15% and 25%) on very-early-age autogenous deformations. This is evidenced by the quite comparable deformations recorded in mixtures with 15 and 25% SF in the presence and absence of CF, alike. Consequently, this may suggest that the adjustment of SF content (at least within the tested quantities) is not efficient in controlling autogenous shrinkage of UHPC at very-early-ages. The above observation can be linked to the two effects through which SF influences autogenous shrinkage: A physical effect (alteration of packing density by filler action), and a chemical effect (dissolution at early-age and pozzolanic activity thereafter) [62]. Higher SF content increases packing density, leads to narrower pores and higher capillary pressures [63] which results in higher autogenous shrinkage [64]. Such effect is, however, not evident at very-early-age when both chemical shrinkage and the subsequent self-desiccations are still to take place as cement hydration proceeds. On the hand, while the dissolution of SF may contribute partially to chemical shrinkage, the pozzolanic activity has to wait until some calcium hydroxide (CH) crystals are produced from the mainstream cement hydration [65]. This may explain why divergence between autogenous deformations in mixtures with 15 and 25% SF in the presence or absence of CF were only observed beyond the very-early-age period.

3.3.2 Determination of the zero-time for measuring autogenous shrinkage

Following the approach proposed by [48] detailed earlier in this manuscript (section 2.4.3), the starting point for measuring autogenous shrinkage in all tested UHPC mixtures was precisely determined. For brevity, two examples (among the four mixtures) are depicted in Figs. 7 and 8 presenting the evolution of the rate of deformation and the thermal flux during the first 48 h in

the mixtures 0CF/25SF and 0.3CF/25SF, respectively. As illustrated in Fig. 7, the rate of deformations in the tested mixture were nil in the first 5 h then followed by a steeply increasing trend (up to $80 \mu\epsilon/h$) between 5 and 18 h before reaching the highest peak at 20 h. Thereafter, the rate of deformation dropped back to the horizontal axis then stabilized. This trend is nontrivial since the thermal flux itself in the same mixture was quite stable during the first 5h when no deformations were observed, then exhibited drastic jump until it recorded the highest peak at a time corresponding to the that of the maximum rate of deformation (~ 20 h) before restablising at zero thereafter.

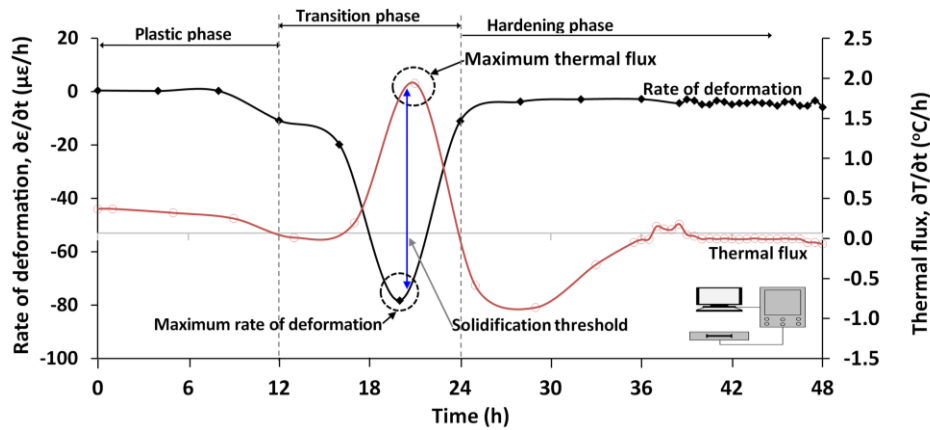


Fig. 7. Determination of solidification threshold from the rate of deformation and thermal flux: mixture 0CF/25SF.

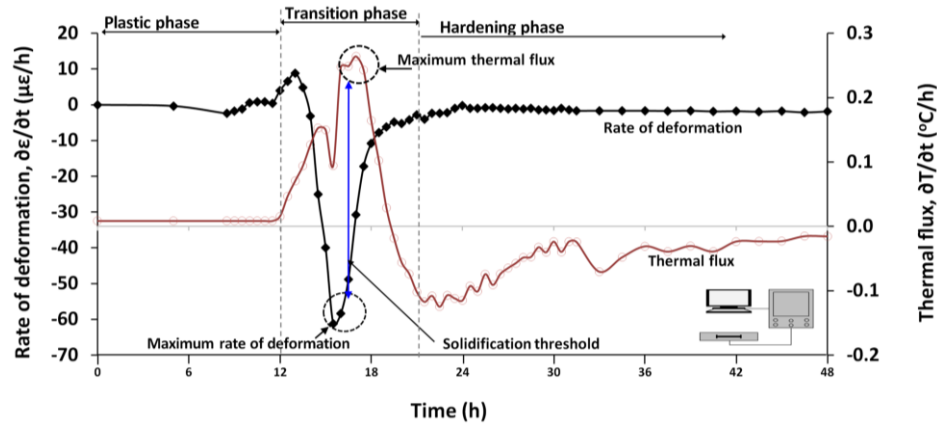


Fig. 8. Determination of solidification threshold from the rate of deformation and thermal flux: mixture 0.3CF/25SF.

The above observations were further supported by the results depicted in Fig.8 for the mixture 0.3CF/25SF. In this mixture, CF was found to flatten the very-early-age deformations until 8.5 h, followed by a sort of expansion between 8 and 13 h. Thereafter, the rate of deformations exhibited the highest peak of $61 \mu\epsilon/h$ at 15.5 h, which is roughly the same time ($\pm 0.5h$) corresponding to the maximum thermal flux. Beyond this time, both the rate of deformation and the thermal flux stabilized at ~ 0 . The coincidence of the maximum thermal flux with the maximum rate of deformation has been identified in the literature as the solidifications threshold [48]. The time corresponding to the solidification threshold was considered as the datum for measuring autogenous shrinkage in this study. This is because prior to this point, as the UHPC is still plastic, deformations are highly influenced by the alterations occurring in the matrix during hydration. These deformations are mainly thermo-chemical resulting from the vigorous exothermal reactions accompanying the hydration of cement actives phases [67]. Most often, such deformations also sprout partially from the deformation of the gauge itself, which (however) have been accounted for herein by using the gauge thermal expansion coefficient and the thermocouple accompanying the gauge. Such approach in determining the time-zero was deemed necessary to yield accurate autogenous shrinkage results. This is because conventional techniques (e.g. penetration resistance test (ASTM C403)) may lead to an overestimation or underestimation of the total magnitude of autogenous shrinkage. Moreover, with nanoinclusions (such as the current case), it is highly possible that matrix reaches percolation due to physical bridging offered by nanomaterials even prior to an actual solidification by structuration of the hydrated system. This renders the penetration resistance techniques quite obsolete. On the other hand, while the time corresponding to the end of matrix expansion has been used in the literature as a datum from measuring autogenous shrinkage, such technique may occasionally be misleading since matrix expansions are not evident in all mixture types. In the current experimental campaign (for instance) and elsewhere [32, 37], matrix expansion at very-early-age were more pronounced in mixtures containing internal curing agents (CF herein and SAP elsewhere).

3.3.3 Effect of CF and SF on early-age autogenous shrinkage

Fig. 9 presents the result of autogenous deformations during the first 180 h. In consistence with the discussion of the previous section, Fig. 9 indicates that autogenous deformations exhibited a phenomenal transformation at the end of the very-early-age period. Between 12 and 24 h, all mixtures exhibited drastic changes in the trend due to the mixture transformation to the hardened state. Beyond 24 h, similar mixtures but with different SF content (showing comparable deformation trend at very-early-age) started to show clearly divergent deformation trend. At 24 h, for instance, in the absence of CF, both mixtures (0CF/25SF and 0CF/15SF) recorded comparable deformation of 160 $\mu\epsilon$. The mixtures with CF (0.3CF/25SF and 0.3CF/15SF) recorded 130 $\mu\epsilon$ and 95 $\mu\epsilon$, respectively. At 48 h, however, the two mixtures without CF (0CF/25SF and 0CF/15SF) recorded 205 and 178 $\mu\epsilon$, respectively, while the mixtures with CF (0.3CF/25SF and 0.3CF/15SF) recorded 160 and 110 $\mu\epsilon$, respectively. At 72 h, the two mixtures without CF (0CF/25SF and 0CF/15SF) recorded 260 and 209 $\mu\epsilon$, respectively, while the mixtures with CF (0.3CF/25SF and 0.3CF/15SF) recorded 197 and 139 $\mu\epsilon$, respectively. At 168 h (7 days), the two mixtures without CF (0CF/25SF and 0CF/15SF) recorded 430 and 310 $\mu\epsilon$, respectively, while the mixtures with CF (0.3CF/25SF and 0.3CF/15SF) recorded 305 and 253 $\mu\epsilon$, respectively. The above trend reflects that while the effect of SF content on very-early-age deformation was not evident as detailed in the previous section, SF has a significant effect on deformations beyond 24h. This can be noticed from the increasing divergence between the deformations of similar mixtures but with different SF content. As such, the effect of SF on autogenous shrinkage is much clearer on mixtures without CF as reflected in the above data and illustrated by the divergence of corresponding graphs in Fig. 9.

To further capture the separate and joint effects of incorporating CF or adjusting the SF content from 25 to 15% on the development of autogenous deformations, the percentage reduction in autogenous deformations pertaining to each of the above two options was calculated relative to the mixture with the highest SF and without CF (0CF/25SF) and plotted in Fig.10. The figure indicates that relative to the reference mixture (0CF/25SF), percentage reduction in autogenous deformation in the mixture 0CF/15SF started with a marginal effect at 1 day but steeply increased in intensity over time until stabilised at $\sim 28\%$ beyond 7 days. On the other hand,

percentage reduction in deformation recorded in the mixture 0.3CF/25SF started with ~20% at 1 day and increased slightly until stabilized at around 30% beyond 7 days. As for the mixture 0.3CF/15SF, the percentage reduction in autogenous deformations were the highest and remained within 40% in the first 7 days before stabilising at 35% thereafter.

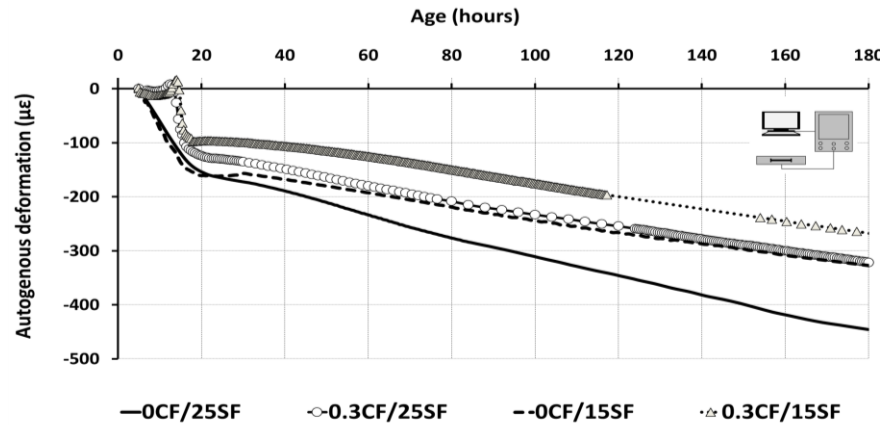


Fig. 9. Evolution of early-age (12 h – 7 days) autogenous deformations in the different ultra high-performance concrete (UHPC) mixtures (as-recorded deformations).

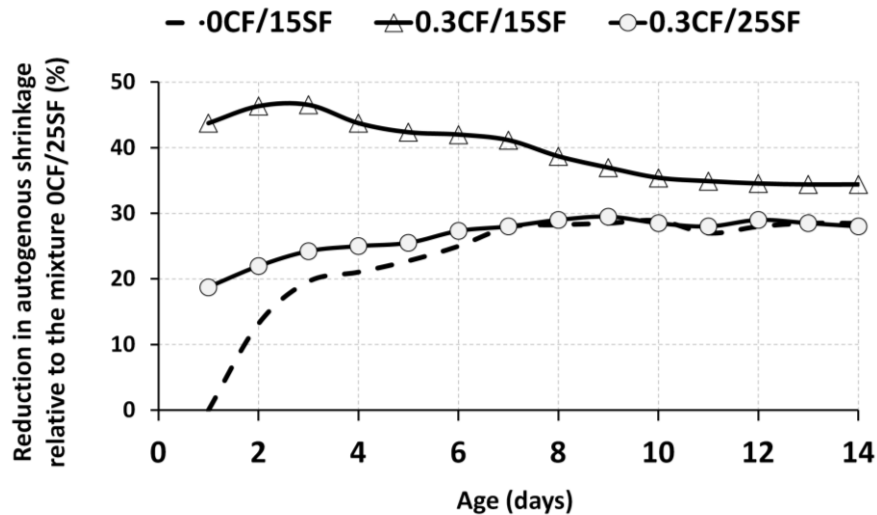


Fig. 10. Profile of percentage reduction in autogenous shrinkage deformations during the first 14 days in the different ultra-high-performance concrete (UHPC) mixtures relative to the mixture 0CF/25SF.

These results indicate that while both the incorporation of CF and the reduction of SF were found influential on controlling autogenous deformations, the effect of each of these two alternatives is, seemingly, dependent on concrete maturity. Incorporating CF appears to be more efficient in controlling the deformations at early-ages while the reduction of SF content seems to be more influential afterwards. The effect of CF on reducing early-age autogenous deformations by up to 20 and 40% for SF contents of 25 and 15% is significant, particularly that autogenous deformations are more critical at early-age when the concrete did not yet develop sufficient strength. This behavior may be correlated with the hydrophilicity/hygroscopicity of CF and its water release capacity which are also time-dependent as explained earlier. The lower efficiency of adjusting SF content on early-age deformations but higher efficiency thereafter may be associated with the time-dependent pozzolanic reaction. When SF content is reduced, autogenous shrinkage is attenuated physically by reducing the extra SF which could refine the pore structure and increase the capillary pressure. Autogenous shrinkage is also attenuated chemically by reducing the excess SF which may have increased the pozzolanic reaction consuming relatively larger CH crystals and yielding relatively less-volumetric CSH gel [63]. In this regard, when the two approaches were considered in the mixtures 0.3CF/15SF, a synergetic effect seems to prevail and the percentage reduction in autogenous shrinkage was the highest at all ages, as expected.

In general autogenous shrinkage is a complex phenomenon and is influenced by such a variety of factors as the capillary pore pressure (or suction), pore-size, the pore solution surface tension, etc., However, within similar conditions for all mixtures, if autogenous shrinkage is considered to be driven by the destabilization of the internal relative humidity as cement hydrates, then a possible link may be established between the effectiveness of CF in reducing autogenous shrinkage at early-ages and the water desorption capacity of CF discussed earlier. If the relative humidity is taken as an influential parameter on autogenous shrinkage among the other different factors appearing in Kelvin's equation [51] (pore radius, temperature, water and gas-related constants), then the water release capacity of a potential internal curing agent exposed to varying levels of relative humidity can be, for simplicity, used to assess the effectiveness of such an internal curing agent. The CF water release capacity described earlier shows that the filaments

can still release almost totally their absorbed water at RH of 90%, even if the desorption is slow and spans for about 14 days.

In retrospect to the above discussion, it can be perceived that CF contributes to reducing autogenous shrinkage by two actions: internal curing and matrix bridging. Within the first 7 days or so, both actions would possibly prevail, thereby leading to the maximum reduction in autogenous shrinkage (about 40 and 20 % in the mixtures with 15 and 25% SF, respectively). Later, as CF dispatches its water to replenish the emptying cement pores, the contribution of CF to attenuating autogenous deformations is more seemingly dominated by matrix bridging. This can also be supported by the higher elastic modulus and tensile strength imparted by CF as reported elsewhere [6].

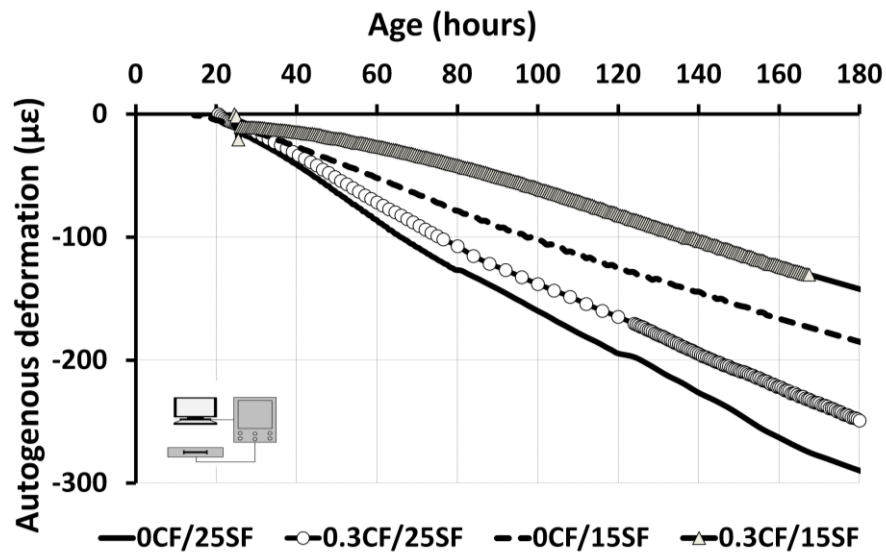


Fig. 11. Evolution of early-age (12 h – 7 days) autogenous deformations (zeroed at the time corresponding to the solidification threshold).

However, it should be elucidated that the effect of CF on autogenous shrinkage is influenced by the matrix expansions (at very-early-age) which were not evident in counterpart mixtures. These expansions, as stated earlier have an effect on lowering net-autogenous deformations. As a result, when as-recorded deformations were zeroed to the solidification threshold (Fig. 11), both early-age and long-term deformations are lowered as shown in Fig 12.

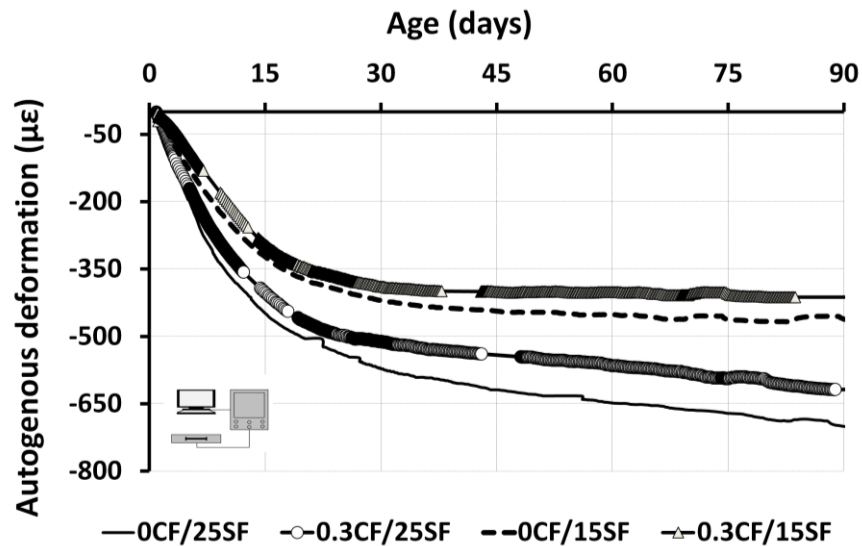


Fig. 12. Long-term deformations in the different ultra-high-performance concrete (UHPC) mixtures.

Long-term deformations shown in Fig. 12 reconfirm that in all mixtures with 25% SF, the autogenous shrinkage readings were the highest, as expected, continued at an increasing trend until the age of 91 days, and reaffirmed the substantial contribution of SF in driving autogenous shrinkage in UHPC. This was reflected by the relatively steeper autogenous shrinkage curves as illustrated by the corresponding graphs. In the mixtures with 15% SF, however, autogenous shrinkage was lower than in their counterparts and plateaued at approximately 28 days after which no significant increase was noticed. This can also be inferred from the corresponding flat curves beyond 28 days. While the effect of CF on autogenous shrinkage was very pronounced at early-age (as discussed earlier), long-term deformations indicate that the effect of CF becomes marginal at extended curing time. This may substantiate that the effect of CF on the autogenous

shrinkage behavior is driven by a twofold mechanism, (i) internal curing and (ii) nanoreinforcing, as detailed elsewhere [8]. While both mechanisms may prevail simultaneously at all curing ages, the former is more evident to be manifested during the early-age period when the matrix undergoes the hydration process and CF still have enough water to contribute towards stabilizing the internal relative humidity. During this period the reinforcing effect may not be optimum; since the adherence of CF with the still hydrating matrix is not evident. At later ages, however, internal curing is not evident as the water retained in CF would have been drained out towards the matrix. As such, dried CF with better adherence to the matrix would provide an enhanced volumetric stability through a bridging or nano-reinforcing effect driven by CF fibrillated morphology and tensile properties. Nonetheless, further work is needed to understand the exact separate and joint effects of these two facets of CF on autogenous shrinkage behavior.

3.4 Mechanical properties

This section presents the effect of CF and SF on mechanical performance of tested UHPC mixtures. Section 3.4.1 addresses the compressive strength at different testing ages (up to 91 days) while section 3.4.2 presents the flexural capacity at 28 and 91 days.

3.4.1 Compressive Strength

The results of compressive strength (f_c) for the tested UHPC mixtures are shown in Fig. 13. The figure indicates the effect of CF on compressive strength of UHPC varies with ages. At early ages (up to 7 days), mixtures with CF showed lower f_c . Nonetheless, beyond 7 days, that adverse effect diminished and mixtures with CF recorded quite comparable performance as their counterparts. The lower f_c measured in systems with CF can be traced-down to the higher air content exhibited in mixtures with CF. While the use of CF has been reported elsewhere to improve compressive strength [6], the excess content of HRWRA in UHPC could lead to a sort of interactions between CF and HRWRA which may have caused the increased air content. However, this possible interaction has not been considered in this study. On the other hand, the reduced compressive strength in mixtures with CF may be associated with the higher amount of

CF purposely selected for the sake of controlling autogenous shrinkage. Our previous works indicated that while mechanical properties are higher at lower CF contents (0.05-0.10%), better control of autogenous deformations was achieved with increasing CF content [6-8]. As for the reduced f_c at early-age (1-7 days) as compared to later age in the presence of CF, this may be linked to the low adherence between the filaments and the matrix at early-age. At later ages, however, as the skeleton of the hydrated system is structuring, it is believed that a better bond is established between the filaments and matrix, thereby enhancing the adherence of the filaments into the skeleton of the hydrated system. Overall, all mixtures satisfied the 120 MPa target compressive strength for the selected UHPC mix design. On the other hand, as for the effect of SF, no clear effect can be captured until the age of 56 days. By the age of 91 days, however, at 25% SF an increment of 8 and 12% in f_c were obtained in mixtures without CF and with CF, respectively. The increased f_c at the age of 91 days with higher SF content can be attributed to a combination of chemical and physical effects which include: (1) a time-dependent pozzolanic reaction of SF with calcium hydroxide from cement hydration to yield secondary C-S-H, thereby refining matrix porosity, strengthening the microstructure, and reducing microcracking [68]; (ii) an increased particle packing, leading to a denser microstructure [69]; and (iii) an increased C-S-H chain length when the mixture contains higher amount of SF [70]. In retrospect to the previous discussion on autogenous shrinkage, where mixtures with 25% SF exhibited higher autogenous shrinkage, which continued in increasing paces up to 91 days and beyond, the increasing trend of the autogenous shrinkage is in harmony with the continuous pozzolanic reaction led by SF and reflected into higher mechanical properties. However, since the autogenous deformations were measured in unrestrained conditions, no adverse effects on mechanical properties were recorded.

On the other hand, in light of the claim that the increased mechanical properties at 90 days in mixtures with 25% SF is driven by the chemical and physical effects of SF, the absence of such effect up to 56 days should be clarified. It is believed herein that there is an interference of a rheological aspect influencing this trend. In fact, in the mixture 15% SF, it is evident that the total net surface area of SF has significantly decreased relative to the mixture with 25% SF. Consequently, the water and HRWRA needed to lubricate and disperse SF particles can decrease

due to lower net surface area of SF particles. This consequently leads to higher slump-flow at the same w/b as previously discussed in fresh properties. The enhanced flowability in the mixture with 15% SF can lead to better dispersion of cement and SF particles, thereby positively influencing the strength gain. On the other hand, the higher rheologically active-water due to the lower SF content can contribute in the solubilisation of more anhydrous particles, thereby enhancing the compressive strength. Such effects are, however, not evident at long-term (beyond 56 days) when the pozzolanic activity will be more dominant [71].

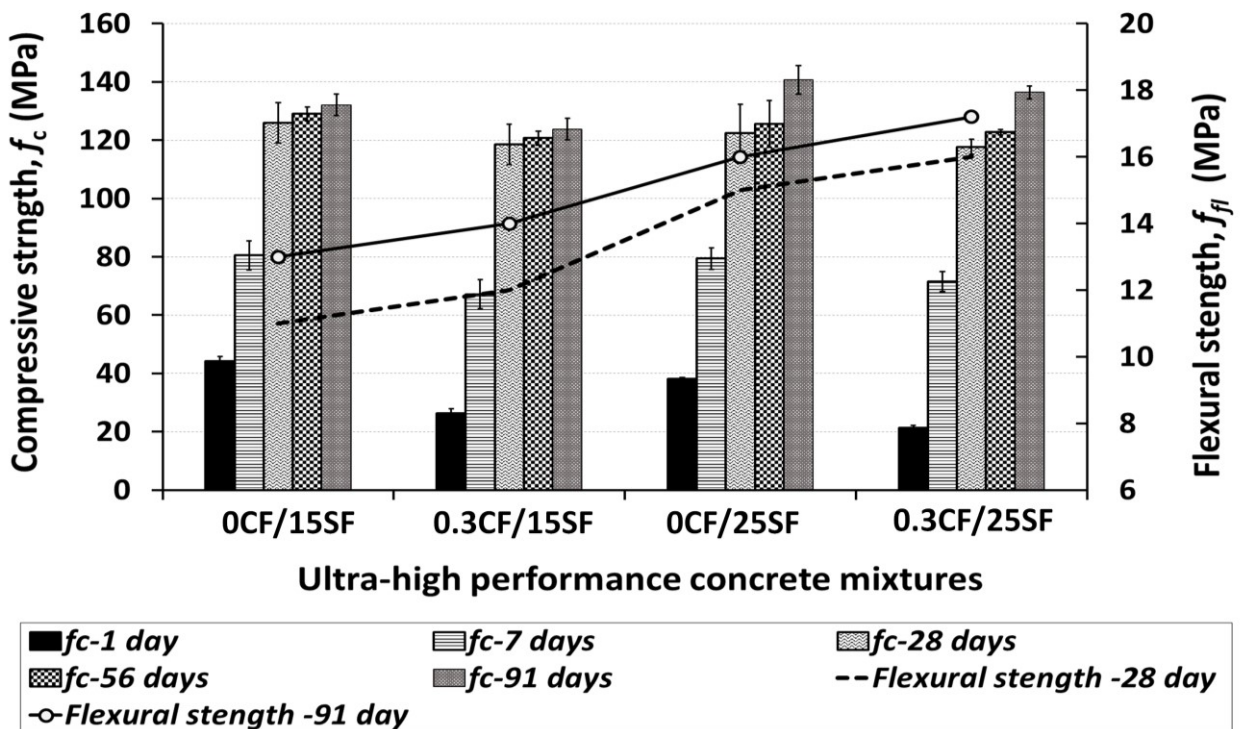


Fig. 13. Compressive and flexural strength results for the different ultra-high-performance concrete (UHPC) after different curing periods

3.4.2 Flexural strength

The results for the flexural capacity (f_{fl}) at 28 and 91 days for all tested UHPC mixtures are depicted in Fig. 13. The figure reveals few major points which can be briefed as follows: (i) mixtures with 25% SF exhibited higher ultimate f_{fl} than that of their counterparts with 15% SF, as expected; (ii) mixtures with CF recorded slightly higher ultimate f_{fl} than that of their corresponding counterparts without CF, and (iii) the f_{fl} is higher at 91 days-in consistence with the compressive strength trend discussed earlier. The higher f_{fl} in mixtures with 25% SF as compared to those with 15% SF is a direct effect of the compressive strength trend for the reasons detailed earlier (higher packing density; pozzolanic activity). This is consistent with mainstream investigations indicating that the optimum SF content to obtain a denser matrix lies around 25% [72].

On the other hand, the higher f_{fl} in mixtures with CF sheds the light on the matrix nanomodification resulting from the incorporation of CF. The incorporation on CF has been proven elsewhere to increase the tensile strength of concrete [6]. Additionally, low water-to-binder ratio cement systems incorporating CF were found to exhibit higher flexural capacity due to an increased amount of chemically-bound water. This led to an enhanced degree of hydration by providing supplementary source of water. Furthermore, nanoindentation assessments [8] indicated that the incorporation of CF in low water-to-binder ratio (0.3) systems enhanced the microstructure phase micromechanical properties which were reflected in higher flexural capacity and elastic modulus.

4 Summary and conclusions

This paper investigated the effectiveness of using cellulose filaments (CF) as a novel approach for mitigating autogenous shrinkage in ultra-high-performance concrete (UHPC). UHPC fresh properties, autogenous shrinkage, and mechanical behavior were evaluated when the mixture incorporated CF at a dosage of 0 and 0.3% as compared to when the mixture content in silica fume (SF) was adjusted from 25 to 15%. Overall, test results reveal that the use of CF reduces autogenous shrinkage with better effectiveness at early age. On the other hand, lowering SF

content also reduces autogenous shrinkage with better long-term effects, but adversely affects mechanical performance. Specific findings can be summarized as follows:

- The incorporation of CF reduced mixture slump-flow due to the increased viscosity imparted by the hydrophilic CF. Nonetheless test observations reveal that mixtures with CF had little resistance to deformation due to a shear thinning effect exhibited in mixtures with CF as demonstrated elsewhere.
- The effectiveness of CF in reducing autogenous shrinkage was more pronounced within the first 7 days owing to the time-dependent water release from CF. A reduction in autogenous shrinkage of 40-45% was maintained between 1 and 7 days before stabilising at 35% at 7-14 days and thereafter. This is of paramount importance since autogenous deformations are more critical at early ages when concrete didn't yet develop a sufficient tensile strength.
- While the incorporation of CF results in slight adverse effect on compressive strength between 1 and 7 days, this effect, however, seems to disappear at later ages (>7 days) as comparable compressive strengths were recorded in all mixtures. On the other hand, the flexural capacity of mixtures with CF was slightly increased. This reduced early-age compressive strength in mixtures with CF can be associated with time dependent development of adhesion between CF and the matrix, while the enhanced flexural capacity may be linked to a combination of an internal curing effect offering supplementary water to foster hydration and nano-bridging effect.
- The reduction of SF content from 25 to 15% slightly favored fresh properties due to the reduction in total surface area to be lubricated by water and HRWRA. On the other hand, while the reduction in SF from 25 to 15% is significant, the effect of this adjustment on early-age autogenous shrinkage was not evident. The percentage reduction in autogenous shrinkage associated with the adjustment of SF content from 25 to 15 started with negligible value (0-4%) at 1 day then gradually increased over time until stabilised at 25-28% at 7 days and thereafter. This indicates that adjusting the SF content in the tested UHPC may be effective in reducing autogenous deformations at later ages but not at

early-ages which are more critical. On the other hand, the reduction in SF content lead to substantial drop in flexural capacity: a drop of up to 32% drop.

Finally, overall results indicate the effectiveness of using CF as a tool for reducing autogenous shrinkage in UHPC, though more work is needed to substantiate the obtained results. The production of UHPC with reduced autogenous shrinkage is expected to contribute to the implementation of UHPC in in-situ applications where autogenous shrinkage are more problematic.

Acknowledgements

This project is jointly supported a Cooperative Research and Development (CRD) grant from the Natural Sciences and Engineering Research Council of Canada (NSERC), Canada Vanier Graduate Scholarship (CGS) program award no: 360284, Kruger Biomaterials Inc. (QC, Canada), and Euclid Chemicals. The authors are grateful to the financial support from all these partners.

References

- [1] F. Sanchez, and K. Sobolev, Nanotechnology in concrete – A review, *Construction and Building Materials*, 24 (11) (2010) 2060–2071.
- [2] M. Ashby, P. Ferreira, and D. Schodek, *Nanomaterials, nanotechnologies and design: an introduction for engineers and architects*, Elsevier Science Ltd, Boston, MA, 2009.
- [3] K. Abe, S. Iwamoto, and H. Yano, Obtaining cellulose nanofibers with a uniform width of 15 nm from Wood, *Biomacromolecules*, 8 (2007) 3276–3278.
- [4] S. Youssefian, and N. Rahbar, Molecular origin of strength and stiffness in Bamboo fibrils, *Scientific Reports*, 5, 11116. <http://doi.org/10.1038/srep11116>
- [5] R. J. Moon, A. Martini, J. Nairn, J. Simonsen, J. Youngblood, Cellulose nanomaterials review: structure, properties and nanocomposites. *Chem. Soc. Rev.* 40 (2011) 3941–3994.
- [6] O.A. Hisseine, A.F. Omran, A. Tagnit-Hamou, Influence of cellulose filaments on cement pastes and concrete, *J. Mater. Civ. Eng.*, 30 (6) 2018: 04018109

- [7] O. A. Hisseine, N. Basic, A. F. Omran, A. Tagnit-Hamou, Feasibility of using cellulose filaments as a viscosity modifying agent in self-consolidating concrete, Article in press, *Cem. Concr. Compos.* (2018), ISSN 0958-9465, <https://doi.org/10.1016/j.cemconcomp.2018.09.009>.
- [8] O.A. Hisseine, W. Wilson, L. Sorelli, A.Tagnit-Hamou, Nanocellulose for improved concrete performance: A macro-to-micro investigation for disclosing the effects of cellulose filaments on strength of cement systems, Article submitted to *Materials and Design*, 2018.
- [9] A.M. Soliman, M.L. Nehdi, Effects of shrinkage reducing admixture and wollastonite microfiber on early-age behavior of ultra-high-performance concrete, *Cem. Conc. Comp.*, 46 (2014) 81–89.
- [10] JCI Technical committee report on Autogenous Shrinkage, *Autogenous Shrinkage of Concrete: Proceedings of the International Workshop*; ed. Tazawa, E and FN Spon. London, 1998, pp. 3-63.
- [11] P.C. Aïtcin, Demystifying autogenous shrinkage, *Concr Int.* 21(11) (1999) 54–56
- [12] H.E. Davis, Autogenous volume change of concrete. *Proceedings of the 43rd annual meeting, American Society of Testing Materials, Atlantic City, N.J., June 1940*, pp. 1103-1113.
- [13] E. Tazawa, S. Miyazawa, Experimental study on mechanism of autogenous shrinkage of concrete, *Cem. Concr. Res.*, 28(8) (1995) 1633-1638.
- [14] K. Habel, J. P. Charron, E. Denarie, E. Bruhwiler, Autogenous deformations and viscoelasticity of UHPFRC in structures-Part 1: experimental results, *Magazine Conc. Res.*, 58 (3) (2006) 135–145.
- [15] P. Richard, M. Cheyrezy, Composition of reactive powder concrete.” *Cem. & Con. Res.*, 25 (7), 1501–1511.
- [16] P.C. Aïtcin, Cements of yesterday and today-concrete of tomorrow, *Cem. & Con. Res.*, 30 (9) (2000) 1349–1359.
- [17] M. Schmidt, E.Fehling, T. Teichmann, K.Bunje, and R. Bornemann, Ultra-high performance concrete: perspective for the precast concrete industry, *Conc. Precasting Plant & Tech*, 69 (3) (2003) 16–29.

- [18] M. Cheyrezy, and M. Behloul, Creep and shrinkage of ultra-high-performance concrete, shrinkage and durability mechanisms of concrete and other quasi-brittle materials, Proc. 6 Int. Conf. CONCREEP-6@MIT, Ed. Ulm, F.-J., Bažant, Z. P., Wittmann, F. H., and Cambridge, M. A., USA, (2001) 527–538.
- [19] A. Loukili, A. Khelidj, and P. Richard, Hydration kinetics, change of relative humidity, and autogenous shrinkage of ultra-high-strength concrete, *Cem. Concr. Res.*, 29 (4) (1999) 577–584.
- [20] V. Baroghel-Bouny, and A. Kheirbek, Effect of mixparameters on autogenous deformations of cement pastes—microstructural interpretations. In: Baroghel-Bouny V, P.C. Aitcin, Proceedings of the international RILEM workshop on Shrinkage of concrete, Shrinkage 2000, RILEM Publications, Paris, 2000.
- [21] Y. Bao, M. Valipour, Meng, W., K. Khayat, G. Chen (2017), Distributed fiber optic sensor enhanced detection and prediction of shrinkage-induced delamination of ultrahigh-performance concrete bonded over an existing concrete substrate, *Smart Mat. Struct.* doi: 10.1088/1361-665X/aa71f4.
- [22] H. Yazıcı, Mert Y.M. Yardımcı, H. Yiğiter, S. Aydın, S. Türkel, Mechanical properties of reactive powder concrete containing high volumes of ground granulated blast furnace slag, *Cem. Concr. Compos.*, 32 (8) (2010) 639-648
- [23] A. Tafraoui, G. Escadeillas, S. Lebaili, T. Vidal, Metakaolin in the formulation of UHPC, *Constr. Build. Mater.* 23 (2) (2009) 669–674.
- [24] N.A. Soliman, Tagnit-Hamou, Development of ultra-high-performance concrete using glass powder — towards ecofriendly concrete, *Constr. Build. Mater.* 125 (2016) 600–612.
- [25] E. Ghafari, S. A. Ghahari, H. Costa, E. Júlio, A. Portugal, L. Durães, Effect of supplementary cementitious materials on autogenous shrinkage of ultra-high-performance concrete, *Construction and Building Materials*, 127 (2016) 43-48.
- [26] N.A. Soliman, and A. Tagnit-Hamou, Study of rheological and mechanical performance of ultra-high-performance glass concrete, *ACI-SP*, 310 (2017) 103–112.
- [27] D. P. Bentz, M.A Peltz, Reducing thermal and autogenous shrinkage contributions to early-age cracking.” *ACI Mat. J.*, 105 (4) (2008), 414–20.

- [28] W. Zhang, W. Sun, Effect of coarse aggregate on early age autogenous shrinkage of high-performance concrete, *Journal of the Chinese Ceramic Society*, 37 (2009) 631-636.
- [29] J. Castro, L. Keiser, M. Golias, W. Weiss, Absorption and desorption of fine lightweight aggregate for applications to internally cured concrete mixtures, *Cem. Conc. Compo.*, 33 (10) (2011) 1001–1008.
- [30] J.J. Park, D. Y. Yoo, S.W. Kim, Y.S. Yoon, Benefits of using expansive and shrinkage-reducing agents in UHPC for volume stability, *Magaz. Concr. Res.* 66 (14) (2014) 745-750.
- [31] S. Meddah, S.Ryoichi, Effect of curing methods on autogenous shrinkage and self-induced stress of high-performance concrete, *ACI Mat. J.*, 107 (1) (2010) 65-74.
- [32] A. Soliman, M. Nehdi, Effect of drying conditions on autogenous shrinkage in ultra-high-performance concrete at early-age, *Materials and Structures/Materiaux et Constructions*, 44 (2011) 879-899. Doi: 10.1617/s11527-010-9670-0.
- [33] S-H. Kang, J-H. Lee, S-G. Hong, J. Moon, Microstructural investigation of heat-treated ultra-high-performance concrete for optimum production, *Materials*, 10 (9) (2017) 1106. Doi:10.3390/ma10091106.
- [34] W. Meng, K. Khayat, Meng, Effect of graphite nanoplatelets and carbon nanofibers on rheology, hydration, shrinkage, mechanical properties, and microstructure of UHPC. *Cem. Concr. Res.* 105 (2018) 64-71.
- [35] J. J. Park, D. Y. Yoo, S. W. Kim, Y. S. Yoon, Drying shrinkage cracking characteristics of ultra-high-performance fibre reinforced concrete with expansive and shrinkage reducing agents.” *Magazine Concr. Res.* 65 (4) (2013) 248–256.
- [36] J. Justs, M. Wyrzykoski, D. Bajare, P. Lura, Internal curing by superabsorbent polymers in ultra-high performance concrete, *Cem. Conc. Res.* 76 (2015) 82–90.
- [37] O.M. Jensen, P.F. Hansen, Water-entrained cement-based materials: I. Principles and theoretical background, *Cement. Concr. Res.*, 31 (4) (2001) 647-654.
- [38] D. Snoeck, D. Schaubroeck, P. Dubruel, N. De Belie, Effect of high amounts of superabsorbent polymers and additional water on the workability, microstructure and

- strength of mortars with a water-to-cement ratio of 0.50.” *Constr. Build. Mater.* 72 (2014) 148–157.
- [39] S. Anshuang, Q. Ling, Z. Shoujie, Z. Jiayang, L. Zhaoyu, Effects of shrinkage reducing agent and expansive admixture on the volume deformation of ultrahigh performance concrete, *Adva. Mat. Scie. & Eng.* (2017) 6384859. Doi: <https://doi.org/10.1155/2017/6384859>
- [40] M.S. Konsta-Gdoutos, Z.S. Metaxa, S. Shah, Multi-scale mechanical and fracture characteristics and early-age strain capacity of high-performance carbon nanotube/cement nanocomposites. *Cem. Concr. Compos.* 32 (2010) 110–115.
- [41] A. Genaidy, T. Tolaymat, R. Sequeira, M. Rinder, D. Dionysiou, Health effects of exposure to carbon nanofibers: Systematic review, critical appraisal, meta analysis and research to practice perspectives, *Science of The Total Environment*, 407 (12) (2009) 3686-3701.
- [42] Y. Liu, Y.L. Zhao, B.Y. Sun, C.Y. Chen, Understanding the toxicity of carbon nanotubes, *Acc. Chem. Res.* 46 (2013) 702-713.
- [43] S. Lanone, P. Andujar, A. Kermanizadeh, J. Boczkowski, Determinants of carbon nanotube toxicity, *Adv. Drug Deliv. Rev.* 65 (2013) 2063-2069.
- [44] J.E. Goodsell, R.J. Moon, A. Huizar, R.B. Pipes, A strategy for prediction of the elastic properties of epoxy-cellulose nanocrystal-reinforced fiber networks, *Nord Pulp Pap. Res. J.* 29 (1) (2014) 85–94.
- [45] Y. Habibi, A. Dufresne, Highly filled bionanocomposites from functionalized polysaccharide nanocrystals, *Biomacromolecules* 9 (7) (2008) 1974–1980.
- [46] A. Passuello, G. Moriconi, S. P. Shah, Cracking behavior of concrete with shrinkage reducing admixtures and PVA fibers, *Cem. Concr. Compos.* 31 (10) (2009) 699–704.
- [47] N. Soliman, A. Tagnit-Hamou, Using particle packing and statistical approach to optimize eco-efficient ultra-high-performance concrete, *ACI Mat. J.*, 114 (06) (2017) 847-858.
- [48] S. Meddah, A. Tahnit-Hamou, Evaluation of rate of deformation for early-age concrete shrinkage analysis and time zero determination, *J. Mater. Civ. Eng.* 23(7) (2011) 1076-1086.

- [49] P.C. Aïtcin, Demystifying autogenous shrinkage. *Concr. Int.*, 21 (11) (1999) 54–56.
- [50] E. Holt, M. Leivo, Cracking risks associated with early age shrinkage. *Cem. Concr. Compos.* 26(5) (2004) 521–530.
- [51] RILEM Commission 42-CEA, (1981), Properties of set concrete at early-ages,” *Materials and Structures*, 84 (14) 399-460.
- [52] E. Tazawa, S. Miyazawa, Experimental study on mechanism of autogenous shrinkage of concrete.” *Cem. & Conc. Res.*, 28 (8) (1995) 1633–1638.
- [53] E.E. Holt, Contribution of mixture design to chemical and autogenous shrinkage of concrete at early-ages, *Cem. Concr. Res.* 35 (3) (2005) 464-472.
- [54] J. Plank, C.Schroefl, M.Gruber, M. Lesti, , R. Sieber, Effectiveness of polycarboxylate superplasticizers in ultra-high strength concrete: the importance of PCE compatibility with silica fume, *J. Adv. Conc. Tech.* 7 (1) (2009) 5–12.
- [55] N. Soliman, and A. Tagnit-Hamou, Using glass sand as an alternative for quartz sand in UHPC, *J. Const. Build. Mat.* 145 (2017) 243–252.
- [56] F. Wang, Y.Zhou, B. Peng, Z. Liu, S. Hu, Autogenous shrinkage of concrete with super-absorbent polymer, *ACI Mater. J.* 106 (2) (2009) 123-127.
- [57] K. Kovler, Why sealed concrete swells, *ACI Mater. J.* 93 (4) (1996) 334-340.
- [58] V. Baroghel-Bouny, P. Mounanga, A. Khelidj, A. Loukili, N. Rafai, Autogenous deformations of cement pastes: Part II. W/C effects, micro–macro correlations, and threshold values, *Cem. Concr. Res.* 36 (1) (2006) 123-136.
- [59] D. Cusson, T.J. Hoogeveen, An experimental approach for the analysis of early-age behaviour of high-performance concrete structures under restrained shrinkage, *Cem. Concr. Res.* 37 (2) (2007) 200-209.
- [60] A. Kamen, E. Denarié, H. Sadouki, E. Brühwiler, Thermo-mechanical response of UHPFRC at early age - Experimental study and numerical simulation, *Cem. Concr. Res.*, 38 (6) (2008) 822-831.
- [61] Weiss, J., Lura, P., Rajabipour, F. and Sant, G., (2008), “Performance of shrinkage-reducing admixtures at different humidities and at early ages, *ACI Mater. J.* 105 (5) (2008) 478-486.

- [62] P. Lura, Autogenous deformation and internal curing of concrete, PhD. Thesis, Technical University Delft, Netherlands, 2003.
- [63] M.H. Zhang, C.T. Tam, M.P. Leow, Effect of water-to-cementitious materials ratio and silica fume on the autogenous shrinkage of concrete, *Cem. Concr. Res.* 33 (10) (2003) 1687-1694.
- [64] M. Mazloom, A. A. Ramezani-pour, J. J. Brooks, Effect of silica fume on mechanical properties of high-strength concrete, *Cem. Concr. Compos.* 26 (4) (2004) 347–357.
- [65] V. Baroghel-Bouny, A. Kheirbek, Effect of mixparameters on autogenous deformations of cement pastes—microstructural interpretations. In: V. Baroghel-Bouny, P. C Aitcin (eds) *Proceedings of the international RILEM workshop on Shrinkage of concrete “Shrinkage 2000”*. RILEM Publications, Paris
- [66] N. V. Tuan, G. Ye, K. V. Breugel, A.L.A. Fraaij, D.D. Bui, The study of using rice husk ash to produce ultra-high performance concrete, *Constr. Build. Mater.* 25 (4) (2011)2030–2035.
- [67] S. Kawashima, S. P. Shah, Early-age autogenous and drying shrinkage behavior of cellulose fiber-reinforced cementitious materials.” *Cem. Concr. Compos.* 33 (2011) 201–208.
- [68] M. Cheyrezy, V. Maret, L. Frouin, Microstructural Analysis of RPC (Reactive Powder Concrete), *Cem. Concr. Res.* 25 (7) (1995)1491-1500.
- [69] A.M. Neville, *Properties of Concrete*, Pearson Education Limited, Fourth Edition, 2005, p. 844
- [70] C. Porteneuve, H., Zanni, C. Vernet, K. O. Kjellsen, J.-P. Korb, D. Petit, Nuclear magnetic resonance characterization of high-and ultrahigh-performance concrete: Application to the Study of Water Leaching, *Cem. Concr. Res.* 31 (12) (2001) 1887-1893.
- [71] N. A. Soliman, A. Tagnit-Hamou , Partial substitution of silica fume with fine glass powder in UHPC: filling the micro gap, *J. Const. Build. Mat.*, 139 (2017) 374–383.
- [72] J. Ma, J. Dietz, F. Dehn, Ultra High-Performance Self Compacting Concrete. 3rd International Symposium on Self-Compacting Concrete, Reykjavik, Iceland, 17-20 August (2003)136-142.

List of Figures

- Fig. 1. Schematic of hierarchical structure of cellulose filaments (CF)
- Fig. 2. Cellulose filaments (CF): (a) aqueous suspension at 0.3%CF; (b) scanning electron microscope (SEM) image of a dried aqueous suspension illustrating the fibrillated morphology of CF
- Fig. 3. Particle-size distribution of granular materials used in this study
- Fig. 4. Schematic diagram of test set-up for autogenous shrinkage (all dimensions in mm)
- Fig. 5. Water release rate of cellulose filaments (CF) in function of duration of exposure to different relative humidity (RH) levels
- Fig. 6. Evolution of very-early-age (0-12 hours) autogenous deformations in the different ultra-high-performance concrete (UHPC) mixtures
- Fig. 7. Determination of solidification threshold from the rate of deformation and thermal flux: (a) example for the mixture 0CF/25SF
- Fig. 8. Determination of solidification threshold from the rate of deformation and thermal flux: mixture 0.3CF/25SF
- Fig. 9. Evolution of early-age (12 h – 7 days) autogenous deformations in the different ultra-high-performance concrete (UHPC) mixtures (as-recorded deformations)
- Fig. 9. Profile of percentage reduction in autogenous shrinkage deformations during the first 14 days in the different ultra-high-performance concrete (UHPC) mixtures relative to the mixture 0CF/25SF
- Fig. 10. Evolution of early-age (12 h – 7 days) autogenous deformations (zeroed at the time corresponding to the solidification threshold)
- Fig. 11. Long-term deformations in the different ultra-high-performance concrete (UHPC) mixtures
- Fig. 12. Compressive and flexural strength results for the different ultra-high-performance concrete (UHPC) after different curing periods

List of Tables

Table 1. Chemical compositions of powders and granular materials used in the study

Table 2. Ultra-high-performance concrete (UHPC) mixture proportions

Table 3. Fresh properties of tested ultra-high-performance concrete (UHPC) mixtures.

CHAPTER 5

Effect of Cellulose Filaments on Properties of Hardened Concrete

5.1 Introduction

In this chapter, the potential of the nanoscale cellulose filaments (CF) for enhancing the strength properties of hardened cement composites is investigated. The goal of the chapter is to quantify the influence of CF on mechanical properties of cement composites. This was undertaken on cement pastes and concrete mixtures where CF was added at up to 0.20% per weight of binder. In cement paste, the effect of CF on mechanical performance was also evaluated under two curing conditions (wet curing and dry-sealed curing). In outcome, with the incorporation of the CF, it was possible to improve the compressive, tensile, and flexural resistance of cement composites without necessary increasing the binder content. Two mechanisms for explaining the strength gain were proposed: (i) a nanoreinforcing effect whereby the intrinsic strengthening effect of nanocellulose would contribute to bridging cracks at the nano/micro scale as evidenced by microstructural analysis, and (ii) an internal curing effect where the hydrophilic CF would provide supplementary water to promote cement hydration or the hygroscopic CF would provide a pathway for water dispatch from the bulk matrix towards anhydrous grains. Therefore, this chapter contributes to providing a new tool for controlling the mechanical performance of cement composites at the nanoscale. Further details are provided below as part of Article 3 published in the context of this research ([Section 5.2](#)) with supplementary evidences on the sources of enhancement in strength of CF-systems to come later in [Chapter 6](#).

5.2 Article 3- Influence of Cellulose Filaments on Cement Paste and Concrete

Article information

Authors and affiliations:

O.A. Hisseine, PhD candidate and Canada Vanier Scholar of NSERC, Cement and Concrete Research Group, Department of Civil Engineering, Université de Sherbrooke

A. F. Omran, Research associate, Cement and Concrete Research Group, Department of Civil Engineering, Université de Sherbrooke

A. Tagnit-Hamou, Professor and director of Cement and Concrete Research Group, Department of Civil Engineering, Université de Sherbrooke

Article status: Published

Journal: ASCE Journal of Materials in Civil Engineering

Reference: Hisseine, O. A., Omran, A.F., and Tagnit-Hamou, A. (2018c) Influence of Cellulose Filaments on Cement Pastes and Concrete. *ASCE Journal of Materials in Civil Engineering*, vol. 30, n° 6: 04018109.

DOI: [https://doi.org/10.1061/\(ASCE\)MT.1943-5533.0002287](https://doi.org/10.1061/(ASCE)MT.1943-5533.0002287)

Titre français: l'effet des filaments de cellulose sur les pates cimentaire et le béton

Contribution of this article: This article provides a comprehensive assessment of the influence of cellulose filaments (CF) on the properties of cement pastes and concrete. It contributes to the thesis by characterising the opportunities to enhance the mechanical properties of cement composites. Therefore, it contributes to partially achieving the objective 4 of this thesis, namely: exploiting the nanoreinforcing ability of CF to nanoengineer the strength properties of hardened concrete (particularly, the elastic modulus, the flexural capacity, and toughness) and to disclose the mechanism underpinning the way CF influences the strength of cement systems.

Influence of Cellulose Filaments on Cement Paste and Concrete

Ousmane A.Hisseine^{a,b,*} Ahmed F.Omran^a, Arezki Tagnit-Hamou^a

^a Cement and Concrete Research Group, Department of Civil Engineering, Université de Sherbrooke, 2500, Boulevard de l'Université, Sherbrooke, QC, J1K 2R1, Canada

^b Vanier Scholar of the Natural Sciences and Engineering Research Council of Canada (NSERC), Canada

*Corresponding author

**Published in the ASCE Journal of Materials in Civil Engineering
Volume 30 Issue 6 - June 2018**

Abstract

In light of the current increasing interest toward nanomaterials for concrete technology, it appears that nanocellulose (with its incredible properties) can shape a promising sustainable candidate. This study investigates the influence of a new type of nanocellulose materials, namely, cellulose filaments (CF), on the properties of cement pastes and self-consolidating concrete (SCC). CFs were found to alter mixture rheology and improve its stability because of the filaments' hydrophilicity. While the compressive strength of CF pastes was adversely affected (because of air entrainment and filament agglomeration), the flexural capacity was increased by up to 25%. In SCC, all measured mechanical properties were enhanced. Strength improvements of up to 16% (in compression), 34% (in splitting tension), 22% (in flexure), and 96% (in energy absorption) were obtained. These improvements were attributed to two effects imparted by CF: nanoreinforcing and internal curing. The former was evidenced by microstructural analysis, while the latter was confirmed by the assessment of autogenous shrinkage, in which CF reduced the shrinkage strains at 7 days by up to 31%. In SCC, CFs also imparted a viscosity-modifying effect, in which the hardened properties were enhanced via improving mixture stability.

Author keywords: Cement paste; Cellulose filaments; Mechanical performance; Microstructure; Nanocellulose; Self-consolidating concrete (SCC) rheology.

Introduction

In the context of sustainable development, the concrete technology community has been striving constantly to enhance the performance of concrete in different dimensions with a particular focus on eco-efficiency perspectives. Fiber-reinforced concrete (FRC) technology is one of the major leaps in this quest, which has led to concretes with enhanced tensile strength, ductility, toughness, and fatigue resistance (Banthia et al. 1994; Khaloo and Afshari 2005; Altoubat et al. 2016). Nonetheless, there are several concerns about fibers conventionally used in FRC. These concerns include low corrosion resistance in steel fibers (Kosa and Naaman 1990), poor bond with the cementitious matrix and degradability under cement's alkaline medium in glass fibers (Rybin et al. 2016), and low cost effectiveness in carbon and polymer fibers (Chung 2000). In this respect, since cellulose is considered to be the most ubiquitous and renewable natural polymeric raw material on the planet, it may be legitimate to believe that plant-based natural fibers (NF) have the potential to offer the most cost-effective and sustainable alternative reinforcement. Unfortunately, many untreated NFs exhibit durability issues, inconsistency in properties, and poor adherence to the matrix (Romido et al. 2000). NFs are very effective in controlling plastic shrinkage [e.g., 99% reduction in crack width and total crack area with only 0.3% by volume (Boghossian and Wegner 2008)], mitigating drying shrinkage [e.g., 86% reduction in crack width with only 1% by volume (Kawashima and Shah 2011)], and improving the mechanical performance of cement composites [e.g., 20–50% enhancement in flexural strength and fracture toughness when a NF dosage of 2–16% by weight was considered (Sedan et al. 2008; Morton et al. 2010; Merta and Tschegg 2013)]. Nevertheless, the industrial production of NF concrete is currently limited. This is due primarily to the inconsistency in fiber properties leading to variations in concrete performance. The variation in concrete performance hinders an accurate prediction of mechanical behavior (Aziz et al. 1981). Additionally, NFs exhibit another handicap, which is the fibers' vulnerability in the cement's alkaline medium (Ardanuy et al. 2011). This is attributable to the alkaline degradation of some fiber components such as lignin, hemicellulose, pectin, and soluble sugars (Onuaguluchi and Banthia 2016). The advantages offered by NFs could have been optimized if some of these issues were addressed.

Recently, research works in nanoscale plant-based materials have led to the emergence of what is called nanostructured cellulose. This includes an array of cellulosic materials such as nanofibrillated cellulose (NFC), cellulose nanocrystals (CNC), bacterial cellulose (BC), and cellulose filaments (CF). NFC consists of alternating crystalline and amorphous domains made of bundles of stretched cellulose chain molecules with long, flexible, and entangled cellulose nanofibers of approximately 1–100-nm diameter and 500–2,000-nm length (Moon et al. 2011). CNC consists of rodlike highly crystalline cellulose particles of 2–20-nm diameter and 50–500-nm length, thereby exhibiting a lower aspect ratio compared to NFC and a limited flexibility due to the absence of amorphous portions (Brinchi et al. 2013). BC particles are microfibrils secreted by various bacteria and have different morphologies, but they are typically rectangularlike, 6–10 nm wide and 30–50 nm long (Eichhorn et al. 2010). CFs are mechanically processed cellulose fibrils with micrometric length and nanometric diameter. CFs exhibit some structural similarities with NFC, but they have an extended length (100–2,000 μm) compared to their diameter (30–400 nm), thereby resulting in a significantly higher aspect ratio (100–1,000). The treatment of natural fibers at the nanoscale to yield these nanostructured cellulose particles increases the consistency in their material properties (lacking at the macroscale) and removes fibers' degradable compounds. Additionally, the use of nanostructured cellulose can allow exploitation of the power of cellulose polymers that imparts inherent strength to plants through the complex hierarchical structure of cellulose. The incorporation of nanocellulose into cement systems has the further potential to obtain what is called nanomodified concrete (Jongvisuttisun et al. 2013).

Nanomodification of concrete refers to incorporating nanosized objects into concrete to manipulate its nanostructure and control its macro behavior (Jennings et al. 2008) in order to develop a new generation of tailored and multifunctional composites with superior mechanical performance and durability (Sanchez and Sobolev 2010). Published studies on nanomodification of concrete have hitherto covered nanometal oxides (e.g., nanosilica, nanotitanium dioxide, nanoiron oxide, nanoalumina, etc.); nanoclay; carbon nanofibers; and carbon nanotubes. Relevant investigations on nanostructured cellulose are scarce. Whereas the incorporation of nanocellulose in polymer matrices is deep rooted (Boldizar et al. 1987; Favier

et al. 1995; Dufresne and Vignon 1998; Al Turaif 2013), its applications in cement and concrete composites are still nascent. Our survey of literature has indicated that very few investigations have reported on the incorporation of NFC, NCC, and BC in cement composites.

In general, the available literature on the use of nanostructured cellulose in cement composites indicates influences on hydration kinetics, rheological properties, and mechanical performance. Reported effects on hydration kinetics include a reduction in mixture conductivity, impediment of early-age hydration kinetics, and acceleration of the hydration process at later ages (Jongvisuttisun et al. 2013). The influences on rheological properties include an increase in viscosity and yield stress in a shear thinning behavior (Hoyos et al. 2013; Cao et al. 2015), an increase in water and superplasticizer demands, and a decrease in workability (Peters et al. 2010). Nanostructured cellulose also alters the microstructure of cement composites and influences their mechanical performance. Onuaguluchi et al. (2014) reported increases in flexural strength and energy absorption of cement pastes containing 0.1% by weight NFC by approximately 106 and 184%, respectively. Cao et al. (2015) reported improvement in flexural strength of 20–30% at an optimum CNC dosage of 0.2% by weight due to an enhanced degree of hydration. Peters et al. (2010) found that a NFC addition of 0.5% by weight was optimal for improving the fracture properties of ultrahigh-performance concrete. Despite several common features between existing nanocellulose materials and the CFs investigated herein, CFs exhibit the highest aspect ratio owing to their micrometric length but nanometric diameter. Initial applications of CF emerged in the paper and pulp industry, where the strength of sheets made from Kraft pulp was improved by 250% at the addition of 10% CF [X. Hua, M. Laleg, K. Miles, R. Amiri, L. Ettaleb, and G. Dorris, “High aspect ratio cellulose nanofilaments and method for their production,” U.S. Patent No. 9051684 B2 (2015)]. The incorporation of CF in cement systems is a new endeavor addressed in this study, in which the effect of CF at dosages of 0.1, 0.15, and 0.2% by weight on the fresh and hardened properties of paste and self-consolidating concrete (SCC) mixtures was investigated. The influence of CF on fresh and rheological properties, heat of hydration, early-age deformations, microstructure, and mechanical performance was examined. For the cement pastes, the mechanical performance was evaluated

in a function of the curing regime (moist versus sealed) in order to disclose the effect of CF on internal curing.

Experimental Program

Materials Properties

Four cement pastes and four SCC mixtures were considered in this study. Type General Use (GU) cement and Class F fly ash (FA) with Blaine fineness values of 431 and 287 m²/kg, respectively, were used. The chemical composition determined by X-ray fluorescence for the cement includes 20.5%SiO₂, 4.0%Al₂O₃, 2.0%Fe₂O₃, 63.2% CaO, 2.2% MgO, 3.4%SO₃, and 1.1%Na₂O_{eq}. For FA, the chemical composition includes 53.7%SiO₂, 17.5%Al₂O₃, 5.6%Fe₂O₃, 12.4% CaO, 2.1% MgO, 1.4%SO₃, and 3.6%Na₂O_{eq}. The CF used in this study was manufactured and provided by Kruger Biomaterials (Trois-Rivières, Québec, Canada) in a semidispersed form (a nominal moisture content of 70%). The filaments were extracted from wood pulp through a process (patent pending) that uses only mechanical energy. Generally, wood pulp is made of a large amount of cellulose macrofibers. The wall structure of cellulose macrofibers is composed of bunches of closely stacked cellulose microfibrils organized around a cavity called a fiber lumen. A single cellulose microfibril is composed of tiny bands of cellulose microfibrils, which, when peeled axially, create CFs. CFs represent an intrinsic part of the hierarchical structure of cellulose (Fig. 1), which imparts intrinsic strength to plant-based materials. The extraction process of CF involves the removal of matrix impurities such as lignin, pectin, wax, and soluble sugars. As a result, CF contains mainly cellulose (>95%) and a small amount of hemicellulose.

To prepare CF suspensions (with different CF concentrations), the as-received CF material was added to the mixing water and homogenized by high shear mixing. Fig. 2 shows pictures of water suspensions with varying CF contents, while Figs. 3 and 4 depict field emission gun-scanning electron microscopy (FEG-SEM) images of a dried CF diluted suspension with 0.1% CF. The figures illustrate the fibrillar morphology for a network of filaments (Fig. 3) and for some individual fibrils (Fig. 4).

In the SCC mixtures, crushed limestone coarse aggregates with 5–14 mm maximum size, 2.77 specific gravity, and 0.52% water absorption rate were used. Natural river sand with a specific gravity of 2.65 and an absorption rate of 0.9% was employed. A polycarboxylate-based high-range water-reducing admixture (HRWRA) with 32% solid content—fulfilling the requirements of ASTM C494 Type F admixtures (2016a)—was added at a constant dosage of 2.5 L/m³ to secure the target flowability of 750 mm in the plain SCC mixture.

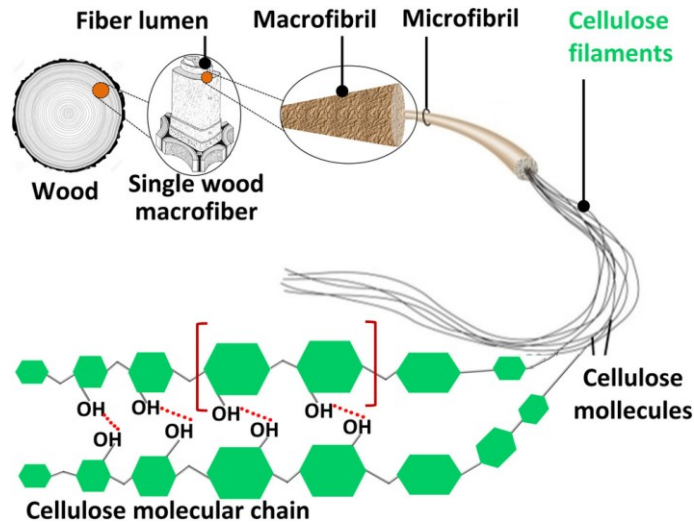


Fig. 1. Schematic of hierarchical structure of cellulose filaments (CFs)

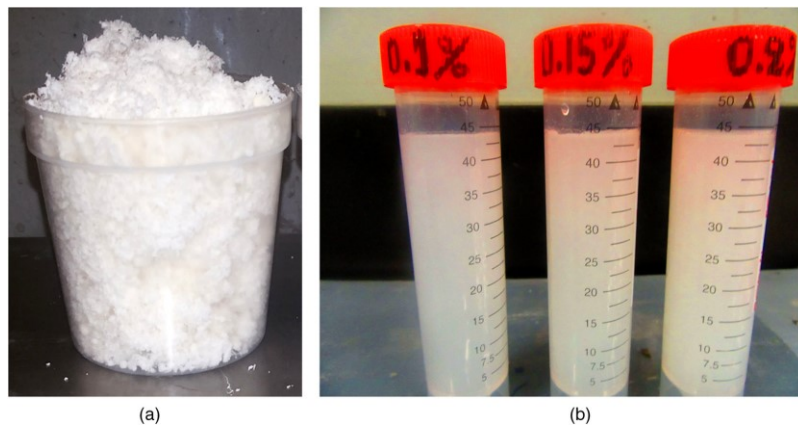


Fig. 2. Cellulose filament (CF) (a) in a semi-dispersed form, as received, and (b) in aqueous suspensions used to prepare the mixes

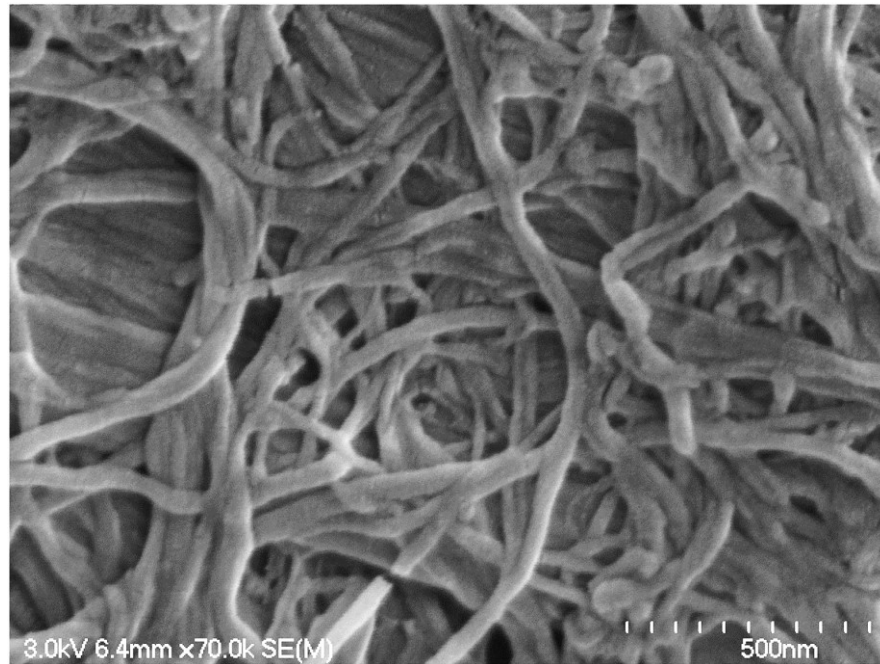


Fig. 3. SEM image of a dried diluted CF aqueous suspension with 0.1% CF: CF network

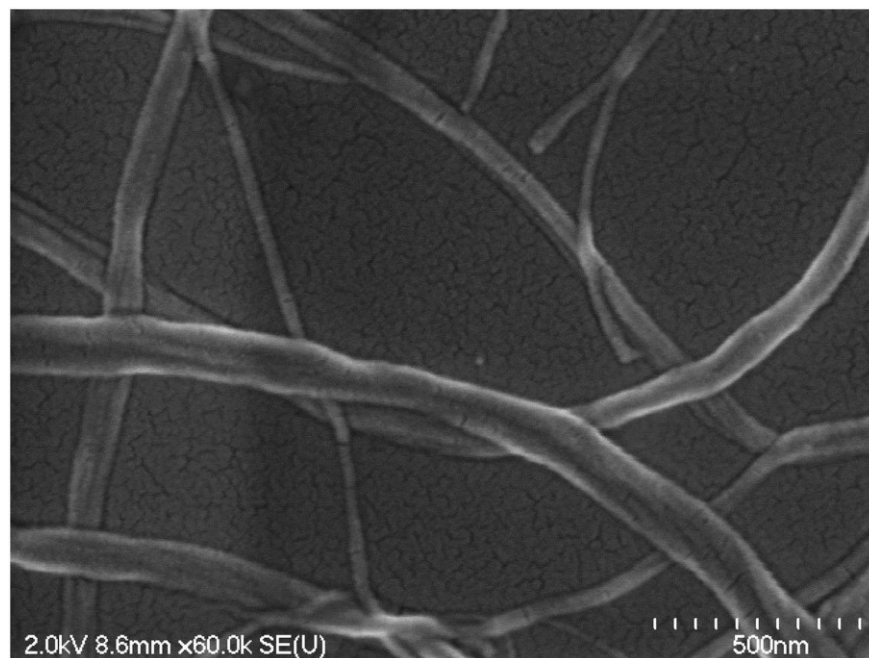


Fig. 4. SEM image of a dried diluted CF aqueous suspension with 0.1% CF: Individual fibrils

Mixture Proportions and Mixing Procedures

Four paste mixtures were designed with cement: FA: water proportions of 1.00: 0.33: 0.50 by mass, respectively. The mixtures contain, respectively, 0, 0.1, 0.15, and 0.2% by weight CF. FA was incorporated in pastes to be consistent with the SCC systems investigated in parallel. The above mixtures were used in all tests conducted on pastes, excluding autogenous shrinkage, where a slightly different recipe was adopted and detailed later in the relevant section. All paste mixtures were prepared following the ASTM C305 guidelines (ASTM 2014a).

Four SCC mixtures were designed with a water-to-binder ratio (W/BW/B) of 0.42: a reference mixture with no CF (designated in this manuscript as Ref.) and three mixtures incorporating CF at dosages of 0.1, 0.15, and 0.2% by weight of binder (Table 1).

Table 1. Concrete mix proportions

Component	Control	0.1% CF	0.15% CF	0.2% CF
Cellulose filament (CF), kg/m ³	-	0.487	0.731	0.974
Type GU cement, kg/m ³			365	
Class F fly ash, kg/m ³			122	
Total binder, kg/m ³			487	
Water, kg/m ³			200	
<i>W/B</i>			0.42	
Sand (0-5 mm), kg/m ³			804	
Coarse Aggregate (5-14 mm), kg/m ³			825	
HRWRA, L/m ³			2.5	

An aqueous suspension of CF was prepared by diluting the as-received material into water by applying high shear mixing for 60 s using a 700-watt blunt-blade blender. CF disintegration was carried out for 10 s at a low speed (100 rps); 20 s at a moderate speed (200 rps); and 30 s at a high speed (300 rps) in an attempt to disentangle filament clumps. To attenuate filament damage during mixing, the blender was carefully selected so as to have a two-tip horizontally laid blade with blunt (less sharp) edges. This was an attempt to foster the disintegration of filaments by the resulting rotational energy created in the suspension rather than by the blades' torque alone.

The above dispersion protocol was adopted by the authors upon investigating the effectiveness of other strategies, namely, magnetic-field shearing, ultrasonication, and dispersion with surfactants.

For paste mixtures where no HRWRA was used, the resulting CF suspension was then added to the total adjusted mixing water. For SCC mixtures, a HRWRA was added to the adjusted mixing water, and the resulting suspension was split into two halves, one of which was mixed with the CF suspension. The ensuing mixture (CF-water-HRWRA) was homogenized by shaking the suspension for approximately 30 s. This step could have also been carried out by stirring since it is simply an extra precaution for an already dispersed CF suspension. Paste systems were prepared using a Globe SP20 mixer, while the SCC mixtures were prepared using a Crown C9 concrete mixer. Detailed mixing procedures for pastes and concrete mixtures are described in Table 2.

Table 2. Mixing procedure

System	Mixing procedure
Pastes	Add mixing water in the form of CF suspension.
	Add cement (and fly ash) to the water and allow 30 sec for water absorption.
	Mix at low speed for 30 sec. Stop the mixer for 15 sec, scrape during this time. Mix at medium speed for 60 sec.
Concretes	Add aggregate and sand, mix for 1 min.
	Add the first half of water containing CF, mix for 1 min.
	Add cement (and fly ash), mix for ½ min.
	During mixing at above step, add the 2 nd half of water, continue mixing for 2.5 min.
	Pause for 2 min to allow air bubbles to evacuate. Remix for 2 min, then start casting.

Curing and Testing Procedures

The influence of two curing regimes (moist versus sealed) on the mechanical properties was investigated for paste mixtures. This was intended to assess the potential effect of CF on internal curing. For moist curing, the paste specimens were kept in a curing room at 100% relative humidity (RH) and 22°C until the time of testing. In the sealed curing condition, the paste specimens were hermetically wrapped with adhesive plastic sheets and kept in a controlled medium (50% RH and 22°C) for 7 days, followed by unwrapping and storing the specimens in the same environment for an additional 21 days.

For concrete mixtures, upon casting, samples were stored in a room with a RH and temperature of approximately 50% and 23°C, respectively, for 24±1 h. Then they were demolded and transferred for storage in a fog room at 100% RH and 22°C temperature until the age of testing. The different test methods adopted to execute the experimental program are elaborated in the following sections.

Tests of Moisture Content and Water Retention/Release Capacity of CF

The moisture content (*MC*) of the as-received CF was determined on five samples of 5.0 g mass kept in an oven at 60°C. The samples were regularly measured during a period of 18 h until the mass loss stabilized at a final mass of 1.7±0.02 g. This corresponds to 34% of the initial 5.0 g mass. To examine the possible effects of the filament's *MC* on the mixing water during the preparation of pastes and concretes, a set of CF samples of 0.3 g were subjected to centrifugation at 2,000; 3,000; and 4,000 rpm. For each centrifugation speed, the mass loss was evaluated after 10, 20, and 30 min of centrifugation. The water retention capacity (*WRC*) of CF was determined using the following methodology: A 30.0 g sample of as-received CF was kept in an oven at 60°C until a final mass of 10.2 g of dry CF (34% of the initial mass) was obtained. Several CF suspensions were prepared by mixing 0.1 g of dry CF (referred to herein as M0M0) with 1.9 g of distilled water. The well-tight samples were then stored at 22°C and 50% RH until tested at predetermined water immersion durations (i.e., 1, 3, 6, 12, 24, 48, or 72 h). For each water immersion duration, four samples were subjected to centrifugation at 3,000 rpm for 25 min using 2-mL centrifugal filters of 100,000 molecular weight cutoff (MWCU) to drain out water.

The resulting CF was accurately weighed for its wetted mass (M_1) and the WRC was determined as

$$WRC = \left(\frac{M_1 - M_0}{M_0} \right) \times 100\% \quad (1)$$

To evaluate the water release rate (WRR) of CF, after the WRC test, the samples for 72-h immersion were exposed to $38 \pm 1^\circ\text{C}$ and $20 \pm 1\%$ RH. The samples were then accurately weighed and their mass (M_2) after moisture loss was recorded after a series of exposure durations (0.17, 0.5, 2, 3, 4, 8, 12, 16, 20, 24, and 48 h). The WRR was calculated as follows:

$$WRR = \left(\frac{M_1 - M_2}{M_1 - M_0} \right) \times 100\% \quad (2)$$

Tests on Paste Mixtures

Fresh and Rheological Properties

The fresh properties of pastes included the mini-slump-cone test [ASTM C230 (ASTM 2014b)], the mini-V-funnel test (EFNARC 2005), the air content [ASTM C185 (ASTM 2015)], and the temperature. In the mini-slump-cone test, the spreading diameter was measured immediately after cone lifting and also after subjecting the sample to 25 blows from the flow table. Moreover, the rheology of all paste mixtures was assessed using a coaxial-cylinder rheometer with a serrated surface and cup and bob diameters of 28.911 and 26.660 mm, respectively, providing a shear gap size of 1.126 mm.

Isothermal Calorimetry

The heat evolution in all paste mixtures was monitored using a TAM air isothermal calorimeter (TA Instruments, New Castle, Delaware) following the guidelines of ASTM C1702 (ASTM 2017). From each mixture, a 3.0 g sample was placed into a calorimetric chamber (kept at a constant temperature of $22 \pm 0.1^\circ\text{C}$). Measurements were collected for a continuous period of 28 h and were used to assess the effect of CF on the heat evolution of different paste mixtures.

Autogenous Shrinkage

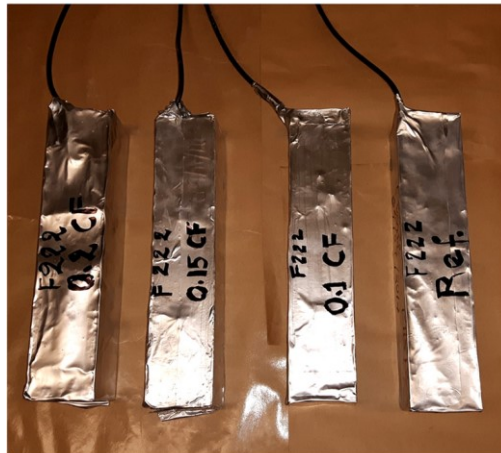
Autogenous deformations were measured to assess the potential effect of CF on internal curing. A plain paste mixture and three mixtures containing CF (at 0.1, 0.15, and 0.2% CF) were considered for this purpose. As is well known, autogenous shrinkage occurs in all cement composites, but it is more evident in systems with a low water-to-cement (W/C) ratio (Tazawa and Miyazawa 1995). Therefore, paste mixtures with a slightly lower W/C (0.35) were designed to mobilize autogenous shrinkage so that the potential effect of CF on this phenomenon can be better captured. The reduction of W/C , however, necessitated the introduction of a water reducer to maintain mixture flowability (a mini-slump flow diameter of 250 ± 15 mm). A HRWRA with a dosage of 0.25% by weight of cement was introduced on a solid basis. This dosage was slightly increased to 0.27, 0.30, and 0.35% by weight in the specimens with 0.1, 0.15, and 0.2% CF, respectively. Paste prisms measuring $80 \times 80 \times 350$ mm were instrumented with embedded vibrating-wire strain gauges of type EM-5 (Roctest, Saint-Lambert, Québec, Canada) of 144Ω resistance and a strain range of $3,000 \mu\epsilon$ [Fig. 5(a)]. Additional to measuring deformations resulting from autogenous shrinkage, the gauge is also equipped with a thermocouple to record temperature evolutions in the paste throughout the testing period so that temperature-borne deformations can be subtracted from the total deformation. To ensure full embedment of the gauge in the paste, the gauge was set centered in the mold (in all directions) using attachment wires so as to allow it a free rotation and axial translation (necessary to respond to the matrix linear deformations). The fresh cement pastes were placed in the mold in two layers and were consolidated following the procedures detailed in ASTM C157 (ASTM 2014d). The molds containing the pastes were hermetically sealed with adhesive plastic wraps immediately after casting and remained so until demolded 24 ± 0.5 h later. Immediately after demolding (within $2 \pm 1/2$ min), the specimens were sealed with an adhesive aluminum foil and kept in a controlled environment (50% RH and 22°C) for 7+days7+days [Fig. 5(b)]. Data were automatically recorded via an acquisition system at a 30 min frequency during the first day and 4 h frequency thereafter.

Parallel to the measurements of autogenous deformations, the setting time of the tested paste mixtures was determined by the Vicat needle test [ASTM C191 (ASTM 2013)]. The final setting

time was used as a datum for the readings of autogenous deformations. This is because, prior to the final setting time, as the paste is still plastic, deformations are predominantly due to (1) the chemical shrinkage resulting from the vigorous exothermal reactions accompanying the hydration of the cement's active phases and (2) the potential deformation of the strain gauge itself due to the rise of temperature as the cement hydrates. Moreover, the splitting-tensile strength (f_{sp}) was evaluated on 100×200 mm paste cylinders at 1, 3, and 7 days in accordance with ASTM C496 guidelines (ASTM 2011) in an attempt to unveil a reinforcing action of CF, if any.



(a)



(b)

Fig. 5. Test set-up for autogenous shrinkage: (a) mold with an embedded vibrating-wire strain gauge, and (b) specimens sealed with adhesive aluminum foil and connected to a data-acquisition

Mechanical Properties

Specimens for mechanical properties were cast from each paste mixture soon after mixing and then demolded 24±1 h later. For each paste mixture, cube samples (50×50×50 mm) and prisms

(50×50×160 mm) were prepared to assess the mechanical performance. The cubes were tested for compressive strength (f_c) at 1, 7, and 28 days according to ASTM C109 guidelines (ASTM 2016c), while the prisms were tested for flexural capacity (f_f) at 28 days according to ASTM C348 guidelines (ASTM 2014c). Mechanical properties at all ages (under both curing regimes) were tested on a minimum of three samples. The average value was used to compare the performance of different mixtures.

Microstructural Analysis

A high-resolution field emission gun (FEG) scanning electron microscopy (SEM) of type Hitachi S-4700 (Tokyo, Japan) equipped with an Oxford energy dispersive spectroscopy (EDS) of type X-Max (Oxford Instruments, Abingdon, United Kingdom) was employed to analyze the microstructure of cement pastes. Analysis was conducted on fresh fractured surfaces to promote the visibility of CF. Test specimens were coated with gold palladium for 60 s to assuage the effect of surface charges induced by the ultrahigh-energy electron beam. A double-faced adhesive carbon film was placed between the specimen and the specimen-holding plate to foster conductivity. A secondary electron (SE) detector, operated at 2.0 or 3.0 kV accelerating voltage and an emission current of 10 μ A, was adopted for the analysis of the fractured specimens.

Tests on Concrete Mixtures

Fresh and rheological properties

For the concrete mixtures, the assessment of fresh properties was carried out using common SCC fresh property tests which included: (i) the slump-flow diameter, the time required to reach a 500 mm spread diameter (T_{500}), and the visual stability index (VSI) [ASTM C1611 (ASTM 2014f)]; (ii) the J-Ring spread diameter and blockage ratio [ASTM C1621 (ASTM 2014e)]; and (iii) the V-Funnel (EFNARC 2005).

The rheology of concrete mixtures was assessed using a ConTec 5 rheometer which consists of a fixed outer cylinder and an inner rotating bladed cylinder. The rotation speed was adjusted to increase from 0.025 to 0.5 rps in 10 points such that 50 resistance-time measurements are

recorded at each point. For the analysis of the rheological measurements, the Bingham model (Bingham and M. Reiner 1933) was adopted to characterize the mixture flow behavior by measuring the rheology data such as yield stress (τ_0), plastic viscosity (μ_{pl}), shear stress (τ), and shear rate ($\dot{\gamma}$).

Mechanical properties

For each concrete mixture, the f_c [ASTM C39 (ASTM 2016b)] at 1, 7, and 28 days and f_{sp} [ASTM C496 (ASTM 2011)] at 28 days were measured using 100×200 mm cylinders. The f_{fl} [ASTM C78 (ASTM 2016d)] and the flexural toughness (T_b) were evaluated using 100×100×400 mm prisms (at 28 days). The flexural tests were performed under four-point bending configuration in a displacement-controlled mode using a displacement rate of 0.0008 mm/s. T_b was determined following the JSCE SF-4 approach (JSCE 1984) where T_b is defined as the area under the load-deflection curve until a deflection of 1/150 of span. It is also defined alternatively as the area immediately before failure if the specified deflection was not reached. The area under the load-deflection curve from flexural testing was calculated using the Trapz built-in function in *MATLAB*.

Microstructural analysis

The microstructural investigations on concrete mixtures were carried out on fresh fractured concrete samples at the age of 28 days following the same testing techniques adopted for paste mixtures described earlier.

Results of Tests for CF Moisture Content and Water Retention/Release

Results of the MC of CFs are presented in Fig. 6. The moisture loss at 60°C was very steep in the first 4 h and then stabilized thereafter until the mass of the dry CF became constant (at 34% of the initial mass) beyond 18 h. The MC of CF at the time of preparing the paste and concrete mixtures can be taken as 66%. However, this suspended water was not considered in calculating the mixing water. In fact, as mentioned earlier, a series of tests were conducted to examine the possible effect of the filament's MC on the mixing water. These tests showed that upon

subjecting the as-received material to centrifugation at 2,000; 3,000; and 4,000 rpm (for up to 30 min), no mass loss was recorded at all. The results of the WRC of CF are shown in Fig. 7. The figure shows that within 1 h of saturation in water, CF can imbibe up to 80% of its mass. The WRC exceeds 100% by 6 h of saturation and stabilizes at 125% when CF was saturated for 72 h. CF samples obtained from WRC tests at 72 h of saturation followed by centrifugation at 3,000 rpm for 25 min released their absorbed water according to the trend shown in Fig. 8. The WRR of CF exceeded 50% by 4 h of exposure to a dry medium ($38 \pm 1^\circ\text{C}$ and $20 \pm 1\%\text{RH}$) and plateaued at 96.8% in 48 h. Whereas this trend gives an indication of the water desorption of CF, a more comprehensive assessment would examine the WRR under variable RH, particularly at higher RH.

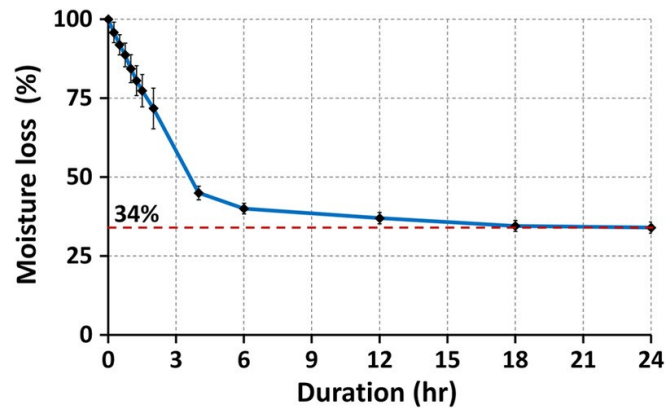


Fig. 6. Moisture content in CF. The figure shows the mass loss at 60°C .

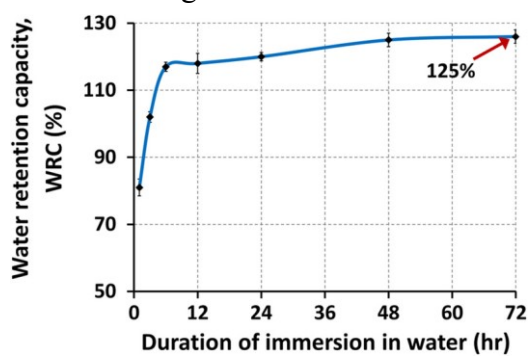


Fig. 7. Water retention capacity of CF in function of the duration of saturation in water.

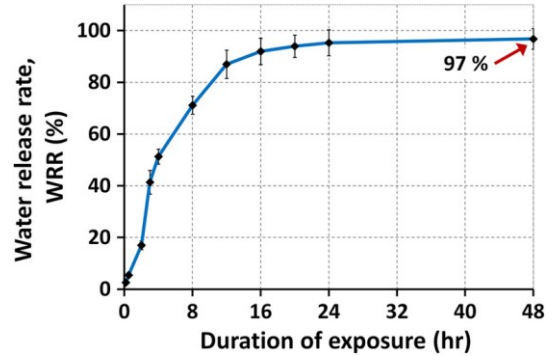


Fig. 8. Water release rate of CF in function of the duration of exposure to a dry medium

Results and Discussion for Paste Mixtures

Fresh Properties and Rheology

The fresh properties of all paste mixtures are presented in [Table 3](#). The results show that CF significantly altered mixture workability. Whereas the slump-flow diameter (before shocking) was 160 mm in the reference paste, the incorporation of CF at dosages of 0.1, 0.15, and 0.2% reduced the slump flow diameter to 100, 90, and 85 mm, respectively. After 25 blows on the flow table, the reference paste had a flow diameter of 330 mm, while the incorporation of CF at dosages of 0.1, 0.15, and 0.2% reduced the slump flow diameter to 290, 270, and 240 mm, respectively. The decrease in workability exhibited in mixtures with CF was directly reflected by a remarkably higher V-funnel passing time. From 3.50 s passing time in the reference mixture, the incorporation of CF at 0.1, 0.15, and 0.2% augmented the passing time to about 13, 25, and 42 s, respectively. This corresponds to about 4, 7, and 12 times the passing time of the reference paste. These observations indicate a significant reduction in workability when CF is used. This is further evidenced by the results in [Fig. 9](#) for the rheological measurements of the plain paste mixture and the mixtures with 0.1 and 0.15% CF. The mixture with 0.2% was not tested as its viscosity was beyond the device limit. [Fig. 9](#) indicates that the incorporation of CF at a dosage of 0.15%, for instance, increased the yield stress and the plastic viscosity of the reference paste by 35 and 42%, respectively. This can be reflected by an increased mixture cohesion and homogeneity and can be attributed to the hydrophilic nature of CF and to its nanometric fibrillar structure. The hydrophilicity of CF leads to water adsorption whereby water molecules adhere peripherally to CFs, thereby fixing some of the mixing water. This is confirmed by the water absorption capacity of CF described in the previous section where CF can imbibe water up to 80% of its mass within 1 h and more than 100% of its mass by 6 h. Additionally, the nanometric fibrillar structure, flexibility, and high aspect ratio of CF promote the intertwining and entanglement of individual filaments and/or the formation of filament networks, which can increase mixture viscosity and enhance its stability. Such effects on mixture flow and rheology have also been observed in some polysaccharide viscosity-modifying agents (VMAs) with a microbial source, such as welan gum ([Khayat 1995](#)). On the other hand,

whereas the addition of CF increased the viscosity, it was observed that mixtures with CF exhibited higher air content. For the three tested CF dosages (0.1, 0.15, and 0.2%), the amount of entrapped air was respectively 1.7, 2.8, and 3.2 times that of the reference paste. While this entrapped air could contribute to attenuating the sharp rise in viscosity (Struble and Jiang 2004) caused by CF, it may lead to adverse effects on mechanical performance.

Table 3. Fresh properties of paste mixtures.

Paste Mixture	Temperature (°C)	Air content (%)	Slump flow diameter (mm)		V-Funnel passing time (s)
			Before	After	
Ref.	26.0	0.68	160	330	3.50
0.1% CF	27.5	1.16	100	290	13.21
0.15% CF	29.3	1.87	90	270	25.42
0.2% CF	29.7	2.18	85	240	42.13

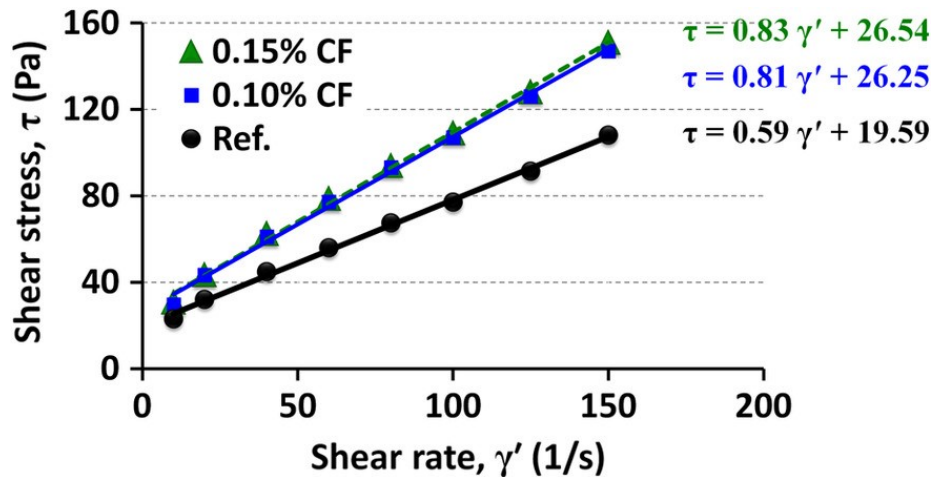


Fig. 9. Rheological measurements of cement pastes.

Isothermal Calorimetry

Heat evolutions in the different paste mixtures are depicted in Fig. 10. The figure reveals two behaviors where the effect of CF varies from insignificant during the first 7 h to a relatively slight increase in heat flow later. The figure also shows slightly higher and broader silicate hydration peaks in the mixtures incorporating CF. This is further confirmed by the cumulative heat release whereby the total released heat was slightly higher in all CF mixtures compared to that of the reference mixture. The mixture with 0.15% CF, for instance, exhibited 7% higher cumulative heat release than that of the reference mixture. Such a trend is common in nanocellulose materials with high purity in cellulose and has been reported in a more pronounced manner in cellulose-based polymers (Mishra et al. 2003), microcrystalline cellulose (Hoyos et al. 2013), cellulose nanofibers (Onuaguluchi et al. 2014), cellulose nanocrystals (Cao et al. 2015), and bacterial nanocellulose (Mohammadkazemi et al. 2015). The increased heat of hydration observed in CF mixtures can be linked to the alkaline hydrolysis of cellulose, which is an exothermic reaction that promotes cement hydration and leads to a sort of acceleration (Knill and Kennedy 2003). This is further confirmed by the reduced setting time recorded in CF-SCC mixtures investigated in parallel.

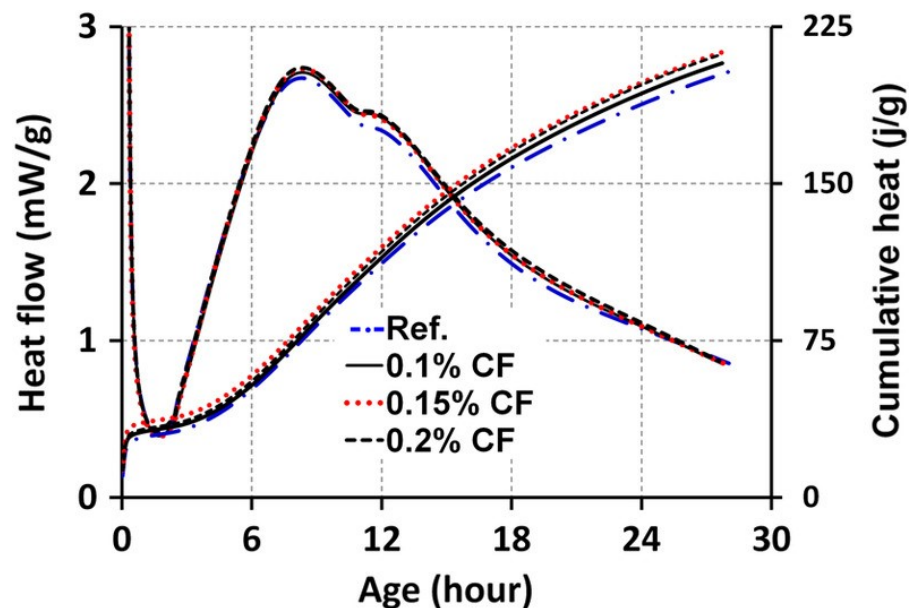


Fig. 10. Hydration heat flow and cumulative hydration heat release in paste mixtures.

Autogenous Shrinkage

Table 4 presents some of the fresh and hardened properties for the pastes considered for autogenous shrinkage. Results from the Vicat setting time indicate that mixtures with CF exhibited some slight retardation. Referring to the aforementioned results of isothermal calorimetry where mixtures with CF exhibited slightly higher heat release, the retardation experienced herein may be attributable to the effect of HRWRA. While the increasing dosage of HRWRA in pastes with CF enabled attaining the target slump flow diameter of 250 ± 15 mm, it may have been responsible for the observed retardation. Such effects are well reported for increasing dosages of polycarboxylate-based HRWRAs (Zingg et al. 2009). Results of autogenous shrinkage measurements showed that the incorporation of CF altered the early-age deformations in the cementitious matrix. Fig. 11 shows that paste mixtures with CF exhibited lower autogenous shrinkage at all ages. At 7 days, for instance, the reference paste recorded a shrinkage strain of $366 \mu\epsilon$. This value was reduced to 340, 257, and $235 \mu\epsilon$ when CF was incorporated at dosages of 0.1, 0.15, and 0.2%, respectively. This corresponds to a reduction in autogenous shrinkage strains of 8, 31, and 36% for the three respective CF addition rates. The observed reduction in autogenous shrinkage deformations in pastes with CF may be associated with an internal curing effect imparted by CF. The CF's hydrophilic and hygroscopic features (discussed earlier) can provide a sort of internal water reservoir. The latter regulates the matrix's internal moisture, which could have otherwise been destabilized by the water loss as cement hydration proceeds. On the other hand, the extremely small size of CF coupled with the omnipresence of hydroxyl groups on its surface may promote CF interactions with the cementitious matrix such that CFs retain water and dispatch it to the matrix to partially replenish the emptying cement pores. This reduces self-desiccation and attenuates early-age deformations, in consequence. This is analogous to the well-reported effect of lightweight aggregates (LWA) and superabsorbent polymers (SAP) on reducing shrinkage deformations in cementitious systems. In this regard, conditional to adequate CF dosage and dispersion, the effectiveness of CFs could be even better. This can be justified by the fact that when CF is used in this perspective, its advantage is twofold. This is because the filaments, additional to their effect on internal curing, may collaterally increase the matrix tensile capacity through filament bridging,

fracture, or pullout. Evidence for this interpretation was found in the splitting-tensile strength (f_{sp}) tests conducted (parallel to the autogenous shrinkage measurements) at 1, 3, and 7 days. Results from those tests indicated that while no effect of CF was noticed on the 1-day strength, increases in f_{sp} of 8 and 17% (relative to the reference) were recorded at 3 and 7 days, respectively, in the mixture with 0.15% CF, for instance (Table 4).

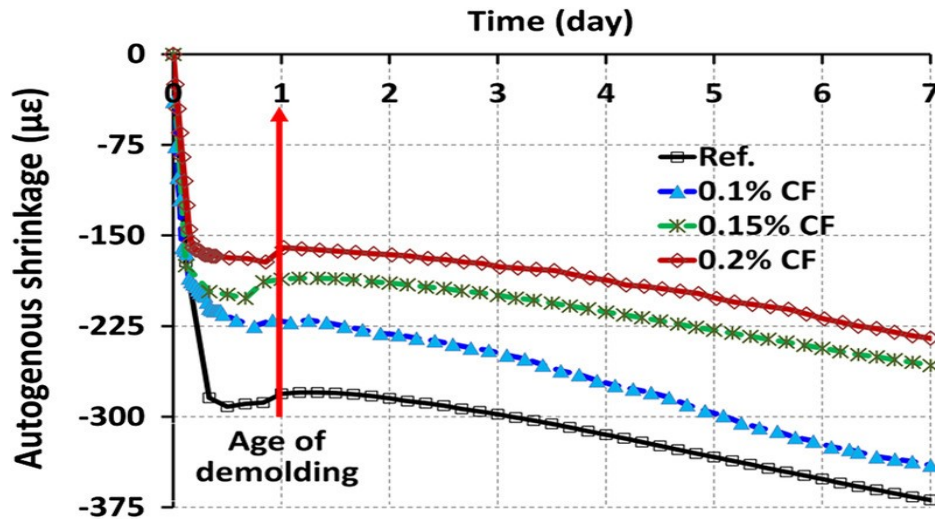


Fig. 11. Early age deformations in paste mixtures

Table 4. Some fresh and hardened properties of paste mixtures studied for autogenous shrinkage

Paste Mixture	Slump (mm)	Vicat final setting-time (min)	Splitting tensile strength (MPa)		
			1 day	3 days	7 days
Ref.	265	418	1.52	2.35	3.18
0.1% CF	255	431	1.45	2.48	3.32
0.15% CF	245	439	1.50	2.54	3.71
0.2% CF	240	442	1.39	2.42	3.68

Mechanical Properties

The compressive strength (f_c) results for all paste mixtures are depicted in Fig. 12. The figure indicates that in cement pastes, the addition of CF adversely affected f_c under both curing regimes (moist and sealed). Furthermore, the reduction in f_c was exacerbated as CF concentration increased. This can be traced to the air entrainment caused by the inclusion of CF as indicated earlier. Such a reduction in f_c was also reported for macrocellulose fibers owing to the amount of entrapped air (Soroushian and Marikunte 1990). Also, the decrease in f_c in paste mixtures can be attributed to the increased likelihood of filament agglomeration (when CF content increases) as supported by our microstructural analysis addressed in the next section. In contrast to f_c , the results of flexural strength (f_{fl}) of cement pastes illustrated in Fig. 13 for both curing regimes reveal that the addition of CF enhanced the flexural capacity—with higher improvements obtained under the sealed curing condition. The reference mixture, for instance, had comparable strengths under both curing regimes. CF mixtures, however, showed higher f_{fl} in sealed curing than in moist curing. For the three CF dosages (0.1, 0.15, and 0.2%), the improvements in f_{fl} under the moist curing condition were 10, 25, and 28%, respectively, relative to reference. For the sealed curing, this corresponded to 19, 34, and 38%, respectively, relative to the corresponding reference. These results suggest that the improvement in f_{fl} can possibly be linked to a combined effect of (1) CF acting as nanoreinforcement owing to CF's fibrillar morphology and (2) CF serving as an internal curing agent for its water affinity and retention/release capacity. This can curtail self-desiccation, thereby leading to a volumetrically stable matrix as supported by the autogenous shrinkage measurements. However, while internal curing can contribute to explaining the increased f_{fl} of dry-sealed CF specimens relative to that of their reference, the reduced f_{fl} measured in the moist condition for all specimens relative to their counterparts in the dry condition suggests that another phenomenon may prevail. This is because if internal curing alone dominates the increase in f_{fl} in the sealed curing regime, it must do so or even better in the moist curing regime (when water is supplied internally and externally). In fact, the reduction of f_{fl} in moist-cured specimens is attributable to the excessive water saturation under this condition. Owing to the hygroscopic nature of CF, its moisture content can considerably influence the mechanical properties of CF-cement composites. This is

due to the well-reported effect of water saturation on reducing the f_{fl} of cementitious matrices incorporating natural fibers. Onuaguluchi and Banthia (2016), for instance, recorded an 18–51% decrease in the f_{fl} of natural fiber–cement systems subjected to water saturation. This reduction is attributable to the deterioration of the interfibrillar hydrogen bonds as well the fiber–matrix interfacial bonds. This softens the fibers and weakens their bonds with the matrix. As a result, the fibers mainly fail in pullout (Coutts and Kightly 1984). The effect of moisture on the f_{fl} of cement systems with natural fibers has also been reported by El-Ashkar et al. (2007) who found that natural fiber–cement mortars dried in an oven exhibited higher f_{fl} than those cured in air or in water.

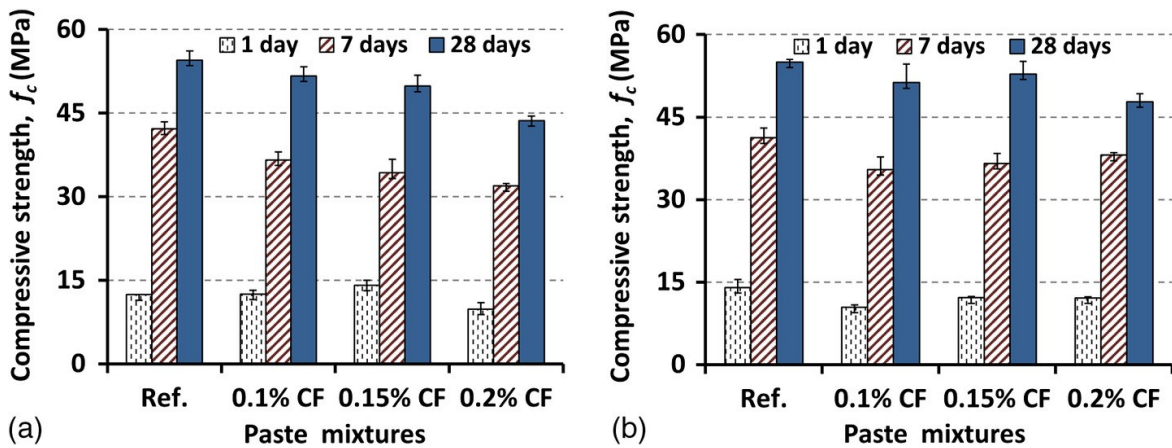


Fig. 12. Compressive strength (f_c) in pastes: (a) moist curing; (b) sealed curing

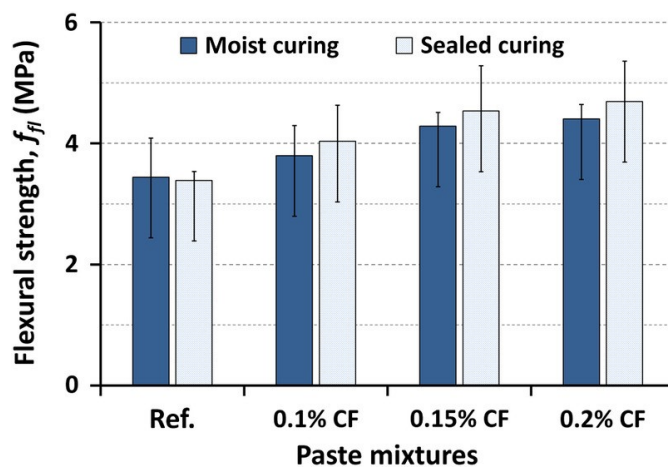


Fig. 13. Flexural strength (f_{fl}) of paste mixtures at 28 days

Microstructural Analysis

Microstructure investigations conducted using FEG-SEM on fresh fractured paste samples revealed that CFs adhere well to the structure of the cementitious matrix. Fig. 14 shows several CFs cemented into the CSH from one side and connected to parts of the matrix from another side. The bottom of the figure also shows several CFs well integrated in the matrix while bridging two parts of the hydrated system and interfering with matrix pores. The adherence of CF in the matrix is further supported by the SEM image of Fig. 15. Moreover, Fig. 16 shows few CFs with protruding ends, which may have been cut during specimen fracture. The figure shows a filament in the middle with an indented cross section, which seems to support the hygroscopic character of CF. The interaction of CFs with the hydrated system may contribute to explaining the enhancement in mechanical properties, particularly f_{sp} and f_{fl} in CF-containing cement systems—elaborated in the previous section. On the other hand, Fig. 17(a) shows some spots in the mixture with 0.2% CF, where CF clumps were observed.

The high surface area of CF and its extremely small size render the dispersion a difficult task, particularly as CF dosage increases. This consequently jeopardizes mechanical performance (particularly in compression) and may result in the reduction in f_c observed in paste mixtures. Under compression, CF entanglements such as the ones depicted in Fig. 17(b) lead to increasing the porous network, thereby reducing f_c . However, this adverse effect may not be the same in flexural loading, where pulling out the entangled filaments or fracturing them necessitates additional energy. This builds up the matrix fracture resistance through the FRC mechanism.

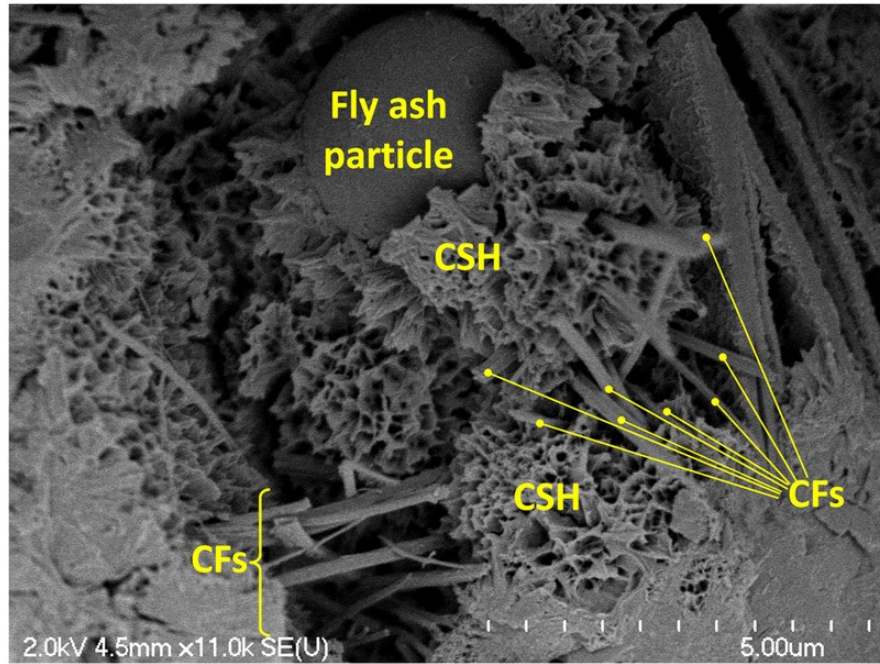


Fig. 14. SEM image of a paste mixture with 0.1% CF.

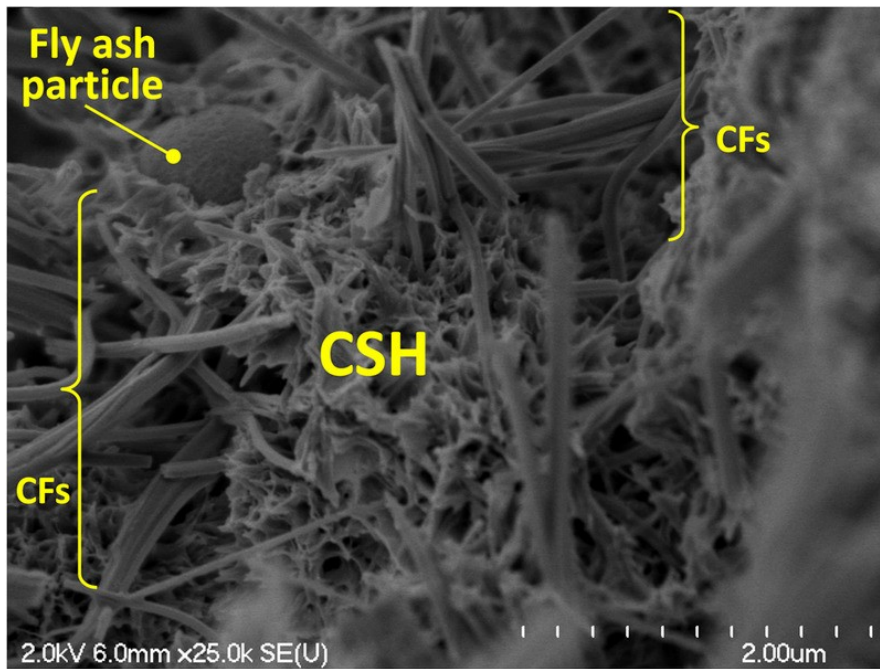


Fig. 15. SEM image of a paste mixture with 0.15% CF

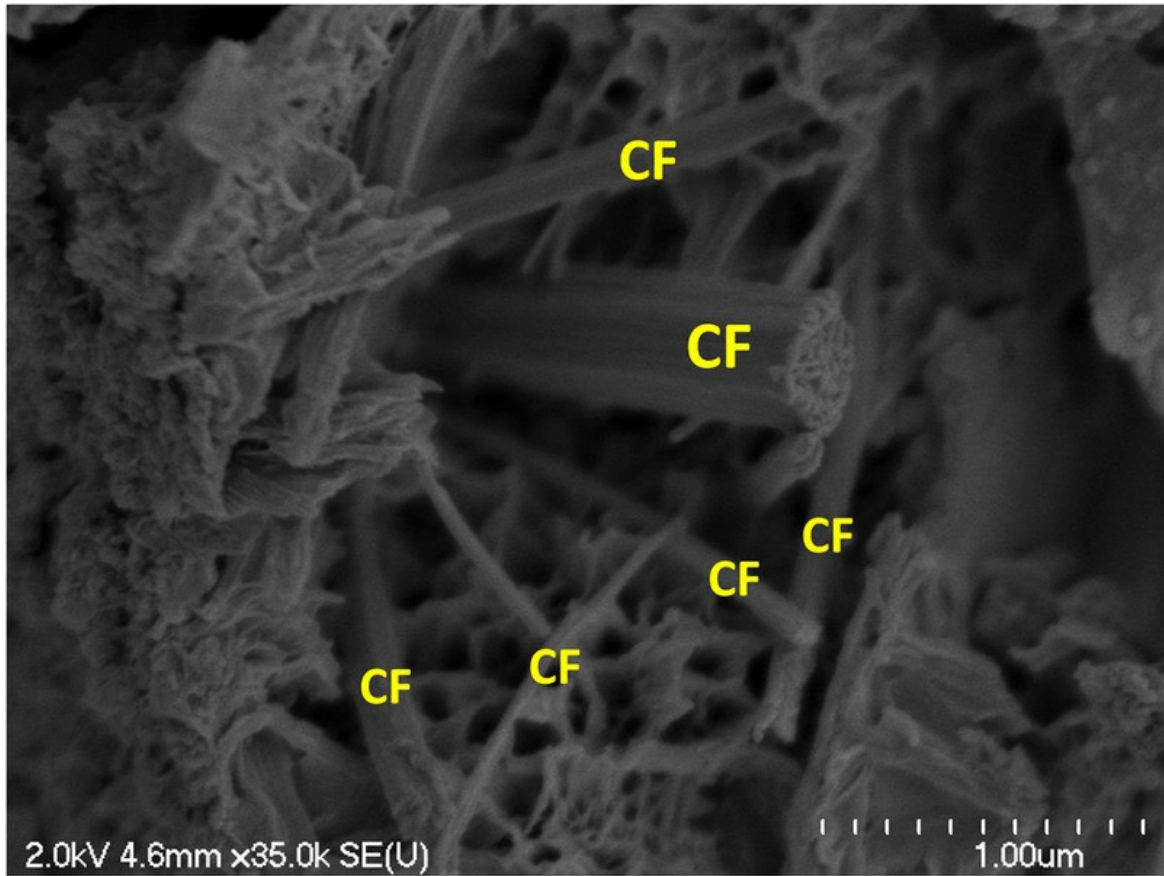


Fig. 16. SEM image of a paste mixture with 0.2% CF.

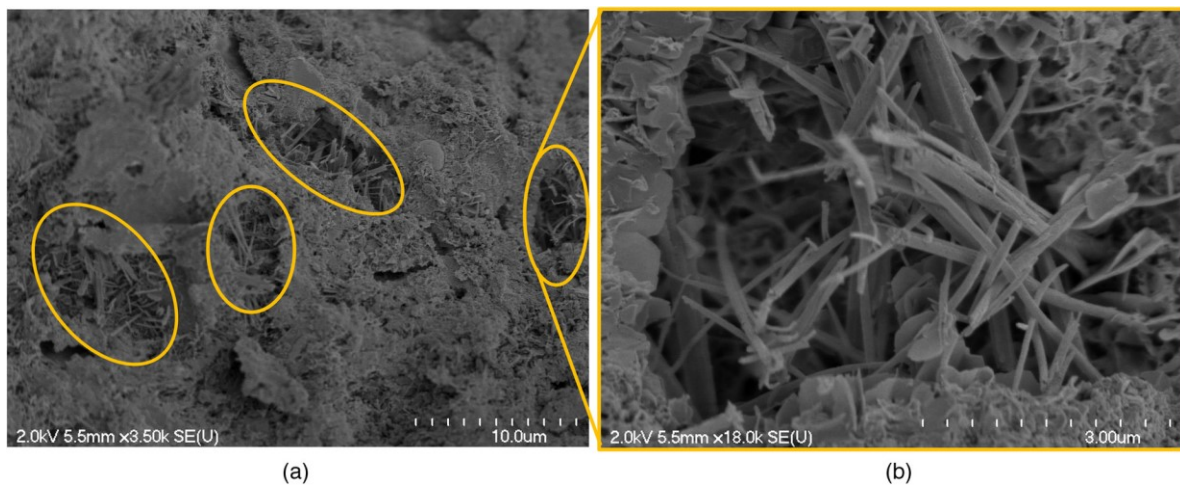


Fig. 17. SEM image of a paste with 0.2% CF: (a) CF agglomeration spots; (b) CF entanglements.

Results and Discussion for Concrete Mixtures

Flow Properties and Rheology

The results of fresh properties of the tested SCC mixtures are presented in [Table 5](#). Data in the table indicate that the addition of CF significantly altered mixture workability. A reduction in the flow diameter (slump and J-ring) of more than 50% relative to the reference mixture and a significant increase in flow time (T_{500} and V-funnel times) were observed for CF additions of 0.15 and 0.2%. This reveals that CFs considerably altered mixture workability and viscosity. This is also confirmed by rheological measurements, which show that the addition of CF significantly increased the evolution of the shear stress (τ) versus shear rate (γ') for all tested SCC mixtures ([Fig. 18](#)). This is accompanied by a significant increase in the yield stress (τ_0) and plastic viscosity (μ_{pl}). For CF dosages of 0.1, 0.15, and 0.2%, the values of τ_0 were, respectively, 2, 5, and 8 times greater than that of the reference mixture. This reflects the increased stability and the consequent high energy necessary to start the flow when CFs are used. Nonetheless, once the flow starts, the increments in μ_{pl} are relatively smaller, as [Fig. 18](#) shows. The figure indicates increments in μ_{pl} of 1.5, 1.8, and 2.1 times that of the reference mix for CF dosages of 0.1, 0.15, and 0.2%, respectively. These are, in fact, lower than the corresponding aforementioned increments in τ_0 . This indicates the reduced mixture resistance to flow once the latter starts. The observed trend of a sharp increase in τ_0 while μ_{pl} remained relatively attenuated is often associated with high apparent viscosity (μ_{app}) at low values of γ' , but low μ_{app} as γ' increases. Such a behavior describes a high degree of pseudoplasticity (or shear thinning behavior), which is an interesting feature in flowable concrete. This is because the increased μ_{app} at low values of γ' contributes to maintaining mixture constituents in suspension (hence more homogenous and stable mixtures). On the other hand, the attenuated μ_{app} at high values of γ' facilitates pumping and consolidation ([Ghio and Monteiro 1997](#)). Such a rheological response in mixtures with CF suggests that the high τ_0 is attributed to the hydrophilic nature of CF, leading to moisture absorption, and to the high aspect ratio and flexibility of CFs, leading to the creation of filament networks. This increases the viscosity buildup at low levels of γ' . At

high levels of γ' , however, CF networks are more likely to be either pulverized or streamlined in the direction of flow, thereby leading to the attenuated rise in viscosity.

Table 5. Fresh properties of SCC mixtures

Mix	Air content, %	Density, kg/m ³	Slump flow		J-Ring		V-Funnel
			Diameter, mm	T_{500} , s	Diameter, mm	Blockage ratio	T (s)
Ref.	1.0	2315	785	1.83	770	0.86	2.13
0.10%	1.5	2373	538	5.12	455	0.67	5.34
0.15%	3.0	2316	320	-	310	0.60	14.75
0.20%	3.1	2320	305	-	300	0.55	20.34

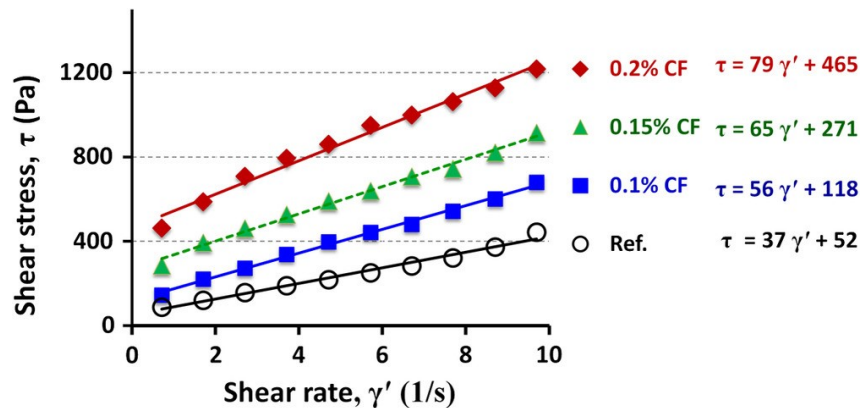


Fig. 18. Flow curves fitted to Bingham model for SCC mixtures

Mechanical Properties

Fig. 19 presents the results of the compressive strength (f_c) of all concrete mixtures where the influence of CF varies from no effect at 1 day, to a marginal effect at 7 days, and to a moderate effect (up to 16% increase) at 28 days. It is observable that the trend of f_c in concrete mixtures is opposite to the decreasing trend noticed in cement pastes. This could be attributable to the fact that the fine and coarse aggregates in concrete mixtures may have partially contributed to increasing the shear mixing energy (imparted by only the mixer in the case of pastes). The effect of aggregates and the overall gradation of mixture constituents on increasing the shear mixing

energy can favor disintegrating CF clumps and/or aligning them in the flow direction. This promotes CF dispersion, which in turn, contributes to the improvement in f_c . This is consistent with the observations made in the previous section on CF-concrete mixtures exhibiting a high degree of shear thinning behavior, where μ_{app} was high at low values of γ' (due to the propensity of CF to water and to the formation of CF networks), but decreased with increasing γ' (due to the breakage of filament networks and/or alignment of individual fibrils in the direction of flow). The shear thinning behavior imparted by CF increases the mixture's ability to maintain its variable-density constituents in suspension and reduces their inherent tendency to segregation. This fosters mixture homogeneity and stability and enhances, in consequence, the properties of the hardened product, including f_c . While the decrease in the f_c of pastes was attributed to the air entrainment and poor dispersion of CF, the latter appears to be more influential because air entrainment by CF was observed in paste and concrete mixtures alike. As such, the HRWRA (used in concrete mixtures but not in pastes) may have positively affected the f_c of concrete mixtures in two ways: the first through dispersing CF, particularly when a suspension of CF-water-HRWRA was prepared and homogenized for that purpose prior to introduction to the mixer, and the second through deflocculating cement flocks, thereby fostering cement dispersion and increasing the degree of cement hydration.

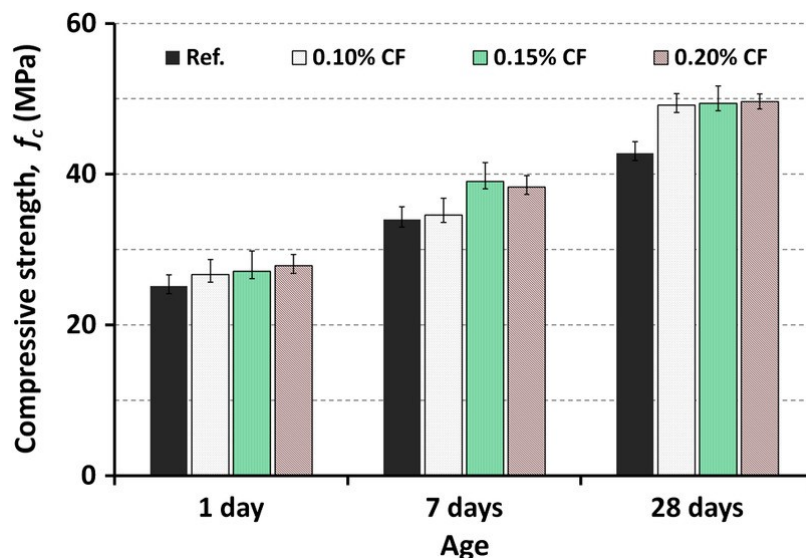


Fig. 19. Compressive strength (f_c) of SCC mixtures

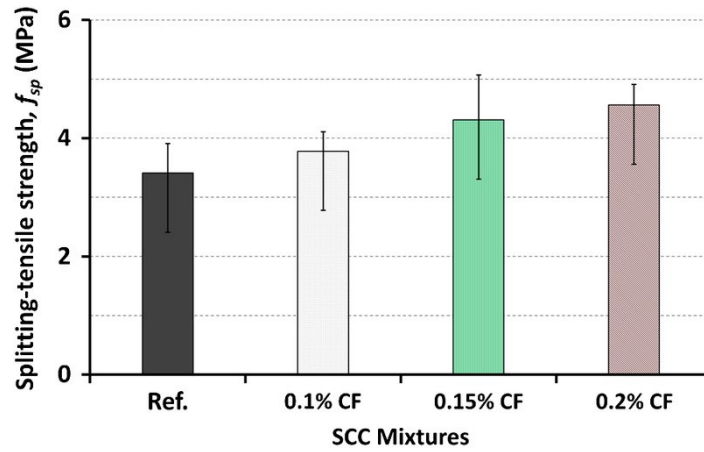
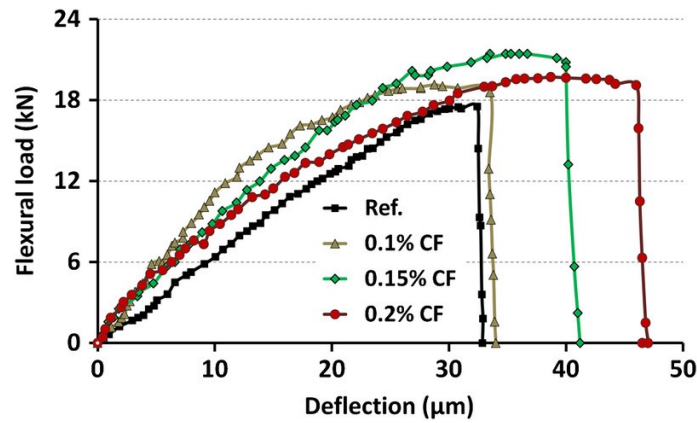
Fig. 20. Splitting-tensile strength (f_{sp}) of SCC mixtures.

Fig. 21. Load-deflection response for SCC mixtures at 28 days.

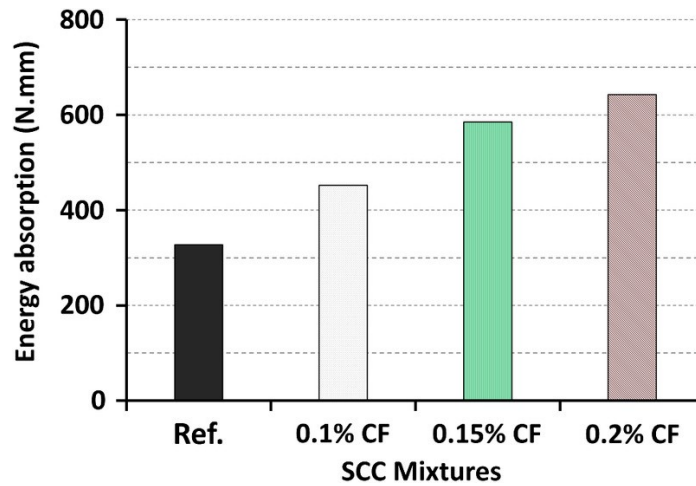


Fig. 22. Energy absorption capacity of SCC mixtures.

The effect of CFs on the mechanical properties of concrete is more pronounced in the splitting-tensile strength (f_{sp}) and flexural capacity (f_{fl}), in which the filaments are more likely to be solicited to serve as nanoreinforcements. Fig. 20 reveals increases in f_{sp} of 11, 26, and 34% (above the reference SCC) for the three respective CF dosages (0.1, 0.15, and 0.2%). These observations are further supported by the results of f_{fl} and the energy-absorption capacity (toughness) depicted in Figs. 21 and 22, respectively. Results from the four-point flexural tests (Fig. 21) indicate that the stiffness of all CF incorporating specimens was higher than that of the reference and that the incorporation of CF at dosages of 0.1, 0.15, and 0.2% increased the load-carrying capacity of the plain SCC by 9, 22, and 13%, respectively.

On the other hand, Figs. 21 and 22 indicate some toughening effects imparted by CF. The reference specimen failed at a relatively lower load than all specimens containing CF, and the drop in its load-carrying capacity was sharp, as expected. Specimens with CF, however, sustained the peak load for some additional range of microdeflections prior to failure as evidenced by the plateauing of the corresponding load-deflection responses. Consequently, the energy-absorption capacity depicted in Fig. 22 shows that the addition of CF at dosages of 0.1, 0.15, and 0.2% enhanced the energy-absorption capacity of the reference specimen by 33, 68, and 96%, respectively. It is observable that whereas the f_{fl} reached a peak value at the CF dosage of 0.15%, higher energy-absorption capacity was recorded at 0.2% CF. This suggests that, under flexural loading, CFs can slightly influence the post-peak behavior by withstanding some tensile stresses little beyond the ultimate load so as to partially enhance sustaining the peak load for some extra microdeflections. Consequently, the enhanced energy-absorption capacity imparted by CF was reflected by an increase in the peak displacement by up to 43% above the plain SCC.

The increased energy-absorption capacity and the resulting increased peak displacement with higher CF dosage while the f_{fl} was relatively low can be juxtaposed to what is often encountered in FRC with macrofibers. In FRC with macrofibers, the flexural capacity (peak load or rupture strength) is often sensitive to f_c , whereas the post-peak behavior, however, is rather influenced by the strengthening and toughening effects imparted by the FRC mechanism (Altoubat et al. 2016). The strengthening and toughening effects in FRC are governed by fiber bridging, the

fiber/matrix interfacial bond, and fiber pullout (Lin et al. 2009). These are known to consume increasing fracture energy depending on fiber characteristics, particularly, length, tensile capacity, bond with the matrix, and fiber count. In spite of the extended CF aspect ratio as compared to other nanocellulose particles, the filaments are extremely short when compared to the conventional fibers used in FRC. This alters the fracture behavior of CF-reinforced concrete in contrast to conventional FRC. As such, in light of the results of the f_t and toughness presented in Figs. 21 and 22, respectively, it is possible that the following scenarios prevail in the fracture behavior in the tested SCC mixtures: Firstly, in the case of the SCC with 0.1% CF, for instance, it can be perceived that once concrete is cracked, the insufficient CF length and fiber count fail to transfer tensile stresses across the matrix microcracks. Consequently, the concrete composite fractures. Secondly, in the specimen with 0.15% CF, it is possible that the slightly higher fiber count allows the transfer of some tensile stresses across the microcracks before they become macrocracks. This instantaneously delays the loss of the load-carrying capacity but cannot alter its sharp drop once started. Finally, in the specimen with 0.2% CF, it can be perceived that the relatively higher fiber count may have allowed the transfer of more tensile stresses across the microcracked section. This results in the observed delayed failure (as more energy is required to pull the filaments out from the cracked surfaces) and reflects the composite's relatively increased fracture resistance. Nonetheless, the toughening effect imparted by CF remains restrained by the CFs' size. While the filaments' micrometric size may allow bridging nano/microcracks, the formation of macrocracks causes an abrupt matrix rupture. As a result, the degradation in the load-carrying capacity (once it starts) has never been gradual (in any CF-containing specimen) as the typical behavior encountered in conventional FRC. Hence, a blend of CF and macrofibers is expected to possibly result in a synergetic effect, such that both pre-peak and post-peak behaviors are improved.

Microstructural Analysis

The microstructure investigations of concrete mixtures are shown in Figs. 23–26. Fig. 23 shows a mixture with 0.2% CF, exhibiting several CFs with their fibrillar morphology quite evident, several protruding ends of CFs that may have been cut during sample fracturing, and a set of traces of filament pullout. This indicates a potential underlying filament bridging/fracturing mechanism contributing to enhancing the mechanical performance. On the other hand, Figs. 24–26 show the presence of several CFs in the interfacial transition zone (ITZ) in the SCC mixtures with 0.1, 0.15, and 0.2% CF, respectively. The ITZ is generally perceived to have lower structural properties, much coarser pores, and easily cleavable highly soluble CH crystals compared to the bulk cementitious matrix (Ollivier et al. 1995; Wang et al. 2009; Erdem et al. 2012). This is generally associated to the wall effect, in which the aggregates appear locally flat relative to the cement grains, which disrupts cement packing (Scrivener et al. 2004), or to the microbleeding effect that leads to the accumulation of mixture water beneath the aggregates during consolidation (Goldman and Bentur 1992). This makes the ITZ the weakest link of the microstructural system, where cracking initiates, and thus it has a phenomenal effect on the mechanical and transport properties of concrete (Nemati et al. 1998; Wong et al. 2009). In this regard, the addition of CFs appears to reinforce the ITZ, thereby contributing to the improved mechanical properties. This could substantiate the enhancement in f_{sp} and f_{fl} in CF mixtures elaborated earlier.

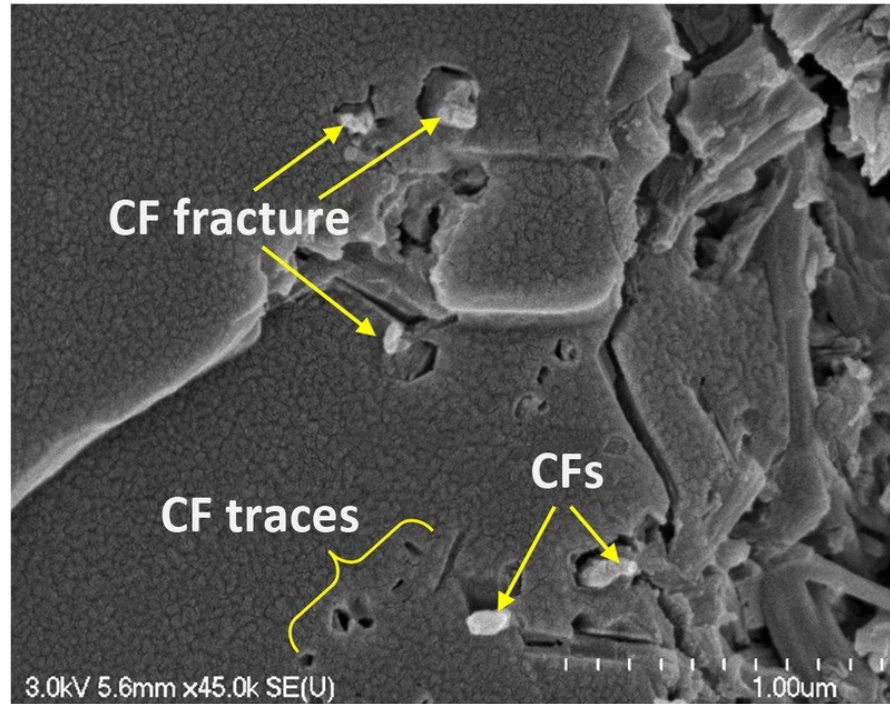


Fig. 23. SEM image of a fractured SCC specimen 0.2% CF.

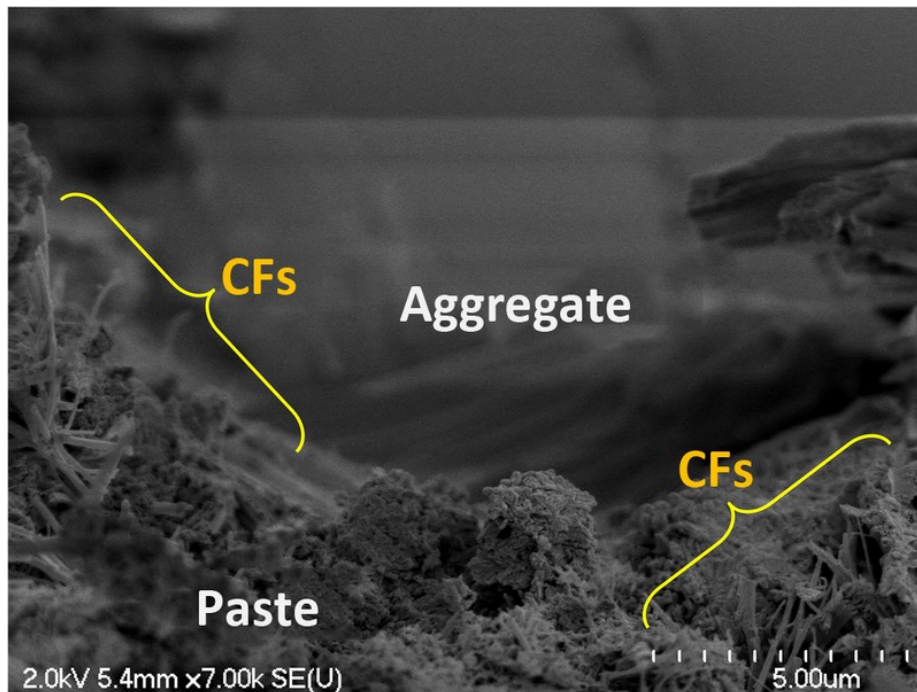


Fig. 24. SEM image illustrating the presence of CFs in the ITZ in the SCC with 0.1% CF.

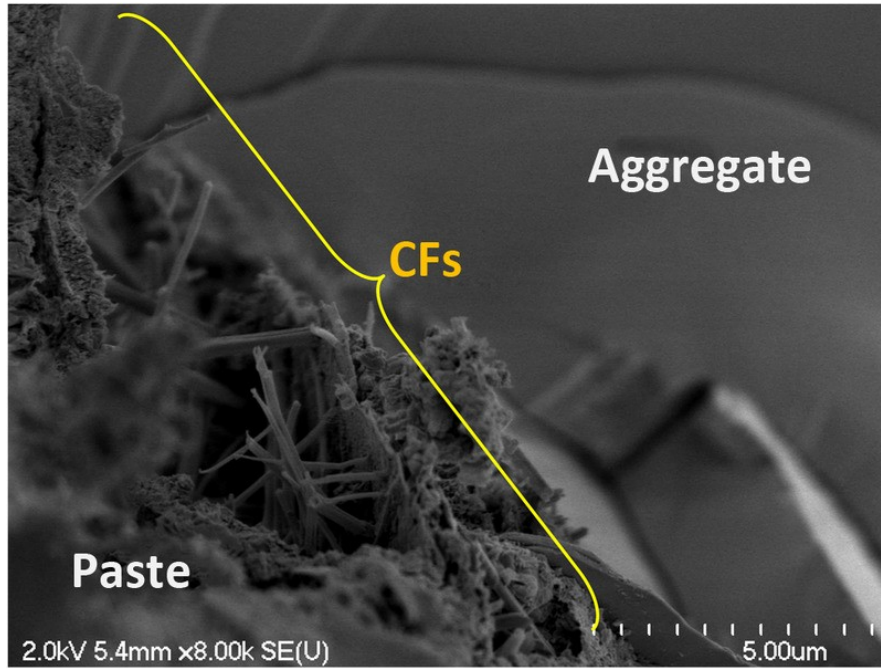


Fig. 25. SEM image illustrating the presence of CFs in the ITZ in the SCC with 0.15% CF.

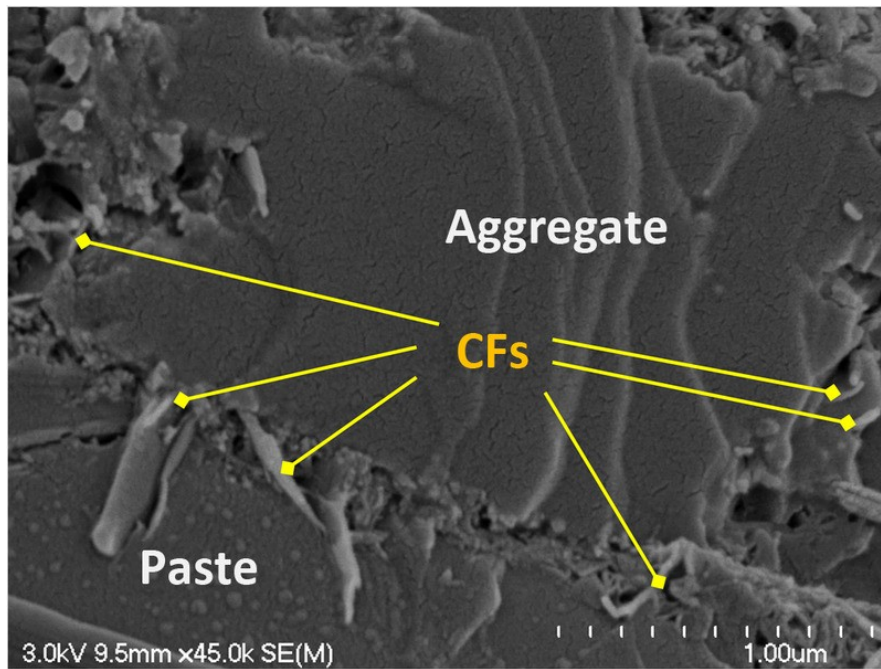


Fig. 26. SEM image illustrating the presence of CFs in the ITZ in the SCC with 0.2% CF.

Conclusions

This study investigated the influence of a new type of nanocellulose materials, namely cellulose filaments, on the performance of cement and concrete systems. The effects of CF addition at 0, 0.1, 0.15, and 0.2% by weight on the properties of cement pastes and SCC mixtures were examined. In paste systems, the mechanical properties were examined in a function of the curing regime (moist versus sealed). The results indicated that CFs altered mixture rheology and improved the stability of SCC mixtures owing to CF's hydrophilicity coupled with its high aspect ratio and flexibility. The improved mixture stability contributed to enhancement of the hardened product. Results from the mechanical performance of cement pastes revealed that the compressive strength was negatively affected. This was traceable to the air entrainment and the formation of filament clumps as CF dosage increased. However, the flexural strength in all CF paste mixtures was higher and improvement of up to 25% relative to the plain mixture was recorded. In SCC mixtures, all mechanical properties were improved. Relative to the plain SCC, strength improvement of up to 16% (in compression), 34% (in splitting tension), 22% (in flexure), and 96% (in energy absorption) were recorded. The enhanced energy-absorption capacity imparted by CF was reflected by an increase in the peak displacement by up to 43% above the plain concrete mixture. This implies a higher strain capacity, which is attractive for applications where structures are required to exhibit such behavior prior to failure, such as in impact- and blast-resisting structures. The improved mechanical performance in paste and concrete mixtures incorporating CF can be attributed to the following mechanisms:

- An internal curing effect, in which CFs act as internal water reservoirs to attenuate self-desiccation and reduce early-age deformations, thereby leading to improved strength. This is supported by the results of the autogenous shrinkage assessment, in which the addition of CF at 0.1, 0.15, and 0.2% reduced the autogenous shrinkage strains of the plain system at 7 days by 8, 31, and 36%.
- A nanoreinforcing effect, in which CFs were found to adhere to the structure of the cementitious matrix and integrate with the hydrated system as supported by the microstructural investigations. For SCC mixtures, the results showed that the CFs'

nanoreinforcing effect is hybridized with a viscosity-modifying effect. In this case, the CFs' hydrophilicity and fibrillar morphology contributed to improving the mechanical properties by enhancing mixture stability and homogeneity and improving the skeleton of the hardened product, in consequence. CFs were also found to reinforce the interfacial transition zone, thereby contributing to improvements in mechanical performance.

Acknowledgments

This project is jointly supported by a Cooperative Research and Development (CRD) grant from the Natural Sciences and Engineering Research Council of Canada (NSERC), Canada Vanier Graduate Scholarship (CGS) program award no: 360284, Kruger Biomaterials, Inc. (QC, Canada), and Euclid Chemicals. The authors are grateful for the financial support from all of these partners.

References

- Altoubat, S., Ousmane, H., and Barakat, S. (2016). "Experimental study of in-plane shear behaviour of fiber-reinforced concrete composite deck slabs." *J. Struct. Eng.*, 10.1061/(ASCE)ST.1943-541X.0001413, 04015156.
- Al-Turaif, H. A. (2013). "Relationship between tensile properties and film formation kinetics of epoxy resin reinforced with nanofibrillated cellulose." *Prog. Org. Coat.*, 76(2–3), 477–481.
- Ardanuy, M., Claramunt, J., García-Hortal, J. A., and Barra, M. (2011). "Fiber-matrix interactions in cement mortar composites reinforced with cellulosic fibers." *Cellulose*, 18(2), 281–289.
- ASTM. (2011). "Standard test method for splitting tensile strength of cylindrical concrete specimens." *ASTM C496/C496M-11*, West Conshohocken, PA.
- ASTM. (2013). "Standard test methods for time of setting of hydraulic cement by Vicat needle." *ASTM C191-13*, West Conshohocken, PA.
- ASTM. (2014a). "Standard practice for mechanical mixing of hydraulic cement pastes and mortars of plastic consistency." *ASTM C305-14*, West Conshohocken, PA.

- ASTM. (2014b). “Standard specification for flow table for use in tests of hydraulic cement.” ASTM C230/C230M-14, West Conshohocken, PA.
- ASTM. (2014c). “Standard test method for flexural strength of hydraulic cement mortars.” ASTM C348-14, West Conshohocken, PA.
- ASTM. (2014d). “Standard test method for length change of hardened hydraulic-cement mortar and concrete.” ASTM C157/C157M-08, West Conshohocken, PA.
- ASTM. (2014e). “Standard test method for passing ability of selfconsolidating concrete by J-ring.” ASTM C1621/C1621M-14, West Conshohocken, PA.
- ASTM. (2014f). “Standard test method for slump flow of self-consolidating concrete.” ASTM C1611/C1611M-14, West Conshohocken, PA.
- ASTM. (2015). “Standard test method for air content of hydraulic cement mortar.” ASTM C185-15, West Conshohocken, PA.
- ASTM. (2016a). “Standard specification for chemical admixtures for concrete.” ASTM C494/C494M-16, West Conshohocken, PA.
- ASTM. (2016b). “Standard test method for compressive strength of cylindrical concrete specimens.” ASTM C39/C39M-16, West Conshohocken, PA.
- ASTM. (2016c). “Standard test method for compressive strength of hydraulic cement mortars.” ASTM C109/C109M-16, West Conshohocken, PA.
- ASTM. (2016d). “Standard test method for flexural strength of concrete (using simple beam with third-point loading).” ASTM C78/C78M-16, West Conshohocken, PA.
- ASTM. (2017). “Standard test method for measurement of heat of hydration of hydraulic cementitious materials using isothermal conduction calorimetry.” ASTM C1702-17, West Conshohocken, PA.
- Aziz, M. A., Paramasivam, P., and Lee, S. L. (1981). “Prospects for natural fibre reinforced concretes in construction.” *Int. J. Cem. Compos. Lightweight Concr.*, 3(2), 123–132.
- Banthia, N., Moncef, A., Chokri, K., and Sheng, J. (1994). “Micro-fiber reinforced cement composites: Uniaxial tensile response.” *Can. J. Civ. Eng.*, 21(6), 999–1011.
- Bingham, E. C., and Reiner, M. (1933). “The rheological properties of cement and cement–mortar–stone.” *Physics*, 4(3), 88–96.

- Boghossian, E., and Wegner, L. D. (2008). "Use of flax fibres to reduce plastic shrinkage cracking in concrete." *Cem. Concr. Compos.*, 30(10), 929–937.
- Boldizar, A., Klason, C., Kubat, J., Naslund, P., and Shah, P. (1987). "Prehydrolyzed cellulose as reinforcing filler for thermoplastics." *Int. J. Polym. Mater.*, 11(4), 229–262.
- Brinchi, L., Cotana, F., Fortunati, E., and Kenny, J. M. (2013). "Production of nanocrystalline cellulose from lignocellulosic biomass: Technology and applications." *Carbohydr. Polym.*, 94(1), 154–169.
- Cao, Y., Zavaterra, P., Youngblood, J., Moon, R., and Weiss, J. (2015). "The influence of cellulose nanocrystal additions on the performance of cement paste." *Cem. Concr. Compos.*, 56, 73–83.
- Chung, D. D. L. (2000). "Cement reinforced with short carbon fibers— A multifunctional material." *Composites, Part B*, 31(6–7), 511–526.
- Coutts, R. S. P., and Kightly, P. (1984). "Bonding in wood fiber cement composites." *J. Mater. Sci.*, 19(10), 3355–3359.
- Dufresne, A., and Vignon, M. R. (1998). "Improvement of starch film performances using cellulose microfibrils." *Macromolecules*, 31(8), 2693–2696.
- EFNARC (European Federation of National Associations Representing Producers and Applicators of Specialist Building Products for Concrete) (2005). "Specification and guidelines for self-consolidating concrete." Surrey, U.K.
- Eichhorn, S. J., et al. (2010). "Review: Current international research into cellulose nanofibres and nanocomposites." *J. Mater. Sci.*, 45(1), 1–33.
- El-Ashkar, N., Nanko, H., and Kurtis, K. (2007). "Effect of moisture state on mechanical behavior and microstructure of pulp fiber-cement mortars." *J. Mater. Civ. Eng.*, 10.1061/(ASCE)0899-1561(2007)19:8(691), 691–699.
- Erdem, S., Dawson, A. R., and Thom, N. H. (2012). "Influence of the micro- and nanoscale local mechanical properties of the interfacial transition zone on impact behavior of concrete made with different aggregates." *Cem. Concr. Res.*, 42(2), 447–458.
- Favier, V., Chanzy, H., and Cavaille, J. Y. (1995). "Polymer nanocomposites reinforced by cellulose whiskers." *Macromolecules*, 28(18), 6365–6367.

- Ghio, V. A., and Monteiro, P. J. M. (1997). "Bond strength of reinforcing bars in reinforced shotcrete." *ACI Mater. J.*, 94(2), 111–118.
- Goldman, A., and Bentur, A. (1992). "Effects of pozzolanic and nonreactive micro fillers on the transition zone in high-strength concretes." *Proc., RILEM Int. Conf. (Toulouse) on Interfaces in Cementitious Composites*, Vol. 18, E & FN Spon, London, 53–61.
- Gomez Hoyos, C., Cristia, E., and Vázquez, C. A. (2013). "Effect of cellulose microcrystalline particles on properties of cement-based composites." *Mater. Des.*, 51, 810–818.
- Jennings, H. M., Bullard, J. W., Thomas, J. J., Andrade, J. E., Chen, J. J., and Scherer, G. W. (2008). "Characterization and modeling of pores and surfaces in cement paste: Correlations to processing and properties." *J. Adv. Concr. Technol.*, 6(1), 5–29.
- Jongvisuttisun, P., Negrello, C., and Kurtis, K. E. (2013). "Effect of processing variables on efficiency of eucalyptus pulps for internal curing." *Cem. Concr. Compos.*, 37, 126–135.
- JSCE (Japan Society of Civil Engineering). (1984). "Method of the test for flexural strength and flexural toughness of fibre-reinforced concrete." *JSCE-SF 4*, Tokyo.
- Kawashima, S., and Shah, S. P. (2011). "Early-age autogenous and drying shrinkage behavior of cellulose fiber-reinforced cementitious materials." *Cem. Concr. Compos.*, 33(2), 201–208.
- Khaloo, A. R., and Afshari, M. (2005). "Flexural behaviour of small steel fibre reinforced concrete slabs." *Cem. Concr. Compos.*, 27(1), 141–149.
- Khayat, K. H. (1995). "Effects of antiwashout admixtures on fresh concrete properties." *ACI Mater. J.*, 92(2), 164–171.
- Knill, C. J., and Kennedy, J. F. (2003). "Degradation of cellulose under alkaline conditions." *Carbohydr. Polym.*, 51(3), 281–300.
- Kosa, K., and Naaman, A. E. (1990). "Corrosion of steel fiber reinforced concrete." *ACI Mater. J.*, 87(1), 27–37.
- Lin, T., Jia, D., He, P., Wang, M., and Liang, D. (2009). "Effects of fiber length on mechanical properties and fracture behavior of short carbon fiber reinforced geopolymer matrix composites." *Mater. Sci. Eng. A*, 497(1–2), 181–185.
- MATLAB [Computer software]. MathWorks, Natick, MA.

- Merta, I., and Tschegg, E. K. (2013). "Fracture energy of natural fibre reinforced concrete." *Constr. Build. Mater.*, 40, 991–997.
- Mishra, P. C., Singh, V. K., Narang, K. K., and Singh, N. K. (2003). "Effect of carboxymethyl-cellulose on the properties of cement." *Mater. Sci. Eng. A*, 357(1–2), 13–19.
- Mohammadkazemi, F., Doosthoseini, K., Ganjian, E., and Mehrdad, A. M. (2015). "Manufacturing of bacterial nano-cellulose reinforced fibercement composites." *Constr. Build. Mater.*, 101, 958–964.
- Moon, R. J., Martini, A., Nairn, J., Simonsen, J., and Youngblood, J. (2011). "Cellulose nanomaterials review: Structure, properties and nanocomposites." *Chem. Soc. Rev.*, 40(7), 3941–3994.
- Morton, J. H., Cooke, T., and Akers, S. (2010). "Performance of slash pine fibers in fiber cement products." *Constr. Build. Mater.*, 24(2), 165–170.
- Nemati, K. M., Monterio, P. J. M., and Scrivener, K. L. (1998). "Analysis of compressive stress induced cracks in concrete." *ACI Mater. J.*, 95(5), 617–630.
- Ollivier, J. P., Maso, J. C., and Bourdette, B. (1995). "Interfacial transition zone in concrete." *Adv. Cem. Based Mater.*, 2(1), 30–38.
- Onuaguluchi, O., and Banthia, N. (2016). "Plant-based natural fibre reinforced cement composites: A review." *Cem. Concr. Compos.*, 68, 96–108.
- Onuaguluchi, O., Panesar, D., and Sain, M. (2014). "Properties of nanofibre reinforced cement composites." *Constr. Build. Mater.*, 63, 119–124.
- Peters, S. J., Rushing, T. S., Landis, E. N., and Cummins, T. K. (2010). "Nanocellulose and microcellulose fibers for concrete." *Transp. Res. Rec.*, 2142, 25–28.
- Romido, D., Toledo Filho, K. S., England George, L., and Ghavami, K. (2000). "Durability of alkali-sensitive sisal and coconut fibres in cement mortar composites." *Cem. Concr. Compos.*, 22(2), 127–143.
- Rybin, V. A., Utkin, A. V., and Baklanova, N. I. (2016). "Corrosion of uncoated and oxide-coated basalt fibre in different alkaline media." *Corros. Sci.*, 102, 503–509.
- Sanchez, F., and Sobolev, K. (2010). "Nanotechnology in concrete— A review." *Constr. Build. Mater.*, 24(11), 2060–2071.

- Scrivener, K. L., Crumbie, A. K., and Laugesen, P. (2004). "The interfacial transition zone (ITZ) between the cement paste and aggregate in concrete." *Interface Sci.*, 12(4), 411–421.
- Sedan, D., Pagnoux, C., Smith, A., and Chotard, T. (2008). "Mechanical properties of hemp fibre reinforced cement: Influence of the fibre/ matrix interaction." *J. Eur. Ceram. Soc.*, 28(1), 183–192.
- Soroushian, P., and Marikunte, S. (1990). Reinforcement of cement-based materials with cellulose fibers, thin-section fiber reinforced concrete and ferrocement, American Concrete Institute, Detroit, 99–124.
- Struble, J., and Jiang, Q. (2004). "Effects of air entrainment on rheology." *ACI Mater. J.*, 101(6), 448–456. Tazawa, E., and Miyazawa, S. (1995). "Experimental study on mechanism of autogenous shrinkage of concrete." *Cem. Concr. Res.*, 25(8), 1633–1638.
- Wang, X. H., Jacobsen, S., He, J. Y., Zhang, Z. L., and Lee, S. F. (2009). "Application of nanoindentation testing to study of the interfacial transition zone in steel fiber reinforced mortar." *Cem. Concr. Res.*, 39(8), 701–715.
- Wong, H. S., Zobel, M., Buenfield, N. R., and Zimmerman, R. W. (2009). "Influence of the interfacial transition zone and micro-cracking on the diffusivity, permeability and sorptivity of cement-based materials after drying." *Mag. Concr. Res.*, 61(8), 571–589.
- Zingg, A., et al. (2009). "Interaction of polycarboxylate-based superplasticizers with cements containing different C3A amounts." *Cem. Concr. Compos.*, 31(3), 153–162.

List of figures

- Fig. 1. Schematic of hierarchical structure of cellulose filaments (CFs)
- Fig. 2. Cellulose filament (CF) (a) semi-dispersed, as received, and (b) suspensions
- Fig. 3. SEM image of a dried diluted CF aqueous suspension with 0.1% CF: CF network
- Fig. 4. SEM image of a dried diluted CF aqueous suspension with 0.1% CF: Individual fibrils
- Fig. 5. Test set-up for autogenous shrinkage: (a) mold with an embedded vibrating-wire strain gauge, and (b) specimens sealed with adhesive aluminum and connected to a data-acquisition
- Fig. 6. Moisture content in CF. The figure shows the mass loss at 60 °C
- Fig. 7. Water retention capacity of CF in function of the duration of saturation in water
- Fig. 8. Water release rate of CF in function of the duration of exposure to a dry medium
- Fig. 9. Rheological measurements of cement pastes
- Fig. 10. Hydration heat flow and cumulative hydration heat release in paste mixtures
- Fig. 11. Early age deformations in paste mixtures
- Fig. 12. Compressive strength (f_c) in pastes: (a) moist curing; (b) sealed curing
- Fig. 13. Flexural strength (f_f) of paste mixtures at 28 days
- Fig. 14. SEM image of a paste mixture with 0.1% CF
- Fig. 15. SEM image of a paste mixture with 0.15% CF
- Fig. 16. SEM image of a paste mixture with 0.2% CF
- Fig. 17. SEM image of a paste with 0.2% CF: (a) CF agglomeration spots; (b) CF entanglements
- Fig. 18. Flow curves fitted to Bingham model for SCC mixtures
- Fig. 19. Compressive strength (f_c) of SCC mixtures
- Fig. 20. Splitting-tensile strength (f_{sp}) of SCC mixtures
- Fig. 21. Load-deflection response for SCC mixtures at 28 days
- Fig. 22. Energy absorption capacity of SCC mixtures
- Fig. 23. SEM image of a fractured SCC specimen 0.2% CF
- Fig. 24. SEM image illustrating the presence of CFs in the ITZ in the SCC with 0.1% CF
- Fig. 25. SEM image illustrating the presence of CFs in the ITZ in the SCC with 0.15% CF
- Fig. 26. SEM image illustrating the presence of CFs in the ITZ in the SCC with 0.2% CF

List of tables

Table 1. Concrete mix proportions

Table 2. Mixing procedure

Table 3. Fresh properties of paste mixtures

Table 4. Some fresh and hardened properties of paste mixtures studied for autogenous shrinkage

Table 5. Fresh properties of SCC mixtures

CHAPTER 6

Effect of Cellulose Filaments on Microstructure of Cement Systems

6.1 Introduction

In light of the effect of cellulose filaments (CF) on enhancing the mechanical performance of cement composites as demonstrated in [Chapter 5](#), the present chapter is devoted to disclosing microstructure-related mechanisms responsible for the increased strength in cement systems incorporating CF. Thus, this chapter aims at fostering new understanding of the macroscale mechanical performance with a top-down multiscale approach. The mechanical properties at macroscale (i.e., compressive strength, flexural capacity, and elastic modulus) of cement pastes incorporating CF at dosages of 0.0%, 0.05%, 0.10%, 0.20% and 0.30 wt% were investigated and supplemented with microstructure assessment and micromechanical evaluation of main microstructure phases. Microstructure assessment included the degree of hydration and analysis of the microstructure and interaction of CF with the hydrated system. Evaluation of micromechanical properties of major microstructure phases includes the hardness (H), indentation modulus (M), and contact creep modulus (C). This was performed using nanoindentation coupled with quantitative energy-dispersive spectroscopy (NI-QEDS).

In outcome, new insights (about the mechanisms contributing to the increased strength in cement systems incorporating nanoscale CF) were provided. This includes: (i) an enhanced degree of hydration (D_h) mobilized by the hydrophilic CF either providing supplementary water to promote hydration and/or an enhanced degree of hydration fostered by the hygroscopic CF providing water pathways to solubilize anhydrous grains. (ii) higher micromechanical properties of in the C-S-H gel matrix possibly due to a stiffening effect offered by the nanoscale CF capable of interacting with hydrates. Further details are provided below as part of Article 4 published in the context of this research ([Section 6.2](#)).

6.2 Article 4- Nanocellulose for improved concrete performance: A macro-to-micro investigation for disclosing the effects of cellulose filaments on strength of cement systems

Article information

Authors and affiliations:

Ousmane A. Hisseine, PhD candidate and Canada Vanier Scholar of NSERC, Cement and Concrete Research Group, Department of Civil Engineering, Université de Sherbrooke

William Wilson, Post-doctoral fellow, Construction Materials Laboratory, Ecole Polytechnique de Lausanne

Luca Sorelli, Professor and director of Materials and Structures Laboratory, Dept. of Civil Eng. and Water Eng., Université Laval, Canada

Balázs Tolnai, General Manager Technology, Kruger Inc.

A. Tagnit-Hamou, Professor and director of Cement and Concrete Research Group, Department of Civil Engineering, Université de Sherbrooke

Article status: Published

Journal: Construction and Buildings Materials

Reference: Hisseine, O. A, Wilson, W., Sorelli, L., and Tagnit-Hamou, A. (2019a). Nanocellulose for improved concrete performance: A macro-to-micro investigation for disclosing the effects of cellulose filaments on strength of cement systems, *Construction and Building Materials*, vol. 206: p. 84–96.

DOI: <https://doi.org/10.1016/j.conbuildmat.2019.02.042>

Titre français: Nanocellulose pour des bétons à performance améliorée : Étude multi échelle (macro-à-micro) pour révéler les effets des filaments de cellulose sur la résistance des composites cimentaires

Contribution of this article: This article provides further understanding of sources of enhanced mechanical performance obtained with CF in Chapter 5. Therefore, together with Chapter 5, the current chapter contributes to realising the objective 4 of the thesis, namely: exploiting the nanoreinforcing ability of CF to nanoengineer the strength properties of hardened concrete (particularly, the elastic modulus, the flexural capacity, and toughness) and to disclose the mechanism underpinning the way CF influences the strength of cement systems.

Nanocellulose for improved concrete performance: A macro-to-micro investigation for disclosing the effects of cellulose filaments on strength of cement systems

Ousmane A.Hisseine^{a,b,*} William Wilson^{b,c}, Luca Sorelli^d, Balázs Tolnai^e, Arezki Tagnit-Hamou^b

^a Vanier Scholar, Natural Sciences and Engineering Research Council of Canada (NSERC), Canada

^b Cement and Concrete Group, Dept. of Civil Eng., Université de Sherbrooke, Canada

^c Construction Materials Laboratory, École Polytechnique de Lausanne

^d Materials and Structures Laboratory, Dept. of Civil Eng. and Water Eng., Université Laval, Canada

^e Kruger Inc., 3285 Bedford Road, Montreal, Quebec H3S1G5, Canada

* Corresponding author

Published in Construction and Building Materials (2019), Vol. 206, Issue 10, pp. 84-96

Abstract

To fulfill further eco-efficiency requirements, concrete technology practitioners are currently challenged to provide concretes with tailored properties to meet sustainability and resilience requirements for infrastructural systems. As such, nano-engineering concrete by incorporating nanocellulose materials (NCM) can disclose new research directions for tailoring properties necessary for sustainable cement composites. The current study investigates the performance of cement systems incorporating cellulose filaments (CF) and aims at fostering new understanding of the macroscale mechanical performance with a top-down multiscale approach. The study investigates the mechanical performance (i.e., compressive strength, flexural capacity, and elastic modulus) at macroscale of cement pastes incorporating CF at dosages of 0.0%, 0.05%, 0.10%, 0.20% and 0.30 wt.%. The findings are supplemented by microstructure investigations, namely, degree of hydration and micromechanical properties (hardness, indentation modulus, and contact creep modulus) of microstructure phases using nanoindentation coupled with quantitative energy-dispersive spectroscopy (NI-QEDS). Results showed that CF incorporation resulted into 15–25% enhancements in macro-mechanical properties with up to 74% enhancement in flexural toughness. These enhancements are driven by a twofold microstructure change, i.e.: increased degree of hydration (15%) and higher micromechanical properties of C-

S-H matrix (~12–25%). CF is a promising nano-reinforcement for engineering cement composites with superior mechanical performance, while promoting the development of ecological construction materials.

Keywords: Cellulose filaments, Mechanical performance, Micromechanical properties, Microstructure, Nanocellulose materials, Nanoindentation

1. Introduction

In the light of the Canadian policy for facing environmental changes, today's concrete technology faces an unprecedented push towards optimizing eco-efficient construction materials. Over the last few years, nanotechnology has emerged as a breakthrough in concrete technology exploring new frontiers for engineering multifunctional properties towards higher eco-efficiency [1]. Thanks to nanotechnology enabling formulating nanomodified concrete; whereby concrete microstructure can be tailored to achieve specific desirable properties [2]. Nanomodified concrete refers to a concrete obtained by incorporating nanometer objects to engineer its nanostructure and control its macrobehavior in order to achieve tailored and multifunctional cementitious composites with superior mechanical performance and durability [1,3]. In this regard, it is largely believed that nanotechnology would elevate nanomodified composites to replicate the features of natural systems improved until perfection during millions of years. This is largely attributable to the complex hierarchical structure exhibited by natural systems [4]. For instance, bones exhibit unique mechanical properties in terms of stiffness, strength and lightweight [5]. Likewise, plants exhibit high tensile strength, and remarkable on-axis stiffness, elastic modulus, and toughness while remaining relatively lightweight through their porous structure allowing for the complex fluid-mechanics and dynamics phenomena associated with liquid transport [6]. The potential for nanotechnology to open new landscapes in composite design to replicate natural systems shapes, in fact, a promising niche market in concrete technology as identified by the RILEM TC 197-NCM report [7]. Major research areas in nanomodification of concrete have so far mainly covered nanosilica (nSiO₂) [8]; nanotitanium dioxide (nTiO₂) [9, 10]; nanoclay [11]; carbon nanotubes (CNT) [12]; and carbon

nanofibers (CNF) [1]. More recently, plant-based cellulosic materials of nano/micro dimensions – referred to throughout this manuscript as nanocellulose materials (NCM) – have emerged as highly promising multifunctional green materials for the development of next-generation high-performance biocomposites. The sustainability aspects of NCM stem from their biodegradability, low toxicity, low environmental and health risks associated with their production, and low production cost [13–15]. Typical NCM include cellulose nanocrystals (CNC) [16]; microfibrillated cellulose (MFC) [13, 14]; nanofibrillated cellulose (NFC) [17, 18]; and cellulose filaments (CF) [19, 20]. Owing to their nanoscale size, fibril morphology, and large surface area, NCM provide new means to engineer superior composite properties necessary for versatile applications such as adhesives, polymer reinforcement, nanocomposites, transparent flexible electronics, cosmetics, bio-based polymer composites, and cement products, etc. [13, 16, 19–23]. The versatility of NCM is mainly driven by the highly functionalizable cellulose polymers. It also sprouts from the remarkable nanoscale reinforcing potential of cellulose chains forming highly ordered domains of nanoparticles [23]. In this context, Moon et al. [13] drafted a comprehensive review on the significant opportunities in composite design offered by the nanoscale NCM, which cannot be achieved by macroscale natural fibers (i.e., too large to exhibit surface reactivity) or with molecular cellulose (i.e., too tiny to impart reinforcing effect). The increased surface area of NCM allows intimate adherence with the host matrix through chemical reactions driven by hydrogen bonding (not evident with macroscale natural fibers), while conserving high transversal isotropic stiffness, which provides an effective nanoscale reinforcement (not evident with molecular cellulose). NCM provide further capabilities to overcome the drawbacks of cement composites reinforced with macroscale natural fibers, such as the low elastic modulus [24], poor compatibility between fiber and matrix [25], and inconsistency in fiber properties leading to variation in concrete quality and performance [26]. Among existing NCM, CF represent the most recent cement additive with promising applications in concrete technology.

CF are cellulosic fibrils with nanometric diameter (30–400 nm) and micrometric length (100–2000 nm). They have some similarities with MFC and NFC but exhibit the highest aspect ratio

(100–1000) among all currently available NCM. Detailed descriptions of properties of NCM are well documented in open literature [13, 27, 28]. CF exhibit an intrinsic hydrophilic nature and a hygroscopic character. The hydrophilicity of CF together with their tendency to form a percolating network of filaments play a fundamental role in their viscosity modifying effect [20]. On the other hand, the hygroscopicity of CF influences the internal curing effect observed with CF [29]. CF have also a significant effect on the mechanical performance of cement composites with flexural strength enhancements up to 25% [19]. As for concrete mechanical properties, CF allow enhancements in strength of up to 16% in compression, 22% in flexure, 34% in splitting tension, and 96% in energy absorption. Those enhancements were ascribed to nanoreinforcing and internal curing effects imparted by CF [19, 20]. While such effects are consistent with similar observations recorded with other nanomaterials such as CNC [16, 29] and NFC [18, 31], a better understanding of the microstructure mechanisms governing the mechanical performance is deemed necessary. To this end, it is hypothesized herein that the enhanced mechanical properties observed at the macrolevel sprout from possible effects imparted by the nanostructured CF at the microstructure level of the cementitious matrix. In light of this hypothesis, the current study aims at disclosing the mechanisms underpinning the effect of CF on mechanical performance of cement-based composites. The study presents a novel top-down multi-scale investigation (from macro to micro) of the mechanical behavior of cement systems incorporating CF at rates 0.0%, 0.05%, 0.10%, 0.20% and 0.30 wt.%. The study assesses the influence of CF on the macrolevel mechanical performance, or engineering properties (compressive strength, elastic modulus, and flexural capacity and toughness) of tested cement systems as well as on the hydration kinetics and mechanical properties of the microstructure phases using nanoindentation coupled with quantitative energy-dispersive spectroscopy (NI-QEDS) method [32, 33]. Not to mention subject novelty, the current study stands out to establish the link between mechanical performance at the engineering scale and microstructure and mechanical properties of major microstructure phases. Research outcomes are expected to substantiate the use of CF as a valuable tool for manipulating concrete properties at the nano/micro scale to control its engineering behavior at the macroscale.

This has the potential to lead to the development of high-performance nano-engineered concrete products using greener materials for sustainable and resilient infrastructure systems

2. Experimental program

The following sections describe material properties and testing methods adopted to characterize the effect of CF on five cement pastes with varying CF contents (0.0%, 0.05%, 0.10%, 0.20% and 0.30 wt%).

2.1. Materials properties

General Use (GU) Portland cement (CSA A3001) [34] equivalent to Type I cement (ASTM C1157) [35] was used in this study. The particle size distribution of this cement is shown in Fig. 1, while its physical properties and oxide-based chemical compositions by X-ray fluorescence analysis are reported in Table 1. The CF used in this study were provided by Kruger Biomaterials Inc. (Trois-Rivières, Québec, Canada). The filaments have a nanometric diameter of 30–400 nm and a micrometric length of 100–2000 μm . This results into their significantly high aspect ratio of about 100–1000 and their high surface area of more than 80 m^2/g . According to the supplier, the filaments were derived from FSC®-certified kraft wood pulp using only virgin fibers to ensure optimum performance and consistent properties. Additional to the intrinsic sustainability features of CF, the extraction process of this material follows a green approach with a yield value of 100%. In fact, as per the supplier, the filaments were extracted through a patented process that uses only mechanical energy and does not involve any chemical or enzymatic treatment, nor does it produce effluent. In addition, the production facility is almost entirely powered by renewable energy; thereby minimizing the carbon footprint of CF. The above-mentioned extraction process of CF involves removal of matrix impurities such as lignin, pectin, wax, and soluble sugars. As such, CF contains mainly cellulose (>95%) and a small amount of hemicellulose (<5%). This is consistent with the two types of saccharides (glucose and xylose) detected by liquid chromatography tests conducted on CF, where typically the former is found in cellulose while the latter is found in hemicellulose. The filaments were received from the supplier in a dispersed form (colloidal suspension with a nominal CF solid content of 1.2%). The CF dispersion carried out by the supplier employed a high-energy

disintegrator with a speed of 3000 rpm (for ~15 min using water at 60 °C) following a procedure adapted from the guidelines set by the Pulp and Paper Technical Association of Canada (PAPTAC). Such CF suspensions were found to result into better composite properties as compared to other dispersion approaches (e.g., high shear mixing for 60 s) adopted in our early works [19, 20]. The as-received suspensions were diluted into water to prepare the CF concentrations for the different cement paste mixtures. As a result, a major challenge in previous works with CF, namely filament agglomerations that jeopardize CF effectiveness in paste systems [19] has been relatively overcome herein by using readily dispersed CF suspensions. Fig. 2(a) shows different CF suspensions, while Fig. 2(b) illustrates a field emission gun-scanning electron microscopy (FEG-SEM) image of a dried CF diluted suspension with 0.10% CF. With the hierarchical and multi-scale structure of cellulose (Fig. 3)—imparting inherent mechanical properties to plant-based materials—coupled with the high surface area of CF, the filaments have high potential to modify the mechanical performance of cement composites such that a nanomodified concrete may be obtained (Fig. 4).

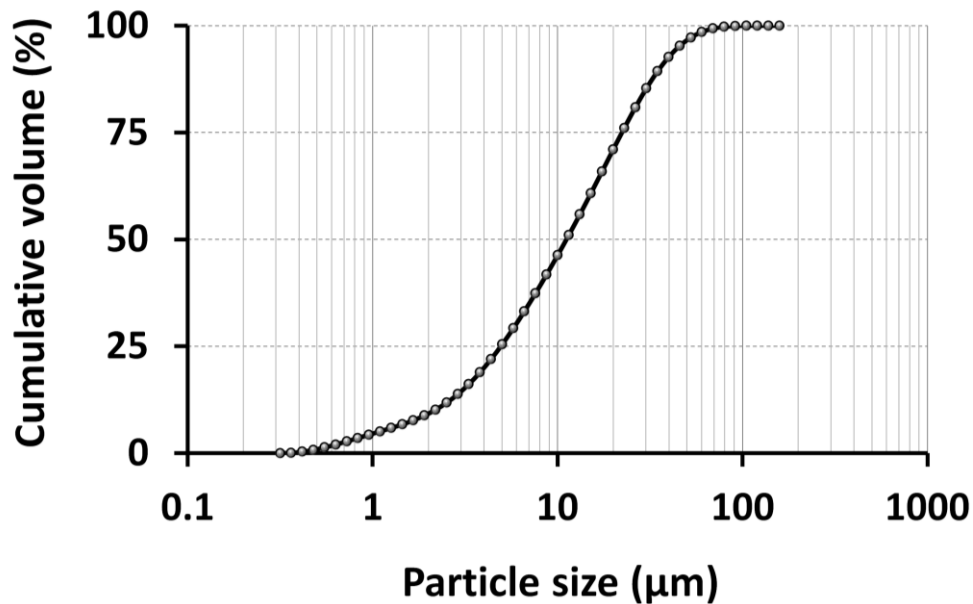


Fig. 1. Particle size distribution of GU cement used in this study

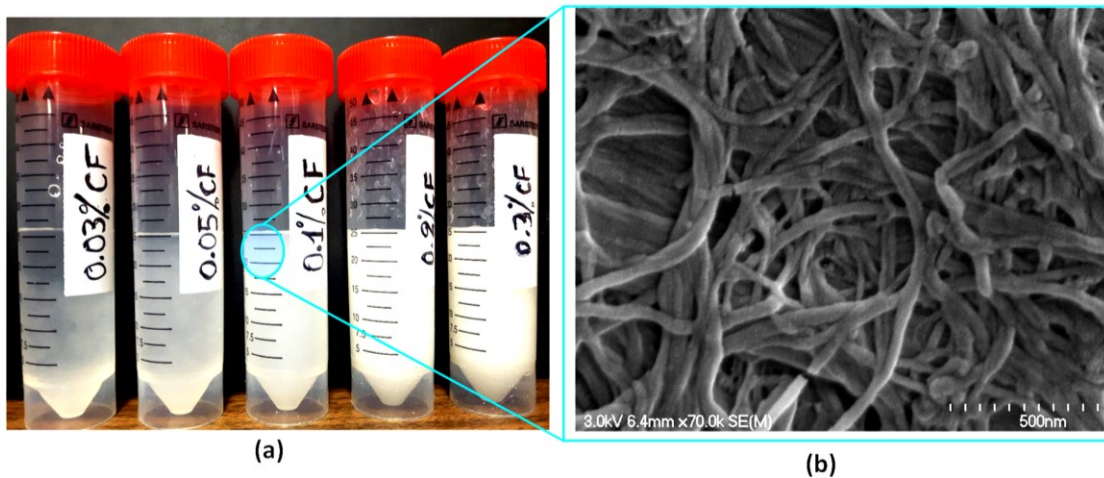


Fig. 2. Cellulose filaments (CF): (a) CF-water suspensions for the different dosages tested in this study, and (b) Scanning electron microscope (SEM) image of a suspension with 0.10% CF (reprinted from [19] with permission from ASCE).

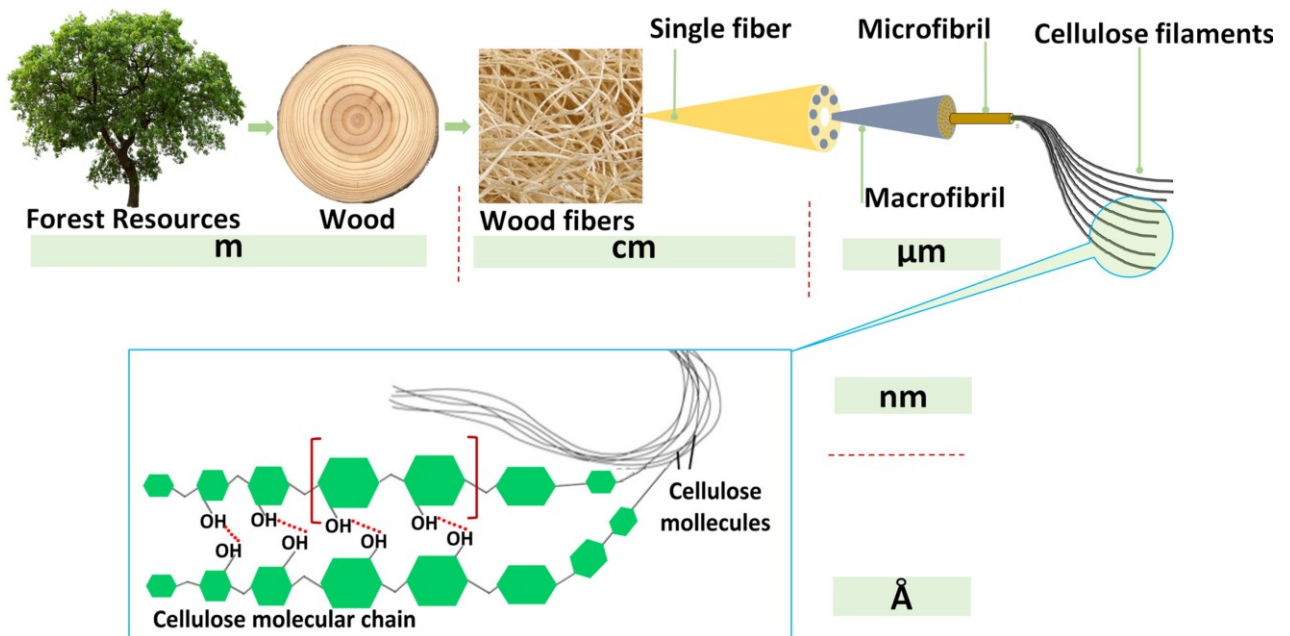


Fig. 3. Schematic illustration of the hierarchical structure of cellulose. The figure depicts cellulose as an intrinsic building block within a structured hierarchy (from the molecular/atomic scale to the macro scale) imparting inherent strength to plant-based systems.

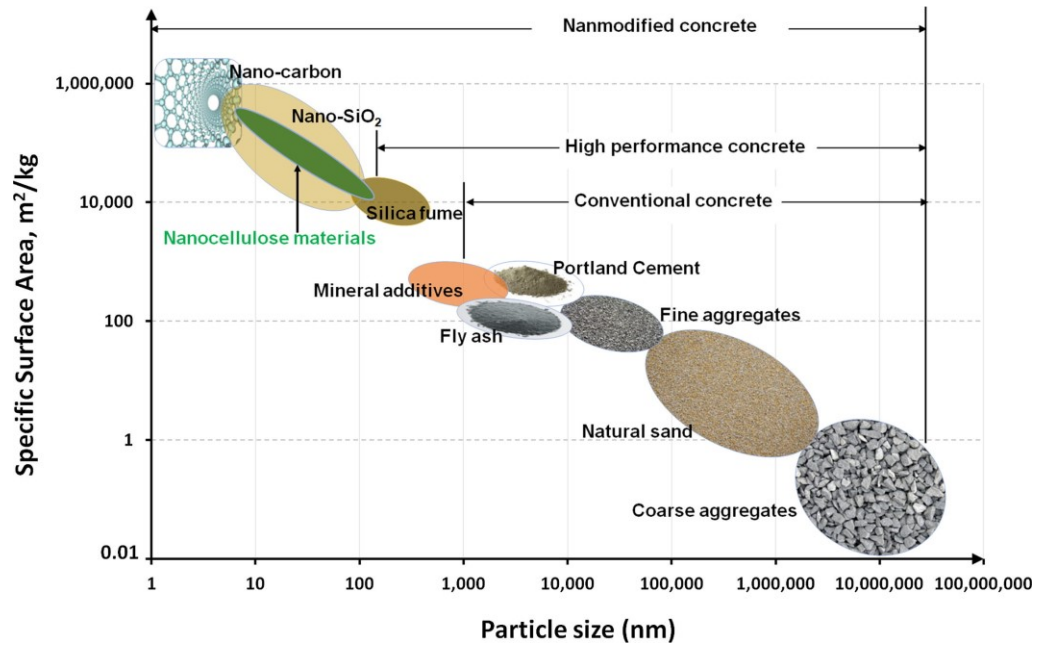


Fig. 4. Relationship between particle size and specific surface area as related to the constituents of different classes of concrete (adapted from [1]).

Table 1. Chemical composition and physical properties of GU cement

Chemical composition	% by mass
SiO ₂	20.5
Al ₂ O ₃	4.0
Fe ₂ O ₃	2.0
CaO	63.2
MgO	2.2
SO ₃	3.4
Na ₂ O	0.2
K ₂ O	0.9
Free lime	1.1
Loss-on-ignition	2.9
Insoluble residues	0.1
Blaine fineness (m ² /kg)	431
Fineness, passing on 45 μm sieve (%)	91

2.2. Mixture proportions, sample preparation, curing, and testing

Table 2 presents the formulation of paste mixtures considered in this study. The water-to-cement ratio (w/c) was kept constant at 0.30 for all mixtures. CF were added at concentrations of 0.0%, 0.05%, 0.10%, 0.20% and 0.30% by mass of cement. A polycarboxylate-based high-range water reducing admixture (HRWRA) with 40% solid content was introduced at different dosages to maintain a target mini-slump flow of approximately 250 ± 15 mm. The net water demand of each mixture was determined after subtracting the amount of water brought by the CF-water suspension (1.2% solid CF content) and the HRWRA (40% solid content). ASTM C305 guidelines [36] were followed in preparing the mixtures. For curing, fresh samples were covered with plastic sheets (in an attempt to control evaporation) and kept at 50% relative humidity (RH) and 23 °C for 24 h. After 24 ± 1 h, the samples were demoulded and transferred for storage in a fog room at 100% RH and 22 °C temperature until the age of testing.

Fresh properties evaluated in this study include the temperature and slump-cone test following a procedure adapted from ASTM C230 [37]. Tested mechanical properties include the compressive strength on $50 \times 50 \times 50$ mm cubes (according to ASTM C109 loading procedure) [38], the flexural capacity on $50 \times 100 \times 400$ mm prisms (width, depth, length) following a procedure adapted from ASTM C78 [39], and the elastic modulus on 100×200 mm cylinders (ASTM C469) [40].

At the microstructure level, thermogravimetric analyses (TGA) were conducted on hardened paste samples at ages of 28 days to evaluate the effect of CF on the degree of hydration. Additionally, the properties of the microstructure phases were further investigated using coupled nanoindentation and quantitative energy dispersive spectroscopy (Fig. 5), following experimental details and the deterministic approach described elsewhere [32, 33].

Table 2. Mix design of pastes based on 1000 g of binder at w/c = 0.3

Component	Ref.	0.05%	0.10% CF	0.20% CF	0.30% CF
GU cement	1000	1000	1000	1000	1000
Net water *	289	244	198	114	24
CF (% dry extract)	0.00	0.50	1.00	2.00	3.00
HRWR (% dry extract)	0.75	1.02	1.39	1.61	2.22

* *N.B.*: The significant drop in net water demand (in mixtures with CF) is due to the considerable amount of free water brought by the CF-water suspension.

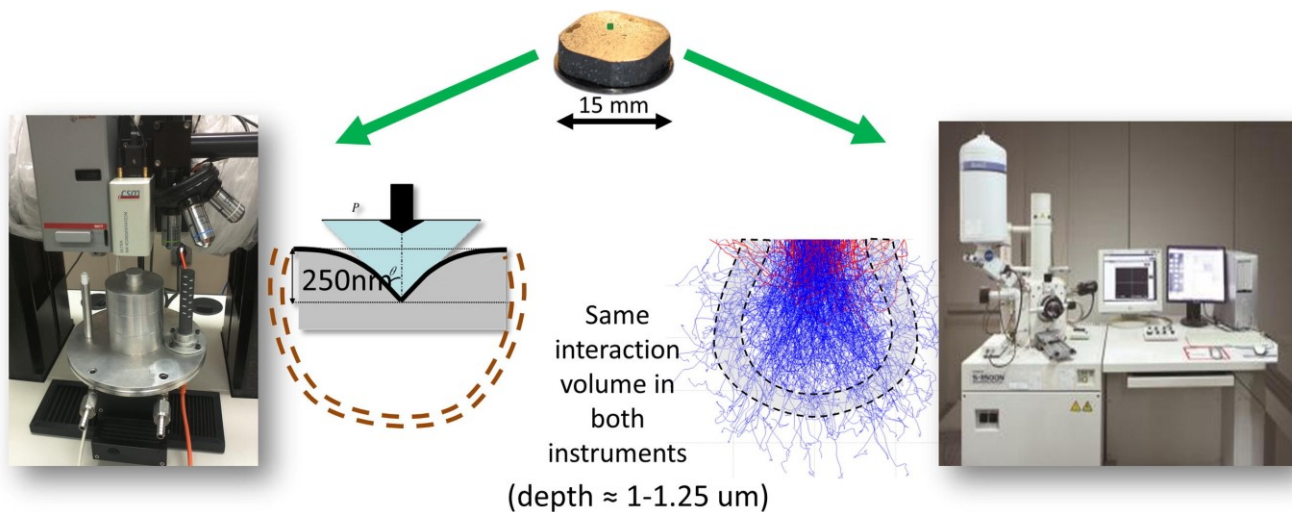


Fig. 5. Illustration of the coupled nanoindentation and quantitative energy-dispersive spectroscopy method (NI-QEDS), adapted from Wilson et al. [32].

3. Results and discussion

3.1. Fresh properties

Fig. 6 presents the variation of slump flow in tested paste mixtures and the corresponding mixture demand in HRWRA. Results indicate that the incorporation of CF led to a remarkable increase in HRWRA demand. To maintain the target slump of 250 ± 15 mm, the incorporation of CF at rates of 0.05, 0.10, 0.20, and 0.30% increased the HRWRA demand by 1.4, 1.8, 2.1

and 3.0 times, respectively, relative to the mixture without CF designated herein as reference (Ref.). The trend for the HRWRA demand is consistent with our previous findings; whereby fresh properties (including yield stress, plastic viscosity, and demand in HRWRA) undergo sudden shift at a CF concentration of $\sim 0.12\%$ where CF dosage reaches a percolation threshold [20]. The percolation threshold, which refers to the minimum CF content necessary to form a continuous network of percolating fibrils, marks noticeable changes in rheological properties as observed herein. The above observations reflect the significant viscosity modifying effect imparted by CF. The viscosity modifying effect of CF sprouts from the hydrophilic nature of cellulose-based fibers emanating from the omnipresence of surface hydroxyl (OH^-) groups [41]. The viscosity modifying effect of CF also originates from the flexible and nanometric fibrillar structure of filaments leading to the creation of nanoscale fibril networks as elaborated elsewhere [20]. In this regard, it is worth noting that the increased viscosity imparted by CF is accompanied by a shear thinning behavior. In the latter, at increasing shear rates, CF networks exhibit high likelihood to be either pulverized or streamlined in the direction of flow, thereby attenuating the viscosity buildup [20]. This reduces mixture resistance to flow while enhancing mixture stability and robustness.

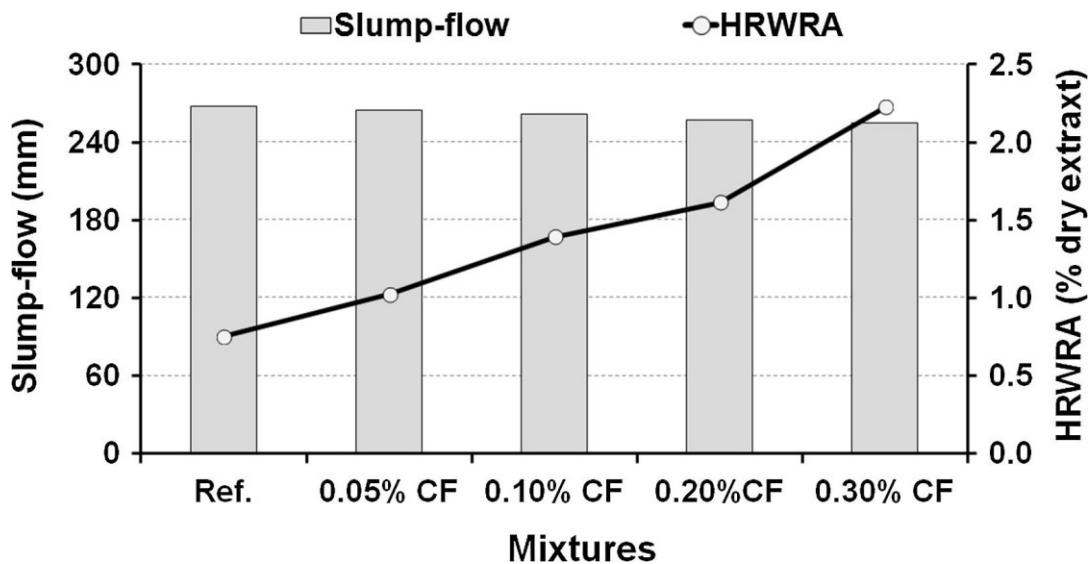


Fig. 6. Effect of CF on slump flow and mixture demand in HRWR (CF=cellulose filaments in % weight of cement content).

3.2. Macroscale mechanical properties

3.2.1. Compressive strength

The compressive strength results depicted in Fig. 7 indicate that the effect of CF on compressive strength varies with curing age. At one day, for instance, the mixtures with 0.05% and 0.10% CF showed, respectively, 22% and 10% higher compressive strength. The mixture with 0.20% CF showed comparable strength to that of the reference, while the mixture with 0.30% CF showed a slightly lower ($\sim 5\%$) compressive strength than that of the plain system. A more significant effect of CF on compressive strength is observed at 7 and 28 days where all mixtures with CF showed higher strength (with better effects noticed between CF contents of 0.05% and 0.10%). At 7 days, CF contents of 0.05% and 0.10% lead to increments in compressive strength of 25% and 15%, respectively. CF contents of 0.20%, however, lead to a marginal increase ($\sim 5\%$) in strength; while at 0.30% CF, no gain in strength over the plain system was noticed. The above trend of the effect CF on compressive strength is further confirmed by the 28-day strength where mixtures with 0.05% and 0.10% CF showed strength improvement of 26% and 17%, respectively, while mixtures with 0.20% and 0.30% CF had less noticeable effects, yet showed enhancement in strength ($\sim 11\%$). The increased compressive strength in the presence of CF may be correlated with the effect of nanocellulose on the hydration kinetics and on the properties of hydrates. It is reported herein and elsewhere [16, 30] that the hydrophilic and hygroscopic nanocellulose may allow dispatching supplementary water to the cementitious matrix to foster the degree of hydration, thereby enhancing the mechanical performance. This effect is, however, not evident at early ages where increased content of nanocellulose may create a viscous suspension interfering with cement solubilisation [18].

In contrast to the dispersion techniques attempted in our previous works (high-shear mixing for 60 s), where the compressive strength of pastes was negatively affected [19], the herein presented results obtained using a readily dispersed CF suspension (~ 15 min of high shear mixing using water at 60°C) substantiate the effect of CF dispersion on composite strength. The effect of CF dispersion may also explain the higher improvement in compressive strength obtained at lower CF concentrations (0.05% and 0.10%) where filaments dispersion is more

likely to be effective. At higher CF dosages (0.20% and 0.30%), the increased CF surface area may lead to filament entanglements, thereby adversely affecting the porous network and jeopardizing mechanical performance including the compressive strength [19].

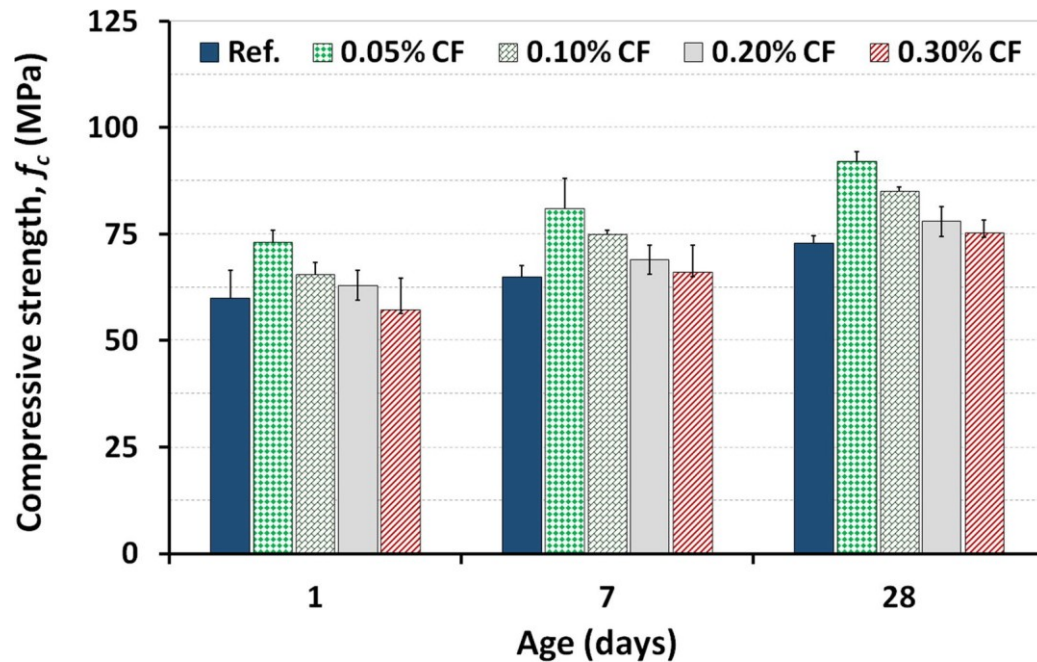


Fig. 7. Evolution of compressive strength (f_c) in tested paste mixtures (CF=cellulose filaments in % weight of cement content).

3.2.2. Elastic modulus

Fig. 8 presents the measurements of elastic modulus (E) at 28 days for the different mixtures considered in this study. Results show that compared to the elastic modulus of plain systems of 18.7 GPa, the incorporation of CF at content 0.05, 0.10, 0.20, and 0.30% resulted into elastic moduli of 22.0, 21.3, 21.1, and 19.0 GPa, respectively. This corresponds to enhancements in the elastic modulus of 18, 14, 6, and 2%, respectively. The highest effects occur once again at lower CF dosages where dispersion (and hence CF effectiveness) is believed to be more prominent. The above observed enhancement in elastic modulus hints that the filaments may have altered the material behavior of the cement paste. This can be contrasted to macroscale fibers, which rather influence the composite behavior and are often beneficial only beyond the elastic limit

where matrix contribution declines and fiber contribution is mobilized by FRC mechanism [42]. In the light of the above enhancements in the elastic modulus in systems with CF, it is perceivable that CF has the potential to increase the matrix-governed first cracking strength.

The CF effect on the elastic modulus can be traced down to the microstructure changes of the cement paste owing to: (i) the higher elastic modulus of the crystalline portion of cellulose nanomaterials approaching 138 GPa [43]; and (ii) the high surface area and omnipresence of surface hydroxyl (OH^-) groups [41] in cellulose nanomaterials leading to surface reactivity and interactions with hydrates containing hydrogen in their structure, namely C-S-H and CH [44]. In this regard, Cao et al. [16] indicated that the use cellulose nanocrystals (CNC) increases the stiffness of high-density calcium-silicate-hydrate (C-S-H) surrounding unhydrated cement particles. Similarly, Flores et al. [30] reported that the incorporation of CNC results into larger volume fraction of high-density C-S-H and a smaller volume fraction of low-density C-S-H. These effects may also influence the micromechanical properties and have direct implications on mechanical performance as to be further examined through microstructure investigations in Section 3.3.2. The increase in elastic modulus in mixtures with CF reveals that there is an opportunity with nanoscale fibers to engineer cementitious composites with higher elastic modulus while maintaining the same water-to-powder ratio. This provides a novel and greener tool for designing concretes with higher elastic modulus necessary for high-rise reinforced-concrete structures. This represents a sustainable alternative option to the conventional means for improving the elastic modulus such as increasing the cement content [45], increasing mixture content in fine powders such as silica fume [29], and using stiffer aggregates [46].

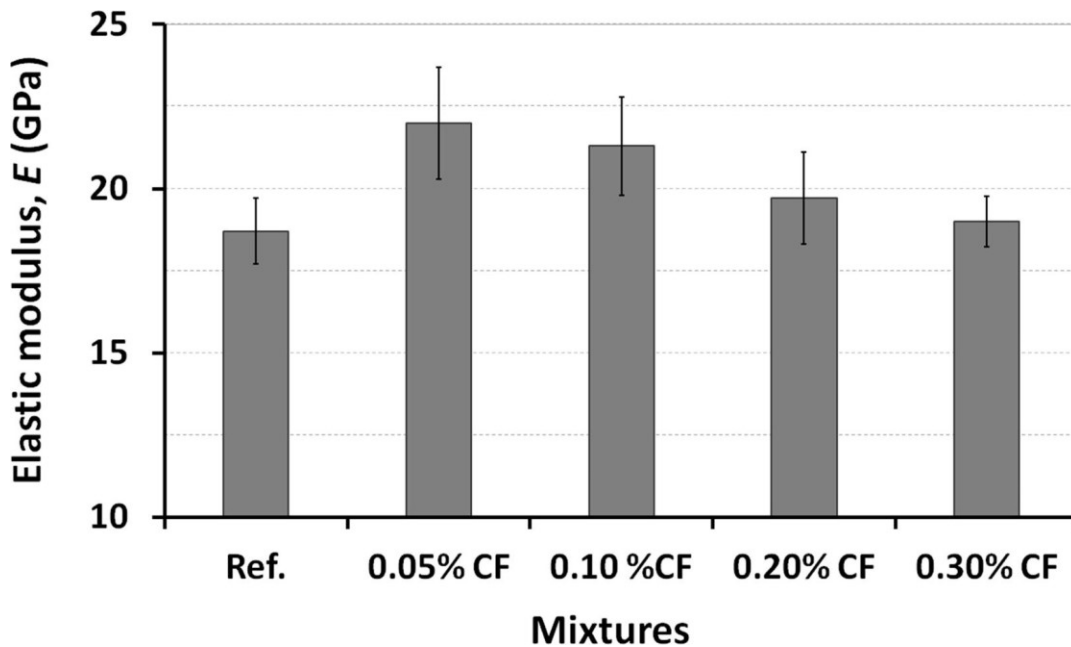


Fig. 8. Elastic modulus (E) of tested cement pastes (CF=cellulose filaments in % weight of cement).

3.2.3. Flexural capacity and toughness

Figs. 9 and 10 present the results of flexural capacity and toughness, respectively. The results indicate that all mixtures with CF exhibit a higher load carrying capacity and an enhanced toughness (or energy absorption capacity, which is measured as the area under the load deflection curve of flexural testing). The reference paste had a flexural capacity of 4.84 MPa, while for CF contents of 0.05, 0.10, 0.20 and 0.30%, the flexural capacities reached 5.62, 5.75, 5.84, and 5.81 MPa, respectively. This corresponds to flexural capacity enhancements of 16, 19, 21, and 20%, respectively, relative to the plain system. On the other hand, the energy absorption capacity of the plain system was 222 N.mm while for CF contents of 0.05, 0.10, 0.20 and 0.30%, the respective energy absorption capacities reached 277, 318, 375, and 386 N.mm. This is equivalent to increases in energy absorption capacity of 25, 43, 69, and 74%, respectively, relative to the plain system. The above results indicate that the flexural capacity and toughness of cement systems with CF exhibit opposing trends. For flexural capacity, the most noticeable

effect of CF appears at the minimum CF content of 0.05%, then for subsequent CF dosages (0.10, 0.20, and 0.30%); the incremental effects are relatively limited. On the other hand, the flexural toughness showed an increasing trend for all CF dosages. As a result, the enchainment in the matrix toughness appears far more important than that on the tensile flexural capacity.

The above results reveal that the effect of CF on flexural capacity is twofold: (i) an increased first peak strength (rupture strength) associated with the nanometric properties of CF. This alters the properties of the cement paste matrix at the microstructure level (as further discussed afterwards). (ii) An enhanced toughness associated with the high aspect ratio and the tensile strength of CF, which contribute towards maintaining the peak load for a prolonged range of micro deflections prior to failure, thereby increasing the cracking resistance. The observed effect of CF on composite fracture behavior is driven by the contribution of the filaments as a nanoreinforcement. Possible mechanisms involved in CF effect on composite fracture behavior may include: (i) filament bridging capacity driven by their high aspect ratio and fibrillated morphology, (ii) filament resistance to rupturing owing to their tensile properties, and (iii) the filament-matrix interfacial bond stemming from the potential interaction between the omnipresent OH^- groups on CF surface and cement hydrates by hydrogen bonding. In this mechanism, irrespective of the effect CF has on peak flexural capacity, the high probability of the fibers intercepting microcracks may play a favorable role in delaying the matrix fracture. The above observations are consistent with previous findings on concrete mixtures [19, 20] and those observed with Kraft pulp fibres (e.g. abaca [47]; sisal [48]; bamboo fibers [49]; and softwood [50]) where the increase in flexural strength reaches a threshold at quite low fiber contents, while the flexural toughness enhancement increases continuously with increasing fiber volume content.

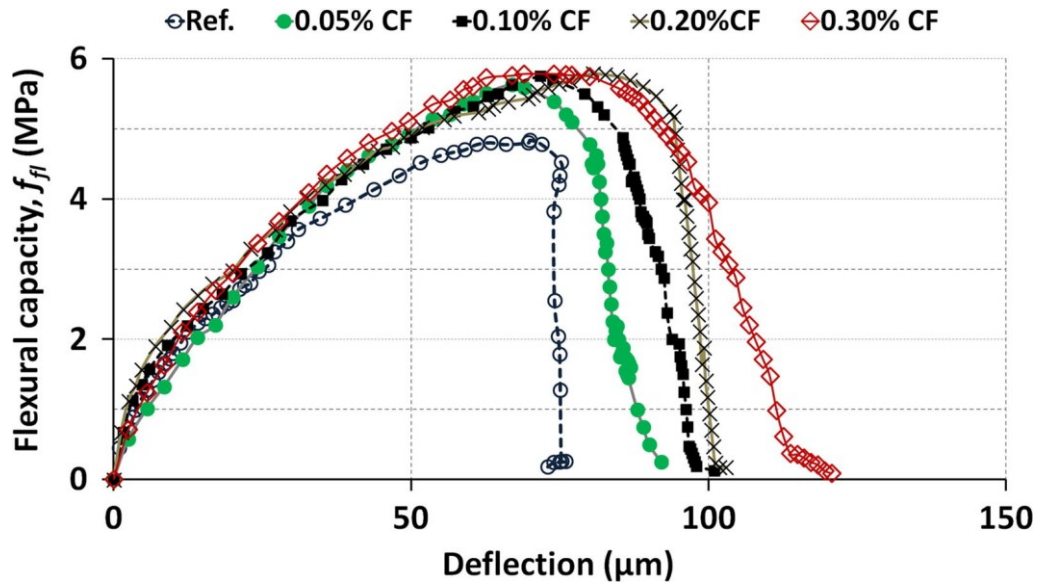


Fig. 9. Flexural capacity (f_{fl}) of tested pastes (CF=cellulose filaments in % weight of cement).

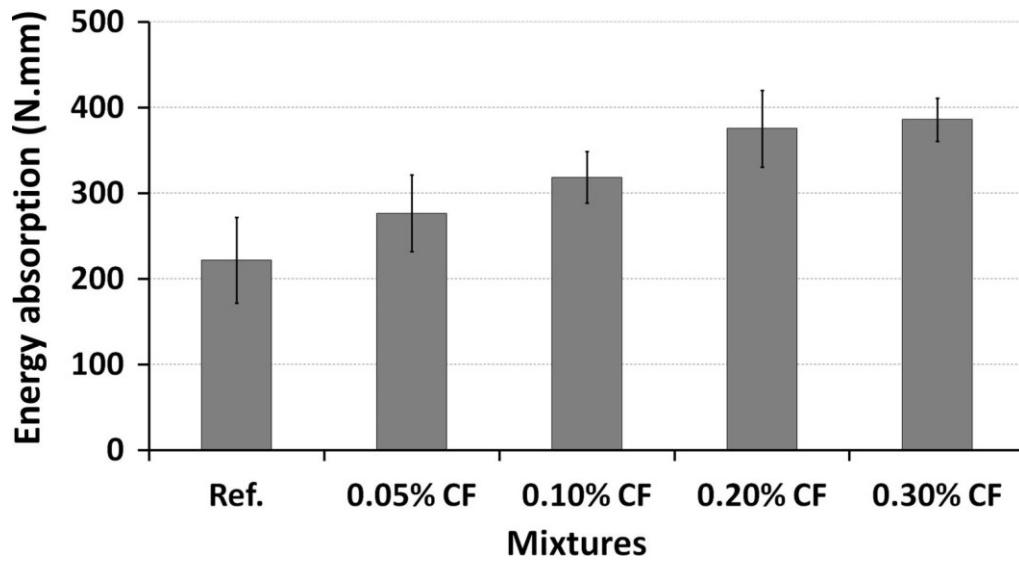


Fig. 10. Energy absorption capacity (CF=cellulose filaments in % weight of cement).

3.3. Microstructural properties

For a better understanding of the origin of CF effect on mechanical performance, the cement paste systems analyzed for macro-mechanical properties were further investigated for their degree of hydration and chemo-mechanical properties of the major phases composing the microstructure.

3.3.1. Degree of hydration

Results of thermogravimetric analysis (TGA) measurements at the ages of 7 and 28 days are depicted in Fig. 11 and Fig. 12, respectively. Both figures indicate that while the initial sample weight (W_i) was constant across all mixtures, reduced final weight (W_f) were recorded in all mixtures containing CF. This resulted into higher weight loss difference (ΔW_{loss}) in mixtures with CF than in the reference mixture. The increased ΔW_{loss} exhibited in mixtures with CF suggests that higher amount of water may have reacted with the cementitious matrix in the presence of CF. To further examine this trend, it was deemed necessary to evaluate the influence of different CF concentrations on the degree of hydration (D_h). The latter was assessed through the chemically bound water (CB_w) determined from ΔW_{loss} between the temperatures of 105 and 1000 °C [51]. In this regard, while some relatively small portions of CB_w may be lost from some hydrates (particularly C-S-H, ettringite, and monosulfate) at temperatures below 105 °C [52], this portion of CB_w was not considered in the current analysis for simplicity. On the other hand, considering that the temperature interval corresponding to decarbonation (CO_{loss}) overlaps with that used to determine the CB_w , the weight loss was corrected by reducing the CO_{loss} (~1.5–2% of total weight loss), which corresponds to ΔW_{loss} between the temperatures of 600 and 780 °C [53]. The CB_w was obtained by dividing the corrected weight loss by the final sample weight (W_f) as presented in Eq. (1). Finally, to obtain the degree of hydration (D_h), the CB_w was normalized to its maximum value (CB_{∞}), which corresponds (for Type I Portland cement) to 0.23 g per g of final of weight, (W_f) [54] as shown in Eq. (2).

$$CB_w = \frac{\Delta W_{loss} - CO_{loss}}{W_f} \quad (1)$$

$$D_h = \frac{CB_w}{CB_\infty} \quad (2)$$

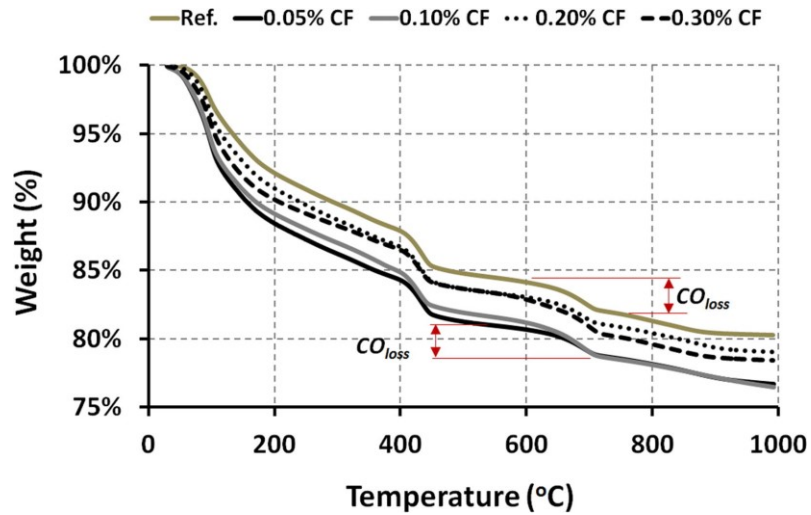


Fig. 11. Thermogravimetric analysis (TGA) at 7 days for the different pastes systems

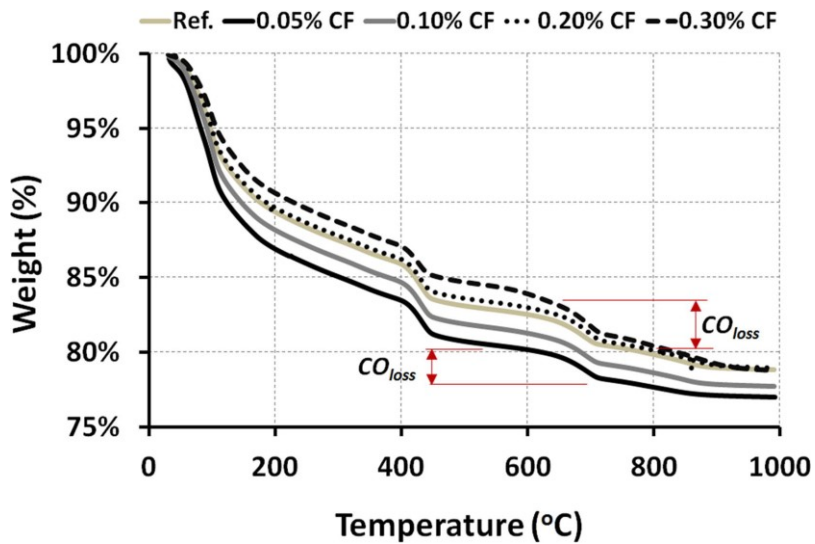


Fig. 12. Thermogravimetric analysis (TGA) at 28 days for the different pastes

The results of D_h thus obtained are plotted in Fig. 13 for the different paste systems. The figure indicates that at 7 days, CF contents of 0.05 and 0.10% enhanced the D_h by 12 and 9%, respectively, while CF contents of 0.20 and 0.30% showed no noticeable effects. At 28 days, however, all CF concentration recorded higher degree of hydration than the plain system. The CF contents of 0.05, 0.10, 0.20 and 0.30% resulted in increments in degree of hydration of 15, 13, 5, and 6%, respectively. The incorporation of CF (at all concentrations) appears to improve the D_h with seemingly more pronounced effect at lower CF concentrations (between 0.05% and 0.10%) possibly due to the dispersion efficiency at low CF concentrations. The higher D_h recorded in systems with CF can be linked with the potential of the hydrophilic and hygroscopic CF to provide a supplementary source of water to promote the solubilisation of more anhydrous cement grains. Such additional water was reported elsewhere to attenuate autogenous shrinkage at 7 days in systems with a $w/c = 0.35$ by up to 36% at a CF content of 0.15% [19].

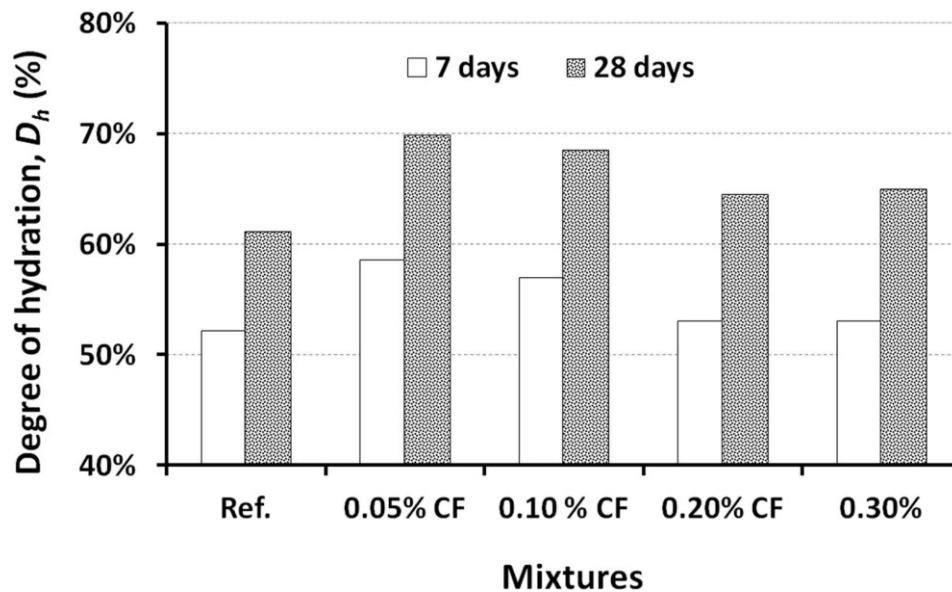


Fig. 13. Degree of hydration (D_h) of the cement in the investigated cement pastes (CF=cellulose filaments in % weight of cement content).

On the other hand, the above results on the effect of CF on the degree hydration can be reconciled with the general trend of the effect of nanocellulose materials (NCM) on hydration kinetics (particularly heat of hydration). Calorimetry tests conducted on cement pastes revealed that CF increases both the silicate hydration peak and the sulfate-depletion peak, thereby leading to higher cumulative heat release [19, 20]. This trend was reported in a more pronounced manner in cement systems incorporating microcrystalline cellulose (MCC) [44], cellulose nanocrystals (CNC) [16], bacterial cellulose (BC) [55], and cellulose-based polymers [56].


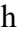
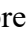

However, it should be elucidated that the above reported effect of cellulose nanomaterials on heat of hydration is more likely to be associated with the alkaline hydrolysis of cellulose whereby the exothermic alkaline hydrolysis reaction of cellulose (producing organic acids and non-acidic products) promotes cement hydration [57].

Therefore, the net effect of cellulose nanomaterials on hydration kinetics is primarily contingent to the product of cellulose alkaline hydrolysis [58]. As such, Onuaguluchi et al. [18] indicated that cellulose nanofibers showed some retardation effect at first few hours (due to the viscous nanocellulose suspension impeding the solubilisation of cement active phases) but lead to higher heat release at later ages (due to water release from nanocellulose). Cao et al. [16] reported slight retardation, but overall higher heat release with CNC when the latter was used in Type V cement (low C_3A) owing to the adherence of CNCs to unhydrated cement particles. Tongfei et al. [59] reported less retardation effects with CNC (compared to that of CaO et al. [16]) when Type I/II cement was used owing to the higher content in C_3A with a possibly higher propensity for adsorbing CNC. On the other hand, they showed that both CNC source and the cement type could significantly influence the hydration kinetics.

3.3.2. Chemo-mechanical properties of the microstructure phases

Fig. 14 and Fig. 15 show composite chemical mappings of surfaces from the reference cement paste and the paste incorporating 0.05% CF, respectively. The composite chemical mappings were obtained by a multilayer combination of single elemental mappings (Si in red, Ca in blue, Al in green and Fe in grey). Both figures show a dense microstructure with significant amounts

of anhydrous clinker grains (bluish-purple and purple grains of anhydrous alite and belite; bright cyan grains of anhydrous aluminate and ferrite), which could be expected due to the low water-to-cement ratio (w/c) and the degree of hydration presented earlier. The hydrates include Portlandite (in blue), Al-rich hydrates (e.g., AFm and AFt phases in greyish green), and the dark-purple C-(A)-S-H matrix which embeds the other phases. Interestingly, very similar chemical mappings were obtained for the reference system without CF (Fig. 14) and the system with 0.05% CF (Fig. 16).

Fig. 14 and Fig. 15 also show grid of markers representing the indented microvolumes investigated by the novel technique NI-QEDS which couples nanoindentation and quantitative energy-dispersive spectroscopy. Data points occurring on “pure” single phases were identified using the deterministic approach presented in Wilson et al. [32]. Thus, the markers , , and  indicates data points with chemistry close to that of “pure” alite, belite, and Portlandite, respectively. The marker  represents the relatively rare occurrence of data points inside the thin C-S-H regions in-between the anhydrous grains and having the “purest” C-S-H composition. In addition, Table 3 compares the two systems in terms of micromechanical properties (indentation modulus M , indentation hardness H , and contact creep modulus C) obtained for the 4 main phases characterized with the NI-QEDS deterministic approach (each with n datapoints). As expected, the anhydrous clinker phases show similar properties in both systems.

The average M and H values for C-S-H in the reference system are in general agreement with the values obtained for several systems with supplementary cementitious materials in previous work, i.e., $M \sim 25\text{--}27$ GPa and $H \sim 0.7\text{--}0.8$ GPa [33]. However, higher average values of $M = 29.2$ GPa and $H = 0.98$ GPa were obtained for the system incorporating 0.05% CF. Thus, the properties of the C-S-H itself appear to be enhanced in the presence of CF (by $\sim 12\text{--}25\%$). This effect could be attributed to both a higher degree of hydration and CF reinforcing the C-S-H matrix (or assemblage). Interestingly, the higher modulus and hardness of the C-S-H matrix with 0.05% CF is in good agreement with the gains previously observed at the macro scale.

Moreover, a higher microscale contact creep modulus C of the C-S-H matrix was observed for the system with 0.05% CF (i.e., the creep of the CF reinforced C-S-H matrix was lower). This

result suggests that the increased ductility of the system at the macroscale depends on a greater micro-scale capacity of the C-S-H to deform upon sustained loading. Thus, other mechanisms such as micro-crack bridging by the filaments themselves may prevail and should be considered for further investigation. The above observation confirms the earlier interpretation that the effect of the filaments on delaying matrix fracture and increasing its energy absorption capacity stems from the contribution of the filaments to enhancing the matrix fracture capacity by FRC mechanism leading to plateauing of load-deflection response prior to failure.

Table 3. Comparison of the reference paste and the paste with 0.05% CF, in terms of micromechanical properties (indentation modulus M , indentation hardness H , and contact creep modulus C , as obtained from n data points deterministically selected with the NI-QEDS method).

	Ref.				0.05% CF			
	M (GPa)	H (GPa)	C (GPa)	n	M (GPa)	H (GPa)	C (GPa)	n
Alite	108±17	10.4±1.6	8840±3009	52	107±17	10.7±1.6	7668±1448	45
Belite	117±13	8.8±1.0	5037±3289	16	111±19	9.2±2.0	4922±2778	19
C-S-H	26.1±3.4	0.78±0.17	146±34	35	29.2±3.5	0.98±0.20	175±31	35
CH	–	–	–	–	44.2±7.3	1.82±0.41	748±517	4

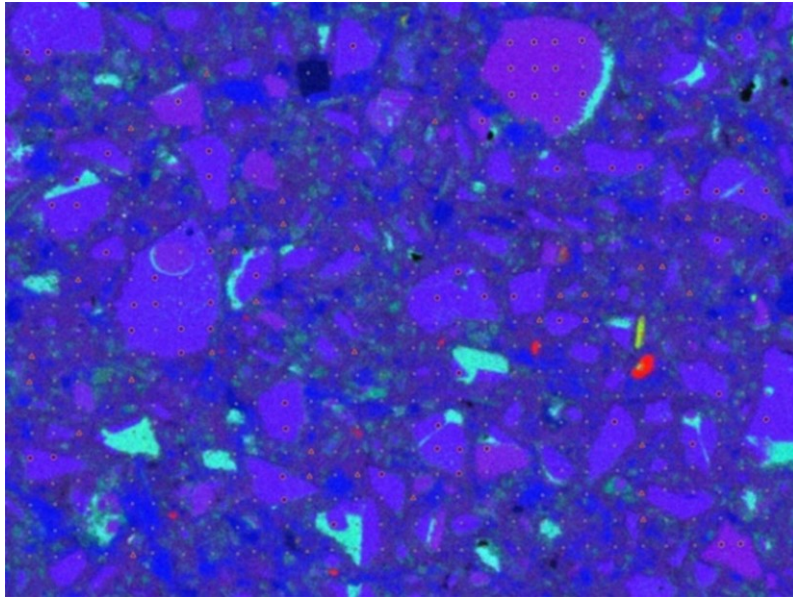


Fig. 14. Composite mapping of the investigated region of interest for the reference system. The mappings represent multilayer combinations of four elemental mappings (Si in red, Ca in blue, Al in green and Fe in grey), and the light grey markers represent the grid of microvolumes chemo-mechanically investigated.

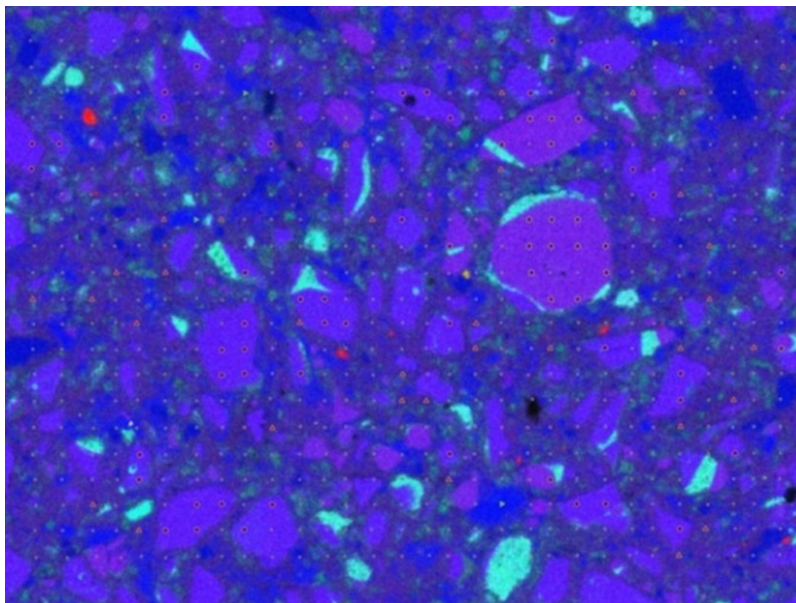


Fig. 15. Composite mapping of the investigated region of interest for the system with 0.05% CF. The mappings represent multilayer combinations of four elemental mappings (Si in red, Ca in blue, Al in green and Fe in grey), and the light grey markers represent the grid of microvolumes chemo-mechanically investigated.

3.3.3. Microstructure evaluation

Fig. 16, Fig. 17, Fig. 18 present SEM micrographs for typical cement pastes incorporating cellulose filaments (CF). Fig. 16 shows the microstructure of a paste with 0.05% CF. Even with such a low CF content, CF appears omnipresent in the form of several needle-like fibrillary particles. Several CF can be observed bridging cracks while some CF can be observed cemented in the hydrated system. Those observations are further confirmed by the micrograph of Fig. 17 for the paste mixture with 0.10% CF. Fig. 17(a), for instance, shows a myriad of protruding filaments with one end embedded in the matrix and the pulled-out end standing free. On the other hand, Fig. 17(b) shows a set of well-identified circular cavities in the matrix corresponding to traces of filaments, which may have been pulled-out from the matrix during fracturing the test sample. Furthermore, Fig. 18(a) for the paste mixture with 0.30% CF illustrates the interaction between the filaments and the hydrated system as the figure shows the germination of hydration products on CF surface. The growth of hydrates on CF surface may support the surface reactivity of CF driven by the omnipresence of OH^- groups. Nonetheless, at increasing CF content, the dispersion of CF clusters such the ones on Fig. 18(b) is not evident, and thus may jeopardize CF effectiveness. This is in consistence with the macroscale mechanical performance which were higher at lower CF dosages (0.05 and 0.10% CF). In light of the above observations on the microstructure of cement pastes incorporating CF, it is possible to explain the effect of CF on the fracture mechanism of tested cement pastes by the well-established fiber-reinforced concrete (FRC) mechanism which involves fiber rupture, fiber pull out, fiber birthing, fiber/matrix debonding, and matrix cracking [60]. Some of the filaments on Fig. 16 crossing the matrix correspond to fiber-bridging which interfere with crack growth. Similarly, some of the CF protruding ends of Fig. 17(a) may correspond to CF fracturing at situations when the rupture energy exceeds the tensile capacity of the filaments. On the other hand, the pulled-out filaments and the traces of pulled-out CF observed in Fig. 17(b) imply the increasing fracture energy involved in deteriorating the filament/matrix interfacial zone where both chemical and frictional bond may prevail. The above different mechanisms contribute to increasing the resistance of the

bulk matrix to fracturing and thus contributes to substantiating the mechanical properties observed at macro scale (particularly flexural capacity and toughness).

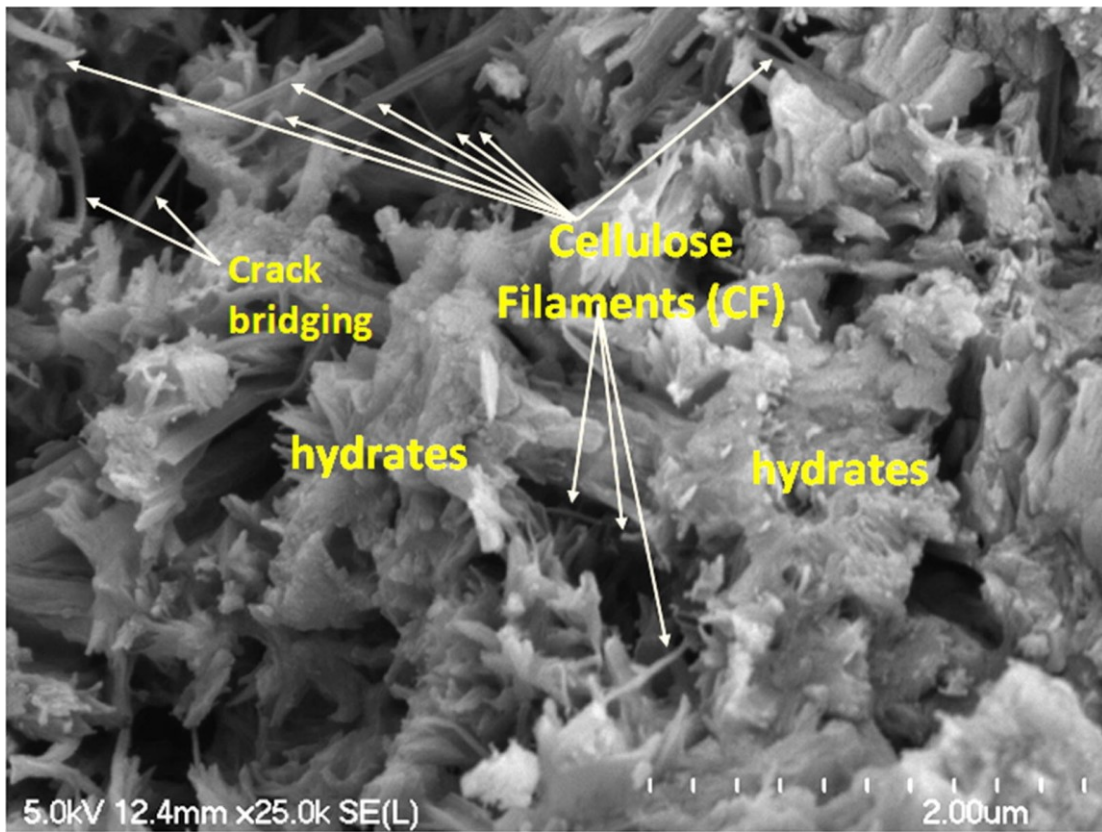


Fig. 16. Scanning electron microscopy (SEM) image of a paste mixture with 0.05% CF. The image shows the omnipresence of CF, and their bridging effect.

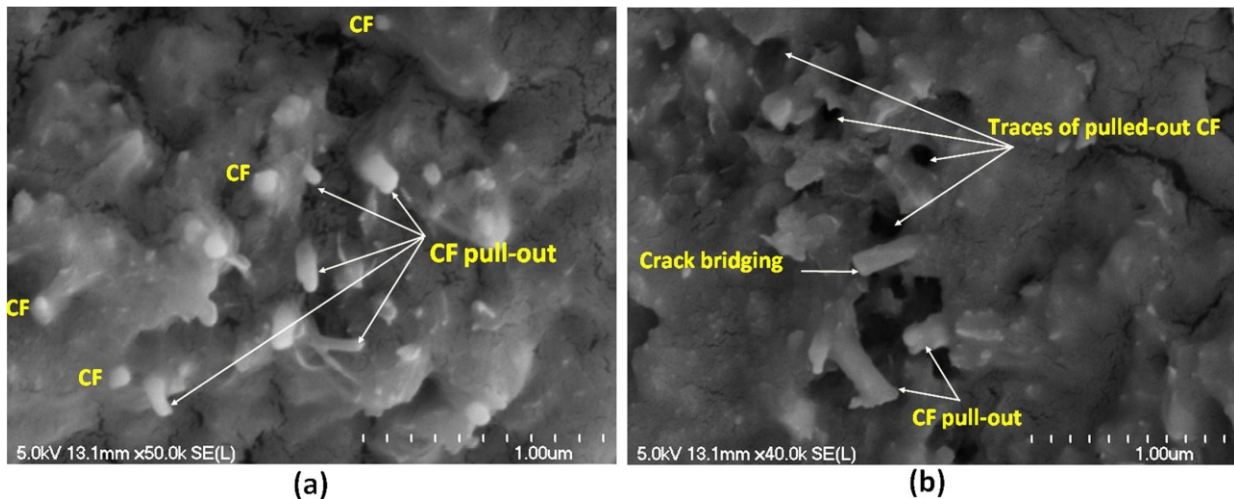


Fig. 17. Scanning electron microscopy (SEM) image of a paste mixture with 0.10% CF: (a) Typical CF pull-out observed on fresh fractured surface, and (b) Traces of pulled-out CF during fracturing the sample.

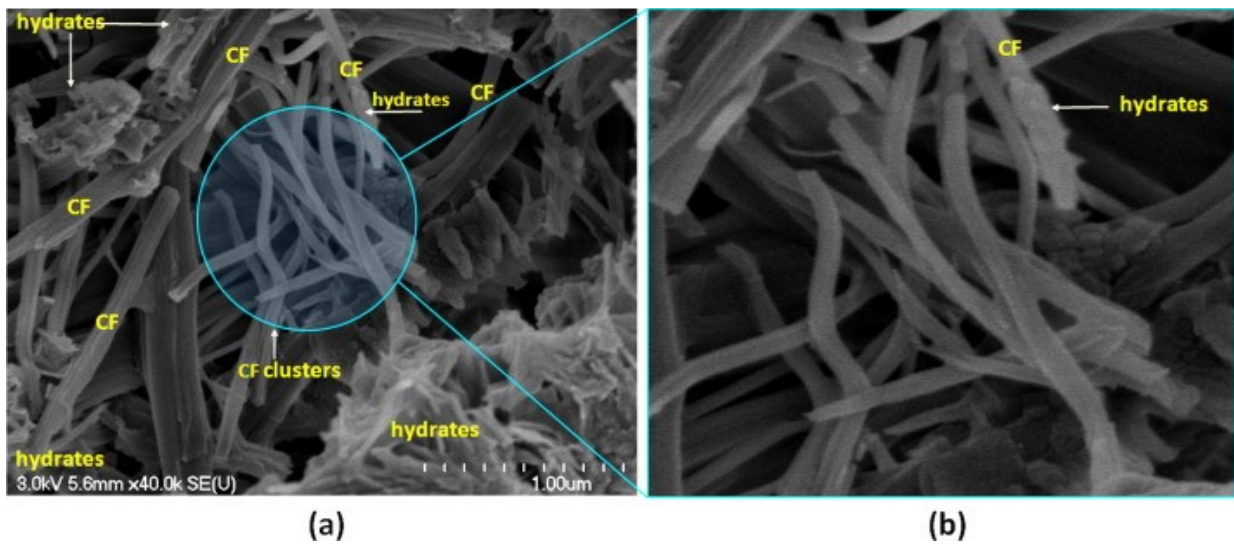


Fig. 18. Scanning electron microscopy (SEM) image of a paste mixture with 0.30% CF: (a) Interaction of CF with hydration products; the figure shows the growth of hydration products on the periphery of CF, and (b) A spot Cellulose filament clusters observed at increasing CF content.

4. Aspects for further consideration

The focus of the current study is to disclose the mechanisms underlying the strengthening effect of CF in cement systems. While overall results demonstrate the potential of CF to allow nano-engineering the properties of cement composites, two common concerns (with the use of all nanocellulose materials (NCM)) remain in suspension: (i) the potential risk hazards to human life posed by the inhalation of NCM and, (ii) the long-term performance of NCM in the corrosive alkaline medium of cement.

- Potential health risks associated with NCM pertain to their nanometric dimensions rendering them susceptible for inhalation. This implies the necessity to highlight the potential human health risks associated with exposure to NCM in the form of respirable nanofibers during production or as a final product [61, 62, 63]. While few studies stress on health hazards from all high-aspect-ratio nanoparticles (HARN) including carbon nanotubes (CNT), carbon nanofibers (CNF), and NCM [64, 65, 66], other researchers prove that the aspect ratio is not the unique parameter involved in the toxicology of fibers. Rather, the biopersistence of a given fiber represents by far an influential factor governing the biological response following chronic exposure [63, 67, 68]. Fiber biopersistence refers to the solubility of the fiber in the lung, and the biological ability of the lung to get rid of it definitively. In this context, an in-vivo study conducted by Warheit et al. [69] involving a 2-week inhalation period, showed no significant pulmonary effects 3 months post exposure to microcellulose. Furthermore, a research (on the ecotoxicological impact of CNC derived from kraft pulp) examined the impact of realistic exposure scenarios (suspension experiments with CNC dosage of 0.03–10 g/L that were based on the potential effluent in the vicinity of a CNC production site) on aquatic organisms from all trophic levels (from bacteria, algae, and crustacean, to fish). Considering all these organisms, the study investigated the acute lethality (LC_{50} = the lethal concentration that reduces the biological system population to 50% viability), reproduction, growth, morphology, embryo development and cytotoxicity (the degree to which a substance is toxic to living cells). In outcome, the study summarized the results as “non-concerning” [70]. Further aspects pertaining to the potential health

hazards of NCM can be found in Endes et al.'s comprehensive review [63]. The latter summarizes that available data in acute exposure scenarios indicate that NCM have far less risk (to human health and environment) than do other HARN commonly used in similar application such as CNT and CNF. While most NCM are currently supplied in water suspensions (reducing the risk of inhalation), this form poses transportation issues. Consequently, recently NCM are also supplied in freeze-dried re-dispersible form. With this, as with any other nanomaterials, extended exposure should be avoided, and personal protection measures should be adopted.

- The second concern about the use of NCM in cement composites is the long-term performance. This concern is particularly mobilized by the potential vulnerability of NCM in the alkaline medium of cement, in analogy to macroscale vegetable fibers. Existing literature ascribes the degradation of macroscale vegetable fibers to the formation of Portlandite (from the cement hydration) inside fiber lumen (the on-axis fiber cavity). This leads to fiber mineralization and subsequent embrittlement [71, 72]. Wei and Meyer [73] suggested that macroscale vegetable fibers degrade in a given sequence where the dissolution of lignin (highly unstable to the increasing pH of cement) is the driving force. The degradation of lignin (serving as a strap for binding cellulose bundles) decreases the integrity and stability of the cell wall of natural fibers. As a result, there remains no binding force between individual cellulose microfibrils. The scenario is, though, quite different with NCM. The latter being obtained by delignification (removal of lignin and other degradable compounds such as pectin, wax, and soluble sugars using also high pH medium), then the vulnerability of lignin to the high alkalinity of cement pore solution shouldn't be a concern. Furthermore, NCM being obtained by axially peeling individual microfibrils, then most probably, there shouldn't be such a concern as fiber lumen where Portlandite would be deposited and lead to fiber mineralization and the consequent embrittlement. In the context of the current project, mechanical properties of ultra-high-performance concrete measured up to 90 days (under laboratory conditions) showed no reduction in strength [29]. Ardanuy et al. [74] evaluated the durability of cement mortars with nanofibrillated cellulose (NFC), (as

compared to mortars reinforced with conventional microscale cellulose fibres from sisal pulp) to withstand accelerated aging (by means of exposure to repeated wet-dry cycles). They found that, though no significant improvement in durability was found in mortars prepared with NFC, no loss in overall mechanical performance was noticed after 5 wet-dry cycles. Rather, NFC-reinforced mortars exhibited significantly higher flexural capacity and flexural modulus, but slightly lower fracture energy as compared to mortars reinforced with conventional sisal fibers. Furthermore, Claramunt et al. [75] investigated the mechanical performance of NFC-reinforced cement mortars subjected to 20 wet-dry cycles as compared to cement mortars with sisal pulp. They reported that sisal-pulp-reinforced-mortars exhibited reduction in mechanical performance due to fiber-debonding from matrix and fiber mineralization none of which was observed in NFC-reinforced mortars. Thus, the latter recorded significant enhancement in durability, flexural capacity, and flexural modulus. While those scant studies on the durability of NCM clear some of the concerns about the long-term performance of NCM in cement composites, the topic remains relatively new and calls for imminent further research.

5. Conclusions

This paper presented a multiscale *top-down* assessment of mechanical properties of cement pastes incorporating cellulose filaments (CF) (from 0.05% to 0.30% by mass of cement). Cement pastes with a water-to-cement ratio of 0.30 were thus investigated in terms of mechanical performances at the engineering scale (compressive strength, elastic modulus, and flexural capacity and toughness) and chemo-mechanical features at the microscale (degree of hydration and micromechanical properties). Interestingly, promising enhancements of macroscale mechanical properties observed in the presence of CF were found to sprout from improvements at microstructure scale. Specific findings can be summarised as follows:

- The incorporation of CF increases the demand in high-range water reducing admixture (HRWRA) due to the viscosity modifying effect of CF. The latter is thought to be associated with CF hydrophilicity leading to water retention and to CF high surface area and high aspect ratio leading to the formation of CF networks.

- The incorporation of CF enhances all tested macroscale mechanical properties. Strength improvement of up to 26% in compression, 18% in elastic modulus, 21% in flexure, and 74% in energy absorption were obtained. Interestingly, improvements in all tested mechanical properties (in the exception of energy absorption) were obtained at low CF concentrations (0.05–0.10%) where CF dispersion (and hence effectiveness) is believed to be more evident.
- The effect of CF on flexural capacity differed from that on toughness: maximum flexural capacity was achieved at relatively low CF contents (0.05–0.10%), whereas higher energy absorption capacity was obtained with increasing CF content (likely due to the contribution of fiber count on the fracture behavior of the matrix).
- The effect of CF on enhancing the above macroscale mechanical properties was found to stem from improvements in microstructure properties of the cement paste system. Microstructure investigations indicated that CF increased the cement degree of hydration by up to 15% at 28 days. The increased degree of hydration was attributed to the hydrophilicity and hygroscopicity of CF leading to, respectively, water retention and water release, thereby providing supplementary water (during hydration) for further reaction of anhydrous cement grains.
- Assessment of micromechanical properties of the main microstructure phases using the NI-QEDS method, revealed that the incorporation of 0.05% CF enhanced the micromechanical properties (indentation modulus M , indentation hardness H , and contact creep modulus C) of the C-S-H gel matrix by about ~12–25%. This enhancement confirms the high altering potential of CF with respect to the C-S-H gel matrix. The enhancement in C-S-H micromechanical properties could be attributed to a combination of a higher degree of hydration and the reinforcing effect imparted by CF on the C-S-H gel matrix. Those change likely drive the gains in elastic modulus and flexural capacity observed at the macroscale.

Finally, these results support the use of CF as a promising material for tailoring concrete properties from the scale of the microstructure phases to obtain a more ductile and tougher

macroscale behavior. Although more works are needed to further explore the enhancement in mechanical performance in systems with CF, it can be retained that CF has the capacity to influence the strength of cement composites at the microstructure scale by contributing to both the hydration kinetics (i.e. by nucleation effects, due to its nanometric diameter) and to the C-S-H gel matrix properties (i.e. as a reinforcing fiber, due to its extremely high aspect ratio).

Acknowledgments

This project is jointly supported by Canada Vanier Graduate Scholarship (CGS) Program, award no 360284; a Cooperative Research and Development (CRD) grant from the Natural Sciences and Engineering Research Council of Canada (NSERC), Kruger Biomaterials Inc. (QC, Canada), and Euclid Chemicals. The authors are grateful for the financial support from these partners.

References

- [1] F. Sanchez and K. Sobolev, Nanotechnology in concrete – a review, *Constr. Build. Mater.*, **24** (11) (2010), pp. 2060–2071
- [2] M. Ashby, P. Ferreira, D. Schodek, Nanomaterials, nanotechnologies and design: an introduction for engineers and architects. Boston, MA: Elsevier Science Ltd, 2009. DOI: <https://doi.org/10.1016/B978-0-7506-8149-0.X0001-3>
- [3] H.M. Jennings, J.W. Bullard, J.J. Thomas, J.E. Andrade, J.J. Chen, G.W. Scherer, Characterization and modeling of pores and surfaces in cement paste: Correlations to processing and properties, *J. Adv. Concr. Technol.*, **6** (1) (2008), pp. 5–29
- [4] P.F. Torgal, S. Jalali, Nanotechnology: Advantages and drawbacks in the field of construction and building materials, *Constr. Build. Mater.*, **25** (2011), pp. 582-590

- [5] L. Filipponi, D. Sutherland, Nanotechnologies: principles, applications, implications and hands-on activities, *European Commission, Directorate-General for Research and Innovation, EUR 24957, 2013*
- [6] H.Z. Wang, R.A. Dixon, On–Off switches for secondary cell wall biosynthesis, *Molecular Plant*, **5** (2) (2012), pp. 297-303
- [7] W. Zhu, P.J.M Bartos, A. Porro A, RILEM TC 197-NCM-Nanotechnology in construction materials- Application of nanotechnology in construction: Summary of a state-of-the-art report, *Mater. Struct.*, **37** (2004), pp.649-658
- [8] A.M. Said, M.S. Zeidan, M.T. Bassuoni, Y. Tian, Properties of concrete incorporating nano-silica, *Constr. Build. Mater.*, **36** (2012), pp. 838-844
- [9] J. Chen, S. C. Kou, C. S. Poon, Hydration and properties of nano-TiO₂ blended cement composites, *Cem. Concr. Compos.*, **34** (5) (2012), pp. 642-649.
- [10] D. Osborn, M. Hassan, and H. Dylla, Quantification of reduction of nitrogen oxides by nitrate accumulation on titanium dioxide photocatalytic concrete pavement, *Trans. Res. Rec.*, **2290** (2012), pp. 147–153.
- [11] N. Tregger, M. Pakula, S. Shah, Influence of micro and nanoclays on fresh state of concrete, *Trans. Res. Rec.*, **2141** (2010), pp. 68-74. DOI: 10.3141/2141-12.
- [12] M. S. Konsta-Gdoutos, Z. S. Metaxa, S. Shah, Multi-scale mechanical and fracture characteristics and early-age strain capacity of high-performance carbon nanotube/cement nanocomposites, *Cem. Concr. Compos.*, **32** (2010), pp. 110–115.
- [13] R. J. Moon, A. Martini, J. Nairn, J. Simonsen, J. Youngblood, Cellulose nanomaterials review: structure, properties and nanocomposites. *Chem. Soc. Rev.*, **40** (7) (2001), pp. 3941–3994.
- [14] J.E. Goodsell, R.J. Moon, A. Huizar, R.B. Pipes, A strategy for prediction of the elastic properties of epoxy-cellulose nanocrystal-reinforced fiber networks, *Nord Pulp Pap. Res. J.*, **29** (1) (2014), pp. 85–94.

- [15] Y. Habibi, A. Dufresne, Highly filled bionanocomposites from functionalized polysaccharide nanocrystals, *Biomacromolecules*, **9** (7) (2008), pp. 1974–1980.
- [16] Y. Cao, P. Zavaterra, J. Youngblood, R. Moon and J. Weiss, The influence of cellulose nanocrystal additions on the performance of cement paste, *Cem. Concr. Compos.*, **56** (2015), pp. 73–83.
- [17] M. Ardanuy, J. Claramunt, R. Arevalo, F. Pares, E. Aracri, T. Vidal, Nanofibrillated-cellulose as a potential reinforcement for high performance cement mortar composites, *BiouResources*, **7** (3) (2012), pp. 3883-3884.
- [18] O. Onuaguluchi, D. Panesar and M. Sain, Properties of nanofibre reinforced cement composites, *Construct. Build. Mater.*, **63** (2014), pp. 119–124.
- [19] O. A. Hisseine, A. F. Omran, A. Tagnit-Hamou, Influence of Cellulose Filaments on Cement Pastes and Concrete, *J. Mater. Civ. Eng.*, **30** (6) (2018), 04018109
- [20] O. A. Hisseine, N. Basic, A. F. Omran, A. Tagnit-Hamou, Feasibility of using cellulose filaments as a viscosity modifying agent in self-consolidating concrete, *Cem. Concr. Compos.*, Volume 94, (2018), pp. 327-340,
- [21] J. Zhou, N. Butchosa, H. S. Jayawardena, J. Park, Q. Zhou, M. Yan and O. Ramstrom, *Biomacromolecules*, **16** (2015), pp. 1426–1432.
- [22] M. A. Laadila, K. Hegde, T. Rouissi, S.K. Brar, R. Galvez, L. Sorelli, R. Ben Cheikh, M. Paiva, K. Abokitse, Green synthesis of novel biocomposites from treated cellulosic fibers and recycled bio-plastic polylactic acid, *J. Cleaner Prod.*, **164** (2017), pp. 575-586.
- [23] E.J. Foster, R.J. Moon, U.P. Agarwal et al., Current characterization methods for cellulose nanomaterials, *Chem. Soc. Rev.*, **47** (2018), pp. 2609-2679.
- [24] R. Jarabo, E. Fuente, M.C. Monte, H. Savastano, P. Mutjé, C. Negro, Use of cellulose fibers from hemp core in fiber-cement production: Effect on flocculation, retention, drainage and product properties. *Ind. Crops Prod.*, **39** (2012), pp. 89–96.

- [25] O. Faruk, A.K. Bledzki, H.S. Fink, M. Mohini Sain, Biocomposites reinforced with natural fibers. *Prog. Polym. Sci.*, **37** (2012), pp. 552– 1596.
- [26] M. A. Aziz, P. Paramasivam, S. L Lee, Prospects for natural fibre reinforced concretes in construction, *Int. J. Cem. Compos. Lightweight Concr.*, **3** (2) (1981), pp.123–132.
- [27] S. J. Eichhorn, A. Dufresne, M. Aranguren, , N. E. Marcovich, J. R.Capadona, S. J. Rowan, C. Weder, W. Thielemans, M. Roman, S. Renneckar, W. Gindl, S. Veigel, J. Keckes, H. Yano, K. Abe, M. Nogi, A. N. Nakagaito, A. Mangalam, J. Simonsen, A. S. Benight, A. Bismarck, L. A Berglund, T. Peijs, Review: current international research into cellulose nanofibres and nanocomposites. *J. Mater. Sci.*, **45** (2010), pp. 1–33.
- [28] L. Brinchi, F. Cotana, E. Fortunati, J.M Kenny, Production of nanocrystalline cellulose from lignocellulosic biomass: Technology and applications. *Carbohydr. Polym.*, **94** (2013), pp. 154–169.
- [29] O. A. Hisseine, N. Soliman, A. Tagnit-Hamou, Cellulose filaments for controlling autogenous shrinkage in ultra-high-performance concrete, Article under review by *Cem. Concr. Res.* (2018)
- [30] J. Flores, M. Kamali, A. Ghahremaninezhad, An investigation into the properties and microstructure of cement mixtures modified with cellulose nanocrystal, *Materials.*, **10** (5), 498. <http://doi.org/10.3390/ma10050498>
- [31] S.J. Peters, T.S. Rushing, E.N. Landis, T.K. Cummins, Nanocellulose and microcellulose fibers for concrete, *Transp. Res. Rec.*, **2142** (2010), pp. 25–28.
- [32] W. Wilson, L. Sorelli, A. Tagnit-Hamou, Automated coupling of NanoIndentation and Quantitative Energy-Dispersive Spectroscopy (NI-QEDS): A comprehensive method to disclose the micro-chemo-mechanical properties of cement pastes. *Cem. Concr. Res.*, **103** (2018), pp. 49–65.
- [33] W. Wilson, L. Sorelli, A. Tagnit-Hamou, Unveiling micro-chemo-mechanical properties of C-(A-) S-H and other phases in blended-cement pastes, *Cem. Concr. Res.*, **107** (2018), pp. 317–336.

- [34] CSA A3000-13 Cementitious materials compendium, CSA, Mississauga, Ontario, Canada, updated 2017.
- [35] ASTM C1157/C1157M-17 Standard Performance Specification for Hydraulic Cement, ASTM International, West Conshohocken, PA, 2017, https://doi.org/10.1520/C1157_C1157M-17
- [36] ASTM C305-14 Standard Practice for Mechanical Mixing of Hydraulic Cement Pastes and Mortars of Plastic Consistency, ASTM International, West Conshohocken, PA (2014). <https://doi.org/10.1520/C0305-14>
- [37] ASTM C230/C230M-14 Standard Specification for Flow Table for Use in Tests of Hydraulic Cement, ASTM International, West Conshohocken, PA, 2014, https://doi.org/10.1520/C0230_C0230M-14
- [38] ASTM C109/C109M-16a Standard Test Method for Compressive Strength of Hydraulic Cement Mortars (Using 2-in. or [50-mm] Cube Specimens), ASTM International, West Conshohocken, PA, 2016, https://doi.org/10.1520/C0109_C0109M-16A
- [39] ASTM C78/C78M-18 Standard Test Method for Flexural Strength of Concrete (Using Simple Beam with Third-Point Loading), ASTM International, West Conshohocken, PA (2018). https://doi.org/10.1520/C0078_C0078M-18
- [40] ASTM C469/C469M-14 Standard Test Method for Static Modulus of Elasticity and Poisson's Ratio of Concrete in Compression, ASTM International, West Conshohocken, PA, 2014, https://doi.org/10.1520/C0469_C0469M-14
- [41] A.C Khazraji, S. Robert (2013) Self-Assembly and Intermolecular Forces When Cellulose and Water Interact Using Molecular Modeling. *Journal of Nanomaterials*, **745979** (2013), Article ID 745979. <http://dx.doi.org/10.1155/2013/745979>
- [42] S. Altoubat, H. Ousmane, S. Barakat, Experimental study of in-plane shear behaviour of fiber-reinforced concrete composite deck slabs, *ASCE J. Struct. Eng.*, **142** (3) (2016): 04015156.
- [43] K. Abe, S. Iwamoto, H. Yano, Obtaining cellulose nanofibers with a uniform width of 15 nm from wood. *Biomacromolecules*, **8** (2007), pp. 3276–3278.

- [44] C.H Gómez, E. Cristia, A. Vázquez, Effect of cellulose microcrystalline particles on the properties of cement-based composites, *Mater. Des.*, **51**(2013), pp. 810–818.
- [45] P.J.M. Monteiro, P.R.L. Helene, S.H. Kang, Designing concrete mixtures for strength, elastic modulus and fracture energy, *Mater. Struct.*, **26** (8) (1993), pp. 443–452. <https://doi.org/10.1007/BF02472804>.
- [46] S.P. Shah, S.H. Ahmad, Structural Properties of high strength concrete and its implications for precast prestressed concrete, *PCI journal*, **6**(30) (1985), pp. 92-119.
- [47] R.S.P. Coutts, P.G. Warden, Air cured, Abaca reinforced cement composites, *Int. J. Cem. Comp. Lightweight Conc.*, **9** (2) (1987), pp. 69-73.
- [48] R.S.P. Coutts, P.G. Warden, Sisal pulp reinforced cement mortar, *Cem. Concr. Compos.*, **14** (1992), pp. 17-21.
- [49] R.S.P. Coutts, Y. Ni, B.C. Tobias, Air-cured bamboo pulp reinforced cement, *J. Mater Sci. Lett.* **13** (1994), pp. 283-285.
- [50] H. Savastano Jr., P.G. Warden, R.S.P. Coutts, Brazilian waste fibres as reinforcement for cement based composites, *Cem. Concr. Compos.*, **22** (2000), pp. 379- 384.
- [51] M. Mouret, A. Bascoul, G. Escadeillas, Study of the degree of hydration of concrete by means of image analysis and chemically bound water, *Adv. Cem. Based Mater.*, **6**(3–4) (1997), pp. 109–115.
- [52] B. Lothenbach, P. Durdziński, K. De Weerd, Thermogravimetric analysis, In K. Scrivener, R. Snellings, & B. Lothenbach (Eds.), *A Practical Guide to Microstructural Analysis of Cementitious Materials*, 2016, (pp. 177-211). CRC Press. <https://doi.org/10.1201/b19074-6>.
- [53] I. Pane, W. Hansen, Investigation of blended cement hydration by isothermal calorimetry and thermal analysis. *Cem. Concr. Res.*, **35** (6) (2005), pp. 1155 – 1164.

- [54] L.E. Copeland, D.L. Kantro, G. J. Verbeck, Chemistry of hydration of Portland cement. Proceedings of the 4th International Symposium on the Chemistry of Cement, National Bureau of Standards, Washington, D. C., 1960, pp. 429-465.
- [55] F. Mohammadkazemi, K.Doosthoseini, E. Ganjian, M. Azin, Manufacturing of bacterial nano-cellulose reinforced fiber-cement composites. *Constr. Build. Mater.* **101** (2015), pp. 958–964.
- [56] P.C. Mishra, V. K. Singh, K. K. Narang, N. K. Singh, Effect of carboxymethyl-cellulose on the properties of cement, *Mater. Sci. Eng. A*, **357** (2003), pp. 13–19.
- [57] C. J. Knill, J.F. Kennedy, Degradation of cellulose under alkaline conditions. *Carbohydr. Polym.*, **51** (2003), pp. 281–300.
- [58] K. Vercammen, M.A. Glaus, L.R. Van Loon, Complexation of calcium by α -isosaccharinic acid under alkaline conditions, *Acta Chem. Scand.*, **53** (1999), pp. 241–246.
- [59] T. Fu, F. Montes, P. Suraneni, J. Youngblood, J. Weiss, The Influence of Cellulose Nanocrystals on the Hydration and Flexural Strength of Portland Cement Pastes, *Polymers* **9** (24) (2017), pp. 424.
- [60] T. L. Anderson, Fracture mechanics: fundamentals and applications: CRC press, FL, USA, 2005.
- [61] M. Roman, Toxicity of cellulose nanocrystals: a review. *Ind Biotechnol.*, **11**(1) (2015), pp. 25–33. doi:10.1089/ind.2014.0024.
- [62] D. B. Warheit, K. L. Reed, T. R. Webb, Man-made respirable-sized organic fibers: what do we know about their toxicological profiles? *Ind Health*, **39**(2) (2011), pp. 119–25. doi:10.2486/indhealth.39.119.
- [63] C. Endes, S. Camarero-Espinosa, S. Mueller et al. A critical review of the current knowledge regarding the biological impact of nanocellulose. *J Nanobiotechnol* (2016) 14:78. <https://doi.org/10.1186/s12951-016-0230-9>.

- [64] C. A. Poland, R. Duffin, I. Kinloch, A. Maynard, W.A.H. Wallace, A. Seaton et al., Carbon nanotubes introduced into the abdominal cavity of mice show asbestos-like pathogenicity in a pilot study. *Nat Nano.*, **3**(7) (2008), pp. 423–8.
- [65] K. Donaldson, F. A. Murphy, R. Duffin, C. A. Poland. Asbestos, carbon nanotubes and the pleural mesothelium: a review of the hypothesis regarding the role of long fibre retention in the parietal pleura, inflammation and mesothelioma, *Particle Fibre Toxicol.* 2010, 7:5.
- [66] J. M. G. Davis, The need for standardized testing procedures for all products capable of liberating respirable fibers—the example of materials based on cellulose. *Br J Ind Med.*, **50**(2) (1993), pp. 187–90.
- [67] M. R. Becklake, Asbestos-related diseases of lung and other organs—their epidemiology and implications for clinical practice. *Am Rev Respir Dis.*, **114**(1) (1976), pp. 187–227.
- [68] Donaldson K, Brown RC, Brown GM. New perspectives on basic mechanisms in lung disease. 5. Respirable industrial fibres: mechanisms of pathogenicity. *Thorax.*, **48**(4) (1993), 390–5. doi:10.1136/thx.48.4.390.
- [69] D. B. Warheit, S. I. Snajdr, M. A. Harstsky, S. R. Frame, Advances in the prevention of occupational respiratory diseases. International Congress Series, Amsterdam: Elsevier Science; 1998, pp. 579–89.
- [70] T. Kovacs, V. Naish, B. O'Connor, C. Blaise, F. Gagne, L. Hall et al. An ecotoxicological characterization of nanocrystalline cellulose (NCC). *Nanotoxicology*, **4**(3) (2010), pp. 255–70. doi:10.3109/17435391003628713.
- [71] B. J. Mohr, H. Nanko, K. E. Kurtis, Durability of kraft pulp fiber–cement composites to wet/dry cycling. *Cem Concr Compos* **27** (2005), pp. 435–48.
- [72] G. H. D. Tonoli, S. F. Santos, P. Joaquim, H. Savastano. Effect of accelerated carbonation on cementitious roofing tiles reinforced with lignocellulosic fibre. *Constr Build Mater.*, **24** (1993), pp. 193–201.

- [73] M. Ardanuy, J. Claramunt, J. A. García-Hortal, M. Barra, Fiber-matrix interactions in cement mortar composites reinforced with cellulosic fibers. *Cellulose* 18 (2011), pp. 281–9.
- [74] M. Ardanuy, J. Claramunt, D. Romildo, T. Filho, Evaluation of durability to wet/dry cycling of cement mortar composites reinforced with nanofibrillated cellulose, Editor(s): A.M. Brandt, J. Olek, M.A. Glinicki, C.K.Y. Leung, *Brittle Matrix Composites* 10, Woodhead Publishing, 2012, Pages 33-41,
- [75] J. Claramunt, M. Ardanuy, L. J. Fernandez-Carrasco, Wet / Dry Cycling Durability of Cement Mortar Composites Reinforced with Micro-and Nanoscale Cellulose Pulps, *Bioresources*, 10 (2) (2015) 3045-3055.

List of Figures

Fig. 1. Particle size distribution of GU cement used in this study

Fig. 2. Cellulose filaments (CFs): (a) CF-water suspensions for the different dosages tested in this study, and (b) Scanning electron microscope (SEM) image of a suspension with 0.1% CF (reprinted from Hisseine et al. (2018) with permission from ASCE.

Fig. 3. Hierarchical structure of cellulose filaments (CF)

Fig. 4. Relationship between particle size and specific surface area as related to the constituents of different classes of concrete (adapted from (Sanchez and Sobolev 2010))

Fig. 5. Effect of CF on slump flow and mixture demand in HRWR (CF=cellulose filaments in % weight of cement content)

Fig. 6. Evolution of compressive strength (f_c) in tested paste mixtures (CF=cellulose filaments in % weight of cement content)

Fig. 7. Elastic modulus (E) of tested cement pastes (CF=cellulose filaments in % weight of cement)

Fig. 8. Flexural capacity (f_{fl}) of tested pastes (CF=cellulose filaments in % weight of cement)

Fig. 9. Energy absorption capacity (CF=cellulose filaments in % weight of cement)

Fig. 10. Thermogravimetric analysis (TGA) at 7 days for the different pastes systems (CF=cellulose filaments in % weight of cement)

Fig. 11. Thermogravimetric analysis (TGA) at 28 days for the different pastes (CF=cellulose filaments in % weight of cement)

Fig. 12. Degree of hydration (D_h) of the cement in the investigated cement pastes (CF=cellulose filaments in % weight of cement content)

Fig. 13. Composite mapping of the investigated region of interest for the reference system.

The mappings represent multilayer combinations of four elemental mappings (Si in red, Ca in blue, Al in green and Fe in grey), and the light grey markers represent the grid of microvolumes chemo-mechanically investigated.

Fig. 14. Composite mapping of the investigated region of interest for the system with 0.05% CF.

The mappings represent multilayer combinations of four elemental mappings (Si in red, Ca in blue, Al in green and Fe in grey), and the light grey markers represent the grid of microvolumes chemo-mechanically investigated.

Fig. 15. Scanning electron microscopy (SEM) image of a paste mixture with 0.05% CF.

The image shows the omnipresence of CF, and their bridging effect.

Fig. 16. Scanning electron microscopy (SEM) image of a paste mixture with 0.10% CF: (a)

Typical CF pull-out observed on fresh fractured surface, and (b) Traces of pulled-out CF during fracturing the sample.

Fig. 17. Scanning electron microscopy (SEM) image of a paste mixture with 0.30% CF: (a)

Interaction of CF with hydration products; the figure shows the growth of hydration products on the periphery of CF, and (b) A spot Cellulose filament clusters observed at increasing CF content.

List of Tables

Table 1. Chemical composition and physical properties of GU cement

Table 2. Mix design of pastes based on 1000 g of binder at $w/c = 0.3$

Table 3. Comparison of the reference paste and the paste with 0.05% CF, in terms of micromechanical properties (indentation modulus M , indentation hardness H , and contact creep modulus C , as obtained from n data points deterministically selected with the NI-QEDS method).

Part III:

Development of multiscale nanomodified strain-hardening cementitious composites incorporating high-volume ground- glass pozzolans (HVGP-SHCC)

- Chapter 7: Characterization and nanomodification of interface properties of HVGP-SHCC.
- Chapter 8: Coupling particle packing optimization with Micromechanical tailoring for the development of HVGP-SHCC
- Chapter 9: Micromechanically guided design of nanoengineered HVGP-SHCC

This part of the thesis contributes towards achieving project objective 5, namely, leveraging the versatile opportunities offered by nanocellulose to develop a novel nanoengineered concrete formulation, namely, a Nanomodified-Strain-Hardening Cementitious Composite (SHCC).

CHAPTER 7

Characterization and Nanomodification of Interface Properties of strain-hardening cementitious composites incorporating high-volume ground-glass pozzolans

7.1 Introduction

In harmony with the overall objective of part III which consists of valorising cellulose filaments (CF) for the development of nanoengineered strain-hardening cementitious composites incorporating high-volume ground-glass pozzolans (HVGP-SHCC), the current chapter is devoted to the characterization and nanomodification of interface properties of HVGP-SHCC. The development of the HVGP-SHCC undertaken herein is guided by two tailoring tools: (i) the optimization of matrix compacity, and (ii) the micromechanical and fracture mechanics tailoring approach. The former has been employed to perform a guided replacement of fly ash (FA) commonly used in SHCC formulation with ground glass pozzolans (GP) such that higher matrix strength may be attained. On the other hand, to optimize the strength to be obtained with packing optimization without jeopardizing ductility, the nanoscale CF were used as a tool to nanoengineer matrix and interface properties towards enhanced complementary energy (J_b) necessary for composite steady state cracking and strain-hardening behavior. In this quest, characterization and tailoring of interface properties is indispensable.

Therefore, the role of this chapter is to (i) characterize the interface properties [frictional bond (τ_0), chemical bond energy (G_d), and slip-hardening effect (β)] of PVA fibers in HVGP-SHCC using single-fiber pull-out test, then (ii) use cellulose filaments (CF) as a nano-modifier to tailor matrix and interface properties, and finally (iii) construct the fiber-bridging stress versus crack opening response [$\sigma(\delta)$] for the different formulations to be subsequently used for assessing the composite pseudo-ductility performance for the different formulation ([Chapter 9](#)).

The work discussed in this chapter (article 5 addressed in [section 7.2](#) below) is being considered for publication in construction and building materials.

7.2 Article 5- Characterization and nano-engineering the interface properties of PVA fibers in strain-hardening cement composites incorporating high-volume ground-glass pozzolans

Article information

Authors and affiliations:

Ousmane A. Hisseine, PhD candidate and Canada Vanier Scholar of NSERC, Cement and Concrete Research Group, Department of Civil Engineering, Université de Sherbrooke

A. Tagnit-Hamou, Professor and director of Cement and Concrete Research Group, Department of Civil Engineering, Université de Sherbrooke

Article status: Under review

Journal: Construction and Building Materials

Initial date of submission: April 18, 2019

Reference: Hisseine, O. A, Tagnit-Hamou, A. (2019). Characterization and nano-engineering the interface properties of PVA fibers in strain-hardening cement composites incorporating high-volume ground-glass pozzolans: Under review by the journal of *Construction and Building Materials*.

Titre français: Caractérisation et nano-modification des propriétés d'interface de bétons écrouissants à teneur élevée en poudre de verre.

Contribution of this article: Contributes towards achieving project object 5, namely, leveraging the versatile opportunities offered by nanocellulose to develop a novel nanoengineered concrete formulation, namely, a Nanomodified-Strain-Hardening Cementitious Composite.

Characterization and nanoengineering the interface properties of PVA fibers in strain-hardening cement composites incorporating high-volume ground-glass pozzolans

Ousmane A. Hisseine; Arezki Tagnit-Hamou

Under Review by Construction and Building Materials

Abstract

In the context of enhancing concrete ecoefficiency through the valorization of domestic materials into concrete design, increasing research attention is being paid to the development of strain-hardening cementitious composites (SHCC) with various supplementary cementitious materials (SCM) in replacement of the commonly used fly ash (FA). In this regard, ground-glass pozzolans [or glass powder (GP)] obtained by grinding post-consumer waste glass can shape a potential candidate. This study is aimed at characterizing the interface properties of polyvinyl-alcohol (PVA) fibers in SHCC incorporating high-volume GP (HVGP) at 0-100% replacement of FA. Single fiber pull-out tests were conducted to characterize the interface properties [frictional bond (τ_0), chemical bond (G_d), and slip-hardening coefficient (β)] necessary for micromechanical tailoring of SHCC. Results indicate that with higher matrix compacity obtained with GP, τ_0 increased significantly, while G_d slightly decreased. Whereas higher τ_0 in HVGP-SHCC was found to increase the maximum pull-out load of PVA fibers, excessive τ_0 causes fiber damage, thereby adversely affecting composite ductility. Therefore, an attempt was made to nanomodify the interface by incorporating nanoscale cellulose filaments (CF) at rates of 0.03–0.10% per cement mass. This allowed to significantly alter the pull-out behavior whereby τ_0 and G_d were relatively attenuated, while a significant increase in β (~ 1.0 - 1.5) was obtained. Thus, the incorporation of CF imparted a characteristic slip-hardening effect that contributed towards enhancing the strain-hardening capacity in HVGP-SHCC as experimentally validated by uniaxial tensile tests.

Author Keywords: Ecological materials, engineered cementitious composites (ECC), recycled glass powder, particle packing optimization, micromechanics, single fiber pull-out, strain hardening

1 Introduction

Strain-hardening cementitious composites (SHCC) also known as engineered cementitious composites (ECC) belong to high-performance fiber-reinforced cementitious composites (HPFRCC) and are characterized by exceptional ductility, significant tensile strain capacity, strain-hardening behavior featured by tight multiple-cracking with relatively low fiber volume, typically $\leq 2\%$ [1–4]. These characteristics are the outcome of a methodical tailoring process which is guided by micromechanical principles such that the mechanical interactions between the fiber, the matrix, and fiber/matrix interface are systematically considered when the composite is subjected to loading [5]. As such, the study of fiber/matrix interface is fundamental for the development of SHCC. The importance of fiber/matrix interface is driven by the fact that in the fiber-bridging concept underpinning the mechanism of action of fiber-reinforced concrete (FRC), fiber rupture is strongly influenced by the magnitude of the interfacial bond, together with fiber length and strength [6]. The importance of fiber/matrix interface also originates from the fact that all composite properties beyond the linear elastic range of deformation (e.g. strength, fracture energy, fatigue, ductility, energy absorption capacities, etc.) are expected to activate the failure of the fiber/matrix interface if fiber failure is prevented [6]. Therefore, the study of fiber/matrix interface is fundamental for tailoring interfacial property towards improving those composite properties. In this regard, single-fiber pull-out (SFP) test (in which an individual fiber is pulled out from its surrounding matrix while continuously recording the pull-out load and the corresponding fiber-slip distance) have been generally recognized as a useful tool for a direct assessment of fiber/matrix interfacial bond properties. The latter are mainly described through the concept of chemical bond (G_d), frictional bond (τ_0), and slip-hardening or slip-softening coefficient (β) [7, 8].

In the context of SHCC with high-volume fly ash (where the use of PVA fibers has been a prevailing practice) [9–12], G_d is associated with the tendency of the hydrophilic PVA fibers to adhere to active cations from the surrounding matrix, particularly Al^{3+} and Ca^{2+} [13, 14]. In this regard, G_d is almost negligible in non-chemically bonded fibers such as steel or polyethylene fibers [15]. In contrast, PVA fibers possess a strong propensity to chemically adhere to cement hydration products. This renders the fibers vulnerable to delamination and rupture which jeopardize strain-hardening behavior as G_d contributes to reducing the complementary energy (J'_b) as well as the multiple-cracking potential [9].

The frictional bond τ_0 is mainly driven by the stiffness, roughness, and compactness of the fiber/matrix interfacial transition zone [11, 16]. High τ_0 values increase the pull-out resistance of fibers and lead to SHCC with higher strength, given the direct correlation between τ_0 and the maximum bringing stress (σ_0) when fiber rupture, slip-hardening, and snubbing effect are ignored [16]. However, excessive τ_0 can cause fiber damage during debonding and lead to decreasing J'_b [9,17]. This significantly reduces matrix ductility. For this reason, with PVA fibers, the fiber/matrix interface properties often exceed the optimal values in typical cement composites [18]. Therefore, the interface properties need to be attenuated such that G_d is the lowest while τ_0 is maintained at moderate levels [9]. The slip-hardening effect β , on the other hand, can be useful to allow fibers to continue resisting further pull-out load even after initial bond deterioration [7, 15] owing to a jamming effect created at the interface.

Therefore, as fiber-pullout confers higher ductility to fiber-reinforced composites [7, 8, 19], it follows that to obtain composites with strain-hardening performance, the interface properties should be optimized rather than maximized. Some of the attempts to optimize interface properties include (i) increasing the FA content, (ii) coating the PVA fibers with an oiling agent, (iii) incorporation of crumb rubber, and (iv) incorporation of nanomaterials such as calcium carbonate nanowhiskers (CaCO_3). Increasing FA content attenuates G_d as well as τ_0 , lowers the crack tip toughness J_{tip} , modifies the PVA fiber-bridging behavior, and results in higher J'_b which favors the strain-hardening response and improves the ductility at the composite level [9]. However, with the reduced J_{tip} associated with excess FA content, reduced composite strength is also observed in HVFA-SHCC [9–12]. Coating the PVA fibers with an oiling agent at an optimum dosage of 1.2 wt.% was reported to allow counteracting excessive G_d , τ_0 , and β and to result into composites with improved performance exhibiting a strain-capacity beyond 4% [18]. However, oiled PVA fibers are very expensive and add to the invoice of SHCC, thereby reducing the potential for large-scale applications of SHCC [19]. Graphene oxide (GO) incorporated at 0.05 - 0.12wt.% were found to increase matrix compactness and lead to higher J_{tip} . While the latter is unfavorable for strain-hardening, the incorporation of GO also enhanced fiber/matrix interface and increased J'_b such that the ratio J'_b/J_{tip} was not adversely affected, thereby leading to higher strain-hardening capacity [20]. The incorporation of CaCO_3 nanowhiskers resulted in a significant decrease in G_d and an improvement in J'_b , thereby enhancing the strain-hardening behavior of SHCC [16].

In the context of the development of HVGP-SHCC attempted herein, the incorporation of GP was intended to optimize the packing density of the matrix to enhance the composite strength lacked in the most commonly used HVFA-SHCC [9–12] while valorizing an otherwise waste material (post-consumer ground-glass). In this regard, it can be perceived that while optimizing matrix compacity allows higher composite strength, it should be noted that too high particle packing densifies fiber/matrix interfacial transition zone and can lead to excessive τ_0 which—when associated with fiber rupture—can jeopardize composite ductility [9, 17]. Therefore, the current study proposes the incorporation of nanoscale cellulose filaments (CF) to serve as a novel tool to nanoengineer matrix and interface properties of HVGP-SHCC towards higher strength and ductility. CF are nanoscale rod-like cellulosic particles with a nanometric diameter (30–400 nm), micrometric length (100–2000 μm), and high aspect ratio (100–1000). CF belong to nanocellulose materials (NCM) such as cellulose nanocrystals (CNC); microfibrillated cellulose (MFC; and nanofibrillated cellulose (NFC) [21].

Precursors of CF as a potential candidate to enhance HVGP-SHCC originate from: (i) strengthening/stiffening features emanating from a combination of internal curing and nanoreinforcing effects leading to higher strength (up to 18% in elastic modulus [22], 25% in flexure, and 96% in energy absorption [23]), (ii) CF effect on the microstructure manifested by an increased degree of hydration of $\sim 15\%$ and enhanced micromechanical properties of C-S-H gel matrix of $\sim 12\text{--}25\%$) [22].

Building upon these findings from our previous research works [17, 22, 23], it is hypothesized herein that while particle packing optimization with the incorporation of GP increases the strength of SHCC at the detriment of ductility, the incorporation of CF as a nanoreinforcing tool can allow obtaining multi-scale fiber-reinforced HVGP-SHCC exhibiting both improved strength and ductility. On the other hand, the high surface area CF may be perceived to interfere at the fiber/matrix interfacial zone such that the excessive bonding of PVA fibers to the matrix (and eventually G_d) may be attenuated, thereby potentially contributing to increasing the complementary energy J_b . For this, the aim of this article is to characterize the interface properties of PVA fibers in HVGP-SHCC along with the nanomodification of matrix and interface properties using CF so that optimized interface properties can be obtained to serve in the micromechanical design of HVGP-SHCC. The study contributes towards the development of multi-scale fiber reinforced SHCC incorporating HVGP and brings new insight on the development of ecological HPFCC using domestic materials.

2 Research Framework

With the aim of increasing composite strength, the SHCC mixtures considered in this study for characterization and nanomodification of interface properties were first screened on the basis of particle packing optimization using the compressible packing model (CPM) proposed by De Larrad [24] where GP replacement of FA of up to 100% was considered [17]. Selected mixtures ensuing from the particle packing optimization (namely with the minimum, moderate, and maximum GP content) were also subjected to nanomodification with CF at dosages of 0.03, 0.05, and 0.10% by mass of cement. Resulting formulations were then considered for the single-fiber pull-out test to compile fiber/matrix interface parameters (namely, chemical bond G_d , frictional bond τ_0 , and slip-hardening coefficient β). In outcome, interface parameters were used to construct the fiber-bridging stress versus crack-opening response $[\sigma(\delta)]$ for the different formulations using micromechanical principles. Uniaxial direct tensile tests were also conducted to validate the results of $\sigma(\delta)$ obtained from micromechanical modeling. Fig. 1 presents an overview of the framework adopted in this study.

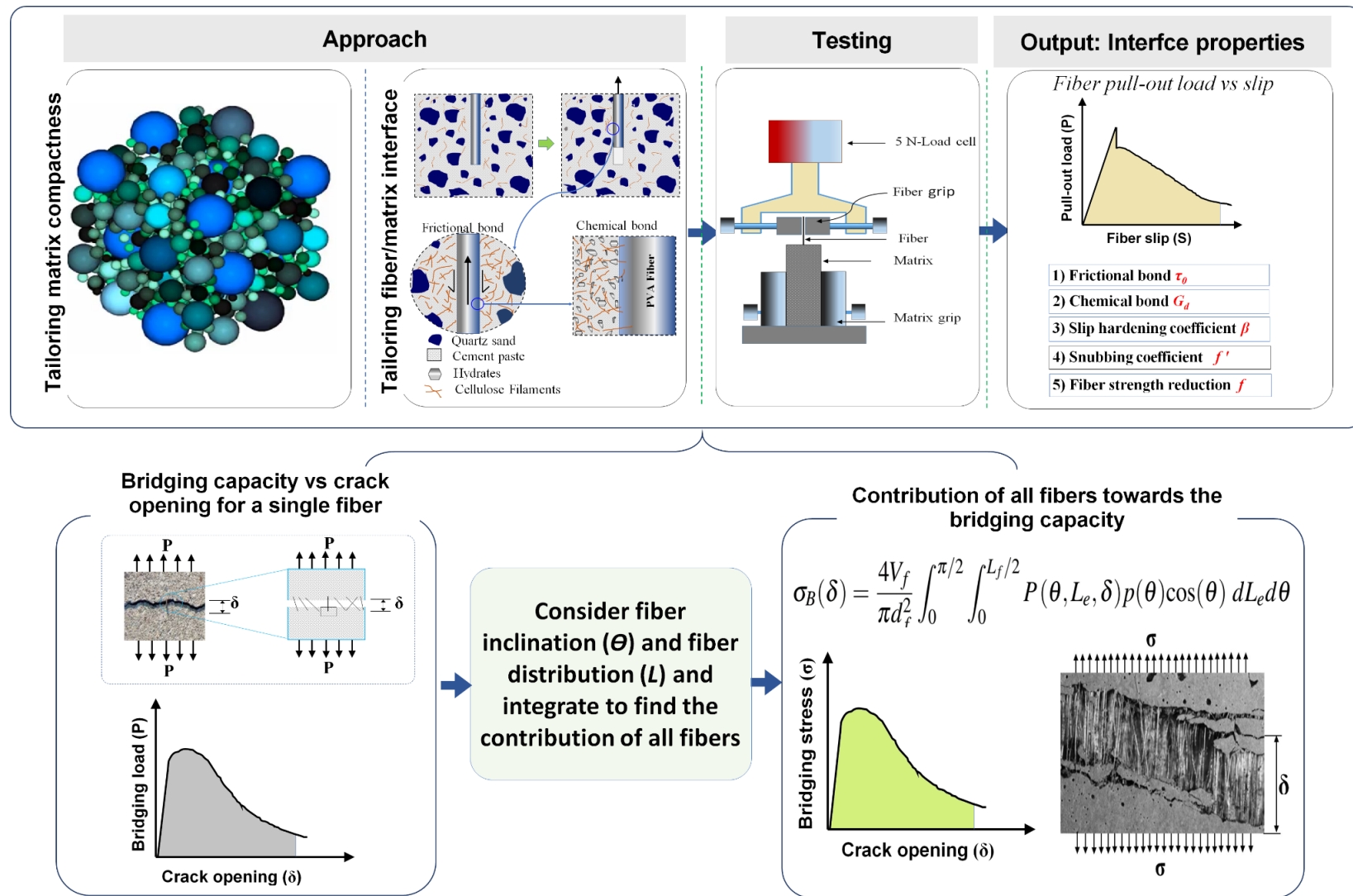


Fig. 1. Research framework for the characterization and nanomodification of interface properties of HVGP-SHCC

3 Experimental Program

3.1 Materials properties

3.1.1 Basic SHCC ingredients

SHCC ingredients include high-sulfate-resistance cement (type HS) with low C_3A and C_3S content (to enhance the rheology), type F- fly ash (FA), type GH glass powder (GP), and quartz sand (QS). The cement has a specific gravity (SG) of 3.18, Blaine fineness of 438 m^2/kg , and mean particle diameter (d_{50}) of 12 μm . The FA used in the study fulfills the requirements of CAN/CSA A3000 specifications and has an SG of 2.55, Blaine surface area of 363 m^2/kg , and d_{50} of 17. The GP used herein has an SG of 2.51 and d_{50} of 27 μm . The QS has an SG of 2.70, maximum particle size (d_{max}) of 600 μm , and mean particle size (d_{50}) of 250 μm . Table 1 presents the chemical composition and physical properties of all granular materials used in this study, Fig. 2 provides their particle-size distribution and Fig. 3 presents scanning electron microscope (SEM) images for FA [Fig. 3 (a)] and GP [Fig. 3 (b)] used in this study. Polyvinyl-alcohol (PVA) fibers [Fig. 4 (a)] were added at 2% per volume of suspended mortar. The fiber has 38 μm diameter, 8 mm length, 40 GPa elastic modulus, and 1400 MPa tensile strength.

3.1.2 Cellulose filaments

The cellulose filaments (CF) were provided by Kruger Biomaterials Inc. (Trois-Rivières, Québec, Canada). CF have 30–400 nm diameter and 100–2,000 μm length. This results in their significantly high aspect ratio of about 100–1,000 and high surface area (80–160 m^2/g). The filaments were received from the supplier in a dispersed form (colloidal suspension with a nominal solid content of 1.2%). Further information about CF characteristics and sustainability features can be found in our former works [22, 23]. Fig. 4 (b) depicts a scanning electron microscope (SEM) image of a CF diluted aqueous suspension at a concentration of 0.10%.

Table 1. Chemical compositions of powders and granular materials used in the study

Composition	Quartz Sand	Type HS Cement	Type F Fly Ash	Type GH Glass Powder
SiO ₂	99.8	22	53.7	73.00
Fe ₂ O ₃	0.04	4.3	5.6	0.40
Al ₂ O ₃	0.14	3.5	17.5	1.50
CaO	0.17	65.6	12.4	11.30
TiO ₂	0.02	0.2	—	0.04
SO ₃	—	2.3	—	—
MgO	0.008	1.9	2.1	1.20
Na ₂ O	—	0.07	1.6	13.00
K ₂ O	0.05	0.8	2.0	0.50
ZnO	—	0.09	—	—
LOI	0.2	1.0	1.8	0.60
C ₃ S	—	50	—	—
C ₂ S	—	25	—	—
C ₃ A	—	2.0	—	—
C ₄ AF	—	14	—	—
Blaine (m ² /kg)		438	363	308

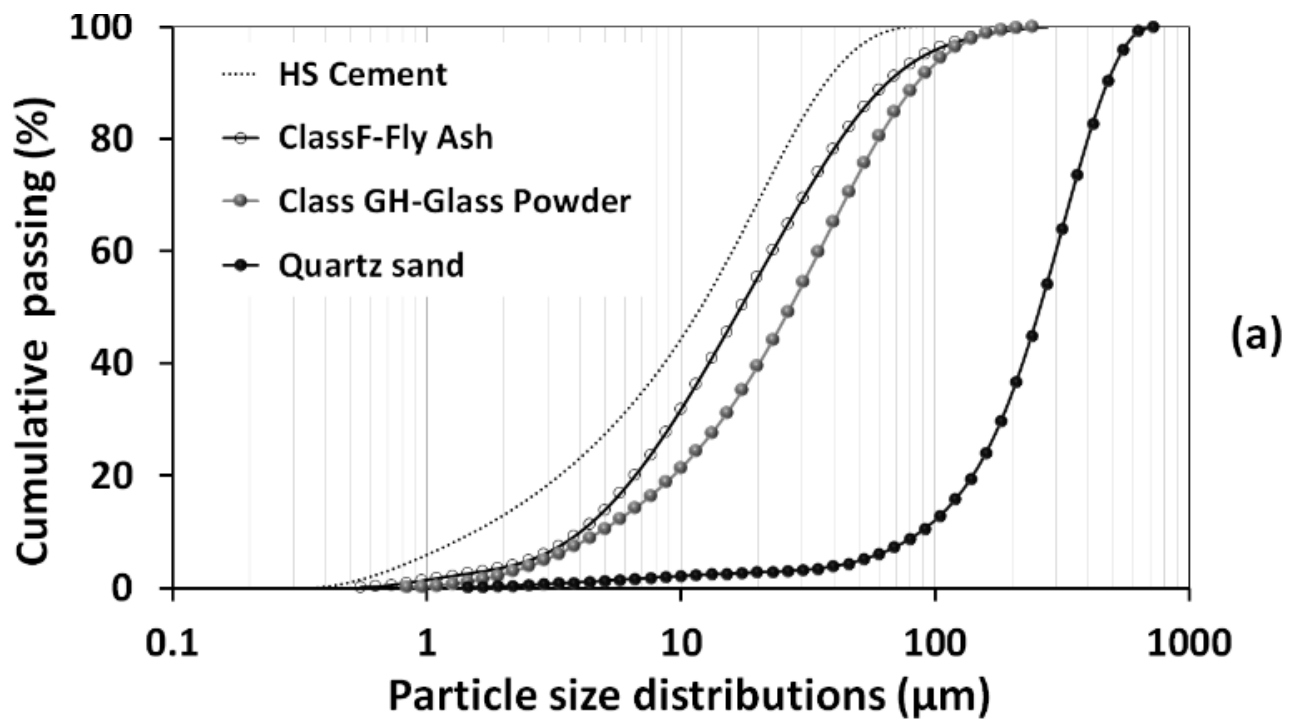


Fig. 2. Particle size distribution of SHCC ingredients

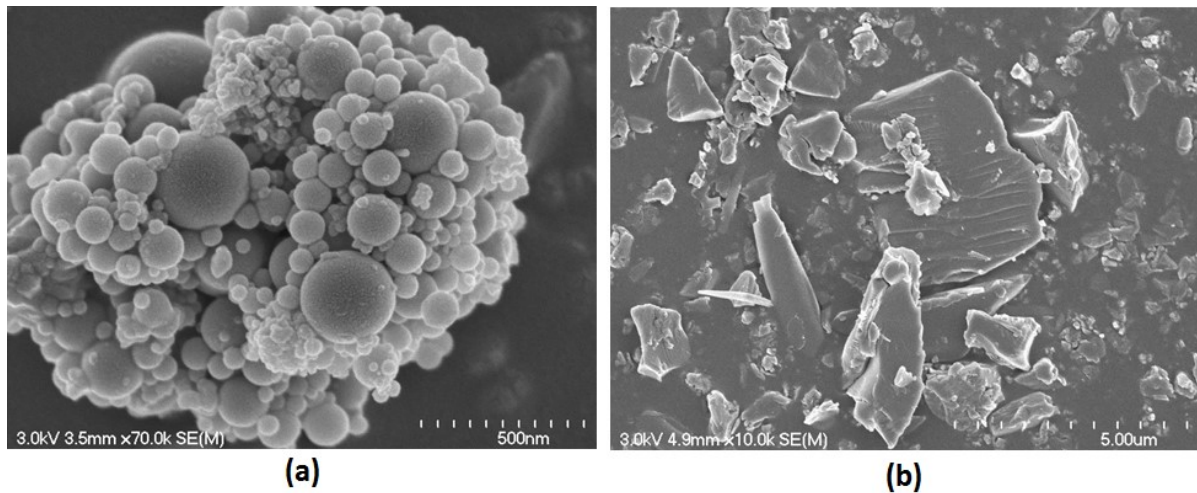


Fig. 3. SEM micrographs of SHCC ingredients: (a) HS Cement, (b) Class F Fly ash, and (c) Glass powder, (d) Quartz sand

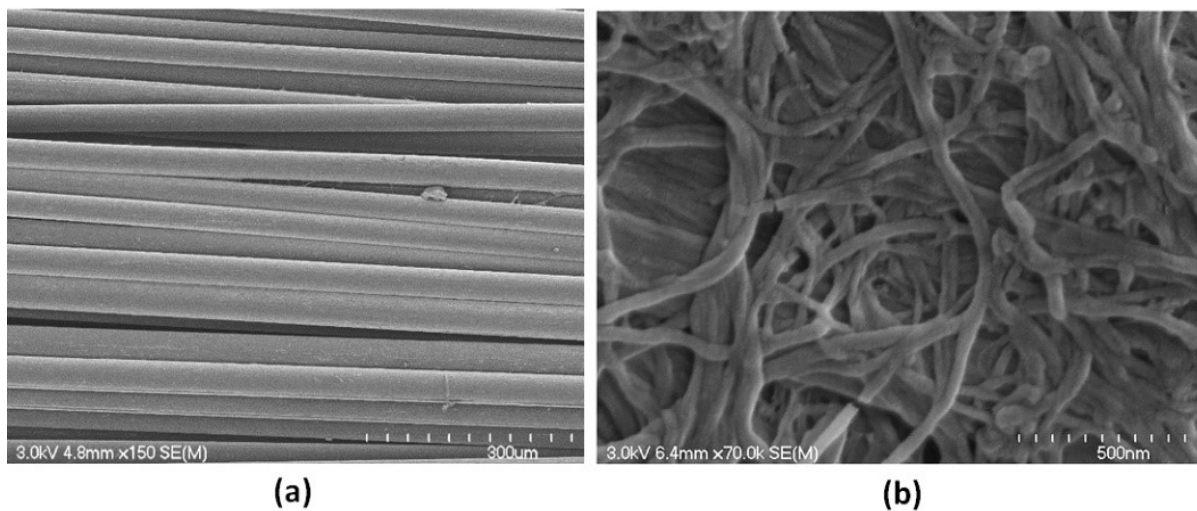


Fig. 4. SEM micrograph of hybrid reinforcement systems used in this study: (a) RECS15 polyvinyl alcohol (PVA) fibers, and (b) nanoscale cellulose filaments (CF)

3.2 Mixture proportions

A basic SHCC mixture with fly ash /cement (FA/c) ratio of 1.2, QS to binder ratio of 0.35 and a water-to-binder (w/b) ratio of 0.28 was considered. A total of fifteen SHCC mixtures (comprised in two mixture series) were developed. In series I, six different ternary mixtures (cement, FA, GP) with variable binary combinations of GP and FA (GP in replacement of FA at 0, 20, 40, 60, 80, and 100%) were developed (Table 2). The replacement of FA by GP was guided by the optimization of matrix packing density using the compressible packing model of De Larrad [24] as detailed elsewhere [17]. The combined particle-size distribution of each of series I-basic mixtures is shown in Fig. 5. In series II, a total of nine nanocellulose-

modified SHCC mixtures were developed. This involves incorporating CF at dosages of 0.03, 0.05, and 0.10% in each of the following series I-SHCC mixtures (0% GP, 40%GP, and 100% GP). The selection of these mixtures was guided by the optimization of particle packing attempted in series I. For all mixtures, a poly-carboxylate (PCE)-based high-range water reducing admixture (HRWRA) with an *SG* of 1.09 and solid content of 40%, fulfilling the requirements of ASTM C494 Type F admixtures [25] was used to secure the target mini-slump flow diameter of 300 ± 20 mm in the suspended mortar. Mixture nomenclature consists of three parts, the first designating the percentage of FA, the second designating the percentage of GP, and the third designating the percentage of CF per cement mass. For instance, the mixture 0FA-100GP-0.10CF refers to the mixture with complete replacement of FA by GP and the addition of CF at 0.10% per cement mass. In any mixture, the binary combination of FA and GP adds up to 100 and corresponds to $(FA+GP)/\text{cement}=1.2$.

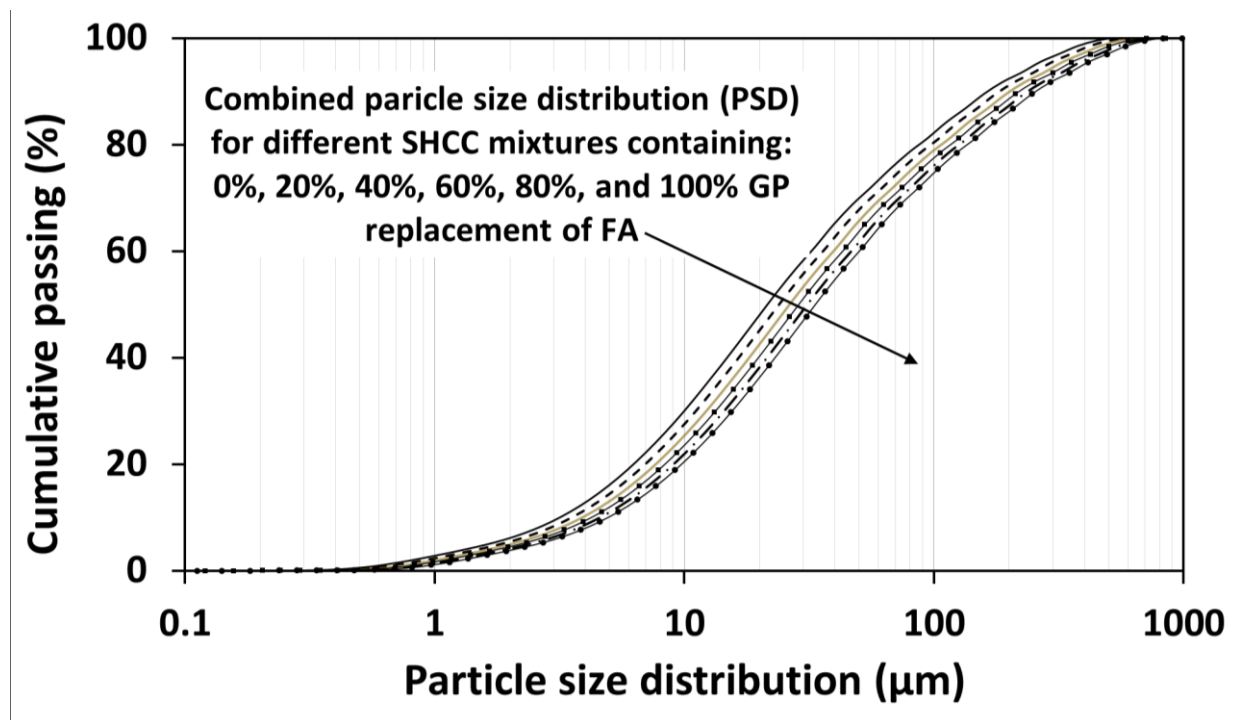


Fig. 5. Combined particle size distribution for the different SHCC formulations

Table 2. Mix design of HVGP-SHCC

Series	No.	Mixture name	Mixture Composition (kg/m ³)								
			Cement	Fly ash (FA)	Glass powder (GP)	Quartz sand (QS)	Water	Water/binder (W/B)	Packing density (PD)	HRWRA (solid extract)	CF (solid extract)
I	1	M100FA-0GP-0CF	597	717	—	460	366	0.28	0.64	3.251	—
	2	M80FA-20GP-0CF	597	576	143	459	365	0.28	0.66	3.609	—
	3	M60FA-40GP-0CF	596	429	286	459	364	0.28	0.70	4.433	—
	4	M40FA-60GP-0CF	595	286	429	458	364	0.28	0.71	4.802	—
	5	M20FA-80GP-0CF	595	143	576	458	363	0.28	0.73	6.172	—
	6	M0FA-100GP-0CF	593	—	717	458	360	0.28	0.74	9.136	—
II	7	M100FA-0GP-0.03CF	597	717	—	459	365	0.28	0.64	4.014	0.175
	8	M100FA-0GP-0.05CF	597	717	—	459	365	0.28	0.64	4.125	0.292
	9	M100FA-0GP-0.10CF	597	717	—	459	365	0.28	0.64	4.589	0.584
	10	M60FA-40GP-0.03CF	596	429	286	459	364	0.28	0.70	5.534	0.175
	11	M60FA-40GP-0.05CF	596	429	286	459	364	0.28	0.70	5.913	0.292
	12	M60FA-40GP-0.10CF	596	429	286	459	364	0.28	0.70	6.084	0.584
	13	M0FA-100GP-0.03CF	593	—	717	457	360	0.28	0.74	9.136	0.175
	14	M0FA-100GP-0.05CF	593	—	717	457	360	0.28	0.74	9.286	0.292
	15	M0FA-100GP-0.10CF	593	—	717	457	360	0.28	0.74	9.479	0.584

3.3 Mixing procedures

In conjunction with other tests conducted on suspended mortar reported elsewhere [17, 26], batching of different SHCC mixtures was carried out using a pan mixer of type Mortartman 360 (Imer, CA, USA). In an attempt to deflocculate powder agglomerates and enhance mixture homogeneity, all powders and granular materials were dry mixed for 7 min prior to adding water and HRWRA. In the second step, 95% of the mixing water (homogenised with 90% of HRWRA) was added to the mixer slowly during ≈ 0.5 min then mixing continued for 2.5 min. For mixtures incorporating CF, a CF-water suspension was first prepared from a readily dispersed CF (colloidal suspensions with 1.2% CF solid content). Thereafter, 90% of the HRWRA was diluted into 95% of CF-water suspension so that the HRWRA further enhances CF dispersion. More details about CF dispersion protocol can be found elsewhere [22]. The remaining 10% of HRWRA is left for final adjustment of mixture flowability. In the third step, the mixer was stopped for ≈ 0.5 min to scrape its blades and edges then mixing continued for another 1 min. The consistency of the suspended mortar was then checked such that when a mini-slump flow diameter of ≈ 300 mm was obtained [27], only the remaining water is added (after adjustment of the amount of water contained in the unused 10% of HRWRA). Otherwise, a gradual amount of HRWRA is added (along with an adjusted amount of the remaining 5% of water) until the desired ≈ 300 mm mini-slump flow diameter is achieved. The resulting mixtures were cast into the required test specimens. A summary of fresh properties for the different mixtures is presented in Table 3, while further details about the fresh state behavior have been reported elsewhere [17, 26].

Table 3. Fresh properties of SHCC plain formulations

Series	No.	Mixture name	Fresh properties			
			Slump-flow diameter (mm)	Air content (%)	Unit weight (kg/m ³)	Temperature (°C)
I: Basic SHHC	1	M100FA-0GP-0CF	315	4.25	2034	21
	2	M80FA-20GP-0CF	310	4.13	2037	20
	3	M60FA-40GP-0CF	310	3.90	2039	22
	5	M40FA-60GP-0CF	305	3.91	2040	21
	5	M20FA-80GP-0CF	305	4.36	2039	21
	6	M0FA-100GP-0CF	300	4.41	2035	23
II: Nanomodified SHCC	7	M100FA-0GP-0.03CF	305	4.22	2021	23
	8	M100FA-0GP-0.05CF	305	4.98	2018	24
	9	M100FA-0GP-0.10CF	300	5.21	2015	25
	10	M60FA-40GP-0.03CF	300	4.18	2032	23
	11	M60FA-40GP-0.05CF	300	4.31	2030	23
	12	M60FA-40GP-0.10CF	295	4.43	2027	23
	13	M0FA-100GP-0.03CF	305	4.24	2025	22
	14	M0FA-100GP-0.05CF	305	5.10	2023	23
	15	M0FA-100GP-0.10CF	295	5.46	2015	22

3.4 Preparation of test samples

Test samples for single-fiber pull-out (SFP) test were cast on tensile coupon molds (Fig. 6). While rectangular molds can be obviously utilized for the same purpose, the authors used dog-bone molds already constructed to perform the direct tensile tests. Existing research on SFP test for SHCC use long continuous fibers such that the fibers are embedded in the molds with the ends stretched to ensure fiber straightness. When the matrix hardens, the PVA fiber is cut at the desired embedment length, typically 1 mm [15, 16, 18]. The issue with this technique is that when the matrix is cut at the desired embedded length (1 mm), there will be usually not enough matrix extension left for efficient (yet safe) gripping during the SFP test. Alternatively, the sample can be glued on an extension plate that will be gripped during testing. To overcome this, a new technique for installing PVA fibers for SFP test was

developed herein (Fig. 6). Small rubber blocks (22×7×6 mm) were prepared and installed in tensile coupon mold such that the 22 × 6 mm cross section aligns with the cross-section of the coupon mold. The 7 mm width hosts the free end of the PVA fiber [Fig. 6 (c) and (d)]. Two notches were made on each rubber block. The notches were placed at the middle third of the rubber piece. They extend in depth to mid-height of the rubber block (3 mm). For each block (except for the ones on the middle of the mold), two PVA fibers were placed such that 7 mm of fiber length stays embedded in the rubber while the remaining 1 mm of fiber length remains hanging [Fig. 6 (d)]. SHCC suspended mortars were cast in two equal layers. The first layer is cast from the mold side opposite to the fiber such that the fresh material flows underneath the hanging fiber-end to support it and minimize fiber bending. The second layer is poured (starting from the fiber side) slowly to avoid causing fiber bending. For mixtures cast at the grip sides of the molds, each mixture contained two fibers while mixtures cast in the middle of the molds had one fiber. This process allowed casting 10 SFP test samples per mixture for the first case and 5 samples for the second case and yield a total of 125 SFP test samples. Upon casting, specimens were sealed and kept in a controlled environment at 50% relative humidity (RH) and 23 °C, then demolded 24±1 h later. Specimens were then sealed inside plastic bags and transferred for storage in a fog room at 100% RH and 22 °C temperature until the age of testing.

A point worth elucidating regarding the current method for preparing test samples for SFP is the straightness of the embedded length L_e inside the fresh mortar. In this regard, while the fiber embedded length L_e of 1 mm is too small to cause significant fiber bending inside the fresh mortar, this feature was verified to ensure that bending of fiber embedded-end caused by fresh mixture weight above L_e remains negligible. For this, L_e has been modeled as a prismatic solid circular beam. Neglecting the effect of surface tension induced by the liquid phase of the mixture, for simplicity, the fiber is principally subjected to the weight of the mortar layer above it. While the mortar layer underneath the fiber provides support hindering fiber bending, this effect has been disregarded to examine the worst case. The fiber end embedded inside the rubber block being far higher than L_e , the latter is considered as a cantilever beam whereby the fiber length embedded in the rubber (7 mm) provides enough rigid support for L_e . Each fiber carries a mortar weight over a tributary length of 7.33 (mold width/3) and a depth of 3 mm (thickness of top mortar layer). The fresh unit weight of each mixture can be used to determine the load per unit length (w) supported by L_e . Using the elastic modulus (E) for the fiber and its moment of inertia [$I_x = \left(\frac{\pi}{4}\right) r^4$, considering circular

cross section], then the maximum deflection at fiber tip can be calculated using the formula:

$$\delta_{max} = \frac{wL_e^4}{EI}$$

Detailed results of fiber deformation at the free end during the fresh state are provided in [Appendix I](#) which proves that the deformation was quite negligible (< 0.1% in all cases). This suggests that the technique used herein for placing the PVA fibers can ensure fiber straightness necessary for SFP test. It can be viewed as an alternative to the current techniques requiring continuous fibers which are not always readily available in the market.

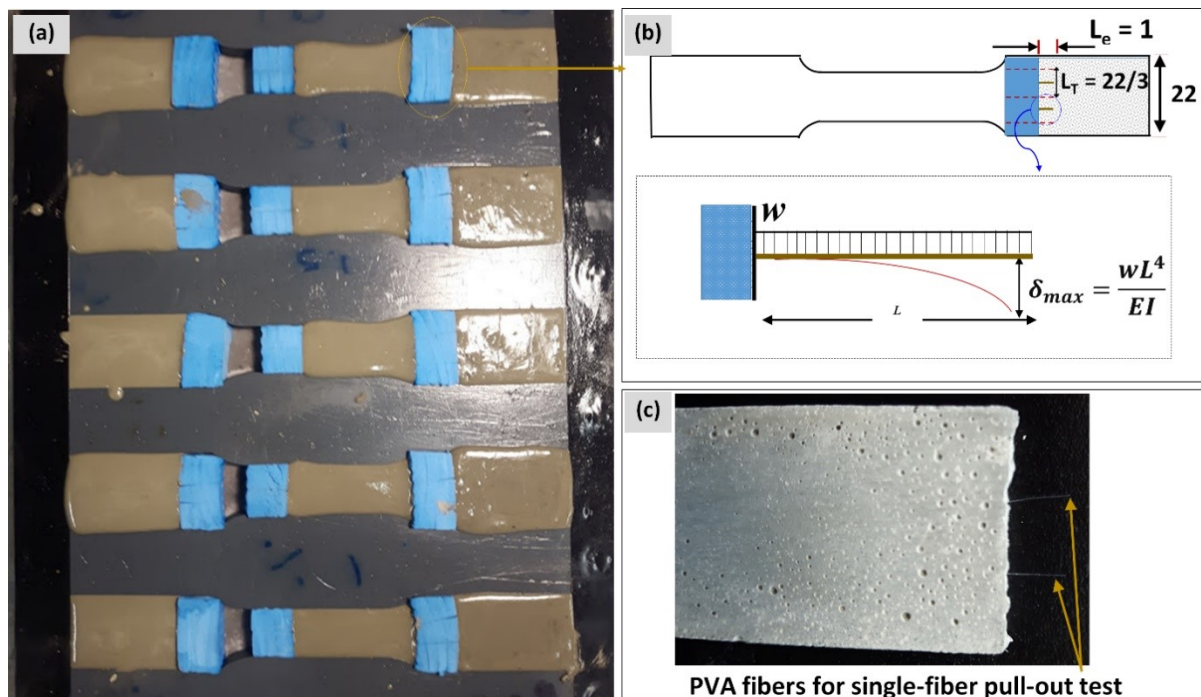


Fig. 6. Preparation of test samples for single-fiber pull-out (SFP) test: (a) fresh samples, (b) verification of fiber embedded-end deformation, (c) SFP test sample at the hardened state (dimensions in millimetres).

3.5 Test set-up and procedure

3.5.1 Single fiber pull-out (SFP) test

The test set-up for the SFP test is shown in [Fig. 7](#). Owing to the high precision requirements in the SFP test, a miniature load cell of 5-N capacity of Zwick type was used for this purpose. The test was conducted under a displacement-controlled mode at a rate of 0.2 mm/s for consistency with the loading rate adopted for the direct tension tests conducted in the assessment of actual SHCC. In an attempt to minimize the elastic stretching, the fiber is gripped at less than 1 mm from the matrix top surface. [Fig. 7 \(a\)](#) shows a schematic of the

test set-up, while Fig. 7 (b) illustrates the actual test configuration where two PVA fibers are visible, one of which being tested. Fig. 7 (b) (at extreme right) also shows a post-test pulled-out PVA fiber with L_e appearing in bright white. Following the above procedures, fiber pull-out load versus fiber slip response was recorded for all mixtures. For each mixture, 5-10 SFP tests were conducted to ensure repeatability. In outcome, 4-7 successful SFP tests were obtained for each mixture.

3.5.2 Uniaxial tensile test

Uniaxial tensile tests were conducted on dog-bone SHCC samples with the dimensions shown in Fig. 8. Tested samples comprise three GP contents (0, 40, and 60%) as optimized elsewhere [17]. For each GP content, SHCC mixtures formulated with the incorporation of CF at the dosage of 0, 0.03, 0.05, and 0.10% of cement mass were also tested. The test was conducted under a displacement-controlled mode at a rate of 0.2 mm/min. The test set-up is equipped with a wire extensometer attached at the middle of the sample. This is supplemented by a laser-type extensometer such that all elastic and plastic deformations are well captured (Fig. 8)

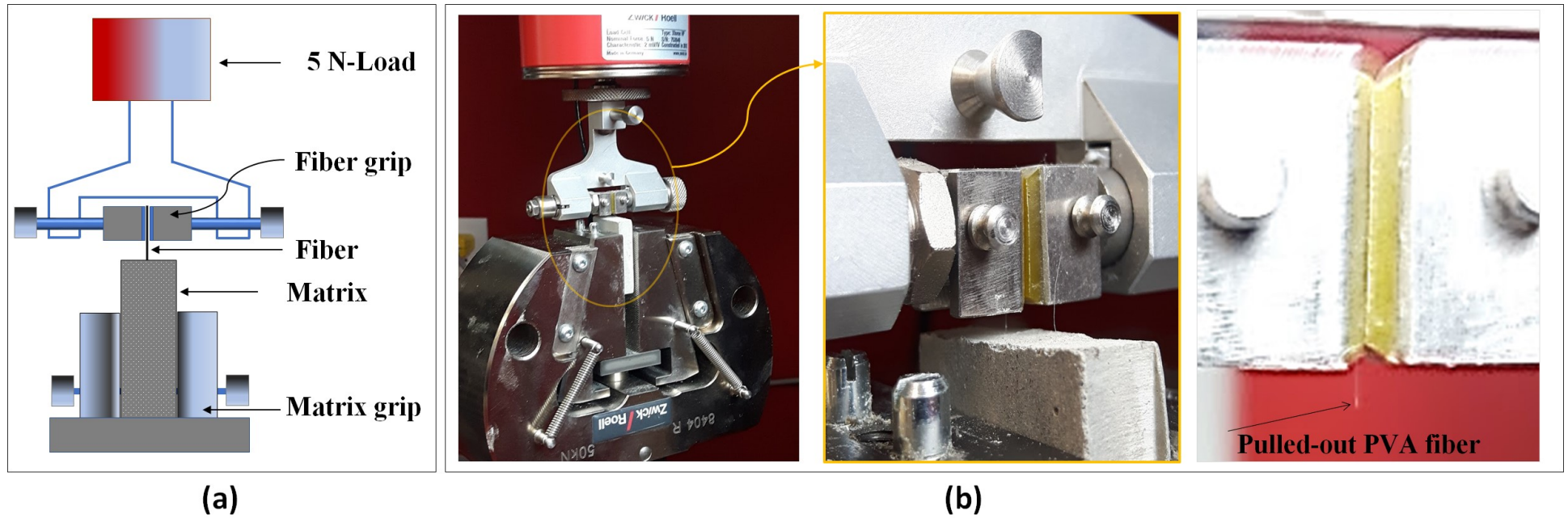


Fig. 7. Single-fiber pull-out (SFP) test: (a) schematic of test set-up; and (b) actual test set-up (left), close view at test sample (middle), and a pulled-out fiber whereby the embedded end appears in bright white (left).

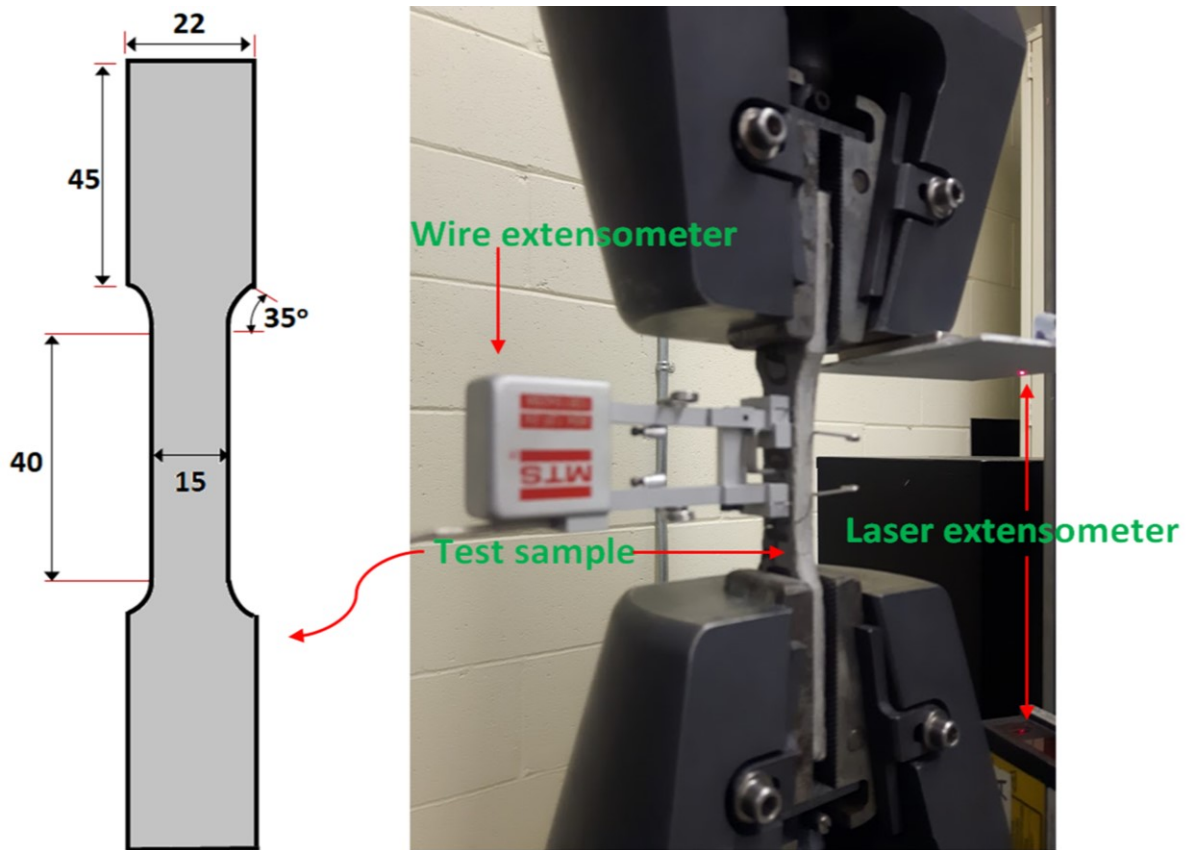


Fig. 8. Test set-up for uniaxial tensile test (all dimensions are in millimeters).

3.6 Data processing

3.6.1 Pull-out slip behavior

The general profile of single fiber pull-out versus slip for PVA fibers (Fig. 9) proposed by Redon et al. [15] has been used to disclose the effect of glass powder (GP) and that of nanomodification by cellulose filaments (CF) on interface properties. Overall, all tests fall within the generic behavior illustrated in Fig. 9 where three distinct phases characterize the fiber pull-out versus slip behavior: (i) full-bond, (ii) fiber-matrix debonding, and (iii) fiber frictional sliding.

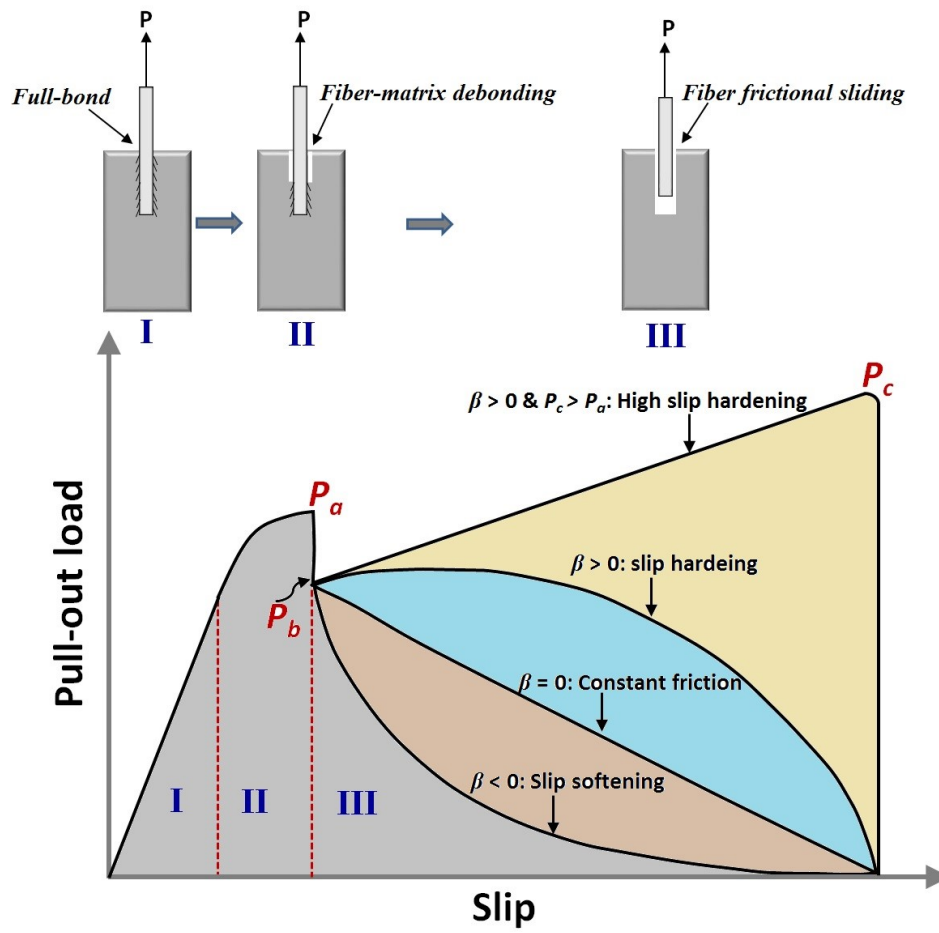


Fig. 9. General pull-out versus slip response obtained with PVA fibers in HVGP-SHCC.

Phase I-Full bond-The linear segment of the pull-out load versus slip response: During this phase, increasing the packing density (by incorporating GP) intensifies the contact points between the fiber and the matrix and roughens the interface [17] as illustrated in Fig. 10. This increases the frictional bond τ_0 and leads to higher pull-out resistance. On the other hand, with the incorporation of CF, the high surface area of these polymers creates a new interface between the PVA fibers and the matrix (Fig. 11). This fosters a polymer-polymer friction (PVA-CF) over a polymer-matrix (PVA-matrix) friction; thereby altering interface properties.

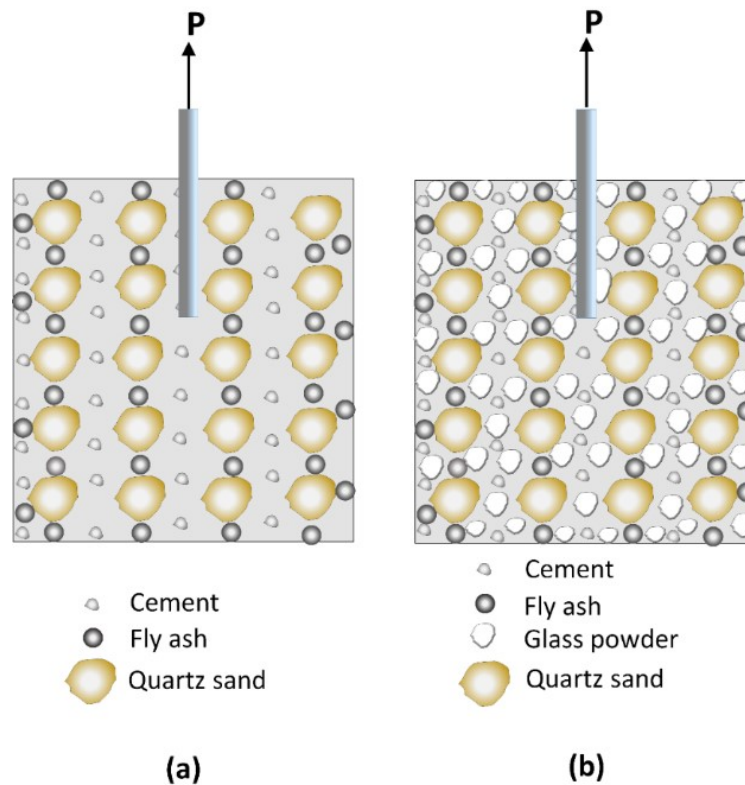


Fig. 10. Illustration of the effect of packing density by GP on interface properties.

Phase II-Fiber-matrix debonding-The concaved-down segment following the linear portion in the pull-out load versus slip response: In this phase, as the pull-out load is resisted by a synergy between chemical adhesion in the undebonded fiber segment and frictional bond in the debonded fiber segment, higher packing density (by incorporating GP) would increase the frictional resistance due to a denser matrix surrounding the PVA fiber (Fig. 10). This can increase the pull-out resistance, but can also lead to fiber rupture, undesirable for strain-hardening [15, 17]. The incorporation of CF, on the other hand, can play a balancing role where the interference of the nanoscale CF polymers would attenuate friction during this phase (Fig. 11).

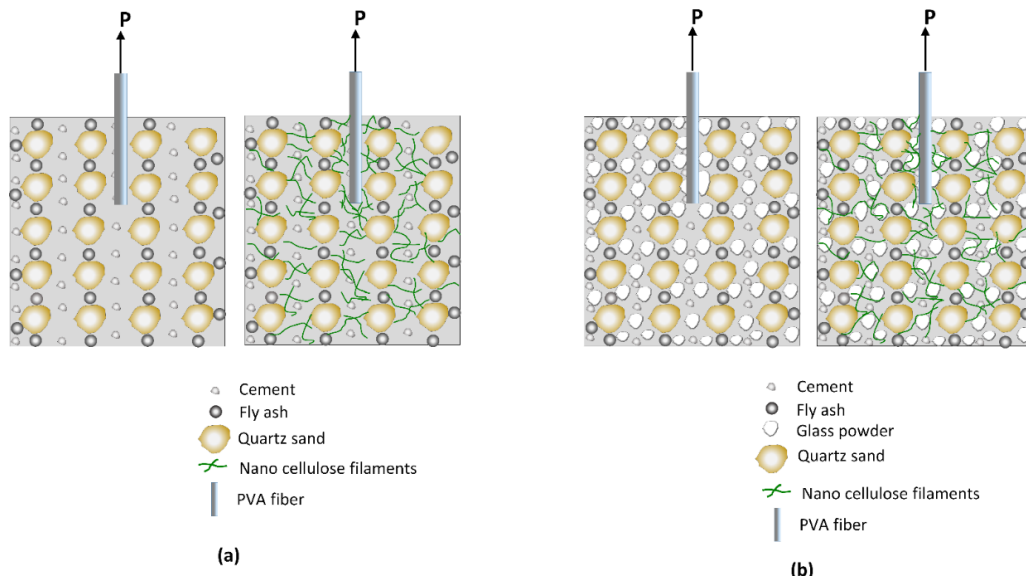


Fig.11. Illustration of the effect of nanoscale CF on interface properties in HVFA-SHCC (a), and in HVGP-SHCC (b). The presence of CF creates a new interface between PVA fibers and the matrix.

Phase III- Fiber frictional sliding-The extended portion of the pull-out load versus slip response beyond point P_b : Fiber sliding during this phase is characterized by three behaviors (slip hardening, constant friction or slip-softening effect) depending on the slip hardening coefficient β which is, respectively, positive, zero or negative [8, 15] as illustrated in Fig. 9. In this regard, the effect of increasing matrix compacity can be viewed from two perspectives: (i) higher packing density increases the friction between the fiber and the matrix and thus leads to higher pull-out resistance, however, (ii) too high packing density can generate frictional stresses exceeding fiber apparent tensile strength. This can cause premature fiber breakage rather than fiber pull-out preferable for strain-hardening [15, 17]. As for CF, the omnipresence of the flexible polymeric fibrils on PVA fiber/matrix interface zone can be perceived to attenuate the friction as the PVA fiber slides-out of the matrix. Moreover, during the fiber-sliding phase, CF can contribute to creating a sort of jamming effect, thereby delaying fiber pull-out. The slip-hardening can be viewed as an advantageous feature as it allows fibers during the sliding phase to continue withstanding load levels (P_c) beyond the debonding load (P_a).

3.6.2 Determination of fiber matrix interface parameters

Following the procedure described in section 3.5.1, the basic data for SFP test were collected. This consists of fiber pull-out load (P) versus fiber slip response (S). To ensure that actual fiber slip (S) is obtained, the as-recorded slip (\dot{S}) was corrected by subtracting the elastic deformation (\ddot{S}) of the fiber caused by fiber stretching using the relationship: $S = \dot{S} - \ddot{S}$,

where the elastic deformation $\delta = PL_e/A_f E_f$, A_f = fiber cross-sectional area, L_e = fiber embedded length, and E_f = fiber elastic modulus. The resulting pull-out versus slip response was plotted and the interface parameters of interest for SHCC micromechanical tailoring were determined. This includes the chemical bond G_d , the frictional bond τ_0 , and the slip hardening coefficient β .

The chemical bond G_d was determined using the relationship:

$$G_d = \frac{2(P_a - P_b)^2}{\pi^2 E_f d_f^3} \quad \text{in J/m}^2 \quad (1)$$

where E_f = fiber axial Young's modulus of elasticity; and d_f = fiber diameter.

The frictional bond τ_0 at the onset of fiber sliding was determined using the following relationship:

$$\tau_0 = \frac{P_b}{\pi d_f L_e} \quad \text{in MPa} \quad (2)$$

where L_e is the embedded fiber length.

The slip hardening coefficient β is a parameter that depends on the slope of the pull-out versus slip curve during the frictional sliding stage (phase III). It was determined from the initial slope of phase III in the pull-out versus slip curve using the formula:

$$\beta = \left(\frac{d_f}{L_f} \right) \left[\left(\frac{1}{\tau_0 \pi d_f} \right) \left(\frac{\Delta P}{\Delta \delta} \right)_{\delta \rightarrow 0} + 1 \right] \quad (3)$$

The term $\left(\frac{\Delta P}{\Delta \delta} \right)_{\delta \rightarrow 0}$ designates the first derivative of the pull-out versus slip response at the onset of fiber sliding.

3.6.3 Linking interface properties to composite behavior

The extrapolation from single fiber response in pull-out to the composite behavior under uniaxial tension goes through linking the above-determined interface parameters to the composite behavior. This necessitates taking into account several factors such as fiber status (bonded, unbonded, frictional sliding phase, or ruptured), fiber orientation, and a set of fiber parameters (i.e., snubbing coefficient, strength reduction factor, and spalling effect).

In this regard, the relationship between the pull-out load (P) of a single fiber and its corresponding fiber debonding length (δ) can be computed from the Lin et al's [8] theoretical model (shown in Eq. (4)) derived on the basis of stress analysis and energy balance principle:

$$P(\delta) = \sqrt{\frac{\pi^2 E_f d_f^3 \tau_0 (1+\eta)}{2} \delta + \frac{\pi^2 E_f d_f^3 G_d (1+\eta)}{2}} \quad (4)$$

where E_f is the elastic modulus of the fibers, d_f is the diameter of the fiber, τ_0 is the frictional bond

strength, G_d is the chemical bond, and $\eta = (V_f E_f)/(V_m E_m)$ where V_f is the volume fraction of fiber, V_m is the volume of the matrix, and E_m is the elastic modulus of the matrix.

Eq. (1) can model the relationship between the load and the debonding length during the fully bonded phase (I) (Fig. 9) combining chemical and frictional bonding. When the fiber is fully debonded and is left sliding over frictional bonding only, the relationship between P and δ is governed by Eq. (5)

$$P(\delta) = \pi d_f \tau_0 \left[1 + \frac{\delta - \delta_0}{d_f} \beta \right] [l_e - (\delta - \delta_0)] \quad (5)$$

where δ_0 is the pull-out length corresponding to full debonding and is defined as in Eq. (6)

$$\delta_0 = \frac{4\tau_0 L_e^2 (1+\eta)}{E_f d_f} + 4 \sqrt{\frac{2G_d L_e^2 (1+\eta)}{E_f d_f}} \quad (6)$$

To include the effect of fiber orientation (being random in the composite) and its consequent implication on frictional forces, Morton and Groves [28] and subsequently Li [29] introduced the snubbing effect $f (> 0)$ as proposed in the following empirical equation [Eq. (7)] to account for the increase in the bridging load P at an inclination angle θ by analogy to a friction pulley at the exit point.

$$P(\theta) = P(0)e^{f\theta} \quad (7)$$

On the other hand, to account for the vulnerability of some fibers to bending and lateral stresses when loaded at an inclined angle, a strength reduction factor f' has been introduced for PVA fibers by Redon et al. [15] as shown in Eq. (8).

$$\sigma_{fu}(\theta) = \sigma_{fu}(0)e^{-f'\theta} \quad (8)$$

A spalling effect (k) has also been introduced by Yang et. [30] as in Eq. (9) to account for some additional forces and stress concentrations exerted by an inclined fiber on the matrix. It is the reaction of the matrix to the pressure created by the inclined fiber such that when the stresses created by the fiber are higher than the strength of the matrix, the latter will experience a spalling of size S .

$$S = \frac{P \sin\left(\frac{\theta}{2}\right)}{k d_f \sigma_{mu} \cos^2\left(\frac{\theta}{2}\right)} \quad (9)$$

where P is the external force acting on the fiber, θ is the orientation of the fiber, σ_{mu} is the matrix tensile strength, and k is the spalling coefficient, a constant which depends on fiber geometry and matrix stiffness.

Finally, to extrapolate from the effect of single fiber orientation to that of multiple fiber orientation in the composite, Kanda and Li [31] proposed the following equation [Eq. (10)] which accounts for this issue in the form of a probability density function for fiber orientation and single fiber pullout load $P(\theta, L_e, \delta)$.

$$\sigma_B(\delta) = \frac{4V_f}{\pi d_f^2} \int_0^{\frac{\pi}{2}} \int_0^{\frac{L_f}{2}} P(\theta, L_e, \delta) p(\theta) \cos(\theta) dL_e d\theta \quad (10)$$

where $p(\theta)$ is the probability density function for fiber orientation.

Thus, starting from interface parameters, Eq. (10) enables to determine the bridging capacity at the composite level for a fixed volume fraction of fibers (V_f). In the current study, basic interface properties (G_d , τ_0 , and β) were collected from SFP test as in section 3.6.2, V_f was fixed at 2%, the snubbing coefficient f for PVA fibers was assumed to be 0.30 [32], fiber strength reduction factor f' was also taken as 0.30 [31], the spalling coefficient was taken as 500 [30]. The parameters f , f' , and k were assumed herein to be insensitive of matrix composition (GP or CF content) for simplicity. This assumption remains conservative for the following reasons: (i) with increased compacity by GP, f is expected to increase while f' is expected to decrease, thereby leading to higher bridging capacity. Similarly, (ii) the nano-bridging effect of CF fostering a stiffer matrix is expected to limit matrix spalling (at exit point of inclined fibers) thereby leading to higher bridging capacity.

By implementing the above equations and following the numerical procedures for the determination of fiber bridging capacity proposed in [30], fiber bridging-stress versus crack opening response for the different formulation was constructed and presented in section 4.3.

4 Results analysis and discussions

4.1 Effect of glass powder on interface properties

Fig. 12 presents the pull-out versus slip response for the different mixtures with varying GP content in replacement of FA. The influence of GP on interface properties can be explained based on the generalized pull-out response depicted earlier in Fig. 9 as well as in light of the

effect of CF on the packing density of the matrix as presented in Table 2. Table 2 indicates that GP increased the packing density from 64% in the reference mixture (with 0 GP) to 66, 70, 72, 73, and 74%, respectively, in the SHCC with 20, 40, 60, 80, and 100% replacement of FA with GP. As such, GP plays a filler effect that can be correlated to the gradation of different granular materials shown earlier in Fig. 2. The latter indicates that GP [with a mean particle size (d_{50}) of 27 μm] as compared to that of cement ($d_{50} = 12 \mu\text{m}$) and that of FA ($d_{50} = 17 \mu\text{m}$), can permit filling the particle gap between the binders (cement and FA) from one side and the QS ($d_{50} = 250 \mu\text{m}$) from another side. This is more evident from the PSD for GP falling between that of binders (cement and FA) from one side and that of QS from another side. In consequence of this observed effect of GP on matrix compactness, Fig. 12 indicates that replacing FA by GP influences the pull-out versus slip response. The most remarkable effect appears on the maximum pull-out load as well as on the frictional sliding phase of the pull-out behavior. The maximum pull-out load [during the fully bonded phase (I)] appears to increase with increasing GP content. It increased from an average of 0.53 N in the reference mixture to an average of 0.86 N in the mixture with 100% GP. This can be perceived to increase the overall fiber bridging capacity (σ_0) to be discussed later in section 4.3. However, the increase in the pull-out load is also accompanied with a relative drop in the slip distance from ~ 0.80 mm in the reference mixture to ~ 0.50 mm in the mixture with 100% GP as can be inferred from the trend of the pull-out versus slip response depicted in Fig. 12. Furthermore, the frictional sliding phase (III) was characterized by constant friction in all tests in the reference mixture. At increasing GP, with higher pull-out load resistance, more tests reveal a sudden sharp drop in the pull-out response.

The above results of pull-out versus slip response were further used to determine the interface properties presented in Fig. 13 [source data provided in Appendix 2]. With increasing GP content, a continuous increase in τ_0 was recorded (from 2.95 MPa in the reference mixture to 3.10, 4.30, 4.62, 5.57, and 6.84 MPa, respectively, in the mixtures with 0, 20, 40, 60, 80, and 100% GP). On the other hand, the chemical bond G_d remained quite comparable (considering the variability of results) but showed an overall decreasing trend with higher GP content (from 2.65 J/m^2 in the reference SHCC to 2.45 J/m^2 in the SHCC with 100% GP). The slip-hardening effect β , on the other hand, remained comparable [≈ 0.005 which corresponds to constant frictional sliding ($\beta=0$)] up to 40%GP, then dropped at increasing GP as more tests revealed sudden drop in the pull-out resistance at higher τ_0 . The significant increase in τ_0 observed with increasing GP is attributed to the increased matrix compacity whereby the fiber/matrix interface becomes denser and rougher. The slight

drop in G_d may be attributed to a dilution effect of GP hindering chemical adhesion between the PVA fiber and the cement. The reduced β at higher GP can be a consequence of the increased τ_0 which rather promotes fiber premature rupture over the frictional sliding mode. Thus, the most significant effect of GP shows on increasing τ_0 . While this has increased the maximum pull-out load observed in systems with high GP content, excessive τ_0 can cause fiber rupture. As a result, a measure for attenuating the interface friction—such that the increase in pull-out load is optimized towards enhanced composite strength and ductility—may be useful. This has been attempted by the incorporation of the nanoscale CF as addressed in the section [4.2](#).

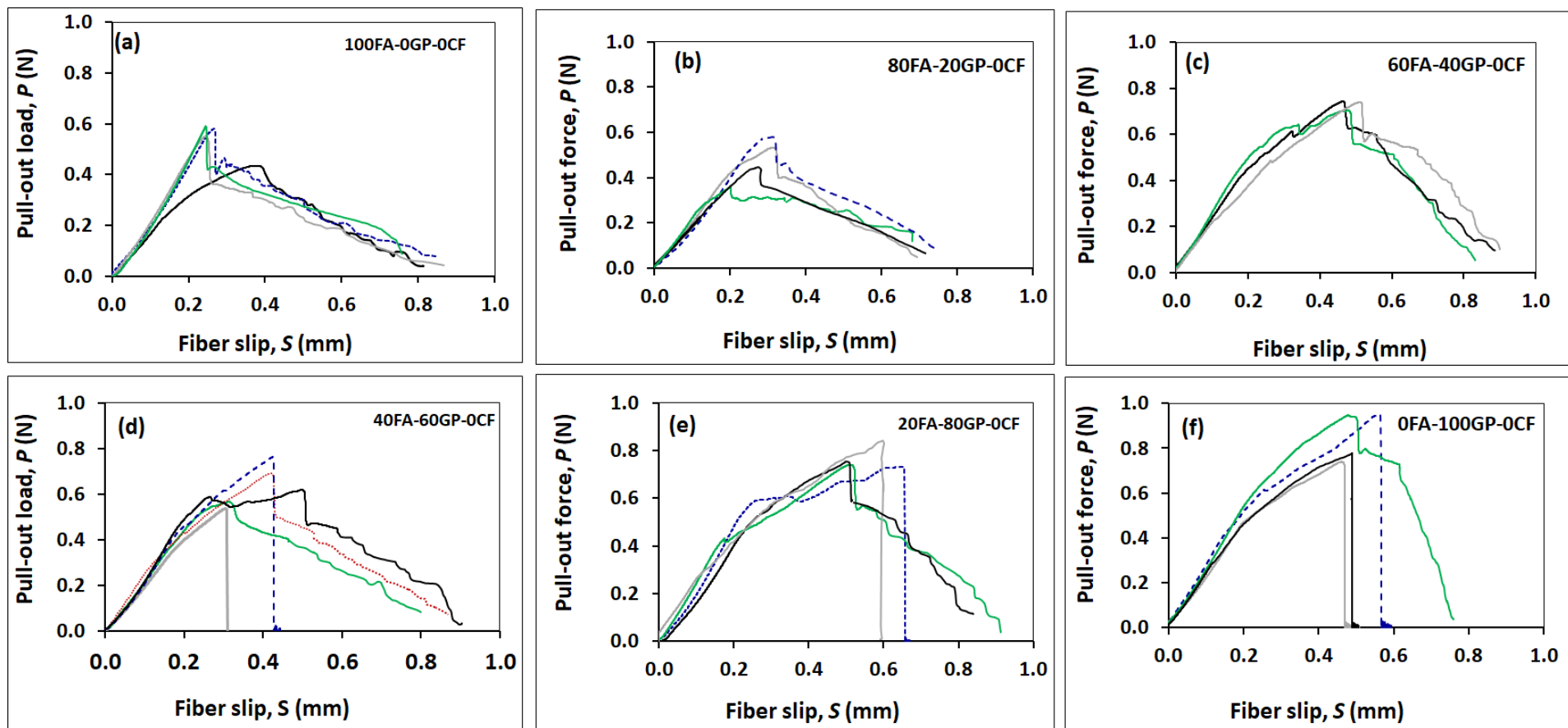


Fig. 12. Pull-out load versus slip response for different GP content in replacement of FA.

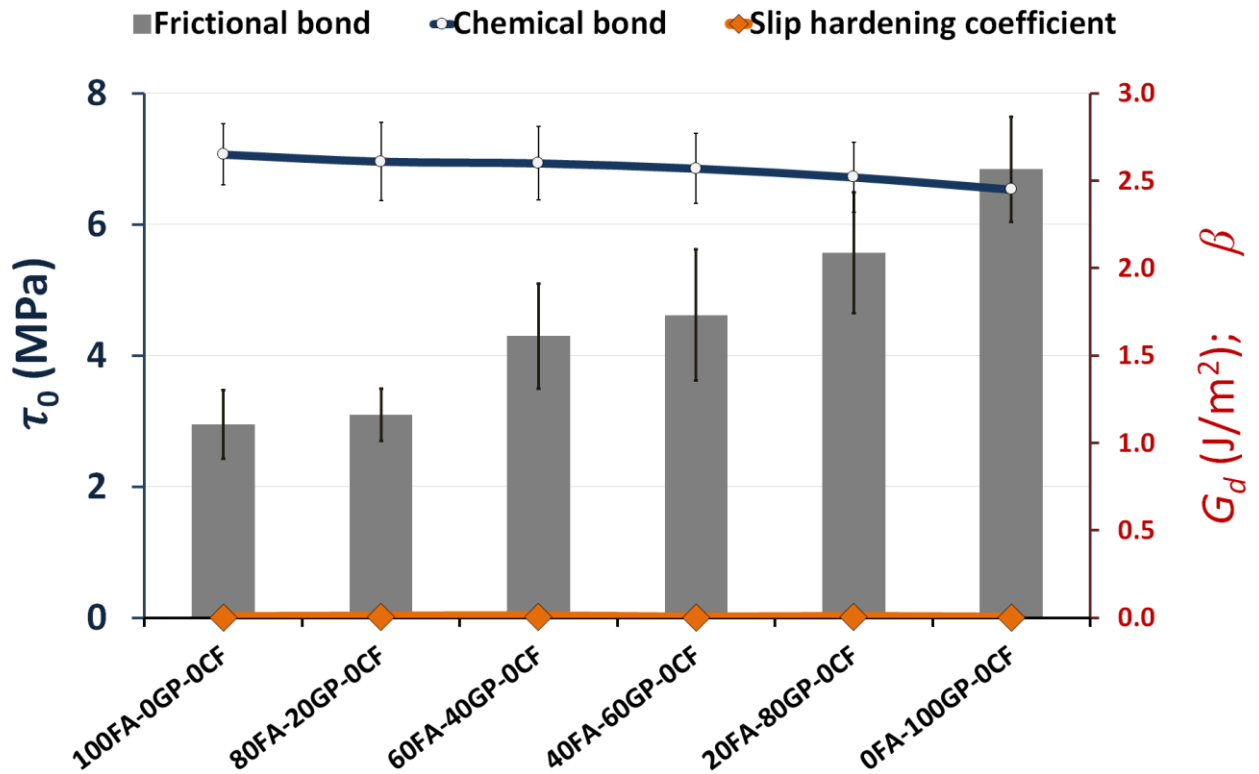


Fig. 13. Effect of GP on interface properties.

4.2 Nano-modifying the interface properties using cellulose filaments

The effect of nanomodification with cellulose filaments (CF) on the pull-out response was assessed on three categories of SHCC, namely the SHCC mixtures with 0, 40, and 100% GP. These mixtures were chosen based on the assessment of packing density [17] such that the effect of CF on interface properties at a scattered range of GP content may be disclosed. Fig. 14 presents the results of SFP tests for the above three systems (0, 40, and 100% GP) along with the corresponding mixtures obtained by incorporating CF at 0, 0.03, 0.05, and 0.10%. Overall results indicate remarkable changes in all the three phases of the pull-out versus slip response described in the generalized pull-out response depicted earlier in Fig. 9. The response of the reference mixture (100FA-0GP-0CF) depicted in Fig. 14 (a), undergoes phase I (fully bonded) by attaining approximately 0.55 N, then undergoes phase II with a quite significant drop from P_a to P_b (implying higher chemical bond). Thereafter, the slip response at phase III (sliding) exhibits constant frictional sliding ($\beta \approx 0$).

The above pull-out response exhibited noticeable change upon the incorporation of CF at 0.03, 0.05, and 0.10% [as shown in Fig. 14(b)-(d), respectively]. Overall, the average peak load attained during phase I (fully bonded) was lower in all systems with CF. The P_a to P_b

difference during phase II of pull-out response was also lower, while a significant-slip hardening effect ($\beta > 0$) was observed during the frictional sliding phase (III).

The above trend of CF effect on altering the pull-out response is further confirmed by the results of systems containing 40% GP. The system without CF (60FA-40GP-0CF) depicted in Fig. 14 (e) had an average peak load in phase I of ~ 0.71 N, a P_a to P_b average difference of 0.17 N, followed by frictional sliding of fiber ($\beta \approx 0$). On the other hand, the systems containing CF depicted in Fig. 14 (f)-(g) recorded an average peak load in phase I in the range of 0.40-0.50 N, a P_a to P_b average difference in the range of 0.03-0.06 N, and remarkable slip-hardening effect as reflected by the rising portion of the graph during the frictional sliding phase. A similar effect of CF was noticed in the mixture with 100% where the incorporation of CF attenuated the peak load during phase I.

In harmony with the above trend recorded in the pull-out versus slip response, the results of interface parameters reported in Fig. 15 indicate that with the incorporation of CF, the frictional bond τ_0 has been attenuated in all mixtures (with a more significant effect in mixtures with high GP). On the other hand, in consequence to the drop in P_a to P_b difference observed in the presence of CF, the chemical bond G_d has been attenuated with the incorporation of CF. Furthermore, the remarkable rising portion of the pull-out response during the sliding phase observed in systems with CF resulted in increasing the slip-hardening effect from $\beta \approx 0$ in systems without CF to $\beta \approx 0.2 - 1.5$ in systems with CF.

While higher interface properties can enhance the maximum pull-out load and increase the bridging capacity, for strain-hardening behavior to prevail, interface properties need to be attenuated such that G_d is the lowest while τ_0 is maintained at moderate levels [9]. As such, the effect of CF on attenuating G_d and τ_0 is advantageous for composite strain-hardening performance.

The effect of CF on attenuating interface frictional bond can be associated with the interference of the omnipresent high-surface area CF at the interfacial transition zone between the matrix and the PVA fiber. In situations where the fiber/matrix is very dense, the resulting higher τ_0 can enhance the maximum pull-out load but can adversely lead to premature fiber rupture or surface damage as shown in Fig. 16. In this regard, Fig. 16 (a) illustrates the status of pulled-out fiber at moderate τ_0 (0GP), Fig. 16 (b) illustrates surface scratch at high τ_0 (40%GP), while Fig. 16 (c) illustrates fiber damage at excessive τ_0 (100%GP). With the increase in τ_0 being attributed to matrix compacity, the latter need to be

optimized to obtain moderate τ_0 to promote fiber pull-out over fiber rupture and foster strain-hardening, in consequence [3, 7, 9].

Therefore, the effect of the nanoscale CF as an interface material can be perceived to promote a polymer-polymer interaction (between CF and PVA) as shown in Fig. 17 (a) and (b). This can reduce the excessive frictional forces between the PVA fiber and the matrix and lead to lower τ_0 . Likewise, the reduction in G_d observed in systems with CF can be attributed to the interference of CF between the PVA fibers and the matrix. This reduces the contact sites between the PVA fibers and the matrix or dilute the concentration of active cations from the matrix (particularly Al^{3+} and Ca^{2+}) responsible for the affinity between the PAV fibers and the matrix [13, 14]. Lowering G_d reduces the likelihood of fiber delamination [15] and contributes towards enhancing the ductility at the composite level. On the other hand, lowering G_d can cause fiber/matrix debonding at relatively lower load (as observed herein in SHCC incorporating CF). This was found elsewhere to contribute towards higher complementary energy J'_b which, in turn allows to fulfil the energy criterion and fosters composite tensile strain capacity [18].

As for the slip hardening effect β , the remarkable impact of CF on this parameter may emerge from a potential jamming effect created by the nanoscale CF coating the PVA fibers [Fig. 17 (a) and (b)] and meshing the matrix at the nanoscale [Fig. 17 (c)]. This can facilitate fibers to debond at lower pull-out load (due to the reduced τ_0 and G_d as explained above), but with the jamming effect created by the surrounding CF, the sliding-out of PVA fibers may consume supplementary pull-out load, thereby leading to the observed significant effect in slip-hardening with β values of in the rage of ≈ 1.5 .

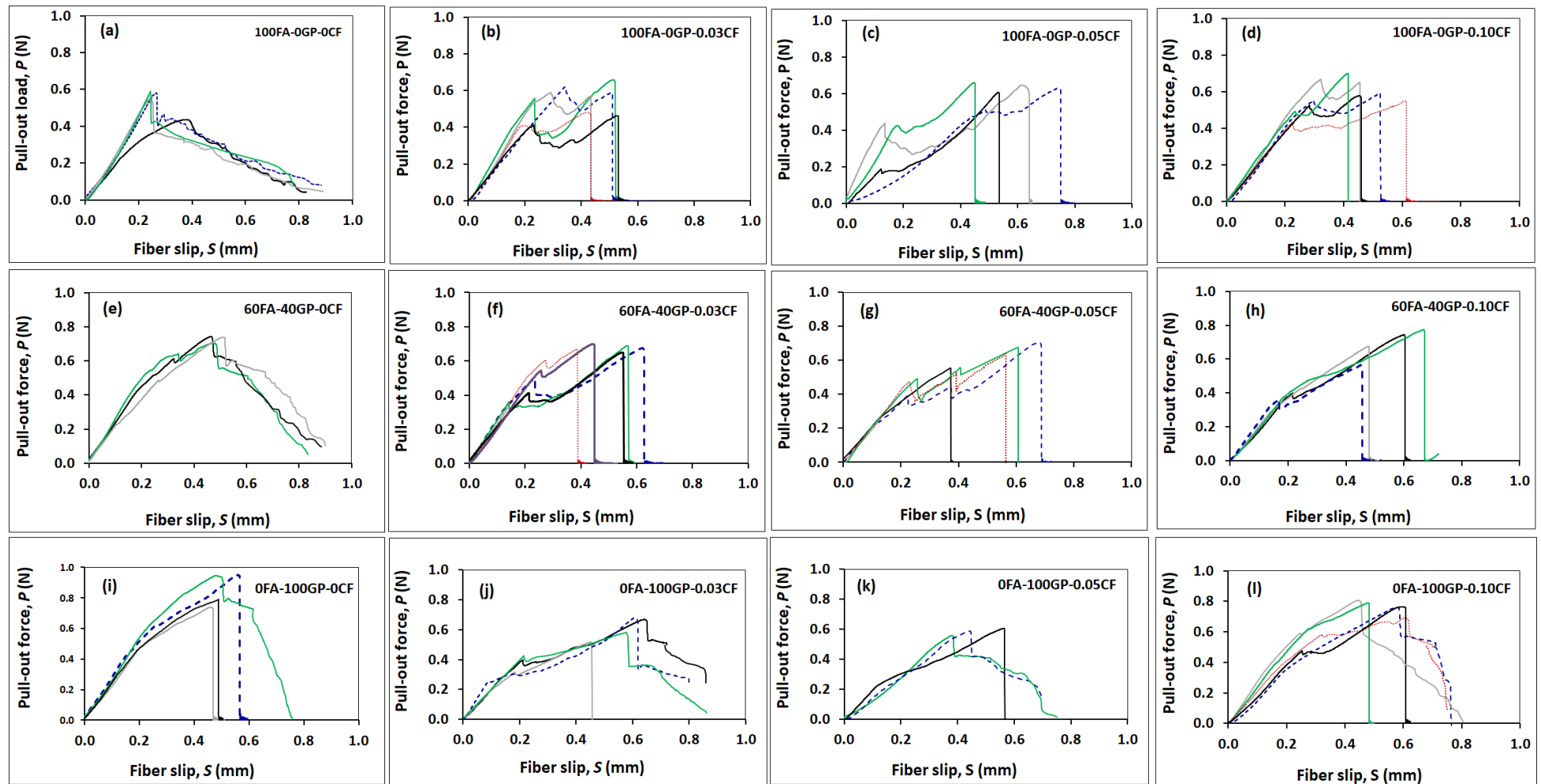


Fig. 14. Effect of nanomodification with cellulose filaments on pull-out response.

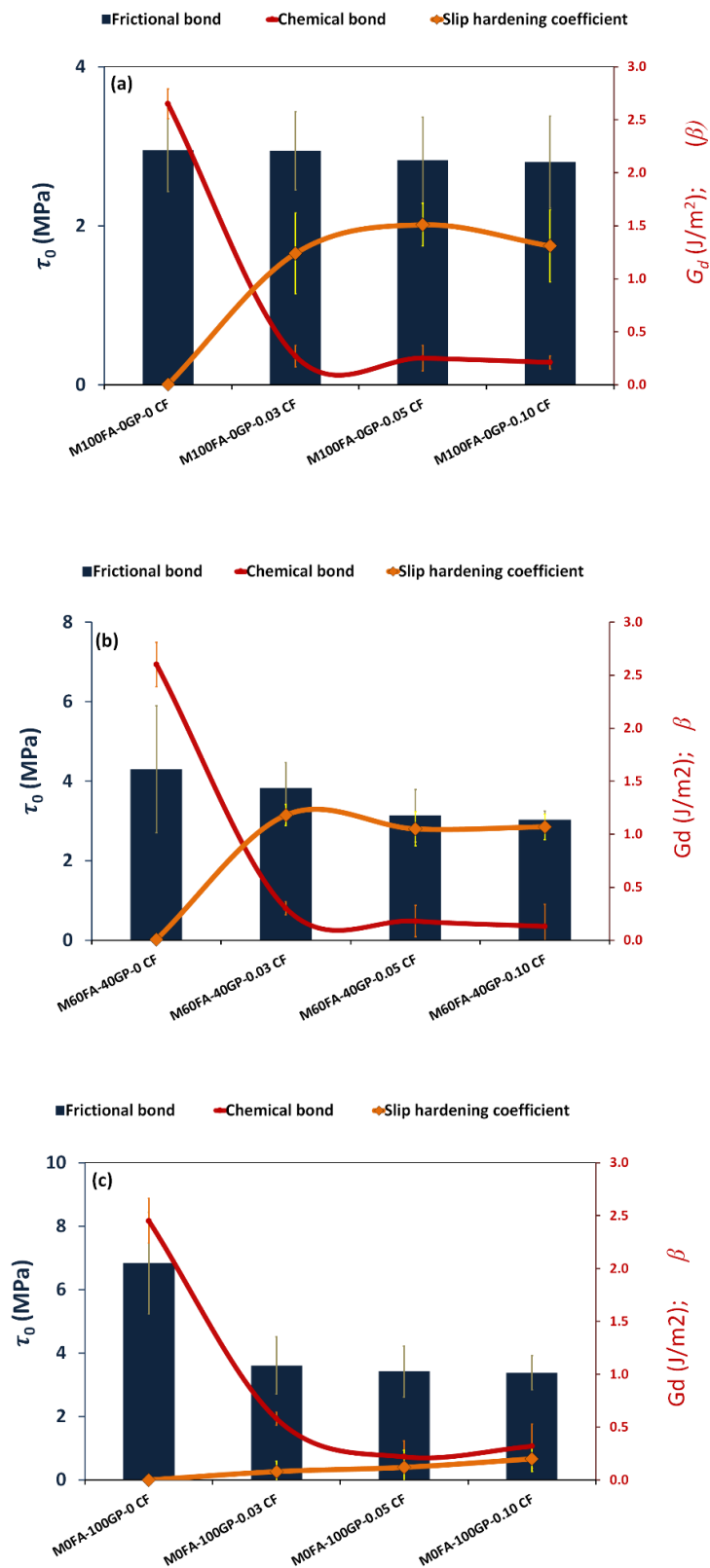


Fig. 15. Effect of nanomodification with cellulose filaments on interface properties.

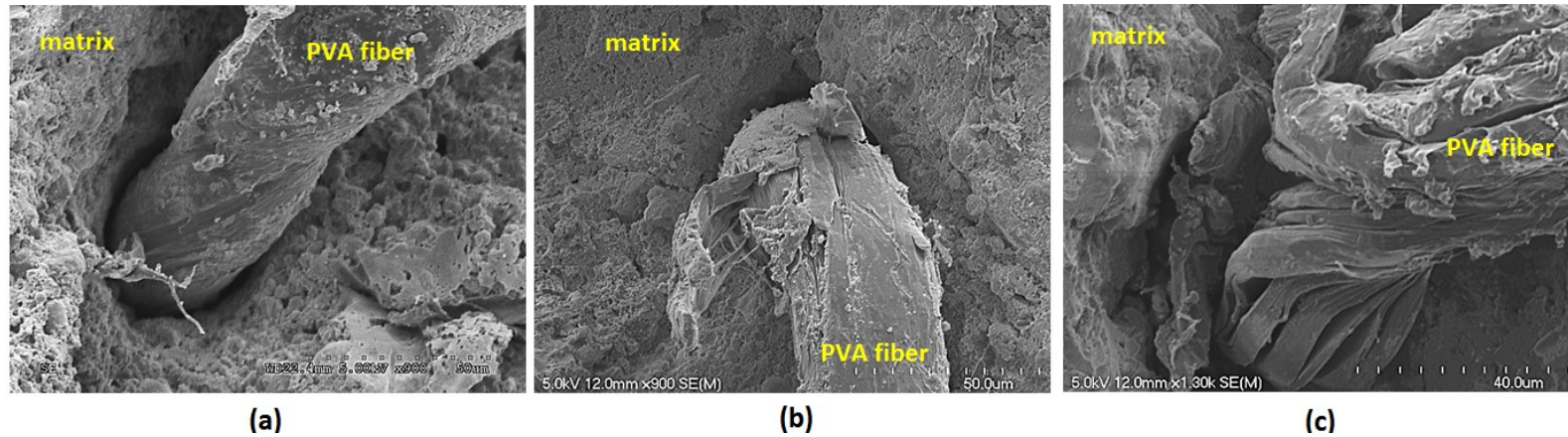


Fig. 16. PVA fiber status post-single fiber-fiber pull-out test in SHCC with: (a) 0% GP, (b) 40% GP, and (c) 100% GP. The figure illustrates fiber damage at increasing GP, which reflects the higher interface friction as well as pull-out load, but the consequent reduced slip at instances of fiber damage.

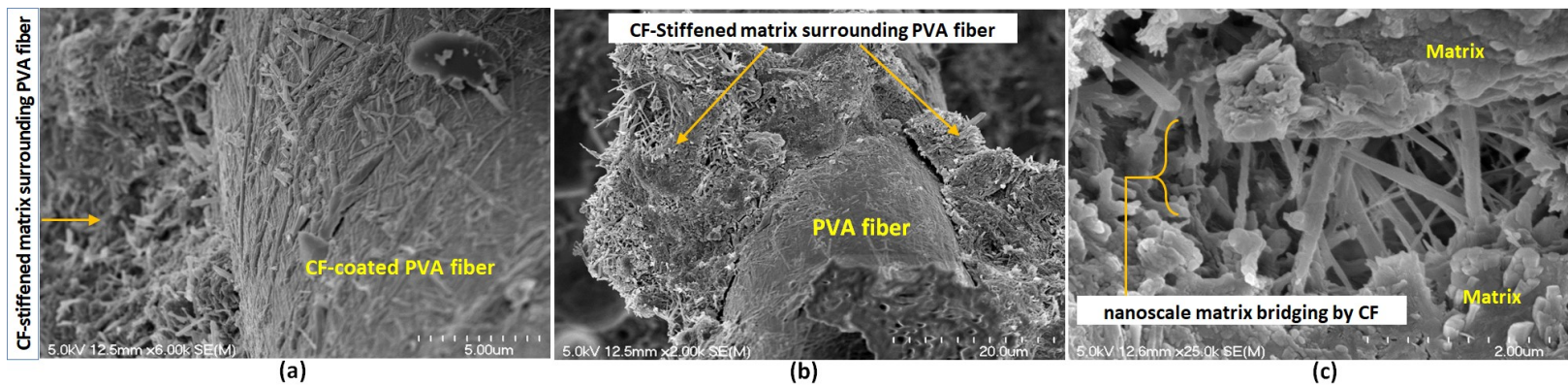


Fig. 17. Effect of CF on SHCC: omnipresence of CF on PVA fiber surface leading to altering interface properties (a and b), nanoreinforcing matrix (c).

4.3 Fiber bridging capacity

Fig. 18 presents the fiber bridging stress versus crack-opening response or $\sigma(\delta)$ for the different SHCC formulations. Fig. 18 (a) illustrates the effect of GP on $\sigma(\delta)$ where higher maximum bridging stress (σ_0) is observed with higher GP content. This is due to the higher frictional bond τ_0 associated with the increased matrix packing density and stiffness at higher GP as highlighted earlier. The figure also indicates a decrease in the crack opening (δ_0) corresponding to the maximum bridging stress at high GP content. As a result, at high GP, the rising branch of $\sigma(\delta)$ is steep while the descending branch shows softening. While this trend implies increased composite strength at high GP content, it can adversely affect the complementary J'_b and lead to a reduced composite ductility.

On the other hand, the $\sigma(\delta)$ for the mixtures incorporating CF indicates that while the incorporation of CF didn't necessarily increase the maximum bridging capacity (σ_0), obviously due to the attenuated frictional bond τ_0 (section 4.2), CF enhance the capacity to withstanding wider crack opening while maintaining higher bridging stress as reflected by the broader stress peak in the $\sigma(\delta)$ curve [Fig. 18 (b)-(d)]. This can culminate into higher complementary energy J'_b [18]. Therefore, while the optimization of matrix packing density in HVGP allows designing SHCC with improved strength, nanomodification with the incorporation of CF offers a multi-scale reinforcing system exhibiting improved ductility. This offers a twofold opportunity for promoting the sustainable development: valorizing an otherwise waste material (GP) into the development of high-performance concrete and exploiting the multifunctional properties of the most abundant (and renewable) natural polymer on the planet (cellulose).

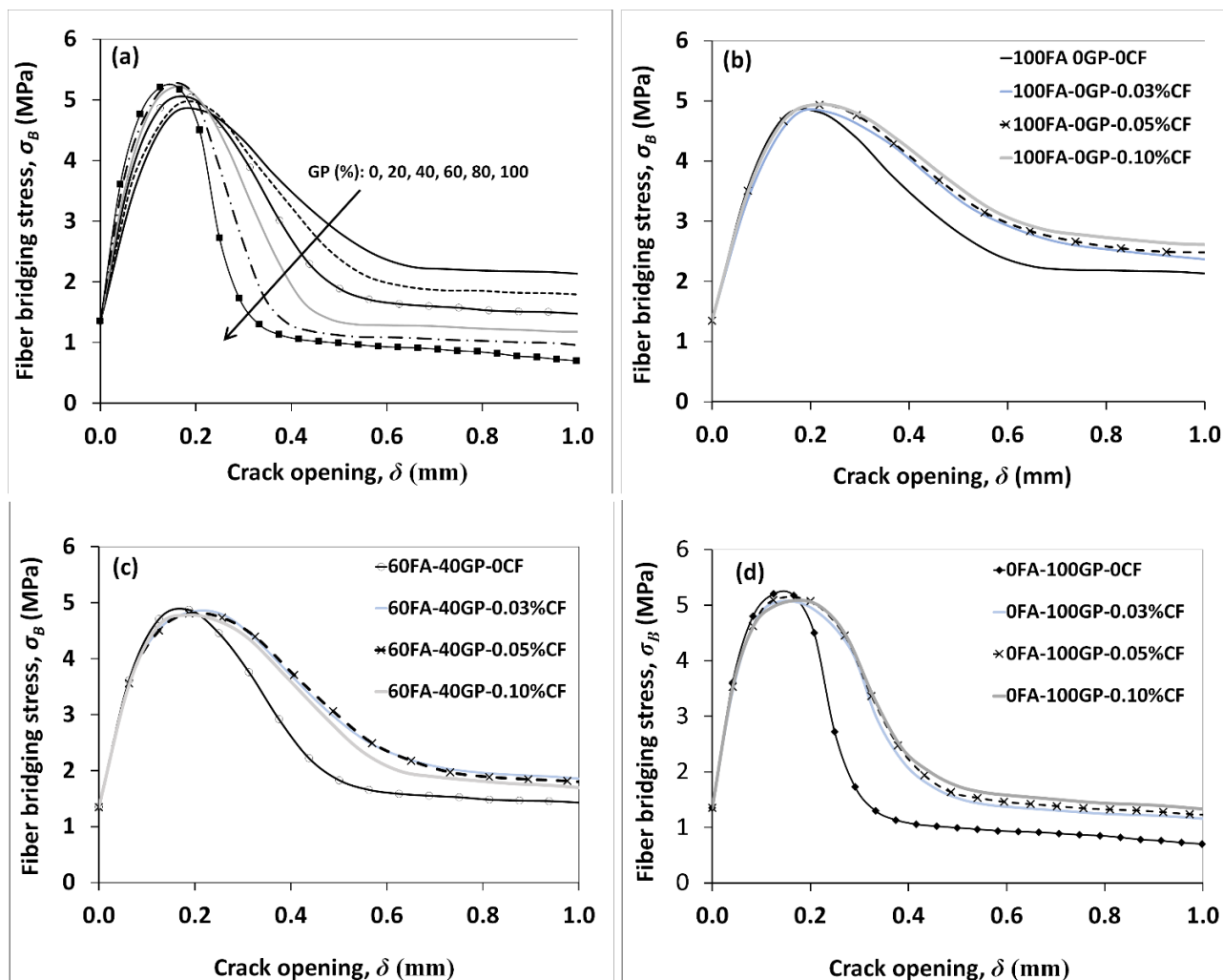


Fig. 18. Computed fiber bridging stress–crack opening relationship [$\sigma(\delta)$]: (a) for varying GP content, (b) effect of CF on the SHCC with 0%GP, (c) effect of CF on SHCC with 40%GP, and (d) effect of CF on the SHCC with 100%GP.

4.4 Experimental validating of SHCC performance

To validate the results of fiber bridging capacity [$\sigma(\delta)$] discussed in the previous section, an experimental campaign involving uniaxial tensile testing was conducted on selected SHCC mixtures. This comprises three GP contents (0, 40, and 60%) and four different CF dosages (0, 0.03, 0.05, and 0.10% of cement mass). The corresponding results are depicted in Fig. 19.

4.4.1 Effect of replacing FA with GP on the uniaxial tensile behavior

The effect of varying GP content from 0 to 40, to 100% (in replacement of FA) on the uniaxial tensile behavior of SHCC are depicted on Figs. 19 (a), (e), (i), respectively. The figures show that the replacement of FA with GP increases the first cracking strength as well as the post-peak strength identified in Fig. 19 (a) by the peaks σ_{cc} and σ_{pc} , respectively. For instance, σ_{cc} has increased from 2.08 MPa in the SHCC with 0 GP to 3.15 and 4.47 MPa in the SHCC mixtures with 40 and 100% GP, respectively. Likewise, σ_{pc} has increased from 3.34 MPa in the SHCC with 0 GP to 4.00 and 5.12 MPa, respectively, in the SHCC mixtures with 40 and 100% GP. While replacing FA with GP shows positive effect on strength properties, the ductility was adversely affected particularly at high GP content. For instance, whereas the ultimate tensile strain capacity (ε_u) was lowered from 3.01% in the SHCC with 0 GP to 2.78% in the SHCC with 40% GP, the drop in ε_u was more significant in the SHCC with 100% GP ($\varepsilon_u = 0.74\%$).

The enhanced σ_{cc} with GP is associated with the increase in matrix strength obtained with the filler effect of GP as detailed elsewhere [17]. On the other hand, the enhanced σ_{pc} is attributable to the higher τ_0 observed with GP. Excessive τ_0 , however, reduces the ultimate strain capacity ε_u as observed herein. This is ascribable to the fact that while higher frictional bond increases the pull-out load, it can also increase the likelihood of fiber damage [Fig. 16 (b), (c)], thereby affecting the post-cracking response and ductility. The above trend in the tensile strength behavior validates the results of fiber bridging stress versus crack opening response $\sigma(\delta)$ (Fig. 18) stemming from the micromechanical theory.

4.4.2 Effect of nano-modification with CF on the uniaxial tensile behavior

Fig. 19 also depicts the uniaxial tensile behavior of nanocellulose-modified HVGP-SHCC. Overall, the incorporation of CF significantly enhanced the tensile strain capacity (ε_u) with a more pronounced effect at high GP content. In the SHCC with 0 GP [Fig. 19 (a)] which has ε_u of 3.01%, for instance, the incorporation of CF at 0.03, 0.05, and 0.10% [(Figs. 19 (b), (c), (d))] increased ε_u to 3.33, 3.60, and 3.78%, respectively. This corresponds to enhancements of 11, 20, and 26%, respectively. In the SHCC with 40% GP [Fig. 19 (e)], the incorporation of CF at 0.03, 0.05, and 0.10% [Fig. 19 (f), (g), (h), respectively] increased ε_u from 2.78 % to 3.12, 3.54, and 3.81%, respectively. This corresponds to enhancements of 12, 27, and 37%. The highest gain in

ε_u was achieved in the SHCC with 100% GP [Fig. 19 (i)] which had initially the lowest ε_u . The incorporation of CF at 0.03, 0.05, and 0.10% [Fig. 19 (j), (k), (l), respectively] increased ε_u in the SHCC with 100% GP from 0.74 % to 1.81, 2.56, and 2.65%, respectively. This corresponds to enhancements of 145, 246, and 258%.

The above results indicate that with the incorporation of CF, the post-peak behavior is significantly enhanced particularly in SHCC with high GP content. The role of CF appears to particularly restore the loss in ductility experienced in HVGP-SHCC. The significant enhancement in tensile ductility obtained with CF can be a result of the effect of CF on the interface properties of HVGP-SHCC as described earlier. In fact, in systems with CF, the interfacial bond is altered due the polymer-polymer (PVA-CF) interface friction attenuating τ_0 and G_d while fostering β . In this regard, as CF imparts a characteristic slip-hardening behavior on fiber pull-out versus slip response, the slip-hardening response can be seen to be transposed from the micromechanical level of individual fibers to the matrix level where an enhanced strain-hardening behavior is reflected by an increased ε_u as observed herein. Beside the effect of CF on interface properties of SHCC, the improved ductility can stem from the effect of CF as a nano-reinforcing agent providing a bridging effect at the scale of hydrates, thereby leading not only to higher elastic modulus in the bulk matrix but also to higher micromechanical properties of the C-S-H gel matrix ($\approx 12\text{-}25\%$ higher indentation modulus M) as demonstrated in our previous work [22]. At increasing elastic modulus, the crack tip toughness J_{tip} can be maintained at moderate levels while the complementary energy J'_b can be improved, thereby leading an enhanced J'_b/J_{tip} ratio, an essential indicator of strain-hardening behavior.

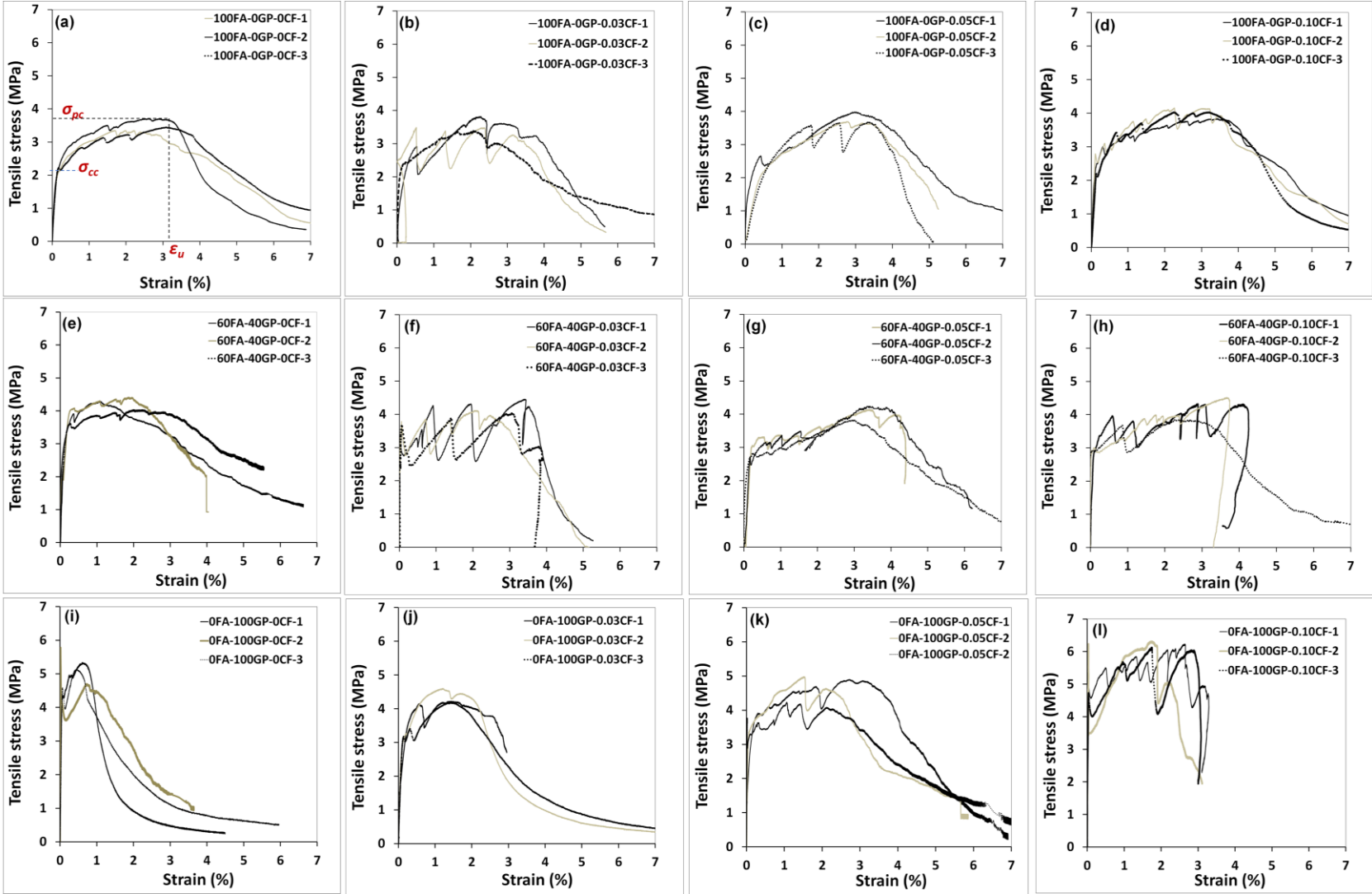


Fig. 19. Uniaxial tensile behavior.

Summary and conclusions

In this study, single-fiber pull-out (SFP) tests were conducted on strain-hardening cementitious composites incorporating high-volume ground pozzolans (HVGP-SHCC) to characterize the interface properties necessary for micromechanical tailoring of SHCC. A new simplified method for preparing SFP test sample was developed. Furthermore, a novel technique for modifying the interface properties of SHCC towards an enhance strain-hardening performance at the composite level has also been presented. This consists of nanomodification of SHCC with the incorporation of nanoscale cellulose filaments (CF). The following specific conclusions can be drawn:

- Replacement of fly ash (FA) with GP in SHCC through packing density optimization resulted in denser matrices. This caused the frictional bond τ_0 to increase significantly (from 2.95 MPa in the system without GP to 6.84 in the system with GP), with no significant effect on the chemical bond G_d and the slip hardening effect β . The increased frictional bond was found to lead to higher pull-out resistance in systems with high GP content, but fiber slip was shorter and fiber damage was more often.
- The incorporation of nanoscale CF at dosages ranging from 0.03-0.10% allowed to significantly alter the pull-out behavior by attenuating τ_0 and G_d while imparting remarkable β . CF allowed creating an interface between the PVA fibers and the matrix (as demonstrated by microstructure investigation). This attenuated the excessive τ_0 and G_d and allowed fiber pull-out at lower loads, but imparted significant β of up to 1.5. this allowed shifting the fiber pull-out (during the sliding phase) from frictional sliding to slip-hardening. In consequence, increased pull-out load was maintained before complete fiber pull-out.
- The effect of GP and CF on interface properties was reflected on the fiber-bridging capacity-versus crack-opening response. Thus, with high GP content, the maximum bridging capacity σ_0 was higher while the corresponding crack opening was lower. Conversely, the incorporation of CF at three ranges of GP (0, 40, 100% replacement of FA) lead to increase the capacity to sustain higher crack opening without significant

response softening. This can be reflected by higher complementary energy and lead to an enhanced strain-hardening at the composite level.

- Validation of micromechanical results through uniaxial tensile tests showed that the incorporation of GP increases both the first crack strength (σ_{cc}) as well as the post crack strength (σ_{pc}) due to the increase matrix compacity. However, reduced tensile ductility was observed in SHCC with high GP content due to excessive τ_0 leading to fiber damage.
- Nano-modification of HVGP-SHCC with the incorporation of CF imparted higher ε_u and contributed towards restoring the loss in ductility experienced in HVGP-SHCC.

Finally, overall results indicate that when GP was incorporated in SHCC through the guidance of particle packing, HVGP can be used to design SHCC with potentially higher strength than that of conventional SHCC with high-volume fly ash (HVFA). Furthermore, nanocellulose offers a new tool to nanomodify matrix and interface properties such that the adverse effect of HVGP-SHCC on ductility can be overcome.

Acknowledgements

This project is jointly supported a Cooperative Research and Development (CRD) grant from the Natural Sciences and Engineering Research Council of Canada (NSERC), Canada Vanier Graduate Scholarship (CGS) program award no: 360284, Kruger Biomaterials Inc. (QC, Canada), and Euclid Chemicals. The authors are grateful to the financial support from all these partners.

References

- [1] V.C. Li, Engineered Cementitious Composites (ECC) – Tailored Composites Through Micromechanical Modeling, Fiber Reinforced Concrete: Present and the Future, Canadian Society for Civil Engineering, Montreal, 1998, pp. 64–97.
- [2] V.C. Li, S. Wang, C. Wu, Tensile strain-hardening behavior of polyvinyl alcohol engineered cementitious composite, ACI Mater. J. 98 (6) (2001) 483–492.
- [3] V.C. Li, On engineered cementitious composites (ECC) – a review of the material and its application, J. Adv. Concr. Technol. 1 (2003) 215–230.
- [4] V.C. Li, C.K.Y. Leung, Steady state and multiple cracking of short random fiber composites, ASCE J. Eng. Mech. 188 (11) (1992) 2246–2264.

- [5] V.C. Li, From micromechanics to structural engineering – the design of cementitious composites for civil engineering application, *J. Struct. Eng. Earthquake Eng.* 10 (2) (1993) 37–48.
- [6] V. C. Li, H. Stang, Interface property characterization and strengthening mechanisms in fiber reinforced cement-based composites, *Adv. Cem. Based Mater.* 6 (1) (1997) 1–20.
- [7] Z. Lin, V. C. Li, Crack bridging in fiber reinforced cementitious composites with slip-hardening interfaces.” *J. Mech. Phys. Solids*, 45(5) (1997) 763–787.
- [8] Z. Lin, T. Kanda, V.C. Li, On interface property characterization and performance of fiber-reinforced cementitious composites, *J. Concrete Sci. and Engrg.* 1 (1999) 173–184.
- [9] S. Wang, V.C. Li, Engineered cementitious composites with high-volume fly ash, *ACI Mater. J.* 104 (3) (2007) 233–241.
- [10] C. Lin, O. Kayali, E.V. Morozov, D.J. Sharp, Development of self-compacting strain-hardening cementitious composites by varying fly ash content, *Constr. Build. Mater.* 149 (2017) 103–110.
- [11] E.H. Yang, Y. Yang, V.C. Li, Use of high volumes of fly ash to improve ECC mechanical properties and material greenness, *ACI Mater. J.* 104 (6) (2007) 620–628.
- [12] M. Sahmaran, V.C. Li, Durability properties of micro-cracked ECC containing high volumes fly ash, *Cement and Concrete Research* 39 (11) (2009) 1033–1043.
- [13] S. A. Rodger, S. A. Brooks, W. Sinclair, G. W. Groves, D. D. Double, High strength cement pastes, *J. Mater. Sci.* 20 (1985) 2853–2860.
- [14] M. A. Gulgun, W. M. Kriven, L. S. Tan, A. J. McHugh, Evolution of mechano-chemistry and microstructure of a calcium aluminate-polymer composite: Part I—Mixing Time Effects,” *J. Mater. Res.* 10 (7) (1995) 1746–1755.
- [15] C. Redon, V. C. Li, C. Wu, H. Hoshiro, T. Saito, A. Ogawa, Measuring and modifying interface properties of PVA fibers in ECC matrix, *ASCE J. Mater. Civ. Eng.* 13 (6) (2001) 399–406.
- [16] H. Ma, J. Cai, Z. Lin, S. Qian, V. C. Li, CaCO₃ whisker modified Engineered Cementitious Composite with local ingredients, *Constr. Build. Mater.* 151 (2017) 1–8.
- [17] O.A. Hisseine, A. Tagnit-Hamou, Coupling particle packing optimization with micromechanical tailoring for the development of ecological strain-hardening cement

- composites (SHCC) with high-volume recycled glass powder (HVGP), Article under review by Cement and Concrete research, March, 2019.
- [18] V. C. Li, C. Wu, S. Wang, A. Ogawa, T. Saito, Interface tailoring for strain-hardening polyvinyl alcohol-engineered cementitious composite (PVA-ECC), *ACI Mater. J.* 99 (5) (2002) 463–472.
- [19] Z. Pan, C. Wu, J. Liu, W. Wang, J. Liu, Study on mechanical properties of cost-effective polyvinyl alcohol engineered cementitious composites (PVA-ECC), *Constr. Build. Mater.* 78 (2015) 397–404.
- [20] C. Lu, Z. Lu, Z. Li, C.K.Y. Leung, Effect of graphene oxide on the mechanical behavior of strain hardening cementitious composites, *Constr. Build. Mater.* 120 (2016) 457–464.
- [21] R. J. Moon, A. Martini, J. Nairn, J. Simonsen, J. Youngblood, Cellulose nanomaterials review: structure, properties and nanocomposites. *Chem. Soc. Rev.* 40 (2011) 3941–3994.
- [22] O. A. Hisseine, William Wilson, Luca Sorelli, Balázs Tolnai, Arezki Tagnit-Hamou, Nanocellulose for improved concrete performance: A macro-to-micro investigation for disclosing the effects of cellulose filaments on strength of cement systems, *Constr. Build. Mater.* 206 (2019) 84–96.
- [23] O.A. Hisseine, A.F. Omran, A. Tagnit-Hamou, Influence of cellulose filaments on cement pastes and concrete, *J. Mater. Civ. Eng.* 30 (6) (2018), p. 04018109.
- [24] F. De Larrard, *Concrete mixture proportioning: A Scientific Approach*, E&FN Spon, London, 1999.
- [25] ASTM C494 / C494M-17, Standard Specification for Chemical Admixtures for Concrete, ASTM International, West Conshohocken, PA, 2017, www.astm.org
- [26] O.A. Hisseine, A. Tagnit-Hamou, Development of ecological nanoengineered strain-hardening cement composites with high-volume ground glass pozzolans, Article under review by Cement and Concrete Composites, March 2019.
- [27] H. Kong, S. G. Bike, V. C Li, Development of a self-consolidating engineered cementitious composite employing electrosteric dispersion/stabilization, *Cem. Concr. Compos.* 25 (3) (2003) 301–309.
- [28] J. Morton, G.W. Groves, The effect of metal wires on the fracture of a brittle matrix composite. *J. Mater. Sci.* 11(1976) 617–622.

- [29] V.C. Li, Post-crack scaling relations for fiber reinforced cementitious composites. *J. Mater. Civil Eng.* 4 (1992) 41–57.
- [30] E.H Yang, S. Wang, Y. Yang, V. C. Li, Fiber-bridging constitutive law of engineered cementitious composites. *J. Adv. Concr. Technol.* 6 (1) (2008) 181–193.
- [31] T. Kanda, V. C. Li, Interface property and apparent strength of high-strength hydrophilic fiber in cement matrix, *J. Mat. in Civ. Engrg. ASCE*, 10 (1) (1998) 5–13.
- [32] C. Wu, Micromechanical tailoring of PVA-ECC for structural application. Ph. D. Thesis, University of Michigan (2001).

List of Figures

Fig. 1. Research framework for the characterization and nanomodification of interface properties of HVGP-SHCC

Fig. 2. Particle size distribution of SHCC ingredients

Fig. 3. SEM micrographs of SHCC ingredients

Fig. 4. SEM micrograph of hybrid reinforcement systems used in this study

Fig. 5. Combined particle size distribution for the different SHCC formulations

Fig. 6. Preparations of test samples for single-fiber pull-out (SFP)

Fig. 7. Single-fiber pull-out (SFP) test

Fig. 8. Test set-up for uniaxial tensile test

Fig. 9. General pull-out versus slip response obtained with PVA fibers in HVGP-SHCC

Fig. 10. Illustration of the effect of GP on interface properties

Fig. 11. Illustration of the effect of CF on interface properties of SHCC

Fig. 12. Pull-out load versus slip response for different GP content in replacement of FA

Fig. 13. Effect of GP on interface properties

Fig. 14. Effect of nanomodification with CF on pull-out response

Fig. 15. Effect of nanomodification with cellulose filaments on interface properties

Fig. 16. PVA fiber status post-SFP test

Fig. 17. Effect of CF on SHCC microstructure

Fig. 18. Computed fiber bridging stress–crack opening relationship (σ – δ) for varying GP content

Fig. 19. Uniaxial tensile behavior

List of Tables

Table 1. Chemical compositions of powders and granular materials used in the study

Table 2. Mix design of HVGP-SHCC

Table 3. Fresh properties of SHCC plain formulations

Appendices

Appendix I. Verification of the deformation (at fresh state) in the fiber embedded end

Appendix II. PVA fiber/matrix interface properties

Appendix I

Verification of the deformation (at fresh state) in the fiber embedded end

Series	No.	Mixture name	Deformation of fiber embedded end				
			Unit weight (kg/m ³)	Mixture weight (10 ⁻⁵ N/mm ³)	weight carried by the fiber embed end (10 ⁻⁴ N/mm)	Fiber deformation at free end (10 ⁻⁴ mm)	Deformation / Embedded length (%)
I	1	M100FA-0GP-0CF	2034	1.99	6.58	8.370	0.084
	2	M80FA-20GP-0CF	2037	2.00	6.59	8.382	0.084
	3	M60FA-40GP-0CF	2039	2.00	6.60	8.391	0.084
	5	M40FA-60GP-0CF	2040	2.00	6.60	8.395	0.084
	5	M20FA-80GP-0CF	2039	2.00	6.60	8.391	0.084
	6	M0FA-100GP-0CF	2035	2.00	6.59	8.374	0.084
II	7	M100FA-0GP-0.03CF	2021	1.98	6.54	8.316	0.083
	8	M100FA-0GP-0.05CF	2018	1.98	6.53	8.304	0.083
	9	M100FA-0GP-0.10CF	2015	1.98	6.52	8.292	0.083
	10	M60FA-40GP-0.03CF	2032	1.99	6.58	8.362	0.084
	11	M60FA-40GP-0.05CF	2030	1.99	6.57	8.353	0.084
	12	M60FA-40GP-0.10CF	2027	1.99	6.56	8.341	0.083
	13	M0FA-100GP-0.03CF	2025	1.99	6.55	8.333	0.083
	14	M0FA-100GP-0.05CF	2023	1.98	6.55	8.325	0.083
	15	M0FA-100GP-0.10CF	2015	1.98	6.52	8.292	0.083

Appendix II

PVA fiber/matrix interface properties

Series	No.	Mixture name	Interface parameters			
			Frictional bond, τ_0 (MPa)	Chemical bond, G_d (J/m ²)	Slip-hardening coefficient (β)	Pull-out work per embedded fiber area (w_p) (N/mm)
I	1	100FA-0GP	2.95±0.52	2.65±0.14	0.0030	1.13±0.21
	2	80FA-20GP	3.10±0.40	2.61±0.18	0.0061	1.28±0.17
	3	60FA-40GP	4.30±0.80	2.60±0.14	0.0057	1.84±0.20
	4	40FA-60GP	4.62±0.89	2.57±0.10	0.0031	2.18±0.18
	5	20FA-80GP	5.57±0.92	2.52±0.16	0.0023	2.76±0.14
	6	0FA-100GP	6.84±0.80	2.45*	—	3.16±0.19
II	7	100FA-0GP-0.03CF	2.94±0.56	0.27±0.10	1.24±0.39	1.52±0.25
	8	100FA-0GP-0.05CF	2.82±0.66	0.25±0.12	1.51±0.20	1.68±0.15
	9	100FA-0GP-0.10CF	2.80±0.78	0.21±0.06	1.31±0.34	1.72±0.15
	10	60FA-40GP-0.03CF	3.83±0.32	0.30±0.02	1.18±0.10	1.92±0.16
	11	60FA-40GP-0.05CF	3.13±0.41	0.18±0.05	1.05±0.16	2.09±0.13
	12	60FA-40GP-0.10CF	3.03±0.33	0.13±0.07	1.07±0.12	2.26±0.18
	13	0FA-100GP-0.03CF	3.61±0.45	0.58±0.10	0.004	1.63±0.12
	14	0FA-100GP-0.05CF	3.42±0.20	0.22±0.12	0.005	2.42 ±0.15
	15	0FA-100GP-0.10CF	3.38±0.14	0.32±0.30	0.007	2.58±0.22

* Chemical bond energy (G_d) calculated from one test as the drop P_a to P_b in pull-out load becomes less frequent at high GP

CHAPTER 8

Coupling Particle Packing Optimization with Micromechanical Tailoring for the Development of Ecological Strain-Hardening Cement Composites Incorporating High-Volume Ground-Glass Pozzolans

8.1 Introduction

In this chapter, a novel formulation for ecological strain-hardening cementitious composites (SHCC) has been developed by valorizing high-volume post-consumer ground-glass pozzolans (HVGP). The development of this HVGP-SHCC was undertaken by coupling particle packing optimization with the micromechanical tailoring approach such that the replacement of fly ash (FA) by ground-glass pozzolans (GP) is systematically guided. HVGP-SHCC with GP replacement of FA at 20, 40, 60, 80, and 100% were produced. Relative to HVFA-SHCC, the resulting formulation exhibited higher strength and improved durability aspects (electrical resistivity). HVGP-SHCC (with the following flow properties and 28 day-strength features) were developed: Mini slump-flow (~250 mm), compressive strength of 60-75 MPa, flexural capacity of 9-15 MPa, tensile strength of 3-6 MPa, and tensile strain capacity of 2-5%. Moreover, HVGP-SHCC have significantly higher electrical resistivity implying improved durability aspects.

These details are reported in section 8.2 in the context of article 6 under reviewed by construction and building materials.

8.2 Article 6- Coupling particle packing optimization with micromechanical tailoring for the development of ecological strain-hardening cement composites incorporating high-volume ground-glass pozzolans

Article information

Authors and affiliations:

Ousmane A. Hisseine, PhD candidate and Canada Vanier Scholar of NSERC, Cement and Concrete Research Group, Department of Civil Engineering, Université de Sherbrooke
A. Tagnit-Hamou, Professor and director of Cement and Concrete Research Group, Department of Civil Engineering, Université de Sherbrooke

Article status: Under review

Journal: Construction and Building Materials

Initial date of submission: April 20, 2019

Reference: Hisseine, O. A, Tagnit-Hamou, A. (2019). Coupling particle packing optimization with micromechanical tailoring for the development of ecological strain-hardening cement composites incorporating high-volume ground-glass pozzolans. Article Under review by *Construction and Building Materials*.

Titre français:

Développement de bétons écrouissants à teneur élevée en poudre de verre en utilisant une nouvelle approche articulant l'optimisation de la compacité granulaire aux modèles d'optimisation micromécanique.

Contribution of this article: Contributes towards achieving project object 5, namely, leveraging the versatile opportunities offered by nanocellulose to develop a novel nanoengineered concrete formulation, namely, a Nanomodified-Strain-Hardening Cementitious Composite.

Development of strain-hardening cementitious composites incorporating high-volume ground-glass pozzolans using a novel approach coupling particle packing optimization with micromechanical tailoring

Ousmane A. Hisseine; Arezki Tagnit-Hamou

Under Review by Construction and Building Materials

Abstract

In line with concrete ecoefficiency requirements for valorizing locally available materials, a novel strain-hardening cementitious composite (SHCC) incorporating high-volume ground-glass pozzolans (HVGP) has been developed herein. The new SHCC was designed using a new approach that couples particle packing optimization with micromechanical tailoring. For the former, the compressible packing density model was adopted, while for the latter, single-fiber pull-out and fracture mechanics tests were conducted to compile model input parameters. This compacity-based formulation yielded SHCC exhibiting higher strength than conventional SHCC containing high-volume fly ash (HVFA). As such, SHCC incorporating HVGP up to 100% replacement of FA were developed. The resulting formulations exhibited (at 28 days) ~60-75 MPa compressive strength, 9-15 MPa flexural capacity, 3-6 MPa tensile strength, 2-5% tensile strain capacity, and significantly increased electrical resistivity. Integrating particle-packing optimization into micromechanical tailoring drives a systematic design of HVGP-SHCC with optimized, strength, ductility, and durability characteristics.

Author Keywords: Engineered cementitious composites (ECC); ground-glass pozzolans (GP); high-performance fiber-reinforced cement composites (HPFRCC); particle packing optimization; recycled glass powder (GP); Strain-hardening cementitious composites (SHCC)

1 Introduction

Strain hardening cementitious composites (SHCC) also referred to as engineered cementitious composites (ECC) represent a relatively new class of high-performance fiber-reinforced cementitious composites (HPFRCC). The most salient features of SHCC are its exceptional ductility, remarkable tensile strain capacity in the range of 2-5% [200–500 times that of normal concrete or conventional fiber reinforced concrete (FRC)], tight multiple

cracking with crack width below 60 μm at 1% strain, and strain-hardening behavior with relatively low fiber volume content, typically $\leq 2\%$ [1-4]. The design of SHCC is guided by micromechanical principles which systematically account for the mechanical interaction between the three major composite constituents (fiber, matrix, and interface properties) when the composite is loaded [5]. This design approach ensures that upon first cracking under uniaxial tension, SHCC strain-hardens in contrast to common FRC which rather tension-soften after first cracking. Thus, SHCC achieves remarkable ductility elevating it to a metal-like composite exhibiting significant fracture toughness approaching that of aluminum alloys [6]. These features were found to be intrinsically maintained across a large range of specimen sizes. This is owing to the fact that SHCC attributes are scale-invariant and can be transposed from centimeter-size specimens to structural scale elements [7]. As a result, SHCC found its way in several structural applications including bridge deck link slabs [8], bridge deck overlays, dam repairs and coupling beams in high rise buildings [9, 10].

Early generations of SHCC used silica fume as supplementary cementitious material (SCM) and polypropylene fibers for reinforcement [1, 11]. Later, for cost-effectiveness and ecoefficiency incentives, SHCC with high-volume fly ash (HVFA) were developed and polyvinyl alcohol fibers (PVA) were utilized [12]. As such, for several years, HVFA has been the most commonly used SCM in SHCC formulation [12, 17-20]. The use of FA in SHCC enhances the workability due to its slower reactivity, additional to its spherically-shaped smooth-textured particles reducing inter-particle friction and enhancing mixture flowability. The use of FA also reduces the heat of hydration (and the associated thermal cracking owing to its slower reactivity) and enhances composite durability by the long-term development of mechanical strength by pozzolanic activity [12, 19, 22]. HVFA in SHCC was also found to dilute the concentration of Al^{3+} and Ca^{2+} cations [12]. Since the latter has a strong propensity for bonding to the hydrophilic PVA fibers [23], the diluting effect of FA turns to reduce fiber/matrix chemical bonding, increase matrix toughness, and contribute towards higher composite ductility [12].

Despite all these benefits, HVFA-SHCC experiences reduced mechanical strength [22]. An investigation on the effect of increasing FA/cement ratio from 1.0 to 1.5 showed that the tensile strength decreases by $\sim 20\%$ as FA content increases [12]. A reduction of 15% in tensile strength and 40% in compressive strength were also recorded when the FA/cement ratio was increased from 1.2 to 2.0 [19]. In the same context, a 35% reduction in tensile

strength and a 30% reduction in elastic modulus were observed when the FA/cement ratio was increased from 1.0 to 2.0 [21]. As such, increasing research attention in SHCC is being directed towards improving the strength characteristics of SHCC by incorporating other SCM or filler materials (e.g.: ground granulated blast furnace slag [13], limestone powder [14, 15], and metakaolin [15]).

On the other hand, due to recent environmental policies in the energy sector in North America, coal-fired power plants are in decline and so is the supply of FA [23]. Therefore, locally available alternative SCMs are becoming more attractive as recommended by the Canadian Standards Association [32]. Locally available alternative SCMs with a potential strength enhancement in SHCC are required for a potential partial or full replacement of FA in SHCC. This can reduce the CO₂ invoice of SHCC and contributes towards localizing its ingredients, hence wide spreading its implementation. One such SCM in Québec (Canada) is the ground glass pozzolan (GP). GP obtained by grinding mixed-waste glass to the same fineness as cement can serve as an SCM. This waste glass cannot be recycled and in the best scenarios, ends landfilled, causing serious environmental problems. In Québec, for instance, only 49 % of glass was recycled in 2008 [25], the rest, which is not recycled due to either breaking, color mixing, or expensive recycling cost, is often landfilled [25]. Thus, valorizing post-consumer glass by grinding it into GP (exhibiting pozzolanic activity) has been proven to be a successful alternative SCM while solving an obvious environmental problem.

Over several years, GP has been valorized in various types of concrete and demonstrated a successful partial replacement of cement in laboratory work and in field applications of regular concrete, self-consolidating concrete, and ultra-high-performance concrete (UHPC) [28-32]. These works and many others catalyzed the acceptance of GP as a standard SCM by CSA [32].

Beside the ecoefficiency aspects of using GP in concrete, further salient features of concretes incorporating GP are (i) the higher strength owing to the pozzolanic activity which forms new pozzolanic C-S-H with very low C/S ratio and high amounts of alkalis (Na + K) and aluminum (Al) [34], (ii) the significantly increased durability owing to the tortuosity, pore refinement, and microstructure densification via pozzolanic activity [35, 37], and (iii) reduced alkali-silica reaction (ASR), particularly when finer GP is used [37] or added in conjunction with fly ash or slag [38].

Therefore, it is legitimate to believe that the above various benefits of GP can be leveraged to produce HVGP-SHCC with enhanced strength characteristics while promoting sustainable development.

For this, it is hypothesized herein that, subject to optimizing GP content in SHCC, the filler effect, the pozzolanic activity, and the intrinsic high strength of GP particles may allow producing SHCC with higher strength while valorizing an otherwise waste material contributing to environmental pollution. With this hypothesis in mind, the current study aims at producing an SHCC with full or partial replacement of FA with GP such that the resulting SHCC exhibits higher strength while responding satisfactorily to pseudo-ductility requirements. Further, the resulting SHCC is expected to exhibit higher durability features, given the effect of GP on durability aspects of all concrete types. To this end, the study adopts a novel approach that combines the packing density optimization commonly used for designing UHPC with the micromechanical tailoring approach commonly used for designing SHCC. This coupled approach is expected to drive a systematic replacement of FA with GP while responding to both strength and pseudo-ductility requirements hardly met with HVFA systems. Likewise, this systematic approach allows avoiding the serendipity of trial and error tests.

While GP has been incorporated successfully in the past in various types of concretes and resulted in enhanced mechanical properties and durability as highlighted above, its utilization in SHCC is rather new. One noteworthy attempt has been made to investigate the microstructure, mechanical performance, durability, and self-healing characteristics of SHCC incorporating GP [39]. However, the study does not present a micromechanically formulated SHCC nor does the study attempt the SHCC behavior under uniaxial tension which is fundamental for this type of concrete [1]. Thus, up to the knowledge of the authors, there is no published research addressing the design of SHCC with GP using the fundamental micromechanical approach. Research outcomes are expected to contribute to the development of high-performance green cement composites necessary for sustainable and resilient infrastructure systems.

2 Framework for the development of HVGP-SHCC

Pseudo-ductility performance criteria require SHCC mixtures to be designed such that the three composite constituents (matrix, fiber, and fiber-matrix interface) are tailored to obtain a composite exhibiting a smooth transition from the quasi-brittle behavior (of conventional

fiber-reinforced cement composites) to a metal-like behavior [11]. This transition is characterized by (i) a sustained or even higher load carrying capacity after matrix first cracking associated with the steady-state cracking, (ii) sequential tight multiple cracking until matrix peak capacity is reached, and (iii) high ultimate tensile strain capacity reaching 2-5% (200-500 times that of plain cement matrices or conventional FRC) [1]. In this study, an HVGP-SHCC was designed under the guidance of micromechanical tailoring. The material development involved tailoring the matrix as well as the fiber/matrix interface properties. Matrix tailoring was undertaken through optimizing matrix compacity (by varying the proportions of GP and FA) followed micromechanical evaluation. This was accompanied by the assessment of the micromechanical response at the fiber/matrix interface using the single-fiber pull-out test. In outcome, fiber bridging capacity for different binary combinations of GP and FA were developed. Fig. 1 presents an overview of the framework adopted in this study for the development of HVGP-SHCC. Further details about SHCC tailoring are provided in sections 3 and 4.

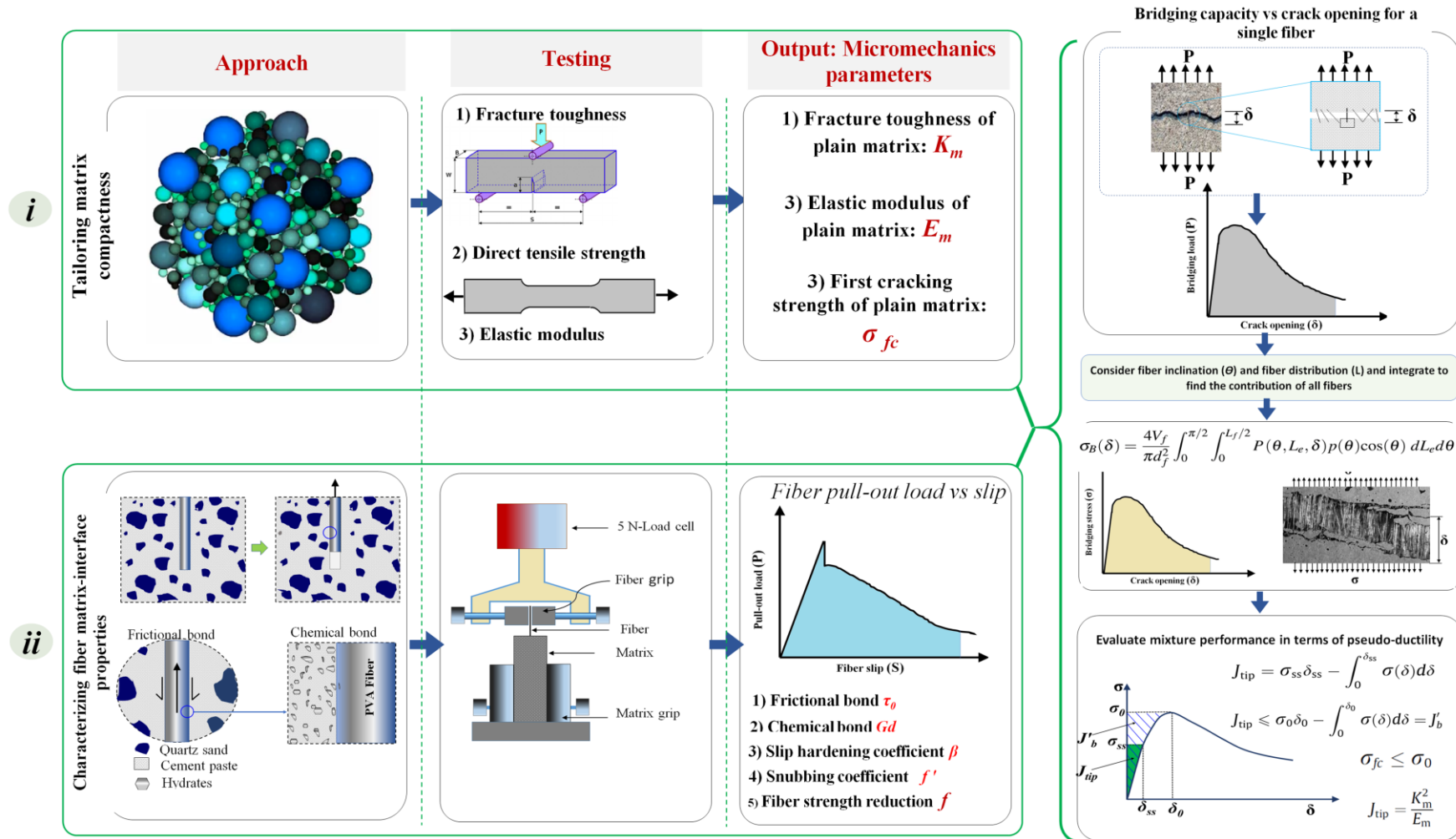


Fig. 1. Multi-scale design framework of SHCC with HVGP

3 Tailoring of HVGP-SHCC

SHCC mixtures developed in this study went through a two-stage tailoring process as highlighted earlier. The first concerns the optimization of matrix packing density whereby particle packing optimization was employed to carry a guided replacement of FA with GP in order to primarily control matrix fracture properties (elastic modulus, tensile strength, and toughness) and implicitly the distribution of initial flow size. Both parameters are intrinsic determinants of pseudo-ductile behavior of SHCC. The second level concerns the implementation of micromechanical tailoring of matrix and the fiber/matrix interface whereby single fiber pull-out test was employed to obtain the fiber bridging capacity of different SHCC mixtures in light of various binary combinations of FA and GP.

3.1 Particle packing optimization

In this study, GP has been used as a replacement of FA under the guidance of particle packing optimization. To optimize particle packing, the compressible packing model proposed by de Larrard [40] was used. Model input parameters consist of (i) the packing density (ϕ) of individual particle groups and their accompanying compaction energy (K), (ii) particle size distribution (PSD) of individual particle sets, and (iii) mixture proportions of individual particle sets [31]. Thus, for a given packing with a given K , the model can predict the theoretical packing density (ϕ) indirectly through Eq. (1)

$$K = \sum_{i=1}^n K_i = \sum_{i=1}^n \frac{\gamma_i \beta_i}{\phi \gamma_i} \quad (1)$$

Where γ_i = overall virtual packing density of the mixture, β_i =residual packing density obtained when the dominant class i is isolated and fully packed.

The values of β_i are defined as in Eq. (2) where y_i is the volume fraction of the size class i .

$$\gamma_i = \frac{\beta_i}{1 - \sum_{j=1}^{i-1} \left[1 - \beta_i + b_{ij} \beta_i \left(1 - \frac{1}{\beta_j} \right) \right] y_j - \sum_{j=i+1}^n \left[1 - a_{ij} \left(1 - \frac{\beta_i}{\beta_j} \right) \right]} \quad (2)$$

where b_{ij} =wall effect, the effect of larger particles on creating voids in the matrix [Eq. (3)], and a_{ij} =loosening effect (the effect of small particles pushing larger particles apart [Eq. (4)])

$$a_{ij} = \sqrt{1 - \left(1 - \frac{d_j}{d_i}\right)^{1.02}} \quad ; \quad d_i > d_j \quad (3)$$

$$b_{ij} = 1 - \left(1 - \frac{d_i}{d_j}\right)^{1.5} \quad ; \quad d_i > d_j \quad (4)$$

where d_i and d_j represent the average particle diameters of the i^{th} and j^{th} size class, respectively.

3.2 Micromechanical tailoring of HVGP-SHCC

The design of SHCC mixtures is built on tailoring matrix, fiber, and fiber-matrix interface along with their associated parameters: [(fiber volume fraction, length, diameter, strength, and elastic modulus, etc. for fiber); (fracture toughness, elastic modulus, and tensile strength etc. for the matrix); and (chemical and frictional bonds, slip-hardening behavior, snubbing effect, etc. for fiber/matrix interface)] [4, 41]. This process elevates composite development from the serendipity of trial-and-error tests to a systematic and guided selection of these micromechanical parameters so that their coupled effect culminates into a composite exhibiting pseudo-ductility at fairly low fiber volume fraction commonly $\leq 2\%$ [1-3]. Emanating from flat crack analyses of ceramics composites reinforced with continuous aligned fibers [42], micromechanical tailoring model was introduced in cement and concrete composites by Li and collaborators [1, 2, 5] and was later improved by Lin et al. [42], Yang et al. [19] and Kanda and Li [41].

The development of pseudo-ductile composites following micromechanics tailoring dictates that for a given composite to exhibit strain-hardening behavior featured by steady-state (flat) crack growth, two criteria must be met, or the more common Griffith crack propagation mode will prevail, leading to quasi-brittle failure of traditional FRC matrices. The two criteria are (i) strength criterion and (ii) energy criterion. Strength criterion requires the matrix first crack strength (σ_{fc}) controlled by matrix fracture toughness (K_m) and initial flaw sizes to be less than fiber bridging capacity (σ_0) on any given potential crack plane as presented in Eq. (5)

$$\sigma_{fc} \leq \sigma_0 \quad (5)$$

On the other hand, the energy criterion stipulates that, for a crack (once generated) to grow in a steady-state mode (the state where tensile strength uncouples from crack length, in

contrast to the well-known Griffith residual strength concept relating a decreasing tensile strength to increasing crack size [42], the following energy balance [Eq. (6)] has to be satisfied.

$$J_{tip} = \sigma_{ss}\delta_{ss} - \int_0^{\delta_{ss}} \sigma(\delta)d\delta \quad (6)$$

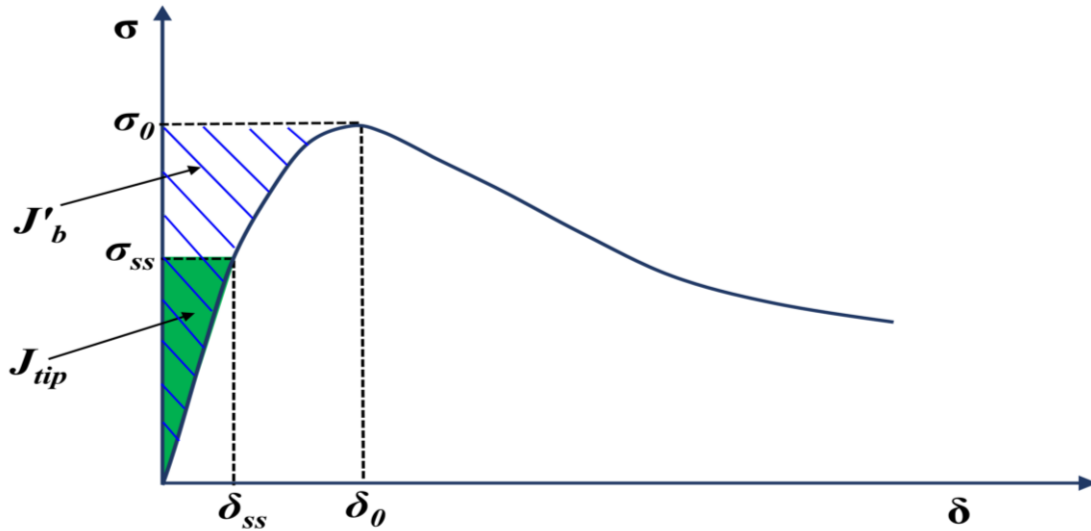


Fig. 2. Fiber bridging stress – crack opening width relationship as linked to pseudo-ductility conditions

In Eq (6), it is observable J_{tip} reaches its upper limit under the following conditions:

$$\begin{cases} \sigma_{ss} = \sigma_0 \\ \delta_{ss} = \delta_0 \\ \sigma_0\delta_0 - \int_0^{\delta_0} \sigma(\delta)d\delta \equiv J'_b \end{cases} \quad (7)$$

where σ_{ss} is the steady-state cracking stress; δ_{ss} is the flat crack opening corresponding to σ_{ss} (Fig. 2); J_{tip} is the crack tip toughness, which can be approximated as the cementitious matrix toughness if fiber volume fraction is less than 5%, calculated as in Eq. (6); σ_0 is the maximum bridging stress which corresponds to the crack opening δ_0 and J'_b is the complementary energy controlled by fiber bridging stress and determined from the $\sigma(\delta)$ curve.

$$J_{tip} = \frac{K_m^2}{E_m} \quad (8)$$

where K_m and E_m are, respectively, the fracture toughness of Young modulus of elasticity of the matrix.

In consequence of Eq. (7), for crack growth to follow a steady-state mode (necessary for pseudo-ductility behavior), the crack tip toughness should not exceed the complementary energy as below:

$$J_{tip} \leq J'_b \quad (9)$$

As such, for a matrix to exhibit a tensile strain-hardening behavior, both criteria (strength and energy) must be satisfied. Otherwise, the tension-softening behavior of traditional FRC will prevail. In this regard, while some conventional FRC may satisfy the strength criteria (governing the range of matrix flaw size), the energy criteria (governing the propagation of steady-state crack) excludes most conventional FRC and is only met with micromechanically tailored SHCC.

In the context of the current study, fiber (RECS 15 PVA fiber) parameters were kept constant, while the matrix and the fiber/matrix interface parameters were subjected to micromechanical tailoring. Matrix parameters (influenced by variable GP replacement of FA) were obtained by fracture toughness, elastic modulus, and direct tensile strength tests of non-fibrillated matrices. On the other hand, fiber/matrix interface parameters were obtained through the single-fiber pull-out test. The compiled micromechanical parameters were used to develop the σ (δ) curve for the different HVGP-SHCC formulations.

4 Experimental Program

The experimental program involves two phases. The first phase was conducted on plain matrices (fibreless or suspended mortars) and deals with the effect of GP on micromechanics parameters (matrix elastic modulus (E), fracture toughness (K_m), ultimate tensile strength (σ_{fc}), and fiber/matrix interface properties). The second phase concerns the composite performance where the effect of different GP content on composite compressive strength, flexural capacity, and direct tensile behavior was evaluated. Details about the experimental program are provided in the following sections.

4.1 Materials properties

SHCC ingredients in both experimental phases include high-sulfate-resistance cement (type HS) with low C_3A content, type F- fly ash (FA), type GH glass powder (GP), and quartz sand (QS). Type HS cement was chosen to optimize mixture flowability, owing to the low C_3A and C_3S contents allowing better flow properties [44]. The cement has a specific gravity (SG) of 3.18, Blaine fineness of 438 m^2/kg , and mean particle diameter (d_{50}) of 12 μm . The

FA used in the study fulfills the requirements of CAN/CSA A3000 specifications and has an SG of 2.55, Blaine surface area of $363 \text{ m}^2/\text{kg}$, and d_{50} of 17. The GP used herein is of high alkali content and has an SG of 2.51 and d_{50} of $27 \mu\text{m}$. As for the QS, it has an SG of 2.70, maximum particle-size (d_{max}) of $600 \mu\text{m}$, and mean particle-size (d_{50}) of $250 \mu\text{m}$. Table 1 presents the chemical composition and physical properties of all granular materials used in this study, Fig. 3 provides their particle-size distribution, and Fig. 4 presents scanning electron microscope (SEM) micrographs of FA [Fig. 4 (a)] and GP [Fig. (b)] used in this study. Polyvinyl-alcohol (PVA) fibers (Fig. 5) were added at 2% per volume of suspended mortar. The fiber has $38 \mu\text{m}$ diameter and 8 mm length, 40 GPa elastic modulus and 1400 MPa tensile strength.

Table 1. Chemical compositions of powders and granular materials used in the study

Composition	Quartz Sand	Type HS Cement	Type F Fly Ash	Type GH Glass Powder
SiO ₂	99.8	22	53.7	73.00
Fe ₂ O ₃	0.04	4.3	5.6	0.40
Al ₂ O ₃	0.14	3.5	17.5	1.50
CaO	0.17	65.6	12.4	11.30
TiO ₂	0.02	0.2	—	0.04
SO ₃	—	2.3	—	—
MgO	0.008	1.9	2.1	1.20
Na ₂ O	—	0.07	1.6	13.00
K ₂ O	0.05	0.8	2.0	0.50
ZnO	—	0.09	—	—
LOI	0.2	1.0	1.8	0.60
C ₃ S	—	50	—	—
C ₂ S	—	25	—	—
C ₃ A	—	2.0	—	—
C ₄ AF	—	14	—	—
Blaine (m ² /kg)		438	363	308

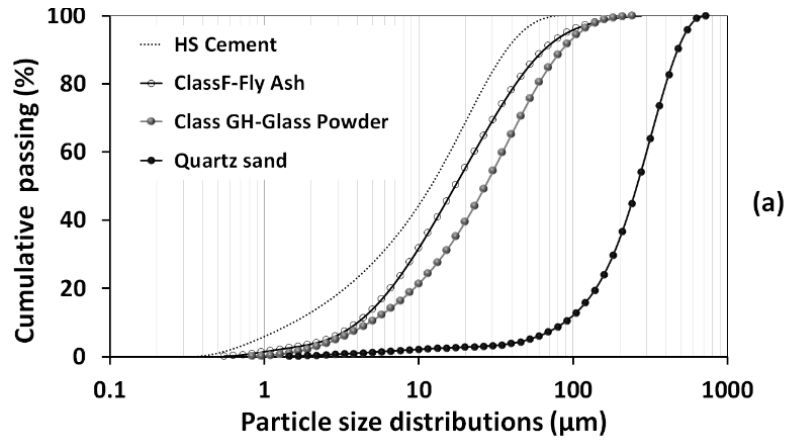


Fig. 3. Particle size distribution of SHCC ingredients

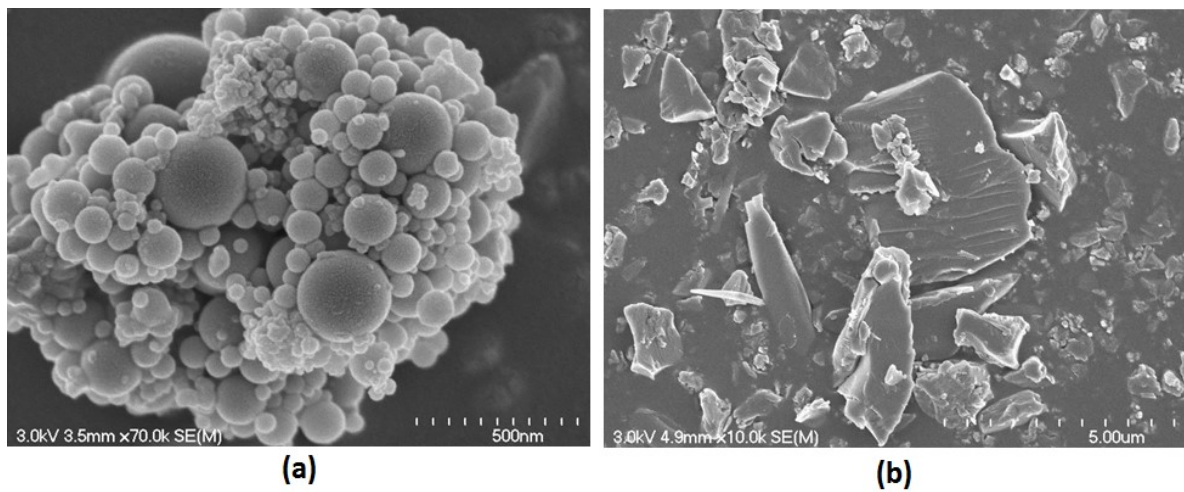


Fig. 4. SEM micrographs of SHCC ingredients: (a) HS Cement, (b) Class F Fly ash, and (c) Glass powder, (d) Quartz sand

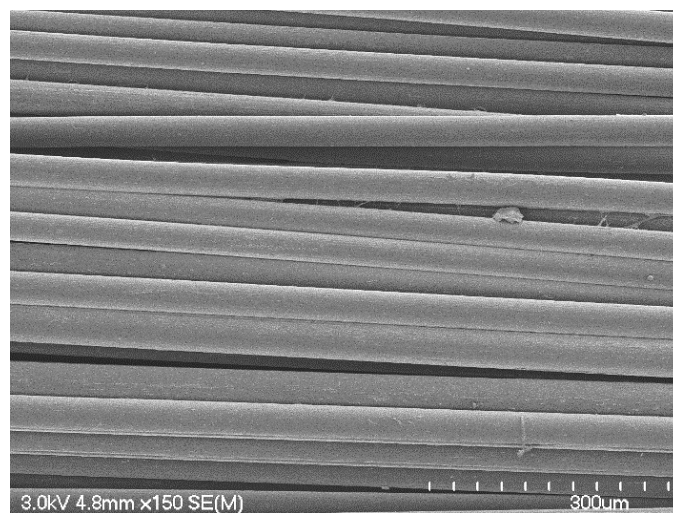


Fig. 5. SEM micrographs of polyvinyl alcohol (PVA) fibers (RECS 15) used in this study

4.2 Mixture proportions

A basic SHCC mixture with FA/cement ratio of 1.2, QS to binder ratio of 0.35 and a water-to-binder (w/b) ratio of 0.28 was considered. A total of six SHHC mixtures were developed. The mixtures consist of different ternary (cement, FA, GP) blends with variable binary combinations of GP and FA (GP in replacement of FA at 0, 20, 40, 60, 80, and 100%) as shown in Table 2. The replacement of FA with GP was guided by the optimization of matrix packing density. The resulting mixtures were then tailored via the micromechanics design approach of SHCC proposed by Li et al. [1, 2, 5]. This resulted in a coupled tool blending the particle packing optimization to ensure high strength, with the micromechanical tailoring approach to ensure high ductility.

Mixture nomenclature consists of two parts, the first designating the percentage of FA (based on FA/cement ratio of 1.2) and the second designating the percentage of GP in replacement of FA. In any mixture, the binary combination of FA and GP adds up to 100 and corresponds to $(FA+GP)/cement = 1.2$. For instance, the mixture 100FA-0GP refers to the reference formulation with FA/cement=1.2 without any GP added. The mixture 60FA-40GP corresponds to 60% FA content with 40% FA content replaced with GP. While the mixture 0FA-100GP refers to complete replacement of FA with GP. A poly-carboxylate (PCE)-based high-range water reducing admixture (HRWRA) with a SG of 1.09 and solid content of 40%, fulfilling the requirements of ASTM C494 Type F admixtures [45] was used to secure the target mini-slump flow diameter of 300 ± 15 mm for phase 1 (suspended mortar) and 250 ± 15 mm for phase 2 (fibrillated matrix).

Table 2. Mix design of HVGP SHCC

No.	Mixture name	Mixture Composition (kg/m ³)							Packing density (PD)	HRWRA (solid extract)
		Cement	Fly ash (FA)	Glass powder (GP)	Quartz sand (QS)	Water	Water/binder (W/B)			
1	M100FA-0GP	597	717	—	460	366	0.28	0.64	3.251	
2	M80FA-20GP	597	576	143	459	365	0.28	0.66	3.609	
3	M60FA-40GP	596	429	286	459	364	0.28	0.70	4.433	
4	M40FA-60GP	595	286	429	458	364	0.28	0.71	4.802	
5	M20FA-80GP	595	143	576	458	363	0.28	0.73	6.172	
6	M0FA-100GP	593	—	717	458	360	0.28	0.74	9.136	

4.3 Mixing procedures and specimen preparations

Batching of different SHCC mixtures was carried out using a pan mixer of type Mortarman 360 (Imer, CA, USA). In an attempt to deflocculate powder agglomerates and enhance mixture homogeneity, all powders and granular materials were dry-mixed for 7 min prior to adding water and HRWRA. In the second step, 90% of the HRWRA diluted into 95% of the mixing water was added to the mixer slowly during 0.5 min then mixing continued for 2.5 min. As the rheology of SHCC is quite delicate, the remaining 10% of HRWRA is left for final adjustment of mixture flowability such that the exact HRWRA would be determined on a performance basis. In the third step, the mixer was stopped for 0.5 min to scrape its blades and edges then mixing continued for another 1 min. The consistency of the suspended mortar was then checked such that when a mini-slump flow diameter of 300 ± 20 mm was obtained [46], only the remaining water is added (after adjustment of the amount of water contained in the unused 10% of HRWRA). Otherwise, a gradual amount of HRWRA is added (along with an adjusted amount of the remaining 5% of water) until the desired 300 ± 20 mm mini-slump flow diameter is achieved.

For phase I experiments (conducted on plain SHCC) to characterize micromechanical parameters (E , K_m and interface properties), the resulting mixture was cast into the required test specimens. On the other hand, for phase II experiments involving the performance of SHCC as a composite (in the presence of PVA fibers), the PVA fibers were added slowly during 1 min. Mixing continued for another 3 minutes to allow PVA fibers to be evenly dispersed. Finally, following 2 minutes of rest, concrete is remixed for 1 minute then cast for the different tests. Specimens for mechanical properties were covered with plastic sheets and kept in a room with relative humidity and temperature of approximately 50% and 23 °C, respectively then demolded 24 ± 1 h later. The specimens were then sealed inside plastic bags then transferred for storage in a fog room at 100% RH and 22 °C temperature until the age of testing. The different test methods adopted to execute the experimental program are elaborated in the following sections.

4.4 Test methods

4.4.1 Packing density

Using the CPM [40], the packing density (ϕ) of different SHCC with varying combinations of FA and GP were determined. Input parameters include: (i) the particle size distribution (PSD) of each granular material, (ii) the packing density (ϕ) of each granular material and the corresponding compaction energy (K), and (iii) mixture proportions [49]. The packing density (ϕ) for the powders, namely, Cement, FA, and GP ($d_{50} < 125 \mu\text{m}$), was indirectly obtained from the Vicat water consistency test [48] which allows to determine the minimum water necessary for normal consistency (a needle penetration of $10 \pm 0.5 \text{ mm}$). According to references [49], this test allows to correlate between the minimum water demand (w) and the void content in the mixture such that the packing density ϕ can be obtained from the following relationship (Eq. 10):

$$\phi = \frac{1}{1 + \rho_s (w/s)} \quad (10)$$

where, ρ_s = density of the solids, w = mass of water mass, and s = mass of solids.

As for the Quartz sand (QS) where $d_{50} \geq 125 \mu\text{m}$, a dry-packing by the gyratory intensive-compaction-test (ICT) method [46] was used to determine the packing density ϕ as in the following equation (Eq. 11):

$$\phi = \frac{w}{V_c \cdot SG} \quad (11)$$

where w = weight of QS, SG = specific gravity of sand, V_c = volume of container

Following these procedures, the value of ϕ for cement, FA, GP, and QS were determined as 0.56, 0.58, 0.49, and 0.61, respectively. The packing index (K) which depends on the compaction method was obtained from [40] as $K = 6.7$ for the powders (cement, FA and GP) and $K = 9.0$ for QS. The value ϕ and the accompanying K , the PSD, as well as mixture

proportions in terms of individual particle groups were used as input in the CPM to calculate the packing density (ϕ) of the different SHCC formulations.

4.4.2 Fresh properties

The unit weight, air content (ASTM C 185) [50], and mini-slump flow test (ASTM C 1437) [51] were measured to evaluate the fresh properties of different SHCC formulations for both test phases.

4.4.3 Phase I Tests: Micromechanics and fracture tests on SHCC matrix

To compile the parameters required for micromechanical tailoring of SHCC mixtures, fracture toughness, direct tension, and single fiber pull-out tests were conducted on the plain (non-fibrous) elements.

4.4.3.1 Matrix elastic Modulus

Elastic modulus of the matrix (E_m) was evaluated on 100×200 cylinders at 28 and 91 days following the procedures described in ASTM C469 [52].

4.4.3.2 Matrix fracture toughness

Fracture toughness (K_m) test was performed following a procedure adapted from ASTM E399 [53]. The test was conducted on 100×100×400 mm prisms (of 25 mm deep, 3 mm central notch) tested in three-point bending configuration in a displacement-controlled mode using a displacement rate of 0.05 mm/min. The notch depth was subsequently remeasured, and K_m was calculated according to Eq. 12 below:

$$K_m = \frac{P_Q S}{B W^{3/2}} * f\left(\frac{a}{w}\right) \quad (12)$$

where P_Q is the applied load, S the span width, B the prism height, w the specimen depth, and $f(a/w)$ is a calibration factor (ranging between 1.91 and 2.18 with respect to the accurate notch depth) [11, 53]. Test set-up for evaluating K_m is depicted in Fig.6 which also illustrates the variable used in Eq. (12). While the adapted test guidelines were initially set for metals and alloys, the fracture toughness obtained based on this method is also reliable for cement composites with maximum aggregate size of 1000 μm [11], such as the case of the SHCC developed herein with maximum QS size of 600 μm .



Fig. 6. Fracture toughness test: (a) Test set-up illustrating the variables used in Eq. (12), and (b) Test samples

4.4.3.3 Direct tensile strength

This test was carried-out on dog-bone shaped coupons (Fig. 7) in order to determine the tensile strength of the plain matrix (σ_{fc}). The test was conducted under a displacement-controlled mode at a rate of 0.2 mm/min. The test set-up is equipped with a 24.4 mm wire extensometer attached at the middle of sample. This is supplemented with a laser-type extensometer such that all elastic and plastic deformations are well captured. This is particularly important for phase II tests where at composite level, SHCC coupons subjected to uniaxial tension develop intensive multiple cracking extending beyond the reading range of the laser extensimeter, which lead to relaxation in the reading. The use of laser extensometer in companion allows correcting such errors.

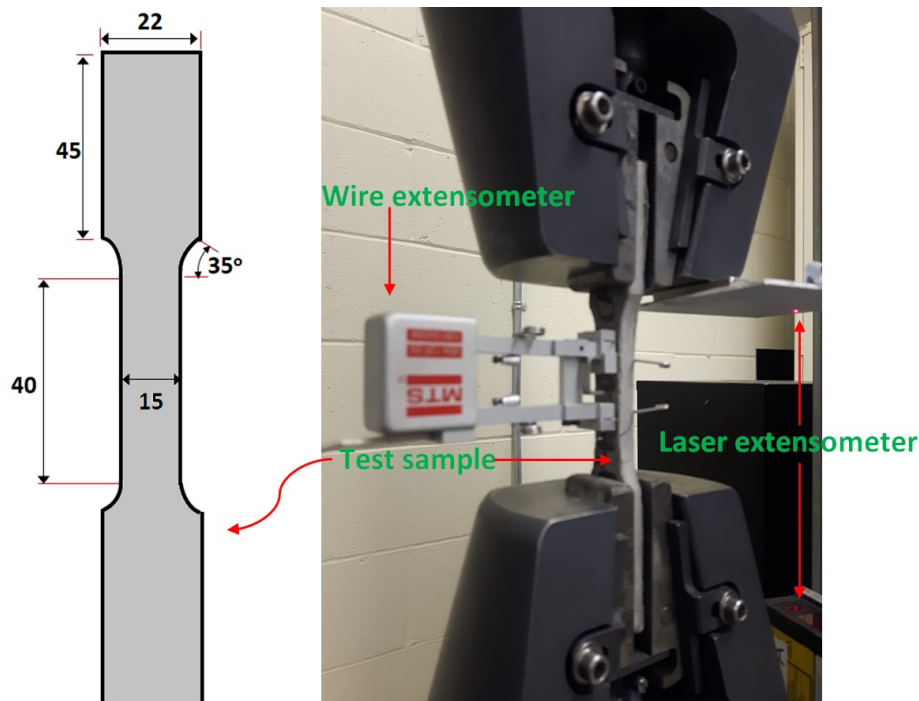


Fig. 7. Uniaxial tension test: The figure illustrates sample dimensions (left) and test configuration (right)

4.4.3.4 Single fiber pull-out

Single fiber pull-out test (SFPT) was conducted to evaluate fiber/matrix interface properties necessary for micromechanical modeling. Owing to the high precision requirements in SFPT, a miniature load cell of 5-N capacity of Zwick type (ZwickRoell, Germany) was used for this purpose. Test was conducted under a displacement-controlled mode at a rate of 0.2 mm/min in consistence with the loading rate adopted for the direct tension coupon tests. To minimize elastic stretching, the fiber was gripped at less than 1 mm from the matrix top surface. Fig. 8 (a) illustrates the test set-up of SFPT, while Fig. 8 (b) depicts the actual test configuration where two PVA fibers are visible one of which being tested. For each mixture, 4-7 successful SFPT were obtained. Following the above procedures, fiber pull-out load versus fiber slip response was recorded for all mixtures. This allowed to determine fiber/matrix interface properties in terms of frictional bond (τ_0), chemical bond (G_d), and slip hardening coefficient (β). These properties were further used to characterize the fiber bridging capacity and develop fiber-bridging stress versus crack-opening response $\sigma(\delta)$ for the different formulations.

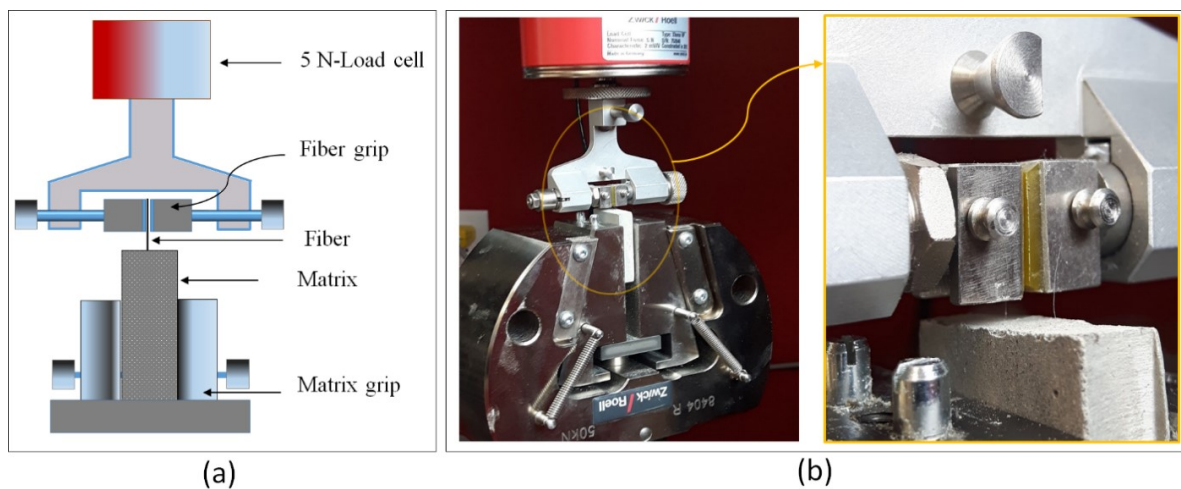


Fig. 8. Single-fiber pull-out test: Schematic of test set-up (a), actual test configuration with a focus on a single fiber being pulled from the matrix (b)

4.4.4 Phase II Tests: Performance of SHCC composites

Tests conducted in Phase I constitute the groundwork for the development of SHCC. The developed SHCC mixtures were then evaluated for hardened performance in terms of direct tensile strength (f_t), flexural capacity (f_{fl}), compressive strength (f_c), and durability aspects (bulk resistivity, ρ). The f_t was evaluated at 28 days following the same procedures and

specimen dimensions described earlier for the case of plain matrix (section 4.4.3.3). The f_{jt} was evaluated on 100×100×400 mm prisms (ASTM C78-18) [54] at 28 days. Flexural tests were performed under four-point bending configuration in a displacement-controlled mode using a displacement rate of 0.05 mm/min. The f_c was assessed on 50×50×50 mm cubes (ASTM C109-16) [55] at 1, 7, 28, 56, and 91 days.

To assess the durability aspects of SHCC as a composite, the electrical bulk resistivity was used as alternative to the most widely adopted rapid chloride permeability (RCP) test. As the RCP test itself relies on measuring the total electrical charge (passing through a specimen subjected to a standard voltage) to provide an indication of the ability of concrete to resist chloride-ion penetration, this test has been argued to directly measure chloride permeability [56]. Rather, RCP test was developed by correlating a measured charge to the total chloride penetrating to a depth of 41 mm of reference slabs subjected to a 90-day ponding test [57]. For this, the electrical bulk resistivity as used in this study can be an alternative tool for performance-based evaluation of concrete resistance to chloride ion penetrability. The electrical resistivity was evaluated on 50×50×50 mm SHCC cubes at 1, 7, 28, 56, and 91 days. All measurements were taken right after removal from the curing room to ensure comparable moisture state. Two electrodes were placed on the two ends of the specimen, a voltage was applied, the potential difference was recorded and electrical resistivity was determined as $\rho = R \cdot (A/l)$, with R being the electrical resistance (Ω), A being the cross-sectional area of the specimen (m^2), and l being specimen length (m). Durability was then assessed based on different electrical resistivity classes [58].

5 Results analysis and discussions

5.1 Results of SHCC matrix used for micromechanical investigation

5.1.1 Optimization of matrix packing density

The packing density for the different SHCC formulations are reported in Table 2. Results indicate that incorporating GP increased the packing density from 64% in the reference SHCC (with no GP) to 66, 70, 72, 73, and 74%, respectively, in the SHCC mixtures with 20, 40, 60, 80, and 100% replacement of FA with GP. This is further substantiated by the combined particle size distribution (PSD) for the different SHCC formulations depicted in Fig. 9. The figure indicates that at increasing replacement of FA with GP, a wider range of

particle size is obtained and higher packing density is achieved, taking into account particle form. The influence of incorporating GP on increasing the packing density can also be explained by the effect of the gradation of different granular materials (PSD) presented earlier in Fig. 2. The figure shows that the PSD curve for GP falls between that of QS from one side that of FA and cement from another side. The incorporation of GP facilitates filling the particle gap between QS and the powders. In other words, GP (with a mean particle size (d_{50}) of 27 μm) being coarser than both cement ($d_{50} = 12 \mu\text{m}$) and FA ($d_{50} = 17 \mu\text{m}$) can allow filling the particle gap between the binders (cement and FA) and the QS ($d_{50} = 250 \mu\text{m}$) at smaller volume than equivalent mass of cement or FA. Additionally, when the larger GP particles replace the relatively smaller FA particles, the space occupied by every single larger GP particle (replacing few FA particles) does not contain voids anymore. As such, more volume becomes occupied by solid particles, thereby reducing the void space and increasing the compacity [59]. While it is largely believed that FA particles with their spherical shape [Fig. 5(b)] would minimize inter-particle friction; thereby increasing packing density, it should be noted that incorporating the irregularly shaped GP particles [Fig. 4 (b)] may not necessary harm packing density. Rather, it can improve compactness by providing more inter-particle friction [59]. The effect of GP on increasing the packing density can also be associated with the tendency of flaky GP particles towards forming a layered stacking [41].

While the increased packing density observed with GP can improve SHCC composite strength commonly lacked with HVFA is used [9, 11, 10, 12], it should be taken into consideration that higher packing density increases matrix fracture strength (K_m) [1, 3, 5]. Increasing K_m results into higher crack tip toughness ($J_{tip} = K_m^2/E_m$) which is a non-favorable feature for maintaining a steady-state cracking necessary for pseudo-ductility behavior of SHCC. Therefore, despite the potential gain in mechanical strength to be obtained by replacing FA with GP, strain-hardening criteria would require matrix packing density to be optimized (rather than maximized) as to be detailed in subsequent sections.

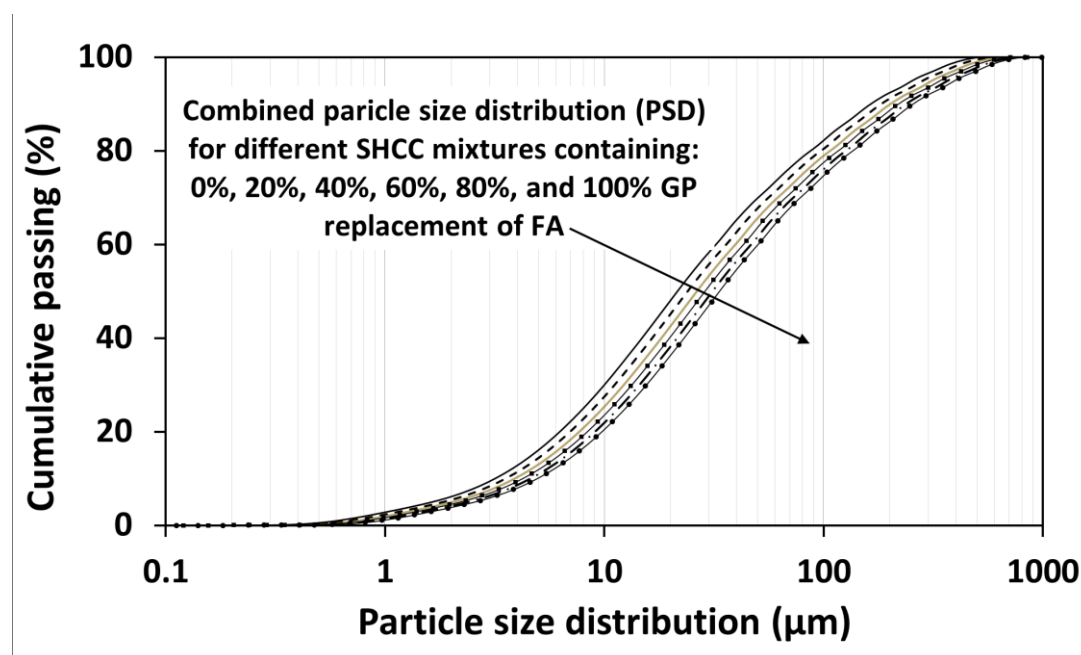


Fig. 9. Combined particle size distribution for the different SHCC formulations

5.1.2 Fresh properties

Table 3 presents the fresh properties of plain SHCC mixtures used for the micromechanical investigation. In retrospect to Table 2, results of fresh properties indicate that the incorporation of GP increases the demand in high-range water reducing admixture (HRWRA). In the presence of GP in SHCC, GP particles tend to fill-up the inter-particle space, thereby decreasing the space available for particle dynamics [59]. Thus, additional to the paste needed to fill-up the inter-particle space, an excess amount of paste is needed to lubricate the mix and give it enough workability. This explains why at increasing GP content, the demand in HRWRA also increased. On the other hand, the increase in HRWRA in the presence of GP may be associated with the excess inter-particle frictional forces generated by the irregularly-shaped, rough-edged glass particles [Fig. 3 (b)] as compared to the spherically-shaped smooth-surfaced FA particles [Fig. 3 (a)]

Therefore, for a target mini-slump flow diameter of 300 ± 20 mm in the suspended mortar, the incorporation of GP led to higher demand in HRWRA. In the context of developing HVGP-SHCC, the slump flow of 300 ± 20 mm in the suspended mortar was established with testing as a key requirement to obtain a flowable and stable SHCC mixture whereby the PVA fibers can be evenly distributed and strain-hardening behavior can be obtained. Thus, with

adequate adjustment of HRWRA, the slump flow of 300 ± 20 mm in the suspended mortar was achieved across all mixtures (Fig. 10). This allowed to obtain SHCC mixtures exhibiting self-consolidating ability with a slump flow of $\sim 250\pm 20$ mm as well a strain-hardening as to be detailed later.

Table 3. Fresh properties of SHCC plain formulations used for the micromechanical investigation

No.	Mixture name	Fresh properties			
		Slump-flow diameter (mm)	Air content (%)	Unit weight (kg/m^3)	Temperature ($^{\circ}\text{C}$)
1	M100FA-0GP	315	4.25	2034	21
2	M80FA-20GP	310	4.13	2037	20
3	M60FA-40GP	310	3.90	2039	22
5	M40FA-60GP	305	3.91	2040	21
5	M20FA-80GP	305	4.36	2039	21
6	M0FA-100GP	300	4.41	2035	23

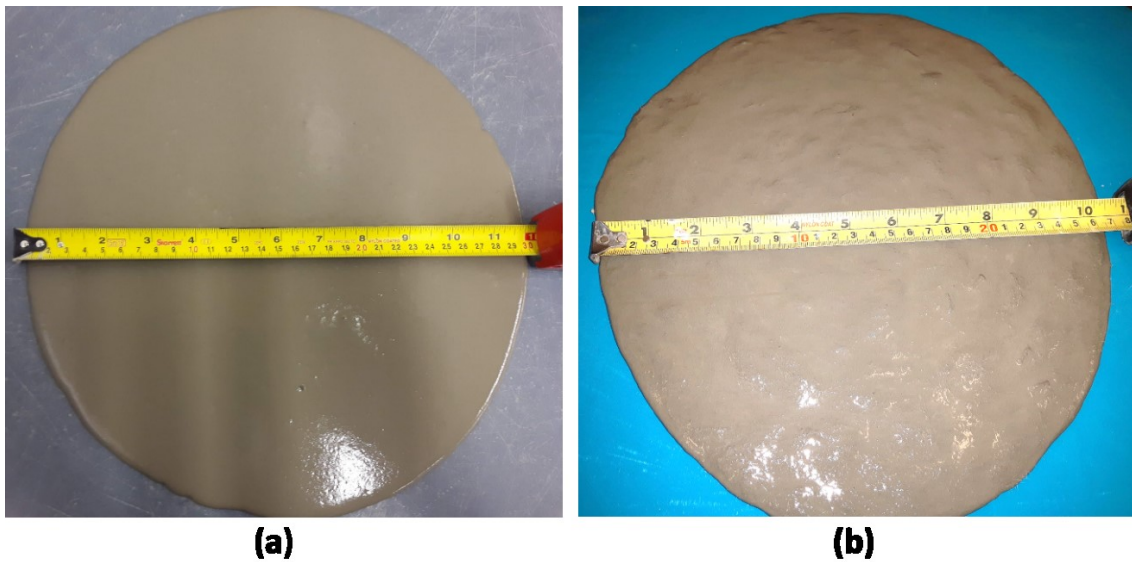


Fig. 10. Typical slump flow in the suspended mortar (a) and in the SHCC as a composite (b)

5.1.3 Micromechanical investigation

5.1.3.1 Effect of glass powder on micromechanical properties

Table 4 presents the results of the micromechanical investigation conducted in this study. With fiber parameters kept constant throughout this study, the table presents matrix and fiber/matrix interface parameters involved in constructing the $\sigma(\delta)$ response for the different SHCC formulations considered herein. Results of matrix parameters indicate that the incorporation of GP results into relatively higher elastic modulus (E_m), and significantly higher fracture toughness (K_m) and first crack strength (σ_{fc}). This can be attributed to both physical and chemical effects imparted by GP whereby the increased matrix compacity discussed in the previous section lowers the porosity and results into higher strength. On the other hand, the pozzolanic activity by GP can contribute towards forming new hydrates contributing to pore refinement and increasing matrix strength [28]. Nonetheless, since GP is used herein in replacement of FA which also exhibits pozzolanic activity and considering the late reactivity of GP [29], the effect of packing density on the observed matrix strength is likely to be more significant.

As for fiber/matrix interface parameters, the chemical bond (G_d) recorded a relatively decreasing trend with increasing GP content. The frictional bond (τ_θ) increased significantly with higher GP, while the slip hardening effect was negligible. The relatively decreasing G_d can be attributed to the effect of GP on altering the concentration of chemical species at the fiber/matrix interface. According to [9], the chemical adhesion between the hydrophilic PVA fibers exhibiting excess bonding to cement and high-volume fly ash (HVFA) matrix is governed by the metal cation concentration at the fiber/matrix interface, in particular Al^{3+} and Ca^{2+} [23, 23]. In this regard, the replacement of FA GP can be perceived to reduce the concentration of Al^{3+} and Ca^{2+} cations at fiber/matrix interface and result into a reduced chemical bonding between the matrix and the fibers as observed herein.

On the other hand, τ_θ increased significantly with the incorporation of GP. The increase in τ_θ is a direct implication of the higher compacity obtained with GP. At increasing GP content, the fiber/matrix interfacial transition zone become denser and stiffer, thereby increasing the frictional forces at pull-out. This feature can be viewed advantageous to increase the pull-out resistance of fibers, hence, to lead to SHCC exhibiting higher strength as targeted in this study. Tantamount, owing to the direct correlation between τ_θ and the maximum bringing stress (σ_0), if fiber rupture is to be ignored, it follows that higher τ_θ has the potential to increase

overall matrix ductility [38]. Nonetheless, it should be noted that excessive τ_0 can lead to fiber rupture or fiber surface damage [63], thereby reducing the slip distance and lowering composite ductility [43].

The effect of varying GP content on the slip hardening behavior is not evident. Negligible slip hardening ($\beta \approx 0$) was noticed at varying GP content. Nonetheless, it was observed that during single fiber pull-out tests, the frictional sliding phase is often characterized by constant friction ($\beta = 0$) at lower GP content. At high GP content, however, this behavior shifted towards fiber premature rupture or surface damage due to excessive frictional bond [63].

5.1.3.2 Effect of glass powder on fiber bridging capacity

The above results pertaining to the matrix and fiber/matrix interface parameters were used to construct the $\sigma(\delta)$ response shown in Fig. 11. The figure indicates that with increasing GP content, the maximum bridging stress (σ_0) increases. This is a direct consequence of the higher τ_0 associated with the increased matrix packing density and stiffness as highlighted earlier. Fig. 11 also indicates that the crack opening (δ_0) corresponding to the maximum bridging stress decreases with increasing GP content. As a result, the commentary energy J'_b [computed from the $\sigma(\delta)$ curve] is lower with higher GP. On the other hand, in consequence to the higher matrix elastic modulus E_m and matrix fracture toughness K_m (with the incorporation of GP) as discussed earlier, the matrix crack tip toughness (J_{tip}) is also higher (Table 4). Considering these micromechanical data, Table 4 indicates that all HVGP-SHCC formulations satisfy well the strength criterion ($\sigma_{fc} \leq \sigma_0$) for strain-hardening behavior as reflected by $\sigma_0/\sigma_{fc} > 1.45$ recommended by [41]. Satisfying the strength criterion of SHCC ensures that the bridging stress σ_0 carried by the fibers across cracked sections remains always higher than the cracking strength of the plain matrix σ_{fc} , or a quasi-brittle failure of conventional fiber reinforced concrete would take place [1, 4, 5]. Table 4 also indicate that all SHCC formulation developed herein satisfy the energy criterion ($J_{tip} \leq J'_b$) for strain-hardening behavior as reflected by $J'_b/J_{tip} > 1.0$ [1]. Satisfying this criterion ensures that, the matrix-cracking governed by the strength criterion (once occurred), propagates in a steady-state mode, otherwise non-stable crack propagation prevails, limiting the development of multiple cracking, thereby failing in quasi-brittle manner [42]. While some conventional FRC may satisfy the strength criterion, only micromechanically tailored cement composites

demonstrate the ability to simultaneously satisfy strength and energy criterion both of which are fundamental requirements of a pseudo-ductile metal like behavior.

Nonetheless, results indicate that the index J'_b/J_{tip} decrease with higher GP content. Strictly speaking, at $J'_b/J_{tip} < 1.0$, no multiple cracking can develop [1]. The reduced J'_b/J_{tip} index in systems with high GP content is a consequence of their higher matrix strength particularly K_m and reduced δ_0 which lead to lower J'_b but higher J_{tip} . These parameters are highly influenced by the fiber/matrix interface parameters. In line with these observations, the $\sigma(\delta)$ responses plotted in Fig. 11 demonstrate that at low GP content, $\sigma(\delta)$ curve have relatively lower σ_0 peak but a broader softening branch in consequence to the reduced τ_0 . On the other hand, at increasing GP, σ_0 peak increases while the softening branch narrows down in consequence to the increased τ_0 .

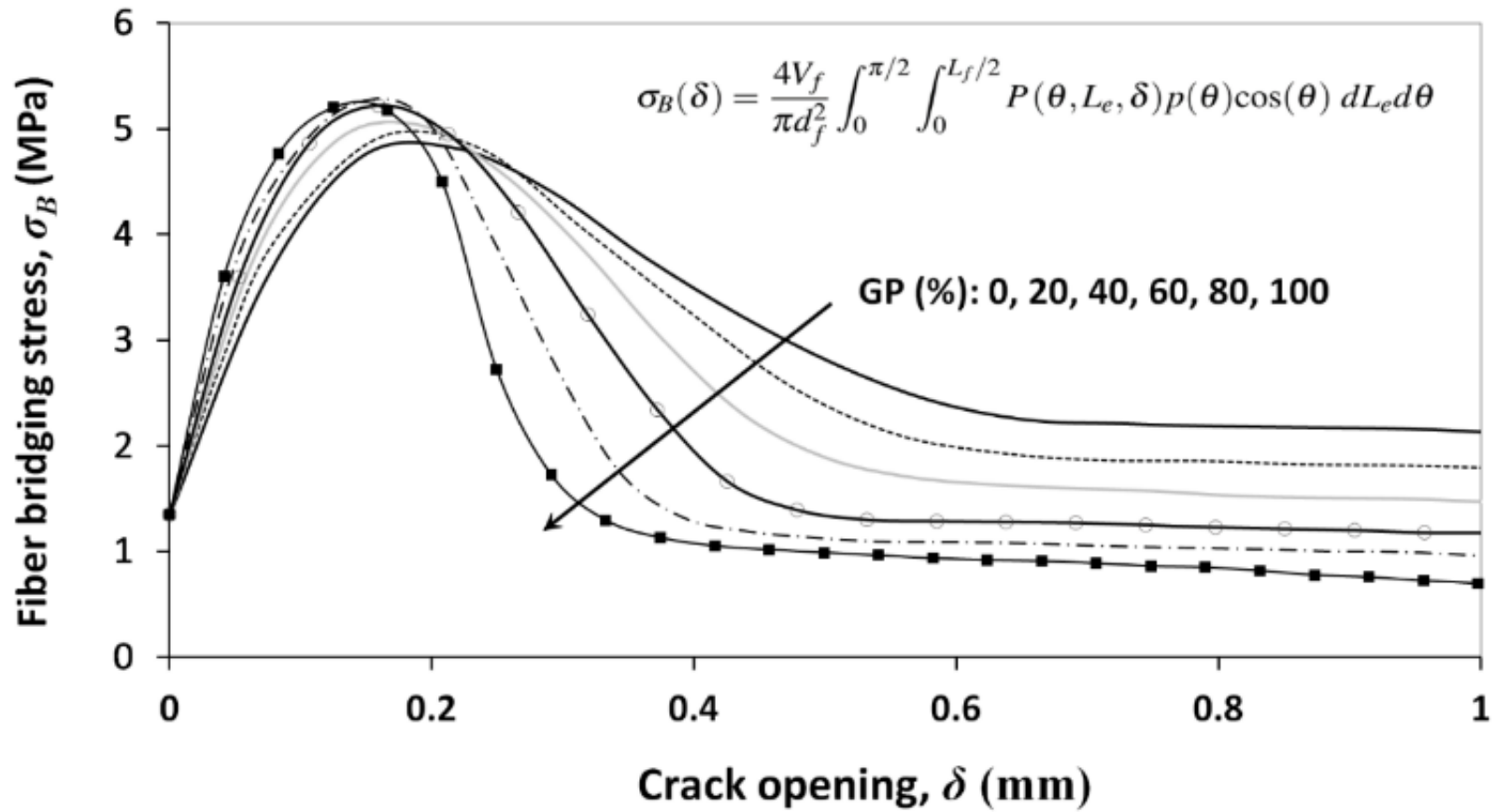


Fig. 11. Computed fiber bridging stress–crack opening relationship (σ – δ) for varying GP content

Table 4. Results of micromechanical investigation and SHCC strain-hardening indicators

No	Mixture name	Matrix parameters			Interface parameters			SHCC composite pseudo-ductility performance				
		Elastic modulus, E_m (GPa)	Fracture toughness, K_m (MPa. \sqrt{m})	First crack uniaxial strength, σ_{fc} (MPa)	Frictional bond, τ_0 (MPa)	Chemical bond, G_d (J/m ²)	slip hardening coefficient, β	Maximum bridging stress, σ_0 (MPa)	Complementary energy, J_b (J/m ²)	Crack tip toughness, J_{tip} (J/m ²)	$\frac{J_b}{J_{tip}}$	$\frac{\sigma_0}{\sigma_{fc}}$
1	M100FA-0GP	22.50±0.48	0.68±0.05	2.59±0.11	2.95±0.52	2.65±0.14	0.003	4.82	64	20.5	3.12	1.86
2	M80FA-20GP	22.75±0.56	0.69±0.04	2.52±0.08	3.10±0.40	2.61±0.18	0.006	4.91	34	20.9	1.63	1.95
3	M60FA-40GP	23.12±0.32	0.71±0.03	2.59±0.05	4.30±0.80	2.60±0.14	0.007	5.04	29	21.5	1.35	1.95
4	M40FA-60GP	23.10±0.55	0.73±0.06	2.74±0.09	4.62±0.89	2.57±0.10	0.001	5.22	27	22.8	1.18	1.91
5	M20FA-80GP	23.00±0.41	0.79±0.07	2.73±0.12	5.57±0.92	2.57±0.16	0.004	5.27	33	26.6	1.23	1.93
6	M0FA-100GP	22.81±0.11	0.81±0.06	2.81±0.10	6.84±0.80	2.56	— **	5.20	31	28.1	1.10	1.85

** No slip hardening was observed as fiber rupture was more common at increasing GP content

5.2 Results of SHCC composite performance

5.2.1 Compressive strength

Fig. 12 presents the development of compressive strength (f_c) up to 91 days for series I SHCC mixtures. The overall trend of strength development is strongly contingent to GP content and curing age. For up to 40% replacement of FA with GP, f_c is comparable (or slightly higher) to that of the reference mixture (0 GP) until 7 days. Beyond 7 days, higher f_c was obtained with GP. On the other hand, starting from 28 days, all GP contents showed higher strength than that of the reference, with the strength enhancement being more significant at lower replacement level of FA with GP ($\leq 40\%$). For instance, at 91 days, up to ~ 14 and 12% higher f_c can be achieved with 20 and 40% GP, respectively. The effect of GP on strength development is linked to both physical and chemical effects. While the increased packing density and the pozzolanic activity led by GP may imply higher strength, this is not evident at early ages when high GP content is used. The reason is that high GP content may dilute cement and reduce the formation of cement hydration products at early-age [30]. On the other hand, given the late pozzolanic activity of GP [29], the strength (comparable or slightly higher than that of the reference) achieved with of GP (≤ 40 replacement of FA) at early ages (1-7 days) can be partially attributed to the packing density, and to a catalyst effect whereby the high alkali content of GP may foster the hydration of FA in HVFA systems [65]. At later curing ages, however, both packing density and pozzolanic activity can influence strength. As such, the observed trend of strength development in systems with GP can also be linked to the strength activity index (SAI) which assesses the strength development of a blended system relative to that of a system with Portland cement [66]. A comparison of SAI of GP (with Blaine values in the range of 264-582 m^2/kg , which includes the Blaine of the tested GP=308 m^2/kg) to that of Class-F FA (with 73.6 % passing 325 mesh) by Shi et al. [32], indicated that, taking into account the effect of fineness [28, 29], GP generally shows lower SAI at early ages (up to 7 days) but comparable or higher SAI to that of FA at later ages (≥ 28 days). The effect of fineness may also explain the slightly higher strength achieved in HVFA system incorporating GP having comparable chemical composition (to the one used in this study) but exhibiting finer particles (Blaine=382 m^2/kg) [39].

Beside the packing density with GP discussed earlier, the contribution of GP into the strength development of FA-rich systems may also sprout from the synergetic effect between FA and GP. In this regard, the high amount of alkalis and aluminum released from dissolution of GP

and FA, respectively, are perceived to contribute towards forming new type of C-S-H close to C-(N, A)-S-H, with low Ca/Si ratio with potentially higher strength [67].

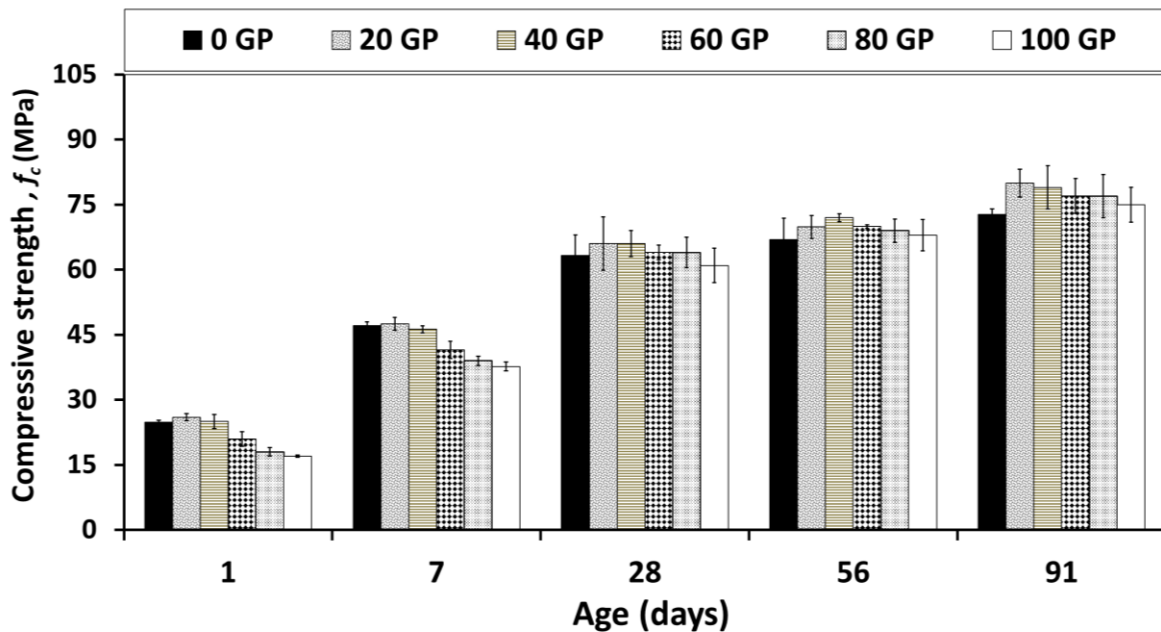


Fig. 12. Evolution of compressive strength in series I SHCC mixtures

5.2.2 Tensile and flexural properties

The composite tensile and flexural properties of the developed SHCC are analyzed based on the generalized composite behavior presented in Fig. 13 and in light of the micromechanical behavior presented in section 5.1.3. Based on Fig 13 (a), a cementitious matrix subjected to uniaxial tension will either exhibit a (i) brittle, (ii) quasi-brittle or (iii) pseudo-ductile response. In the first case, the tensile response is limited by the first cracking strength (σ_{cc}) which is the case of plain concrete (PC). In the latter two cases, the tensile response is rather controlled by the post-peak strength (σ_{pc}) whereby for a strain-hardening behavior to prevail, the condition $\sigma_{pc} \geq \sigma_{cc}$ must be met [68]. For this, a multiple cracking stage is an intrinsic feature manifested by a significant increase in the ultimate tensile strain (ε_u) before damage localization and response softening occur. Otherwise, a quasi-brittle failure (whereby beyond σ_{cc} , immediate softening follows) will prevail such as the case of conventional FRC. An analogous scenario exists when a cementitious matrix is subjected to flexural loading [Fig. 13 (b)]. In this case, beyond the brittle failure at first cracking load f_{cc} , the post peak behavior is rather characterized by either deflection softening or deflection hardening. In

spite of this analogy, strain-hardening is more of a material property and may be taken into account in structural design as it is scale-invariant [7]. Deflection-hardening, on contrast, is a structural property (influenced by the dimension and cross-sectional geometry of test specimen) and therefore is not a material property in the strict sense [68]. As such, strain-hardening composites are also deflection-hardening ones, but the vice-versa is does forcedly hold [7].

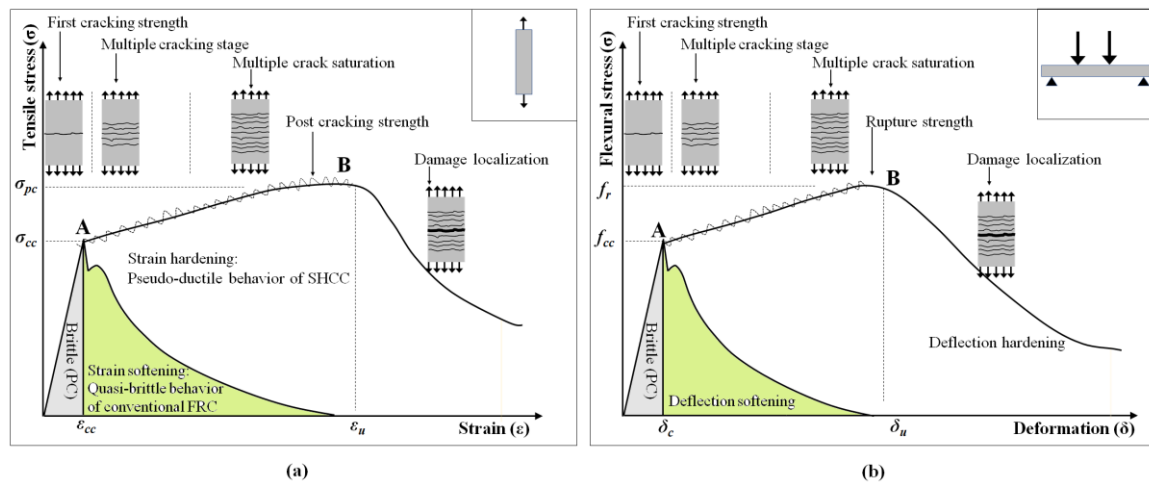


Fig. 13. Generalized response in uniaxial tension (a) and in flexure (b) for strain-hardening cementitious composites (SHCC) as compared to conventional fiber reinforced-concrete (FRC) and plain concrete (PC)

5.2.2.1 Direct tensile strength

Fig. 15 presents the results of uniaxial tensile behavior of series I SHCC mixtures. The figure shows the uniaxial behavior for three test samples per mixture for each of the six replacement rates of FA by GP (0, 20, 40, 60, 80, and 100%) [Fig. 15 (a)-(f), respectively]. As a general observation, GP allows achieving higher first cracking strength (σ_{cc}) as well as higher post-peak strength (σ_{pc}). For the above respective GP contents, σ_{cc} has increased from 2.08 MPa in the reference SHCC (0 GP) to 2.28, 3.15, 3.58, 3.82, and 4.47 MPa in the SHCC mixtures with 20, 40, 60, 80, and 100% GP. This corresponds to, respectively, 10, 48, 70, 81, and 112% higher σ_{cc} . Similarly, σ_{pc} increased from 3.34 MPa in the reference SHCC to 3.65, 4.00, 4.09, 4.18, and 5.12 MPa, respectively, in the SHCC mixtures with 20, 40, 60, 80, and 100% GP. This corresponds to, respectively, ~9, 20, 22, 26 and 53% higher σ_{pc} . Thus, with $\sigma_{pc} \geq \sigma_{cc}$ in all formulations, a strain-hardening behavior is expected for all tested SHCC mixtures.

In terms of ultimate tensile strain capacity (ε_u), SHCC with GP (up to 40%) have also demonstrated satisfactory ductility as reflected by ε_u values comparable to that of the reference SHCC with HVFA. The latter had ε_u of 3.01%, while for SHCC with 20, 40, and 60% GP, ε_u of 2.95, 2.78 and 2.62%, respectively, were recorded. This reveals that with HVGP (up to 40%), there is an opportunity to increase the strength characteristics of SHCC without dramatically jeopardizing the ductility. Nevertheless, at increasing GP content ($\geq 60\%$), lower ε_u was recorded. The average ε_u dropped from 3.01% in the reference SHCC, to respectively, 1.0 and 0.74% in the mixtures with 80 and 100% GP replacement of FA.

The above results can be interpreted in light of matrix and interface properties in the context of HVGP-SHCC discussed earlier. With the incorporation of GP, the increased matrix strength (driven by the packing density enhancement and pozzolanic reactivity) justifies the observed increase in σ_{pc} predominantly influenced by the matrix [68, 69]. On the other hand, given the partial contribution of fiber and interface properties towards σ_{cc} [70], the increased matrix compactness additional to the inherent irregular shape and rough-texture of GP particles lead to higher frictional bond between matrix and PVA fibers. This resulted into higher pull-out load, hence higher σ_{cc} . In contrast to the significantly increasing trend of σ_{cc} with higher GP content, the post peak strength (σ_{pc}), being governed by the fiber bridging capacity, showed a relatively lower trend. This can be associated with the effect of interface parameters on fiber bridging capacity whereby the higher frictional bond increases the likelihood of fiber damage (Fig. 14), thereby affecting the post-cracking strength σ_{pc} . This can also limit composite ductility [71] as demonstrated by the reduced ultimate tensile strain ε_u , particularly at higher GP content. Therefore, given the tight inverse relationship between strength and ductility in cement composites [1, 72, 74], the recorded lower ε_u at increasing GP content may be justified. Additional to the increased matrix strength and the higher frictional bond observed with GP, the inherent higher hardness (and the consequent intrinsic brittleness) of glass particles [75] can transpose a reduced ε_u in HVGP mixture.

In line with the tensile strain behavior, the multiple cracking behavior in the SHCCs with 20 and 40% GP was quite comparable to that with HVFA. However, multiple cracking slightly decreased at 60%GP, and significantly dropped at 80 and 100% GP. This is reflected by the frequency and intensity of load peaks inferred from the corresponding tensile stress-strain curves. In this regard, the tensile stress-strain response in the reference and in the mixtures with up to 60%GP were found to align with the general profile of the strain-hardening

behavior depicted in Fig. 13 (a), while for the mixtures with 80 and 100% GP, the tensile response was observed to shift from the strain-hardening profile of pseudo-ductile composites towards the quasi-brittle behavior of common FRC.

These above results on the uniaxial tensile performance of SHCC at the composite level are well in harmony with the results of our micromechanical investigation (section 5.1.3). Thus, at higher GP content, in agreement with the trend of increasing σ_{fc} and σ_{pc} (but decreasing ε_u) at the composite level, higher fiber bridging stress (σ_θ) accompanied with lower maximum crack opening (δ_θ) was observed at the micromechanical level. This was found to reduce the complementary energy J'_b . In light of the increasing J_{tip} driven by the higher matrix strength in HVGP, a reduced J'_b/J_{tip} was obtained at increasing GP content. The index J'_b/J_{tip} being a key indicator for steady-state crack growth can be cross-linked with the tensile strength behavior discussed above. Thus, the ratio J'_b/J_{tip} has dropped from 3.12 in the reference SHCC to 1.63, 1.35, 1.18, 1.23, and 1.1 in the SHCCs with 20, 40, 60, 80, and 100% GP. This is quite in good agreement with overall composite tensile performance in terms of tensile strain capacity ε_u and strain-hardening behavior.

On the other hand, composite tensile properties are also in consistence with the fiber/matrix interface properties indicating significant increase in frictional bond (with increasing GP) at the micromechanical level. This was found to lead to higher pull-out resistance carried by individual fibers, but, in contrast, resulted into shorter fiber slip. The latter was also accompanied, at instances, with higher likelihood of fiber rupture. This can be transposed into a deceased tensile strain capacity ε_u at the composite scale [71].

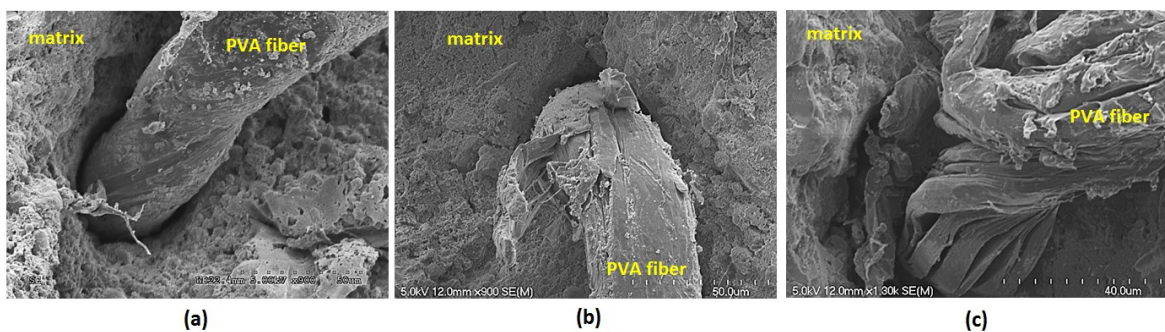


Fig. 14. PVA fiber status post-single fiber-fiber pull-out test in SHCC with: (a) 0% GP, (b) 40% GP, and (c) 100% GP. The figure illustrates fiber damage at increasing GP, which reflects the higher interface friction as well as pull-out load, but the consequent reduced slip at instances of fiber damage

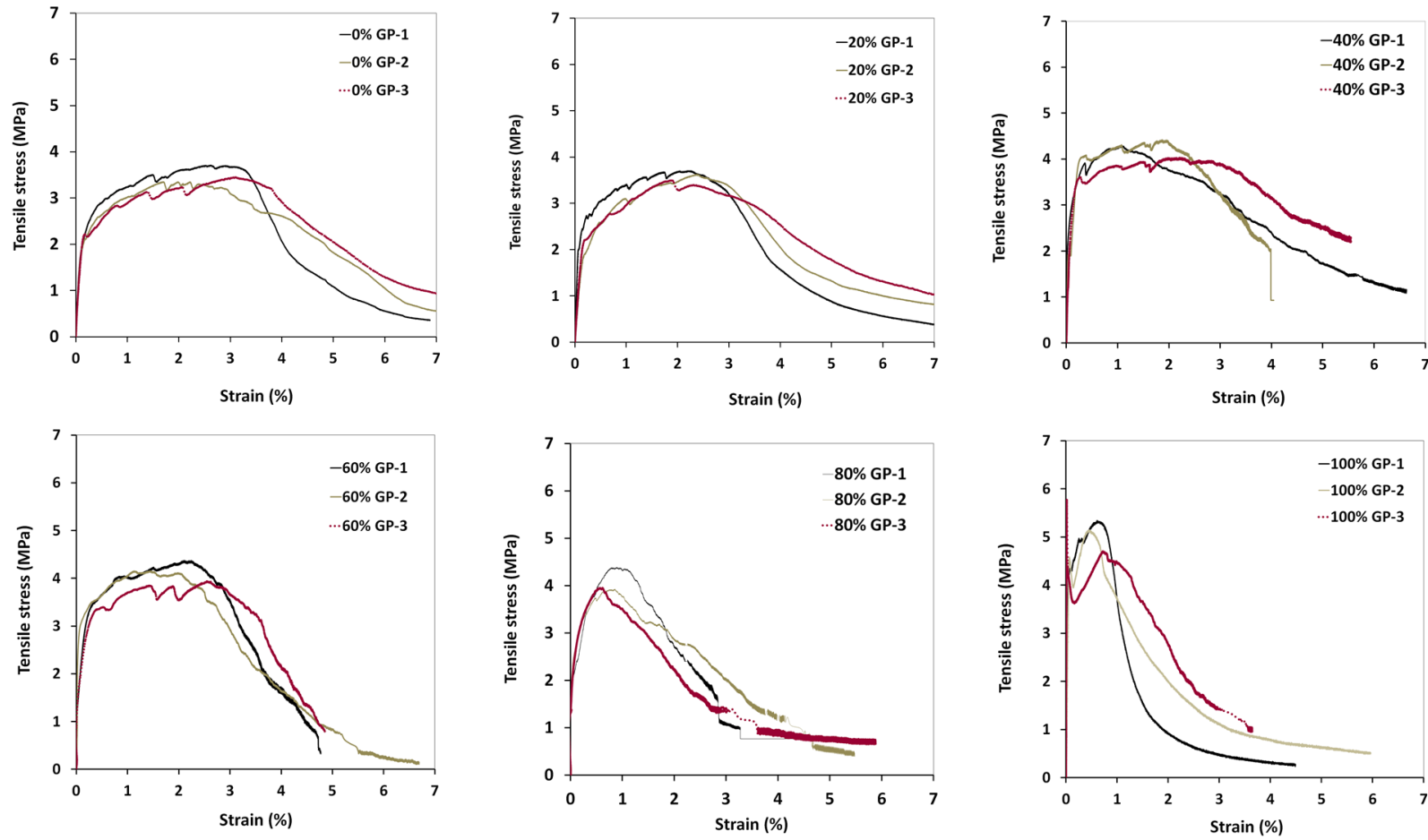


Fig. 15. Uniaxial tensile behavior of Series I SHCC mixtures

5.2.2.2 Flexural capacity

Fig. 16 presents the results of flexural capacity. Replacing FA with GP influenced both the flexural first cracking strength (f_{cc}) as well as the flexural post-cracking strength (f_{pc}) identified, respectively by A and B peaks in the generalized flexural response depicted earlier in Fig. 13 (b). However, the effect of GP on f_{cc} and f_{pc} are not similar. Increasing f_{cc} was observed with increasing GP, while for f_{pc} , up to 40% GP comparable values to the that of the reference were recorded. At $GP \geq 60\%$, f_{pc} experienced a decreasing trend. As such, for FA replacement with GP at 20, 40, 60, 80, and 100%, f_{cc} has been enhanced from 8.47 MPa in the reference SHCC to, respectively, 8.79, 9.10, 9.55, 10.52, and 11.14 MPa, which correspond to 4, 7, 13, 24, and 31% higher f_{cc} . On the other hand, as compared to the f_{pc} value of 14.41 MPa in the reference SHCC, f_{pc} values for the above respective GP contents were 14.83, 14.61, 11.20, 10.57, and 9.53 MPa. The above trend is in good agreement with the uniaxial tensile response described in the previous section where the first cracking strength (under uniaxial tension), σ_{cc} , recorded a significantly continuous increase with higher GP content, while the post peak strength (σ_{pc}), showed a relatively lower trend. The cracking strength in both cases are predominantly governed by the matrix where the increased packing imparted by GP plays an influential role as stated earlier. Furthermore, the higher frictional bond obtained with GP can partially contribute to withstanding higher load. In contrast, the post-peak strength in both tension and flexure (σ_{pc} and f_{pc}) are governed by fiber bridging capacity. As such, the response beyond matrix rupture (f_{cc}), is driven by the ability of fibers to resist the pull-out effect. Thus, at cracked sections the load is entirely transferred from the matrix via the interfacial bond to the bridging fibers. The latter transfer the applied load to uncracked sections in the matrix, which, at event of cracking transmit their load to available (non-puled-out or ruptured) fibers. This sequential process drives the extended deflection capacity (Fig. 17) and the associated development of multiple cracking (Fig. 18) and continues until no more fibers can transfer the applied load whereby the matrix fails by damage localization (widening of single crack at a stress corresponding to f_{pc}) [9].

In this sequence, it can be perceived that, while the higher frictional bond obtained with GP may foster higher pull-out load, the increased likelihood of fiber rupture may limit post-peak strength f_{pc} (as observed herein). This can explain the reduced ultimate mid-span deflection δ_u . The latter remained comparable to that of the reference SHCC for up to 40% GP, but decreased in intensity at higher GP content. This aligns well with the trend of the ultimate strain capacity ε_u observed in uniaxial tensile response presented earlier. As a result, the

flexural response of Fig. 16 reveals that with up to 40% GP, the deflection-hardening response as described in Fig. 13 (b) can be achieved. At $GP \geq 60$, despite the higher first cracking strength f_{cc} , the flexural response approaches a quasi-brittle behavior commonly encountered in conventional FRC due to matrix and interface parameters detailed above.

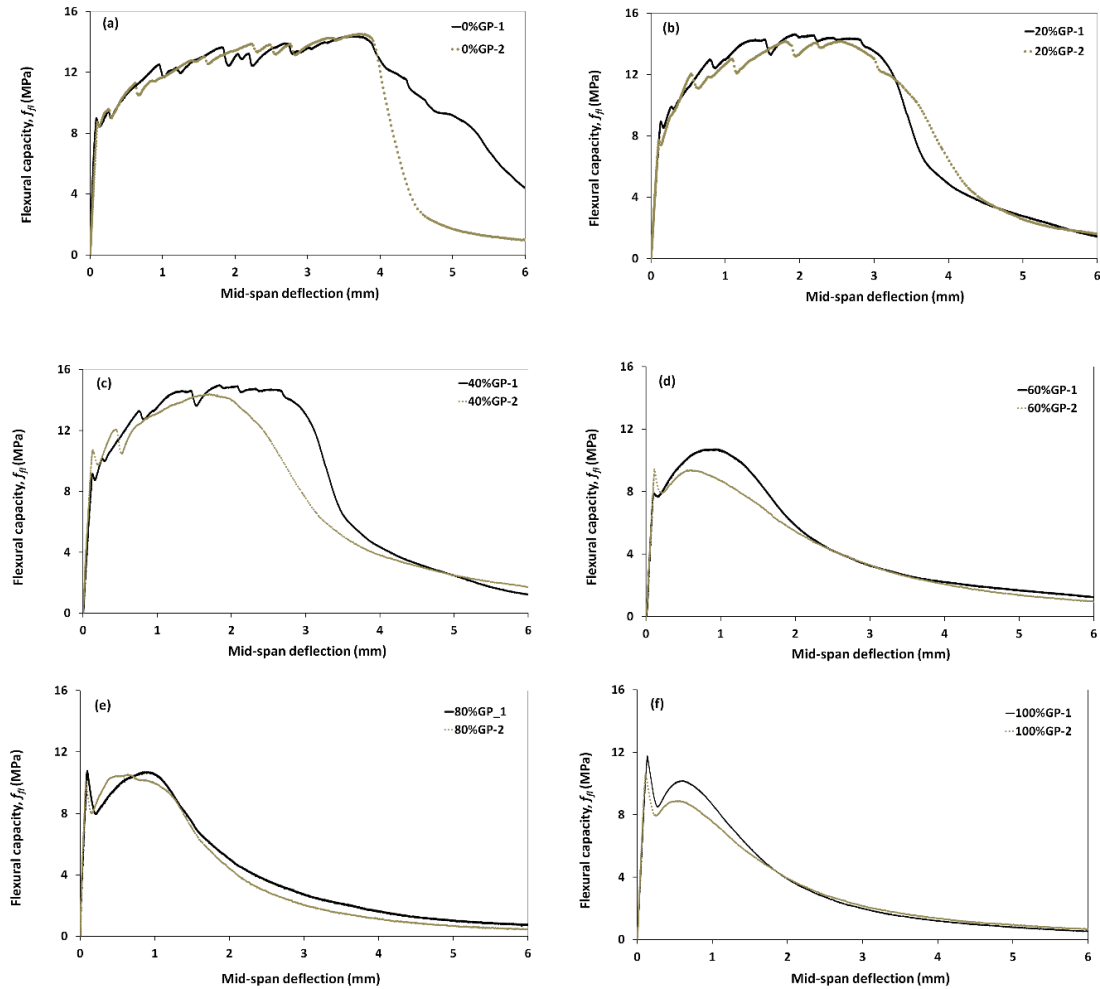


Fig. 16. Flexural response of Series I SHCC mixtures

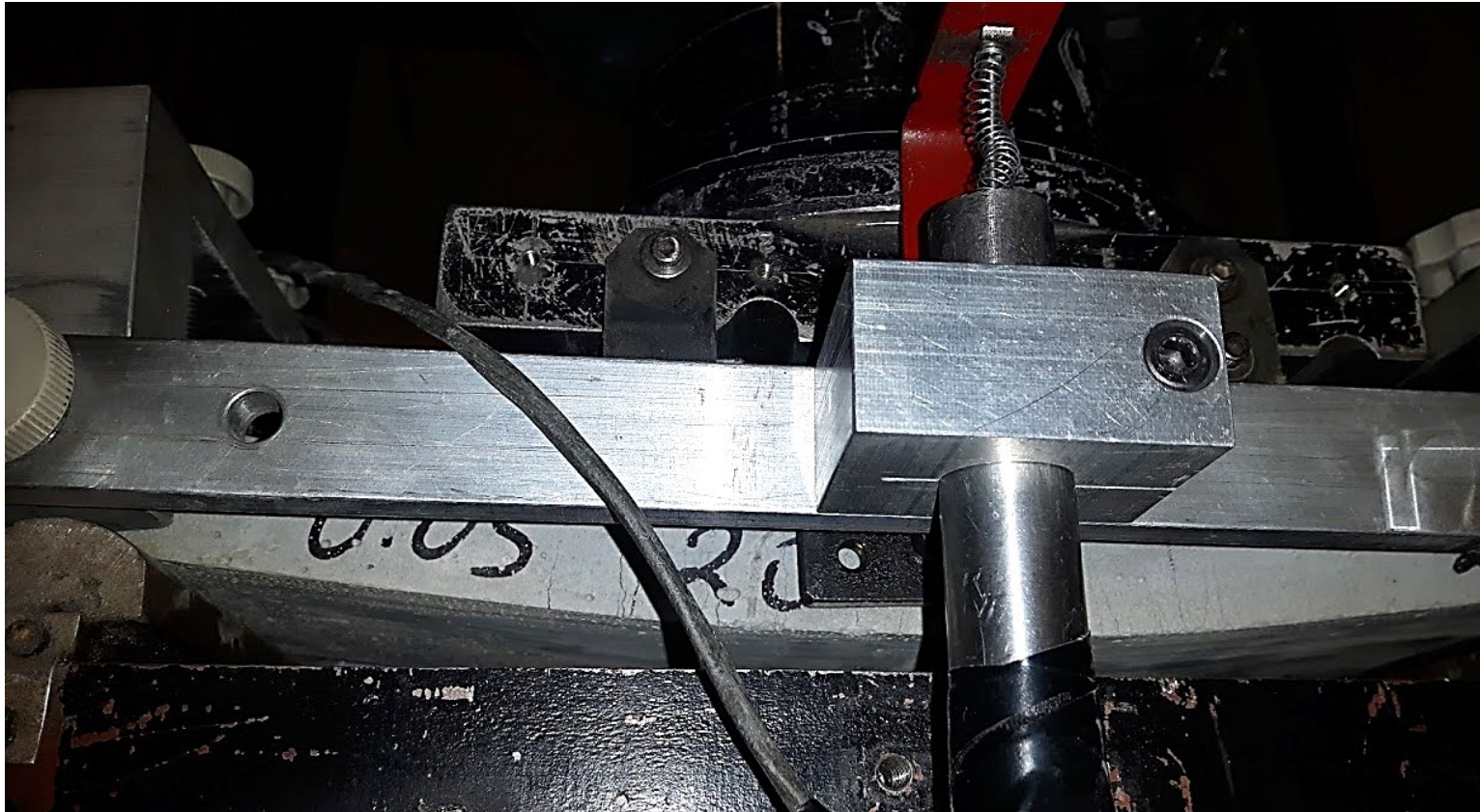


Fig. 17. Multiple cracking and deflection capacity in HVGP-SHCC. The figure illustrates the significant deflection capacity reflected by the remarkable curvature and tight multiple cracking while maintaining the peak post-cracking load for extended deformation

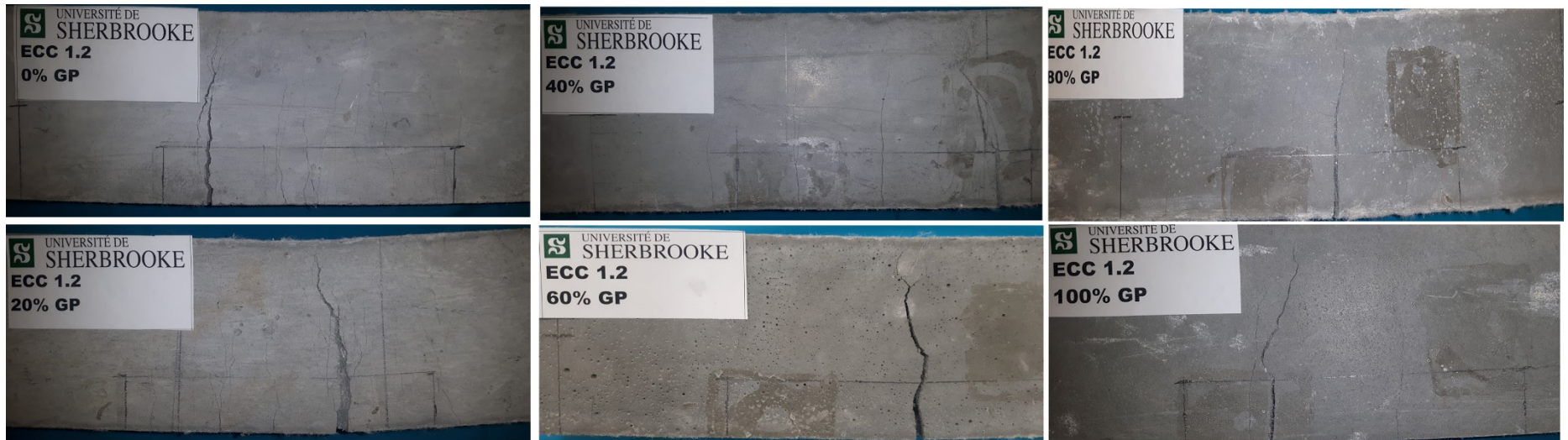


Fig. 18. Development of cracking pattern in the different SHCC systems. Lower GP content exhibit higher multiple cracking but reduced flexural load, while higher GP content increases the flexural capacity but experience lower ductility. SHCC with up to 40% GP record enhanced strength and ductility. Higher GP content tend towards the quasi-brittle failure of conventional FRC

5.2.3 Electrical resistivity

The results of electrical bulk resistivity are presented in Fig. 19. The electrical resistivity (ρ) of concrete is linked to the corrosion likelihood of reinforcing bars because corrosion itself is an electro-chemical process where the rate of flow of ions between the anode and cathode (and thus the rate of corrosion), is affected by the resistivity of concrete. As such, higher resistivity values imply less likelihood of corrosion occurrence while lower values of resistivity imply that corrosion occurrence is high [76]. Fig. 19 depicts the development of ρ for tested SHCC up to 91 days. Based on different durability levels as related to chloride-ion penetrability reported in ASTM C1202 [77] and their relation to electrical resistivity [58]. At early age (1 day), no clear distinction between the different formulations can be made owing to the effect of moisture content of the still-hydrating matrices. The effect of GP becomes evident from the age of 7 days whereby higher ρ was measured. This became more noticeable at 28, 56, and 91 days whereby an enhancement in ρ of up to 17% was achieved in the SHCC with 60% GP at 28 days, 63% enhancement in the SHCC with 80% GP at 56 days, and 33% higher ρ in the SHCC with 60% GP at the age of 91 days. Thus, while all SHCC formulations represent resistivity levels (at 28 day) corresponding to low penetrability of Cl^- , systems with GP were found to exhibit significantly higher resistivity compared to HVFA-SHCC. The enhanced electrical resistivity in systems with GP can be correlated with the strength gain explained earlier and can also be ascribed to the enhanced packing density, tortuosity, and pore refinement through pozzolanic activity [25, 34]. The pozzolanic activity, in particular, can be inferred from the age-dependence of the increase in resistivity. The latter is thus highly associated with the formation of additional C-S-H products densifying the interfacial transition zone, and hindering the ionic flow in the pore network [78], despite the increased alkalinity of GP [30].

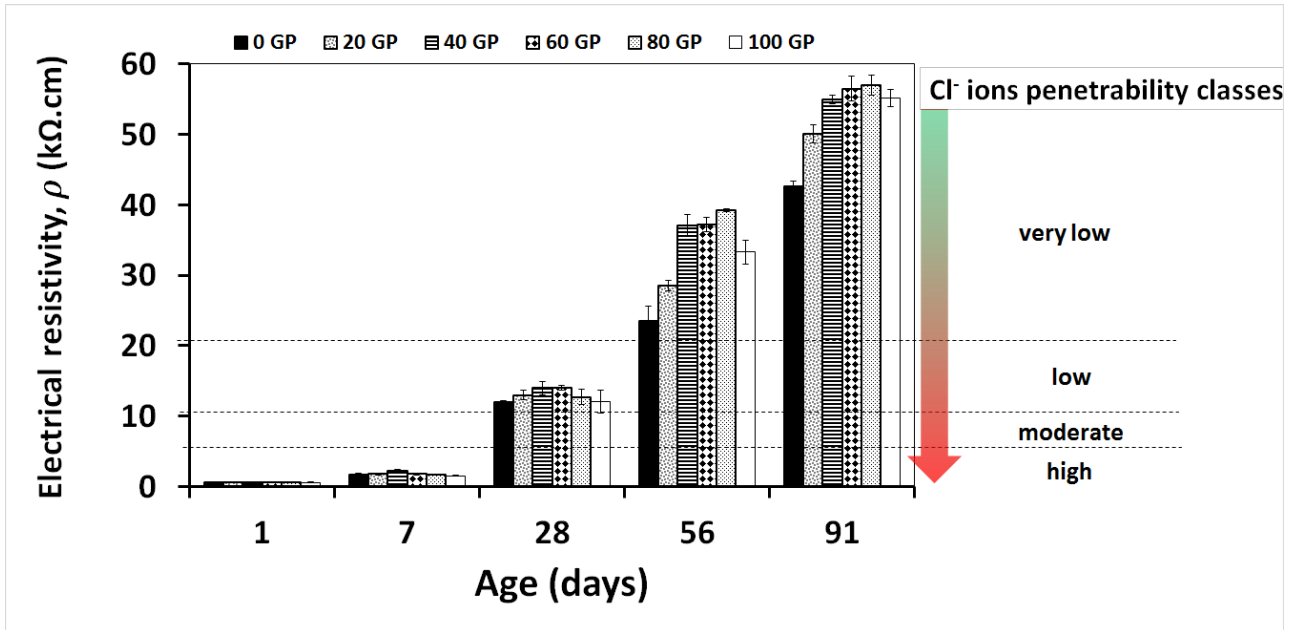


Fig. 19. Electrical resistivity of SCC mixtures

Summary and conclusions

This study presented the development of a new strain-hardening cementitious composite (SHCC) using high-volume ground-glass pozzolans (HVGP). The development of SHCC (considering fly ash (FA) replacement by ground-glass pozzolans (GP) of up to 100%) went through a novel two-stage tailoring that couples packing density optimization with the principles of micromechanical modeling. The compressible packing density model was used to optimize matrix compactness while for micromechanical modelling, single fiber pullout tests and fracture tests were conducted to compile model input. Results indicate that the incorporation of GP increases matrix compactness and results into higher strength and fracture properties. HVGP-SHCC incorporating up to 40% GP replacement of FA were developed. The resulting SHCC formulations have self-consolidation ability and exhibited (at 28 days) 60-75 MPa compressive strength, 9-15 MPa flexural capacity, 3-6 MPa tensile strength, 2-5% tensile strain capacity, and significantly increased electrical resistivity. Overall result support the use of GP for enhancing the strength characteristic of SHCC with specific findings as follows:

- The incorporation of GP increases matrix strength by a combined filler and pozzolanic effects rendering the matrix denser. As such, composite strength has been enhanced by up to 112% in the uniaxial first crack strength, 53% in uniaxial post-cracking strength, 31% in flexural first cracking strength, 15 and 25% in 28- and 91-days compressive strength, respectively. The increased strength obtained with GP, however, lead to reduced ductility. Nonetheless, up to 40% GP, comparable higher strength and ductility comparable to that of HVFA-SHCC can be achieved.
- In line with the increased strength in HVGP-SHCC, the durability aspects as evaluated by the electrical resistivity have also been enhanced. The following enhancement in the electrical resistivity were recorded: 17% at 28 days in the SHCC with 60% GP, 63% at 56 days in the SHCC with 80% GP, and 33% at 90 days in the SHCC with 60% GP. This is was found to stem from the increased compacity as well the pozzolanic activity imparted by GP.
- The increased strength in HVGP-SHCC, though, was found to a reduced matrix ductility, particularly at high GP content ($\geq 40\%$). This found to originate from the increased frictional bond imparted by the inclusion of GP. Higher frictional bond increases the maximum brdging capacity, but reduces slip distance, thereby limiting the strain-hardening ability whereby the crack tip toughness (J_{tip}) increases at the expense of the complementary energy (j'_b). Therefore, for optimum utilisation of GP in SHCC, the interface properties have to be tailored such that the frictional bond is rather optimised.

Finally, overall results demonstrate the effectiveness of using GP for enhancing the strength of HVFA-SHCC by replacing FA by up to 40% GP to obtain composite with enhanced strength and comparable ductility and better durability aspects. This shapes a new avenue for developing high-performance cement composite while promoting the sustainable development.

Acknowledgements

This project is jointly supported a Cooperative Research and Development (CRD) grant from the Natural Sciences and Engineering Research Council of Canada (NSERC), Canada Vanier Graduate Scholarship (CGS) program award no: 360284, Kruger Biomaterials Inc. (QC, Canada), and Euclid Chemicals. The authors are grateful to the financial support from all these partners.

References

- [1] V.C. Li, Engineered Cementitious Composites (ECC) – Tailored Composites Through Micromechanical Modeling, *Fiber Reinforced Concrete: Present and the Future*, Canadian Society for Civil Engineering, Montreal, 1998, pp. 64–97.
- [2] V.C. Li, S. Wang, C. Wu, Tensile strain-hardening behavior of polyvinyl alcohol engineered cementitious composite, *ACI Mater. J.* 98 (6) (2001) 483–492.
- [3] V.C. Li, On engineered cementitious composites (ECC) – a review of the material and its application, *J. Adv. Concr. Technol.* 1 (2003) 215–230.
- [4] V.C. Li, C.K.Y. Leung, Steady state and multiple cracking of short random fiber composites, *J. Eng. Mech., ASCE* 188 (11) (1992) 2246–2264.
- [5] V.C. Li, From micromechanics to structural engineering – the design of cementitious composites for civil engineering application, *J. Struct. Eng. Earthquake Eng.* 10 (2) (1993) 37–48.
- [6] M. Maalej, T. Hashida, V.C. Li, Effect of fiber volume fraction on the off- crack-plane fracture energy in strain-hardening engineered cementitious composites, *J. Amer. Ceramics Soc.*, 78 (12) (1995) 3369-3375.
- [7] H. Stang and V.C. Li. Classification of Fibre Reinforced Cementitious Materials for Structural Applications. In 6th RILEM Symposium on Fibre- Reinforced Concretes (FRC), pages 197–218, Varenna, Italy, September 2004. RILEM Publications.
- [8] S. Qian, M.D. Lepech, Y.K. Yun, V.C. Li, Introduction of transition zone design for bridge deck link slabs using ductile concrete, *ACI Struct. J.* 106 (1) (2009) 96–105.

- [9] V.C. Li, Strategies for high performance fiber reinforced cementitious composites development, in: S. Ahmad, M. di Prisco, C. Meyer, G.A. Plizzari, S. Shah (Eds.), *Fiber Reinforced Concrete: From Theory to Practice*, Proceedings of the North American/European Workshop on Advances in Fiber Reinforced Concrete, Bergamo, Italy 2004, 93–98.
- [10] M. Kunieda, K. Rokugo, Recent progress on HPFRCC in Japan required performance and applications, *J. Adv. Concr. Technol.* 4 (1) (2006) 19–33.
- [11] V.C. Li, D. K. Mishra, H. C. Wu, Matrix design for pseudo strain-hardening fiber reinforced cementitious composites, *RILEM J. Materials and Structures*, 28 (183) (1995) 586-595.
- [12] S. Wang and V.C. Li, Engineered Cementitious Composites with High-Volume Fly Ash, *ACI Materials Journal*, 104 (3) (2007) 233-241.
- [13] J. K. Kim, J. S. Kim, Ha G. J. Ha, Y. Y. Kim, Tensile and fiber dispersion performance of ECC (engineered cementitious composites) produced with ground granulated blast furnace slag. *Cem. Concr. Res.* 37(7) (2007) 096–1105.
- [14] J. Zhou, S. Qian, M. G. S. Beltran, G. Ye, K. Breugel, V. C. Li, Development of engineered cementitious composites with limestone powder and blast furnace slag, *Materials and Structures*, 43(6) 803–814.
- [15] K. Turk, M. L. Nehdi, Coupled effects of limestone powder and high-volume fly ash on mechanical properties of ecc, *Constr. Build. Mater.* 164 (2018) 185-192.
- [16] E. Özbay, O. Karahan, M. Lachemi, K.M.A. Hossain, C. Duran Atis, Investigation of properties of engineered cementitious composites incorporating high volumes of fly ash and metakaolin, *ACI Mater. J.* 109 (5) (2012) 565-571.
- [17] Y. Al-Najjar, S. Yes_ilmén, A.M. Al-Dahawi, M. S_ahmaran, G. Yıldırım, M. Lachemi, L. Amleh, Physical and chemical actions of nano-mineral additives on properties of high-volume fly ash engineered cementitious composites, *ACI Mater. J.* 113 (6) (2016) 791-801.
- [18] Y. Zhu, Y. Yang, Y. Yao, Use of slag to improve mechanical properties of engineered cementitious composites (ECCs) with high volumes of fly ash, *Constr. Build. Mater.* 36 (2012) 1076–1081.

- [19] E.H. Yang, Y. Yang, V.C. Li, Use of high volumes of fly ash to improve ECC mechanical properties and material greenness, *ACI Mater. J.* 104 (6) (2007) 620–628.
- [20] E. Ozbay, M. Sahmaran, M. Lachemi, H.E. Yucel, Self-healing of microcracks in high-volume fly-ash-incorporated engineered cementitious composites, *ACI Mater. J.* 110 (1) (2013) 33–43.
- [21] C. Lin, O. Kayali, E.V. Morozov, D.J. Sharp, Development of self-compacting strain-hardening cementitious composites by varying fly ash content, *Constr. Build. Mater.* 149 (2017) 103–110.
- [22] M. Sahmaran, V.C. Li, Durability properties of micro-cracked ECC containing high volumes fly ash, *Cement and Concrete Research* 39 (11) (2009) 1033–1043.
- [23] S. A. Rodger, S. A. Brooks, W. Sinclair, G. W. Groves, D. D. Double, High strength cement pastes, *J. Mater. Sci.* 20 (1985) 2853–2860.
- [24] M. A. Gulgun, W. M. Kriven, L. S. Tan, A. J. McHugh, Evolution of mechano-chemistry and microstructure of a calcium aluminate-polymer composite: Part I—Mixing Time Effects,” *J. Mater. Res.* 10 (7) (1995) 1746–1755.
- [25] R. M. Flores, Chapter 1 - Introduction and Principles, Editor(s): Romeo M. Flores, *Coal and Coalbed Gas*, Elsevier, 2014, Pages 1–40.
- [26] A. Shayan, A. Xu, Value-Added Utilisation of Waste Glass in Concrete, *Cem. Concr. Res.* 34 (1) (2004) 81–89, [https://doi.org/10.1016/S0008-8846\(03\)00251-5](https://doi.org/10.1016/S0008-8846(03)00251-5).
- [27] Recyc-Québec, “Le Verre Fiches Informatives (in French),” Recyc-Québec, Québec City, Canada, 2010, 8p.
- [28] A. Zidol, Optimization of the fineness of glass powder in binary cementitious systems, M.S. thesis, Université de Sherbrooke, Sherbrooke, Canada, 2009.
- [29] R. Idir, Mécanismes d’action des fines et des granulats de verre sur la réaction alcali-silice et la réaction pouzzolanique, Ph.D. thesis, Université de Sherbrooke, Sherbrooke, Canada, 2009.
- [30] A. Omran, A. Tagnit-Hamou, Performance of glass-powder concrete in field applications, *Constr. Build. Mater.* 109 (2016) 84–95, <https://doi.org/10.1016/j.conbuildmat.2016.02.006>.

- [31] N. A. Soliman, A. Tagnit-Hamou, Development of ultra-high-performance concrete using glass powder—Towards ecofriendly concrete,” *Constr. Build. Mater.* 125 (2016) 600–612, <https://doi.org/10.1016/j.conbuildmat.2016.08.073>.
- [32] C. Shi, Y. Wu, C. Riefler, H. Wang, Characteristic and pozzolanic reactivity of glass powders, *Cem. Concr. Res.* 35 (5) (2005) 987–993.
- [33] CSA A3001-18, Cementitious Materials for Use in Concrete, Canadian Standards Association, Toronto, ON, 2018.
- [34] H. Siad, M. Lachemi, M. Sahmaran, K.M.A. Hossain, Effect of glass powder on sulfuric acid resistance of cementitious materials, *Constr. Build. Mater.* 113 (2016) 163–173.
- [35] N. Schwarz, H. Cam, N. Neithalath, Influence of a fine glass powder on the durability characteristics of concrete and its comparison to fly ash, *Cem. Concr. Compos.* 30 (6) (2008) 486–496.
- [36] O. Bonneau, M. Lachemi, E. Dallaire, J. Dugat, P.-C. Aïtcin, Mechanical properties and durability of two industrial reactive powder concretes, *ACI Mat. J.* 94 (4) (1997) 286–290.
- [37] Y. Shao, T. Lefort, S. Moras, D. Rodriguez, Studies on concrete containing ground waste glass, *Cem. Concr. Res.* 30 (1) (2000) 91–100.
- [38] H. Du, K.H. Tan, Use of waste glass as sand in mortar: Part II. Alkali–silica reaction and mitigation methods, *Cem. Concr. Compos.* 35 (1) (2013) 118–126.
- [39] H. Siad, M. Lachemi, M. Sahmaran, H. A. Mesbah, K. M. A. Hossain, Use of recycled glass powder to improve the performance properties of high-volume fly ash-engineered cementitious composites, *Construction and Building Materials*, 163(2018) 53-62.
- [40] F. de Larrard, *Concrete Mixture Proportioning: A Scientific Approach*, E&FN Spon, London, 1999.
- [41] T. Kanda, V.C. Li, Multiple cracking sequence and saturation in fiber reinforced cementitious composite, *Concr. Res. Technol., JCI* 9 (2) (1998) 19–33.
- [42] D.B. Marshall, B.N. Cox, A J-integral method for calculating steady-state matrix cracking stresses in composites, *Mech. Mater.* 8 (1988) 127–133.

- [43] Z. Lin, T. Kanda, V.C. Li, On interface property characterization and performance of fiber reinforced cementitious composites, *Concrete Science and Engineering*, 1, RILEM, 1999. pp. 173–184.
- [44] P.C. Aïtcin, Cements of yesterday and today-concrete of tomorrow, *Cem. & Con. Res.*, 30 (9) (2000) 1349–1359.
- [45] ASTM C494 / C494M-17, Standard Specification for Chemical Admixtures for Concrete, ASTM International, West Conshohocken, PA, 2017, www.astm.org
- [46] H. Kong, S. G. Bike, V. C Li, Development of a self-consolidating engineered cementitious composite employing electrosteric dispersion/stabilization, *Cem. Concr. Compos.* 25 (3) (2003) 301-309.
- [47] F. V. Muellera, O. H. Wallevika, K. H. Khayat, Linking Solid Particle Packing of Eco-SCC to Material Performance,” *Cem. Concr. Compos.*, 54 (2014) 117-125.
- [48] ASTM C187-16 Standard Test Method for Amount of Water Required for Normal Consistency of Hydraulic Cement Paste, ASTM International, West Conshohocken, PA, 2016, www.astm.org
- [49] J. P. Bigas, , J. L. Gallias, Effect of fine mineral additions on granular packing of cement mixtures,” *Mag. Concr. Res.* 54 (3) (2002) 155-164.
- [50] ASTM C185-15a, Standard Test Method for Air Content of Hydraulic Cement Mortar, ASTM International, West Conshohocken, PA, 2015, www.astm.org
- [51] ASTM C1437-15, Standard Test Method for Flow of Hydraulic Cement Mortar, ASTM International, West Conshohocken, PA, 2015, www.astm.org
- [52] ASTM C469 / C469M-14, Standard Test Method for Static Modulus of Elasticity and Poisson’s Ratio of Concrete in Compression, ASTM International, West Conshohocken, PA, 2014, www.astm.org
- [53] ASTM E399-12, Standard test method for linear-elastic plane-strain fracture toughness K_{Ic} of metallic materials, ASTM International, West Conshohocken, PA, 2012, www.astm.org
- [54] ASTM C78 / C78M-18, Standard Test Method for Flexural Strength of Concrete (Using Simple Beam with Third-Point Loading), ASTM International, West Conshohocken, PA, 2018, www.astm.org

- [55] ASTM C109 / C109M-16a, Standard Test Method for Compressive Strength of Hydraulic Cement Mortars (Using 2-in. or [50-mm] Cube Specimens), ASTM International, West Conshohocken, PA, 2016, www.astm.org
- [56] P. Azarsa, R. Gupta, Electrical resistivity of concrete for durability evaluation: a review, *Adv. Mater. Sci. Eng.* 2017, Article ID 8453095, 30 pages, <https://doi.org/10.1155/2017/8453095>.
- [57] AASHTO T 259, Method of Test for Resistance of Concrete to Chloride Ion Penetration, American Association of State Highway and Transportation Officials, Washington, DC, 2006, 3 pp.
- [58] V. Baroghel-Bouny, Concrete design for a given structure service life - Durability management with regard to reinforcement corrosion and alkali-silica reaction. Paris: AFGC Scientific and Technical Documents (AFGC) 2004. p. 252.
- [59] S.A.A.M. Fennis, J. C. Walraven, J. A. Uijl J (2006), Optimizing the particle packing for the design of ecological concrete, Proceedings of the 16th Internationale Baustofftagung, Weimar, Bunderepublik Deutschland. 1(2006)1313 -1320.
- [60] R.M. German, Particle packing characteristics, Princeton: Metal Powder Industries Federation (1989)
- [61] Y. Jiao, F. H. Stillinger, S. Torquato, Optimal packings of superballs, *Phys. Rev. E* 79, 041309 – Published 23 April 2009; Erratum *Phys. Rev. E* 84, 069902 (2011)
- [62] A. Zidol, Optimization of the Fineness of Glass Powder in Binary Cementitious Systems, M.S. thesis, Université de Sherbrooke, Sherbrooke, Canada, 2009.
- [63] H. Ma, J. Cai, Z. Lin, S. Qian, V. C. Li, CaCO₃ whisker modified Engineered Cementitious Composite with local ingredients, *Constr. Build. Mater.* 151 (2017) 1-8.
- [64] O.A. Hisseine, A. Tagnit-Hamou, Interface properties of high-volume ground glass pozzolans strain-hardening cementitious composites: characterization and nanomodification, article under review by cement and concrete research (March 2019)
- [65] Y.M. Zhang, W. Sun, H.D. Yan, Hydration of high-volume fly ash cement pastes, *Cem. Concr. Compos.* 22 (6) (2000) 445–452.

- [66] ASTM C311 / C311M-18, Standard Test Methods for Sampling and Testing Fly Ash or Natural Pozzolans for Use in Portland-Cement Concrete, ASTM International, West Conshohocken, PA, 2018, www.astm.org
- [67] I. Jawed, J. Skalny Alkalies in cement: a review: II. Effects of alkalies on hydration and performance of Portland cement *Cem. Concr. Res.*, 8 (1) (1978) 37-51.
- [68] A. E. Naaman, H. W. Reinhardt, Setting the stage: Toward performance-based classification of FRC composites, In 'High Performance Fiber Reinforced Cement Composites (HPFRCC4). Proceedings of the Fourth International RILEM Workshop'. (eds.) A.E. Naaman and H.W. Reinhardt. Rilem Publications S.A.R.L. 2003, 1-4.
- [69] C. K. Yi, C. P. Ostertag, Strengthening and toughening mechanisms in microfiber reinforced cementitious composites. *J Mater Sci* 36(6) (2001) 1513–1522, doi: 10.1023/A:1017557015523.
- [70] P. Balaguru, H. Najm H, High-performance fiber-reinforced concrete mixture proportions with high fiber volume fractions. *ACI Mater J* 101(4) (2004) 281–286.
- [71] Y. Geng, C. K. Leung, A microstructural study of fibre/mortar interfaces during fibre debonding and pull-out. *J Mater Sci* 31(5) (1996), 1285–1294, doi: 10.1007/BF00353108.
- [72] M.S. Sahmaran, H.E. Yücel, S. Demirhan, C.V. Li, Combined effect of aggregate and mineral admixtures on tensile ductility of engineered cementitious composites, *ACI Mater. J.* 109 (6) (2012) 627-638.
- [73] A. Hillerborg, Analysis of One single crack, in *Fracture Mechanics of Concrete*, edited by F.H. Wittmann, Elsevier Science Publishers B.V., Amsterdam, pp. 223-249, 1983.
- [74] N.M. Altwair, M.M. Johari, S.S. Hashim, Flexural performance of green engineered cementitious composites containing high volume of palm oil fuel ash, *Constr. Build. Mater.* 37 (2012) 518–525.
- [75] J. Sehgal, S. Ito, Brittleness of glass, *Journal of Non-Crystalline Solids*, Volume 253, Issues 1–3, 1999, Pages 126-132, ISSN 0022-3093,
- [76] W. J. McCarter, H. M. Taha, B. Suryanto, G. Starrs, Two-point concrete resistivity measurements: interfacial phenomena at the electrode–concrete contact zone, *Meas. Sci. Technol.* 26 (2015).

-
- [77] ASTM C1202-19, Standard Test Method for Electrical Indication of Concrete's Ability to Resist Chloride Ion Penetration, ASTM International, West Conshohocken, PA, 2019, www.astm.org
- [78] A.M. Matos, T. Ramos, S. Nunes, J. Sousa-Coutinho Durability enhancement of SCC with waste glass powder Mater. Res., 19 (1) (2016), pp. 67-74

List of Figures

- Fig. 1. Multi-scale design framework of SHCC with HVGP
- Fig. 2. Fiber bridging stress – crack opening width relationship as linked to pseudo-ductility conditions
- Fig. 3. Particle size distribution of SHCC ingredients
- Fig. 4. SEM micrographs of SHCC ingredients
- Fig. 5. SEM micrographs of polyvinyl alcohol (PVA) fibers (RECS 15)
- Fig. 6. Fracture toughness test
- Fig. 7. Uniaxial tension test
- Fig. 8. Single-fiber pull-out test
- Fig. 9. Combined particle size distribution for the different SHCC formulations
- Fig. 10. Typical slump flow in the suspended mortar
- Fig. 11. Computed fiber bridging stress–crack opening relationship (σ – δ)
- Fig. 12. Evolution of compressive strength in series I SHCC mixtures
- Fig. 13. Generalized response in uniaxial tension and in flexure in FRC
- Fig. 14. PVA fiber status post-single fiber-fiber pull-out test in SHCC
- Fig. 15. Uniaxial tensile behavior of Series I SHCC mixtures
- Fig. 16. Flexural response of Series I SHCC mixtures
- Fig. 17. Multiple cracking and deflection capacity
- Fig. 18. Development of cracking pattern in the different SHCC systems.
- Fig. 19. Electrical resistivity of SCC mixtures

List of Tables

- Table 1. Chemical compositions of powders and granular materials used in the study
- Table 2. Mix design of HVGP SHCC
- Table 3. Fresh properties of SHCC plain formulations used for the micromechanical investigation
- Table 4. Results of micromechanical investigation and SHCC strain-hardening indicators

CHAPTER 9

Nanocellulose for the Development of Nano-engineered Strain-Hardening Cementitious Composites incorporating High-Volume Ground-Glass Pozzolans

9.1 Introduction

In this chapter, the nanoreinforcing cellulose filaments (CF) are utilised as a tool to nano-engineer the properties of strain-hardening cementitious composites (SHCC) incorporating high-volume post-consumer ground-glass pozzolans (HVGP) addressed in Chapter 8. In the latter, the optimisation of matrix packing density resulted in SHCC with improved strength relative to SHCC incorporating high-volume fly-ash (HVFA). However, at high replacement levels of fly ash (FA) by ground-glass pozzolans (GP), namely ($> 40\%$), the ductility of the composite is adversely affected due to the increase in matrix strength associated with higher compacity.

Therefore, the role of this chapter is to nanoengineer the SHCC matrix by the reinforcing ability of the nanoscale CF to provide a sub-level crack bridging mechanism. On the other hand, bearing in mind the high surface area of CF, their use here is also intended to modify the interface properties between PVA fiber and the matrix towards enhanced composite performance. Due to CF effect of increasing matrix elastic modulus (thereby reducing the crack tip toughness) and also due to the effect of CF on altering the interface properties, composites with CF exhibited significant increase in ductility. This allowed SHCC with as high GP content as 100% replacement of FA to exhibit adequate ductility while demonstrating superior tensile and flexural strength. These details are reported in [section 9.2](#) in the context of Article 7 under reviewed by Cement and Concrete Composites.

9.2 Article 7- Nanocellulose for the development of nano-engineered strain-hardening cementitious composites incorporating high-volume ground-glass pozzolans

Article information

Authors and affiliations:

Ousmane A. Hisseine, PhD candidate and Canada Vanier Scholar of NSERC, Cement and Concrete Research Group, Department of Civil Engineering, Université de Sherbrooke

A. Tagnit-Hamou, Professor and director of Cement and Concrete Research Group, Department of Civil Engineering, Université de Sherbrooke

Article status: Under review

Journal: *Cement and Concrete Composites*

Initial date of submission: April 23, 2019

Reference: Hisseine, O. A, Tagnit-Hamou, A. (2019). Nanocellulose for the development of nano-engineered strain-hardening cementitious composites incorporating high-volume ground-glass pozzolans. Article Under review by *Cement and Concrete Composites*.

Titre français:

Nano-filaments de cellulose pour le développement de bétons écouissants nano-modifiés à teneur élevée en poudre de verre.

Contribution of this article: Contributes towards achieving project object 5, namely, leveraging the versatile opportunities offered by nanocellulose to develop a novel nanoengineered concrete formulation, namely, a Nanomodified-Strain-Hardening Cementitious Composite.

Development of nano-engineered strain-hardening cement composites with high-volume ground glass pozzolans (HVGP)

Ousmane A. Hisseine; Arezki Tagnit-Hamou

Under Review by Cement and Concrete Composites

Abstract

Nanomodification of concrete has a promising potential to allow engineering concrete properties for specific applications. This study shows how nanoscale cellulose filaments (CF) can be used as a novel tool to tailor the properties of strain-hardening cementitious composites (SHCC) incorporating high-volume ground-glass pozzolans (HVGP) towards improved strength and ductility. CF was introduced (at dosages of 0, 0.03, 0.05 and 0.10% by weight of cement) into SHCC incorporating ground-glass pozzolans (GP) in replacement of fly ash (FA) at 0, 40, and 100%. Micromechanical guidelines were adopted for tailoring the formulations. The performance of resulting SHCC was then validated by uniaxial-tensile and flexural tests. Results indicate that CF allows nanoengineering matrix and interface properties by increasing matrix elastic modulus and imparting a significant slip hardening effect. Consequently, higher complementary energy and lower crack tip toughness were obtained, thereby leading to enhanced ductility. Thus, while an increase in uniaxial post-peak strength of up to 23% can be achieved with CF, the most significant effect of CF, however, was on the ultimate tensile strain capacity (ε_u) which was more pronounced in the SHCC mixtures with 40 and 100%GP. Thus, improvements in ε_u of up to 26, 37, and 258% were achieved for the three respective GP contents (0, 40, and 100%). Consequently, the energy absorption capacity was enhanced with CF by up to 52, 83, and 238%, respectively. Thus, with the incorporation of CF, it was possible to produce SHCC with up to 100%GP replacement of FA exhibiting higher strength and ductility, while contributing to promoting ecoefficiency.

Author Keywords: Ecological concrete, strain-hardening cementitious composites, engineered cementitious composites, recycled glass powder, particle packing optimization, micromechanics, single fiber pull-out, strain-hardening

1 Introduction

In line with the eco-efficiency requirements set by the Canadian Standards Association (CSA) [1], the use of locally available materials for concrete production is believed to foster sustainable development [2]. In this context, a new type of strain-hardening cementitious composites (SHCC) also known as engineered cementitious composites (ECC) has been recently developed at the University of Sherbrooke (Canada) using high-volume ground-glass pozzolans (HVGP) by coupling particle packing optimization with micromechanical tailoring [3]. SHCC belong to the class of high-performance fiber-reinforced cementitious composites (HPFRCC) and are characterized by: (i) exceptional ductility, (ii) remarkable tensile strain capacity (3-11%), (iii) tight multiple cracking with crack width below 60 μm at 1% strain, and strain-hardening behavior with relatively low fiber volume content, typically $\leq 2\%$ [4-11]. Unlike conventional FRC, SHCC are typically designed through micromechanical principles such that the mechanical interactions between the fiber, the matrix, and fiber/matrix interface are systematically considered when the composite is subjected to loading [12]. As a result of these strict design guidelines, upon first cracking, SHCC strain-hardens, develops multiple cracking, and achieves significant ultimate strain capacity of 300–500 times that of normal concrete or conventional fiber-reinforced concrete (FRC), which rather tension-softens after first cracking [7]. These remarkable metal-like ductility characteristics accompanied by substantial fracture toughness were found to elevate SHCC to closely replicate the features of aluminum alloys [13] and promote the use of SHCC in several real-life structural applications [14-17].

Initially developed with silica fume as a supplementary cementitious material (SCM) [4,18], most of today's SHCC formulations use high-volume fly ash (HVFA) for such several reasons as cost-effectiveness [19], enhanced mixture workability associated with the slower reactivity of fly ash (FA) as well as to the spherically-shaped smooth-textured FA particles (reducing inter-particle friction) [20], increased ductility attributed to the diluting effect of FA (reducing fiber/matrix chemical bonding and increasing matrix toughness) [19]. However, with the current policies in the energy sector leading to limiting coal-powered electrical stations, the supply of fly ash is diminishing particularly in North America. Thus, SHCC with other materials other than fly ash may be more attractive. This justifies the emerging new types of SHCC such as the ones with ground granulated blast furnace slag [21, 22], nanomineral additives [23], limestone powder [24, 25], and metakaolin [26].

In this context, in a recent contribution of ours, a novel type of SHCC incorporating high-volume ground-glass pozzolans (HVGP) was developed through an innovative approach coupling particle packing optimization with micromechanical tailoring; such that strength and ductility can be optimized [3]. Ground-glass pozzolan (GP) obtained by grinding mixed-waste glass to a fineness closer to that of cement can serve as an SCM while solving a serious environmental and socioeconomical burden; because postconsumer glass recycling is often restrained by either glass breakage, color mixing, or expensive recycling. Thus, more than 50% of postconsumer glass in Québec ended in landfills in 2008 [27]. With an enhanced mechanical performance (associated with pozzolanic activity) as well as durability aspects (attributed to tortuosity, pore refinement, and microstructure densification) [28] demonstrated in several types of concrete in laboratory as well as *in-situ* applications [28-31], GP has been very recently accepted as a standard SCM by CSA [1].

When these advantages of GP were leveraged for producing HVGP-SHCC, the adopted approach that couples particle packing optimization with micromechanical tailoring allowed obtaining composites with superior strength characteristics than conventional HVFA-SHCC [3]. HVGP-SHCC formulations with a self-consolidation ability (a mini slump-flow of ~ 250 mm) and exhibiting (at 28 days) 60-75 MPa compressive strength, 9-15 MPa flexural capacity, 3-6 MPa tensile strength, 2-5% tensile strain capacity, and significantly increased electrical resistivity were developed [3]. The enhancement in uniaxial tensile strength and flexural capacity were particularly significant. Relative to conventional HVFA-SHCC, enhancement of up to 112% in the first-crack strength, 53% in uniaxial post-peak strength, and 31% in flexural first-crack strength were achieved with HVGP-SHCC [3]. The gain in strength emerges from the optimization of matrix packing density [31, 32] as well as from the pozzolanic activity by GP [33]. However, considering that the above gain in tensile strength was accompanied by a decrease in ductility, particularly at $GP \geq 60\%$ replacement of FA, the optimum gain in tensile strength (while maintaining comparable ductility to HVFA-SHCC) was located at $\sim 20\%$. The reduction in ductility in HVGP-SHCC is primarily driven by the higher matrix strength whereby the crack tip toughness (J_{tip}) increases at the expense of the complementary energy (j'_b). It also sprouts from the excessive frictional bond (imparted by the denser matrix of HVGP-SHCC) contributing to fiber damage and limiting the strain-hardening ability [34].

One possible way to enhance the ductility of HVGP-SHCC is to consider multi-scale reinforcement whereby nonreinforcement can be added to foster composite ductility. Considering the microscale nature of the cracking process, the nanoscale spacing, and high specific surface areas of nanomaterials may allow effective inception of micro-cracks [35]. As such, nanoscale reinforcement in the form of graphite nanoplatelets (GNP) and carbon nanofibers (CNF) incorporated (at rates of 0–0.30% per cement mass) into ultra-high-performance concrete (UHPC) increased the tensile strength and energy absorption capacity by 56% and 187%, respectively [36]. Furthermore, at an optimum GNP addition of 0.2%, strain-hardening in tension and in flexure were observed [36]. In a similar manner, a multi-scale reinforced SHC containing 0.08 wt.% graphene oxide (GO) and 2% vol. of PVA fibres recorded 25% higher compressive strength, 38% higher tensile strength, and 81% flexural capacity [37]. Likewise, the synergy between nanocellulose and microcellulose fibers was found to increase the fracture energy of reactive powder concrete by more than 50% [38]. On the other hand, the incorporation of nano-carbonate whiskers (CaCO_3) at 0.5% vol. in HVFA-SHCC reduced the chemical bond (by limiting the adhesion of PVA fibers to the matrix), increased the compressive strength by 30%, the ultimate tensile strength by 53%, and the tensile strain capacity by 114% [39].

Therefore, it may be legitimate to believe that the incorporation of nanoscale cellulose filaments (CF) can enhance the ductility of HVGP-SHCC. Cellulose filaments (CF) are nanoscale rod-like cellulosic particles with a nanometric diameter (30–400 nm), micrometric length (100–2000 μm), and high aspect ratio (100–1000). CF belong to nanocellulose materials (NCM) such as cellulose nanocrystals (CNC); microfibrillated cellulose (MFC); and nanofibrillated cellulose (NFC) [40]. NCM have recently emerged as highly promising multifunctional green materials (for the development of next-generation high-performance bio composites) fostering concrete sustainability. This is attributable to their biodegradability, low toxicity, low environmental and health risks associated with their production, and low production cost [41–43]. Owing to their nanoscale size, fibril morphology, and large surface area, NCM provide new means to nanoengineer superior composite properties necessary for versatile applications [41, 42], including cement composites [43–47].

Previous investigations with CF indicate a viscosity modifying effect associated with the tendency of the hydrophilic and flexible CF fibrils to form a percolating network of filaments

bridging cement particles [45]. CF also influence the mechanical performance of cement campsites through a combination of internal curing and nanoreinforcing effect whereby strength enhancements of up to 18% in elastic modulus [46], 25% in flexure, and 96% in energy absorption [44] were recorded. These effects were found to stem from higher microstructure properties (increased degree of hydration of $\sim 12\%$ and enhanced micromechanical properties of C-S-H gel matrix of $\sim 12\text{--}25\%$) [46].

Considering the advantages offered by NCM as demonstrated in our former works [44-46] and elsewhere [43, 47], it is perceivable that these advantage may be leveraged towards enhancing the ductility performance of HVGP-SHCC. To this end, it is hypothesized herein that the effect of CF on increasing the elastic modulus (E_m) of cement matrix may allow attenuating the crack tip toughness ($J_{tip} = K_m^2/E_m$), while the effect of CF as a nanoreinforcement may enhance the complementary energy J'_b such that the condition for steady-state cracking ($J_{tip} \leq J'_b$) may be fostered over the common Griffith cracking. This can contribute towards enhancing the strain-hardening behavior. Furthermore, the potential omnipresence of the high-surface area CF ($\geq 80 \text{ m}^2/\text{g}$) at the interface between the cementitious matrix and the PVA fibers, may reduce the excessive bonding of PVA fibers to the matrix, whereby CF-PVA interactions would attenuate matrix-PVA interactions. This may contribute towards reducing excessive frictional bonding and consequently lowering the likelihood of fiber damage during pull-out, thereby enhancing composite ductility. In light of the above hypothesis, the current study aims at valorizing the advantages offered by CF towards enhancing the ductility of HVGP-SHCC such that the incorporation of CF as a nanoscale reinforcement in conjunction with the mainstream PVA fibers may result into a hybrid reinforced system with improved performance. The resulting HVGP-SHCC have the potential to exhibit higher strength and ductility relative to conventional HVFA-SHCC. Research outcomes are expected to contribute towards the localisation of ingredients of high-performance cement composites while developing greener concrete products with superior performance.

2 Framework for the development of nanoengineered HVGP-SHCC

For the development of nanoengineered HVGP-SHCC, the current study relies on our former work on the design of HVGP-SHCC based on coupling particle packing optimization with micromechanical tailoring [3]. With the aim of enhancing the ductility of HVGP-SHCC, selected formulations (with the minimum, optimum, and maximum packing density

corresponding to, respectively, FA replacement by GP of 0, 40, and 100%) from the previous work were considered in the current study. In light of the reduced ductility at high GP content [3], the above mixtures were modified by the incorporation of nanoscale cellulose filaments (CF) at rates of 0.03, 0.05, and 0.10% by mass of cement. The incorporation of CF was intended to provide a nanoreinforcing system to the matrix as well as to attenuate the excessive frictional bond encountered with increasing GP [34], thereby allowing for nanotailoring matrix and interface properties. Single-fiber pull-out and fracture mechanics tests were conducted to compile the parameters necessary for constructing fiber-bridging stress versus crack-opening response which was used for micromechanical tailoring. In outcome, pseudo-ductility performance as dictated by the micromechanical design approach of SHCC was assessed for the different formulations. Finally, the performance of the different formulations (transposed from the micromechanical investigations) was validated by uniaxial tension and flexural tests conducted on SHCC at the composite level. Fig. 1 presents an overview of the framework adopted in this study for the development of HVGP-SHCC.

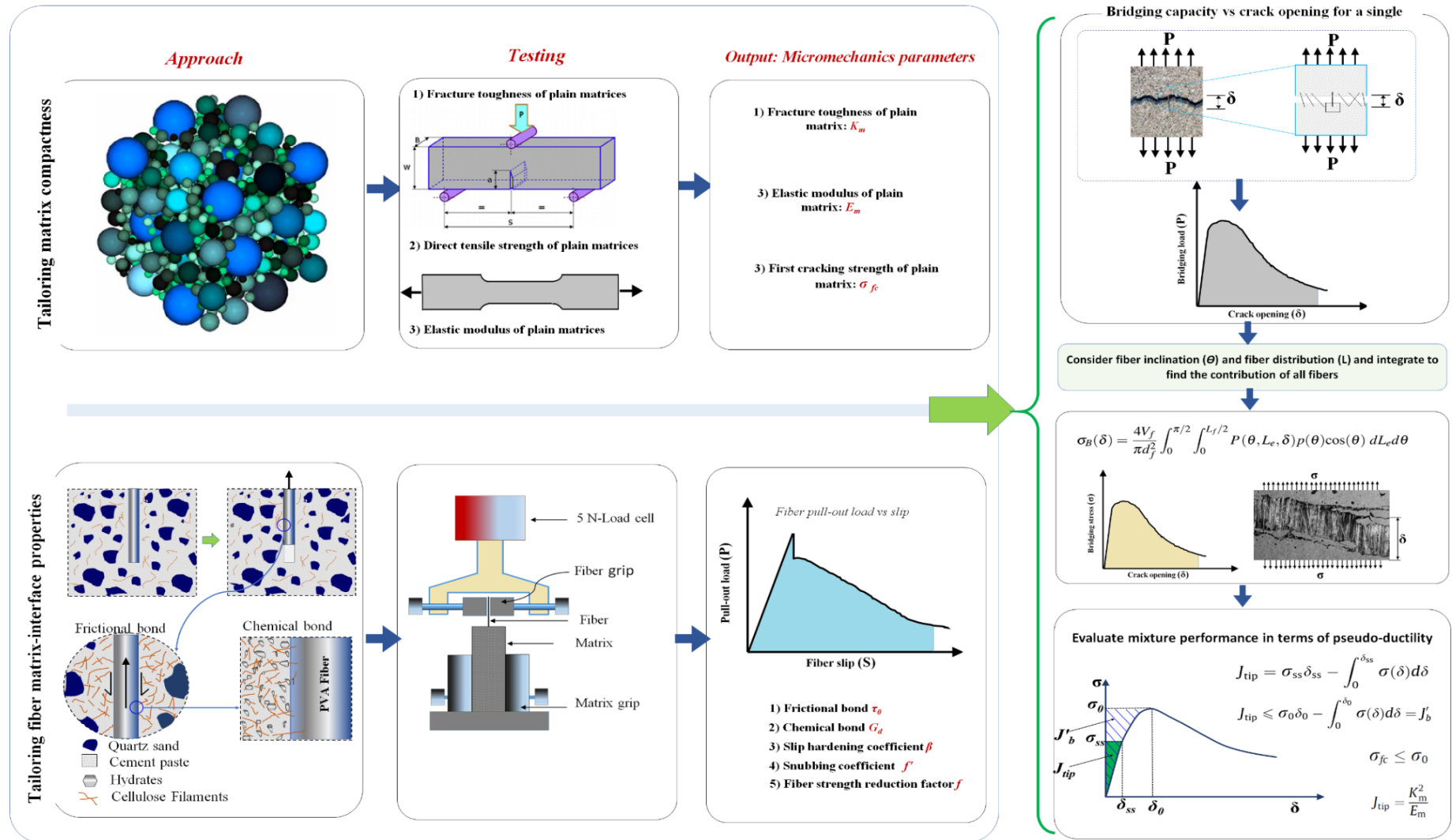


Fig. 1. Multi-scale design framework of nanoengineered HVGP-SHCC

3 Micromechanical tailoring of HVGP-SHCC

The design of SHCC mixtures is built on tailoring matrix, fiber, and fiber-matrix interface along with their associated parameters: [(fiber volume fraction, length, diameter, strength, and elastic modulus, etc. for fiber); (fracture toughness, elastic modulus, and tensile strength etc. for the matrix); and (chemical and frictional bonds, slip-hardening behavior, etc. for fiber/matrix interface)]. The process of micromechanical tailoring is thus the one that quantitatively accounts for the mechanical interaction between these three groups of composite constituent parameters when the composite is subjected to loading [7, 48]. This process elevates composite development from the serendipity of trial-and-error tests to a systematic and guided selection (or otherwise modification) of these micromechanical parameters so that their coupled effect culminates into a composite exhibiting pseudo-ductility at fairly low fiber volume fraction commonly $\leq 2\%$ [4-11]. Emanating from flat crack analyses of ceramics composites reinforced with continuous aligned fibers [49], micromechanical tailoring model was first introduced in cement and concrete composites by Li and collaborators [4-7, 12] and was later improved by Kanda and Li [48], Lin et al. [50], and Yang et al. [51].

The development of pseudo-ductile composites following micromechanics tailoring dictates that for a given composite to exhibit strain-hardening behavior featured by steady-state (flat) crack growth, two criteria must be met, or the more common Griffith crack propagation mode will prevail, leading to quasi-brittle failure of traditional FRC matrices. The two criteria are (i) strength criterion and (ii) energy criterion. Strength criterion requires the matrix first-crack strength (σ_{fc}) controlled by matrix fracture toughness (K_m) and initial flaw sizes to be less than fiber bridging capacity (σ_0) on any given potential crack plane as presented in Eq. (1)

$$\sigma_{fc} \leq \sigma_0 \quad (1)$$

On the other hand, the energy criterion stipulates that, for a crack (once generated) to grow in a steady-state mode (the state where tensile strength uncouples from crack length, in contrast to the well-known Griffith residual strength concept relating a decreasing tensile strength to increasing crack size [49]), the following energy balance [Eq. (2)] has to be satisfied.

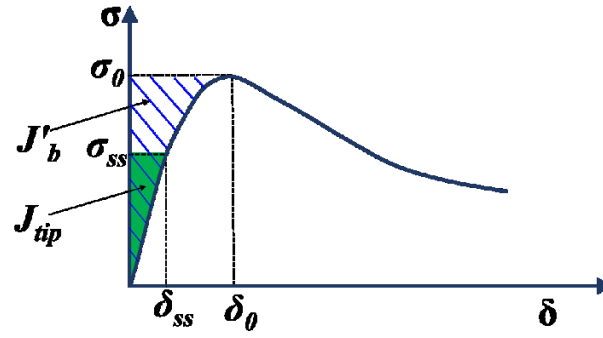


Fig. 2. Fiber bridging stress – crack opening width relationship as linked to pseudo-ductility conditions

$$J_{tip} = \sigma_{ss} \delta_{ss} - \int_0^{\delta_{ss}} \sigma(\delta) d\delta \quad (2)$$

In Eq. (2), it is observable J_{tip} reaches its upper limit under the following conditions:

$$\begin{cases} \sigma_{ss} = \sigma_0 \\ \delta_{ss} = \delta_0 \\ \sigma_0 \delta_0 - \int_0^{\delta_0} \sigma(\delta) d\delta \equiv J'_b \end{cases} \quad (3)$$

where σ_{ss} is the steady-state cracking stress; δ_{ss} is the flat crack opening corresponding to σ_{ss} (Fig. 2); J_{tip} is the crack tip toughness, which can be approximated as the cementitious matrix toughness if fiber volume fraction is less than 5%, calculated as in [Eq. (2)]; σ_0 is the maximum bridging stress which corresponds to the crack opening δ_0 and J'_b is the complementary energy controlled by fiber bridging stress and determined from the σ - δ curve.

$$J_{tip} = \frac{K_m^2}{E_m} \quad (4)$$

where K_m is the matrix fracture toughness and E_m is the matrix Young modulus of elasticity.

In consequence of Eq. (3), for crack growth to follow a steady-state mode (necessary for pseudo-ductility behavior), the crack tip toughness should not exceed the complementary energy as below:

$$J_{tip} \leq J'_b \quad (5)$$

As such, for a matrix to exhibit a tensile strain-hardening behavior, both criteria (strength and energy) must be satisfied. Otherwise, the tension-softening behavior of traditional FRC

will prevail. In this regard, while some conventional FRC may satisfy the strength criteria (governing the range of matrix flaw size), the energy criteria (governing the propagation of steady-state crack) excludes most conventional FRC and can be satisfied only when micromechanical principles are taken into account [4-6].

In the context of the current study, fiber (RECS 15 PVA fiber) parameters were kept constant, while the matrix and the fiber/matrix interface parameters were subjected to micromechanical tailoring. Matrix parameters (influenced by variable GP replacement of FA as well as by the incorporation of CF) were obtained by fracture toughness, elastic modulus, and direct tensile strength tests of the non-fibrillated matrix. On the other hand, fiber/matrix interface parameters (also influenced by variable GP replacement of FA as well as by the incorporation of CF) were obtained through the single-fiber pull-out test. The compiled micromechanical parameters were used to develop the fiber bridging stress versus crack opening relationship for the different SHCC formulations.

4 Experimental Program

The experimental program involves two phases conducted on, respectively, SHCC mortar and SHCC as a composite. The first phase addresses the effect of GP as well as the influence of nanomodification with CF on matrix-related parameters [matrix elastic modulus (E_m), fracture toughness (K_m), ultimate tensile strength (σ_{fc})], and fiber/matrix interface properties [frictional bond (τ_0), chemical bond (G_d), and slip-hardening effect (β)]. The second phase addresses SHCC performance as a composite where the effect of different GP content as well that of nanomodification with CF on composite compressive strength, flexural capacity, and direct tensile behavior was evaluated. GP content in replacement of FA consists of 0, 40, and 100% as inferred from our previous work [3]. CF was incorporated at rates of 0.0, 0.03, 0.05, and 0.10% per cement mass, as inferred from our former investigations [44-46].

4.1 Materials properties

4.1.1 Basic SHCC ingredients

SHCC ingredients in both experimental phases include high-sulfate-resistance cement (type HS) with low C_3A content, type F- fly ash (FA), type GH glass powder (GP), and quartz

sand (QS). Type HS cement was chosen to optimize mixture flowability, owing to the low C_3A and C_3S contents allowing better flow properties with this type of cement [52]. The cement has a specific gravity (SG) of 3.18, Blaine fineness of $438 \text{ m}^2/\text{kg}$, and mean particle diameter (d_{50}) of $12 \text{ }\mu\text{m}$. The FA used in the study fulfills the requirements of CAN/CSA A3000 specifications and has an SG of 2.55, Blaine surface area of $363 \text{ m}^2/\text{kg}$, and d_{50} of 17. The GP used herein is of high alkali content and has an SG of 2.51 and d_{50} of $27 \text{ }\mu\text{m}$. As for the QS, it has an SG of 2.70, maximum particle size (d_{max}) of $600 \text{ }\mu\text{m}$, and mean particle size (d_{50}) of $250 \text{ }\mu\text{m}$. Table 1 presents the chemical composition and physical properties of all granular materials used in this study, Fig. 3 provides their particle size-distribution, and Fig. 4 presents scanning electron microscope (SEM) micrographs of FA [Fig. 4 (a)] and GP [Fig. 4 (b)] used in this study. Polyvinyl-alcohol (PVA) fibers [Fig. 5 (a)] were added at 2% per volume of suspended mortar. The fiber has $38 \text{ }\mu\text{m}$ diameter and 8 mm length, 40 GPa elastic modulus and 1400 MPa tensile strength.

4.1.2 Cellulose filaments

The cellulose filaments (CF) were provided by Kruger Biomaterials Inc. (Trois-Rivières, Québec, Canada). CF are characterized by a nanometric diameter of 30–400 nm and a micrometric length of 100–2,000 μm . This results in their significantly high aspect ratio of about 100–1,000 and high surface area of more than $80 \text{ m}^2/\text{g}$. According to the supplier, the filaments were derived from FSC®-certified Kraft wood pulp using only virgin fibers to ensure optimum performance and consistent properties. The filaments were received from the supplier in a dispersed form (colloidal suspension with a nominal CF solid content of 1.2%). Further information about CF characteristics and sustainability features can be found in our former works [44–46]. Fig. 5 (b) depicts a scanning electron microscope (SEM) image of a CF diluted aqueous suspension at a concentration of 0.10%.

Table 1. Chemical compositions of powders and granular materials used in the study

Composition	Quartz	Type HS	Type F Fly	Type GH Glass
	Sand	Cement	Ash	Powder
SiO ₂	99.8	22	53.7	73.00
Fe ₂ O ₃	0.04	4.3	5.6	0.40
Al ₂ O ₃	0.14	3.5	17.5	1.50
CaO	0.17	65.6	12.4	11.30
TiO ₂	0.02	0.2	—	0.04
SO ₃	—	2.3	—	—
MgO	0.008	1.9	2.1	1.20
Na ₂ O	—	0.07	1.6	13.00
K ₂ O	0.05	0.8	2.0	0.50
ZnO	—	0.09	—	—
LOI	0.2	1.0	1.8	0.60
C ₃ S	—	50	—	—
C ₂ S	—	25	—	—
C ₃ A	—	2.0	—	—
C ₄ AF	—	14	—	—
Blaine (m ² /kg)		438	363	308

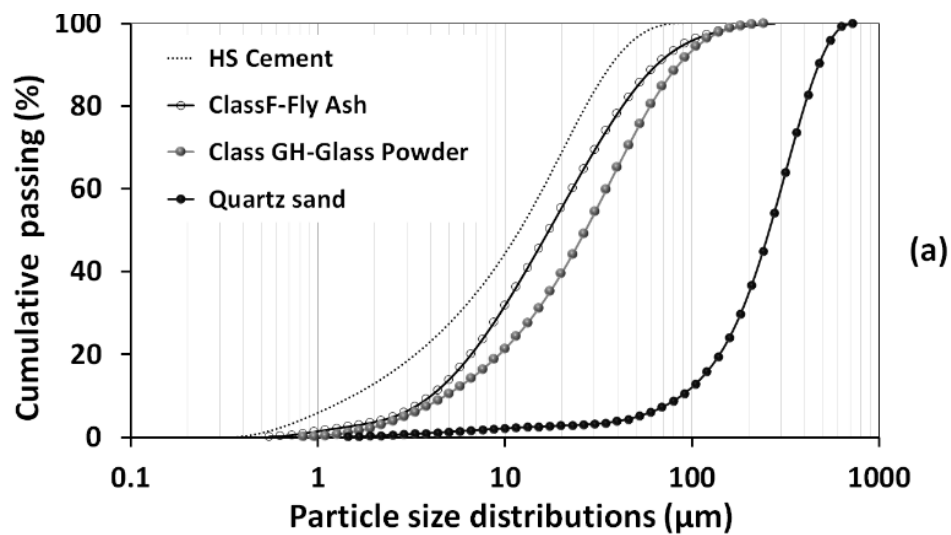


Fig. 3. Particle size distribution of SHCC ingredients

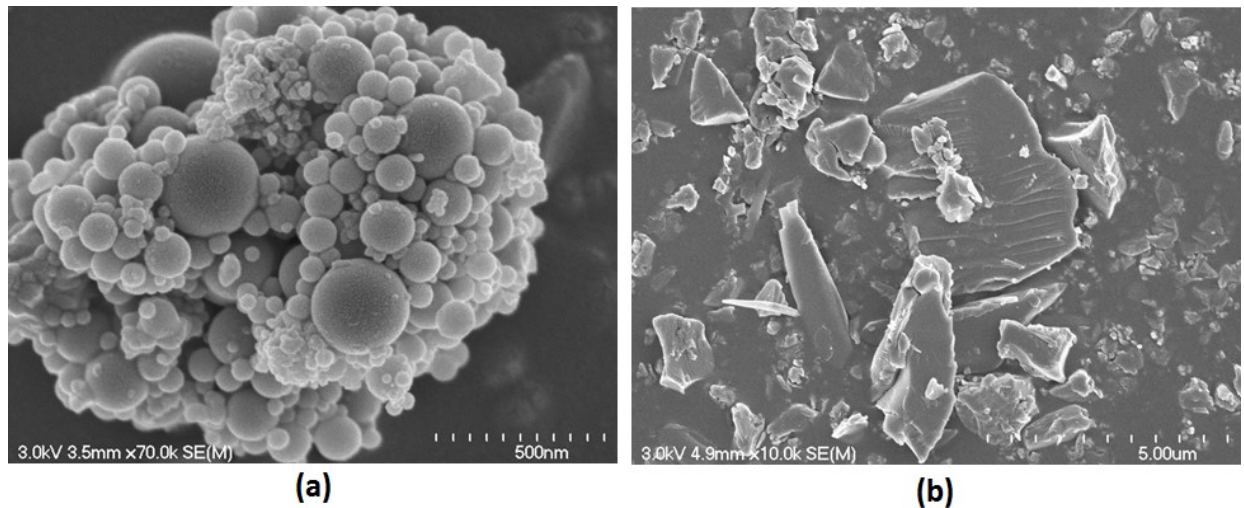


Fig. 4. . SEM micrographs of SHCC ingredients: (a) HS Cement, (b) Class F Fly ash, and (c) Glass powder, (d) Quartz sand

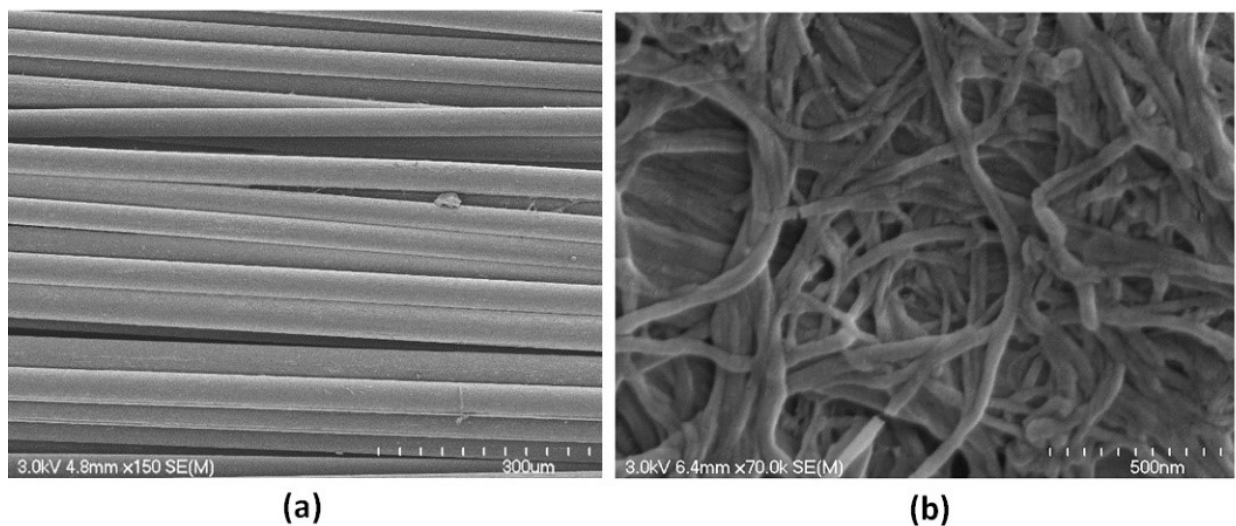


Fig. 5. SEM micrograph of hybrid reinforcement systems used in this study: (a) RECS15 polyvinyl alcohol (PVA) fibers, and (b) nanoscale cellulose filaments (CF)

4.2 Mixture proportions

A basic SHCC mixture with FA/cement ratio of 1.2, QS to binder ratio of 0.35 and a water-to-binder (w/c) ratio of 0.28 was considered. A total of 12 SHHC mixtures (comprised in three mixture series based on GP content of 0, 40, and 100% as inferred from our former work [3]) were developed. Series I involves the mixture with 0% GP (which corresponds to a conventional HVFA-SHCC). Series II involves the mixture with 40% GP (corresponding to the optimum GP content for strength and ductility as described in [3]). Series III involves

the mixture with 100% GP (corresponding to maximum GP content, but reduced ductility). Each of these series includes three additional mixtures obtained by incorporating CF at dosages of 0.03, 0.05, and 0.10% on the basic mixture with either 0, 40, or 100% GP as shown in Table 2. Resulting mixtures were tailored via the micromechanics design approach of SHCC proposed by Li et al. [4,5,12].

Mixture nomenclature consists of three parts, the first designating the percentage of FA (based on FA/cement ratio of 1.2), the second designating the percentage of GP, and the third designating the percentage of CF per cement mass. In any mixture, the binary combination of FA and GP adds up to 100 and corresponds to $(FA+GP)/\text{cement}=1.2$. For instance, the mixture 100FA-0GP-0.00CF refers to the reference HVFA-SHCC formulation with FA/cement=1.2 without neither GP nor CF added, while the mixture 0FA-100GP-0.10CF refers to complete replacement of FA with GP and the addition of CF at 0.10% per cement mass. A poly-carboxylate (PCE)-based high-range water reducing admixture (HRWRA) with a *SG* of 1.09 and solid content of 40%, fulfilling the requirements of ASTM C494 Type F admixtures [53] was used to secure the target mini-slump flow diameter of 300 ± 20 mm for phase 1 (suspended mortar) and 250 ± 20 mm for phase 2 (fibrillated matrix). The effect of these different formulations on SHCC salient characteristics represents the main theme of this study.

Table 2. Mix design of HVGP SHCC

Series	No.	Mixture name	Mixture Composition (kg/m ³)								
			Cement	Fly ash (FA)	Glass powder (GP)	Quartz sand (QS)	Water	Water/binder (W/B)	Packing density (PD)	HRWRA (solid extract)	CF (solid extract)
I	1	M100FA-0GP-0.00CF	597	717	—	460	366	0.28	0.64	3.251	—
	2	M100FA-0GP-0.03CF	597	717	—	460	366	0.28	0.64	4.014	0.175
	3	M100FA-0GP-0.05CF	597	717	—	460	366	0.28	0.64	4.125	0.292
	4	M100FA-0GP-0.10CF	597	717	—	460	366	0.28	0.64	4.589	0.584
II	5	M60FA-40GP-0.00CF	596	429	286	459	364	0.28	0.70	4.433	—
	6	M60FA-40GP-0.03CF	596	429	286	459	364	0.28	0.70	5.534	0.175
	7	M60FA-40GP-0.05CF	596	429	286	459	364	0.28	0.70	5.913	0.292
	8	M60FA-40GP-0.10CF	596	429	286	459	364	0.28	0.70	6.084	0.584
III	9	M0FA-100GP-0.00CF	593	—	717	458	360	0.28	0.74	9.136	—
	10	M0FA-100GP-0.03CF	593	—	717	458	360	0.28	0.74	9.180	0.175
	11	M0FA-100GP-0.05CF	593	—	717	458	360	0.28	0.74	9.286	0.292
	12	M0FA-100GP-0.10CF	593	—	717	458	360	0.28	0.74	9.479	0.584

4.3 Mixing procedures and specimen preparations

Batching of different SHCC mixtures was carried out using a pan mixer of type Mortarman 360 (Imer, CA, USA). In an attempt to deflocculate powder agglomerates and enhance mixture homogeneity, all powders and granular materials were dry-mixed for 7 min prior to adding water and HRWRA. In the second step, 90% of the HRWRA diluted into 95% of the mixing water was added to the mixer slowly during 0.5 min then mixing continued for 2.5 min. For mixtures incorporating CF, a CF-water suspension was first prepared from readily dispersed CF (colloidal suspensions with 1.2% CF solid content). Thereafter, 90% of HRWRA was diluted into 95% of CF-water suspension so that the HRWRA further enhances CF dispersion. Further details about CF characteristics and dispersion protocol can be found elsewhere [46]. Since SHCC formulation is quite challenging and the threshold between a stable mixture and a segregating one is very delicate, the remaining 10% of HRWRA is left for final adjustment of mixture flowability such that the final HRWRA content would be determined on a performance basis. In the third step, the mixer was stopped for 0.5 min to scrape its blades and edges then mixing continued for another 1 min. The consistency of the suspended mortar was then checked such that when a mini-slump flow diameter of 300 mm was obtained [54], only the remaining water is added (after adjustment of the amount of water contained in the unused 10% of HRWRA). Otherwise, a gradual amount of HRWRA is added (along with an adjusted amount of the remaining 5% of water) until the desired 300 mm mini-slump flow diameter is achieved.

For phase I experiments involving tests required for micromechanical modeling (E , K_m and interface properties from single-fiber pull-out tests) using plain SHCC, the resulting mixture was sampled into the required test specimens. On the other hand, for phase II experiments involving the performance of SHCC as a composite (in the presence of PVA fibers), the PVA fibers were added slowly during 1 min. Mixing continued for another 3 minutes to allow PVA fibers to be evenly dispersed. Finally, following 2 minutes of rest, concrete is remixed for 1 minute then sampled for the different tests. Specimens for mechanical properties were covered with plastic sheets and kept in a room with relative humidity and temperature of approximately 50% and 23 °C, respectively then demoulded or 24±1 h later. The specimens were then sealed inside plastic bags then transferred for storage in a fog room at 100% RH and 22 °C temperature until the age of testing.

4.4 Test methods

4.4.1 Packing density

The packing density for the basic formulations containing GP at 0, 40, and 100% were determined following the compressible packing model (CPM) proposed by De Larrad [55] as detailed in our former work [3] in the context of developing HVGP-SHCC.

4.4.2 Fresh properties

The unit weight, air content (ASTM C 185) [56], and mini-slump flow test (ASTM C 1437) [57] were measured to evaluate the fresh properties of different SHCC formulations for both test phases.

4.4.3 Phase I Tests: Micromechanics and fracture tests on SHCC matrix

To compile the parameters required for micromechanical tailoring of SHCC mixtures, fracture toughness, direct tension, and single fiber pull-out tests were conducted on fibreless SHCC matrix (mortar).

4.4.3.1 Matrix elastic Modulus

Elastic modulus (E) was evaluated on 100×200 cylinders at 28 days following the procedures described in ASTM C469 [58].

4.4.3.2 Matrix fracture toughness

Fracture toughness (K_m) test was performed following a procedure adapted from ASTM E399 [59]. The test was conducted at 28 days on 100×100×400 mm plain (non-fibrous) prisms (of 25 mm deep, 3 mm central notch) tested in three-point bending configuration in a displacement-controlled mode using a displacement rate of 0.05 mm/min. The notch depth was subsequently remeasured, and K_m was calculated according to Eq. (6) below:

$$K_Q = \frac{P_Q S}{BW^{3/2}} * f\left(\frac{a}{w}\right) \quad (6)$$

where P_Q is the applied load, S the span width, B the prism height, w the specimen depth, and $f(a/w)$ is a calibration factor (ranging between 1.91 and 2.18 with respect to the accurate notch depth) [18, 59]. Test set-up for evaluating K_m is depicted in Fig. 6 which also illustrates the variables used in Eq. (6). While the above-mentioned test guidelines were initially set for metals and alloys, the fracture toughness obtained based on this method is also reliable for cement composites with a maximum aggregate size of 1000 μm [18], such as the case of the SHCC developed herein with maximum QS size of 600 μm .



Fig. 6. Fracture toughness test: (a) Test set-up illustrating the variables used in Eq. (6), and (b) Test samples

4.4.3.3 Direct tensile strength

This test was conducted on plain (non-fibrous) dog-bone shaped coupons (Fig. 7) in order to determine the tensile strength of the plain matrix (σ_{fc}). The test was conducted under a displacement-controlled mode at a rate of 0.2 mm/min. The test set-up is equipped with a 24.4 mm wire extensometer attached at the middle of the sample. This is supplemented by a laser-type extensometer such that all elastic and plastic deformations are well captured. This is particularly important for phase II tests where at composite level, SHCC coupons subjected to uniaxial tension develop intensive multiple cracking extending beyond the reading range of the laser extensometer, which lead sometimes to relaxation in the reading captured by the wire extensometer. The use of laser extensometer in companion, allows correcting such errors.

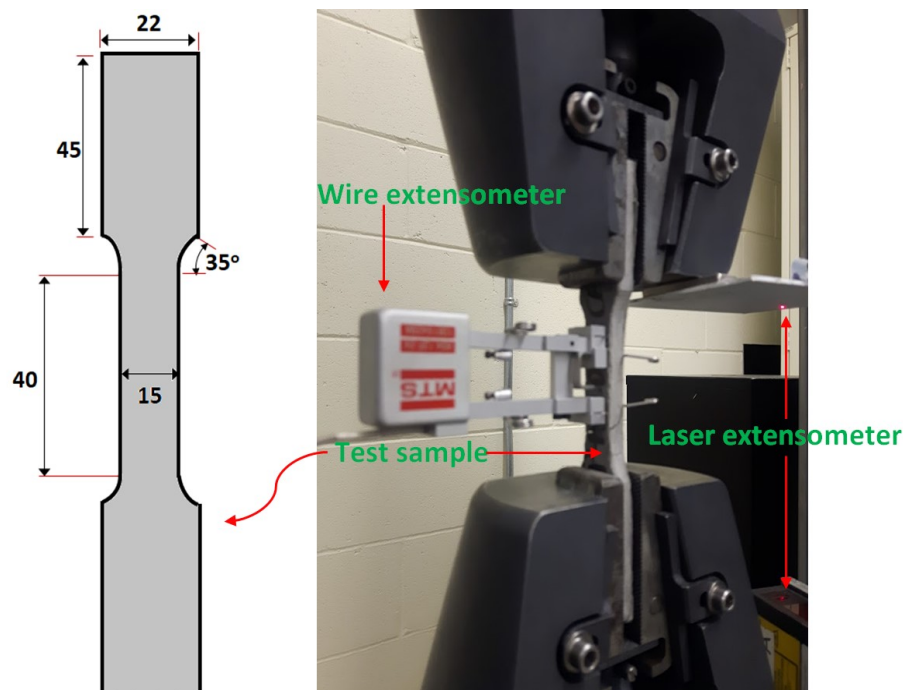


Fig. 7. Uniaxial tension test: The figure illustrates sample dimensions (left) and test configuration (right)

4.4.3.4 Single fiber pull-out

Single fiber pull-out test (SFPT) was conducted to evaluate fiber/matrix interface properties necessary for micromechanical modeling. Owing to the high precision requirements in SFPT, a miniature load cell of 5-N capacity of Zwick type (Zwick Roell, Germany) was used for this purpose. The test was conducted under a displacement-controlled mode at a rate of 0.2 mm/min. To minimize elastic stretching, the fiber was gripped at less than 1 mm from the matrix top surface. Fig. 8 (a) illustrates the test set-up of SFPT, while Fig. 9 (b) depicts the actual test configuration where two PVA fibers are visible one of which being tested. For each mixture, 4-7 successful SFPT were obtained. Following the above procedures, fiber pull-out load versus fiber slip response was recorded for all mixtures. This allowed to determine fiber/matrix interface properties in terms of frictional bond (τ_0), chemical bond (G_d), and slip hardening coefficient (β). These properties were further used to characterize the fiber bridging capacity and develop fiber stress crack opening response (σ - δ) for the different formulations. Elaborated details about specimen preparation, test procedures, and method of determining interface parameters are provided elsewhere [34].

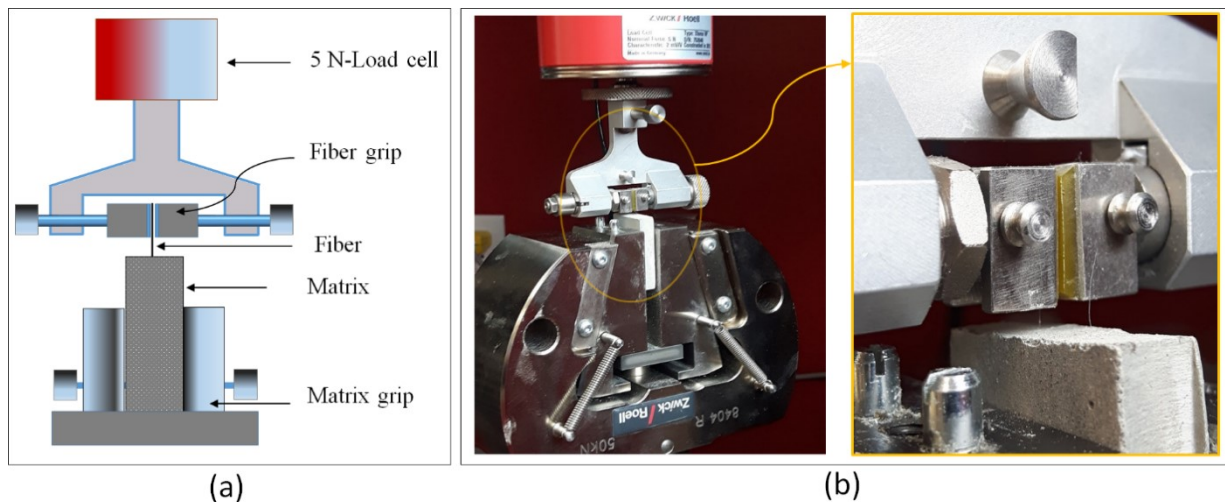


Fig. 8. Single-fiber pull-out test: Schematic of test set-up (a), actual test configuration with a focus on a single fiber being pulled from the matrix (b).

4.4.4 Phase II Tests: Performance of SHCC composites

Tests conducted in Phase I constitute the groundwork for the development of SHCC. The performance of the developed SHCC mixtures was then validated at the composite level in terms of compressive strength (f_c), direct tensile strength (f_t), and flexural capacity (f_{fl}). The

f_c was assessed on 50×50×50 mm cubes (ASTM C109-16) [60] at 1, 7, 28, 56, and 91 days. The f_t was evaluated at 28 days following the same procedures and specimen dimensions described earlier for the case of the plain matrix (section 4.4.3.3). The f_{fl} was evaluated on 100×100×400 mm prisms (ASTM C78-18) [61] at 28 days. Flexural tests were performed under four-point bending configuration in a displacement-controlled mode using a displacement rate of 0.05 mm/min.

5 Results analysis and discussions

5.1 Results of SHCC matrix used for micromechanical investigation

5.1.1 Matrix packing density

Table 2 displays the packing density for the three SHCC categories (0, 40, and 100%GP replacement of FA) considered in the current study. Results indicate that GP plays a filler effect whereby with increasing GP content, mixture compactness increases. Thus, incorporating GP increased the packing density from 64% in the reference SHCC (with no GP) to 70 and 74%, respectively, in the SHCC mixtures with 40, and 100% replacement of FA with GP. In agreement with this trend, the combined particle-size distribution (PSD) for the three basic SHCC mixtures (Fig. 9) also indicates that at increasing replacement of FA by GP, a wider-range of mixture particle-size is obtained. This implies a better gradation of granular materials [62]. In this regard, the filler effect imparted by GP and the subsequent higher packing density can also be correlated with the gradation of different granular materials shown earlier in Fig. 3. The latter indicates that GP [with a mean particle size (d_{50}) of 27 μm] as compared to that of cement ($d_{50} = 12 \mu\text{m}$) and FA ($d_{50} = 17 \mu\text{m}$), can permit filling the particle gap between the binders (cement and FA) from one side and the QS ($d_{50} = 250 \mu\text{m}$) from another side. This is more evident from the PSD curve for GP falling between that of QS from one side that of FA and cement from another side. The increasing packing density with the irregularly shaped (but larger) GP particles as opposed to the spherically-shaped (but relatively smaller) FA particles can also be ascribed to the reduced voids obtained when larger particles leading to wider gradation are used [32, 62]. This has been reported to lead to higher packing density than when perfect-geometry particles leading to narrow gradation are used [63, 64]. Furthermore, the tendency of flaky GP particles towards forming a layered stacking may explain the increased packing density obtained with

GP [65]. This trend has been observed in a more pronounced manner when various rates of GP replacement of FA were considered in our former work [3] and is believed to drive higher composite strength commonly. However, in light of the increasing matrix fracture strength (K_m) accompanying the enhanced matrix compactness, caution must be paid to the consequent rise in crack tip toughness ($J_{tip} = K_m^2/E_m$) [4, 6,12]. The latter jeopardises steady-state cracking necessary for pseudo-ductility behavior of SHCC.

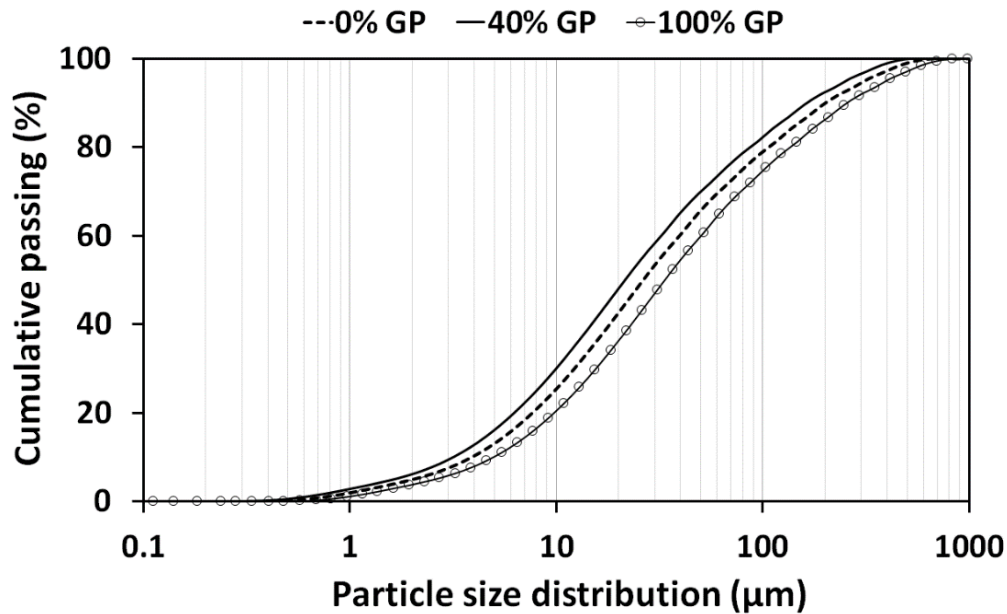


Fig. 9. Combined particle size distribution for the different SHCC formulations

5.1.2 Fresh properties

The fresh properties of plain SHCC mixtures used for the micromechanical investigation are presented in Table 3. While all mixtures had comparable slump flow 300 ± 20 mm, mixture proportions presented earlier in Table 2 indicate that to maintain the above target slump-flow, increasing demand in high-range water reducing admixture (HRWRA) was observed with the replacement of FA by GP. This can be linked to higher packing density imparted by GP as discussed in the previous section. In this regard, the GP particles (with their filler effect) tend to fill-up the inter-particle space, thereby decreasing the space available for particle dynamics [32]. Thus, additional to the paste needed to fill-up the inter-particle space, an excess amount of paste is needed to lubricate the mix and give it enough workability. Another explanation of the increase in HRWRA in the presence of GP can be the excess inter-particle frictional forces generated by the irregularly-shaped, rough-textured glass

particles [Fig. 4 (b)] as compared to the spherically-shaped smooth-surfaced FA particles [Fig. 4 (a)].

While the GP filler effect, particle morphology, and surface texture [32] may contribute towards explaining the increasing demand in HRWRA observed with GP, former works conducted with GP showed opposite trend and reported that the incorporation of GP does not affect mixture rheology [31, 66-69]. The reconciliation between the two trends is possible when it is observed that GP influences rheology through both physical and chemical effects. The physical effect emerges from GP irregular particle shape and rough surface texture, while the chemical effect emerges from the high alkali content whereby the elevated concentration of alkali ion is expected to accelerate the solubility of Ca^{+2} ions, thereby serving as a hydration catalyst [70]. In this regard, both physical and chemical effects are expected to be significant at high GP content, while most previous investigations were conducted on low GP content $\sim 20\text{-}30\%$ where the effect of GP on rheology may not be clearly captured. Thus, in the current study and elsewhere [71], the high-volume content of GP may mobilise a synergetic effect between the high alkali content and the morphology effect of GP, thereby leading to reduced flowability.

On the other hand, results also indicate that the incorporation of CF increases the demand in HRWRA owing to the viscosity modifying (VMA) effect of CF. The latter stems from CF hydrophilicity together with CF propensity for forming a percolating nanoscale network contributing to the viscosity buildup as demonstrated elsewhere [45]. In this regard, the VMA effect of CF is also accompanied by a shear thinning effect leading to reduced mixture resistance to flow at increasing shear rates [45]. Thus, for a target mini-slump flow diameter in the suspended mortar of 300 ± 20 mm (which was found to correspond to optimum flowability to enable fiber dispersion), the incorporation of GP and that of CF lead to higher demand in HRWRA. Adequate adjustment of HRWRA allowed achieving the slump flow of 300 ± 20 mm in the suspended mortar and facilitated achieving SHCC mixtures with a self-consolidating ability (slump flow of $\sim 250\pm 20$ mm).

Table 3. Fresh properties of SHCC plain mix used for the micromechanical investigation

Series	No.	Mixture name	Fresh properties			
			Slump-flow diameter (mm)	Air content (%)	Unit weight (kg/m ³)	Temperature (°C)
I	1	M100FA-0GP-0.00CF	315	4.25	2034	21
	2	M100FA-0GP-0.03CF	305	4.22	2021	23
	3	M100FA-0GP-0.05CF	305	4.98	2018	24
	4	M100FA-0GP-0.10CF	300	5.21	2015	25
II	5	M60FA-40GP-0.03CF	300	4.18	2032	23
	6	M60FA-40GP-0.00CF	310	3.90	2039	22
	7	M60FA-40GP-0.05CF	300	4.31	2030	23
	8	M60FA-40GP-0.10CF	295	4.43	2027	23
III	9	M0FA-100GP-0.00CF	300	4.41	2035	23
	10	M0FA-100GP-0.03CF	305	4.24	2025	22
	11	M0FA-100GP-0.05CF	305	5.10	2023	23
	12	M0FA-100GP-0.10CF	295	5.46	2015	22

5.1.3 Micromechanical investigation

5.1.3.1 Effect of glass powder on micromechanical properties

Table 4 depicts the results of the micromechanical investigation conducted in this study. The table presents matrix and fiber/matrix interface parameters involved in constructing the fiber-bridging stress versus crack opening response (σ - δ curve) for the three SHCC series considered herein. Regarding matrix parameters, results reveal that the variation of GP across the three basic SHCC mixtures (0, 40, and 100% GP) has slightly enhanced the elastic modulus (E_m), but significantly increased the fracture toughness (K_m) and first crack strength (σ_{fc}). This is ascribable to the contribution of GP on increasing matrix compacity as discussed earlier as well as to the pozzolanic activity of GP which can foster forming new hydrates contributing to pore refinement and increasing matrix strength [28].

Regarding interface parameters, the most obvious effect of GP was reflected by a higher frictional bond (τ_0) which increased from 2.9 MPa at 0 GP to 4.30 and 6.84 MPa at 40 and 100%GP, respectively. This corresponds to increases of, respectively, 1.5 and 2.3 times and can be a direct implication of the higher compacity obtained with GP whereby the fiber/matrix interfacial transition zone becomes denser and stiffer and leads to increasing τ_0

[34]. High τ_0 values may augment the pull-out resistance of fibers and lead to SHCC with higher strength [3] given the direct correlation between τ_0 and the maximum bridging stress (σ_0), provided that fiber rupture is ignored [39]. However, excessive τ_0 can lead to fiber damage [34], thereby reducing the slip distance and lowering composite ductility [50]. Thus, for achieving strain-hardening behavior, interface properties need to be optimized rather than maximized [34]. The chemical bond (G_d) on the other hand, showed a relatively decreasing trend with higher GP content most likely due to the dilution effect of GP reducing the concentration of Al^{3+} and Ca^{2+} cations responsible for chemical adhesion between the cementitious matrix and PVA fibers [72, 73], while the slip hardening coefficient (β) was non-significant ($\beta \approx 0$). The effect of GP on the above micromechanical parameters was observed in a more pronounced manner when more varied GP contents were considered [3].

5.1.3.2 Effect of glass powder on fiber bridging capacity

Fig. 10 shows the fiber bridging stress versus crack opening response (σ - δ) in function of GP content. The major observation from the figure is that the maximum bridging stress (σ_0) increases with higher GP (as a consequence of the higher τ_0 observed with higher GP content), while the crack opening (δ_0) corresponding to the maximum bridging stress decreases with increasing GP content. As a result, the complementary energy J_b is lower with higher GP. On the other hand, regarding matrix strength and bridging capacity, Table 4 shows that the three basic SHCC formulations satisfy well the strength criterion ($\sigma_{fc} \leq \sigma_0$). The energy criterion ($J_{tip} \leq J_b'$) is also satisfied, but the ratio J_b' / J_{tip} was observed to drop with higher GP content. This seems to be a penalty of the higher matrix fracture toughness K_m and the reduced δ_0 (observed with high GP) which lead to lower J_b' but higher J_{tip} . As such, higher GP content adversely affected the ductility.

5.1.3.3 Effect of nano-modification with CF on micromechanical properties

As presented in Table 4, the results of matrix parameters indicate that tailoring of SHCC by the incorporation of the nanoscale cellulose filaments (CF) turned to significantly influence both matrix and interface properties for the three SHCC categories considered for nanomodification.

Regarding matrix parameters, CF increases matrix mechanical properties, namely the elastic modulus (E_m), the fracture toughness (K_m), and the first cracking strength (σ_{fc}). For instance, the incorporation of CF lead to an increase of up to 15, 10, and 12% in the SHCC mixtures

with 0, 40, and 100%GP, respectively. The effect of CF on increasing E_m can be attributed to the microstructure changes led by the nanoscale CF owing to its high surface area ($>80 \text{ m}^2/\text{g}$) and to its high surface reactivity driven by the omnipresent hydroxyl groups (OH-). This has been reported to foster CF interaction with hydration products containing hydrogen in their structure such as calcium-silicate-hydrate (C-S-H) and calcium hydroxide (CH) [74]. A micro-to-macro investigation by Hisseine et al. [46] indicated that CF enhances overall mechanical performance and particularly E_m by a coupled effect of an increased degree of hydration (driven by the hydrophilic and hygroscopic CF) and by a nanoreinforcing effect. In the latter, assessment of micromechanical properties of the main microstructure phases using the NI-QEDS method [75], revealed that CF enhanced the micromechanical properties (indentation modulus M , indentation hardness H , and contact creep modulus C) of the calcium-silicate-hydrate (C-S-H) gel matrix by about $\sim 12\text{--}25\%$. In the same context, cellulose nanocrystals (CNC) were found to foster the formation of a larger volume fraction of high-density C-S-H relative to a smaller volume fraction of low-density C-S-H [76] as well as to result in stiffer high-density C-S-H [77]. As a result, the nanoscale cellulose reinforcement influences composite performance by altering the material properties.

The above-discussed effect of CF on increasing the elastic modulus can influence the strain-hardening behavior of the composite. Given the definition of crack tip toughness (J_{tip}) as a function of the elastic modulus and the fracture toughness ($J_{tip} = K_m^2/E_m$), it can be seen that the increase in E_m is fundamental for reducing J_{tip} and fulfilling the energy criterion ($J_{tip} \leq J_b$) for SHCC [4-6,12].

While PVA fibers in HVFA-SHCC generally exhibit slip hardening effect [78], this was not recorded in this study. Rather, the results discussed in the previous section indicate that with HVGP, interface properties are mainly characterized by: (i) a significant increase in frictional bond τ_0 , (ii) slight drop in chemical bond G_d , and (iii) a marginal effect on slip-hardening behavior β . In the presence of CF, however, fiber/matrix interface properties exhibited unexpected behavior. The frictional bond τ_0 was lowered in all tested three categories of SHCC. This was more evident in mixtures with GP (exhibiting higher packing density, namely 40%GP and 100%GP). By the incorporation of CF, the reduction in τ_0 in these two mixtures reached up to, respectively, ~ 30 and 50% . The incorporation of CF also reduced the chemical bond G_d in all tested SHCC mixtures. Interestingly, all mixtures with CF recorded a significantly higher slip hardening with $\beta > 1.0$. The slip hardening behavior

is a characteristic feature that polymeric fibers demonstrate during the frictional sliding phase of their pull-out response, once the chemical and frictional bonds have already gone and fibers undergo sliding with either slip hardening, constant friction or slip-softening effect, characterized by the coefficient β , which is, respectively, positive, zero or negative [79]. Slip-hardening in polymeric fibers is associated with their reduced hardness as compared to that of the surrounding matrix which leads to fiber damage or surface scratch leaving behind a jamming effect in the fiber channel [78, 79]. This can increase fiber resistance to pull-out as recorded in the current study.

The above results on the effect of CF on interface properties are driven by the influence of CF on altering the fiber/matrix interfacial transition zone (ITZ). The reduced τ_0 is most probably a result of the reduced fiber/matrix friction owing to the interference of the omnipresent, high surface area ($> \text{m}^2/\text{g}$) nanoscale filaments at the ITZ (Fig. 11). In the presence of CF at fiber/matrix interface, frictional forces are expected to be reduced due to polymer-polymer friction (CF-PVA) at the expense of polymer-matrix friction (PVA-matrix). In a similar manner, G_d is reduced in the presence of CF, most likely due to the reduction of contact sites between the PVA fibers and active cations from the matrix, particularly Al^{3+} and Ca^{2+} governing the propensity of the hydrophilic PVA fibers to the cementitious matrix [72, 73]. Such an effect on SHCC interface properties has also been also observed on nanoscale calcium carbonate whiskers (CaCO_3) by Hui et al. [39] Excessive bond between PVA fibers and the matrix were reported by Redon et al. [78] to cause fiber delamination such as the scenario observed in this study (Fig. 12). This could reduce fiber bridging capacity and influence composite ductility in consequence. Therefore, attenuated τ_0 and G_d as obtained herein may be preferable.

On the other hand, the featured slip hardening behavior exhibited in the presence of CF can be attributed to a jamming effect created by the nanoscale CF inside the PVA fiber tunnel during fiber pull-out. In this regard, it was observed that with nanocellulose-modified HVGP-SHCC, the lower values of τ_0 allowed the PVA fibers to withstand (without rupturing) the deterioration of the frictional bond at loads lower than fiber apparent tensile strength. This can significantly foster multiple-cracking and ductility. Briefly, tailoring SHCC with CF appears to allow attenuating the excessive frictional bond τ_0 encountered in HVGP-SHCC, reduce the chemical bond, and impart a characteristic slip-hardening

behavior. These effects were found to underpin the contribution of CF towards improved ductility in SHCC.

5.1.3.4 Effect of nano-modification with CF on fiber bridging capacity

In light of the above micromechanical parameters of nanocellulose-modified SHCC, the fiber bridging stress-crack opening response (σ - δ) shown in Figs. 11 (a), (b), and (c) corresponding respectively to SHCC with 0, 40, and 100% GP replacement of FA were constructed and the relevant strain hardening performance indicators were extracted and presented in Table 4. Figs. 11 indicate that at for all SHCC categories, while the incorporation of CF didn't necessarily increase the maximum bridging capacity (σ_0), seemingly due to the reduce frictional bond τ_0 , the wider crack opening in CF matrices led to higher complementary energy J'_b . With the former discussion on CF effect on increasing the E_m and decreasing J_{tip} , it follows that the index J'_b/J_{tip} has been enhanced in all CF systems while preserving a ratio of $\sigma_0/\sigma_{fc} > 1.45$. This demonstrates that with nanomodification, the conventional HVFA-SHCC can achieve a further enhancement in ductility. This can be possibly leveraged for reducing the critical volume fraction of PVA fibers necessary for the transition from quasi-brittle behavior to strain-hardening behavior. On the other had, HVGP mixtures (which initially exhibited higher strength but lower strain-hardening performance), benefited from the nanomodification as evidenced by the improved J'_b/J_{tip} . This indicates that HVGP-SHCC can benefit from nanocellulose modification to yield acceptable strain hardening performance. Beyond the SHCC performance transposed from the micromechanical investigation as discussed in this section, the performance of the actual matrix is the ultimate target. Thus, next section is devoted to validating the performance at the composite level of all SHCC formulations in terms of compressive strength, uniaxial tension, and flexural capacity.

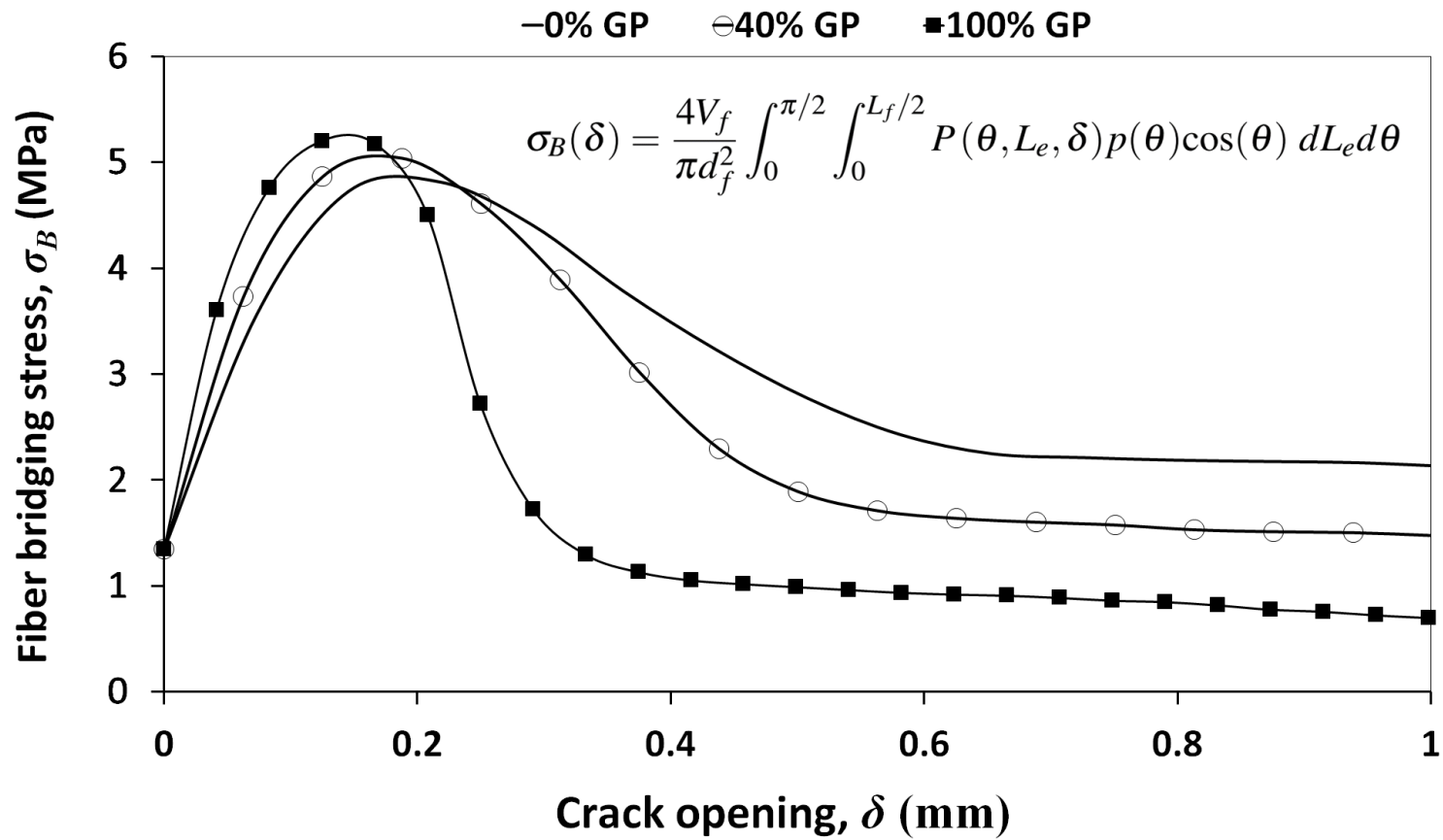


Fig. 10. Computed fiber bridging stress–crack opening relationship (σ – δ) for varying GP content

Table 4. Results of micromechanical investigation and SHCC strain-hardening indicators

Series	No	Mixture name	Matrix parameters			Interface parameters			SHCC composite pseudo-ductility performance				
			Elastic modulus, E_m (GPa)	Fracture toughness, K_m (MPa. \sqrt{m})	First crack uniaxial strength, σ_{fc} (MPa)	Frictional bond, τ_0 (MPa)	Chemical bond, G_d (J/m ²)	slip hardening coefficient, β	Maximum bridging stress, σ_0 (MPa)	Complementary energy, J_b (J/m ²)	Crack tip toughness, J_{tip} (J/m ²)	$\frac{J_t}{J_c}$	$\frac{\sigma_0}{\sigma_{fc}}$
I	1	100FA-0GP-0.00CF	22.50±0.48	0.68±0.05	2.59±0.11	2.95±0.52	2.65±0.14	0.003	4.82	64	20.5	3	1.86
	2	100FA-0GP-0.03CF	25.74±0.21	0.70±0.08	2.90±0.12	2.94±0.56	0.27±0.10	1.24±0.39	5.03	67	19.0	3	1.73
	3	100FA-0GP-0.05CF	25.50±0.19	0.71±0.04	2.90±0.08	2.82±0.66	0.25±0.12	1.51±0.20	5.15	66	19.8	3	1.78
	4	100FA-0GP-0.10CF	24.69±0.32	0.71±0.07	2.92±0.04	2.80±0.78	0.21±0.06	1.31±0.34	5.18	67	20.4	3	1.77
II	5	60FA-40GP-0.00CF	23.12±0.32	0.71±0.03	2.59±0.05	4.30±0.80	2.60±0.14	0.007	5.04	29	21.5	1	1.95
	6	60FA-40GP-0.03CF	24.22±0.14	0.75±0.05	2.69±0.19	3.83±0.32	0.30±0.02	1.18±0.10	5.12	42	23.1	1	1.98
	7	60FA-40GP-0.05CF	24.80±0.24	0.77±0.03	2.73±0.10	3.13±0.41	0.18±0.05	1.05±0.16	5.09	39	23.6	1	1.86
	8	60FA-40GP-0.10CF	25.00±0.21	0.76±0.09	2.80±0.12	3.03±0.33	0.13±0.07	1.07±0.12	5.06	45	23.4	1	1.81
III	9	0FA-100GP-0.00CF	22.81±0.11	0.78±0.06	2.81±0.10	6.84±0.80	2.56*	—**	5.20	31	26.7	1	1.85
	10	0FA-100GP-0.03CF	25.50±0.13	0.81±0.02	2.92±0.13	3.61±0.45	0.58±0.10	0.004	5.20	53	25.5	2	1.76
	11	0FA-100GP-0.05CF	25.34±0.17	0.82±0.02	2.95±0.08	3.42±0.20	0.22±0.12	0.005	5.15	52	26.4	1	1.78
	12	0FA-100GP-0.10CF	24.85±0.15	0.84±0.07	3.00±0.04	3.38±0.14	0.32±0.30	0.007	5.27	51	28.6	1	1.70

*Only one sample exhibited the Pa to Pb drop necessary for determining the chemical bond.

** No slip hardening was observed as fiber rupture was more common at increasing GP content

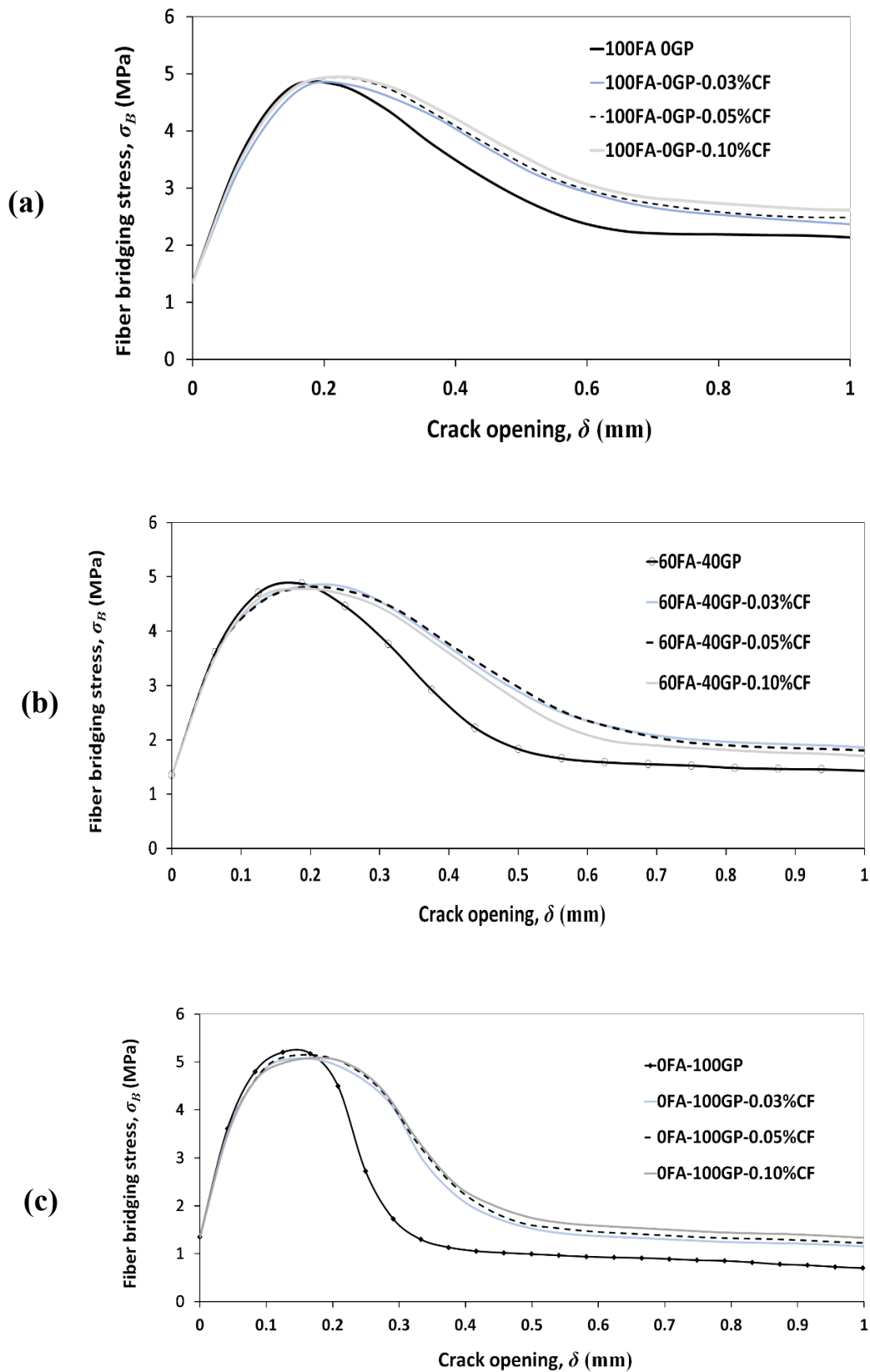


Fig. 11. Computed fiber bridging stress–crack opening relationship (σ – δ) for varying nanocellulose content in the SHCC with: (a) 0% GP, (a) 40% GP, and (c) 100% GP.

5.2 Results of SHCC composite performance

5.2.1 Compressive strength

Fig. 12 presents the development of compressive strength (f_c) up to 91 days for the three categories of tested SHCC in function of the dosage in cellulose filaments (CF). The figure indicates two trends related to, respectively, the effect of GP and that of CF on strength development. As for the effect of GP, early age strength (until 7 days) in the mixture with 40%GP (60FA-40GP-0CF) is comparable (or slightly higher) to that of the reference mixture (100FA-0GP-0CF). Beyond 7 days, higher f_c was observed in the mixture with 40%GP. The SHCC with 100%GP (0FA-100GP-0CF), on the other hand, had lower strength (at 1 and 7 days) than that the reference mixture (00FA-0GP-0CF). From 28 days, both mixtures with GP, recorded higher compressive strength than that of the reference. This trend has been recorded in a more evident manner when different GP contents were considered where strength enhancement with GP of 15–25% was achieved [3]. The effect of GP on strength development can be linked to both physical and chemical effects. GP can physically enhance the strength through a filler effect attributable to the higher packing density as detailed earlier. GP can also contribute to the strength through a pozzolanic activity, particularly at later ages [29] While GP could also contribute to early-age strength development through a catalyst effect owing to its high alkali content [70], the observed reduced strength at early ages particularly at 100%GP may be associated with a dilution effect whereby excessive GP content may physically interfere with the formation of cement hydration products at early-age [31].

On the other hand, CF appears to increase the compressive strength in all three categories of SHCC with a particularly more noticeable effect beyond 7 days. The effect of CF on strength development is also in agreement with previous findings [44] attributing it to a combination of nanoreinforcing and internal curing effects. In the former, the high-aspect ratio fibrillated CF contributes to reinforcing the microstructure, while in the latter, the hydrophilic and hygroscopic CF may contribute to increasing the degree of hydration by providing supplementary water to promote the solubilization of more anhydrous cement particles [46].

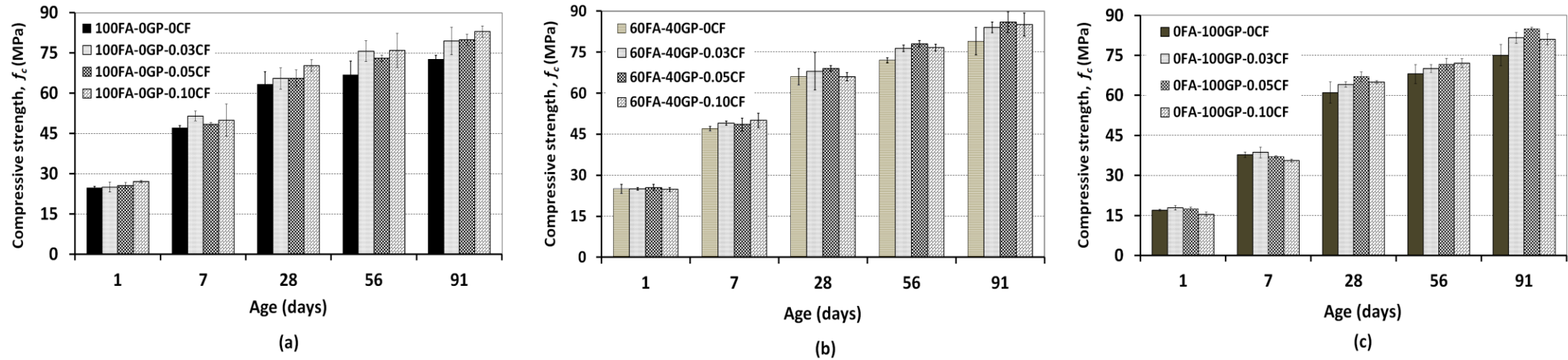


Fig. 12. Evolution of compressive strength: Effect of nanocellulose on: reference SHCC (a), SHCC with 40%GP (b), and the SHCC with 100%GP (c)

5.2.2 Tensile and flexural properties

The composite tensile and flexural properties of the developed SHCC are analyzed based on the generalized composite behavior presented in Fig. 13 and is light of the micromechanical investigation presented in section 5.1.3. Based on Fig. 13 (a), a cementitious matrix subjected to uniaxial tension will either exhibit: (i) a brittle, (ii) a quasi-brittle or (iii) a pseudo-ductile response. In the first case, the tensile response is limited by the first-crack strength (σ_{cc}) which is the case of plain concrete (PC). In the latter two cases, the tensile response is rather controlled by the post-peak strength (σ_{pc}) whereby for a strain-hardening behavior to prevail, the condition $\sigma_{pc} \geq \sigma_{cc}$ must be met [80]. For this, a multiple-cracking stage is an intrinsic feature manifested by a significant increase in the ultimate tensile strain (ϵ_u) before damage localization and response softening occur. Otherwise, a quasi-brittle failure (whereby beyond σ_{cc} , immediate softening follows) will prevail such as the case of conventional fiber-reinforced concrete (FRC). An analogous scenario exists when a cementitious matrix is subjected to flexural loading [Fig. 13 (b)]. In this case, beyond the brittle failure at first-crack load in flexure f_{cc} , the post peak behavior is rather characterized by either deflection softening or deflection hardening. In spite of this analogy, strain-hardening is more of material property and may be taken into account in structural design [14]. Deflection-hardening, on contrast, is a structural property (influenced by the dimension and cross-sectional geometry of test specimen) and therefore is not a material property in the strict sense [80].

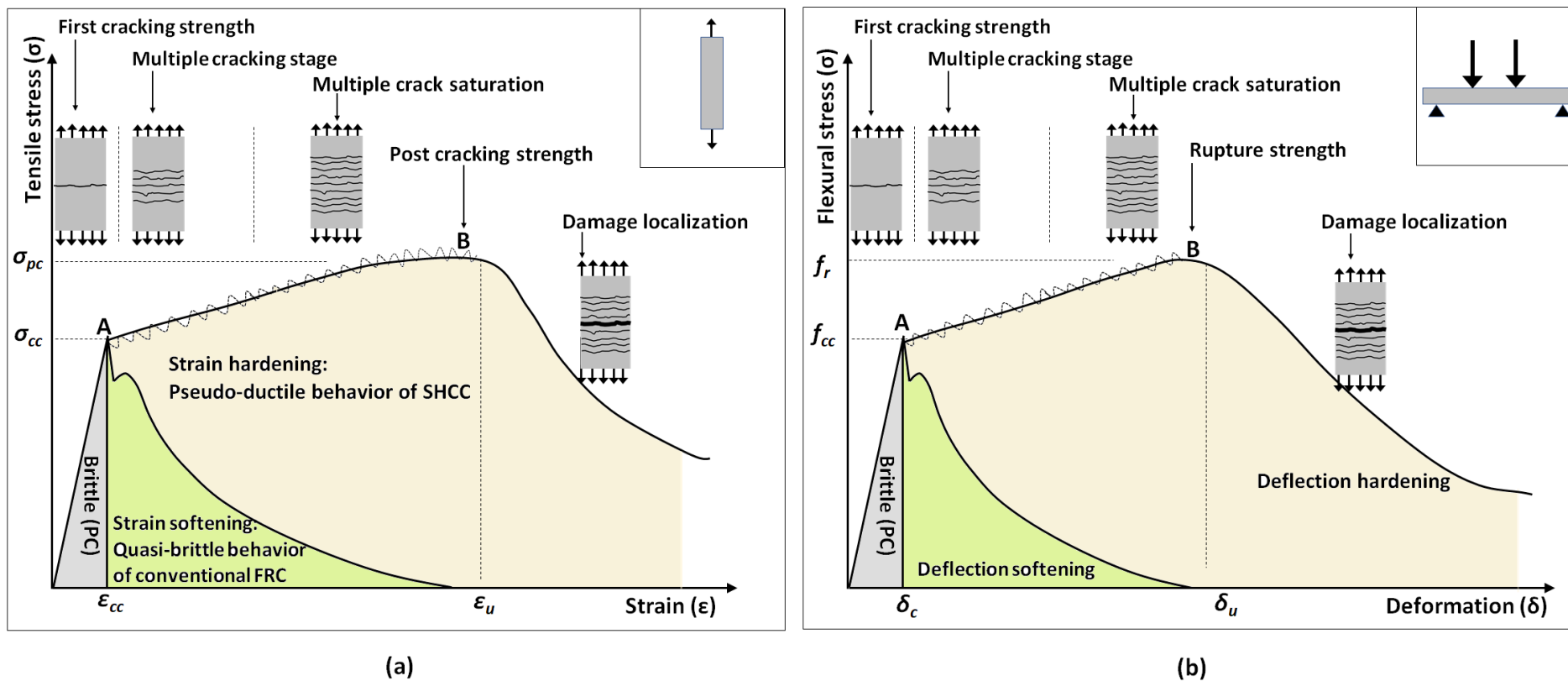


Fig. 13. Generalized response in uniaxial tension (a) and in flexure (b) for strain-hardening cementitious composites (SHCC) as compared to conventional fiber reinforced-concrete (FRC) and plain concrete (PC)

5.2.2.1 Direct tensile strength

5.2.2.1.1 Effect of replacing FA with GP

Fig. 14 presents the results of uniaxial tensile behavior of the three SHCC categories (with 0, 40, and 100%GP) considered for modification with CF. Fig. 14 (a), (e), (f) indicate that GP allows achieving higher first cracking strength (σ_{cc}) as well as higher post-peak strength (σ_{pc}) identified by the peaks A and B, respectively, in the generalized response show in Fig. 13. Thus, σ_{cc} has increased from 2.08 MPa in the reference SHCC (0 GP) to 3.15 and 4.47 MPa in the SHCC with 40 and 100%GP, respectively. This corresponds to, respectively, 48 and 112% higher σ_{cc} . Similarly, σ_{pc} has increased from 3.34 MPa in the reference SHCC to 4.00, and 5.12 MPa, respectively, in the SHCC mixtures with 40 and 100% GP. This corresponds to, respectively, 20 and 53% higher σ_{pc} . As all formulation recorded $\sigma_{pc} \geq \sigma_{cc}$, theoretically speaking, strain-hardening behavior is expected in all three mixtures.

However, the ultimate tensile strain capacity (ε_u) was slightly lowered from 3.01% in the reference SHCC to 2.78% in the SHCC with 40% GP. The drop was more significant in the SHCC with 100% GP (0.74%). While these results can be explained by the tight inverse relationship between strength and ductility in cement composites [4, 81, 82], further interpretation can be found in the effect of GP on the matrix and interface properties discussed earlier. The increased matrix strength with the incorporation of GP drives the increase in σ_{pc} influenced by the matrix [83, 84]. On the other hand, given the contribution of fibers and interface properties towards σ_{cc} [85], the increased matrix compactness can lead to a higher frictional bond between matrix and PVA fibers. This can result in higher pull-out load, hence higher σ_{cc} as observed herein. On the other hand, the reduced ultimate strain capacity ε_u can be correlated to the fiber/matrix interface properties where the increased frictional bond with high GP content may increase fiber bridging capacity but lead to lowering the corresponding crack opening. Additionally, while higher frictional bond increases the pull-out load, it can also increase the likelihood of fiber damage [Fig. 15 (b), (c)], thereby affecting the post-cracking strength σ_{pc} and ductility [86, 87]. In agreement with the above trend, as GP content was increased from 0 to 40 to 100%, higher fiber bridging stress (σ_0) accompanied with a lower crack opening (δ_0) was observed at the micromechanical level (section 5.1.3). This was found to reduce the complementary energy J'_b . In light of the increasing J_{tip} driven by the higher matrix strength of HVGP, a reduced J'_b/J_{tip} was obtained at increasing GP content. The index J'_b/J_{tip} being a key indicator

for steady-state crack growth, can be correlated with the tensile strength behavior discussed above. Thus, the ratio J_b^i/J_{tip} dropped from 3.12 in the reference SHCC to 1.35 and 1.10 in the SHCC mixtures with 40 and 100% GP. This appears to concord with overall composite tensile performance in terms of tensile strain capacity ε_u and strain-hardening behavior.

5.2.2.1.2 Effect of nanomodification with CF

Fig. 14 also presents the results of uniaxial tensile behavior of nanocellulose-modified HVGP-SHCC where the effect of CF on matrix and interface properties was investigated on three SHCC categories, namely at FA replacement with GP of 0, 40, and 100%. For each of these formulations, CF was incorporated at 0, 0.03, 0.05, and 0.10% per mass of cement. The result of Fig. 14 indicate that the influence of CF varies depending on the above SHCC categories due to the significant difference in matrix and interface properties. In the SHCC with 0GP, the effect of CF on the first-crack strength σ_{cc} is not evident. However, in the SHCC mixtures with 40 and 100% GP, σ_{cc} was reduced with the incorporation of CF, but the post-peak strength σ_{pc} was enhanced. Furthermore, CF generally led to remarkably higher ultimate tensile strain capacity (ε_u). For instance, the reference SHCC [Fig. 14 (a)] had ε_u of 3.01%, while incorporating CF at 0.03, 0.05, and 0.10% [(Figs. 14 (b), (c), (d))] in the same system increased ε_u to 3.33, 3.60, and 3.78%, respectively corresponding to 11, 20, and 26% enhancement. The three respective CF dosages also led to moderate increase in the post-crack tensile strength (from 3.34 MPa in the reference SHCC to 3.48, 3.65, and 4.10 MPa), respectively corresponding to enhancements of 5, 10, and 23%. At increasing GP where reduced ε_u was initially observed, the incorporation of CF becomes more advantageous. In the SHCC with 40% GP [Fig. 14 (e)], the incorporation of CF at 0.03, 0.05, and 0.10% [Fig. 14 (f), (g), (h)] increased ε_u from 2.78 % to 3.12, 3.54, and 3.81%, respectively corresponding to 12, 27, and 37% enhancement. The highest gain in ε_u was achieved in the SHCC with 100% GP [Fig. 14 (i)] which had initially the lowest ε_u . The incorporation of CF at 0.03, 0.05, and 0.10% [(Fig. 14 (j), (k), (l))] increased ε_u in the SHCC with 100% GP from 0.74 % to 1.81, 2.56, and 2.65%, respectively corresponding to 145, 246, and 258% higher ε_u . This can be observed to significantly improve the energy absorption capacity (the integration of the area under the stress-strain curve) by up to 238%.

These results indicate that the incorporation of CF remarkably alters the strain-hardening performance with particularly pronounced effects at high GP content. The effect of nanomodification with CF on the strain-hardening behavior can be explained in light of the

effect of CF on matrix and interface properties discussed earlier (section 5.1.3). The observed significant enhancement in ε_u stems from the increased slip hardening effect imparted by CF, while the relatively lower effect on σ_{pc} can be linked to the reduced frictional bond in the presence of CF [34]. The reduced frictional bond in systems with CF is driven by the polymer-polymer (PVA-CF) interface friction (Fig. 16 (a)) attenuating both τ_0 and G_d while fostering the slip hardening effect β . On the other hand, given the increased matrix elastic modulus (E_m) in systems with CF, a reduced crack tip toughness J_{tip} is obtained while the slip hardening effect β imparted by CF promotes fibers to maintain increasing pull-out load at higher slip distance. This implies matrix resistance of higher crack opening (δ_0) at maximum bridging stress (σ_0). As a result, higher complementary energy J'_b is obtained in systems with CF. In light of the reduced J_{tip} in systems with CF versus the increased J'_b , it follows that the incorporation of CF fosters maintaining steady-state crack growth (once cracks occur) as demonstrated by the higher J'_b/J_{tip} which is fundamental for SHCC [5, 12].

In this regard, the significant gain in composite ε_u obtained at increasing GP (particularly at 100% GP) can be explained by a threefold effect of CF. The first is the enhancement of matrix elastic modulus E_m , thereby contributing to lowering the crack tip toughness. The second is the reduction of the excessive frictional bond contributing to fiber rupture and fiber surface damage. The third, at reduced frictional bond, PVA fibers tend to slide-out of the matrix at lower pull-out load levels (below fiber apparent tensile strength), but the presence of the nanoscale CF surrounding the PVA fibers fosters a slip hardening by a jamming effect leading to increasing slip distance [34]. These effects can significantly increase composite strain capacity and translate into multiple cracking reflected by the increased frequency and intensity of load peaks in the tensile response of CF-reinforced systems.

The above results are in good agreement with the uniaxial tensile response and should be viewed with one regard on CF effect on the plain matrix and another regard on CF effect on fiber/matrix interface properties. CF enhances the strength of the plain matrix as evidenced by the higher elastic modulus (E_m), the fracture toughness (K_m), and the first cracking strength (σ_{fc}) recorded in the plain matrix in section 5.1.3.3 owing to a coupled effect of an increased degree of hydration (driven by the hydrophilic and hygroscopic CF) and a nanoreinforcing effect [44], as well as enhanced C-S-H micromechanical properties [46]. This increased strength, however, shouldn't be in conflict with the reduced first cracking load in CF-SHCC systems incorporating HVGP particularly at 100% GP observed herein.

In fact, in HVGP-SHCC, the effect of CF on interface properties appears to overcome its matrix strengthening effect. The incorporation of CF reduces both the frictional bond τ_0 and the chemical bond G_d as the omnipresent, high-surface-area, hydrophilic CF promotes polymer-polymer interactions with the hydrophilic PVA fibers at the expense of PVA-matrix interactions. This reduces the contact sites between PVA fibers and the matrix and results in lower τ_0 . Reduction of τ_0 lowers the likelihood of fiber rupture while promoting fibers to undergo higher slip hardening [34], but it also reduces the maximum pull-out load as well as the maximum bridging capacity as highlighted earlier. Consequently, the first crack-strength f_{cc} may be reduced by the lower τ_0 , while the post-peak strength f_{pc} may be improved by the slip hardening effect imparted by CF, possibly due to a jamming effect created by the omnipresence of CF at the fiber/matrix interface. This, additional to the reinforcing effect provided by CF to the matrix, may explain the higher ductility obtained with CF even in systems with high strength such as the SHCC with 100% GP.

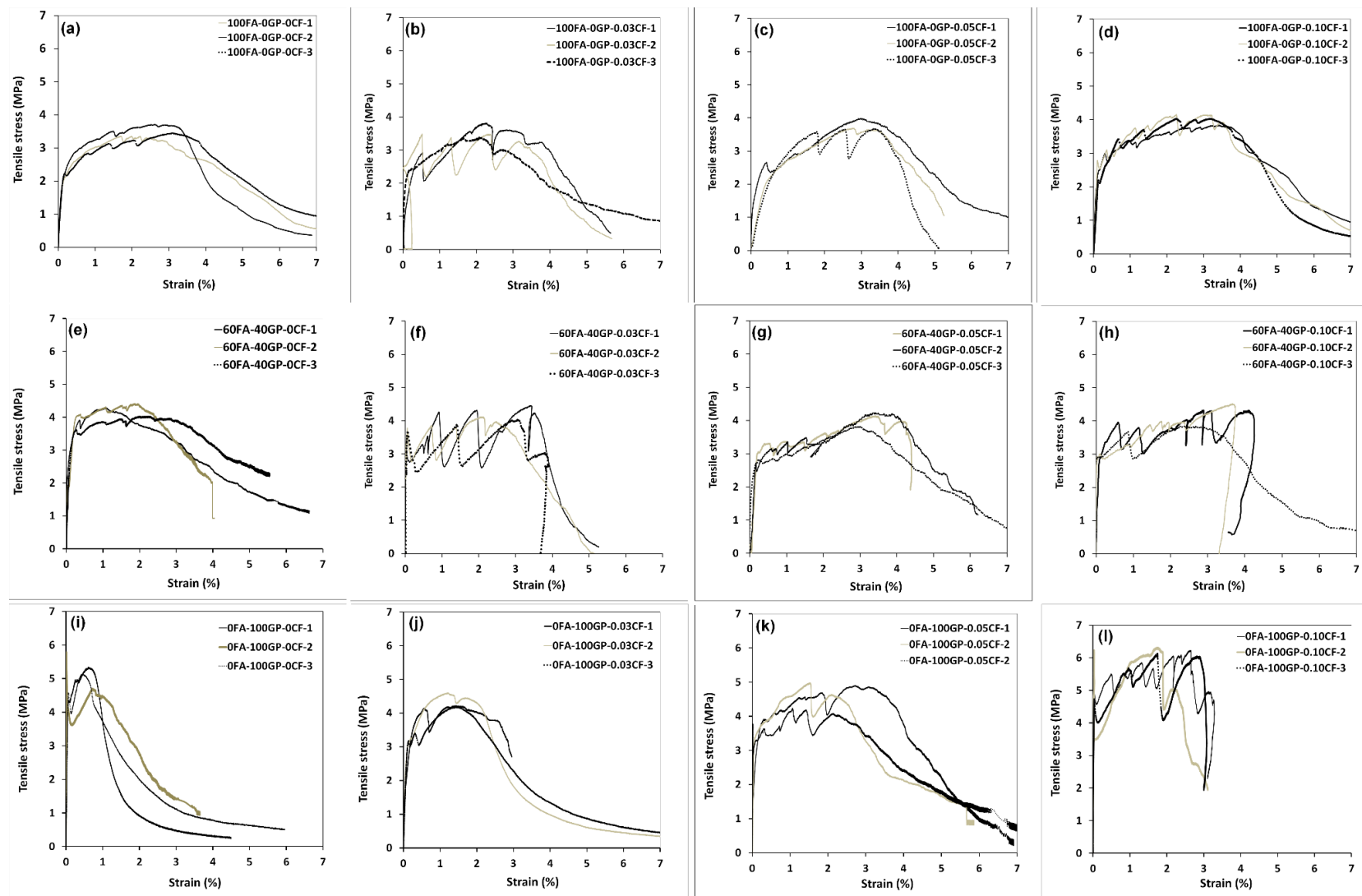


Fig. 14. Uniaxial tensile behavior of nanocellulose-modified HVGP-SHCC

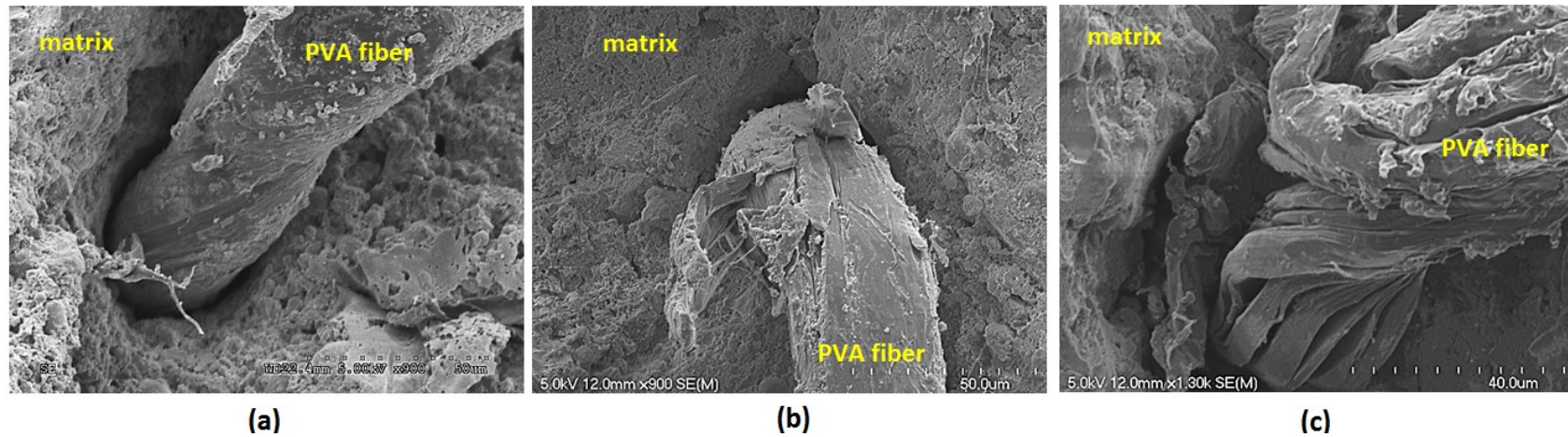


Fig. 15. PVA fiber status post-single fiber-fiber pull-out test in SHCC with: (a) 0% GP, (b) 40% GP, and (c) 100% GP. The figure illustrates fiber damage at increasing GP, which reflects the higher interface friction as well as pull-out load, but the consequent reduced slip at instances of fiber damage

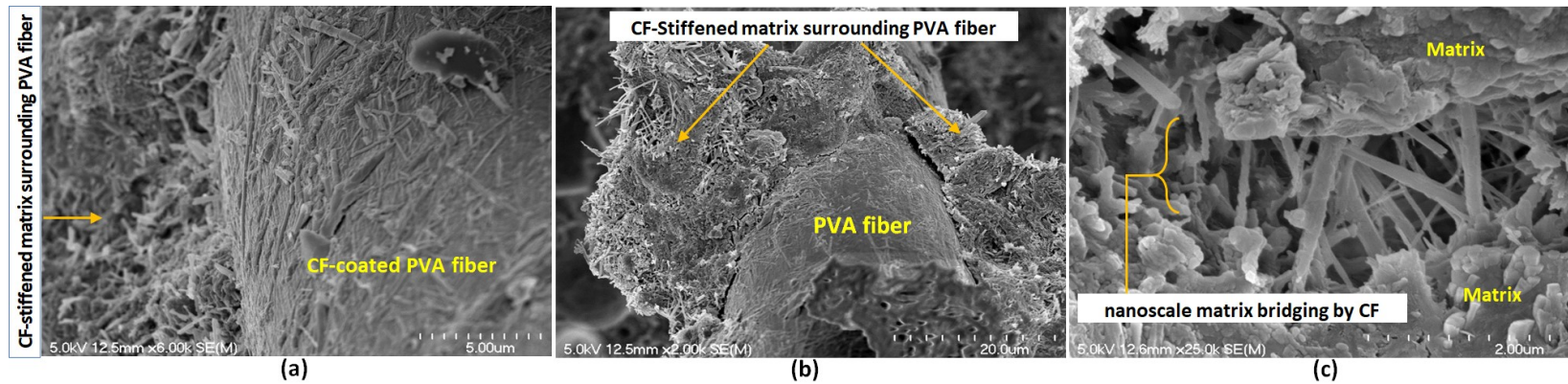


Fig. 16. Effect of CF on SHCC: omnipresence of CF on PVA fiber surface leading to altering interface properties (a and b), and nanoreinforcing matrix (b)

5.2.2.2 Flexural capacity

5.2.2.2.1 Effect of replacing FA with GP

Fig. 17 presents the results of the flexural response of SHCC with 0, 40, and 100%GP along with the respective mixtures resulting from incorporating CF at 0.03, 0.05, and 0.10% per mass of cement in the above three formulations. On the other hand, Fig. 18 illustrates the exceptional deflection capacity of a typical HVGP-SHCC, while Fig. 19 shows the multiple-cracking behavior in the above three respective SHCC categories. Overall, the flexural results recorded herein followed a pattern comparable to that observed in the direct tensile response and indicate that replacing FA with GP influenced both the flexural first cracking strength (f_{cc}) as well as the flexural post-cracking strength (f_{pc}) identified, respectively by A and B peaks in the generalized flexural response depicted in Fig. 13 (b). Higher f_{cc} was observed with increasing GP. Thus, f_{cc} was enhanced from 8.47 MPa in the reference SHCC to, respectively, 9.10 and 11.14 MPa in the SHCC with 40 and 100%GP. This is equivalent to, respectively, 7 and 31% higher f_{cc} . The post cracking strength f_{pc} of the reference SHCC (14.41 MPa), on the other hand, was not significantly affected in the SHCC with 40%GP (14.61 MPa) but experienced reduction in the SHCC with 100 %GP (9.53 MPa). The above trend of f_{cc} and f_{pc} are analogous to that observed in σ_{cc} and σ_{pc} in uniaxial tension where the former was dominated by the matrix strength transposed from the effect of GP on the compactness, while the latter was further influenced by the fiber/matrix interface properties where the increased frictional bond τ_0 with high GP content increases the likelihood of fiber damage [Figs. 15 (b) and (c)]. This may reduce post-peak strength f_{pc} and lead also to a lower ductility as reflected by the decreased deflection capacity δ_u (ultimate mid-span deflection). The latter was reduced from 3.91 mm in the reference SHCC to 2.45 mm in the SHCC with 40% GP. The drop in δ_u was more significant in the SHCC with 100% GP (0.64 mm). Therefore, next section attempts to overcome this through the incorporation of the nanoscale CF.

5.2.2.2.2 Effect of nanomodification with CF

The flexural response SHCC with 0, 40, and 100%GP subjected to nanomodification with CF are also depicted in Fig. 17. The major effect of CF appeared in the improved deflection capacity δ_u reflected by the ultimate mid-span deflection corresponding to post-cracking strength σ_{pc} . This was particularly phenomenal in the SHCC with 40 and 100% GP which have initially lower δ_u . As such, considering the reference SHCC [Fig. 17 (a)], the

incorporation of CF at 0.03, 0.05, and 0.10% [Fig. 17 (b)-(d)] resulted in δ_u of 4.51, 4.92, and 5.31 mm as compared to 3.91 mm in the reference SHCC. This corresponds to 15, 26 and 36% higher δ_u . In the SHCC with 40% GP [Fig. 17 (e)], the system without CF had a δ_u of 2.45 mm while the incorporation of CF at the above three respected dosages led to δ_u of 2.94, 3.97, and 4.56 mm [Fig. 17 (f)-(h)] (or an enhancement in δ_u of 20, 62, and 86%, respectively). The highest gain was obtained in the system with 100%GP [Fig. 17 (i)] where δ_u has increased from 0.64 in the system without CF to 1.73, 1.95, and 3.31 mm, respectively in the systems with 0.03, 0.05 and 0.10% CF [Fig. 17 (j)-(l)] which correspond to 162, 195, and 400% higher δ_u . This can be perceived to significantly improve the energy absorption capacity (the integration of the area under the load-deformation curve) by up to 293%.

In line with the above observations, the effect of CF on first-crack strength in flexure f_{cc} in the reference SHCC and in the SHCC with 40%GP was not evident. Rather a subtle reduction in f_{cc} was noticed, but a slightly higher post-cracking strength was recorded. This trend was more obvious in the SHCC with 100% GP where in the system without CF, f_{cc} was 11.14 MPa, while the incorporation of CF at 0.03, 0.05, and 0.10% reduced the f_{cc} to 7.65, 7.5, and 7.11 MPa, respectively. However, the post-peak cracking f_{pc} was enhanced. For CF contents of 0.03, 0.05, and 0.10%, the system with 100%GP, the f_{pc} was 10.12, 10.94, and 11.23 MPa as compared to 9.53 MPa in the system without CF. This is equivalent to 6, 15 and 18% enhancement in the post-peak strength f_{pc} . These results are in concord with the uniaxial tensile response discussed earlier.

Thus, the flexural and uniaxial response of SHCC demonstrates that nanomodification with CF enabled enhancing the deflection and strain capacity of all SHCC categories with a more remarkable effect at high GP systems initially deficient in ductility. The enhanced deflection and strain capacity in the reference SHCC can be leveraged for reducing the critical volume fraction of PVA fibers necessary for a strain-hardening response. On the other hand, for HVGP-SHCC, nanomodification with CF allowed significant enhancement in deflection and strain capacity leading to shifting the response from an initially strain-softening (at 100%GP) towards the desirable strain-hardening response, thereby making possible the use of GP as SCM in the design of SHCC with potentially better eco-efficiency. This can be inferred from the valorization of an otherwise waste material (waste glass) into concrete development and the valorization of the multifunctional properties of nanocellulose towards enhancing concrete performance

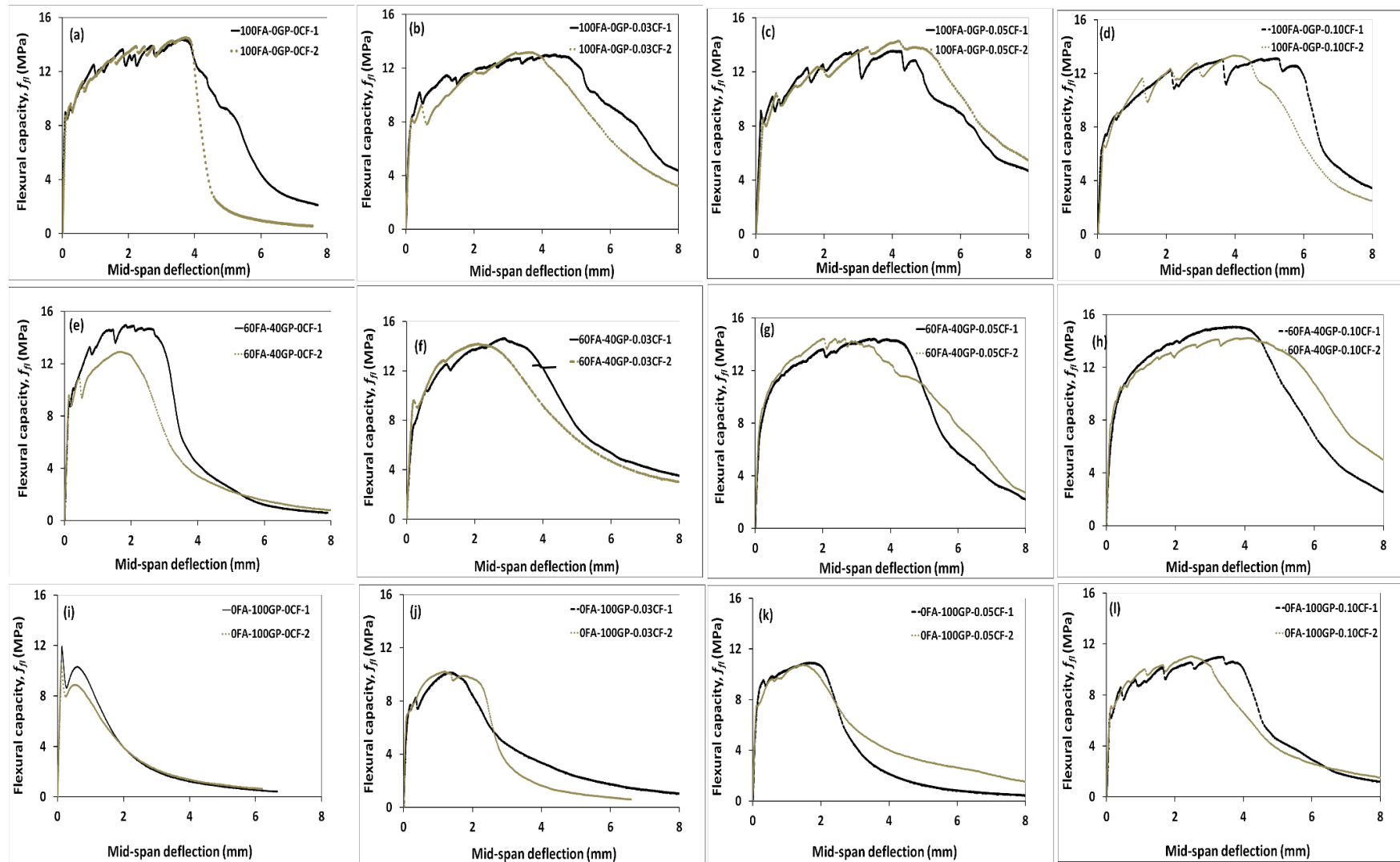


Fig. 17. Flexural response of SHCC with 0, 40, and 100% GP subjected to nanomodification with CF.

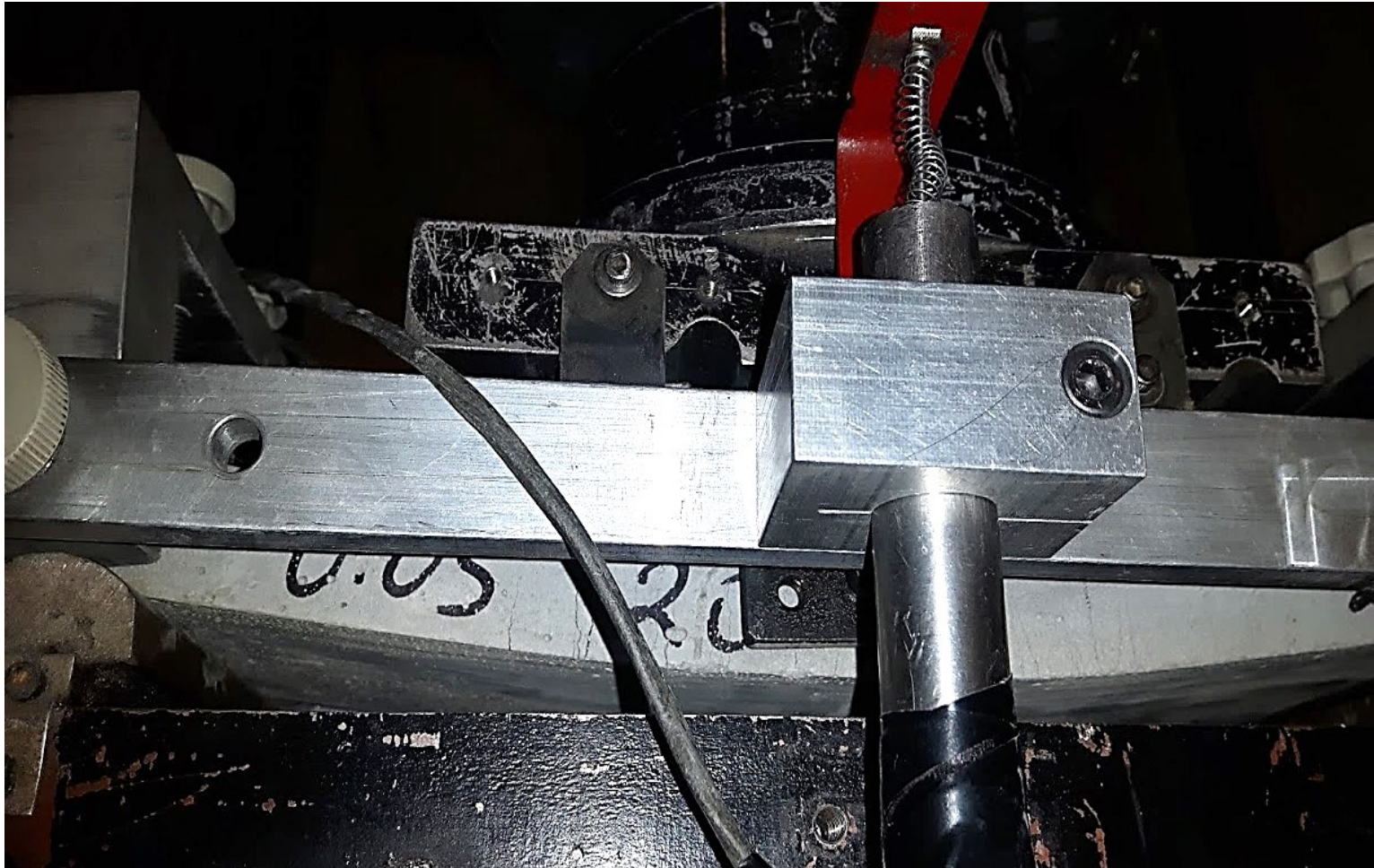


Fig. 18. Multiple cracking and deflection capacity in HVGP-SHCC. The figure illustrates the significant deflection capacity reflected by the remarkable curvature and tight multiple cracking while maintaining the peak post-cracking load for extended deformation

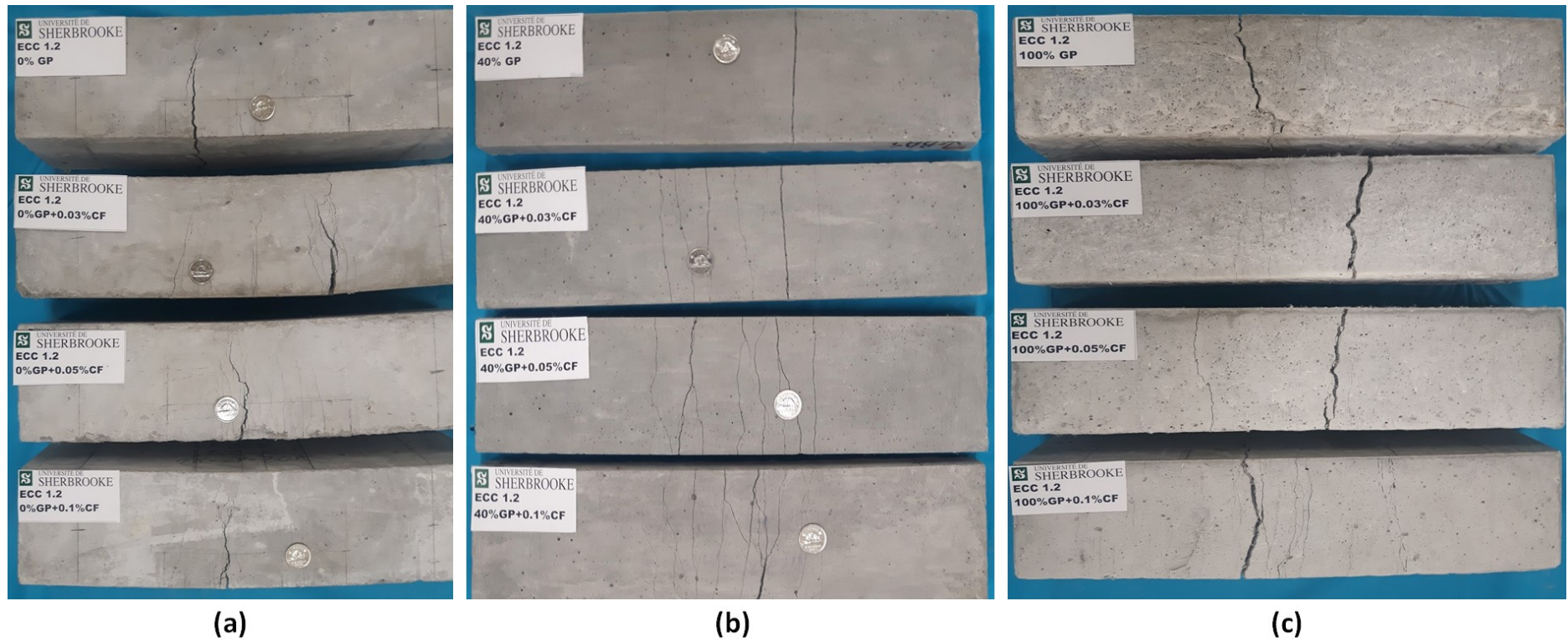


Fig. 19. Multiple cracking pattern in the different SHCC systems incorporating CF. (a) 0%GP, (b) 40%GP, and (c) 100%GPLower GP

6 Summary and conclusions

In this study, nanoscale cellulose filaments (CF) were used as a tool to nanotailor the properties of strain-hardening cement composites incorporating high-volume ground-glass pozzolans (HVGP-SHCC). The objective was to enhance the ductility of HVGP-SHCC exhibiting increased strength but reduced ductility. CF was incorporated at dosages of 0.03, 0.05, and 0.10% in SHCC mixtures containing 0, 40 and 100% ground-glass pozzolans (GP) in replacement of fly ash (FA). Single-fiber pull-out and fracture mechanics tests were conducted to construct fiber-bridging stress versus crack-opening response. Micromechanical guidelines were adopted to assess the performance of different formulations. Uniaxial-tensile and flexural capacity tests were conducted to validate the performance of different formulations. The findings of this study are summarised below:

- The incorporation of GP increased matrix strength by a combination of filler and pozzolanic effects rendering the matrix denser. Composite strength has been increased by up to 112% in the uniaxial first-crack strength, 53% in uniaxial post-peak strength, and 31% in flexural first-crack strength. The increased strength obtained with GP, however, led to reduced ductility. For instance, at 40% GP, SHCC showed comparable ductility to that of HVFA-SHCC, while exhibiting higher strength (48% higher first-crack strength in tension and 20% higher post-crack strength in tension). At 100% GP, however, the significant increase in first-crack strength (112%) resulted in a substantial drop in ultimate strain capacity (from 3.01% in the reference SHCC to 0.74%).
- The incorporation of the nanoscale CF significantly affected the strain-hardening behavior of SHCC with a more pronounced effect in systems with high GP content (100%). As such, CF was found to influence both matrix and interface properties. CF increased the elastic modulus of the matrix (~15%), and reduced the crack tip toughness, thereby contributing to improving the strain-hardening characteristics of SHCC. CF also influenced the strain-hardening behavior of SHCC by attenuating the frictional and chemical bonds and imparting a significant slip-hardening effect ($\beta > 1.0$). This was found to marginally affect the first-crack strength but enhanced the post-peak strength by up to 23%.

- The effect of CF was more pronounced on improving the ultimate strain capacity (in uniaxial tension) and the deflection capacity (in flexure). For this, the effect of CF was even more significant in the SHCC mixtures with 40 and 100%GP which had initially higher strength but reduced ductility. Thus, the incorporation of CF in the SHCCs with 0, 40, and 100%GP improved the ultimate tensile strain capacity by 26, 37, and 258%, respectively. Likewise, the deflection capacity (in flexure) in the mixtures with 0, 40, and 100% GP was improved by up to 36, 86, and 400%, respectively. As a result, the energy absorption capacity (in tension) for the above three GP contents can be enhanced with CF by up to 52, 83, and 238%, respectively. Likewise, the energy absorption capacity (in flexure) for the three GP contents (0, 40, and 100%) was enhanced with CF by up to 65, 92, and 293%, respectively.

Finally, overall results demonstrate the usefulness of CF as a tool to impart ductility to HVGP-SCHH while serving as a nanoreinforcement altering both matrix and interface properties towards improved strain-hardening characteristics. As such, nanotailoring SHCC with the incorporation of CF allowed obtaining strain-hardening behavior even with as high-volume GP as 100% replacement of FA. This can be viewed as a useful tool for designing high-performance fiber-reinforced cement composite with superior strength and ductility while promoting sustainable development.

Acknowledgements

This project is jointly supported a Cooperative Research and Development (CRD) grant from the Natural Sciences and Engineering Research Council of Canada (NSERC), Canada Vanier Graduate Scholarship (CGS) program award no: 360284, Kruger Biomaterials Inc. (QC, Canada), and Euclid Chemicals. The authors are grateful to the financial support from all these partners.

References

- [1] CSA A3001-18, Cementitious Materials for Use in Concrete, Canadian Standards Association, Toronto, ON, 2018.

- [2] M. Sonebi, Y. Ammar, P. Diederich, 15 - Sustainability of cement, concrete and cement replacement materials in construction, Editor(s): Jamal M. Khatib, In Woodhead Publishing Series in Civil and Structural Engineering, Sustainability of Construction Materials (Second Edition), Woodhead Publishing, 2016, Pages 371-396.
- [3] O.A. Hisseine, A. Tagnit-Hamou, Development of strain-hardening cementitious composites incorporating high-volume ground-glass pozzolans using a novel approach coupling packing density optimization with micromechanical tailoring, Article under review by Cement and Concrete Research, April 2019.
- [4] V.C. Li, Engineered Cementitious Composites (ECC) – Tailored Composites Through Micromechanical Modeling, Fiber Reinforced Concrete: Present and the Future, Canadian Society for Civil Engineering, Montreal, 1998, pp. 64–97.
- [5] V.C. Li, S. Wang, C. Wu, Tensile strain-hardening behavior of polyvinyl alcohol engineered cementitious composite, *ACI Mater. J.* 98 (6) (2001) 483–492.
- [6] V.C. Li, On engineered cementitious composites (ECC) – a review of the material and its application, *J. Adv. Concr. Technol.* 1 (2003) 215–230.
- [7] V.C. Li, C.K.Y. Leung, Steady state and multiple cracking of short random fiber composites, *ASCE J. Eng. Mech.* 188 (11) (1992) 2246–2264.
- [8] X. Guan, Y. Li, T. Liu, C. Zhang, H. Li, J. Ou, An economical ultra-high ductile engineered cementitious composite with large amount of coarse river sand, *Constr. Build. Mater.*, 201 (2019) 461-472.
- [9] K. Q. Yu, J. T. Yu, J. G. Dai, Z. D. Lu, S. P. Shah, Development of ultra-high performance engineered cementitious composites using polyethylene (PE) fibers, *Constr. Build. Mater.*, 158 (2018) 217-227.
- [10] Y. Ding, J. Yu, K. Q. Yu, S. Xu, Basic mechanical properties of ultra-high ductility cementitious composites: From 40 MPa to 120 MPa, *Composite Structures*, 185 (2018) 634-645.
- [11] K. Yu, L. Li, J. Yu, Y. Wang, J. Ye, Q. Xu, Direct tensile properties of engineered cementitious composites: A review, *Constr. Build. Mater.*, 165 (2018) 346-362.

- [12] V.C. Li, From micromechanics to structural engineering – the design of cementitious composites for civil engineering application, *J. Struct. Eng. Earthquake Eng.* 10 (2) (1993) 37–48.
- [13] M. Maalej, T. Hashida, V. C. Li, Effect Of Fiber Volume Fraction On The Off- Crack-Plane Fracture Energy In Strain-Hardening Engineered Cementitious Composites, *J. Amer. Ceramics Soc.* 78 (12) (1995) 3369-3375.
- [14] H. Stang, V.C. Li. Classification of Fibre Reinforced Cementitious Materials for Structural Applications. In 6th RILEM Symposium on Fibre- Reinforced Concretes (FRC), pp. 197–218, Varenna, Italy, September 2004. RILEM Publications.
- [15] S. Qian, M.D. Lepech, Y.K. Yun, V.C. Li, Introduction of transition zone design for bridge deck link slabs using ductile concrete, *ACI Struct. J.* 106 (1) (2009) 96–105.
- [16] V.C. Li, Strategies for high performance fiber reinforced cementitious composites development, in: S. Ahmad, M. di Prisco, C. Meyer, G.A. Plizzari, S. Shah (Eds.), *Fiber Reinforced Concrete: From Theory to Practice*, Proceedings of the North American/European Workshop on Advances in Fiber Reinforced Concrete, Bergamo, Italy 2004, pp. 93–98.
- [17] M. Kunieda, K. Rokugo, Recent progress on HPFRCC in Japan required performance and applications, *J. Adv. Concr. Technol.* 4 (1) (2006) 19–33.
- [18] V. C. Li, D. K. Mishra, H. C. Wu, Matrix design for pseudo strain-hardening fiber reinforced cementitious composites, *RILEM J. Materials and Structures*, 28 (183) (1995) 586-595.
- [19] S. Wang, V.C. Li, Engineered Cementitious Composites with High-Volume Fly Ash, *ACI Mater. J.* 104 (3) (2007) 233-241.
- [20] C. Lin, O. Kayali, E.V. Morozov, D.J. Sharp, Development of self-compacting strain-hardening cementitious composites by varying fly ash content, *Constr. Build. Mater.* 149 (2017) 103–110.
- [21] J. K. Kim, J. S. Kim, Ha G. J. Ha, Y. Y. Kim, Tensile and fiber dispersion performance of ECC (engineered cementitious composites) produced with ground granulated blast furnace slag. *Cem. Concr. Res.* 37(7) (2007) 096–1105.

- [22] Y. Zhu, Y. Yang, Y. Yao, Use of slag to improve mechanical properties of engineered cementitious composites (ECCs) with high volumes of fly ash, *Constr. Build. Mater.* 36 (2012) 1076–1081.
- [23] Y. Al-Najjar, S. Yes_ilmén, A.M. Al-Dahawi, M. S_ahmaran, G. Yıldırım, M. Lachemi, L. Amleh, Physical and chemical actions of nano-mineral additives on properties of high-volume fly ash engineered cementitious composites, *ACI Mater. J.* 113 (6) (2016) 791-801.
- [24] J. Zhou, S. Qian, M. G. S. Beltran, G. Ye, K. Breugel, V. C. Li, Development of engineered cementitious composites with limestone powder and blast furnace slag, *Materials and Structures*, 43(6) 803–814.
- [25] K. Turk, M. L. Nehdi, Coupled Effects of Limestone Powder and High-Volume Fly Ash on Mechanical Properties of ECC, *Constr. Build. Mater.* 164 (2018) 185-192.
- [26] E. Özbay, O. Karahan, M. Lachemi, K.M.A. Hossain, C. Duran Atis, Investigation of properties of engineered cementitious composites incorporating high volumes of fly ash and metakaolin, *ACI Mater. J.* 109 (5) (2012) 565-571.
- [27] A. Zidol, Optimization of the fineness of glass powder in binary cementitious systems, M.S. thesis, Université de Sherbrooke, Sherbrooke, Canada, 2009.
- [28] A.M. Matos, T. Ramos, S. Nunes, J. Sousa-Coutinho, Durability enhancement of SCC with waste glass powder, *Mater. Res.* 19(1) (2016) 67-74.
- [29] R. Idir, Mécanismes d'action des fines et des granulats de verre sur la réaction alcali-silice et la réaction pouzzolanique, Ph.D. thesis, Université de Sherbrooke, Sherbrooke, Canada, 2009.
- [30] A. Omran, A. Tagnit-Hamou, Performance of glass-powder concrete in field applications, *Constr. Build. Mater.* 109 (2016) 84–95, <https://doi.org/10.1016/j.conbuildmat.2016.02.006>.
- [31] N. A. Soliman, A. Tagnit-Hamou, Development of ultra-high-performance concrete using glass powder—Towards ecofriendly concrete,” *Constr. Build. Mater.* 125 (2016) 600–612, <https://doi.org/10.1016/j.conbuildmat.2016.08.073>.

- [32] S.A.A.M. Fennis, J. C. Walraven, J. A. Uijl J (2006), Optimizing the particle packing for the design of ecological concrete, Proceedings of the 16th Internationale Baustofftagung, Weimar, Bunderepublik Deutschland. 1(2006)1313 -1320.
- [33] C. Shi, Y. Wu, C. Riefler, H. Wang, Characteristic and pozzolanic reactivity of glass powders, *Cem. Concr. Res.* 35 (5) (2005) 987–993, <https://doi.org/10.1016/j.cemconres.2004.05.015>.
- [34] O.A. Hisseine, A. Tagnit-Hamou, Characterization and nano-engineering the interface properties of PVA fibers in strain-hardening cementitious composites incorporating high-volume ground-glass pozzolans, Article under review by *Construction and Building Materials* (2019).
- [35] M.S. Konsta-Gdoutos, Z.S. Metaxa, S.P. Shah Multi-scale mechanical and fracture characteristics and early-age strain capacity of high-performance carbon nanotube/cement nanocomposites, *Cem Concr Compos*, 32 (2) (2010), pp. 110-115.
- [36] W. Meng, K. H. Khayat, Mechanical properties of ultra-high-performance concrete enhanced with graphite nanoplatelets and carbon nanofibers, *Composites Part B: Engineering*, 107 (2016) 113-122.
- [37] C. Lu, Z. Lu, Z. Li, C.K.Y. Leung, Effect of graphene oxide on the mechanical behavior of strain hardening cementitious composites, *Constr. Build. Mater.* 120 (2016) 457-464.
- [38] S.J. Peters, T.S. Rushing, E.N. Landis, T.K. Cummins, Nanocellulose and microcellulose fibers for concrete, *Transport. Res. Rec.*, 2142 (2010), 25-28.
- [39] H. Ma, J. Cai, Z. Lin, S. Qian, V. C. Li, CaCO₃ whisker modified Engineered Cementitious Composite with local ingredients, *Constr. Build. Mater.* 151 (2017) 1-8.
- [40] R.J. Moon, A. Martini, J. Nairn, J. Simonsen, J. Youngblood Cellulose nanomaterials review: structure, properties and nanocomposites, *Chem. Soc. Rev.*, 40 (7) (2001) 3941-3994.
- [41] J.E. Goodsell, R.J. Moon, A. Huizar, R.B. Pipes, A strategy for prediction of the elastic properties of epoxy-cellulose nanocrystal-reinforced fiber networks, *Nord. Pulp Pap. Res. J.*, 29 (1) (2014) 85-94.
- [42] Y. Habibi, A. Dufresne Highly filled bionanocomposites from functionalized polysaccharide nanocrystals, *Biomacromolecules*, 9 (7) (2008) 1974-1980.

- [43] Y. Cao, P. Zaverri, J. Youngblood, R. Moon, J. Weiss, The influence of cellulose nanocrystal additions on the performance of cement paste, *Cem. Concr. Compos.* 56 (2015) 73-83.
- [44] O.A. Hisseine, A.F. Omran, A. Tagnit-Hamou, Influence of cellulose filaments on cement pastes and concrete, *J. Mater. Civ. Eng.* 30 (6) (2018), p. 04018109.
- [45] O.A. Hisseine, N. Basic, A.F. Omran, A. Tagnit-Hamou, Feasibility of using cellulose filaments as a viscosity modifying agent in self-consolidating concrete, *Cem. Concr. Compos.* 94 (2018), pp. 327-340.
- [46] O. A. Hisseine, William Wilson, Luca Sorelli, Balázs Tolnai, Arezki Tagnit-Hamou, Nanocellulose for improved concrete performance: A macro-to-micro investigation for disclosing the effects of cellulose filaments on strength of cement systems, *Constr. Build. Mater.* 206 (2019) 84-96.
- [47] H. Kolour, M. Ahmed, E. Alyaseen, E. N. Landis, An investigation on the effects of cellulose nanofibrils on the performance of cement paste and concrete, *Adv. in Civil Eng. Mater.* 7 (1) (2018) 463–478, <https://doi.org/10.1520/ACEM20180048>. ISSN 2379-1357.
- [48] T. Kanda, V.C. Li, Multiple cracking sequence and saturation in fiber reinforced cementitious composite, *Concr. Res. Technol., JCI* 9 (2) (1998) 19–33.
- [49] D.B. Marshall, B.N. Cox, A J-integral method for calculating steady-state matrix cracking stresses in composites, *Mech. Mater.* 8 (1988) 127–133.
- [50] Z. Lin, T. Kanda, V.C. Li, On interface property characterization and performance of fiber reinforced cementitious composites, *J. Concrete Sci. and Engrg.* 1 (1999) 173–184.
- [51] E.H. Yang, Y. Yang, V.C. Li, Use of high volumes of fly ash to improve ECC mechanical properties and material greenness, *ACI Mater. J.* 104 (6) (2007) 620–628.
- [52] P.C. Aïtcin, Cements of yesterday and today-concrete of tomorrow, *Cem. & Con. Res.* 30 (9) (2000) 1349–1359.
- [53] ASTM C494 / C494M-17, Standard Specification for Chemical Admixtures for Concrete, ASTM International, West Conshohocken, PA, 2017, www.astm.org.
- [54] H. Kong, S. G. Bike, V. C Li, Development of a self-consolidating engineered cementitious composite employing electrosteric dispersion/stabilization, *Cem. Concr. Compos.* 25 (3) (2003) 301-309.

- [55] F. De Larrard, *Concrete mixture proportioning: A Scientific Approach*, E&FN Spon, London, 1999.
- [56] ASTM C185-15a, *Standard Test Method for Air Content of Hydraulic Cement Mortar*, ASTM International, West Conshohocken, PA, 2015, www.astm.org
- [57] ASTM C1437-15, *Standard Test Method for Flow of Hydraulic Cement Mortar*, ASTM International, West Conshohocken, PA, 2015, www.astm.org.
- [58] ASTM C469 / C469M-14, *Standard Test Method for Static Modulus of Elasticity and Poisson's Ratio of Concrete in Compression*, ASTM International, West Conshohocken, PA, 2014, www.astm.org.
- [59] ASTM E399-12, *Standard test method for linear-elastic plane-strain fracture toughness K_{Ic} of metallic materials*, ASTM International, West Conshohocken, PA, 2012, www.astm.org.
- [60] ASTM C109 / C109M-16a, *Standard Test Method for Compressive Strength of Hydraulic Cement Mortars (Using 2-in. or [50-mm] Cube Specimens)*, ASTM International, West Conshohocken, PA, 2016, www.astm.org.
- [61] ASTM C78 / C78M-18, *Standard Test Method for Flexural Strength of Concrete (Using Simple Beam with Third-Point Loading)*, ASTM International, West Conshohocken, PA, 2018, www.astm.org.
- [62] K. Sobolev, A. Amirjanov, The simulation of particulate materials packing using a particle suspension model, *Adv. Powder Technol.* 18 (3) (2007), pp. 261-271, ISSN 0921-8831.
- [63] K. Sobolev and A. Amirjanov, The development of a simulation model of the dense packing of large particulate assemblies, *Powder Technol.* 141(2004)155–160.
- [64] K. Sobolev and A. Amirjanov, A simulation model of the dense packing of particulate materials, *Adv. Powder Technol.* 15 (2004) 365–376.
- [65] Y. Jiao, F. H. Stillinger, S. Torquato, Optimal packings of superballs, *Phys. Rev. E* 79, 041309 – Published 23 April 2009; Erratum *Phys. Rev. E* 84, 069902 (2011).
- [66] A. Shayan, A. Xu, Value-Added Utilisation of Waste Glass in Concrete, *Cem. Concr. Res.* 34 (1) (2004) 81–89, [https://doi.org/10.1016/S0008-8846\(03\)00251-5](https://doi.org/10.1016/S0008-8846(03)00251-5).

- [67] A. A. Aliabdo, M. A. Abd Elmoaty, A. Y. Aboshama, Utilization of waste glass powder in the production of cement and concrete,” *Constr. Build. Mater.* 124 (2016) 866–877, <https://doi.org/10.1016/j.conbuildmat.2016.08.016>
- [68] M. H. Shehata, M. D. Thomas, Use of ternary blends containing silica fume and fly ash to suppress expansion due to alkali–silica reaction in concrete,” *Cem. Concr. Res.* 32 (3) (2002) 341–349.
- [69] A. Tagnit-Hamou, A. Bengougam, Glass powder as a supplementary cementitious material, *Concr. Int.* 34 (3) (2012) 56–61.
- [70] Y.M. Zhang, W. Sun, H.D. Yan, Hydration of high-volume fly ash cement pastes, *Cem. Concr. Compos.* 22 (6) (2000) 445–452.
- [71] H. Siad, M. Lachemi, M. Sahmaran, H. A. Mesbah, K. M. A. Hossain, Use of recycled glass powder to improve the performance properties of high-volume fly ash-engineered cementitious composites, *Constr. Build. Mater.* 163 (2018) 53-62.
- [72] S. A. Rodger, S. A. Brooks, W. Sinclair, G. W. Groves, D. D. Double, High strength cement pastes, *J. Mater. Sci.* 20 (1985) 2853-2860.
- [73] M. A. Gulgun, W. M. Kriven, L. S. Tan, A. J. McHugh, Evolution of mechano-chemistry and microstructure of a calcium aluminate-polymer composite: Part I—Mixing Time Effects,” *J. Mater. Res.* 10 (7) (1995) 1746-1755.
- [74] C.H. Gómez, E. Cristia, A. Vázquez Effect of cellulose microcrystalline particles on the properties of cement-based composites, *Mater. Des.* 51 (2013) 810-818.
- [75] W. Wilson, L. Sorelli, A. Tagnit-Hamou Automated coupling of nanoindentation and quantitative energy-dispersive spectroscopy (NI-QEDS): a comprehensive method to disclose the micro-chemo-mechanical properties of cement pastes, *Cem. Concr. Res.* 103 (2018) 49-65.
- [76] J. Flores, M. Kamali, A. Ghahremaninezhad An investigation into the properties and microstructure of cement mixtures modified with cellulose nanocrystal, *Materials*, 10 (5) (2017), p. 498, [10.3390/ma10050498](https://doi.org/10.3390/ma10050498).
- [77] Y. Cao, N. Tian, D. Bahr, P. D. Zavattieri, J. Youngblood, R. J. Moon, J. Weiss, The influence of cellulose nanocrystals on the microstructure of cement paste, *Cem. Concr. Compos.* 74 (2016) 164-173.

- [78] C. Redon, V. C. Li, C. Wu, H. Hoshiro, T. Saito, A. Ogawa, Measuring and modifying interface properties of PVA fibers in ECC matrix, *ASCE J. Mater. Civ. Eng.* 13 (6) (2001) 399-406.
- [79] Z. Lin, V. C. Li, Crack bridging in fiber reinforced cementitious composites with slip-hardening interfaces, *J. Mech. Phys. Solids*, 45(5) (1997) 763–787.
- [80] A. E. Naaman, H. W. Reinhardt, Setting the stage: Toward performance-based classification of FRC composites, In ‘High Performance Fiber Reinforced Cement Composites (HPFRCC4). Proceedings of the Fourth International RILEM Workshop’. (eds.) A.E. Naaman and H.W. Reinhardt. Rilem Publications S.A.R.L. 2003, 1-4.
- [81] A. Hillerborg, Analysis of one single crack, In *Fracture Mechanics of Concrete*, edited by F.H. Wittmann, Elsevier Science Publishers B.V., Amsterdam, pp. 223-249, 1983.
- [82] N.M. Altwair, M.M. Johari, S.S. Hashim, Flexural performance of green engineered cementitious composites containing high volume of palm oil fuel ash, *Constr. Build. Mater.* 37 (2012) 518–525.
- [83] C. K. Yi, C. P. Ostertag, Strengthening and toughening mechanisms in microfiber reinforced cementitious composites, *J. Mater. Sci.* 36(6) (2001) 1513–1522, doi: 10.1023/A:1017557015523.
- [84] P. Balaguru, H. Najm H, High-performance fiber-reinforced concrete mixture proportions with high fiber volume fractions, *ACI Mater J* 101(4) (2004) 281–286.
- [85] Y. Geng, C. K. Leung, A microstructural study of fibre/mortar interfaces during fibre debonding and pull-out. *J Mater Sci* 31(5) (1996), 1285–1294, doi: 10.1007/BF00353108.
- [86] M.S. Sahmaran, H.E. Yücel, S. Demirhan, C.V. Li, Combined effect of aggregate and mineral admixtures on tensile ductility of engineered cementitious composites, *ACI Mater. J.* 109 (6) (2012) 627-638.
- [87] N. Banthia, A. Moncef, K. Chokri, J. Sheng, Micro-fiber reinforced cement composites: Uniaxial tensile response, *Can. J. Civ. Eng.* 21(6) (1994) 999–1011.

List of Figures

- Fig. 1. Multi-scale design framework of HVGP-SHCC
- Fig. 2. Fiber bridging stress – crack opening relationship
- Fig. 3. Particle size distribution of SHCC ingredients
- Fig. 4. SEM micrographs of SHCC ingredients
- Fig. 5. SEM micrograph of hybrid reinforcement systems used in this study
- Fig. 6. Fracture toughness test
- Fig. 7. Uniaxial tension test
- Fig. 8. Single-fiber pull-out test
- Fig. 9. Combined particle size distribution for the different SHCC formulations
- Fig. 10. Computed fiber bridging stress–crack opening relationship
- Fig. 11. Fiber bridging stress–crack opening relationship (σ – δ) for CF-SHCC
- Fig. 12. Evolution of compressive strength
- Fig. 13. Generalized response in flexure and uniaxial tension
- Fig. 14. Uniaxial tensile behavior of nanocellulose-modified HVGP-SHCC
- Fig. 15. PVA fiber status post-single fiber-fiber pull-out test in CF-HVGP-SHCC
- Fig. 16. Effect of CF on matrix and interface properties of HVGP-SHCC
- Fig. 17. Flexural response of SHCC
- Fig. 18. Multiple cracking and deflection capacity in HVGP-SHCC
- Fig. 19. Multiple cracking pattern in the different SHCC systems incorporating CF

List of Tables

Table 1. Chemical compositions of powders and granular materials used in the study

Table 2. Mix design of HVGP SHCC

Table 3. Fresh properties of SHCC plain formulations used for the micromechanical investigation

Table 4. Results of micromechanical investigation and SHCC strain-hardening indicators

Part 4

Application of Nanoengineered Strain-Hardening Cementitious Composites incorporating High-Volume Ground-glass Pozzolans (nHVGP-SHCC):

High performance composite deck slabs constructed with nHVGP-SHCC

Chapter 10: Nanoengineered strain-hardening cementitious composites incorporating high-volume ground-glass pozzolans for composite slabs with high resistance to shear bond failure under static and fatigue loading

This part of the thesis has the objective of scaling-up the enhanced performance demonstrated by the newly developed nanoengineered HVGP-SHCC towards a structural application, namely composite deck slabs with an improved shear-bond resistance. Preliminary results are reported herein while the complete results can be consulted in the finalized version of the article

CHAPTER 10

Nanoengineered HVGP-SHCC-Based Composite Slabs for High Resistance to Shear Bond Failure

10.1 Introduction

In light of the enhanced strength and ductility characteristics obtained with the newly developed nanoengineered strain-hardening cementitious composites incorporating high-volume ground-glass pozzolans (nHVGP-SHCC) as presented in [Chapter 9](#), the current chapter is intended to exploring the viability of transposing the enhanced mechanical performance demonstrated by nHVGP-SHCC towards a structural scale. For this, full-scale composite deck slabs (with dimensions of up to 2400 × 900 mm) were constructed with the new SHCC as a concrete topping. The slabs will be subjected to cyclic loads often encountered in industrial applications (effect of machineries, effect of forklifts) as well as in parking structures (moving load of vehicles). This is in order to leverage the enhanced mechanical strength and ductility of the new concrete to promote compatibility between the steel deck and its concrete topping to improve slab resistance to shear bond failure (associated with the deterioration of steel-concrete interfacial bond), one of the main failure modes in composite slabs. Details of this chapter are included in [Section 10.2](#) as part of an article under preparation to appear in the *Journal of Engineering Structures*.

10.2 Article 8 - High performance composite slabs constructed with nanoengineered strain-hardening cementitious composites for improved resistance to shear bond failure.

Article information

Authors and affiliations:

Ousmane A. Hisseine, PhD candidate and Canada Vanier Scholar of NSERC, Cement and Concrete Research Group, Department of Civil Engineering, Université de Sherbrooke

A. Tagnit-Hamou, Professor and director of Cement and Concrete Research Group, Department of Civil Engineering, Université de Sherbrooke

Article status: Under preparation

Potential Journal: *Journal of Engineering Structures*

Titre français:

Béton écrouissant nanomodifié pour des dalles composites à haute performance

Contribution of this article: This article contributes towards providing a platform for validating the performance of the newly developed SHCC at the structural scale.

Nano-engineered strain-hardening cement composites with high-volume ground glass pozzolans for high-performance composite slabs with improved shear-bond capacity

Ousmane A. Hisseine; Arezki Tagnit-Hamou

Under preparation to be submitted to Journal of Engineering Structures

Abstract

Longitudinal shear failure associated with steel-concrete slip in composite slabs represents one of the major failure types as transposed by the shear bond method for the structural design of composite slabs. Steel-concrete slip in composite slabs emerges from the loss of composite action exacerbated by the inherent discrepancy between the ductility of the steel deck and its concrete topping. This study investigates how a newly developed nanoengineered strain-hardening cementitious composite incorporating high-volume ground-glass pozzolans (nHVGP-SHCC) can be used as a ductile topping in composite slabs to improve the load-carrying capacity and resistance to shear bond failure. The study involved testing fourteen full-scale slabs. This includes seven SHCC slabs and seven slabs constructed with a conventional high-performance concrete (HPC) having a compressive strength comparable to that of their counterparts. Slabs were tested under flexural static/fatigue load until failure. Test variables include type of concrete topping (SHCC and HPC) steel deck geometry (reentrant and trapezoidal), shear span (520 and 665, 770 mm), and loading type (static and fatigue). Results indicate that with a similar compressive strength in both HPC and SHCC, the latter leads to increasing the ultimate load-carrying capacity by up to 55% and imparts a ductile failure characterized by multiple cracking spread over the effective span as contrasted to the localized cracks observed in composite slabs with HPC.

Author Keywords: Composite deck slabs, engineered cementitious composites (ECC), shear bond failure, strain-hardening cementitious composites (SHCC), recycled glass powder (GP), ground glass pozzolans (GP), high-performance concrete, fatigue behavior

1 Introduction

Composite steel floor deck-slabs (also referred to throughout this work as composite slabs, for simplicity) represent the most widely used slab system in the construction of multistory steel-framed buildings. This is motivated by their numerous advantages such as light weight, economy, and ease of erection. A composite slab (Fig. 1) consists of a structural concrete topping placed permanently over cold-formed steel deck in which the role of steel deck is threefold: (i) a platform during construction, (ii) a permanent formwork for the young concrete, and (iii) a positive tensile reinforcement for the slab during service. To control temperature and shrinkage cracks, composite slabs also incorporate welded wire mesh (WWM) which has theoretically no structural function.

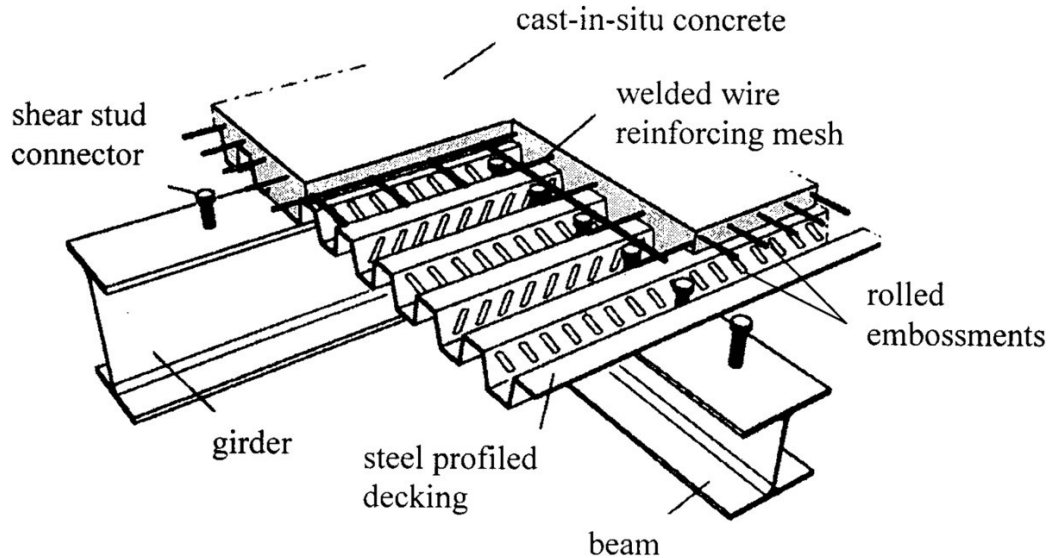


Fig. 1: Schematic of composite slab reinforced with profiled steel decking [Mohammed and Abdullahi, 2011].

At service, an adequate composite action should be developed between the steel deck and its concrete topping. However, due to the slip at the steel-concrete interface, the longitudinal shear bond between the steel deck and its concrete topping varies along the span. Among other failure types commonly encountered in composite slabs (namely, flexure failure, vertical shear failure at support, and longitudinal shear failure between the steel and concrete), the longitudinal shear failure is considered the most common one [Wright and Evans, 1990].

This common failure type in composite slabs is manifested by the formation of diagonal tension crack in the concrete at or near the load application points. The formation of diagonal tension crack is subsequent to a loss of bond between the steel deck and the concrete. Therefore, proper composite action is necessary to transfer the shear forces between the steel deck and its concrete topping. The composite action between the steel and concrete can be enhanced by means of mechanical interlocking such as headed shear studs, embossments (the indentations on steel sheet surface), and enhanced deck profile and geometry.

While significant research [Schuster, 1976; Porter and Ekberg, 1976; Wright and Evans, 1990; Abdulla and Easterling, 2009] has already been invested during the last few decades to disclose the overall behaviour of composite slabs, the relative steel-concrete slip remains a concern. As a result, the effect of shear bond between the profiled steel and its concrete topping has been transposed in code practice as one of two methods for composite design adopted by ASCE [ASCE, 1992], British Standards [BS, 1994], and Eurocode 4 [Eurocode, 1994], namely: (i) the shear bond method (or m-k method), and (ii) the partial shear connection (PSC) method.

The shear bond failure between the ductile steel deck as compared to the highly brittle concrete topping may be mobilized by the significant variation between the ductility of the two materials. However, with the conventional concrete used (the performance of which in composite slabs is now well established), it is quite challenging to elevate the ductility of concrete topping. Concrete topping with higher ductility can increase the compatibility between the two major composite constituents (steel deck and concrete), lead to higher composite action, and reduce the shear bond failure. Few recent attempts have addressed the behavior of composite slabs with high performance concrete [Mohammed, 2010; Mohammed *et al.*, 2011; Mohammed *et al.*, 2016; Hossain *et al.* 2016]. Among these investigations, the work of Mohammed *et al.* [2016] and that of Hossain *et al.* [2016] have also evaluated the shear bond behavior of composite slabs constructed with SHCC subjected to static loading. Composite slabs constructed with SHCC subjected to static flexural loading exhibited higher pre-peak strength as well as enhanced post-peak ductility as a result of the intrinsic strain-hardening feature of SHCC. This mobilized higher composite action and resulted in improved shear bond capacity in SHCC slabs than in slabs constructed with conventional concrete [Hossain *et al.*, 2016]. Comparable results were

obtained by [Mohammed *et al.* \[2016\]](#) on full-scale testing of composite slabs constructed with SHCC topping subjected to static flexural load.

While these investigations demonstrate the effectiveness of SHCC topping to allow enhancing the shear bond capacity in composite slabs subjected to static flexural loading, it should be noted that repeated loading (where the loss of composite action can be expediated by the effect of fatigue) can clearly elucidate the importance of improving the performance of composite slabs by using SHCC topping. This is because the steel-concrete shear bond failure in composite slabs can be even more problematic under repeated loading causing fatigue failure. This can be of major concern in elevated composite deck slabs, particularly in industrial applications (forklift, freight loading and unloading, machinery, etc.) as well as in parking steel-framed parking structure (repeated moving load from vehicles). In such scenarios, fatigue can expedite the loss of composite action and exacerbate shear bond failure even when the individual static loads (being lower than the ultimate capacity of the composite slab) may not cause shear bond failure [[McCuaig and Schuster, 1988](#)].

In light of the above research question, it is hypothesized herein that the shear bond behavior of composite slabs can be significantly enhanced should the ductility of the concrete topping be improved. To this end, the current study proposes for concrete topping in composite slabs the use of a newly developed nanoengineered strain-hardening cementitious composite (SHCC) incorporating high-volume ground-glass pozzolans (nHVGP-SHCC) presented elsewhere [[Hisseine *et al.* 2019b](#); [Hisseine *et al.* 2019c](#), [Hisseine *et al.* 2019d](#)]. The most important characteristics of this SHCC is that it couples particle packing optimization with micromechanical tailoring to produce composites exhibiting higher strength while incorporating locally available materials. On the other hand, this SHCC incorporates nanoscale cellulose filaments (CF) such that the resulting multiscale reinforcing system further enhances the ductility. Therefore, the objective of the current study is to valorise the enhanced strength and ductility of this newly developed nHVGP-SHCC as a concrete topping to produce high-performance composite slabs exhibiting improved resistance to shear bond failure. To achieve this objective, an experimental program involving construction and testing of fifteen full-scale slabs (nine with nHVGP-SHCC and six with a high-performance concrete (HPC) designed with compressive strength comparable to that of their counterparts) was established. All slabs were

tested to failure under either a static flexural or under flexural fatigue to provide details on the shear-bond resistance of SHCC-composite slabs as compared to their counterparts. Research outcomes contribute towards the valorization of nanoengineered high-performance composite for the development of high-performance structural systems.

2 Research methodology

To achieve the aforementioned project objective, an experimental program involving construction and testing of fifteen full-scale composite slabs was established. This includes a set of 9 composite slabs constructed with the newly developed nanoengineered strain-hardening cementitious composite (SHCC) incorporating high-volume ground-glass pozzolans (nHVGP-SHCC) as well as another set of 6 composite slabs constructed with a commercially supplied high-performance concrete (HPC). The slabs were tested under static/fatigue flexure load until failure. Test variables include type of concrete topping (SHCC and HPC) steel deck geometry (reentrant and trapezoidal), shear span (520, 665, and 770 mm), and loading type (static and fatigue). The study provides an assessment of the structural performance of nHVGP-SHCC composite slabs in terms of load-deflection response, shear response, load-slip behaviour, steel-concrete shear bond resistance, ductility, and failure modes to assess nHVGP-SHCC as a promising material for constructing high-performance composite slabs with a particularly improved resistance to fatigue-induced shear-bond failure. The following sub-sections provide further details about the experimental program in terms of materials properties, preparation of slabs, and testing.

2.1 Materials properties

Two surface-galvanized steel decking profiles were used (a trapezoidal profile named P3615 and a re-entrant profile named reveal series) provided by CANAM (Canada). Both decks are 1.21 mm thick and made from standard steel grade conforming to ASTM A 653M SS. The former is of Grade 230 with a minimum yield strength of 230 MPa, while the latter is of Grade 275 having a minimum yield strength of 275 MPa. The PVA fibers used in SHCC have 38 μm

diameter and 8 mm length, 40 GPa elastic modulus and 1400 MPa tensile strength. Fig. 2 show presents the geometry of these two profiles.

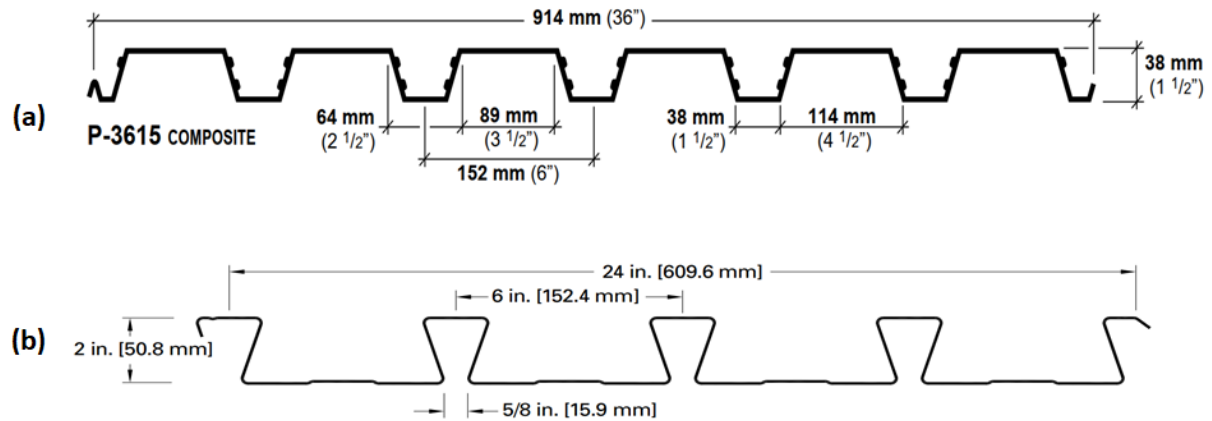


Fig. 2. Geometry of the steel decking used in this study: (a) the trapezoidal profile (P3615), and (b) the reentrant profile (reveal series)

2.2 Mixture proportions

2.2.1 nanoengineered strain-hardening cementitious composite incorporating high-volume ground-glass pozzolans (nHVGP-SHCC)

The strain-hardening cementitious composite (SHCC) used herein incorporates high-volume ground-glass pozzolans (HVGP) in replacement of high-volume fly ash (FHVFA). The original formulation of this nHVGP-SHCC was developed by coupling particle-packing optimization with micromechanical tailoring additional to the incorporation of nanoscale cellulose filament (CF) imparting higher ductility. This resulted into different designs having a water-to-binder ratio of 0.28, a quartz sand-to-binder ratio of 0.35 and various replacement levels of fly ash (FA) by ground-glass pozzolans (GP) [Hisseine *et al.* 2019b; Hisseine *et al.* 2019c, Hisseine *et al.* 2019d]. Later, for the purpose of scaling-up this SHCC to structural applications, further optimization of SHCC formulation was undertaken by performing a full-factorial design (2^3). Based on the above studies, three design parameters influencing composite strength and ductility were chosen as: (i) the replacement level of fly ash (FA) by ground-glass pozzolans (GP)

[20–60%] responsible for increasing compacity and strength but reducing ductility, (ii) volume fraction of PVA fibers [1.2–2%], and (iii) the content of CF [0.03–0.10%]. On the other hand, the effect of these parameters on compressive strength, direct tensile strength, and flexural capacity were evaluated experimentally in eight basic mixture supplemented by three repeatability mixtures as well as four verification mixtures. In outcomes, contour lines for several combinations of the various ranges included in the above three parameters were established some of which satisfying strength and ductility at low PVA fiber content (This is described in full detail in a separate work: [Hisseine *et al.* 2019e]). One such formulation has been used for constructing the composite slabs. This formulation consists of 20% GP replacement of fly ash, 1.6% PVA fibers and 0.10% CE. Table 1 shows the detailed mixture proportions of the SHCC used herein.

Table 1. SHCC mix proportions, kg/m³

Component	Quantity (Kg)
Water	308.9
Cement	584.4
Class F fly ash	561.0
Glass powder	140.3
Quartz sand	450.0
HRWRA (6.4
Cellulose filaments (CF)	48.7
PVA fibers	20.8

2.2.2 High-performance concrete

The high-performance concrete (HPC) used in this study was provided by a local ready-mix supplier [Carrière St. Dominique, Sherbrooke, QC]. The mix design has 14 mm maximum aggregate size, a water-to-binder (w/b) ratio of 0.41, 2-4% nominal air content, 650±40 mm target slump-flow diameter, and a target 28-day strength of 50 MPa. On site fresh properties

consists 680 mm slump, 2% air content, and 2316 kg/m³ fresh unit weight. Table 2 shows the mixture proportions along with on-site fresh properties.

Table 1. HPC mix proportions, kg/m³

Component	Quantity (Kg)
Water	194
GU cement-Type GUb-S/SF	470
Aggregates (5-20 mm)	600
Aggregates (5-10 mm)	223
Sand	807
Water reducer (140M-Grace)	1600 ml/100kg
Air entraining agent (Air Mac12-Euclid)	10 ml/100 kg
Set retarder [Eucon 727-Euclid]	100 ml/100 kg
Viscosity modifying agent [Visctrol- Euclid]	0.23 kg

2.3 Mixing procedures and specimen preparations

Mixing procedure for SHCC followed a protocol adapted from the mixing sequence described in details in our former studies [Hisseine *et al.* 2019c; Hisseine *et al.* 2019d]. However, to produce the large volume required to construct the slabs (a minimum of 200 L per slab), the time for dry-mixing the powders was extended from 7 minutes in regular size batches to 15 minutes in the current study to allow better dispersion of powders and sand. SHCC slabs were cast such that each slab was cast with one batch. HPC slabs were cast all from the same batch delivered by the ready mixer. Upon casting, slabs were covered with plastic sheets in an attempt to maintain a controlled environment and were then kept in the laboratory [at approximately 22° C and 55% relative humidity (RH)] for 24 hours. Later, the slabs were covered with burlap and water-cured constantly for 7 days. After the 7th day, the slabs remained exposed to the lab environment until the age of testing at 91 days. Figs. 3-6 illustrate the different stages of preparing the slabs.

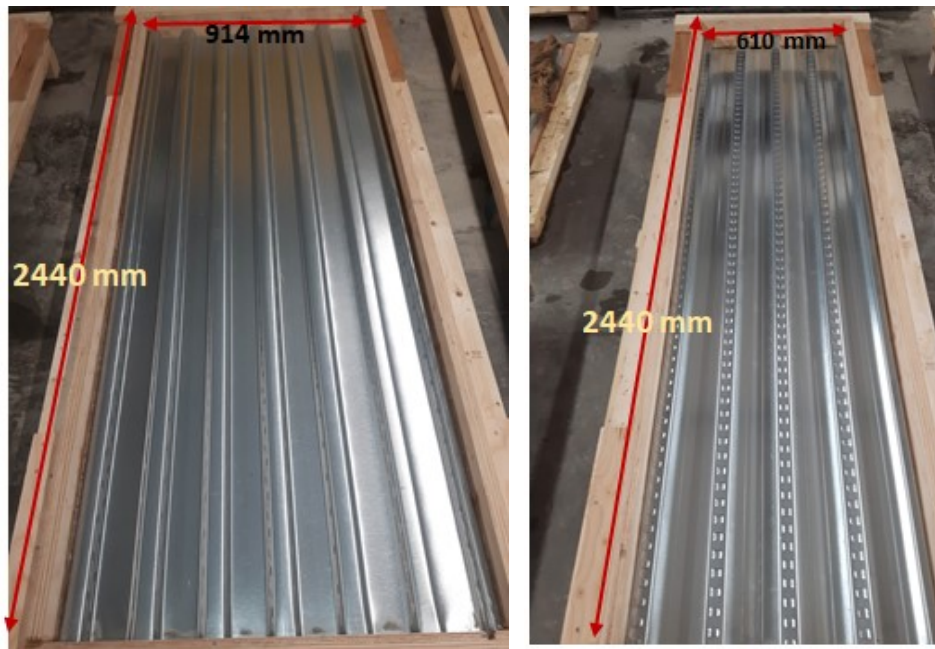


Fig. 3. Molds used for casting the slabs for: (a) trapezoidal profile, and (b) reentrant profile



Fig. 4. Casting of SHCC slabs: The figure depicts the exceptional texture, rheology, and self-consolidating ability of nHVGP-SHCC. The figure shows an SHCC slab where no WWM are used.



Fig. 5. Casting of high-performance concrete (HPC) slabs using a readily supplied mix



Fig. 6. Curing of composite deck slabs using wet burlap during the first 7 days.

2.3 Test matrix

Fourteen full-scale slabs were tested. This includes seven slabs cast with the newly developed nanomodified strain-hardening cementitious composite incorporating high-volume ground pozzolans (nHVGP-SHCC) and seven slabs with a conventional high-performance concrete (HPC). For each concrete type (SHCC vs HPC) six slabs were subjected to monotonic static flexural test while one slab was subjected to flexural fatigue test. Static flexural test for each concrete type included two sets based on the decking profile (trapezoidal or reentrant). Each set involves testing three different shear spans (L_s) of 520, 665, and 770 mm. For both corner types, dynamic test was conducted only on the trapezoidal profile at L_s value of 770 mm. In this thesis, only the static tests conducted on the trapezoidal profile for both concrete types will be reported. The reader is invited to the full article to appear soon [[Hisseine et al. 2019f](#)]. Specimen identification codes includes three parts, the first designating the concrete type, the second designating the geometry of the steel deck, and the third designating the shear span. For instance, SHCC-Trap-520 designates the slab with strain hardening cementitious composites tested with a trapezoidal profile at a shear span of 520mm.

2.4 Instrumentation and testing

[Fig. 7](#) show a schematic of the test set-up used in this study. The set-up consists of a simply supported configuration allowing to test the slabs in four-point bending. Slab supports consists a roller and hinge to allow rotation but prevent translation. Each slab was instrumented with two extensometers placed at mid-span (to measure the central deflection) and four Linear Voltage Displacement Transducers (LVDTs) installed in pairs at each side of the slab (left and right) to measure end-slip between steel and concrete. Each slab also has two steel strain-gauges (SSG) of 10 mm length mounted at the soffit of the steel deck (at mid span) to measure deck strains, and two other concrete strain-gauges (CSG) of 50 mm length mounted on the top surface of concrete at mid-span, right above the SSGs, to measure concrete strain. [Fig. 7](#) (a) shows a side view of the set-up and the instrumentation while further details are provided in [Fig. 7](#) (b) showing a top view of the slab. An actual scenario is also provided in [Fig. 8](#).

To obtain a given response (central deformation, steel deck strain, concrete strains, end-slip), the measurements recorded by the corresponding pair of instrumentation devices

(extensometers, SSGs, CSGs, LVDTs) were averaged. The load was applied through an actuator equipped with a 500 kN load cell. For static testing, test was conducted in displacement-controlled mode using a loading rate of 2 mm/minute until complete failure. Slab testing continued until the load-carrying capacity drops to more than 50% of the ultimate capacity. For dynamic testing, the slabs were subjected to a sinusoidal waveform fatigue load between a minimum load applied at 25% of the ultimate static load-carrying capacity and a maximum load at 75% of the static load-carrying capacity. All instrumentation devices were connected to a data acquisition system allowing a continuous data record throughout the test. Load versus central deformation, load versus strain response in the deck, load versus strain response in the concrete topping, load versus end slip, and cracking pattern were recorded.

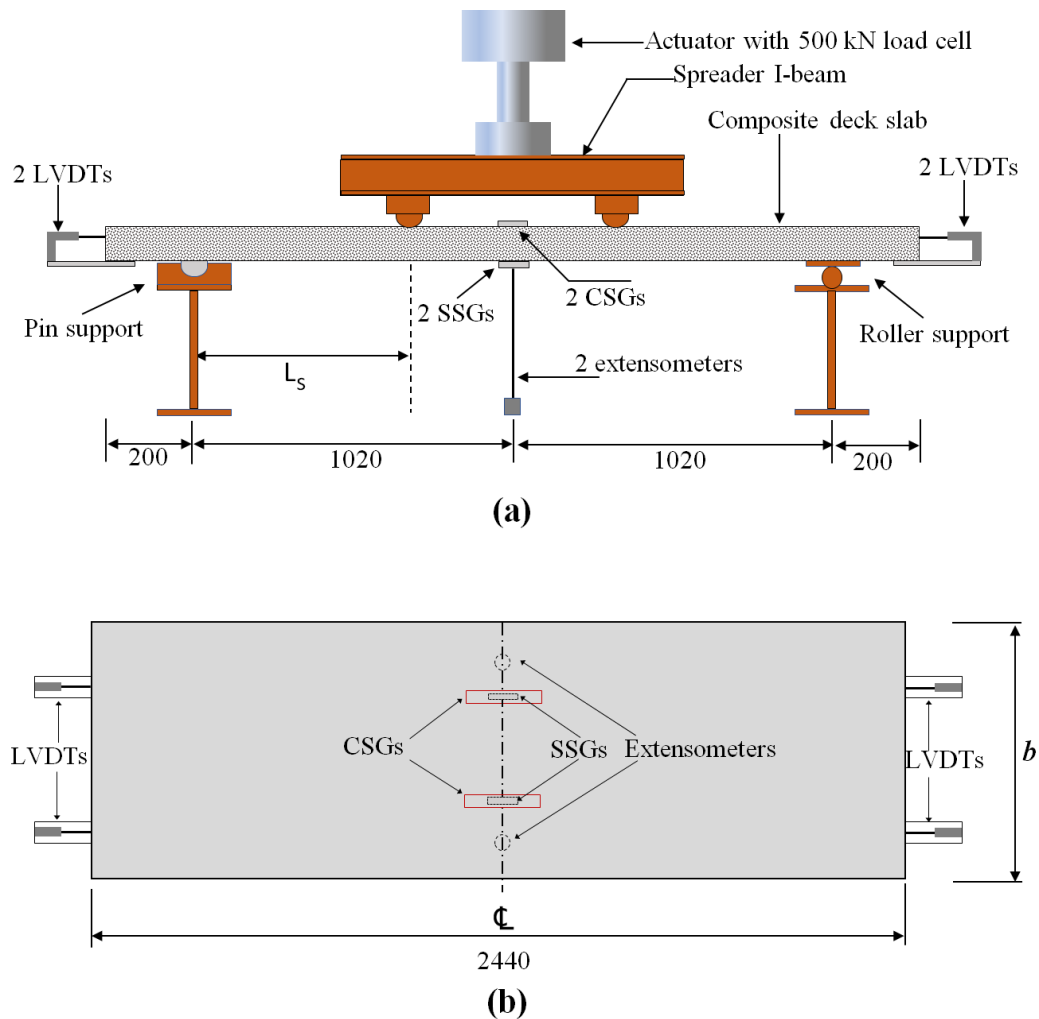


Fig. 7. Schematic illustration of test set-up: front view (a), and top view of slab (b)



Fig. 8. Actual test set-up: Front view (top), and side view (bottom)

3 Results and discussion

3.1 Load-deflection response, slip response and cracking pattern

Fig. 9 shows the load-deflection response of slabs with trapezoidal profile for both the conventional high-performance concrete (HPC) [Fi. 9 (a)] as well as for the strain-hardening cementitious composite [Fi. 9 (b)] developed in this study.

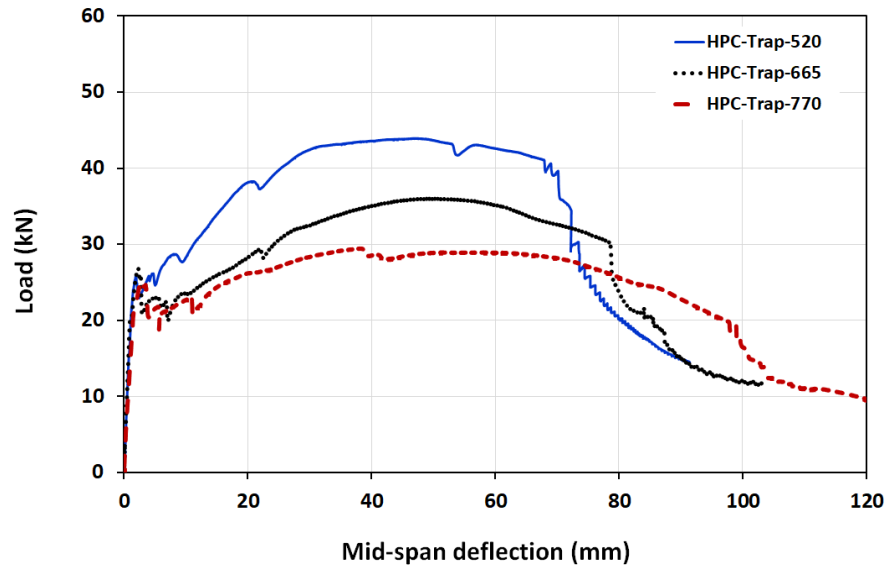
3.1 Slabs with conventional HPC

In the slabs with the conventional HPC [Fi. 9 (a)], for the three shear spans of 520, 665, and 770, the first crack appeared at approximately 25, 22, and 16 kN, respectively. While the first cracking load varied as function of shear span, the load-deflection response remained linear and comparable for all slabs up to a load value of about 25 kN. Beyond 25 kN, increasing deflection caused cracks to coalesce and eventually led to a remarkable steel-concrete slip as demonstrated in Fig. 10 (a) where significant slip was recorded beyond a load value of 25 kN. After the steel-deck concrete separation, the load-deflection behavior of slabs differed depending on the shear span. At the shear span of 770 mm the higher lever arm caused abrupt drop in the load carrying capacity whereby the load-deflection response appeared to be controlled mainly by the steel deck. At the shear span of 665 mm, the moderate lever arm caused drop in the load carrying capacity, but the post-cracking response was higher than that at shear span of 770 mm. At the shear span of 520 mm, the reduced lever arm allowed smoother transfer of load from the concrete to the steel deck. Thus, the post-cracking response was the highest. Beyond 25 kN, increasing deflection caused cracks to coalesce and eventually led to a remarkable steel-concrete slip as demonstrated in Fig. 11 where significant slip was recorded beyond a load value of 25 kN. After the steel-deck concrete separation, the load-deflection behavior of slabs differed depending on the shear span. At the shear span of 770 mm the higher lever arm caused abrupt drop in the load carrying capacity whereby the load-deflection response appeared to be controlled mainly by the steel deck. At the shear span of 665 mm, the moderate lever arm caused drop in the load carrying capacity, but the post-cracking response was higher than that at shear span of 770 mm. At the shear span of 520 mm, the reduced lever arm allowed smoother transfer of load from the concrete to the steel deck. Thus, the post-cracking response was the highest.

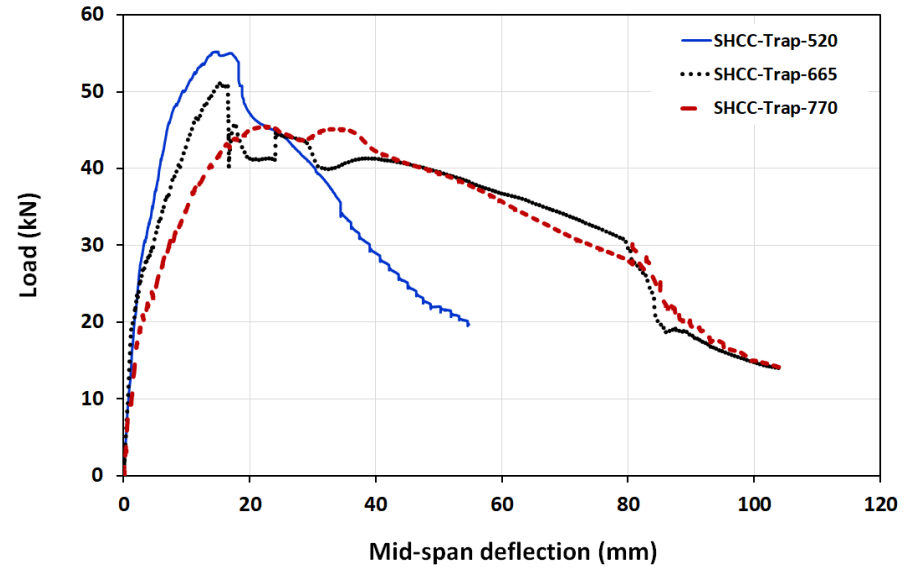
As such, the ultimate capacity for the three respective shear spans corresponded to 44, 36, and 29 kN. Therefore, it was observed that composite slabs demonstrate higher load-carrying at shorter shear span than at longer ones. This associated with the effect of shear span on the steel-concrete interaction and consequently on the overall composite action. The observed behavior in load-deflection is also confirmed by the load-strain response depicted in Fig 11 (a) where higher strains were recorded in both the steel deck and the concrete topping for shorter shear spans than for longer shear spans. Nevertheless, it was observed all HPC slabs failed by developing localized cracks concentrated at the points of load application (Fig. 12).

3.1 Slabs with conventional HPC

As for SHCC slabs, the load-deflection response depicted in Fig. 9 (b) shows a remarkably different behavior than the one observed in their counterparts with conventional HPC. For all three shear spans (520, 665, and 770 mm), the load-deflection response remained linear until around 20 kN for the shear span of 770 mm and around 30 kN for the shear spans of 665 and 520 mm. For the three shear spans of 520, 665, and 770 mm, the visible crack appeared at 45, 40, and 30 kN, respectively. Beyond the load level corresponding to the first crack, a raising portion was observed in the load-deflection response which led to delaying the coalescence of cracks until a significantly high ultimate load was achieved. The ultimate load-capacity for the three respective shear spans (520, 665, and 770 mm) was 56, 51, and 45 kN. The above results confirm the effect of shear span on the ultimate capacity of composite slabs addressed in the previous section. On the other hand, while HPC and SHCC were designed to exhibit comparable compressive strength, slabs with SHCC demonstrated a higher first cracking strength. Slabs with SHCC exhibited a strain-hardening behavior which helped in maintaining a composite action up to higher load levels, thereby reducing steel-concrete slip [Fig. 10 (b)] and eventually leading to higher load-carrying capacity as well as higher strain capacity as demonstrated in Fig. Fig 11 (b). Furthermore, the ductile feature of SHCC lead to a failure pattern characterized by multiple cracking spread over the whole effective span (Fig 13). These observations indicate that the use of newly developed ecological SHCC in composite slabs can boost the performance of composite slabs. Further analysis of the performance of composite slabs with SHCC in terms of shear bon capacity as well as the fatigue response can be found in [Hisseine *et al.* 2019f].



(a)



(a)

Fig. 9. Load-central deflection response: (a) slabs with conventional HPC, and (b) slabs with SHCC

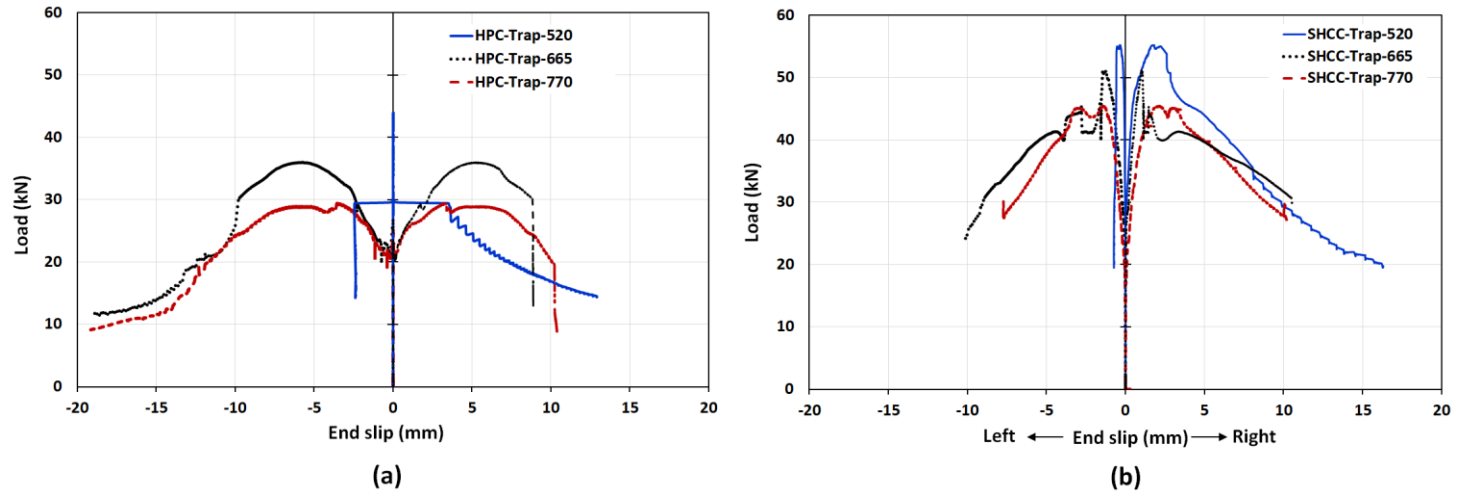


Fig. 10. Load-end slip: (a) slabs with conventional HPC, and (b) slabs with SHCC

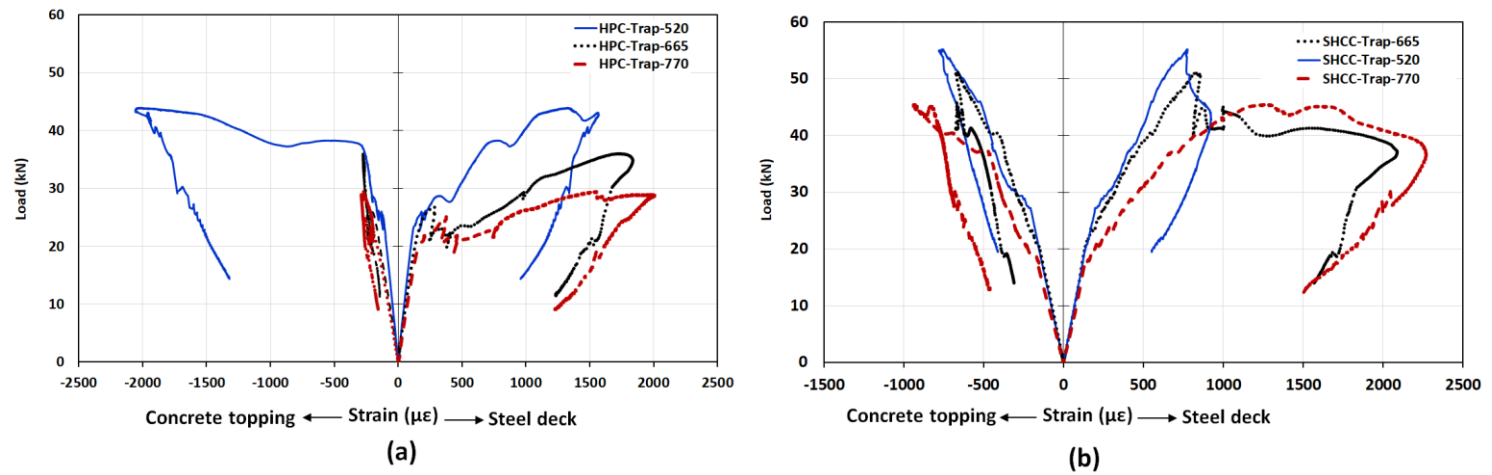


Fig. 11. Load-strain response: (a) slabs with conventional HPC, and (b) slabs with SHCC

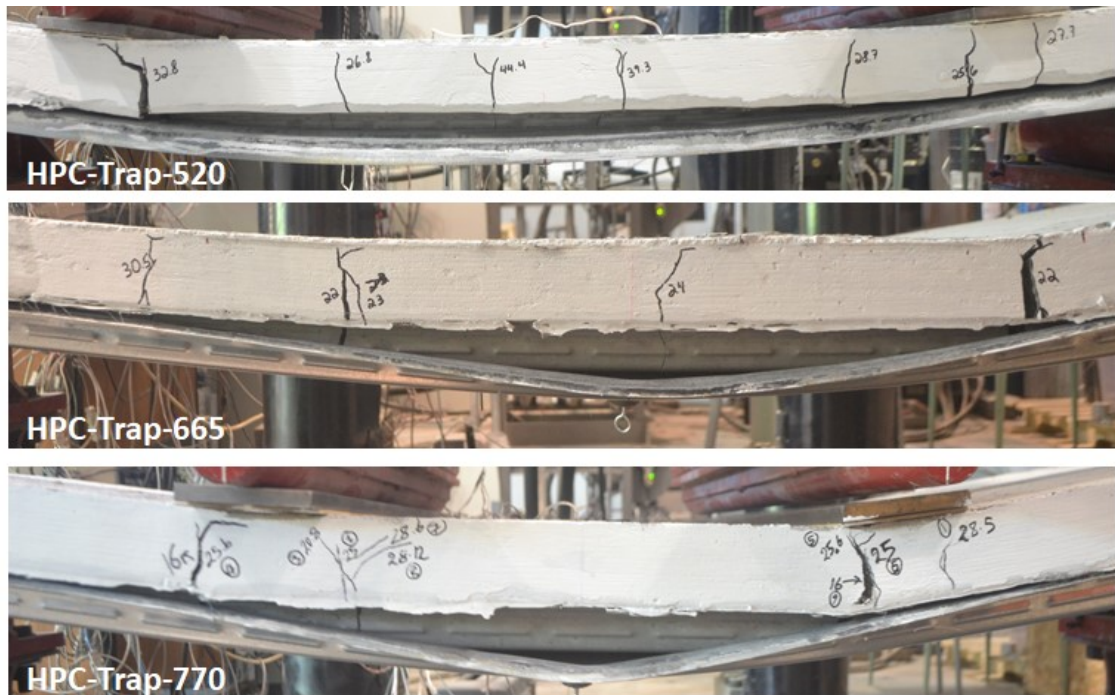


Fig. 12. Cracking pattern in composite slab with conventional HPC

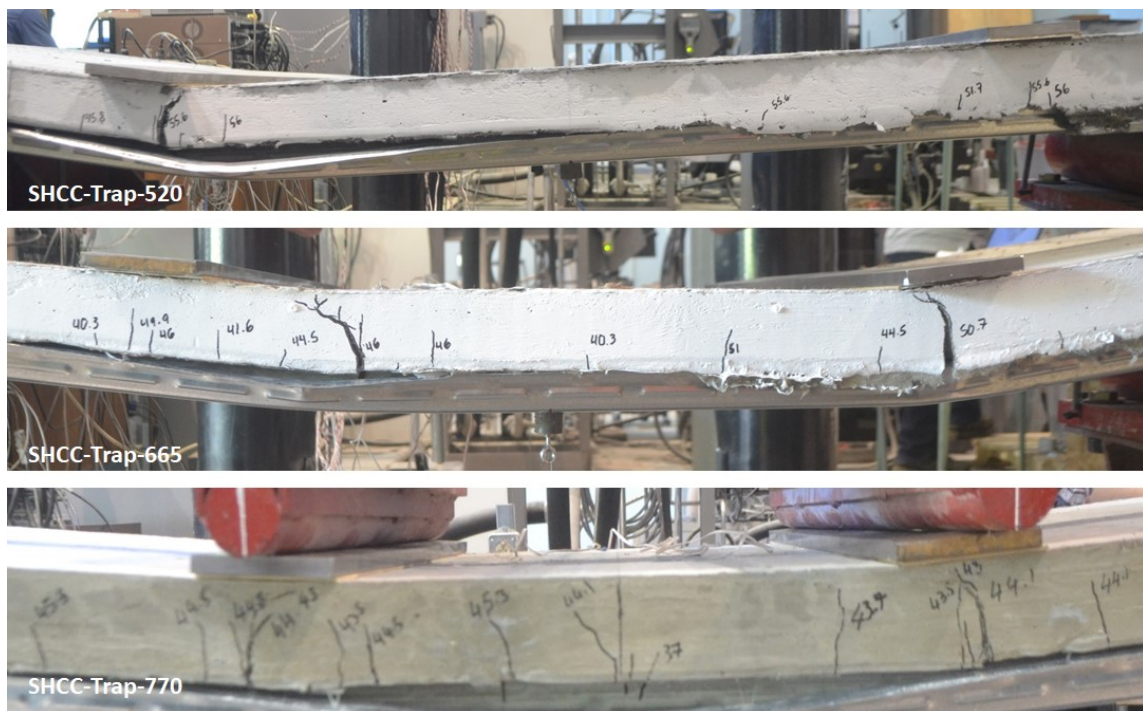


Fig. 13. Cracking pattern in composite slab with SHCC topping

4 Summary and conclusion

In this study, a newly developed ecological strain-hardening cementitious composite (SHCC) incorporating high-volume ground-glass pozzolans and modified at nanoscale with nano cellulose filaments has been used in structural application as a novel concrete to develop high-performance composite slabs. Fourteen composite deck slabs were constructed and tested under either static or fatigue loading. This includes seven SHCC slabs and seven slabs with a conventional high-performance concrete (HPC). Test variables include type of concrete topping (SHCC and HPC) steel deck geometry (reentrant and trapezoidal), shear span (520 and 665, 770 mm), and loading type (static and fatigue). The study provides an assessment of the structural performance of SHCC composite slabs as promising a material for constructing high-performance composite slabs with an improved performance. The specific portion of the study included in this thesis focuses on the load-deflection strain response, slip response as well as the cracking pattern for slabs with trapezoidal profile. Particular findings are as follows:

- For both HPC and HPC, composite slabs with shorter shear span exhibit higher load-carrying capacity as well as higher strain capacity.
- Compared to composite slabs with conventional HPC, SHCC exhibited higher first cracking load (by more than 100%) as well higher ultimate load-carrying capacity (up to 55%)
- The use of SHCC increased the load level corresponding to steel-concrete debonding, thereby contributed to increasing both the load and strain capacity.
- In SHCC composite slabs, the ductile feature of their SHCC topping was translated into a failure mode characterized by multiple cracking spread over the effective span as contrasted to the localized cracks observed in composite slabs with HPC.

Overall the study reveals that the use of SHCC in composite slabs increase the compatibility between the steel deck and its concrete topping thereby enhancing the composite action and resulting into improved load-carrying capacity.

Acknowledgement

The authors acknowledge the support from Canada Vanier Graduate Scholarship (CGS) program award no: 360284, Kruger Biomaterials Inc. (QC, Canada), Euclid Chemicals, and CANAM Canada

References

- ASCE Standard for the Structural Design of Composite Slabs. ANSI/ASCE 3-91 American Society of Civil Engineers, New York (1992).
- ASCE Standard for the Structural Design of Composite Slabs. ANSI/ASCE 3-91 American Society of Civil Engineers, New York (1992).
- B.S. Mohammed, M.A. Al-Ganad, M. Abdullahi, Analytical & experimental studies on composite slabs utilising palm oil clinker, *Constr. Build. Mater.* 25 (8) (2011) 3550–3560.
- BS 5950, Part 4: Code of Practice for Design of Floors with Profiled Steel Sheeting, British Standards Institution, London (1994).
- Eurocode 4-1994 Design of Composite Steel and Concrete Structures, Part 1. 1: General Rules and Rules for Buildings. EN1994-1-1 European Committee for Standardization, Brussels (2004).
- H.D. Wright, H.R. Evans, A review of composite slab design, in: *Proceedings of the Tenth International Specialty Conference on Cold-Formed Steel Structures*, St. Louis, Missouri, USA, 1990, pp. 27–47.
- H.D. Wright, H.R. Evans, P.W. Harding; The use of profiled steel sheeting in floor construction *J. Constr. Steel Res.*, 7 (4) (1987), pp. 279-295.
- Hisseine, O.A., and Tagnit-Hamou, A. (2019b). Characterization and nano-engineering the interface properties of high-volume glass powder strain hardening cement composites: Under review by the journal of Composites Part B.
- Hisseine, O.A., and Tagnit-Hamou, A. (2019c). Development of high volume-glass powder strain-hardening cement composites: Under review by the journal of Cement and Concrete Research
- Hisseine, O.A., and Tagnit-Hamou, A. (2019d). Development of nano-engineered strain-hardening cement composite with high volume-glass powder using cellulose filaments: Under review by Cement and Concrete Campsites.
- Hisseine, O.A., and Tagnit-Hamou, A. (2019e). Factorial design for the optimization of nano-engineered strain-hardening cement composite with high volume-glass powder and cellulose filaments: Under preparation, to be submitted to the journal of cement and concrete research.
- Hisseine, O.A., and Tagnit-Hamou, A. (2019f). Nano-engineered strain-hardening cement composites with high-volume ground glass pozzolans for high-performance composite slabs with improved shear-bond capacity: Under preparation, to be submitted to the journal of Engineering Structures.
- K.M.A. Hossain, S. Alam, M.S. Anwar, K.M.Y. Julkarnine, High performance composite slabs with profiled steel deck and Engineered Cementitious Composite – Strength and shear bond characteristics, *Construction and Building Materials*, Volume 125, 2016, Pages 227-240,
- McCuaig, Laurence A. and Schuster, R. M., "Repeated Point Loading on Composite Slabs" (1988). *International Specialty Conference on Cold-Formed Steel Structures*. 3.
- McCuaig, Laurence A. and Schuster, R. M., "Repeated Point Loading on Composite Slabs" (1988). *International Specialty Conference on Cold-Formed Steel Structures*. 3.
- R. Abdulla, W.M. Easterling, New evaluation and modeling procedure for horizontal shear bond in composite slabs, *J. Constr. Steel Res.*, 65 (4) (2009), pp. 891-899
- R.M. Schuster, Composite steel-deck concrete floor systems, *J. Struct. Div. ASCE*, 102 (5) (1976), pp. 899-917.

Part 5

Concluding messages

Chapter 11: Conclusions, recommendation, and perspectives (English)

Chapter 12: Conclusions, recommandation et perspectives (Français)

CHAPTER 11

Conclusions and Perspectives (English)

11.1 Conclusions

In the present thesis, the viability of using a new type of nanocellulose material (NCM), namely cellulose filaments (CF) for nanoengineering the properties of cement and concrete composite has been undertaken through a comprehensive experimental program extending from nanoscale measurement with nanoindentation assessment to full-structural scale elements. Through this research, CF were demonstrated promising for nanoengineering concrete properties at its three major states (fresh, hardening, and hardened). As such, in relation to these three states of concrete, three potential applications of CF were identified: (i) viscosity modifying agent (VMA) for fresh concrete, (ii) shrinkage reducing admixture (SRA) for hardening concrete, and (iii) nanoreinforcing tool for hardened concrete. While these effects of CF can be interacting within the same mixture, the scope of the current project focused on characterising the separate effects. Specific conclusions are as follows:

- CF can serve as an alternative VMA without noticeable drawback on hydration kinetics while serving for collateral functions such as fiber bridging and internal curing (as transposed by the multifunctional aspects of natural systems). This is in contrast to most of commercially available VMAs which interfere with cement hydration and lead to significant set retardation and drop in strength gain when high dosages are used.
- Beside CF hydrophilicity, the basic mechanism underpinning the VMA effect of CF is its high aspect ratio (up to 1000) as well as its flexibility. Thus, a geometry-based percolation model indicated that CF fibrils can form a percolated network of connected fibrils which can bridge cement particle and increase mixture consistency. The minimum CF dosage necessary to reach the percolation threshold was identified as ≈ 0.12 wt.% which coincided with an inflection point in the trend of mixture demand in high-water reducing admixture (HRWRA) as well as in the trend of rheological properties in terms of Bingham parameters (yield stress and plastic viscosity). Therefore, to obtain a VMA effect of CF without excessively increasing the HRWRA demand, a maximum CF

content of 0.12% is recommended. However, this dosage can be exceeded in situations where internal curing is the target.

- The hydrophilic and hygroscopic features of CF can enhance the properties of hardening concrete. This effect can be better captured in low water-to-cement systems where autogenous shrinkage is more pronounced. In this context, CF was found to contribute towards reducing the autogenous shrinkage in ultra-high-performance concrete (UHPC) with a particular effect at early ages (due to the time dependent water dispatch from CF). CF can reduce the autogenous shrinkage during the early age (within the 1st 24 hours) by up to 45% and during the first 7 days by up to 35%. This is advantageous as compared to the effect of adjusting the mixture content in silica fume (25-15%) which lead to a significant drop in flexural capacity (32% lower).
- CF enhances the mechanical properties of cement pastes and concrete by a coupled effect of internal curing and nanoreinforcing. The internal curing can also be accompanied by the hygroscopic CF providing pathways to diffuse water from water-saturated parts of the matrix towards anhydrous cement grains as demonstrated by SEM micrographs supporting the likelihood of this hypothesis. On the other hand, the nanoreinforcing effect was found to provide bridging at the scale of hydrates and a reinforcing tool to the porous network at the interfacial transition zone. As a result, it is possible to increase the elastic modulus of cement and concrete composites by around 18%, and the flexural capacity and toughness by up to 25 and 96% respectively.
- CF effects on mechanical performance sprout from its ability to nano-modify the microstructure properties. As such, the improved mechanical properties at the macroscale were found to be buttressed by an increased degree of hydration at the microstructure level as well as increased micromechanical properties (indentation modulus, hardness, and contact creep) of major microstructure phases where the micromechanical properties of C-S-H can be improved by up to 25%.
- Salient opportunities offered by CF for altering the properties of cement systems were leveraged towards the development of nano-engineered strain-hardening cementitious composite (SHCC). For this, firstly, a new SHCC was developed via a new approach coupling particle packing optimization with micromechanical tailoring. Here, the new

approach provided a systematic replacement of FA by GP. In this quest, replacing the commonly used fly ash (FA) with ground-glass pozzolans (GP) under the guidance of packing density optimization lead to mixtures with enhanced strength. However, for mixtures incorporation GP in excess of 40%, the ductility is relatively lower. With CF incorporated at ranges from 0.03-0.10, it was possible to enhance the elastic modulus of the plain matrix and reduce the crack tip toughness. On the other hand, the high surface of CF high allowed attenuating excessive interfacial frictional bond between PVA fibers and the matrix (as encountered at high GP content) while imparting a characteristic slip-hardening effect which contributed towards imparting a more ductile composite behavior.

- The characteristic slip-hardening effect imparted by CF at the micromechanical behaviour of interface properties was translated into higher complementary energy. When the latter is paralleled with the increased matrix elastic modulus (and reduced crack tip toughness offered by CF), enhanced complementary energy and ductility were obtained, particularly in mixtures with high GP content. Thus, for selected SHCC mixtures with GP content of 0, 40, and 100% in replacement of FA, the improvements in ultimate strain capacity were respectively 26, 37, and 258%. Consequently, the energy absorption capacity was enhanced with CF by up to 52, 83, and 238%, respectively. Thus, with the incorporation of CF, it was possible to produce SHCC with up to 100%GP replacement of FA exhibiting higher strength and ductility, while contributing towards promoting ecoefficiency.
- Scaling-up the newly developed SHCC to structural application by using this SHCC as concrete topping in composite deck slabs increased the compatibility between the steel deck and its concrete topping, led to resisting higher load prior to steel-concrete separation, and eventually resulted into slabs with improved ultimate flexural load carrying capacity by up to 55%. This improvement in ultimate capacity was accompanied by a ductile failure characterized by multiple cracking spread over the effective span as contrasted to the localized cracks observed in composite slabs constructed with conventional high-performance concrete.

11.2. Perspectives

While CF offers several opportunities to enhance the performance of cement systems, the following aspects need be carried over for further research:

- The effectiveness of CF in the enhancement of most properties appears to be at low dosages typically 0.03-0.15%. While this can be justified by the increased CF surface area, it is almost undebatable that effective dispersion at high CF content is a challenge. Currently the dispersion protocol involves high shear mixing. Ultrasonication has been proven effective with several nanomaterials but its use in field application is not evident. For this, it is recommended that CF may be functionalized by grafting onto its surface surfactant molecules with a twofold effect to: (i) enhance CF dispersion, and (ii) play a dispersing role in the mix by replacing the HRWRA.
- Develop effective dispersion techniques adoptable with in-situ casting. Current dispersion techniques and tool are adapted to laboratory-scale specimens. At industrial scale, much more effective dispersion protocols are needed. This can be attempted at the same time with the former proposition on grafting surfactants on CF surface to promote dispersion. This will reduce the amount of water being used now to make readily dispersed CF suspension where the cost of transporting suspensions (majorly water) is perceived to add to the concrete invoice.
- While market-based applications of CF-concrete has just started (upon the findings of this research) in one industrial sector (in cement-based sewer pipes by a Quebec-based firm), further markets should be explored to valorise the multifunctional aspects of the material. For instance, the VMA effect of CF associated with the formation of nanoscale filament networks bridging cement particle and fostering mixture stability, may be exploited in shotcrete applications, in extruded concrete, and in printable concrete.
- Characterize the interaction between the different roles of CF and how these interactions can influence composite properties so that adequate CF dosage for specific desirable functions may be determined. For instance, separating the nano-bridging effect from the internal curing effect in autogenous shrinkage control, may allow determining the adequate CF dosage necessary to provide a given tensile resistance to the matrix to

withstand volumetric instabilities. Or vice-versa this can allow quantifying the amount of water needed for stabilize matrix internal relative humidity and consequently control self-desiccation.

- The synergy between CF and macro-fibers detected in strain-hardening cementitious composites (SHCC) can be explored further with other FRC types such that FRC incorporating CF can be made with reduced macrofiber content, thereby reducing the cost of producing conventional FRC.
- Characterise the coupled effect of CF and other shrinkage reducing admixtures such as those responsible for reducing pore surface tension and those acting by expansion such as sulfo-aluminate-based expansive agents.
- Valorise the water carrying capacity of CF to explore the coupled effect of CF and self-healing agents necessitating water supply to be efficient.
- The long-term durability of CF in cement systems is a concern requiring further studies. Major concerns in this matter relate to the potential degradation of CF inside the high pH and alkaline medium of cement.

CHAPTER 12

Conclusions et Recommendation (Français)

12.1. Résumé et Conclusion

Cette étude a pour but de valoriser un nouveau type de matériau nano-cellulosique, notamment, les filaments de cellulose (FC) pour développer des bétons nano-modifiés à performances améliorées. Au cours de cette recherche, l'incorporation des CF a été démontrée efficace pour une nano-ingénierie des propriétés du béton dans ses trois états principaux (frais, durcissant et durci). Ainsi, en relation avec ces trois états, trois applications potentielles de FC ont été identifiées: (i) l'utilisation des FC comme agent modificateur de viscosité (VMA) pour le béton frais, (ii) utilisation de FC comme un adjuvant réducteur de retrait (SRA) pour le béton durcissement, et (iii) l'utilisation de FC comme un renforcement nanométrique. Les conclusions spécifiques suivantes sont tirées de cette étude:

- Les FC peuvent servir comme un agent modificateur de viscosité (VMA) ainsi offrant une option alternative aux VMA traditionnels, sans avoir des inconvénients sur la cinétique d'hydratation tout en conférant des fonctions collatérales telles que le pontage de fissures et la cure interne. Ceci est difficile à obtenir avec la plupart des VMA couramment utilisés tels que ceux à base de Welan Gum (qui interfèrent avec l'hydratation du ciment et entraînent un retard de prise important et une perte de résistance lorsque des teneurs élevées sont utilisées).
- Outre le caractère hydrophile des FC, le mécanisme de base qui sous-jacent l'effet VMA de la CF est le ratio d'aspect élevé (jusqu'à 1000) ainsi que la flexibilité des fibrilles cellulosiques nanométriques. Ainsi, un modèle de percolation basé sur la géométrie a indiqué que les FC forment un réseau de fibrilles connectées (percolées) pouvant relier les particules de ciment et augmenter la consistance du mélange. La teneur minimale de FC nécessaire pour atteindre le seuil de percolation a été identifiée à environ 0,12% en poids de liant, ce qui coïncide avec un point d'inflexion de la tendance de la demande des pâtes cimentaire et bétons en superplastifiant ainsi que sur la tendance des propriétés

rhéologiques. Par conséquent, pour obtenir un effet VMA des FC sans une augmentation excessive en teneur de superplastifiant, un dosage maximal en FC de 0,12% est recommandée. Cependant, ce dosage peut être dépassé dans les cas où l'effet de cure interne est visé.

- Les caractéristiques hydrophiles et hygroscopiques des FC peuvent améliorer les propriétés du béton durcissant. Ces potentiels peuvent être exploités dans des systèmes à faible rapports eau-sur-liant (E/L). Dans ce contexte, il a été constaté que les FC contribuent à la réduction du retrait autogène dans les bétons à ultra hautes performances avec un effet particulier à jeune-âge (en raison d'une action synergétique articulant le dégagement de l'eau contenue dans les FC au pontage des fissuration): Des réductions en retrait endogène jusqu'à 45% et 35% ont été obtenues au cours des premiers 24 heures et 7 jours, respectivement. Ceci est avantageux par rapport à l'effet de l'ajustement de la teneur de la fumée de silice (25-15%) qui conduit à une chute significative de la capacité de flexion (une réduction de 32%).
- Les FC améliorent les propriétés mécaniques des composites cimentaires par un effet double : (i) un effet de renforcement, et (ii) un effet de cure interne. Le premier peut également être accompagné par l'effet des FC (étant hygroscopiques) fournissant des voies pour diffuser de l'eau à partir des particules saturées en eau vers des particules anhydres. D'autre part, l'effet de nanoreinforcement permet un pontage des fissures à l'échelle des hydrates et de renforcer la zone de transition interfaciale. Pour ce, avec l'incorporation de FC, il était possible d'augmenter le module d'élasticité des composites cimentaire jusqu'à 18%, ainsi que la résistance à la flexion (25%) et la ténacité (96%).
- L'effet des FC sur les performances mécaniques discutées ci-haut, provient de la capacité de FC à nano-modifier les propriétés de la microstructure. Ainsi, l'amélioration des propriétés mécaniques à l'échelle macroscopique est supportée par un degré d'hydratation amélioré au niveau de la microstructure ainsi que par des propriétés micromécaniques plus importantes (module d'indentation, dureté, et fluage du contact)

des phases majeures de la microstructure où les propriétés micromécaniques de CSH été améliorées jusqu'à 25%.

- Pour une mise en valeur des différents apports de la nano-modification des composites cimentaires par l'incorporation des FC, une nouvelle formulation d'un béton de haute performance de type béton écouissant a été développée. La conception de ce nouveau béton a suivi une nouvelle approche articulant l'optimisation de la compacité granulaire avec les modèles micromécaniques. Ainsi, la poudre verre (PV) provenant du concassage des bouteilles de verre a été incorporée en remplacement de la cendre volante (CV) – souvent utilisée dans cette application – de manière à optimiser la compacité de la matrice pour améliorer la résistance mécanique. Par la suite, les FC ont été introduits comme un renforcement nanométrique permettant d'obtenir un béton renforcé à multi-échelle.
- Les résultats démontrent que les FC ont permis de nano-renforcer la matrice ainsi que d'améliorer les propriétés d'interface entre la matrice et les macro-fibres d'alcool polyvinylique (PVA), permettant ainsi d'améliorer le comportement d'écrouissage. Ainsi, des bétons écouissants contenant jusqu'à 100% de PV en remplacement de CV ont été développés. Les formulations obtenues ont un caractère autoplaçant (≈ 250 mm d'étalement) et présentent (à 28 jours) une résistance à la compression de 60-75 MPa, une capacité de flexion de 9-15 MPa, une résistance à la traction directe de 3-6 MPa, une capacité de contrainte de traction de 2-5% et une résistivité électrique améliorée. Les bétons formulés présentent, alors, des performances mécaniques supérieures à celles des bétons écouissants contenant la CV. Néanmoins, bien que l'amélioration de la résistance mécanique obtenue avec la PV ne compromette pas la ductilité du composite jusqu'à 40% de PV, une ductilité réduite a été observée quand la teneur en PV dépasse 40%. Pour ce, le FC a été utilisé pour conférer un effet nano-renforçant ainsi que pour améliorer les propriétés d'interface entre la matrice et les macro-fibres. L'incorporation des FC a démontré un double effet sur le comportement des bétons écouissants : (i) le module d'élasticité de la matrice plane des bétons écouissant est très important en présence des FC. Ceci a contribué à réduire la ténacité de la fissuration, (ii) les FC ont

atténué la friction excessive—entre les macrofibres et la matrice—rencontrée à des teneurs élevées en PV (limitant la ductilité du béton). Les FC ont aussi conféré un effet écrouissant à l'arrachement des macro-fibres de PVA permettant ainsi d'accroître la capacité de contrainte en traction. Une amélioration de la capacité de déformation et de la ductilité au-delà de 200% par rapport aux systèmes sans FC a été obtenue. Ainsi, avec l'incorporation de FC, il était possible de produire des bétons écrouissant contenant jusqu'à 100% de PV en remplacement de CV tout en présentant des résistances mécaniques et ductilités plus importantes.

12.2 Recommandations

Bien que les FC offrent plusieurs possibilités d'améliorer les performances des composites cimentaires, les aspects suivants doivent être considérés dans les travaux ultérieures:

- L'efficacité des FC à améliorer les propriétés de bétons semble -dans la majorité des cas- se situer à des dosages très faibles, généralement de 0,03 à 0,15%. Des teneurs élevées en FC sont moins efficaces et parfois causent des résultats négatifs. Ceci est due principalement à la dispersion qui devient de plus en plus difficile en haute teneurs en FC. Actuellement, le protocole de dispersion (mélange à haute cisaillement et dispersion en utilisant des polycarboxylate) demeure efficace pour des quantités de béton à l'échelle du laboratoire, pour des applications de chantier, des nouveaux protocoles doivent être développés. La fonctionnalisation des FC (en y-greffant des molécules dispersant) est l'un des sujets à explorer pour améliorer la dispersion.
- Alors que l'applications de béton incorporant des FC au marché vient tout juste de commencer (d'après les résultats de cette recherche) dans un secteur industriel (tuyaux à béton), d'autres marchés devraient être explorés pour valoriser les aspects multifonctionnels des FC. Par exemple, l'effet VMA et thixotropique des FC peut être exploité dans les applications des béton projetés, des béton extrudés et bétons imprimés.
- Caractériser l'interaction entre les différents rôles de FC et la manière dont ces interactions peuvent influencer sur les propriétés de béton, de manière à pouvoir déterminer

un dosage adéquat de FC pour des fonctions spécifiques visées. Par exemple, en ce qui concerne le retrait endogène, le fait de séparer quantitativement l'effet de nano-renforcement de celui de la cure interne pourra permettre de déterminer le dosage adéquat de FC nécessaire pour fournir une résistance à la traction donnée à la matrice afin de résister aux instabilités volumétriques. En outre, cela pourra permettre de quantifier la quantité d'eau nécessaire pour contribuer à la stabilisation de l'humidité relative interne de la matrice et par conséquent de contrôler l'auto-dessiccation.

- La synergie entre les FC et les macrofibers telle que détectée dans les bétons écrouissant peut être transposée vers d'autres types de bétons fibrés, de telle sorte à produire des bétons fibrés plus écologiques (incorporant moins de macrofibers)
- Caractériser l'effet synergétique entre les FC et d'autres agents réducteurs de retrait, tels que ceux responsables de la réduction de la tension de surface des pores et ceux agissant par expansion tels que les agents d'expansion à base de sulfo-aluminate.
- La durabilité à long terme des FC dans les composites cimentaires est une préoccupation qui nécessite des études supplémentaires. Les principales préoccupations à cet égard concernent la dégradation potentielle des FC dans le milieu alcalin à pH élevé du ciment.



**DÉVELOPPEMENT DES BÉTONS NANO-MODIFIÉS AUX
PERFORMANCES AMÉLIORÉES**

*(NANO-ENGINEERING CONCRETE PROPERTIES FOR
ENHANCED PERFORMANCE)*

